FLOW AND HEAT TRANSFER MEASUREMENTS INSIDE A HEATED MULTIPLE ROTATING CAVITY WITH AXIAL THROUGHFLOW

Nicolas D. D. Miché

Submitted for the degree of Doctor of Philosophy

Department of Engineering, School of Science and Technology
University of Sussex
September 2008

DECLARATION

I hereby declare that this thesis has not been submitted, either in the same or different form, to this or any other University for a degree.

Nicolas D. D. Miché
September 2008

PREFACE

The work reported in this thesis was carried out at the Thermo-Fluid Mechanics Research Centre (TFMRC), a Rolls-Royce University Technology Centre for aero-thermal systems. The experimental program was funded by the European Union and a consortium of European gas turbine manufacturers under the BRITE-EURAM Framework V scheme ICAS-GT2. Inevitably, certain aspects of the rig design and instrumentation, as well as the forming of the testing programme were carried out in collaboration with the author's colleagues in the industry and within the Centre. However, the experiments and evaluation of the results reported in this thesis were carried out by the author, except where indicated in the text.

UNIVERSITY OF SUSSEX

Nicolas D. D. Miché **Doctor of Philosophy**

FLOW AND HEAT TRANSFER MEASUREMENTS INSIDE A HEATED MULTIPLE ROTATING CAVITY WITH AXIAL THROUGHFLOW

SUMMARY

This thesis discusses experimental results of measurement of heat transfer and velocity flow in a heated multiple cavity test rig with axial throughflow. Of particular interest are the internal cylindrical cavities formed by adjacent discs and the interaction of these with a central axial throughflow of cooling air. Tests were carried out for a range of non-dimensional parameters representative of gas-turbine high pressure compressor internal air system flows (Re_Φ up to $5x10^6$ and Re_z up to $2x10^5$). One configuration of the test rig was tested in the course of the reported study (Build 3) and test data from a previous rig configuration (Build 2) were processed, analysed and compared with the tested data. The most significant difference between the two builds of test rig was the size of the annular gap between the (non-rotating) shaft and the disc bores. Build 3 had a wider annular gap ratio, $d_h/b=0.164$, while Build 2 featured a gap ratio of $d_h/b=0.092$. Heat transfer data were obtained from thermocouples and a conduction analysis. Heat transfer results show differences between the versions of the rig, with the higher Nusselt number values in Build 3 attributed to the wider annular gap allowing more of the throughflow to penetrate into the cavity compared to Build 2. An attempt is made to correlate the average disc Nusselt numbers and this indicates the existence of different regimes. A two-component Laser Doppler Anemometry system was used on both rigs to measure cavity axial and tangential velocity components. Optical access in Build 3 also allowed for measurement of radial velocities. The axial and radial velocities inside the cavities are virtually zero. The size of the annular gap between disc bore and shaft has a significant effect on the radial distribution of tangential velocity. An analysis of the frequency spectrum obtained from the tangential velocity measurements shows evidence of periodicity in the flow consistent with the current understanding of the flow structure in a heated rotating cavity with axial throughflow.

TABLE OF CONTENTS

LIST OF APPENDICES

LIST OF FIGURES

LIST OF TABLES

NOMENCLATURE

a, b		inner and outer radii of a disc
A		area
C_p		specific heat at constant pressure
d		diameter
d_h		hydraulic diameter of the inlet
D		rotor outer diameter
f		frequency
G	$= s/b$	gap ratio
Gr_{sh}		shroud Grashof number
Gr_y		Grashof number
h		heat transfer coefficient
k		thermal conductivity
L		appropriate length scale
$\dot{m}$		mass flow rate of the throughflow
n		number of subcases
N		number of disc or shroud surfaces, or number of LDA fringes
Nu	$= q\ r / \Delta T\ \mathrm{k}$	local Nusselt number
$Nuav$	$= q_{av}\ b / \Delta T_{av}\ \mathrm{k}$	average Nusselt number
$Nush$	$= q_{sh}\ (s/2) / \Delta T_{av}\ \mathrm{k}$	shroud Nusselt number
Nuy	$= q\ y / \Delta T\ \mathrm{k}$	Nusselt number based on y
p		pressure
Pr	$= \mu\ C_p / \mathrm{k}$	Prandtl number
q		heat flux
r, z, Φ		radial, axial and tangential coordinates
r_I, r_o		inner and outer radii for evaluation of average disc heat transfer
r_s		shaft radius
Re_z	$= W\ d_h / \nu$	axial Reynolds number
Re_Φ	$= \Omega\ b^2 / \nu$	rotational Reynolds number
Ro	$= W / \Omega\ a$	Rossby number

s		axial width of cavity, standard deviation
Sk		Stokes number
t		thickness of disc
T		temperature
$\overline{u}$		mean value of velocity component
u,U		normal component velocity, standard uncertainty
U_α		uncertainty in the quantity α
V_r V_z, V_φ		radial, axial and tangential velocity components
W		bulk mean axial velocity of the throughflow
x	= r/b	non dimensional radial coordinate
y	= $b - r$	distance radially inward from shroud
α		angle
β	= $1/T$	volume expansion coefficient
δ		spacing or interval
ΔT		appropriate temperature difference
ε		emissivity
θ		angle
λ		wavelength
μ		dynamic viscosity
ν		kinematic viscosity
ρ		density
σ		R.M.S value
τ		characteristic response time
ω		angular frequency
Ω		rotational speed of the cavity

Subscripts and superscripts

air	value for air
av	radially weighted average
b	value at r = b
c	constant, cut-off value
cav	value inside the cavity
conv	pertaining to convective heat transfer
d	pertaining to the downstream disc of the cavity,

	Doppler
f	pertaining to the LDA fringes, fluid
fin	pertaining to fin solution
g	gravitational acceleration
i, o	values on the inside and the outside of the shroud, respectively, increment value
in	value at inlet
j	increment value
p	particle
rad	pertaining to radiative heat transfer
r	value at radius r
ref	appropriate reference value
s	denotes a value at the surface
sh	pertaining to the shroud
T	total
t	pertaining to time
u	pertaining to the upstream disc of the cavity
95	95% interval

ACKNOWLEDGEMENTS

First of all, I would like to thank my supervisors Dr. Christopher Long and Prof. Peter Childs for their help, support and guidance throughout this project.
My gratitude also extends to the sponsors of this project: Rolls Royce Plc, the European Union and participating companies in the 5th Framework of the BRITE-Euram scheme.

I am grateful to Dr. Alex Alexiou, now at the Technical University of Athens, for his experimental work on Build 2 of the Multiple Cavity Rig and for showing me the ropes on Build 3. Dr. Steven Begg at Brighton University was also extremely helpful with his advice and training on laser measurements.

On a more personal level, I would like to acknowledge my former colleagues and friends at Sussex University's TFMRC who made my time there so much more enjoyable.

Finally, my thanks go to my family for all their help and encouragement over the years, as well as to Douglas J. Oliver MIMechE for proof reading this thesis and to my wife Philippa for editing and general moral support.

1. Introduction

Gas turbines are internal combustion heat engines that use the thermal energy rise from a continuous combustion process on a mass flow of air to be converted into useful work such as thrust or shaft mechanical power. Engines operating at higher combustor output temperature also have a higher thermal efficiency. The obstacle to this maximisation of the power output of gas-turbines lies within the resistance of the turbine blade material and nozzle guide vanes to extreme temperatures and combined high tensile stresses induced by the turbine rotation (10000 rev/min for a typical high pressure turbine on a 0.6 m diameter). The use of air-cooled blades in the turbine assembly allows the heat (typically in the order of 1800 K in a modern civil engine such as the Rolls-Royce Trent 1000 featured in Fig1.1) that would compromise the material integrity of the turbine components to dissipate locally.

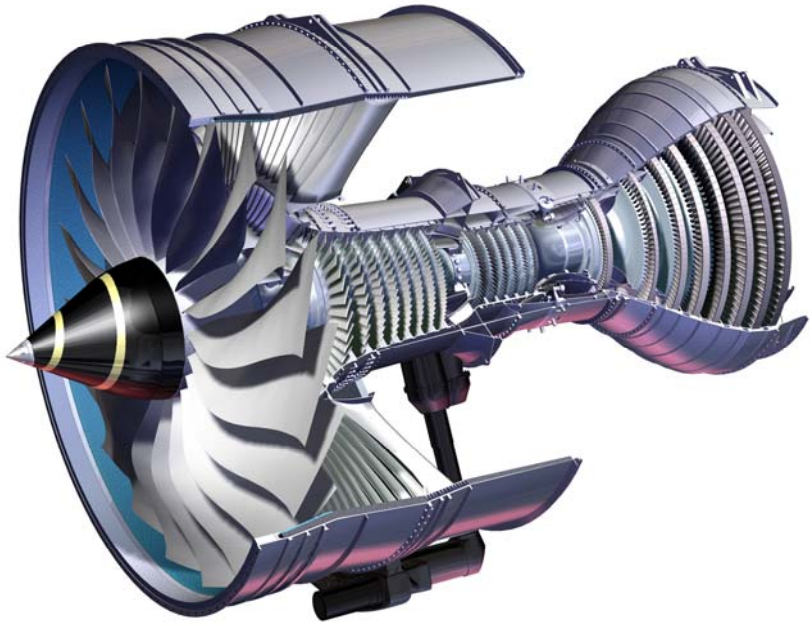

Fig 1.1 Trent 1000 engine cut-away, courtesy of Rolls-Royce plc.

Air cooled turbine blades and nozzle guide vanes are constructed with air passages in their cores being fed by a flow of cooling air allowing convective heat transfer to extract excessive heat from the material to the cooling air.

Part of this cooling air flow can also exit on the blade/vane and form a cooling film of air on the surfaces. Heat conduction from the turbine blade to its supporting disc also requires some cooling of the disc to prevent excessive mechanical growth and fatigue. The cooling air supply to the turbines originates from the internal part of the turbine assembly, away from the main stream of gases, in a zone where the cooling flow will act on the turbine assembly disc and be fed through holes on the blade stem into the blade itself. The pressure of this cooling air should be higher than the main gases pressure at the point in the turbine stages where it would exit in order to ensure positive flow and effective cooling. The mass flow rate of air to be fed to the cooled components, although small compared to the mainstream of gases, is by no means negligible. Gas-turbine manufacturers generally divert part of the airflow from the compressor stages to feed the air cooling system downstream of the combustors. This avoids the need for an external compressor system to power the cooling air path, it saves weight and simplifies the overall design of the gas-turbine.

However, the work carried out to compress the cooling air and the fact that this air does not participate directly in useful power generation are parasitic to the overall cycle of the engine (to the order of up to 6% of the specific fuel consumption in a modern turbofan engine according to Rolls-Royce, 2005). There is therefore a trade-off between thermal efficiency gains from increased turbine inlet temperatures and parasitic losses from cooling air and compression work to be provided for protection of the turbine assembly components from melting and excessive thermal distortion. A direct action in order to reduce the thermal efficiency losses due to the use of cooling air is to minimise the amount of this air required to ensure an effective and reliable use of the gas-turbine. An effective way to reduce the flow rate of cooling air is to deliver the cooling air at the lowest temperature possible in order to increase the cooling, thus using less air for the same cooling effectiveness.

Fig 1.2 shows the typical routes taken by this cooling air across a gas-turbine. This internal air path is referred to as the secondary air system of a gas-turbine because, as explained above, this air does not participate directly in the gas and thrust production.

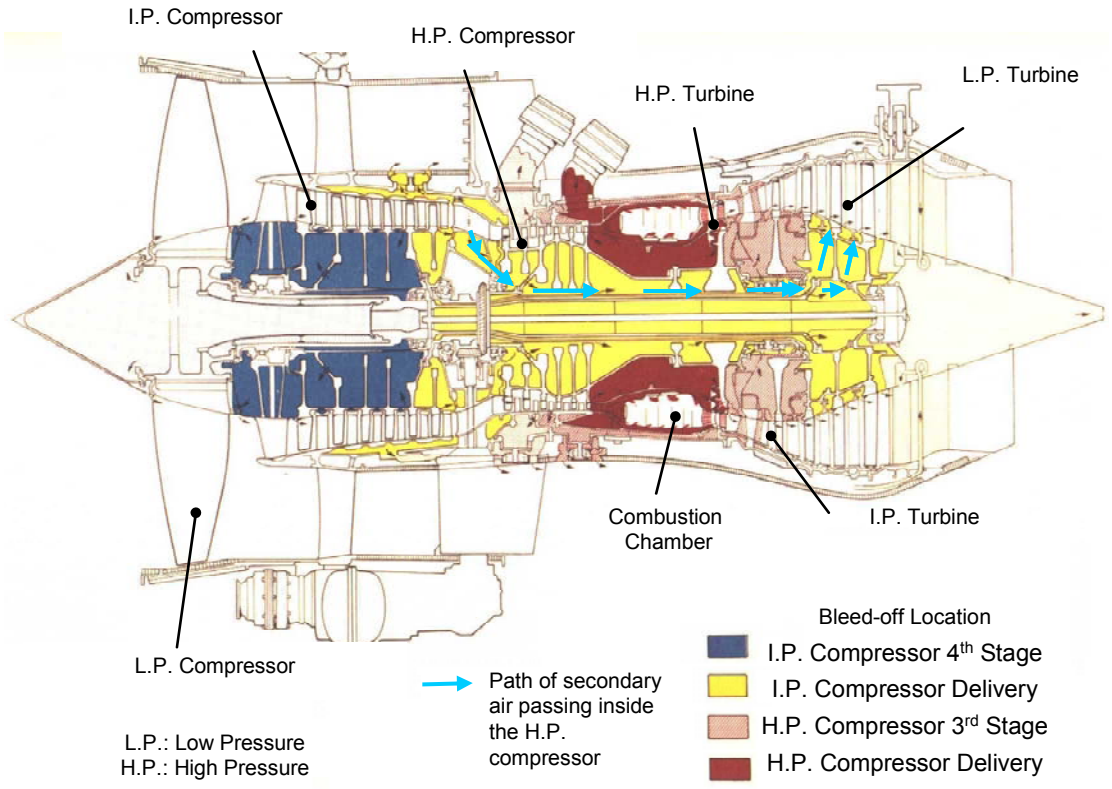

Fig 1.2 A typical gas-turbine aero-engine internal air system (Rolls-Royce plc.)

Of particular relevance to the subject of this thesis, is the air that is extracted from stages of the intermediate pressure compressor and used for the cooling and sealing of the low pressure turbine stages. This air travels from the compressor to the turbine area in the central part of the rotor and drive shafts as shown in Fig 1.3.

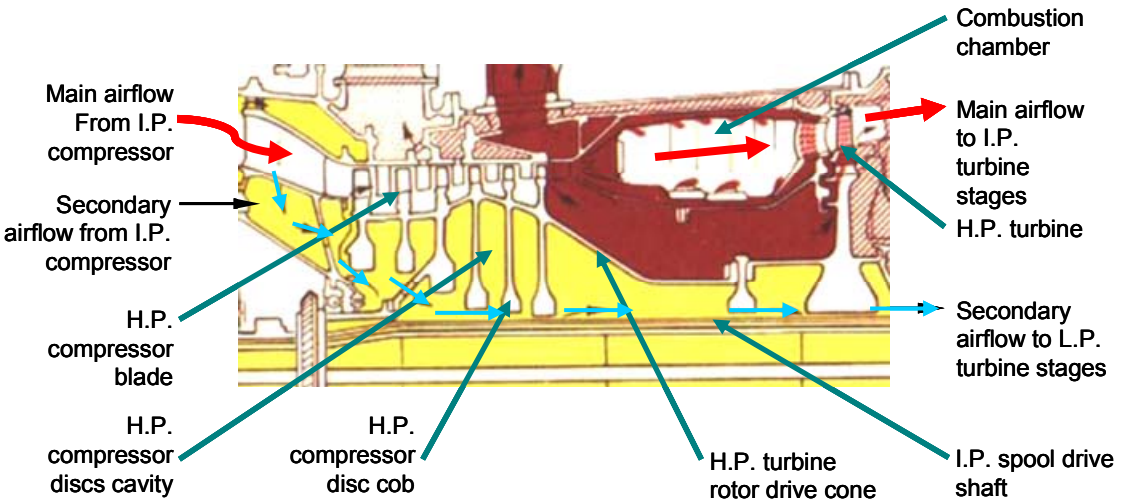

Fig 1.3 Typical layout of a H.P. compressor and turbine stage (Rolls-Royce plc.)

The rotor comprises a succession of narrow annular passages and cavities formed by the disc and hollow drive shafts. All these components also are subject to rotation, sometimes in different relative speeds and directions to each other. Viscous forces acting on the air through these flow obstacles and rotational forces also impair the pressure ratio across the internal air system and hence reduce the cooling air flow on the turbine side. Higher pressures in the compressor stage will also induce more heat rise of the air due to compression. As the cooling air passes through the internal components of the rotor, viscous dissipation ensues from the interaction of the cooling air with the various rotating parts (termed windage). Heat gain or losses are induced depending on the heat conducted through the metal of the components by the actual temperature of the main gas stream in the vicinity (e.g. heat conduction through the drive cone as a result of high temperatures in the combustion chamber). A knowledge of the heat transfer from the internal surfaces of the rotor components to the cooling air in the secondary air system is therefore important for the engine designer in order to predict not only the cooling efficiency of the turbine but also the thermal growth and metal stress and fatigue of the engine components.

The internal air system therefore provides sealing of the gas-turbine and acts on the overall safety and reliability of the gas-turbine. It is therefore of importance to understand the mechanisms involved with the flow characterisation and heat transfer occurring inside the secondary air system. The subject of the current thesis focuses on an investigation of the heat transfer and flows encountered inside the rotating cavities formed by the discs of the high pressure compressor stages of a typical gas-turbine engine. The surface temperatures and flow velocity measurements of the engine components were performed in an experimental apparatus representing the internal components of a high pressure compressor disc stack with a throughflow of air. The conditions of operation such as heating, secondary flow supply and rotational speed were near engine representative conditions.

This study follows on more than twenty years of previous studies, mostly performed at the TFMRC at the University of Sussex.

Notably Farthing et al. (1992 a and b) and Long (1994) established the fundamental and influential parameters governing convective heat transfer in cavities with superposed radial and axial flow on an idealised geometry experimental apparatus. Later, Alexiou (2000) performed experimental studies on engine representative geometry and operating conditions multiple cavity rig.

The present work follows on from Alexiou's in a later generation of near engine geometry experimental rig with heat transfer instrumentation and provision for non-invasive airflow velocity measurement within the represented cooling air flow.

This work reported here is the embodiment of a leading edge experimental research programme which has successfully investigated the flows existing in the internal air systems of gas turbine engines. The results from this study have highlighted a dependency on the annular gap between the shaft and the discs on the in-cavity tangential velocity flow field and the discs heat transfer. Radial velocity flow measurements show evidence of periodicity in the flow, consistent with the passage of circulating bodies within the cavities. The shroud heat transfer measurements were consistent with earlier work and showed similarities to natural convection from a horizontal plate. The adoption of precision instrumentation and techniques, including LDA, has facilitated the quantification of highly complex flow structures which expands the understanding of the heat transfer mechanisms which are influenced by such flows. Such improvements are beneficial for the prediction of component temperature and life. The new data is also useful for the validation of CFD codes, where unsteady effects or buoyancy driven flows are inherently difficult to model accurately, which are used in the development of new engines.

In chapter 2, an introduction to the subject of flow and heat transfer in rotating cavities is provided. A description of the current literature is presented detailing the governing parameters and the current understanding of the flow and heat transfer characteristics. Chapter 3 provides a description of the experimental equipment used in this study, its instrumentation, operation and procedures used for the data recording. In chapter 4, a description of how the collected experimental data has been post-processed is presented. Then Chapter 5 will discuss the data analysis and uncertainties. Chapters 6 and 7 will exhibit and

discuss the flow and heat transfer results. Finally the conclusions and recommendations for future work will be provided in Chapter 8.

The work presented in this thesis also resulted in the publication of a journal article (Long et al. 2007) which is reproduced in Appendix 1.

2. Literature review

2.1 Generalities on Rotating Cavity Systems

2.1.1 Gas Turbine Co-rotating Discs Systems

Air delivery in a gas turbine is achieved in the compressor stage by the combined action of successive rows of rotating blades driven by a turbine downstream of the combustion chamber and static blades mounted on the external casing, as shown in Fig 2.1. Relative speed between the rotating and static blades ensures positive pressure rise of the inlet air to feed into the combustion chamber. Typically, rotating blades are individually dove-tail mounted onto the periphery of an assembly disc holding in place a row of blades. Rows of rotating blades are bolted to each other along the direction of the axis of rotation, forming what is referred to as a compressor disc stack and mechanically linked to their driving turbine. The ensemble of discs, turbines, links, and bearings under rotation represent the rotor of the gas turbine.

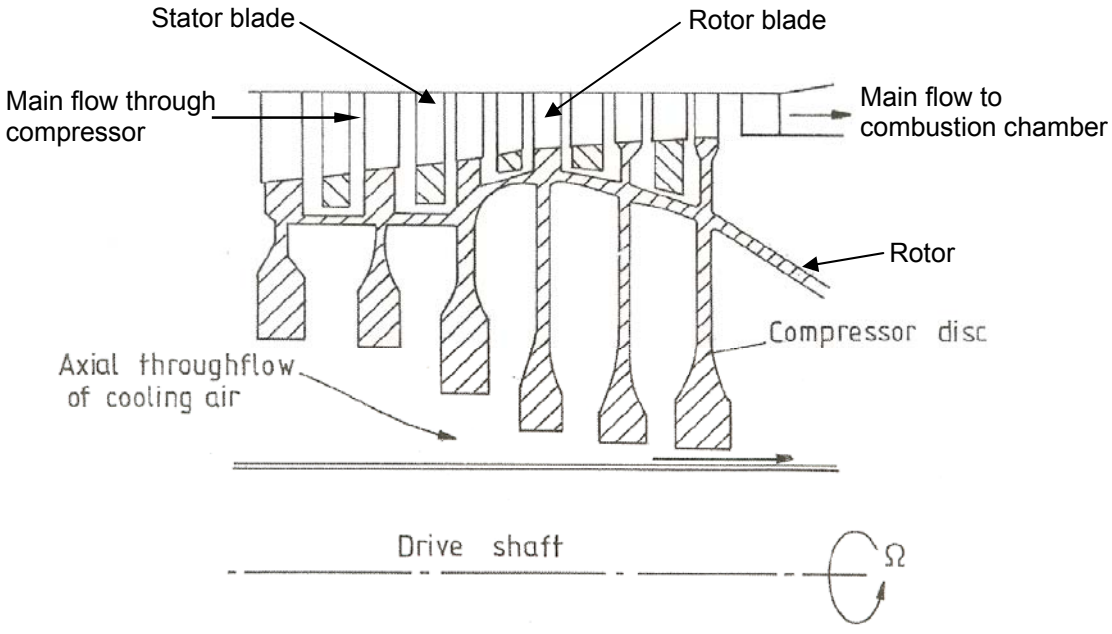

Fig 2. 1 Schematics of the internal layout of a H.P. compressor (Long 1994)

Mechanical damage to the blades while the gas turbine is operating is prevented by leaving a gap between the rotor blade tip and the casing (conversely for the stator blade and rotor). The efficiency of the compressor stages being affected by the blade tip clearance by about 1.5% of the affected stage efficiency for 1% of blade clearance change according to Freeman (1985), it is important to keep this value to a minimum. However, temperature rise of the air across the compressor, typically of 600 °C for a 30:1 compression ratio inevitably conducts heat through the rotor and stator components and affects their geometrical properties by thermal expansion; thus affecting blade tip clearance and overall power efficiency. Moreover hoop stresses on the rotor, thermal stress and high centripetal forces, with the typical magnitude of centrifugal acceleration in the order of 10^4g, justify the diametrical thickness of the discs and the expanded shape at their inner bore referred as the “cob” whose increase in material accommodates the hoop stress concentration of the bore.

In between rows of rotor blades lies a zone where the outer surface of the rotor acts as an end wall to the row of stator blades for axial flow sealing. This part is not mechanically submitted to such levels of mechanical stress as the disc, having no mechanical resistance requirements for securing blades in position and therefore presents the shape of a thin-walled cylinder compared to the disc’s geometry. This cylinder, by design, is typically manufactured as part of a disc and is referred to as a shroud. Therefore, the typical geometry of a compressor disc as a whole comprises of a thick-walled cylinder part where the cylinder blades are mounted with material concentration at the core for increased mechanical resistance, and of a thin-walled cylinder part for the compressor stator blades sealing. Series of these two-part discs in a compressor stack will form distinct volumes between two discs and a shroud that are referred to as compressor disc stack cavities.

Rotating cavities can be of several types in gas turbines, depending on their location in the engine.

These cavities are the result of construction design, and their presence could also be put to use to the secondary air system as a point of collection, conveyance, or extraction of cooling air through the engine. The main types of rotating cavities are briefly described below and illustrated in Fig 2.2.

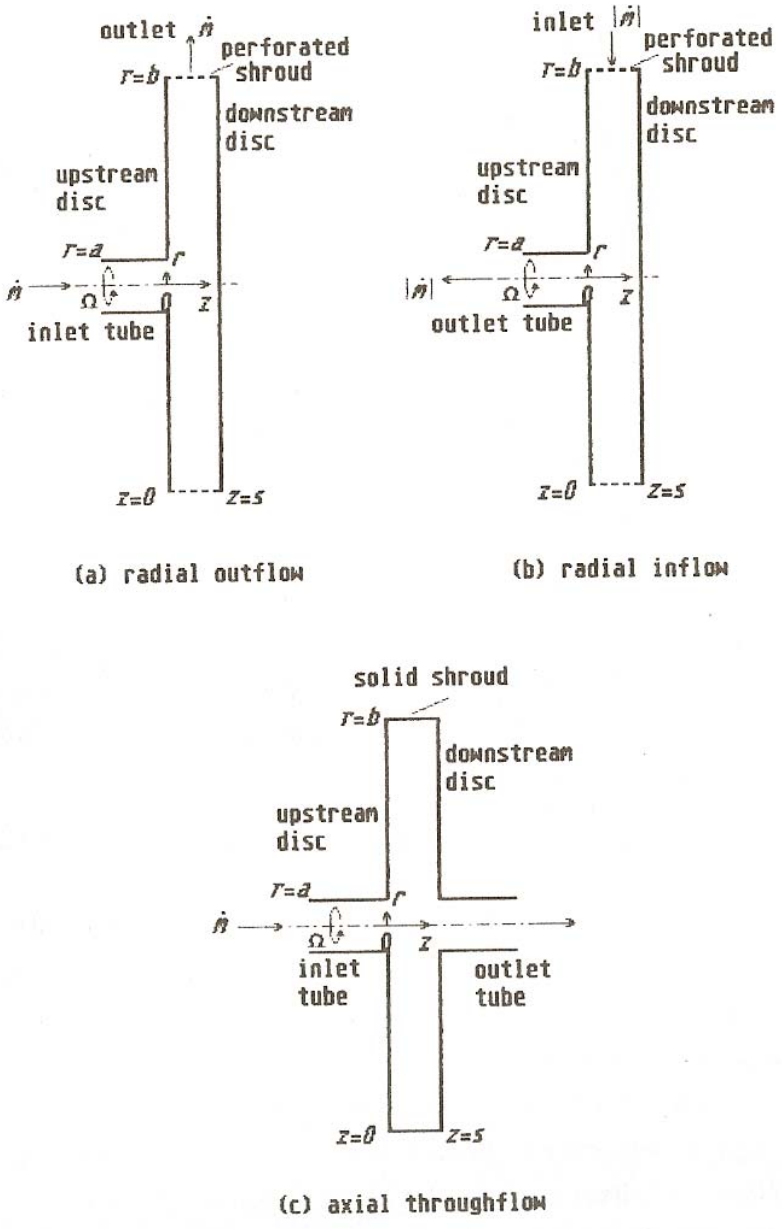

Fig 2. 2 Main types of cavity flow from Owen and Rogers (1995)

Totally enclosed cavities are sometimes found in turbine construction and less commonly in compressors where air flow across the components is generally encouraged as part of the secondary air system.
This configuration presents, however, by its simplicity a good base for modelling and understanding rotating cavity flows and has been studied in the literature as described in section 2.2.

Radial outflow cavities are a type of rotating cavity whereby air is introduced into the cavity near the centre of revolution and extracted through perforations in the shroud, as illustrated in Fig 2.2(a). This type of cavity is generally found in the turbine where it forms part of the turbine cooling air delivery system.

Conversely, radial inflow cavities are formed when the air circulation within the cavity originates from perforations in the shroud periphery and leaves the cavity by the centre of revolution, as shown in Fig 2.2(b). This is the arrangement found in some compressor stages to collect the pressurised air required by the secondary air system.

Both configurations of radial inflow and radial outflow cavities have been extensively described in the research literature and their internal flow and heat transfer mechanisms are now fairly well understood. Although a very interesting subject, this is beyond the scope of the current thesis. Therefore, the author suggests the reader wanting to know more about radially opened cavities to seek more information firstly in chapter 3 and 4 of the book by Owen and Rogers (1995), where a full description of these configurations' characteristics is provided, together with a selection of relevant publications.

Finally, the rotating cavity with axial throughflow configuration refers to when the air enters and leaves the cavity by the central axis. Fig 2.2(c) shows the schematics of a rotating cavity with axial throughflow when now a central shaft is also present. This type of cavity is commonly found within compressor stages of gas turbine engines. This configuration is the main focus of the present study and further description of its flow and heat transfer mechanisms will be found in sections 2.3 and 2.4.

2.1.2 Parameters and Dimensionless Groups

Below is a general nomenclature of the basic parameters pertaining to rotating cavities and particularly to the case of rotating cavities with axial throughflow as explained before.

Let us consider the schematics of a rotating cavity with axial throughflow as shown in Fig 2.3(a).

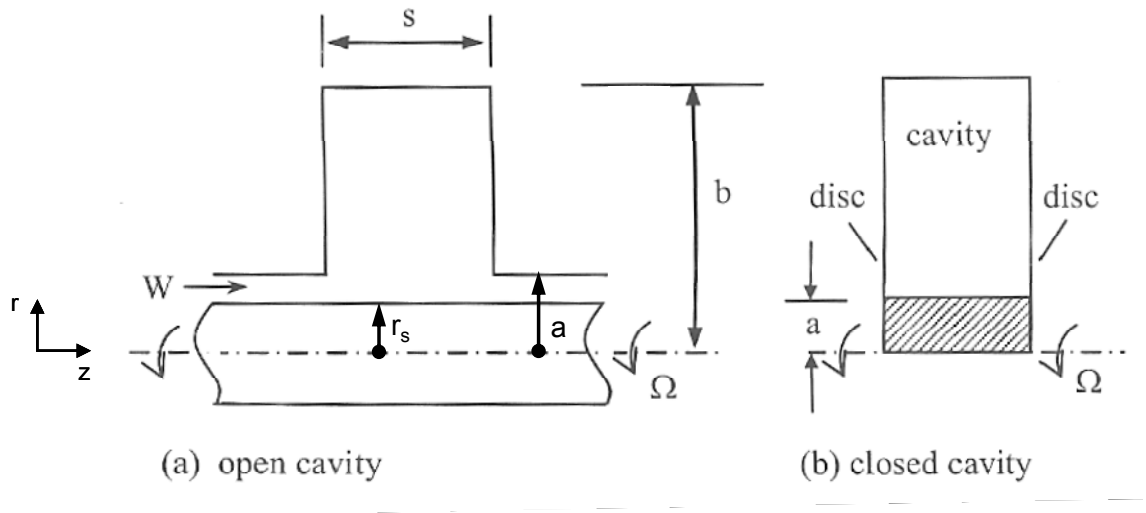

Fig 2. 3 Nomenclature of rotating cavities from King et al. (2005)

Two discs separated from each other by a shroud of axial gap s, rotate around the axis of revolution z at a rotational speed Ω. The outside radius of the discs is b, whereas the inside radius of the discs, or bore, is a. The gap ratio of the cavity G is defined as:

$$G = s/b \qquad \textbf{Eq. 2.1}$$

The cavity generally rotates around a central shaft of diameter r_s, which can be stationary or rotate at a speed Ω_s. The axial throughflow of air runs across the cavity at a bulk average velocity W defined as:

$$W = \frac{\dot{m}}{\rho \times A_{an}} \qquad \textbf{Eq. 2.2}$$

Where $\dot{m}$ =mass flow rate of air delivered through the cavity

ρ =density of inlet air

$A_{an} = \pi \times \left(a^2 - r_s^2\right)$=shaft annulus area

The parameter relevant to the rotation of the cavity is the rotational Reynolds number, Re_ϕ defined as:

$$Re_\phi = \frac{\Omega \times b^2}{\nu} \qquad \textbf{Eq. 2.3}$$

Likewise, the axial Reynolds number Re_z characterises the axial throughflow of air as:

$$Re_z = \frac{W \times d_h}{\nu} \qquad \textbf{Eq. 2.4}$$

Where $d_h = 2\left(a - r_s\right)$ = hydraulic diameter

Relating the effects of the axial flow and the rotational flow can be expressed as the Rossby number Ro:

$$Ro = \frac{W}{\Omega \times a} \qquad \textbf{Eq. 2.5}$$

This ratio of the axial velocity of the tangential solid body velocity at the disc's bore may also be expressed from equation 2.3 and equation 2.4 as:

$$Ro = \frac{b^2 \times Re_z}{2a \times (a - r_s) \times Re_\phi} \qquad \textbf{Eq. 2.6}$$

The Grashof number Gr is a parameter relevant to buoyancy induced flow. In a rotating cavity application the expression of Grashof number based on the radial distance along the disc surface is based on the local surface temperature and its relative centripetal acceleration was expressed by Farthing et al. (1992b) by taking y as a height reference from the shroud as: .

$$Gr_y = \frac{\beta \Delta T \times \Omega^2 r \times y^3}{\nu^2} \qquad \textbf{Eq. 2.7}$$

Where $\beta = 1/T_{in}$ is the volume expansion coefficient with T_{in} the inlet temperature of the throughflow air. ΔT is the temperature difference between the supply air and the local surface temperature at the radius r considered, $\Delta T = (T_s - T_{in})$.

Also, $y = (b - r)$ is the distance radially inward from the shroud which is taken as the length parameter for this instance of Grashof number, with its value increasing against the gravitational field direction.

The Prandtl number is a ratio of the kinematic viscosity to the thermal diffusivity at a given point.

$$Pr = \frac{\nu}{\alpha} \qquad \textbf{Eq. 2.8}$$

Where $\alpha = \frac{k}{\rho \times \mathrm{Cp}}$

The Prandtl number is considered as the characteristic number for thermal boundary layers and heat transfer in forced convection. The kinematic viscosity (ν) is in relation with the transport properties of the fluid in respect to momentum, and is related to the thickness of the velocity boundary layer δ (non-slip condition). An increase of viscosity meaning an increase of δ. Similarly, the thickness of the thermal boundary layer is in relation with the thermal diffusivity. Hence, Schlichting and Gersten (2000) remark that the Prandtl number for forced convection is a direct measure of the ratio of the two boundary layers.

The Rayleigh number Ra is a parameter related to the heat transfer within the fluid. It is expressed as the product of the Grashof number and the Prandtl number.

$$Ra = Gr \times Pr \qquad \textbf{Eq. 2.9}$$

The Nusselt number Nu is the non dimensional parameter related to the heat flux on a surface. For the case of a heat flux on a cavity disc, the Nusselt number is expressed as.

$$Nu_y = \frac{q \cdot y}{k \cdot \Delta T} \qquad \textbf{Eq. 2.10}$$

Where q is the heat flux from the surface of the disc to the cavity fluid at location y

Following is a review of previous work related to flow and heat transfer in the sealed cavity configuration and an introduction on buoyancy induced flow.

2.2 Sealed cavities

2.2.1 Isothermal

A sealed cavity refers to the configuration shown in Fig 2.3(b) whereby the enclosure formed by the two disks is bounded on the disks' outer radius by the shroud and also at the inner diameter of the disks, if any, forming a cavity in which no air either enters or leaves. The cavity rotates about its axis of revolution and the trapped air within is accelerated as a result of friction with the cavity walls. When no temperature difference across the cavity and its walls exists (isothermal condition) the fluid within the cavity fluid is only subjected to mechanical forces and will end-up rotating at the same speed as the discs, which is referred as solid body rotation.

2.2.2 Axial heat flow

A sealed rotating cavity is subjected to axial heat flow when one of the discs is hotter than its opposite and the inner and outer cylindrical surfaces are considered adiabatic. The hotter disc is referred to as the hot disc and the cooler one as the cold disc. The lower cavity air density by the hot disc side induces greater buoyancy forces (directed against the centrifugal acceleration) than on the cold disc side. The circulation flow resulting from this buoyancy forces imbalance to the cavity air will be such as it will circulate centripetally oriented by the hot disc and centrifugally oriented by the cold disc, as illustrated by Fig 2.4.

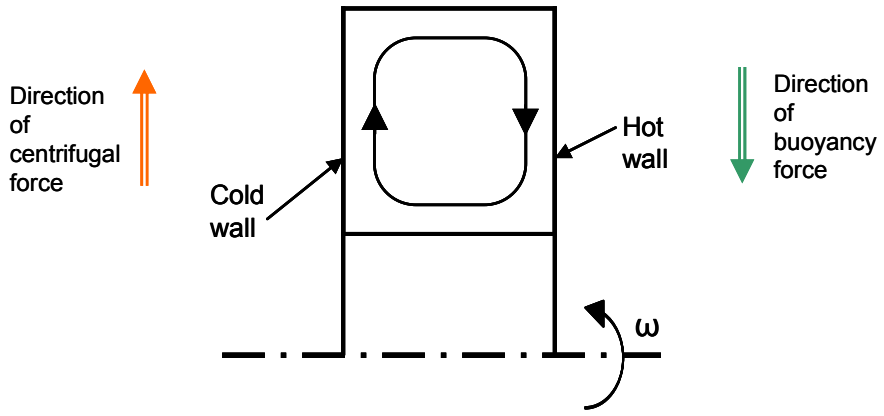

Fig 2. 4 Sealed rotating cavity with axial heat flow

Bohn et al. (1994) performed computations for a rotating sealed annulus with axial flow of heat. The temperature distributions on the discs were uniform and the inner and outer cylindrical surfaces were considered adiabatic. A fixed Prandtl number and up to 300 K temperature difference between the hot and cold discs were considered in the computations. Their results showed that the fluid within the cavities was circulating around the walls in the boundary layers, with nearly no motion occurring in the core region. The sudden transportation of a fluid element from the outer surface towards the inner radii from the buoyancy force will see its relative circumferential speed increasing from the shroud tangential velocity as the radius decreases (minus the reduction in the absolute speed due to viscous friction). In the solid body rotation frame of speed reference, this increase of tangential velocity will show the element to be spiralling towards the centre at increasing relative tangential speed, thus highlighting an outwards Coriolis force seen to balance against the centripetal buoyancy force (Fig 2.5). Similarly the Coriolis force will be seen to work against the radially-outwards circulating flow as shown in Fig 2.6.

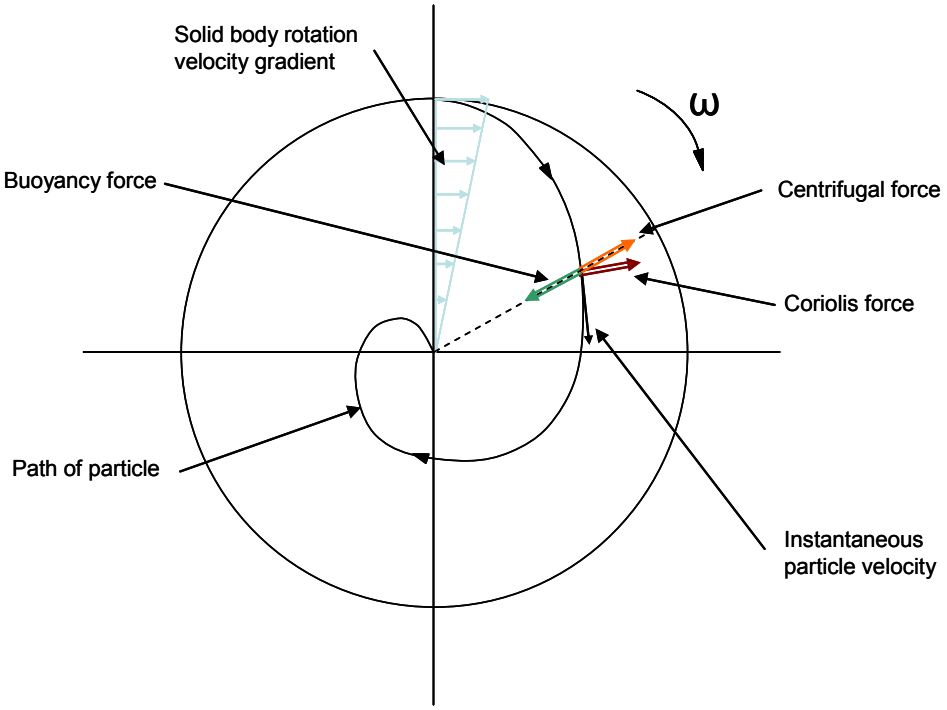

Fig 2. 5 Path of a particle driven inwards of cavity as result of buoyancy seen in rotating frame of reference with directions of acting forces upon it

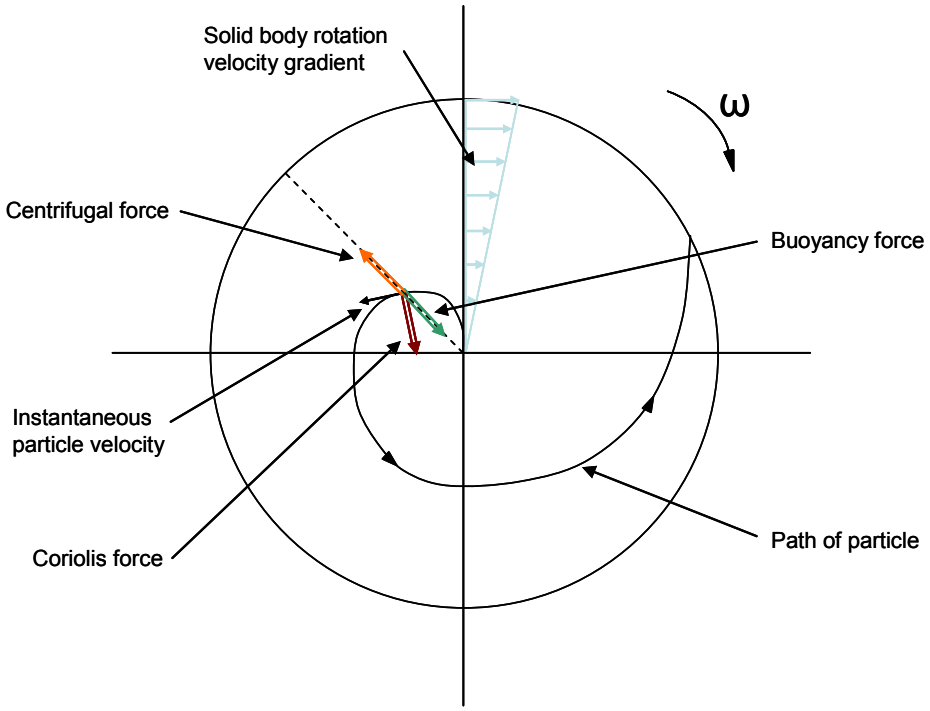

Fig 2. 6 Path of a particle driven outwards of cavity as result of centrifugal force seen in rotating frame of reference with directions of acting forces upon it

Thus Bohn et al. (1994) affirmed that the fluid motion in a rotating annulus with axial flow of heat is driven by buoyancy force and damped by the Coriolis effect. As a result their computations showed that an increase of the rotational Reynolds number at constant Grashof number reduced the flow circulation within the cavity (and consequently the heat transfer) from the damping effect of the Coriolis effect increasing with rotational speed. This can be seen in Fig 2.7, where:

$$Nu = \frac{q_{av} \times s}{k_{ref} \times \left(T_H - T_C\right)} \qquad \textbf{Eq. 2.11}$$

Where T_H = hot disc temperature

T_C = cold disc temperature

$$Re_\phi = \frac{\Omega \times r_m \times s}{\nu_{ref}} \qquad \textbf{Eq. 2.12}$$

Where r_m = average radius

$$Gr = \frac{\Omega^2 \times r_m \times s^3}{\upsilon_{ref}^2} \times \beta\left(T_H - T_C\right) \qquad \textbf{Eq. 2.13}$$

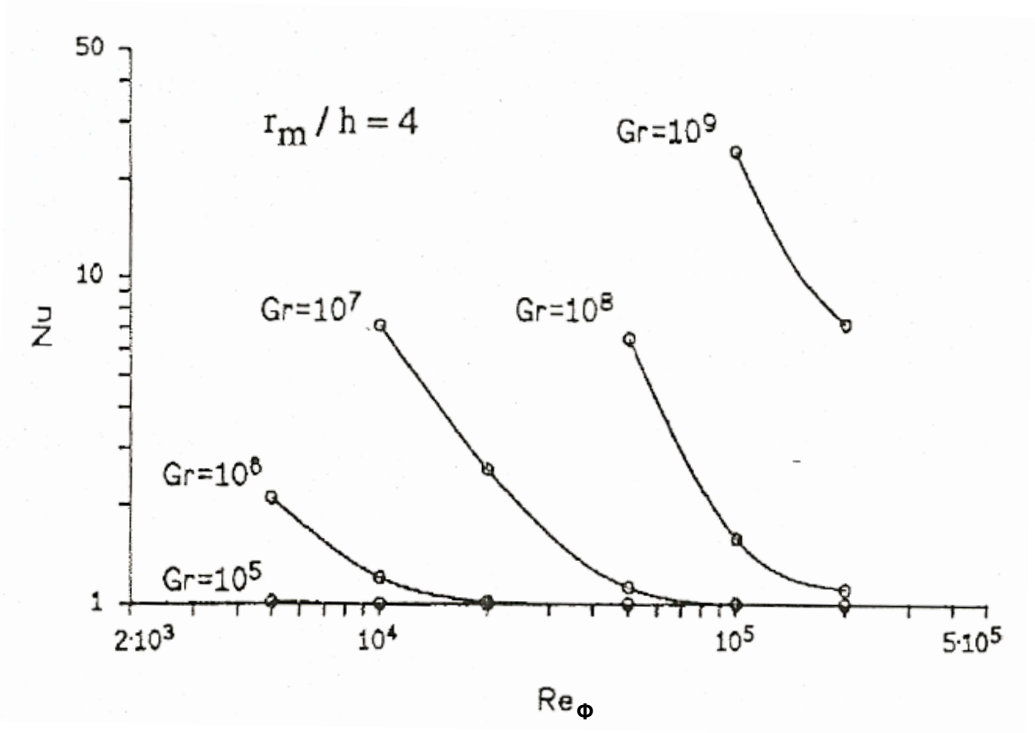

Fig 2. 7 Nu vs Re_Φ for various Gr in an enclosed cavity from Bohn et al. (1994)

In Fig 2.7 it can be seen that an increase of Re_Φ at constant Gr attenuates the heat transfer as it tends towards $Nu \rightarrow 1$ (pure conduction) at higher Re_Φ values. Also Bohn et al. (1994) obtained heat transfer correlation for their stationary laminar model on experimental data up to values of Ra=10^{11} which is significantly higher a value than the normally considered Ra=10^9 transition value from laminar to turbulent free convection on a stationary vertical plate. Later, Bohn and Gier (1998) confirmed by a combined computational and experimental study the dependence of the cavity heat transfer on Re_Φ. Their experimental measurements were correlated for an air filled rotating annulus with axial flow of heat for G=0.5, a/b=0.52 and 2x10^8 < Ra < 5x10^{10} by:

$$Nu = 0.346 \times Ra^{0.124} \qquad \textbf{Eq. 2.14}$$

2.2.3 Sealed cavity with radial flow of heat

A sealed cavity is subjected to a radial flow of heat when the annulus presents a temperature difference between the shroud and the inner cylinder walls (the discs being considered as adiabatic).

Bohn et al. (1995) conducted an experimental study on a sealed rotating annulus for the case of a radial heat flow where the shroud surface is hot and the inner cylindrical surface is cooler. The two discs were insulated. For conditions of $10^7<Ra<10^{12}$ the Nusselt numbers were correlated.

For a cavity with G=0.34 and a/b=0.35:

$$Nu = 0.246 \times Ra^{0.228} \qquad \textbf{Eq. 2.15}$$

For a cavity with G=0.5 and a/b=0.52

$$Nu = 0.317 \times Ra^{0.213} \qquad \textbf{Eq. 2.16}$$

Where $Nu = \dfrac{q_{av} \times b \times \ln(b/a)}{k(T_H - T_C)}$

$$Ra = Gr \cdot Pr = \frac{r_m \cdot \Omega^2 \cdot \Delta T \cdot (b-a)^3}{1/2 \cdot (T_H + T_C) \cdot \nu^2} \times \frac{\mu \cdot \mathrm{C_p}}{k} \qquad \textbf{Eq. 2.17}$$

$$\mathrm{Re} = \frac{\Omega \cdot r_m \cdot (b-a)}{\nu} \qquad \textbf{Eq. 2.18}$$

With $r_m = \dfrac{(a+b)}{2}$ the mean annulus radius

As seen previously, in the case of a sealed rotating annulus with axial flow of heat the cavity air was being driven into a tumbling motion going radially outwards on the hot disc side as a combined effect of buoyancy and centrifugal acceleration. In the typical case of radial heat flow where the shroud is hotter than the inner cylindrical wall of the annulus however, the temperature gradient generates centripetal buoyancy forces across the cavity length. As a result the flow can only circulate from the onset of flow instabilities allowing re-circulating flows oriented in the axis of rotation of the annulus to appear as illustrated by Fig 2.8.

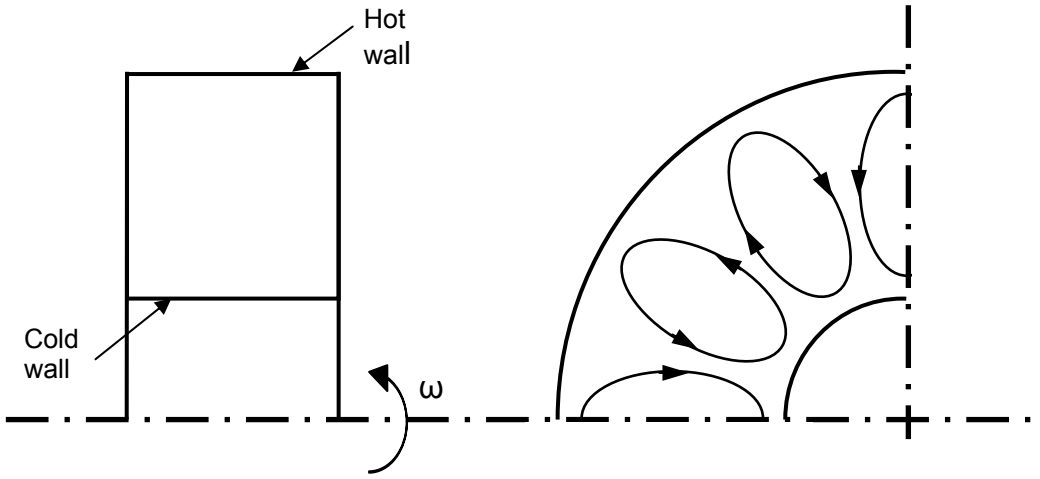

Fig 2. 8 Sealed rotating cavity with radial flow of heat

This flow behaviour is reminiscent of the Rayleigh-Bénard convection flow between two plates with a temperature gradient in the opposite direction to the gravitational force. Fig 2.9 shows the Rayleigh-Bénard convection flows in a horizontal stationary enclosure.

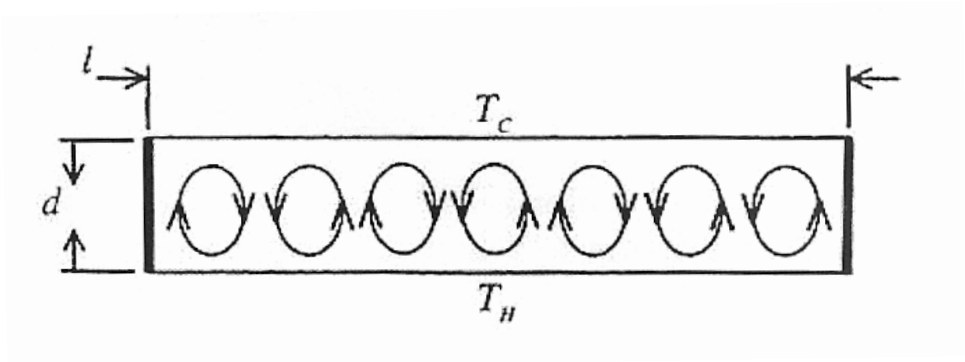

Fig 2. 9 Rayleigh-Bénard convection flow between two plates from King et al. (2005)

King et al. (2005)'s flow computations showed pairs of cyclonic and anti cyclonic vortices were created in the tangential plane of an inwardly heated sealed rotating cavity for Rayleigh number values up to Ra=10^9. Fig 2.10 shows their computed velocity contours and temperature isotherms. They remarked that the flow was in state of vacillation as the number of vortices pairs varied with time. The 3-D computations highlighted axial components of velocities associated to the vortices.

Their presence is linked to the cyclonic and anti-cyclonic nature of these vortices and show axial velocities away from the discs for a cyclonic vortex (low pressure) and towards the discs for an anti-cyclonic vortex as shown in Fig 2.10.

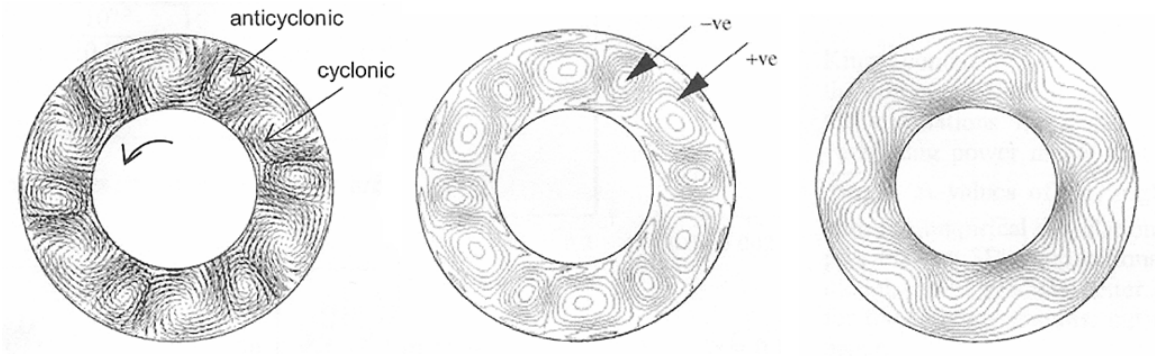

Fig 2. 10 Sealed cavity with radial flow of heat computations from King et al. (2005) for Re_{Φ}=546

The Nusselt number computations of King et al. were in good agreement with heat transfer from Rayleigh-Bénard convection in stationary enclosures but were significantly higher than the empirical correlations for a closed rotating annulus.

In summary in can be noted that the buoyancy forces influencing the flow structure within a sealed rotating annulus submitted to an inwardly radial flow of heat can induce time dependent three-dimensional pairs of cyclonic and anti-cyclonic vortices similar to Rayleigh-Bénard convection in a horizontal plate enclosure.

2.3 Rotating cavity with axial throughflow

2.3.1 Isothermal throughflow

Farthing et al. (1992a) reported on their flow observations and measurements in a cavity under isothermal throughflow conditions. They used Laser Doppler Anemometry (LDA) in an experimental set-up reproducing a rotating cavity without central shaft which gap ratio G was varied from 0.133 to 0.533 and had a radius ratio a/b≈0.1. For a non-rotating condition ($Ro\rightarrow\infty$), the interaction of the throughflow of air with the cavity air was found to generate one or more toroidal vortices in the cavity with virtually no penetration of the throughflow into the cavity. The typical flow schematics for the case of throughflow of air with no rotation of the cavity for different values of G can be seen in the cases indexed as (i) in Fig 2.11.

At lower gap ratios (G=0.267 and G=0.133) Farthing et al. observed multiple contra-rotating vortices inside the cavity. The increase of rotational speed had the initial observed effect of suppressing the toroidal vortex in the cavity, plausibly as the result of vortex motion damping caused by generated Coriolis forces from the tumbling air motion driven by the interaction with the central throughflow. The central throughflow itself is also affected by rotational speed that would give a tendency to centrifuge the central flow out; and axi-symmetric and non axi-symmetric vortex breakdown were observed. The type of vortex breakdown and radial extent to which the throughflow penetrates the cavity was found to depend principally on the values of G and Ro, and that the transition from one type of vortex breakdown to another was subject to hysteresis.

For a case with G=0.533 in turbulent flow (Re_z>2000), Farthing et al. observed no discernible signs of influence on the vortex and the central jet with rotational speed for values of Rossby number higher than 100.

For 100>Ro>21, non axi-symmetric vortex breakdown where the jet of air gets diverted into the cavity could be observed. This is sketched in Fig 2.11 as condition (b). This mode of vortex breakdown was referred to as mode 1a shown in Fig 2.12.

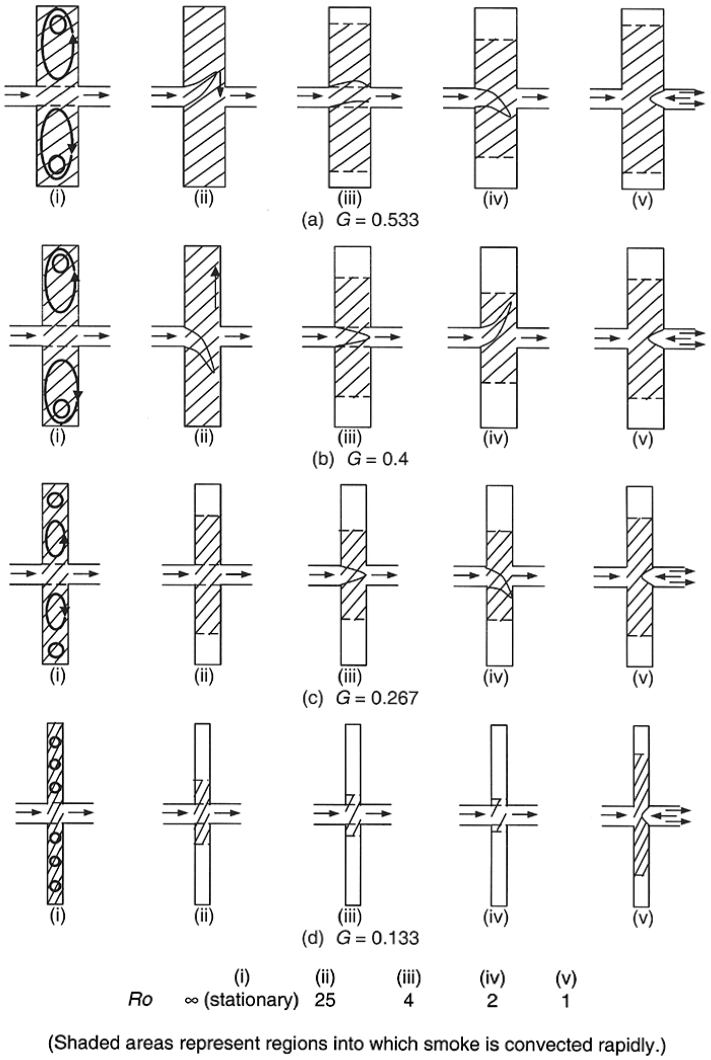

Fig 2. 11 Visual impressions of smoke patterns in an isothermal rotating cavity with axial throughflow: Re_z=5000 (Farthing et al. 1992a)

For 21>Ro>2.6, as the rotational speed increased, the jet would become axi-symmetric again but with occasional oscillations (mode IIa in Fig 2.12, illustrated as case c in Fig 2.11).

2.6>Ro>1.5 showed a “flickering flame” appearance of the central jet with occasional excursions into the cavity.

For Rossby values below Ro=1.5 the flow turned axi-symmetric again and signs of reversed flow at the downstream edge of the jet was observed (case e in Fig 2.11).

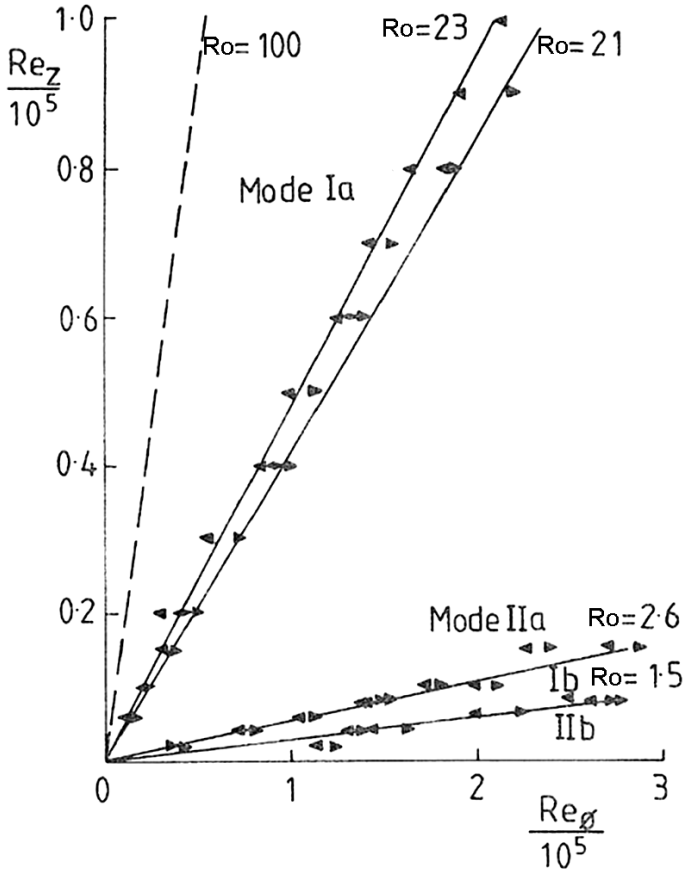

Fig 2. 12 Vortex breakdown modes in an isothermal rotating cavity according to Ro from Farthing et al. (1992a)

Observations in cavities with smaller gap ratio showed a weakening of the strength of the cavity vortex and vortex breakdown as G reduced.

These observations were made in a cavity without a central shaft. The presence of a central shaft within the throughflow is likely to act as a flow straightener to the central jet and therefore further reduce the effects of vortex breakdown.

Farthing et al.'s LDA measurements were performed for a fixed Re_z=8x10^4, varying Ro and G in the radial and tangential velocity components. The effects of Ro and G on the time averaged radial velocity across the cavity at r/b=0.8 is shown in Fig 2.13.

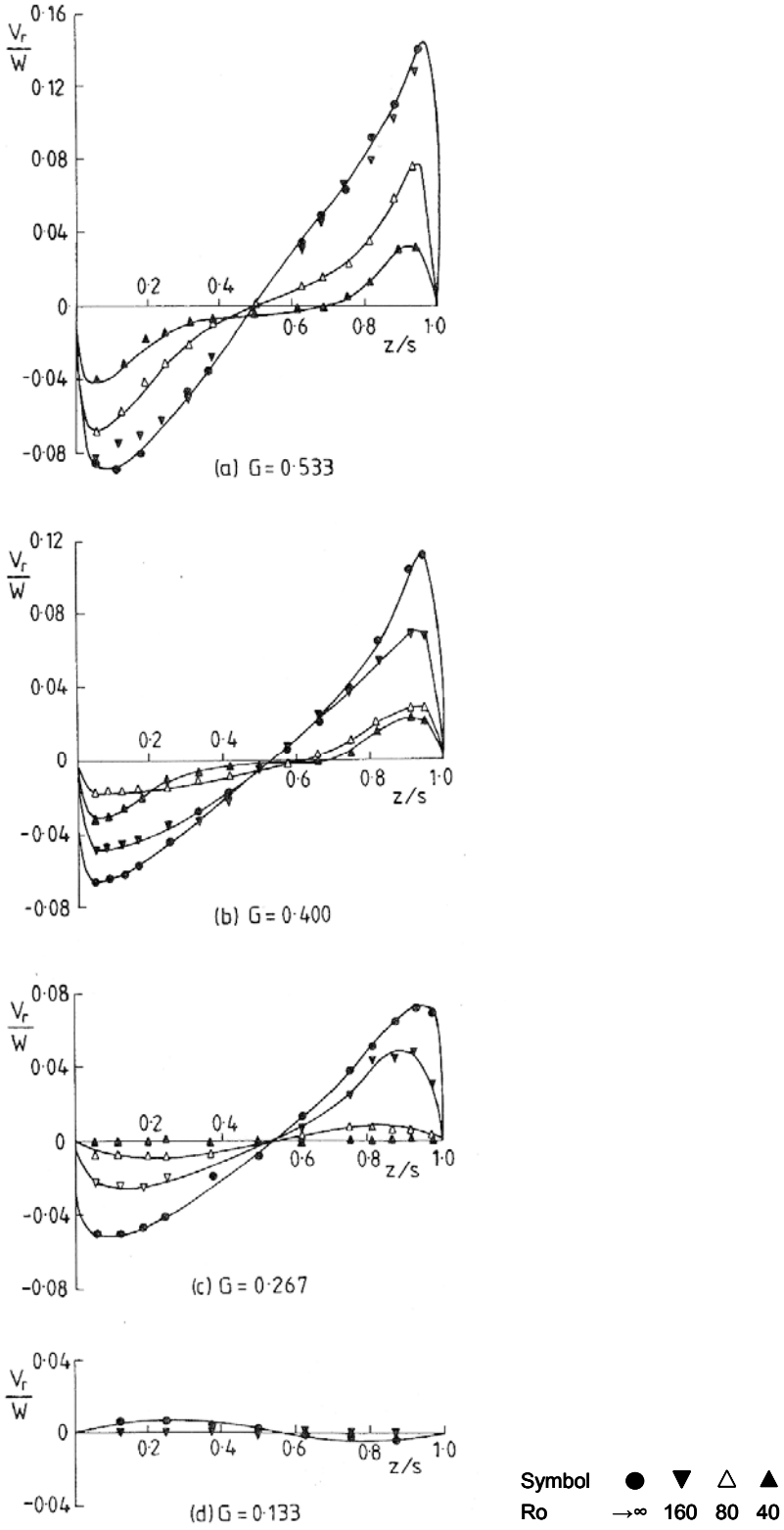

Fig 2. 13 Effects of Ro and G on radial velocities across an isothermal rotating cavity from Farthing et al. 1992a

Figure 2.13 shows, as seen before, that an increase in rotational speed or a reduction in gap ratio has the effect of weakening the toroidal vortex.

For G=0.533, G=0.4 and G=0.267, the radial flow is consistent with a toroidal vortex driven by the central throughflow, with radial outflow by the downstream disc, radial inflow by the upstream side of the cavity and a quiescent point of rotation by mid-cavity. For G=0.133 they observed a reverse flow consistent with a condition when contra-rotating vortices are present in the cavity; and the weakness of this circulation as a result of small gap ratio was further highlighted by the fact that at Ro≤160 zero velocity radial flow indicated stratification of the cavity flow in this outer region.

Tangential velocity flow measurements were also reported by Farthing et al. measured in the mid plane of cavity (z/s=0.5) for different gap ratio and Ro along the radial span of the cavity.

Fig 2.14 shows the effect of Ro and G on the normalized tangential velocity with Ωr for Re_z= 4 x 10^4.
They observed that for all conditions, the outer part of the cavity air was at solid body rotation velocity and that the size for this zone was increasing with decreasing G. A free vortex flow where $V_\Phi/\Omega r$>>1 is created by the centre of the cavity is said to be created by the inward coming part of the toroidal vortex by the upstream disc which turns to conserve its angular momentum.
As the toroidal vortex strength is weakened by decreasing Ro and G, so will the central vortex swirl be affected.The effect of z/s on the tangential velocities was found to be small in the zone outside the boundary layers of the discs.

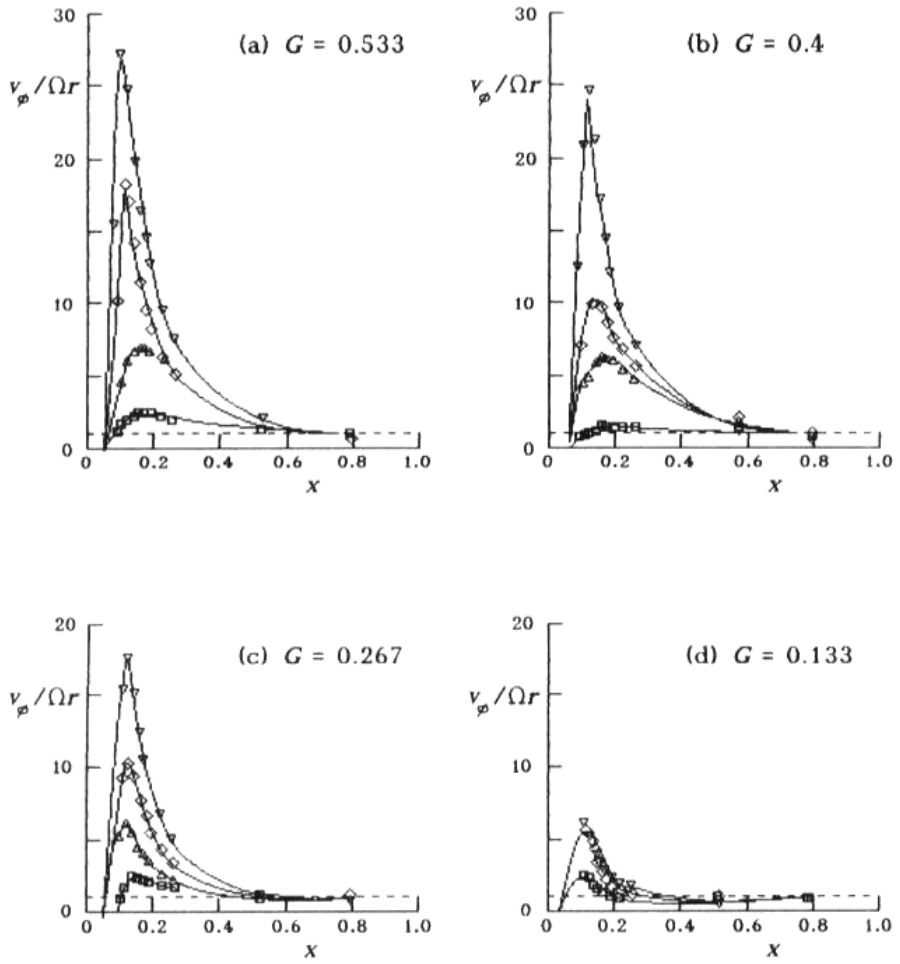

Fig 2. 14 Effects of Ro and G on the tangential velocity components across an isothermal rotating cavity from Farthing et al. 1992a

2.3.2 Non-isothermal throughflow

Farthing et al. (1992a) used the same rig as described in 2.3.1 to produce flow visualisation inside a rotating cavity where the discs could be heated independently to produce temperature distributions that could increase, decrease or remain approximately constant with increasing radius. The shroud

was unheated. For G=0.27, 2.2x10^3 ≤ Re_z ≤ 7.7x10^3 , 1.3x10^4 ≤ Re_Φ ≤ 8.7x10^4 they observed for all temperature distributions similar on both discs that the flow inside the cavity was seen to be non axi-symmetric. The throughflow was seen to enter the cavity in a “radial arm” and was then divided by the outer radii and tangentially transported around two contra-rotating re-circulation vortices towards a “dead zone” where a more diffusive inwards motion of the air would be seen. Fig 2.15 illustrates schematically their observations.

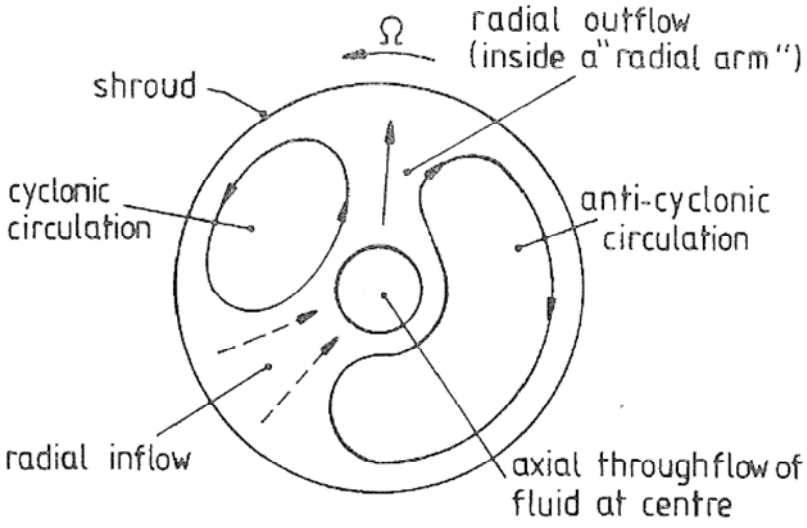

Fig 2. 15 Schematic of flow structure from Farthing et al. (1992a)

The flow ensemble was found to rotate at a speed ω slightly inferior to solid body rotation in the order of 0.9≤ω/Ω≤1 which decreases with increasing G and temperature difference between max disc temperature and inlet air temperature. The relative speed of the circulation system was also found to reach a minimum at Ro≈2. For a symmetrically heated cavity (at G=0.138) with the temperature of the discs increasing with radius, Farthing et al. correlated the measured local Nusselt numbers on the discs by:

$$Nu_y = 0.0054 \times Re_z^{0.3} \times Gr_y^{0.25} \qquad \textbf{Eq. 2. 19}$$

The 0.25 exponent of Gr_y in equation 2.19 suggests laminar free convection occurring in the narrow gap cavity by relation to the correlations for free convection for a stationary vertical plate for:

-laminar flow

$$Nu = 0.36 \times Gr^{0.25} \qquad \textbf{Eq. 2. 20}$$

-turbulent flow

$$Nu = 0.022 \times Gr^{0.4} \qquad \textbf{Eq. 2. 21}$$

Having the downstream disc heated while the upstream was not, showed broadly similar flows but unsymmetrical about the axial plane. A similar improvement in flow stability than in the case of an enclosed cavity with radial outflow of heat was seen in the axial throughflow condition with discs temperature decreasing with radius. Conversely, having a temperature profile increasing with radius would set an unstable density distribution like in the case of a closed cavity with radially inward heat flow.

Long (1994) used the same experimental rig geometry as described by Farthing et al. but where the disks and shroud could be symmetrically heated with the discs' temperature profiles increasing with radius and gap ratios of G=0.36 or G=0.13. He estimated the proportion of axial throughflow entering the cavity from a heat balance calculation using measured values of average disc heat transfer and cavity temperature. For Ro<1, approximately 50% of the throughflow of air was estimated to be diverted into the cavity. For Ro>10, this decreased to about 10%. These values were found to be broadly independent of gap ratio.

For conditions of Ro>4, at G=0.36 the heat transfer was found to be increasing by several times compared to the case at G=0.13. Long concluded that the rotationally induced buoyancy and direct influence of the central throughflow are the two mechanisms responsible for the heat transfer inside a heated rotating cavity with axial throughflow.

Burkhardt et al. (1992) carried out heat transfer measurements on an engine geometry and running conditions representative five cavity rig involving measured surface temperatures and a conduction solution method. A central shaft was present and could rotate in either direction of the rotor. The

experimental conditions were in the range $2.7\text{x}10^4 \leq Re_z \leq 9.5\text{x}10^4$ and $1.9\text{x}10^6 \leq Re_\Phi \leq 5.6\text{x}10^6$. They observed that under identical tests conditions the heat transfer for an upstream disc tended to be greater than that of its downstream disc. The temperatures of the discs tended to decrease as the shaft rotational speed approached the discs speed, implying higher heat transfer on the discs at this condition.

Alexiou et al. (2000) carried out engine representative heat transfer measurements on an experimental rig representing the last two cavities of the high-pressure compressor including the turbine drive cone on a scaled down version of a typical engine geometry. A central shaft could be stationary or either co-rotate or contra-rotate with the discs. Up to 85% of the throughflow could also be diverted away through peripheral holes located on the downstream side of the shaft. Surface temperatures of the last disc and cone were measured and a conduction solution method was applied in order to derive heat fluxes. The disc was instrumented on one face only, therefore a symmetrical temperature distribution across the disc thickness was assumed. Farthing et al. (1992b), Burkhardt et al. (1993) and Long et al. (1997) previously used this assumption on relatively thin discs experiencing a relatively large radial temperature gradient. Hence the name “fin solution” sometimes used for the description of an adiabatic plane assumed conduction solution on a thin disc.

Two regimes of heat transfer were revealed from the heat transfer measurements on the inner surface of the cone: a rotationally dominated and a throughflow dominated regime of heat transfer.

The rotationally dominated regime is when the heat transfer occurs by free convection induced by flow stratification on the outer part of the cone cavity with rotationally induced buoyancy forces. The local Nusselt numbers were correlated for Ro<3.5 by:

$$Nu = 0.0243 \times Re_z^{0.086} \times \left\{ Re_\phi^2 \times \beta \Delta T \right\}^{0.326} \times X^{-1.89} \times \left\{ X^{-1} - 1 \right\}^{-0.082} \qquad \textbf{Eq. 2. 22}$$

Where $X = r/b$, is the non dimensional radial coordinate

The throughflow dominated regime on the cone heat transfer was suggested to be the result of a large vortex filling the cavity. The local Nusselt numbers were correlated for Ro>3.5 by:

$$Nu = 8.93 \times 10^{-5} \times Re_z^{1.301} \times X^{-3.523} \qquad \textbf{Eq. 2. 23}$$

Where $X = r/b$, is the non-dimensional radial coordinate

It was reported by Alexiou et al. (2000) that in the rotationally dominated regime higher heat transfer on the cone inner surface was found when the shaft was co-rotating with the cone. The disc heat transfer was however found to be relatively insensitive to the sense of rotation of the shaft and was found to be significantly lower than the heat transfer at the inner surface of the cone.

Long et al. (2003) extended their investigation on the previously cited rig to the heat transfer through the cavity shroud area. A variation of this engine representative multiple cavity rig was also used featuring four cylindrical cavities, a stationary shaft and no drive cone. This rig was referred to as the Multiple Cavity Rig, Build 2. Shaft and disc bore diameters remained identical to Build 1 used by Alexiou (2000). Figure 2.16 outlines the major geometrical differences between the different builds of the Multiple Cavity Rig.

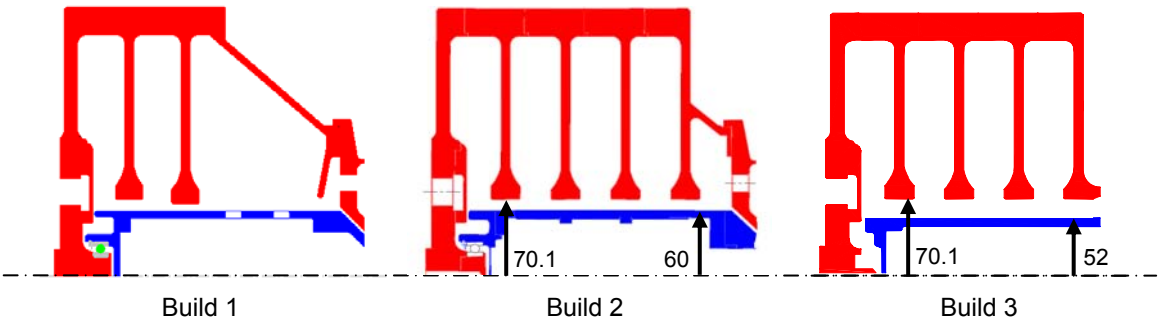

Fig 2. 16 Outline views of the Multiple Cavity Rig build 1, 2 and 3

Surface temperature measurements on the inner and outer surface of the shroud allowed heat flux calculations assuming one-dimensional radial conduction through the shroud. A total relative temperature of the cavity air by the shroud at $r=b$ was estimated as:

$$T_{T,rel,b} = T_{in} + \frac{\Omega^2 \times (b^2 - a^2)}{2 \times Cp} \qquad \textbf{Eq. 2. 24}$$

This was then used in order to derive Nusselt numbers at the shroud's inner face. The characteristic length in the calculation of the shroud Nusselt and Grashof numbers was the ratio of the shroud area to the perimeter (resulting as $s/2$) consistent with the definitions used for correlations of free convection from a heated horizontal plate. The measurements were carried out in the range of $4x10^4 \leq Re_z \leq 1.7x10^5$ and $1.6x10^8 \leq Gr_{sh} \leq 4x10^9$. Experiments showed that the shroud heat transfer was governed by rotationally induced free convection and was increasing with Grashof number. The shroud Nusselt numbers showed similarities to correlations for free convection on a horizontal plate with a gravitational field; with a transition to turbulent free convection possibly occurring at $Gr_{sh}>10^9$. Variations of Re_z appeared not to visibly influence the shroud heat transfer. Similarly so was the variation of the shaft rotation direction in the case of tests on Build 1 of the Multiple Cavity Rig. This indicates cavity air flow stratification at the outer cavity radii, making the air in the shroud vicinity impervious to the central flow influence. No differences in the shroud heat transfer between the two instrumented cavities in Build 2 were noticed. Following on this, Long and Childs (2007) extended their shroud heat transfer analysis on Build 3 of the Multiple Cavity Rig which was similar in operating and geometrical characteristics to Build 2 but with the difference of a smaller diameter shaft (104 mm diameter against 120 mm for Build 2) resulting in an annular gap almost twice as big as on Build 2. Similar conclusions were made as in Long et al. (2003). The shroud Nusselt number values of Build 3 were found to be greater than those of Build 2. This was attributed to a difference in throughflow interaction on the cavity flow as a result of an increased annular gap in Build 3. This is related to the increased measured tangential velocities found in Build 3's cavities compared to Build 2 as reported in Long et al. (2007).

Recent flow velocity measurements were performed by Owen and Powell (2004) inside a single cavity rig with a heated downstream disc while the shroud and upstream disc were adiabatic. The shaft was co-rotating at disc speed. Their experiments covered the following range of axial and rotational Reynolds numbers, $0.147x10^4 \leq Re_z \leq 4.78x10^4$ and $0.299x10^6 \leq Re_\Phi \leq 3.2x10^6$. The dimensional characteristics of the cavity were a/b=0.4 and s/b=0.2. Non-simultaneous LDA measurements for the radial and tangential velocity components were obtained through a Perspex upstream disc. The

measurements showed that for the case of a downstream heated disc, the core of fluid within the cavity tended to rotate at a slightly slower rate than solid-body rotation (by about 4%) and that the ratio of tangential fluid core velocity to solid body rotation tended to reduce even further as the fluid to disc surface temperature difference (ΔT) increased. This is in broad agreement with Farthing et al. (1992b)'s observations. Spectral analysis of the tangential velocities highlighted a multi-cell flow structure comprising one, two, or three pairs of vortices. This indicates complex three-dimensional flow within the cavity featuring vortex breakdown of the central flow which could perhaps be accentuated by the influence of a relatively big shaft diameter and an assymetrical disc heating. Radial velocity measurements were unfortunately not presented in Owen and Powell (2004) paper to illustrate this further.

Long et al. (2007) reported LDA measurements in the Multiple Cavity Rig for Build 2 and Build 3. Simultaneous axial and tangential velocity component measurements were performed on Build 2 from a window aperture inside the shaft. Build 3 featured a similar optical access for the axial and tangential velocity measurements, while also being able to perform simultaneous radial and tangential velocity measurements in the two last cavities through windows embedded in the last disc and downstream rotor casing. Radial velocities inside the cavities were found to be typically two orders of magnitude lower than the tangential velocity component. Tangential velocity spectra showed evidence of periodicity in the flow structure. The difference in flow structure between cavity 3 and 4 was attributed to differences in exit conditions from the cavities. A difference in tangential velocity profiles along the radii was also noted between Build 2 and Build 3.

This is attributed to a difference in the influence of the central throughflow and its breakdown on the flow inside the rotating cavities from the difference in annular gap size between Build 2 and Build 3. More details on the flow measurements are to be found in the present thesis.

Table 2.1 below summarises the reviewed experiments and operating conditions in rotating cavity with axial throughflow, while Figure 2.17 compares the range of experimental conditions to the operating condition of a typical engine in cruise.

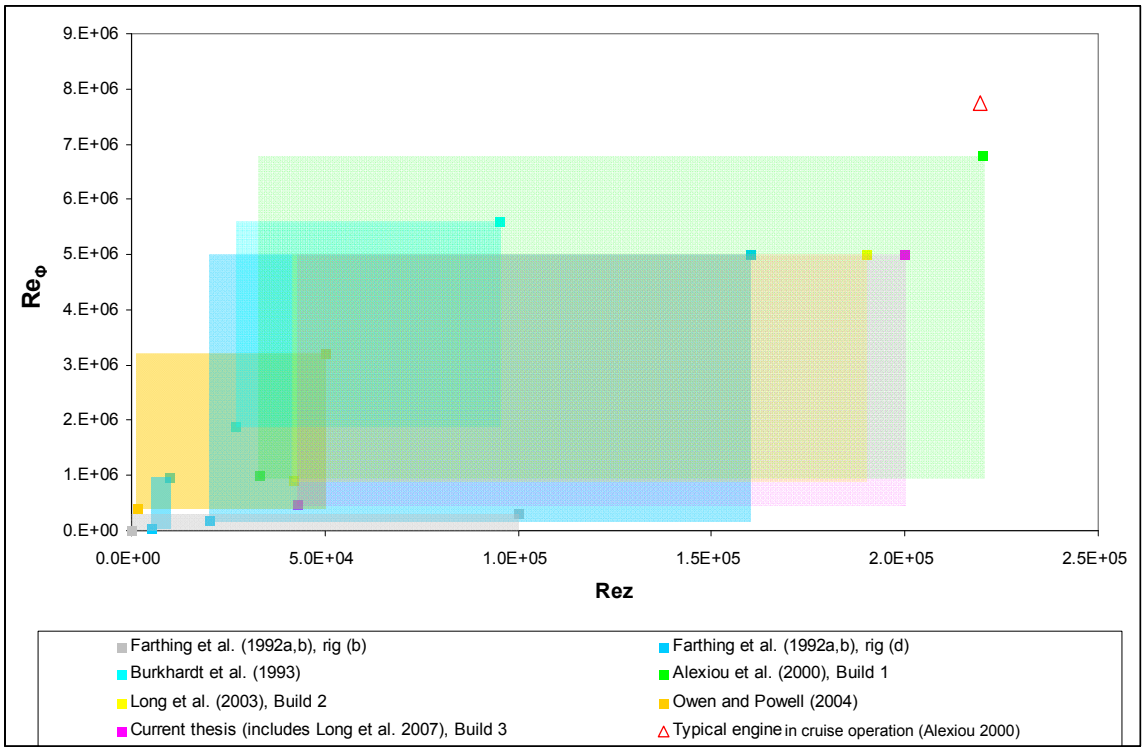

Fig 2. 17 Comparison of ranges of previous experiments to a typical engine in cruise operation

Experiment	Number of cavities	Geometric description	Shaft	G	a/b	Heating	H/T	LDA	Re_ϕ range	Re_z range
Farthing et al. (1992a,b)	rig a 1 cavity	idealised	no	0.27	0.1	air impingement 70°C max.	no	high speed photography	$1.3x10^4 \le Re_\phi \le 8.7x10^4$	$2.2x10^3 \le Re_z \le 7.7x10^3$
	rig b 1 cavity	idealised	no	0.133, 0.267, 0.4, 0.533	0.1	isothermal	no	Vr, VΦ	$0 \le Re_\phi \le 3x10^5$	$0 \le Re_z \le 1x10^5$
	rig c 1 cavity	idealised	yes	0.267	0.1	downstream disc	no	high speed photography	$0.5x10^5 \le Re_\phi \le 9.5x10^5$	$0.5x10^4 \le Re_z \le 1x10^4$
	rig d 1 cavity	idealised	no	0.12, 0.24, 0.36	0.1	discs	no	VΦ	$0.5x10^5 \le Re_\phi \le 9.5x10^5$	$0.5x10^4 \le Re_z \le 1x10^4$
							yes	no	$2x10^5 \le Re_\phi \le 5x10^6$	$2x10^4 \le Re_z \le 1.6x10^5$
Burkhardt et al. (1993)	5 cavities	engine parts	yes rotating	0.256	0.286	air impingement shroud, discs	yes	no	$1.9x10^6 \le Re_\phi \le 5.6x10^6$	$2.7x10^4 \le Re_z \le 9.5x10^4$
Long (1994)	1 cavity	idealised	no	0.13, 0.36	0.1	shroud, discs	yes	no	$2x10^5 \le Re_\phi \le 5x10^6$	$2x10^4 \le Re_z \le 1.6x10^5$
Alexiou et al. (2000)	2 cavities + turbine drive cone	geom.. similar (70% full size)	yes rotating	0.195	0.3	air impingement shroud, discs, cone	yes	no	$1x10^6 \le Re_\phi \le 6.8x10^6$	$0.33x10^5 \le Re_z \le 2.2x10^5$
Long et al. (2003)	Build 1 2 cavities + cone	geom.. similar (70% full size)	yes rotating	0.195	0.3	air impingement shroud, discs, cone	yes	no	$1.1x10^6 \le Re_\phi \le 7.7x10^6$	$0.33x10^5 \le Re_z \le 2.2x10^5$
	Build 2 5 cavities	geom.. similar (70% full size)	yes static	0.195	0.32	air impingement shroud, discs	yes	not reported	$0.9x10^6 \le Re_\phi \le 5x10^6$	$0.42x10^5 \le Re_z \le 1.9x10^5$
Owen and Powell (2004)	1 cavity	idealised	yes synchro nous	0.2	0.4	shroud, downstream disc	yes	VΦ Vr not reported	$4x10^5 \le Re_\phi \le 3.2x10^6$	$1.4x10^3 \le Re_z \le 5x10^4$
Current thesis (includes Long et al.2007)	Build 2 5 cavities	geom.. similar (70% full size)	yes static	0.195	0.32	air impingement shroud, discs	yes	VΦ, Vz	$4x10^5 \le Re_\phi \le 5x10^6$	$4.2x10^4 \le Re_z \le 1.9x10^5$
	Build 3 4 cavities	geom.. similar (70% full size)	yes static	0.195	0.32	air impingement shroud discs	yes	VΦ, Vz, Vr	$4.7x10^5 \le Re_\phi \le 5x10^6$	$4.3x10^4 \le Re_z \le 2x10^5$

Table 2. 1 Review of previous experiments in rotating cavities with axial throughflow

Progress in CFD modelling of gas turbines' components has been supported by experimental studies used to validate models and the parallel evolution of computing equipment. Sun et al. (2004) explained the difficulty involved in modelling buoyancy driven heat transfer in rotating cavities, whereas forced convection situations are comparatively easier to model accurately in CFD (due

to a lower importance of fluid density variations). The three-dimensional and unsteady nature of the flow within the compressor cavities requires a high-level of computational detail in order to define the overall behaviour of the flow and heat transfer. Cheaper computing facilities allow finer grids and smaller time steps to be used to try defining the flow better. However, the level of details provided by CFD simulations often falls within the measurement uncertainty zone of the experimental measurements they are trying to match. Therefore a somewhat paradoxical situation could occur in which a highly refined and detailed computation is necessary in order to be able to predict broader observations accurately. Tian et al. (2004)'s computations reproduced the geometry of the experimental rig used by Farthing et al. (1992a). Their modelling was three-dimensional, steady and a k-ε turbulence model was applied. In isothermal conditions, for a fixed Re_z and $\beta\Delta T$ (based on shroud temperature), rotational conditions were varied and the investigation was related to the flow structure evolution over a range of increasing rotational Rayleigh number. The simulations showed that the cavity flow and heat transfer could be separated into an outer radius zone where Rayleigh-Bénard type of convection could be encountered, and in the lower radius zone forced convection would occur. The Rayleigh-Bénard type zone size would increase with increasing Ra and a critical Rayleigh number Ra_c would mark the value over which the flow would become unstable and time dependent. From a stable axi-symmetric flow (Ra_c=6.5x10^5 in their case) the flow begins to oscillate and becomes more non axi-symmetric as Ra increases and three pairs of cyclonic and anti-cyclonic circulations would appear (Ra≈8.5x10^6).

Increasing further the value of Rayleigh number, two pairs of circulations would be found at Ra=2.4x10^7 and the flow would establish itself to one pair of circulations at Ra≥2.6x10^7.

Fig 2.18 shows a circulation pattern from Tian et al.'s computations for high Rayleigh number (Ra=4.1x10^8) very similar to the experimental observations of Farthing et al. (1992a).

Owen et al. (2006) performed CFD computations based on Owen and Powell (2004)'s experimental rig's geometry on three different running conditions. Similar circulating flow patterns to Farthing et al (1992a)'s observations were also highlighted in the simulations. The computed tangential velocity distribution

and radial Nu distribution were qualitatively similar to the experimental data. However, the computation's results at low Re_{Φ}, Re_z, and Ro did not match its experimental equivalent, over predicting the tangential velocities and under predicting heat transfer values. The reason for this was not known by the authors.

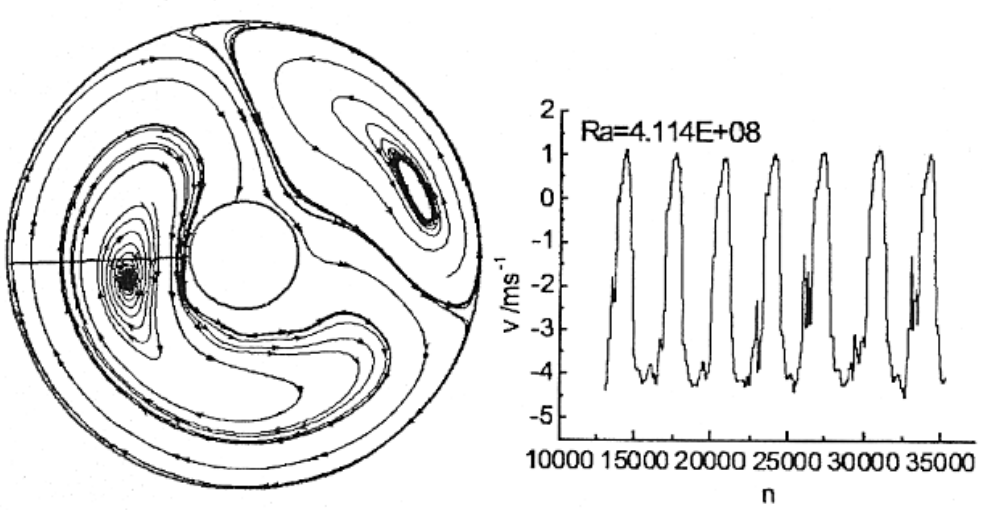

Fig 2. 18 Flow velocity field computations fron Tian et al. 2004

Sun et al. (2006) performed a comparison simulation study on the computational ability of Large Eddy Simulation (LES) to obtain a better agreement with experimental measurements in buoyancy affected rotating cavity flow with axial throughflow, against a "regular" Navier-Stokes based computation using a k-ε type averaging turbulence model.

The geometry used was a 120 degree sector of a cavity geometry based on the Build 2 of the Multiple Cavity Rig. Three operating conditions were investigated in the range $1.87 \times 10^8 \leq Gr \leq 7.41 \times 10^8$ and $1.65 \leq Bo \leq 11.5$ (Gr being based on the shroud) from the experimental measurements performed by Alexiou (2002). Computations highlighted large Rayleigh-Bénard type flow structures within the cavity with the presence of unsteady circulating flows and radial arms. Overall, LES provided a finer flow structure description than the k-ε model and the velocity and temperature computations were in much better agreement with the experimental data, although still diverging on the computed heat transfer values by about 25%.

3. Experimental apparatus

As mentioned in the introduction, the experimental rig used in the present study follows on several generations of cavity rigs that were used in the TFMRC at the University of Sussex over the years. More precisely, the experimental rig used has several rotating cavities, and being the third variation of this rig set-up, is referred to as Multiple Cavity rig, Build 3, pictured in Figure 3.1.

Build 3 represents the internal set-up of a high pressure compressor on a 0.7 scale. A disc stack geometrically similar to a real engine is featured, forming the internal cavities. A shaft is represented in the inner radius, although it is stationary. Compressed air is blown across the rig as cooling air would inside a real high pressure compressor and thus forms the secondary air system in a compressor stack to be studied.

Build 2 will be seldom mentioned in this thesis. It was geometrically identical to Build 3 although the static shaft had a slightly bigger diameter. Results from Build2 were reported in Alexiou (2001), Alexiou (2002) and Long et al. (2003). It is worth noting that some LDA measurement data had been produced in Build 2 but had not been published. Build 1 was the subject of the thesis of Alexiou (2000) and featured a shaft that could be rotated with or against the rotor direction at various speeds. Holes in the shaft allowed a portion of the cooling air to exit away from the cavity area. The rotor represented one compressor cavity and the turbine drive cone found on the end side of the high pressure compressor.

At the start of the work reported in this thesis, the Multiple Cavity Rig Build 3 had just finished being designed and manufactured by the technical team at the TFMRC and predecessor experimentalist on the Multiple Cavity Rigs, A. Alexiou. The author and A. Alexiou performed the commissioning of this rig with the LDA system using the shaft as optical access similarly to Build 2. Initial commissioning results were mentioned in Alexiou (2002) before the rig and project were handed over to the author late 2002. Provision for optical access through the discs had already been included in the design of Build 3. It was the author's subsequent task to source and set-up a suitable traverse system for LDA access through the discs before the experimental work would start. In the course of the currently reported experimental work, the author expanded the

flow measurement definition in greater details within the cavities. Measurements by the author within the shaft, cavity entrance and cob areas, together with the radial velocity measurements in cavities were the first of their kind to be reported.

Following is a description of the experimental apparatus. It is worth noting that most design features, instrumentation and test cell equipment related to Build 3 of the Multiple Cavity Rig had already been implemented and detailed in previous versions of the rig. More details on these are described in Alexiou (2000).

3.1 The Multiple Cavity Rig

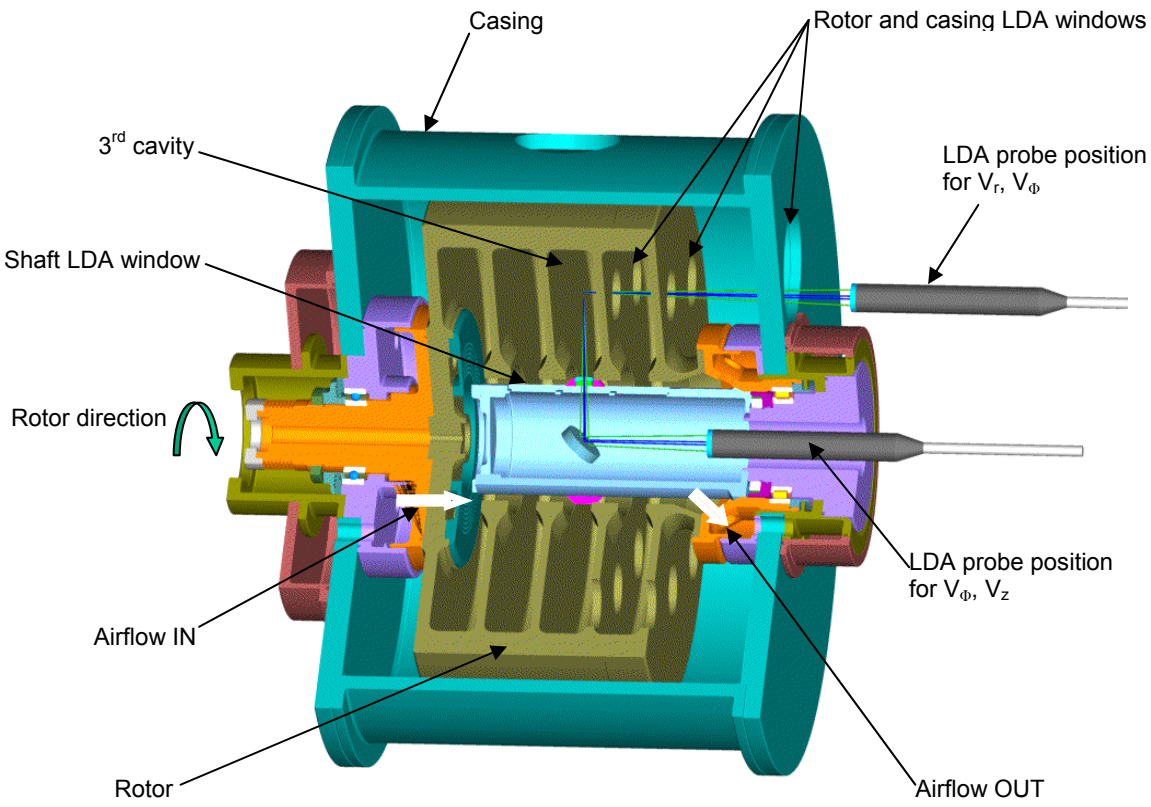

Fig 3 . 1 Cut-out view of the Multiple Cavity Rig build 3

Fig 3.1 shows a general view of the Multiple Cavity Rig Build 3. Figure 3.2 show a schematic of the multiple cavities and their dimensional parameters. The rotor is made of titanium 318 and forms four cylindrical cavities with an inner radius a= 70.1mm, an outer radius b= 220.0mm (a/b= 0.32) and with a disc spacing s= 42.9mm ($G= s/b=$ 0.195). The last two discs carry glass windows to allow velocity measurements (radial and tangential components) in the last two cavities at 0.51< r/b < 0.96, also shown in Fig 3.3.

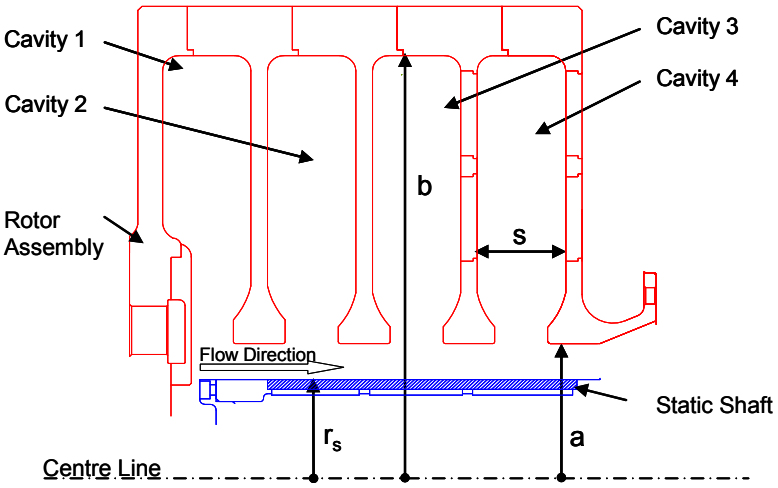

Fig 3. 2 Dimension parameters in the Multiple Cavity Rig, Build 3

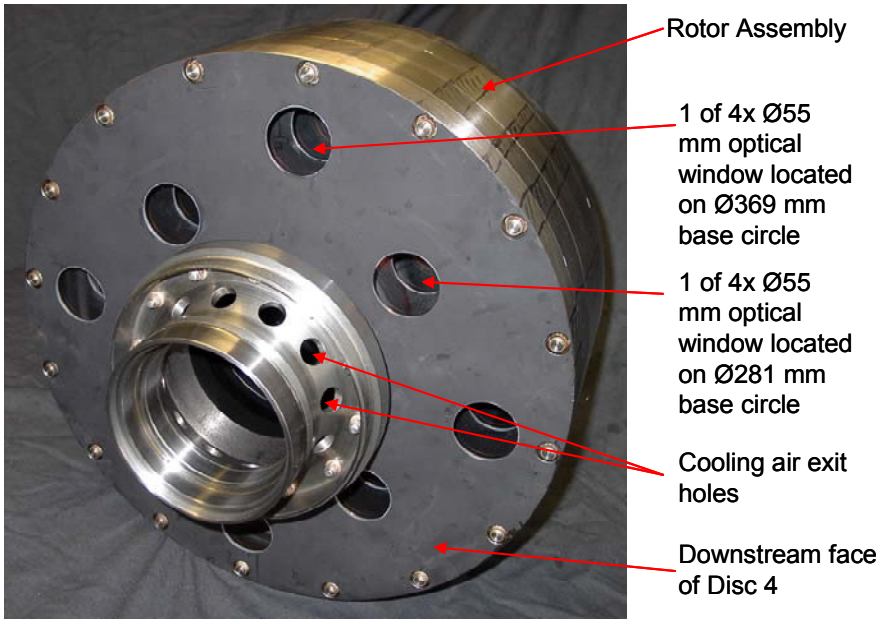

Fig 3. 3 External view of the downstream side of the rotor assembly showing the discs optical access windows

The non-rotating inner shaft has an outer radius r_s= 52.0mm (Δr= a-r_s= 18.1mm). An axi-symmetric sleeve can be placed over the shaft as shown in Fig3.4. Its section geometry is shown in Fig 3.5.

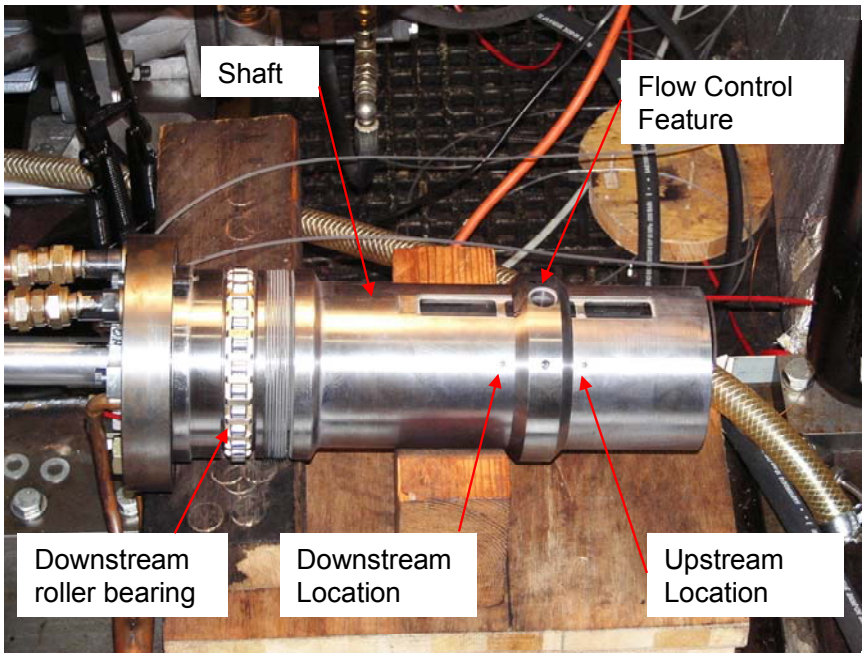

Fig 3. 4 View of the shaft and Flow Control Feature installed at mid-position

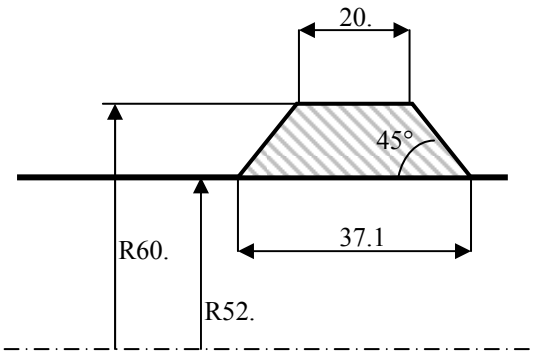

Fig 3. 5 Cross section sketch of the Flow Control Feature

This sleeve, named the 'Flow Control Feature', was aimed at influencing the behaviour of the central airflow and attempted to modify the amount of throughflow being diverted inside the third cavity. The Flow Control Feature could be positioned at three different axial locations as indicated in Fig 3.6, i.e. under disc 2, in the middle of cavity 3, or under disc 3.

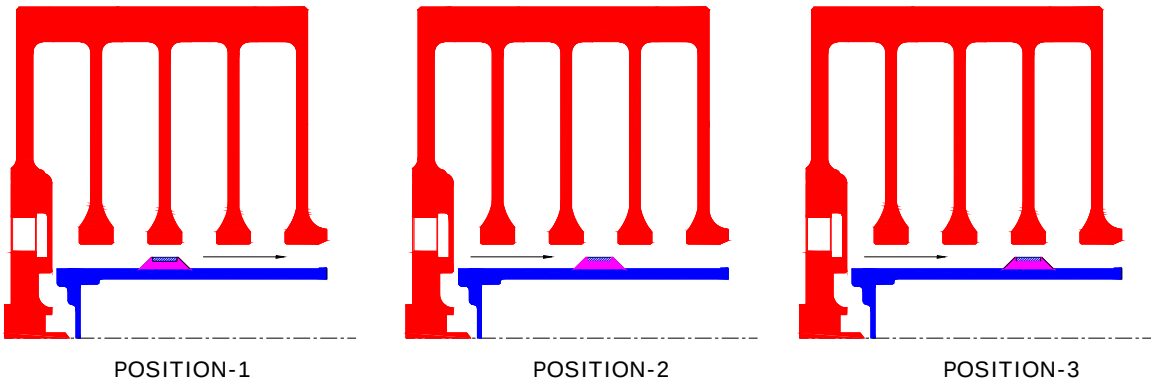

Fig 3. 6 Possible positions of the Flow Control Feature

The shaft has a glass window covering the axial length of the last three cavities. Through this window, the tangential and axial components of velocity in these cavities can be measured. The rig was designed so that the shaft can be removed without dismantling the rig. This allows for cleaning the optical access windows and positioning (or removing) the Flow Control Feature.

The rotor assembly is housed within a steel, non-pressurised casing and supported by a high precision grease lubricated ball bearing on the upstream side and an oil lubricated cylindrical roller bearing on the downstream side.

A 3 kW A/C motor was used to rotate the rotor in the clockwise direction (according to the direction of the cooling flow) via a 2.6 kW TR Tasc Unit driving a poly-vee belt. Operating speeds achieved were varied up to 6000 rev/min. A single pulse Hall effect sensor on the drive shaft provides speed feedback to the control desk.

The control desk, pictured in Fig 3.7, provides access to the data loggers, pump controls, speed controls, and includes the computer controlling the LDA system and the pressure and temperature data loggers.

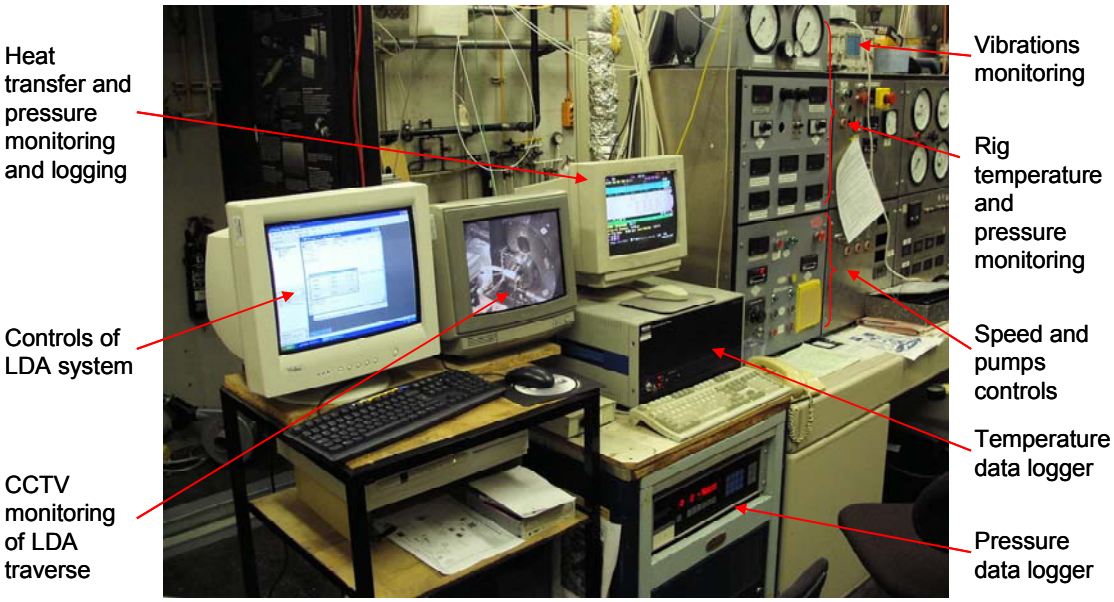

Fig 3. 7 Control desk of the Multiple Cavity Rig, Build 3

3.2 Air Supply

Air inside the rotor assembly is supplied to the rig by a single stage 275 kW Howden compressor which can deliver up to 1.1 kg/s of air at 4 bar abs. and 200°C, pictured in Figure 3.8.

Fig 3. 8 Photograph of the Howden screw compressor

Before entry to the rig, the air was cooled to typically 30-55°C (varied depending on air relative humidity and supply pressure in order to avoid condensation) by passing it through a single flow, shell and tube heat exchanger, with water flowing over the tubes at a variable rate to obtain the desired output air temperature. The air is delivered inside the rig via six circumferentially distributed holes of 25mm diameter in the upstream rotor disc, followed by a diffuser plate bolted onto the rotor in order to help create a uniform inlet velocity profile as described in Alexiou (2000) (pictured in Fig 3.9).

Fig 3. 9 Multiple Cavity Rig inlet diffuser plate

The air exits the rig in the downstream bearing support via 12 holes of 16mm diameter at 60° orientation outward to the axis of rotation. Sealing in the bearing supports and flanges of the pressurised rotor was provided by an arrangement of labyrinth seals designed to Rolls-Royce standard (Rolls-Royce, 1983), with the stator part lined with abradable material to increase sealing effectiveness. The labyrinth seals prevented lubricating oil ingestion into the rig provided the rotor was pressurised by at least 0.35 bar before the oil pressure pump was activated. More details on the lubrication and sealing systems can be found in Alexiou (2000).

The pressurisation of the rig was achieved by a manually operated ball valve downstream of the rig on the exhaust pipe leading to the outlet orifice plate.

Airflow across the rig was measured by an inlet and outlet orifice plate made to BS1042 specifications. The difference of the inlet and outlet airflows provided a measurement of the leakage flow through the rig's seals. Figure 3.11 illustrates the air system of the Multiple Cavity Rig.

The outer surface of the rotor assembly is heated by the impingement of hot air blown inside the rotor casing by two 10 kW Leister hot air heaters; each supplying up to 0.01 kg/s of air at 800 K.

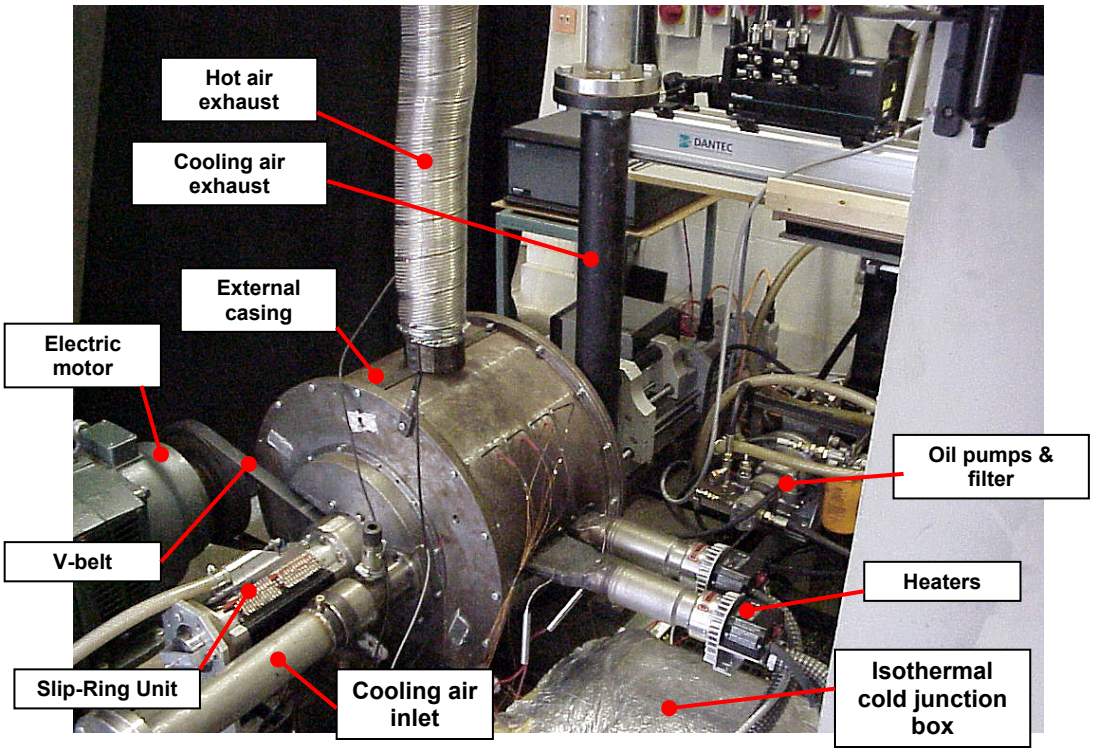

Fig 3. 10 External view of the Multiple Cavity Rig, Build 3

Fig 3.10 provides a general view of the rig. Fig 3.11 and 3.12 summarise the air supply and cooling layout of the rig.

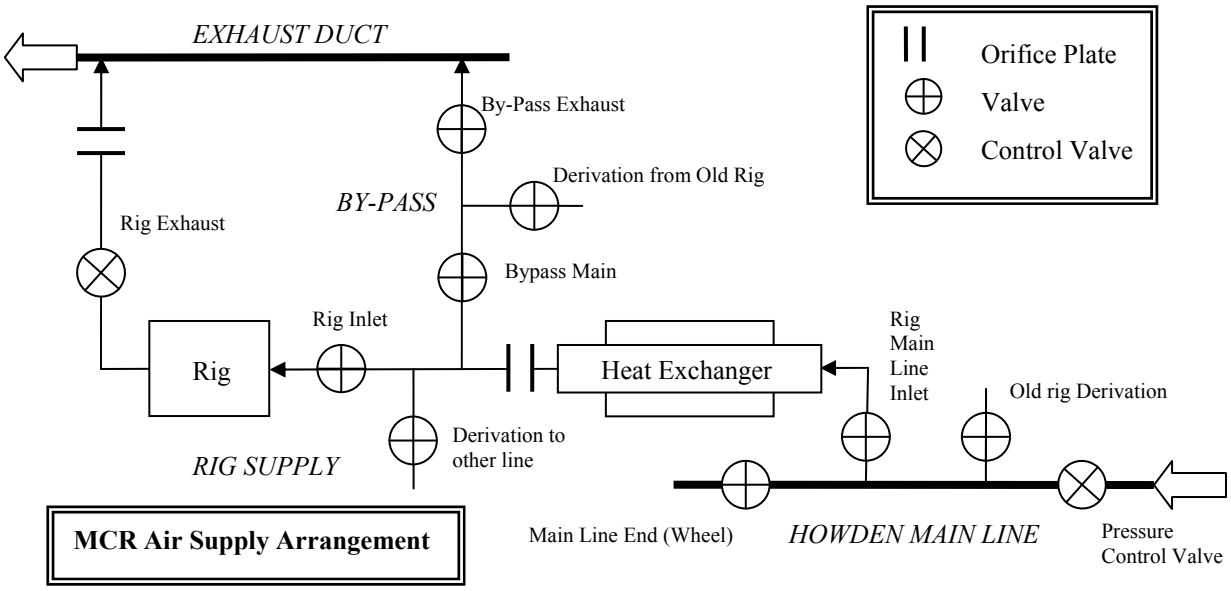

Fig 3. 11 Air supply diagram of the Multiple Cavity Rig, Build 3

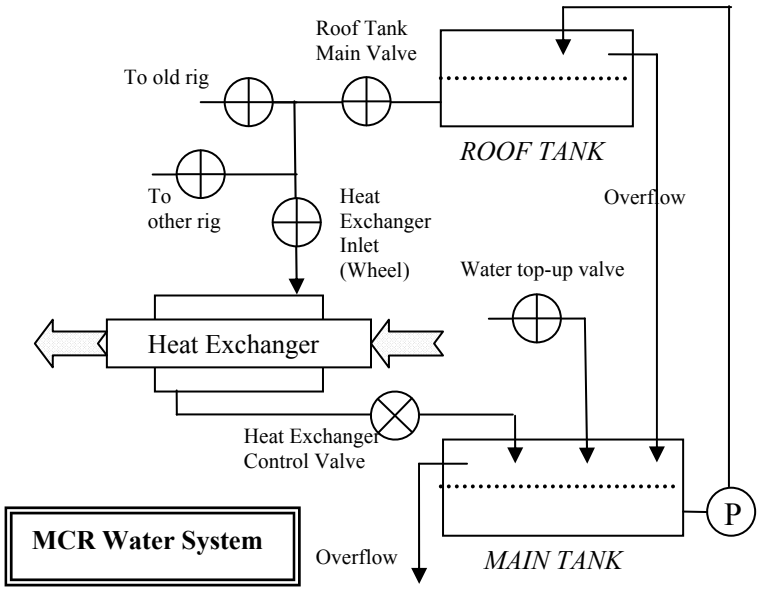

Fig 3. 12 Water cooling system diagram of the Multiple Cavity Rig, Build 3

3.3 Temperature measurement

Fig 3.13 shows the internals of the Multiple Cavity Rig and its points of instrumentation.

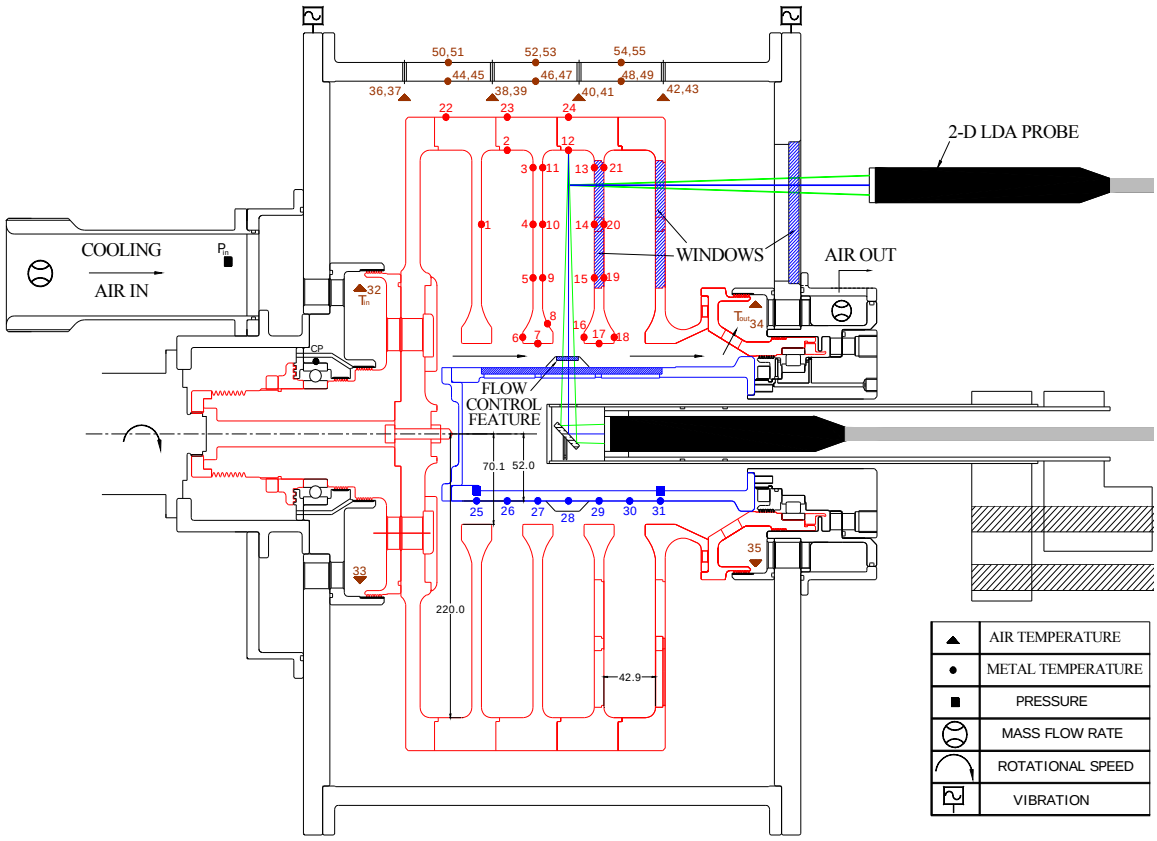

Fig 3. 13 Instrumentation of the Multiple Cavity Rig, Build 3

Temperature measurement can be distinguished between air-temperature measurements and surface temperature measurements. All temperatures were measured using calibrated 0.25 mm diameter wire K-type (NiCr-NiAl) thermocouples.

The air temperature thermocouples used for the inlet, exhaust and rotor casing airspace temperatures were placed inside a stainless steel tube protruding from the flanges or casing surfaces and holding the thermocouple bead at a distance of 5 mm from them.

Surface temperature thermocouples were cemented inside narrow channels in order to reduce thermal disturbances and titanium straps were welded on top of the channels to ensure that the leads could not be centrifuged out in the rotor parts as described in Alexiou (2000). The wires leading out from the beads in the rotor assembly were taken out tangentially in a 6 mm slot before bifurcating

into a radial channel in order to reduce the measurement errors due to heat conduction along the thermocouple wires in the radial direction. The thermocouple beads were punched into their slots so that they were flush with the surface and in intimate contact with the surrounding material in order to reduce thermal disturbances.

Referring to the numbering of the thermocouples in Fig 3.13, the thermocouple instrumentation of the Multiple Cavity Rig comprises an inlet cooling air temperature measurement comprising two diametrically opposed air temperature thermocouples located in the upstream part of the casing (thermocouples 32 and 33). Similarly, the cooling air exit temperature is measured by the air thermocouples 34 and 35. The rotor thermocouples relating to the heat transfer of disc 2 were located on the disc's surface temperature (thermocouples 3, 4, 5 and 9, 10, 11). The thermocouples related to the heat transfer of disc 3 were the surface thermocouples 13, 14, 15 on the upstream face of disc 3 and thermocouples 19, 20, 21 on the downstream face of disc 3. The shroud heat transfer of cavity 2 was obtained via the measurement of surface thermocouples 23 and 2, while the surface thermocouples 24 and 12 provided the data necessary to derive the heat transfer characteristics of the shroud in cavity 3. More details on the radial and relative circumferential locations of the rotor thermocouples are provided in table 3.1 below.

Rotor thermocouple No.	Radial position (mm)	Circumferential position (°)
1	162.5	90
2	220.0	135
3	206.5	225
4	162.5	45
5	121.0	0
6	75.0	180
7	70.1	0
8	85.5	90
9	121.0	270
10	162.5	315
11	206.5	135
12	220.0	90
13	206.5	135
14	162.5	315
15	121.0	45
16	75.0	225
17	70.1	45
18	75.0	225
19	121.0	180
20	162.5	0
21	206.5	270
22	245.65	270
23	245.65	315
24	246.45	180

Table 3. 1 Location of the rotating instrumentation (thermocouple numbers according to Fig. 3.13)

All the rotor thermocouple leads were led through instrumentation holes in the periphery of the rotor down to a hole in the upstream rotor drive flange to a Wendon 48 way Slip Ring Unit (SRU) linked to the end of it. The thermocouples and junction boxes had previously been made for Build 1 as detailed in Alexiou (2000). The calibration of this batch of thermocouple had previously been determined against a platinum resistance thermocouple in a thermostatically controlled water bath. A voltage characteristic of this batch was determined by a least squares quadratic curve in Alexiou (2000). A K-type thermocouple from the same batch as the rotating thermocouples was measuring the cold junction temperature at the leads connection of the slip ring unit. The non-rotating thermocouples had also previously been calibrated similarly to the rotating ones, and all leads were connected into an isothermal cold junction box. The temperature in the connection box was measured by a pair of RS components LM35CZ precision temperature sensors. The voltage signals from the slip ring unit thermocouples and from the isothermal junction box were measured by a Solartron Orion data logger with a sensitivity of ±1 μV, corresponding to ±0.025 °C for the thermocouples used. The uncertainty level associated with the thermocouples measurement, calibration and cold junction compensation will be explained in Chapter 4. The Orion channels list is provided in Appendix 3.1.

A Q-BASIC program was used to control remotely the data logger and convert and record the temperatures from the calibration equations and the cold junction signals.

Fig 3.14 shows the layout of the instrumentation of the Multiple Cavity Rig. The thermocouples and Orion data logger arrangement can be seen in the left part of the diagram.

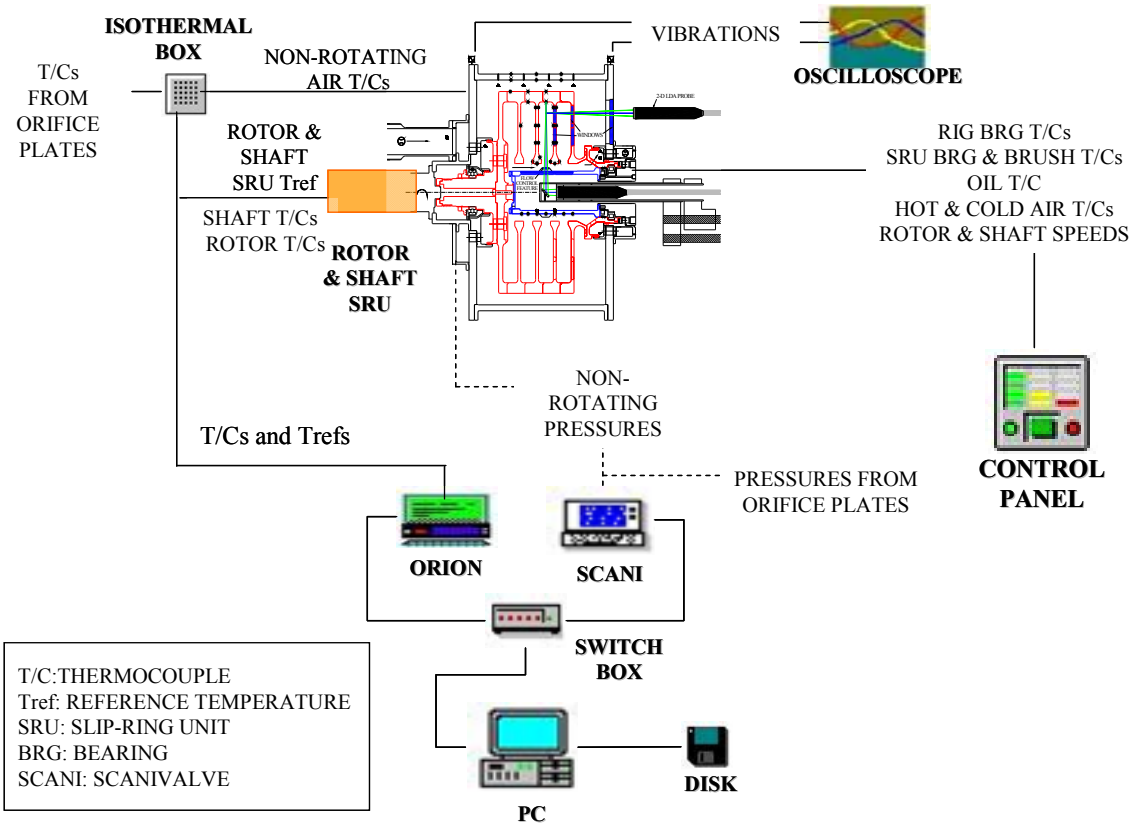

Fig 3. 14 Instrumentation layout of the Multiple Cavity Rig, Build 3

3.4 Pressure measurement

Static air pressures were measured by a Scanivalve system controlled remotely by the same computer used for the temperature data logging. The layout of the pressure measuring equipment is featured in Fig 3.14. The static pressures measured included the orifice plates, inlet and outlet cooling air pressure and shaft pressures. A detailed list of the logged channels can be found in appendix 3.2.

The Scanivalve pressure channels were calibrated against a dead-weight tester as per Alexiou (2000) and displayed an accuracy of 0.1%.

3.5 Air velocity measurement

Air flow velocity measurements within the Multiple Cavity Rig were performed by Laser Doppler Anemometry (LDA). This method of measurement allows a high spatial and temporal resolution. It requires no calibration as the output signal is a function of velocity, and is able to measure reverse flows with a suitable frequency shifting technique.

The main elements of an LDA system consist of:

- a continuous wave laser
- a beam splitter
- a frequency shift device
- transmitting optics (mirrors, fibre optic etc.)
- receiving optics
- a photomultiplier
- a signal processor
- a computer to remotely control the processor and log the data

LDA systems allow the determination of a velocity component from moving particles in a fluid. The intersection of a moving particle (be it dust naturally present in the air or a purposely introduced tracking particle), commonly referred to as a seeding particle, into a coherent source of light (laser beam) will scatter light around from reflection or refraction with the seeding particle. Due to the movement of the particle relative to the beam direction, the scattered light will show an apparent frequency shift compared to its source, also known as Doppler shift. The frequency shift is in direct relation to the relative displacement speed of the seeding particle's component of velocity along the laser beam direction. The scattered light signal therefore needs to be detected and compared to the source signal, so that the component of velocity can be determined.

Splitting the source beam into two separate beams directed so that the beams cross each other at a known angle allows the detection of velocities along the two beam directions, thus allowing a plane of measurement to be defined.

The known crossing angle will permit the definition of the direction of the velocity component measured from the addition of the two Doppler shift vectors. The resulting vector will run along the line perpendicular to the bisection of the crossing beams belonging to the plane of intersection. This represents the working principles of a one-dimensional differential Doppler system, shown in Fig 3.15.

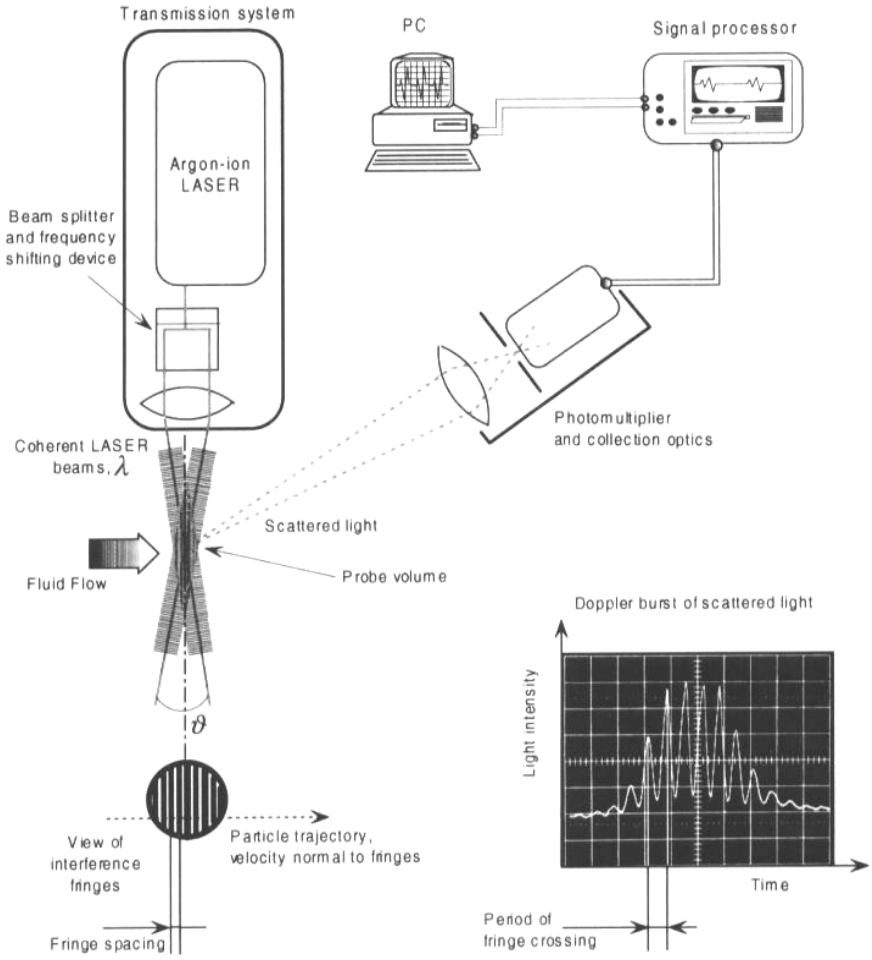

Fig 3. 15 Working principle schematics of a one-dimensional LDA system (from Begg 2003)

The two split beams of equal intensity cross into a focal point of high light intensity. This intersection region is referred to as the measurement volume, or probe volume. The laser beams cross sectional intensity pattern is in a bell shape with the maximum light intensity in the centre of the beam. This Gaussian mode of emission is also known as the TEM 00 transverse laser mode.

The high light intensity zone of the probe volume will therefore show an ellipsoidal shape as shown in Fig 3.16.

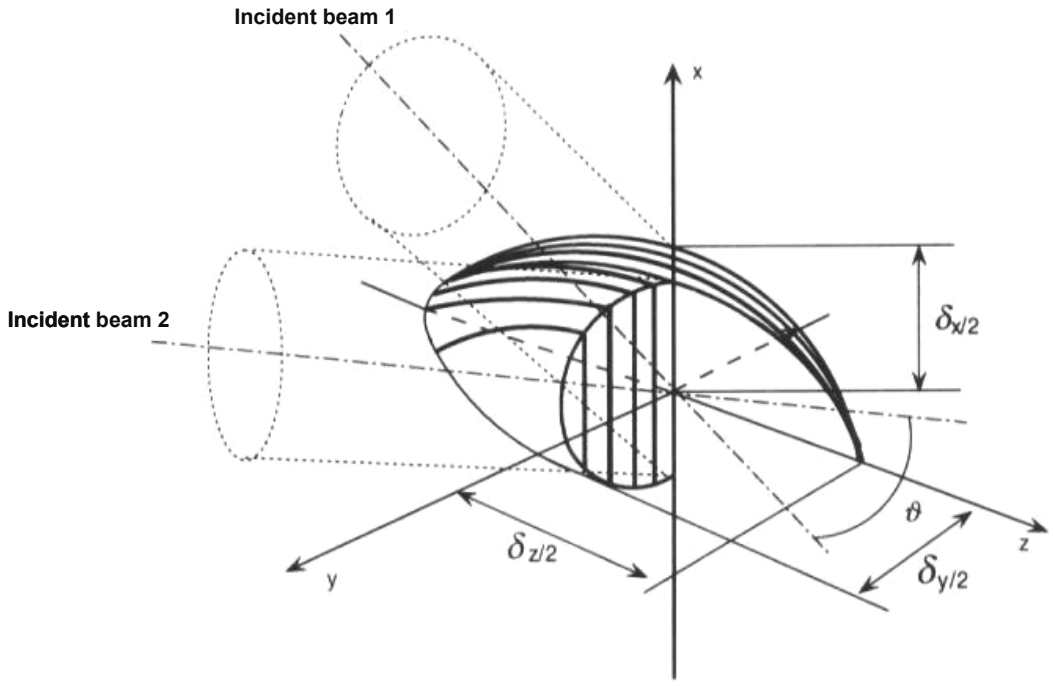

Fig 3. 16 Probe volume construction and dimensions (from Begg 2003)

The dimensions of the probe volume shown in Fig 3.13 can be expressed as:

-Height $$\delta_x = \frac{4 \times F \times \lambda}{\pi \times E \times d_g \times \cos\left(\theta/2\right)}$$ **Eq. 3.1**

-Width $$\delta_y = \frac{4 \times F \times \lambda}{\pi \times E \times d_g}$$ **Eq. 3.2**

-Length $$\delta_z = \frac{4 \times F \times \lambda}{\pi \times E \times d_g \times \sin\left(\theta/2\right)}$$ **Eq. 3.3**

Where F is the focal length of the incident beams

λ is the wavelength of the emitted laser light

E is the beam expansion factor

d_g is the beam Gaussian diameter

and θ is the angle of incidence of the beams

Considering the “interference fringe model” commonly found in the literature, at the point crossing the probe volume the two coherent light waveforms meet and add to each other when in phase or cancel each other when in opposite phase. The resulting interferences produce a series of equally spaced constructive and destructive interference fringes which materialise as bright and dark stripes. Fig 3.17 represents a simplified interference model of interfering wave fronts.

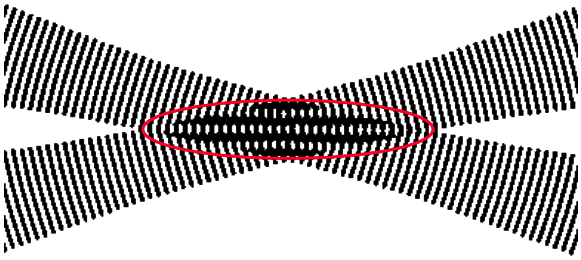

Fig 3. 17 Interference fringe model (Dantec 2004)

The fringe spacing is a function of the angle of incidence of the beams and their wavelength. It is expressed as:

$$\delta_f = \frac{\lambda}{2 \times \sin\left(\theta/2\right)} \qquad \textbf{Eq. 3.4}$$

The interference fringes in the probe volume are formed parallel to the bisector of the beams and in a plane perpendicular to the plane of the beams intersection. The number of fringes in the probe volume is calculated as:

$$N_f = \frac{8 \times F \times \tan\left(\theta/2\right)}{\pi \times E \times d_g} \qquad \textbf{Eq. 3.5}$$

The fringes in the probe volume offer a zone of high contrast compared to the light intensity of the incident beams. A seeding particle passing through the fringes will therefore scatter light at a level that can be detected and filtered out from other scattering not occurring in the probe volume.

A collection lens pointed at the probe volume is used to transmit the scattered light of seeding particles to a Photo Multiplier Tube (PMT) that will convert the fluctuating light intensity into an electric signal.

Seeding particles scatter light by refraction or reflection in all directions. However the highest light intensity of scattering is observed in the direction away from the laser source. This is referred to as forward scatter mode and is illustrated by the polar plot in Fig 3.18 for a particle size equal to the wavelength of the laser source.

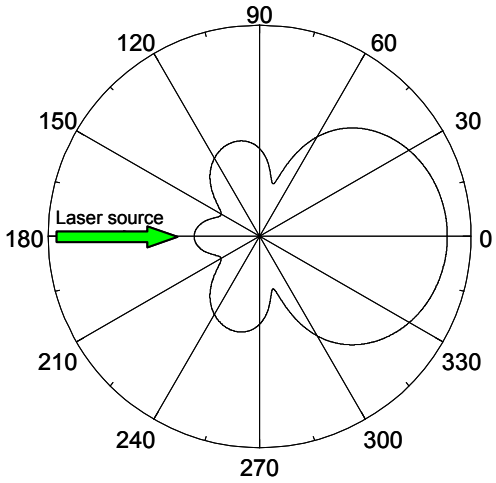

Fig 3. 18 Polar plot of light scattering from a particle of size equal to the wavelength of the laser source with the light intensity shown on a logarithmic scale (Dantec 2004)

The positioning of the receiving optics would therefore preferably be in the forward scatter mode (i.e. pointing towards the laser source) in order to improve the signal to noise ratio (SNR) of the measured scattered light through the probe volume. However, for practical reasons, it is often more convenient to locate the receiving optics pointing from the same direction as the laser sources as this configuration offers the convenience of having only one optical access required on the experimental set-up. Even though the scattering light intensity in back scatter configuration is less than in forward scatter, the signal to noise ratio of the scattered light from the probe volume is still strong enough for practical signal measurement and is widely used in commercial systems. As a seeding particle passes through the probe volume fringes, the scattered light from the particles will be seen to fluctuate from the succession of constructive and destructive wavefront interferences.

Due to the Gaussian transverse power distribution of the incident beams, the overall power intensity will be higher by the centre fringes of the probe volume.

The detected scattered light intensity signal of the seeding particle passing through the probe volume will typically look like the signal shown in Fig 3.19 below, with an oscillating pattern whose period corresponds to the travel time between a light and a dark fringe. The overall light intensity varies in a bell shape as the particle progresses through the fringes.

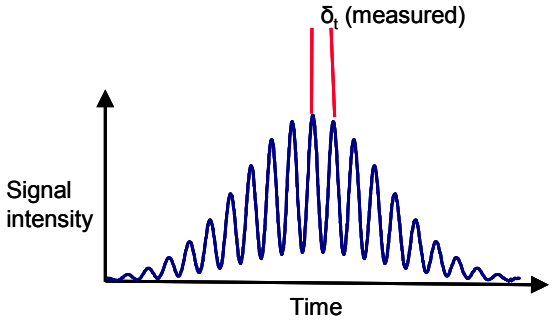

Fig 3. 19 Typical Doppler burst signal of scattered light (Dantec 2004)

Knowing the distance between the fringes, δ_f, and the time, δ_t, it took the seeding particle to cross them, the speed of the particle in the component normal to the fringes, U, can be deduced as:

$$U = \frac{\delta_f}{\delta_t} \qquad \textbf{Eq. 3.6}$$

The frequency at which the light is scattered is equal to the Doppler frequency of a dual beam anemometer (Albrecht et al. 2003) and is expressed as:

$$f_d = \frac{U}{\delta_f} = \frac{2 \times U \times \sin\left(\theta/2\right)}{\lambda} \qquad \textbf{Eq. 3.7}$$

Modern signal processors determine the Doppler frequency from the photo multiplier signal using correlation or Fast Fourier Transform (FFT) algorithms. Some high pass and low pass filtering is also applied to differentiate the randomly arriving frequency modulations of a seeding particle passing through the probe volume, named “burst” from the general optical and electronic noise collected by the PMTs. Signal filtering is also applied to discard bursts produced by multiple particles passing simultaneously into the probe volume.

The velocity component calculation being in direct relation to an induced frequency of passage through equally spaced fringes, it is not possible to distinguish whether the passage occurred in one direction or the other of the velocity component. This directional ambiguity can be eliminated by introducing a frequency shift to one of the incident beams. An acoustic-optical modulator, a "Bragg cell", is commonly found in modern LDA systems in the transmitting optics in order to add a known frequency shift to one of the incident beams. The frequency modulation of one beam compared to the other produces variations in the interference patterns in the probe volume. As the beams are unequally shifted, the fringes will appear to be scanning across the probe volume at a constant velocity. Knowing the direction of the frequency shift, a particle moving in the direction of the shift at a certain speed will produce a burst signal of lower frequency than the frequency that would have been produced in a non-shifted probe volume. Conversely, a particle going against the fringes will produce a higher frequency burst. Additionally, a stationary particle will now be able to be detected as the burst frequency produced will correspond to the frequency shift.

Seeding particles introduced into the fluid of which velocity is to be measured must be sufficiently small in order to accurately follow the flow velocity field, yet be sufficiently large in order to scatter enough light to produce Doppler bursts strong enough to give an acceptable signal to noise ratio. Various materials and forms can be considered as suitable seeding particles, such as oxide powders or atomised oil. The type of seeding and size of seeding particles will depend on the type of flow to be studied, its environment, and the optical set-up of the LDA system used. Typically, atomised oil particles of diameter size in the order of 1µm are used in airflow measurements. The fidelity of motion of a flow tracer particle in turbulent flow can be quantified by its Stokes number (Sk) as explained in Tropea et al. (2007). It is defined as the ratio between the characteristic particle response time, τ_p, and the characteristic particle flow time scale τ_f. For Stokes numbers $Sk = 1$ the particles will follow the flow closely.

Considering a particle material density ρ_p = 870 kg.m^{-3} (quenching oil, RS 184-7939), a particle diameter produced by the seeder of d_p=1µm, into air of

properties μ_f = 15x10^{-6} Pa.s and ρ_f =1.2 kg.m^{-3}, the particle characteristic response time is given in Albrecht et al. (2003) as:

$$\tau_p = \frac{\rho_p \cdot d_p^2}{18\mu_f} \qquad \textbf{Eq. 3.8}$$

The cut-off dynamic frequency at which the particles still follow the velocity oscillation of the flow, allowing for 1% slip, can be calculated as (Albrecht et al. 2003):

$$f_c = \frac{0.0227}{\tau_p} \qquad \textbf{Eq. 3.9}$$

An expression of the Stokes number as a characteristic non-dimensional frequency of the particle response was shown in Melling (1997) from the solution of Hjelmfelt and Mockros (1966) as:

$$Sk_c = \left(\frac{\rho_f \cdot \omega_c}{\mu_f} \right)^{1/2} \cdot d_p \qquad \textbf{Eq. 3.10}$$

Where $\omega_c = 2\pi f_c$

In the case of the presented LDA experiments, the cut-off frequency is estimated as f_c = 70.5 kHz for a 1μm seeding particle. This corresponds to Stoke numbers of the seeding of Sk < 0.19 at flow frequencies up to f_c; which is considered as acceptable in the current experiment.

When selecting the optical set-up and seeding Begg (2003) recommends a fringe spacing about four times bigger than the mean particle diameter as best practice. The density of seeding is also important in order to increase the rate of burst sample occurrence, but too much seeding would also be increasing the likelihood of rejected data due to Doppler bursts from simultaneous particles within the probe volume. Longer seeding duration, especially in dense atomisation can also cause the optical access windows in the experimental rig to become dirty faster, adding optical glare in the emission and collection optical path, hence lowering the signal to noise ratio.

A two velocity component LDA system is easily obtained by adding another dual beam system and burst signal processing channel to the original system so that the second pair of beams' probe volume coincides with the first probe volume. By having the second pair of beams orthogonally positioned to the first one, a direct measurement of planar velocity components is possible. Distinguishing

the Doppler signals one component from another is achieved by using different wavelengths (colours) for each pair of beams. A colour separator after the collection optics filters the scattered light into two different optical components which in turn become converted into electrical signals by a PMT and processing unit per velocity component.

Ease of use and money savings can be provided from a dual frequency laser source such as the Stabilite 2017 laser from Spectra-Physics that was used on the Multiple Cavity Rig's LDA system. The described LDA equipment and 'in-shaft' coaxial traverse system have been used since Build 2 of the Multiple Cavity Rig and were previously mentioned in Alexiou (2001) and Alexiou (2002). The water cooled Argon-Ion laser was emitting in the green colour mode (514.5 nm wavelength) and blue (488 nm) at a power output of up to 5 Watts.

The transmitting and receiving equipment's configuration schematic is shown in Fig 3.20.

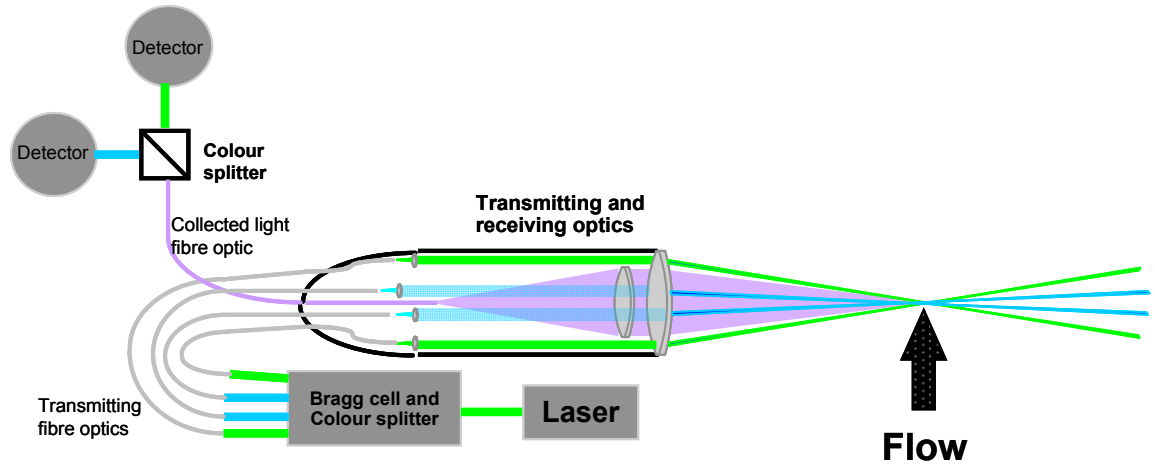

Fig 3. 20 Typical layout of a 2-D backscatter LDA system (adapted from Dantec 2004)

The laser source is emitted into a DANTEC Fiberflow 2D system. The laser source is split and a frequency shift of 40 MHz added by a Bragg cell. A colour separator outputs a pair of non-shifted and shifted beams for each colour frequency of the laser source. The beam pairs are then transmitted via a 10 m long fibre optic cable to an integrated back-scatter two dimensional probe.

The total output at the fibres was about 30% of the supplied power at the laser source. The 27 mm diameter Fiberflow probe allowed the transmission of the measurement beams in a factory aligned sealed casing. The front optic was

modified to provide a 250 mm focal length to the probe. This allowed a sufficient reach of the probe volume deep inside the rig's cavities. The 27 mm external diameter of the probe permitted its insertion inside the Multiple Cavity Rig's shaft as will be explained below. The probe volume characteristics are shown below in Table 3.2 together with other relevant LDA parameters.

Parameter	**Value**
Transmitting lens focal length	250 mm
Beam spacing	15 mm
Frequencies Tangential velocity (green) Axial velocity (blue)	 514.5 nm 488 nm
Laser beam diameter	1.35 mm
Beam half angle	1.718 °
Expansion factor	1
Probe volume diameter	0.121 mm (for λ = 514.5 nm)
Probe volume length	4.046 mm (for = 514.5 nm)
Number of fringes	14
Fringe spacing	8.579 μm
Frequency shift	40 MHz

Table 3. 2 LDA parameters

The 15 mm beam spacing and 250 mm focal length produced a length of the probe volume of about 4 mm. The relatively large length of the probe volume had the consequence of reducing the ability to measure near walls. The resulting fringe spacing of about 8 μm also meant that multiple measurement occurrences could be more frequent due to the 8 to 1 ratio of fringe spacing to seeding particle size of 1 μm provided by the TSI 9306A six jet atomiser seeding RS components RS184-7939 quenching oil into the rig.

Therefore, the seeding density had to be kept to a minimum for acceptable validated data rate. In order to reduce glare and optical noise while measuring, the internal surfaces of the rig were painted matt black and the optical access

windows were made out of BK7 optical grade glass treated with an anti-reflecting coating for the 480-520 nm wavelength range. The scattered light signals were sent to the photomultipliers from the probe via a fibre optic and colour separator.

The photomultipliers' signals were fed to a DANTEC BSA70 Burst Spectrum Analyser which processed the Doppler signals and managed the power supplies to the PMT and Bragg cell. The signal processor features automatic surge protection of the photomultipliers, a hardware Fast Fourier Transform algorithm capable of handling and validating Doppler bursts at rates of up to 100 kHz. A Baumer BHG06-25W360 encoder driving a Texas Instrument 74HCT240W logic transceiver mounted at the end of the slip ring unit of Build 3 as shown in Figure 3.21. The encoder driver, which connection diagram is shown in Appendix 3.3, provided a TTL level synchronisation input to the LDA signal processor. Although the encoder could provide 360 pulses per revolution, only the reset pulse was used as is normal practice in rotating machinery where the rotational speed can be considered steady.

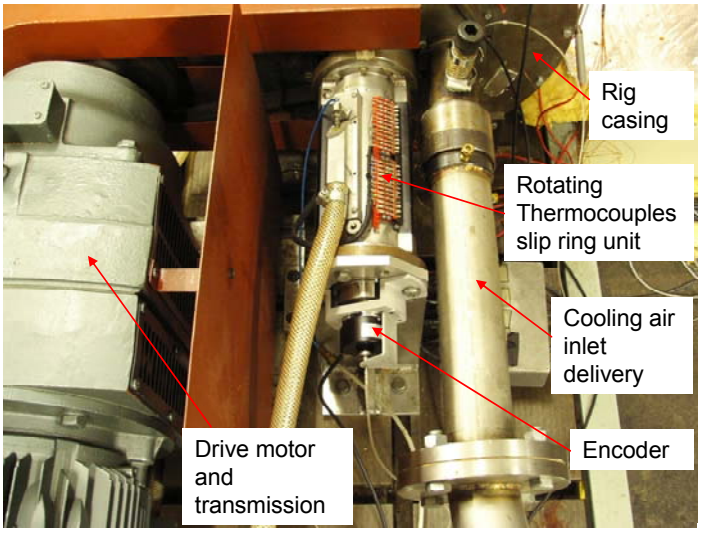

Fig 3. 21 View of the shaft encoder mount and slip ring unit

The BSA Flow software (v3.0) provided the user interface and data collection facility of the LDA system. It features an online Doppler monitoring window and indications of data rates and validation percentages. Controls over the different filtering and photomultipliers voltages were provided and the number of samples

to be acquired could be set as an end condition of measurement. A range of data calculations such as velocity moments, RMS and intervals of confidence could be applied as the samples were collected or in post-processing. Additional calculations such as spectral analysis were also included in the package. Traverse systems could be controlled automatically, allowing an easier and precise locating of the probe volume in a user-defined experimental spatial grid.

Two different traverse systems were used for the LDA measurements on the Multiple Cavity Rig depending on the type of cavity velocity component to be measured. For the measurements of axial and tangential components, the 2D LDA probe was mounted along the rig's centre line with the traverse system already developed for Build 2 (Alexiou 2001) represented in Fig 3.22.

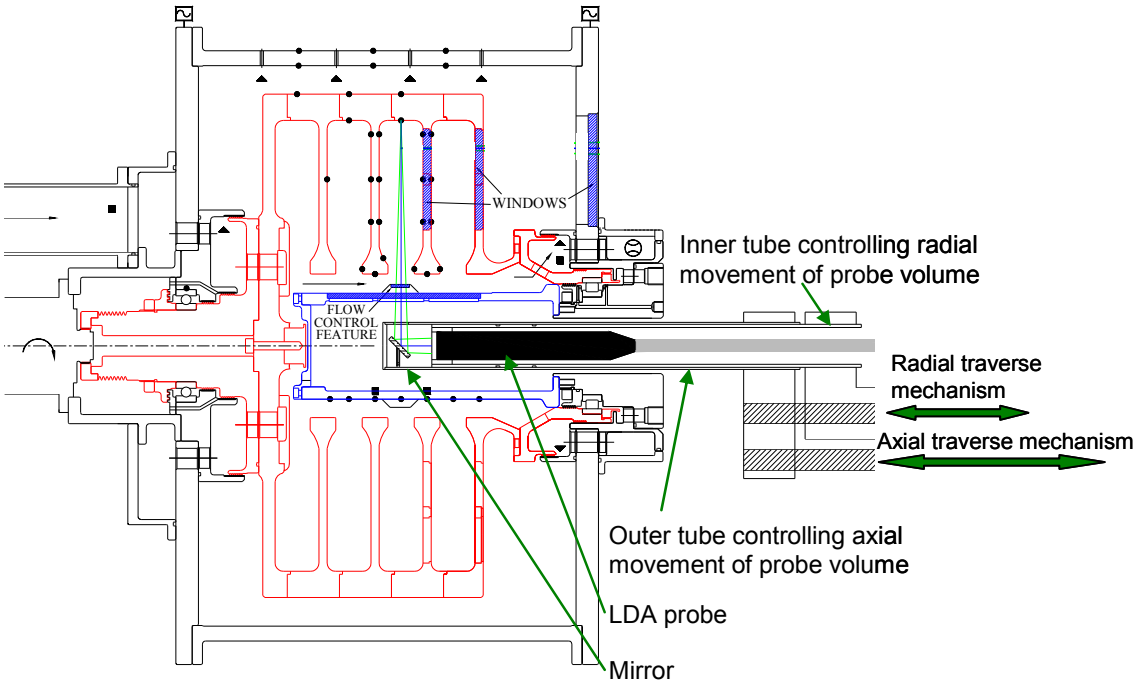

Fig 3. 22 Schematics of LDA traverse system for measurements of V_Φ and V_z velocity components

A 45° mirror in line with the probe reflected the beams up inside the rig's cavities and allowed collection of the scattered light back to the probe. A longitudinal traverse system driving two co-axial tubes provided an accurate positioning of the probe volume within the rig. The inside tube supported the

probe while the outside tube held the mirror on its end. Moving the inside tube along the centre line relative to the outside tube modified the distance of the probe to the mirror, which resulted in the probe volume changing position accordingly in the vertical axis, thus changing the radial location. Moving both tubes together in the longitudinal axis resulted in the displacement of the probe volume across the cavities. The displacement of the tubes was controlled by stepper motors which were directly commanded from the LDA software, allowing the positioning of the points of measurement from a pre-determined positions grid. Figure 3.23 shows an outside view of the LDA system configuration for the measurements of tangential and axial velocities.

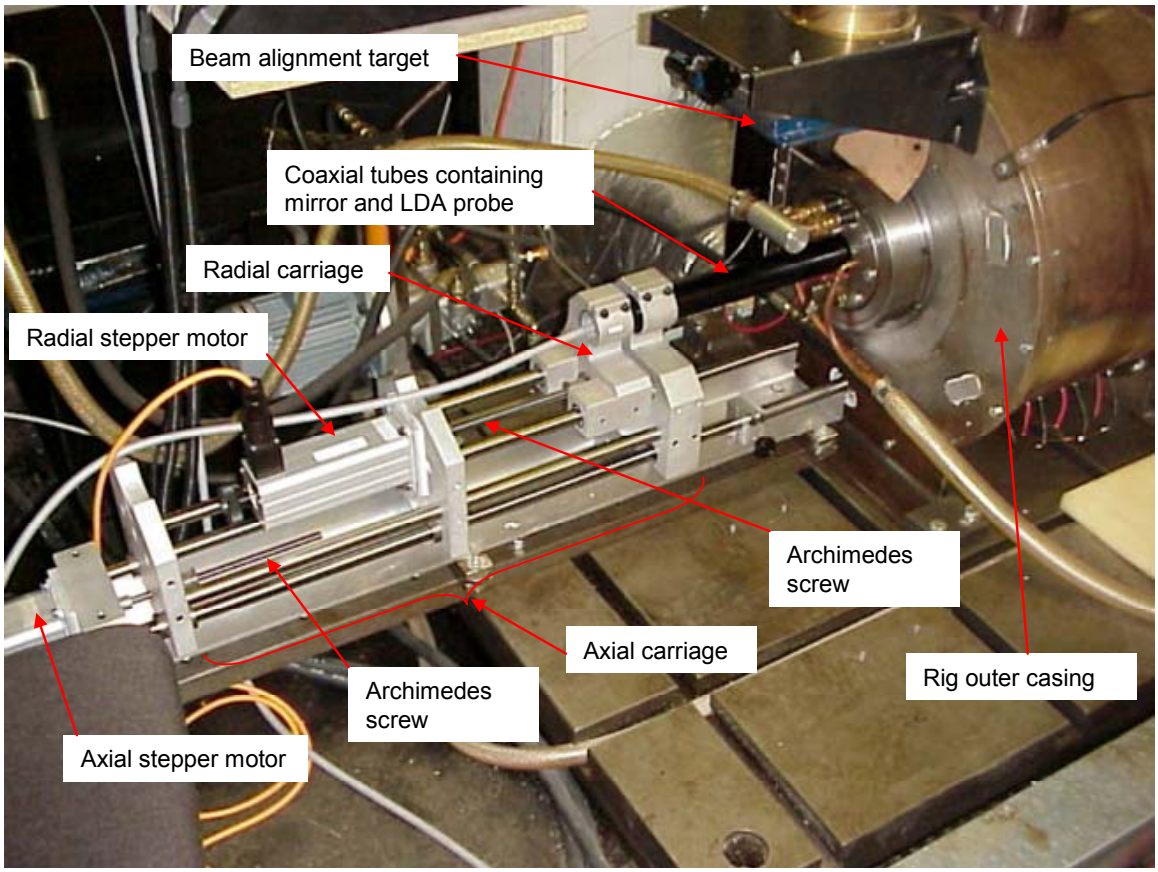

Fig 3. 23 External view of the traverse system for measurements of V_Φ and V_z velocity components

The angular alignment of the probe was ensured by pulling out the traverse system so that the beams would shoot onto a horizontal external target referenced to the geometry of the rig, shown in Figure 3.23. The measuring areas allowed by this probe configuration are shown in Fig 3.24.

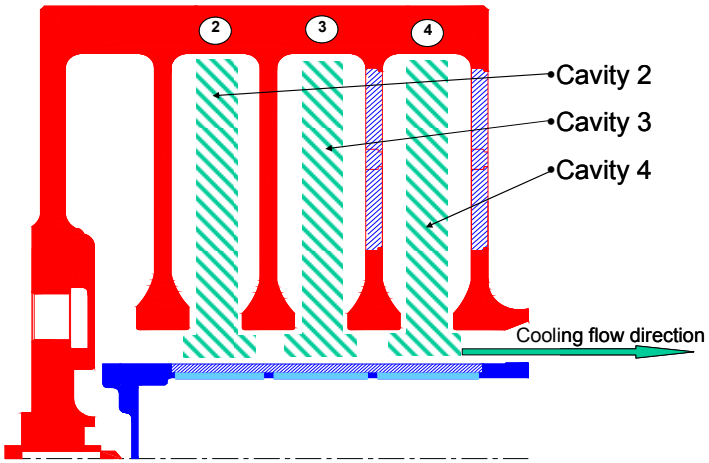

Fig 3. 24 Measurement zones for LDA V_z,V_Φ in the Multiple Cavity Rig, Build 3

Due to the presence of the cobs, there was a limit on how close to the discs the measurements could be made. Had the optical access through the discs not been feasible in this rig, a useful modification on the through shaft LDA configuration would have been to allow the tube mirror angle to be varied in order to get the probe volume nearer to the disc wall without interference from the protruding cobs. This option would have however provided only valid tangential velocities as the axial velocity measurement would have been difficult to resolve with a tilted frame of reference, especially given the low radial and axial measured velocity values described in Chapter 6.

For the reported series of experiments, the measurement zone across the cavities were in the range 0.345 < z/s < 0.671. Measurements across the whole radius of the cavities from the shaft surface to the shroud were possible, with the limitation of proximity to the surfaces only due to the excessive glare from the relatively long probe volume (~4 mm) getting in proximity with the surfaces. In these experiments, the closest points of measurement from the shaft, cob or shroud were set at least 3 mm away from the surfaces, giving a measurement range within the cavities of 0.264 < r/b < 0.955. Similarly, measurements under the cobs were possible but limited to a range 0.264 < r/b < 0.305.

The accuracy of positioning was considered as ±0.5 mm in the longitudinal and radial axis.

Measurements of the tangential and radial velocity components were achieved by positioning the LDA probe off axis so that the beams would shoot across the discs' windows as shown in Fig 3.25. Optical access through the discs had already been integrated into the manufacturing of Build 3 (Alexiou 2002).

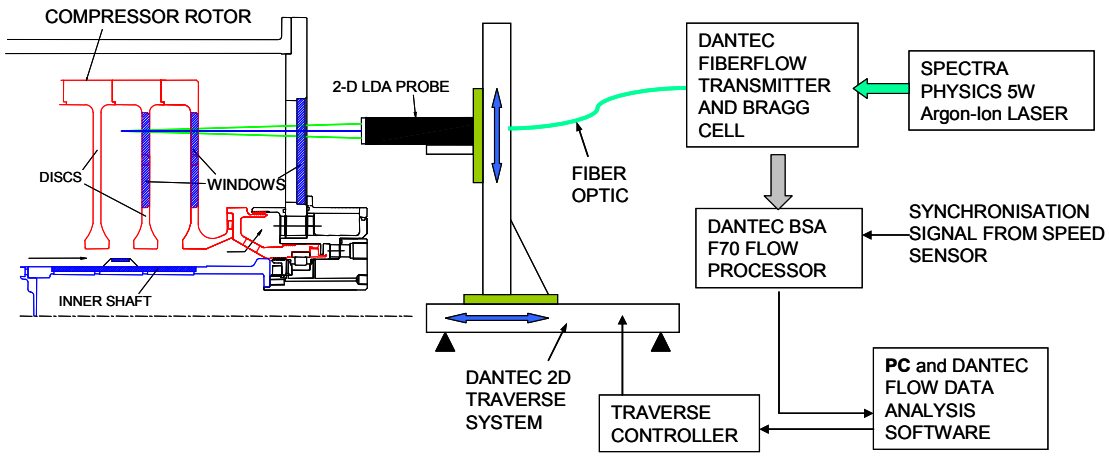

Fig 3. 25 Schematics of LDA traverse system for measurements of V_Φ and V_r velocity components

A DANTEC 2D traverse system, implemented by the author, allowing 600 mm travel on both axes and an adjustable probe mount were used for the positioning of the probe volume as shown in Fig 3.26.

The volume taken by the traverse system and its location according to the rig required the re-location of the laser and ancillaries to a different bench pictured in Fig 3.27.

Position referencing of the probe volume according to the rig was achieved by the insertion of a locating target disc instead of the rig casing optical access window as shown in Fig 3.28.

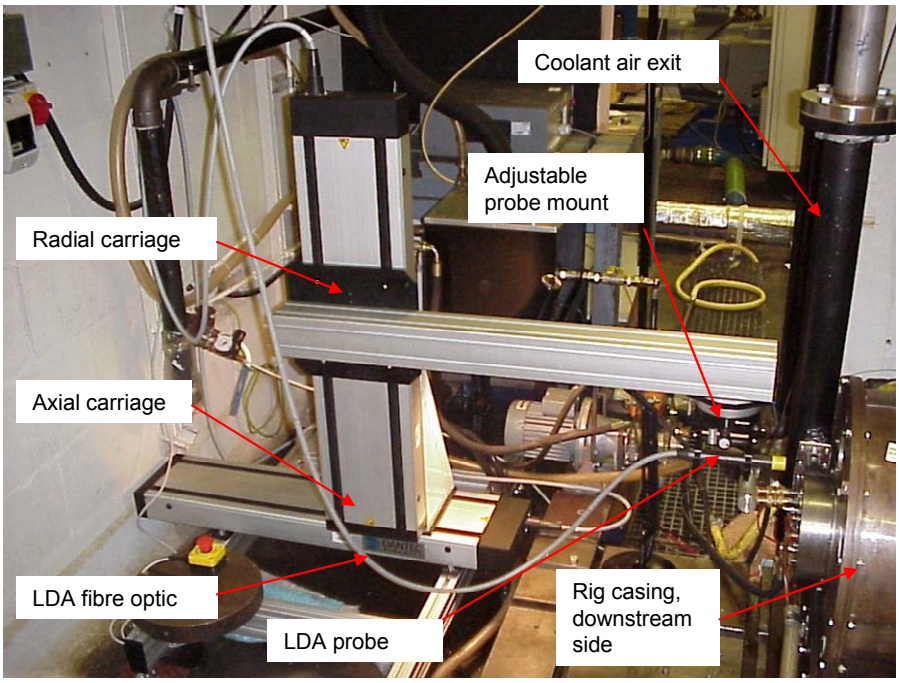

Fig 3. 26 External view of the traverse system for measurements of V_Φ and V_r velocity components

The angular referencing of the target disc was maintained by a common punch mark alignment on the casing and the target. Longitudinal alignment of the probe was checked by actuating the traverse system along its full longitudinal displacement range and monitoring that the beam pairs would not drift from their horizontal and vertical respective planes represented as lines in the reference target. The accuracy of positioning of the probe volume was considered as ±0.5 mm in the longitudinal and radial axis. The measurement zones inside cavities 3 and 4 were limited by the discs windows' radial locations and by a minimum clearance of the length of the probe volume from the discs' surfaces. The measurement zones in cavities 3 and 4 were determined as $0.067 \leq z/s \leq 0.964$ and $0.565 \leq r/b \leq 0.925$ as shown in Fig 3.29.

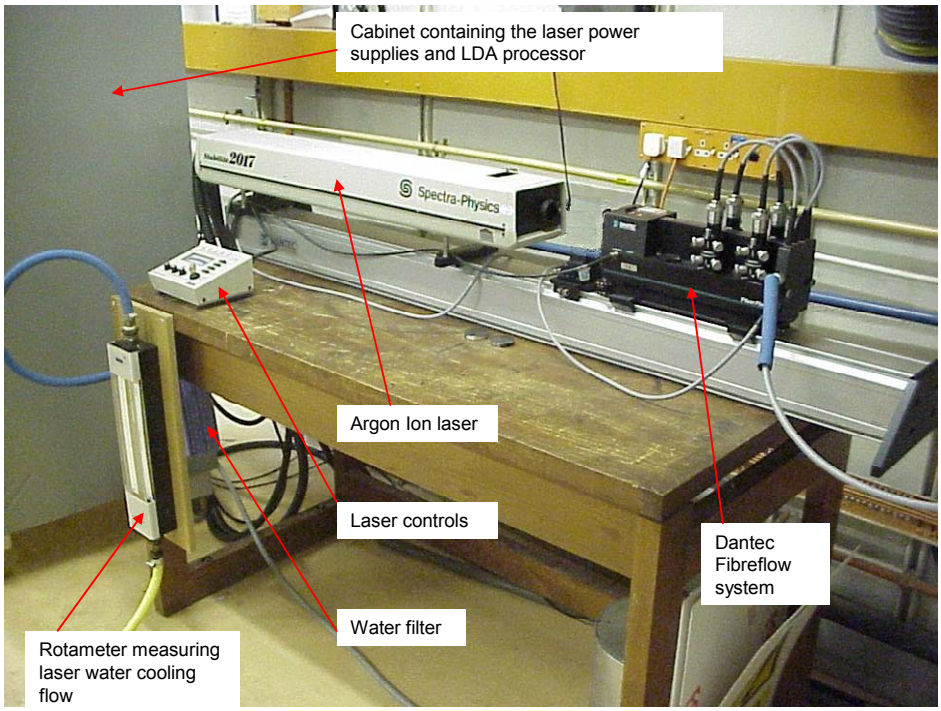

Fig 3. 27 View of the laser bench as installed for the measurements of V_Φ and V_r velocity components

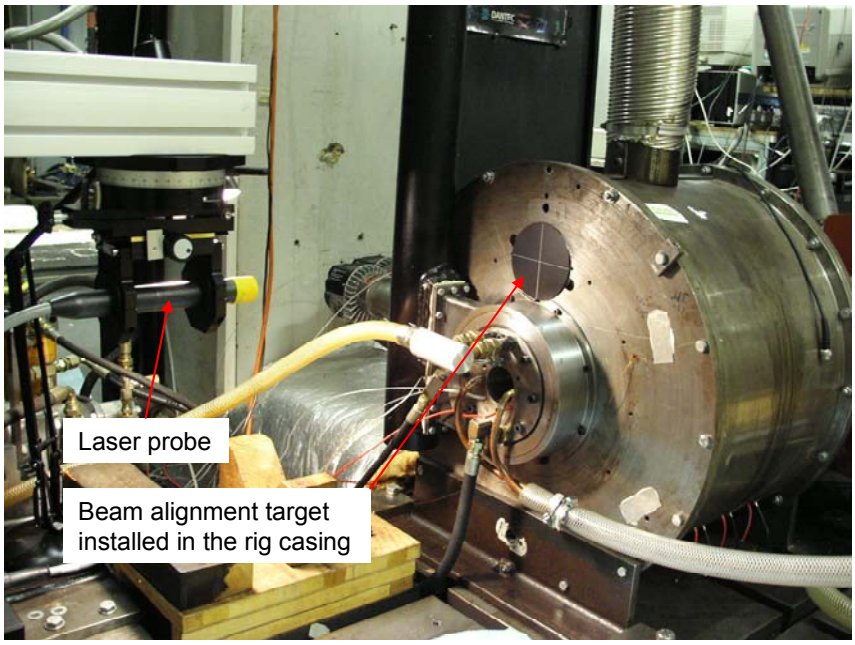

Fig 3. 28 View of the beam alignment target for the measurements of V_Φ and V_r velocity components

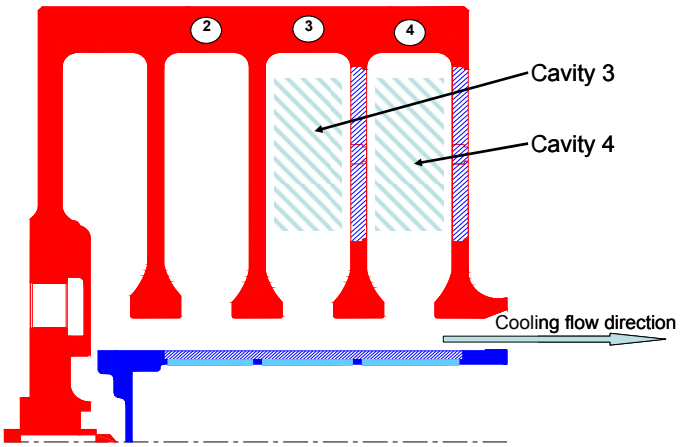

Fig 3. 29 Measurement zones for LDA V_r,V_Φ in the Multiple Cavity Rig, Build 3

Before each experimental run, the traverse system was aligned and the probe volume position referenced. All optics were thoroughly cleaned with an optical grade lint free chamois pad soaked in methylated spirit. The internal surfaces of the optical access windows required the shaft to be dismantled in order to allow access for cleaning. The LDA set-up routine is described in Appendix 3.4 for the case of the longitudinal traverse configuration measuring the axial and tangential velocity components. On a weekly basis, the laser source output was checked and the mirrors and transmitting fibre optics re-aligned as required.

4. Experimental procedure and data processing

4.1 Experimental procedure

4.1.1 Pre-start

As mentioned in Chapter 3, the rig's LDA system, including the optical access windows, was cleaned, tuned and referenced prior to an experimental session (typically the day before). While the shaft was removed for cleaning of the windows, the rig's downstream roller bearing was inspected together with its pressurised lubrication system, and topped-up as necessary (Shell Tellus 22 oil). The air supply cooling water was circulated between the roof tank (5 m^3 capacity) and the underground main water tank (10 m^3 capacity) in order to ensure the water temperature was uniform. This required the circulating pump to be run for several hours, typically one full afternoon, especially if the rig had not been run for several weeks and the outdoor temperature was very different from the ambient temperature underground of the test cell. The pre-start operations on a day of running would typically consist in powering up the laser first according to the procedure in Appendix 4.1, so that the laser source temperature would have time to stabilise. The rig's air cooling and compressor were prepared following the procedure described in Appendix 4.2.

The rig air supply line operating positions were checked and set to isolate the rig through a by-pass line used at first when operating the compressor to clean-up the pipes of the air system for a few minutes before the rig would be pressurised as described in Appendix 4.3. All power supplies, control computers, data loggers and electrical ancillaries were powered-up and relevant control software loaded-up. When ready to start, the lab ventilation, shop air cooling to the slip ring unit, and Howden cooling air compressor would be started-up as described in the pre-start checklist in Appendix 4.4. The LDA atomiser air supply was provided by a standalone Hydrovane compressor. The atomiser was pressurised in standby non-atomising mode.

4.1.2 Start up and running

With the rig control software monitoring the temperatures, supply pressures, rotational speed and flow rates, the rig would be first pressurised to a minimum pressure by closing the air supply bypass and adjusting the compressor pressure control valve according to the procedure described in appendix 4.5 until the desired value of Re_z for the experiment has been achieved. The oil lubrication pump would then be switched on as there would no longer be a risk of oil leaks inside the rig through the labyrinths seals as the rig's rotor was now pressurised. The rig could then be set to rotate at the required speed to achieve the target value of Re_Φ. The shroud heaters would then be switched on. The full starting procedure is described in Appendix 4.6.

While the rig heated up, the air supply temperature would be monitored and adjusted to remain constant by varying the water supply rate on the heat exchanger. The first thermal steady-state would typically be achieved after 45 minutes to 1 hour (30 to 45 minutes for subsequent conditions) and was confirmed by monitoring a change in surface temperatures of less than 0.2 °C in a period of 5 minutes. The rig shut down procedure is described in Appendix 4.7.

4.1.3 Data acquisition

Once the thermal steady-state of the desired experimental condition was achieved, the data acquisition could be initiated. The pressure logging consisted of running the acquisition program that operated remotely the scanivalve unit (scani.bas). Three scans of the pressure channels were performed and the pressure results for each scan were recorded on the computer disk as a text file. The temperature and transducer signals were recorded from the rig monitoring program (orion.bas) previously mentioned. This was driving the Orion data logger remotely and would record 100 separate scans (each taking 1.3 seconds) with a delay of 2.5 seconds between scans. The logged data was written into a test file to be used for post-processing. The standard deviation from the steady-state temperature logging was found to be always less than 0.2 °C, and typically less than 0.1°C across all the experiments.

The velocity measurements through the shaft in the V_Φ,V_z velocity components were performed on typically 37 different points in the rig as represented in Fig 4.1.

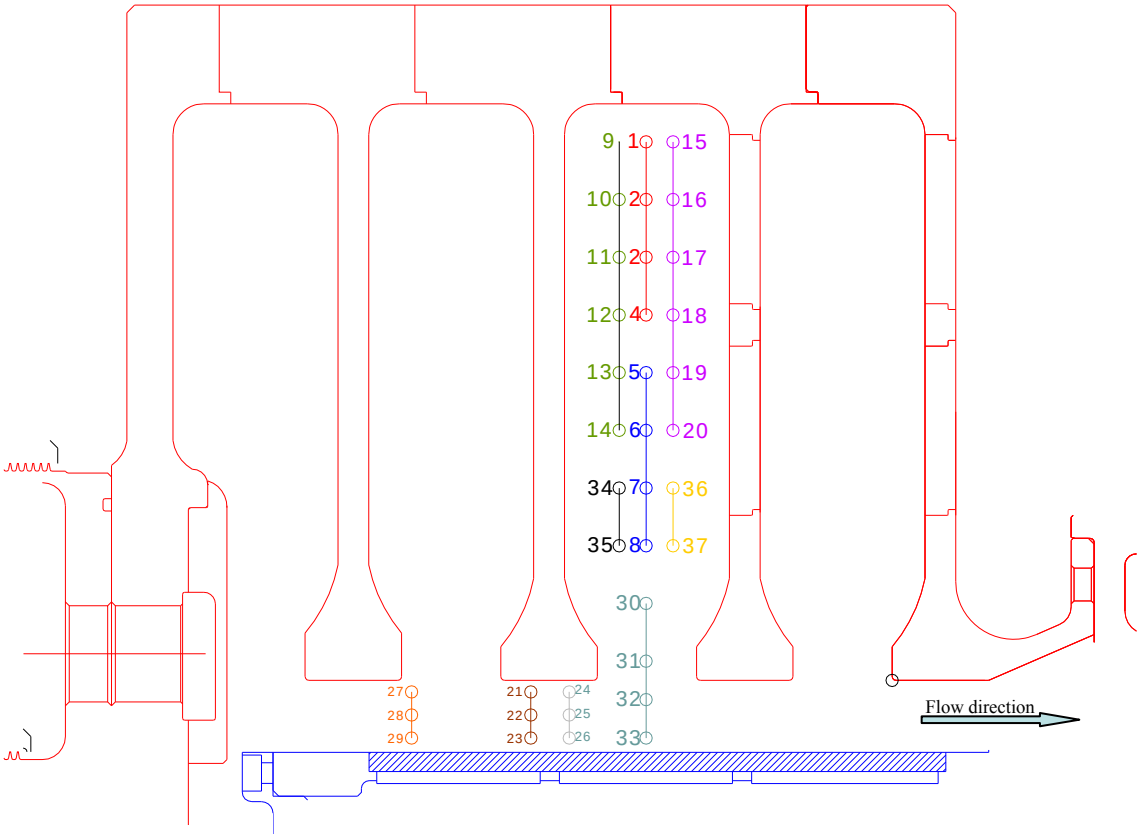

Fig 4. 1 LDA measurement points for V_Φ,V_z configuration

4.2 Heat transfer data processing

Following is a description of the equations employed for the heat transfer related calculated parameters and the way they were derived from dedicated software.

4.2.1 Data processing method

Experimental measurements described in Chapter 3 resulted in output files comprising steady state data averaged over 100 scans for the temperature and rotational speed data, and three scans for the pressure related data, together with standard deviations. Cooling air mass flow rates were calculated from the orifice plates data on the rig and appropriate leakage through the rig deduced according to the method described in Alexiou (2000).

From these sets of data, the rotational Reynolds number for the discs was defined as:

$$Re_{\phi} = \frac{\Omega \times b^2}{\nu} \qquad \text{Eq. 4.1}$$

Where ν is evaluated for $T_{in} = \frac{T_{32} + T_{33}}{2}$

The axial Reynolds number was defined as:

$$Re_z = \frac{W \times d_h}{\nu} \qquad \text{Eq. 4.2}$$

Where d_h is the hydraulic diameter of the cavities annulus inlet: $d_h = 2\left(a - r_s\right)$,

$W = \frac{\dot{m}}{\rho \times \pi \left(a^2 - r_s^2\right)}$ is the mean axial velocity of the cooling flow in the intra cavity annulus.

The Rossby number was expressed as:

$$Ro = \frac{W}{\Omega \times a} = \frac{Re_z \times b^2}{2 \times Re_{\phi} \times a^2 \times \left(1 - \frac{r_s}{a}\right)} \qquad \text{Eq. 4.3}$$

The conduction solution method used to derive local disc's heat transfer using finite differences in order to solve the two-dimensional steady-state conduction equation in cylindrical coordinates below:

$$\frac{\partial^2 T}{\partial z^2}+\frac{\partial^2 T}{\partial r^2}+\frac{1}{r}\times\frac{\partial T}{\partial r}=0 \qquad \text{Eq. 4.4}$$

Where T is the temperature at radius r and axial coordinate z

A calculation domain grid was defined through the cross section of the disc limited by the surface thermocouples as shown in Fig 4.2.

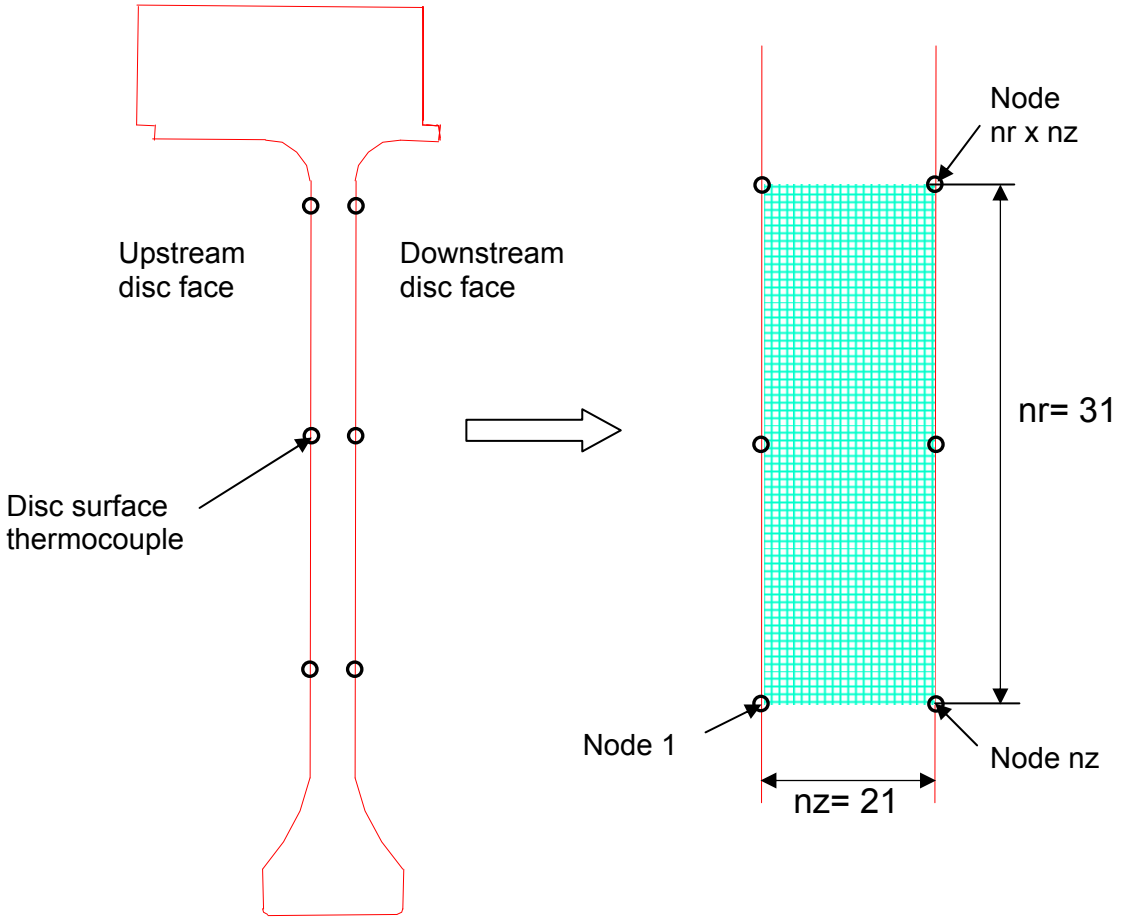

Fig 4. 2 Disc heat transfer grid

The cross section was divided into a 21 x 31 node matrix with the node numbering shown in Fig 4.2.

The two-dimensional steady-state conduction equation (Eq. 4.4) can be written in finite difference terms for a point node p within the calculation grid as:

$$A_n \cdot T_n + A_s \cdot T_s + A_p \cdot T_p + A_e \cdot T_e + A_w \cdot T_w = 0 \qquad \text{Eq. 4.5}$$

Where: n, s, e, w, refer to the node relative to node p as defined in Fig 4.3

$$A_n = \left\{ \frac{1}{\partial r^2} + \frac{1}{2 \times r_{(p)} \times \delta r} \right\}$$

$$A_s = \left\{ \frac{1}{\delta r^2} - \frac{1}{2 \times r_{(p)} \times \delta r} \right\}$$

$$A_p = \left\{ \frac{-2}{\delta r^2} - \frac{2}{\delta z^2} \right\}$$

$$A_e = \left\{ \frac{1}{\delta z^2} \right\}$$

$$A_w = \left\{ \frac{1}{\delta z^2} \right\}$$

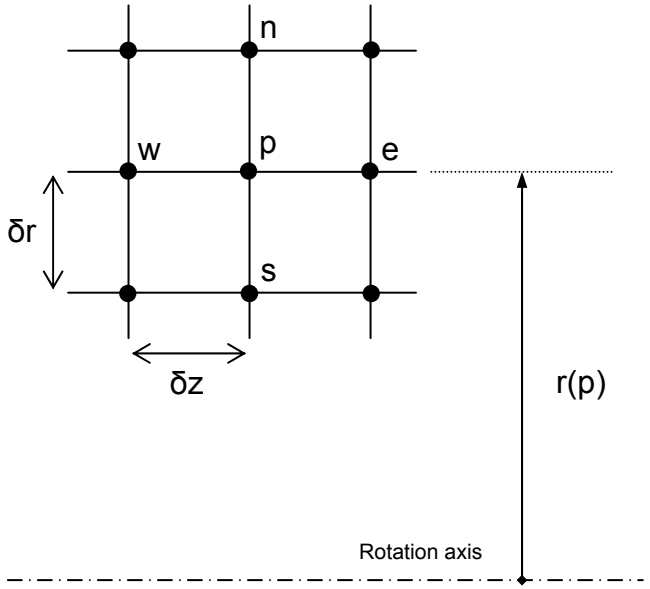

Fig 4. 3 Finite difference grid terminology

The boundary nodes on the periphery of the grid are directly defined by the surface temperature interpolated from the measured surface temperatures. The disc's surface temperatures were interpolated from the three surface thermocouples (e.g. between thermocouples 3, 4, and 5 for the upstream face of Disc 2, shown in Fig 3.13) using a third order polynomial curve fitting as explained in detail in Chapter 5. Inside disc temperatures at the inner and outer radii of the discs (e.g. between thermocouples 5 and 9 for the inner radius of disc 2) were derived by linear interpolation.

All the nodes temperature expressions put together formed a system of 21 x 31 simultaneous algebraic equations which were solved by Gaussian elimination. Once the internal temperatures in the grid were derived, the local total heat fluxes on the discs surfaces could be expressed by second order backward difference as:

$$q_T(j) = -k\left(\frac{-3T_j + 4T_{j+1} - T_{j+2}}{2\delta_z}\right) \qquad \text{Eq 4.6}$$

Where k is the thermal conductivity of the disc material, δ_z is the axial distance between two nodes, T_j is the local disc temperature surface, T_{j+1} and T_{j+2} are respectively the next and second adjacent axial cell temperatures into the disc surface

A variation of the conduction solution method above (Eq. 4.4 to 4.6) was also employed to numerically derive the local total heat fluxes, based on the assumption of an adiabatic mid-plane in the disc thickness (following on Farthing et al. 1992b and Alexiou 2000 as explained in section 2.3.2). This was referred to as the fin solution and was solved using the same method as the two-dimensional solution above, only the adiabatic plane assumption was fulfilled by considering both faces of the disc to have a symmetrical temperature profile boundary condition. An average of the upstream and downstream local temperature profiles was therefore applied as boundary condition on both disc faces (Eq. 4.7) in order to fulfil the symmetrical temperature distribution and numerically resolve the fin solution of local heat fluxes.

$$T_{fin}(r) = \frac{T_{upstream}(r) + T_{downstream}(r)}{2} \qquad \text{Eq. 4.7}$$

A radiation correction was then applied to the total calculated heat flux values for the 2D conduction solution and the fin conduction solution in order to deduce the convective local heat fluxes on the discs' surfaces such as:

$$q_{conv} = q_T - q_{rad} \qquad \text{Eq. 4.8}$$

Where q_{rad} is the estimated radiative heat flux

The radiative heat flux calculation in Cavity 3 was based on the grey body method described in Long (1999), applied to the same number of annular surfaces as there were surface grid nodes. The remaining surfaces on the discs were modeled as bigger annular surfaces, as shown in Fig 4.4.

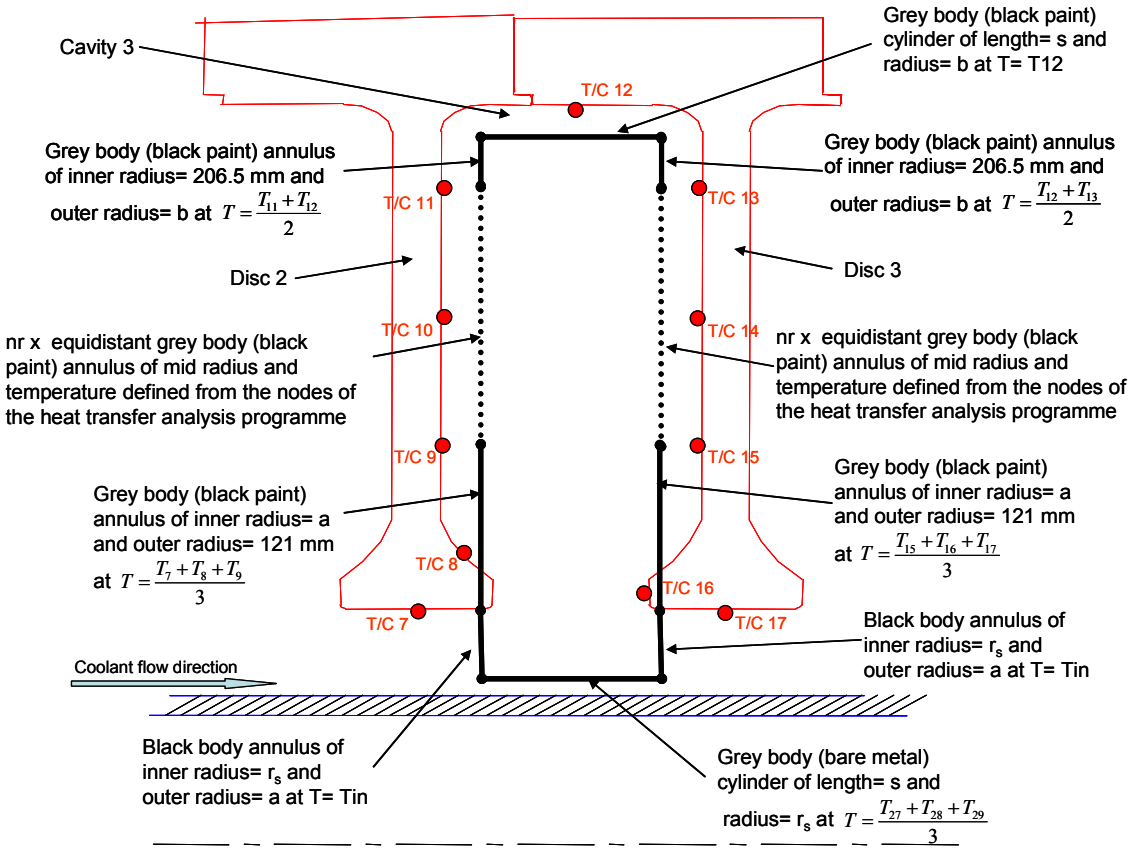

Fig 4. 4 Description of the radiation enclosure model of Cavity 3 (not to scale)

The view factors of the enclosure defined in Fig 4.4 were obtained from the catalogue of Howell (1982). The Stefan Boltzman constant was fixed at $\sigma=56.7\times10^{-9}$ W/m^{2}K^4, and the emissivity values used on the different sections of the cavity enclosure model were set as:

-Non-painted titanium: $\varepsilon_1=0.2$ (from Alexiou 2000)

-Black-painted surfaces: $\varepsilon_2=0.95$ (from Touloukian 1972)

-Annulus gap under discs: $\varepsilon_3=1$ (black body)

The view factors were written in a square matrix form F(i,j) of dimensions equal to the number of surfaces considered in the radiation model, where i denotes the index of the emitting surface in relation to the receiving surface j. “Self

viewing" surfaces, either flat or convex, F(i,i), being not able to see parts of themselves, were therefore assigned a view factor F(i,i)=0. Shaft-to-disc annulus view factors were then defined from Rea (1975).

The shaft to shroud view factors could then be deduced using the summation rule (stating that the sum of the view factors in an enclosure equals to unity), hence:

$$F_{shaft,shroud} = 1 - \sum F_{shaft,all\ surfaces\ except\ shroud} \qquad \text{Eq. 4.9}$$

After having defined the view factors from the shaft to all the other surfaces of the enclosure, the view factors from the enclosure surfaces to the shaft could be calculated from the reciprocity rule:

$$A_i \cdot F_{ij} = A_j \cdot F_{ji} \qquad \text{Eq 4.10}$$

Where A_x is the area of the considered surface

The disc to disc view factors were then calculated from Minning (1979) and their counterparts also deduced by reciprocity. Then the summation rule was applied to obtain the discs to shroud view factors (and shroud to discs view factors by reciprocity). Finally, the summation rule was applied for the calculation of the shroud to shroud view factors.

From Long (1999) the radiation exchange between grey bodies in an enclosure is expressed as:

$$q_{rad,i} = \frac{E_{b,i} - J_i}{\left(1-\varepsilon_i\right)/\varepsilon_i} = \sum_{j=1}^{N} F_{ij}\left(J_i - J_j\right) \qquad \text{Eq. 4.11}$$

Where J_i is the radiosity of the considered surface (W/m^2)

E_b is the surface black body emission (W/m^2)

$E_{b,i} = \sigma \cdot T_i^4$, with σ =56.7x10^{-9} W/(m^2.K^4)

ε_i is the emissivity of the surface

N is the total number of surfaces of the radiation enclosure

The radiosities are determined from the second part of equation 4.11 for each surface which develops as (as an example for i=1 to 3 and j=1 to 3):

$$E_{b,1} = \frac{1-\varepsilon_1}{\varepsilon_1}\left[0 + F_{12}\left(J_1 - J_2\right) + F_{13}\left(J_1 - J_3\right)\right] + J_1$$
$$E_{b,2} = \frac{1-\varepsilon_2}{\varepsilon_2}\left[F_{21}\left(J_2 - J_1\right) + 0 + F_{23}\left(J_2 - J_3\right)\right] + J_2 \qquad \text{Eq. 4.12}$$
$$E_{b,3} = \frac{1-\varepsilon_3}{\varepsilon_3}\left[F_{31}\left(J_3 - J_1\right) + F_{32}\left(J_3 - J_2\right) + 0\right] + J_3$$

Re-arranging into:

$$\left[\frac{1-\varepsilon_1}{\varepsilon_1}\left(0 + F_{12} + F_{13}\right) + 1\right]\cdot J_1 + \left[-\frac{1-\varepsilon_1}{\varepsilon_1}\cdot F_{12}\right]\cdot J_2 + \left[-\frac{1-\varepsilon_1}{\varepsilon_1}\cdot F_{13}\right]\cdot J_3 = E_{b,1}$$
$$\left[-\frac{1-\varepsilon_2}{\varepsilon_2}\cdot F_{21}\right]\cdot J_1 + \left[\frac{1-\varepsilon_2}{\varepsilon_2}\left(F_{21} + 0 + F_{23}\right) + 1\right]\cdot J_2 + \left[-\frac{1-\varepsilon_2}{\varepsilon_2}\cdot F_{23}\right]\cdot J_3 = E_{b,2}$$
$$\left[-\frac{1-\varepsilon_3}{\varepsilon_3}\cdot F_{31}\right]\cdot J_1 + \left[-\frac{1-\varepsilon_3}{\varepsilon_3}\cdot F_{32}\right]\cdot J_2 + \left[\frac{1-\varepsilon_3}{\varepsilon_3}\left(F_{31} + F_{32} + 0\right) + 1\right]\cdot J_3 = E_{b,3}$$

Eq. 4.13

Which re-organised in a general matrix form is expressed as:

$$\left[A\right]\cdot\left(J\right) = E_b \qquad \text{Eq. 4.14}$$

Where [A] is the coefficient matrix function of F_{ij} and ε_i for each J_i in vector (J)

Equation 4.14 results in a system of N simultaneous equations that can be solved to find the unknown J_i.

Once the radiosities J_i are determined, the first part of equation 4.11 is used to determine the value of q_{rad} for each of the surfaces of the cavity.

The local Nusselt numbers are calculated at each radius location from the corrected heat flux in equation 4.8 as:

$$Nu_r = \frac{q_{conv,r} \cdot r}{k \cdot \Delta T} \qquad \text{Eq. 4.15}$$

Where $\Delta T = T_{(r)} - T_{ref}$ with $T_{ref} = T_{in} + \frac{\Omega^2 \left(b^2 - a^2\right)}{2\,\mathrm{Cp}}$ the adiabatic wall fluid temperature estimation from Long et al (2003)

The average Nusselt numbers on the discs calculation zones were defined from the area weighted parameters $q_{conv,av}$ and ΔT_{av} as:

$$Nu_{av} = \frac{q_{conv,av} \cdot b}{k \cdot \Delta T_{av}} \qquad \text{Eq. 4.16}$$

With

$$q_{conv,av} = \frac{2\pi}{A} \int_{r_i}^{r_o} q_{conv,r} \cdot r \cdot dr \qquad \text{Eq. 4.17}$$

$$\Delta T_{av} = \frac{2\pi}{A} \int_{r_i}^{r_o} \Delta T \cdot r \cdot dr \qquad \text{Eq. 4.18}$$

Where A is the area between the inner radius of the calculation grid r_i and outer radius r_o.

The integrals in equations 4.17 and 4.18 were numerically calculated using Simpson's rule.

A one-dimensional conduction solution equation was used to derive the heat flux through the shroud, using the measured temperatures on the inner and outer surfaces of the shroud, respectively $T_{sh,I}$ and $T_{sh,o}$.

The shroud total heat fluxes were calculated as:

$$q_{T,sh} = \frac{k\left(T_{sh,o} - T_{sh,i}\right)}{b \cdot \ln\left(D/2b\right)} \qquad \text{Eq. 4.19}$$

The shroud convective heat flux was then corrected for radiation contribution as above such as:

$$q_{conv,sh} = q_{T,sh} - q_{rad,sh} \qquad \text{Eq. 4.20}$$

The shroud Nusselt number is defined as:

$$Nu_{sh} = \frac{q_{conv,sh} \cdot (s/2)}{(T_{sh,i} - T_{ref}) \cdot k} \qquad \text{Eq. 4.21}$$

With

$$T_{ref} = T_{in} + \frac{\Omega^2 (b^2 - a^2)}{2Cp} \qquad \text{Eq. 4.22}$$

The shroud Grashof number is defined as:

$$Gr_{sh} = \frac{\rho^2 \cdot \Omega^2 \cdot b \cdot \beta \cdot \Delta T_{sh} \left(s/2\right)^3}{\mu^2} \qquad \text{Eq. 4.23}$$

Where $\beta \Delta T_{sh} = \frac{1}{T_{in}} (T_{sh} - T_{in})$

4.2.2 Processing software

As mentioned in chapter 3, the recorded temperature and pressure data were pre-processed in a Q-BASIC programme described in Alexiou (2000) which gave average values of rotational speed, pressure and temperature from the recording scans (100 scans for temperature and 3 scans for pressure), together with the associated standard deviations values for the rotational speed and temperatures. A listing of this programme is provided in Appendix 4.8.

The mass flow through the rig was corrected for leakage through the labyrinth seals according to Curzons (1991). From this raw data file, an example of which can be found in appendix 4.9, the lab atmospheric pressure, test identification and comments were manually added for each experimental condition and the output files were collated onto an excel worksheet as a list.

With all the experimental data in a file list, the post-processing programme could be run. This programme was written in Matlab and would take the raw data from the list file in MCRexcel.xls, process the relevant heat transfer and flow related calculations and then write the results back into a results worksheet

in MCRexcel.xls where they could be further post-processed into standard test reports by using a Visual Basic code and worksheet template described later. The overall architecture of the post-processing software is shown in Fig 4.5.

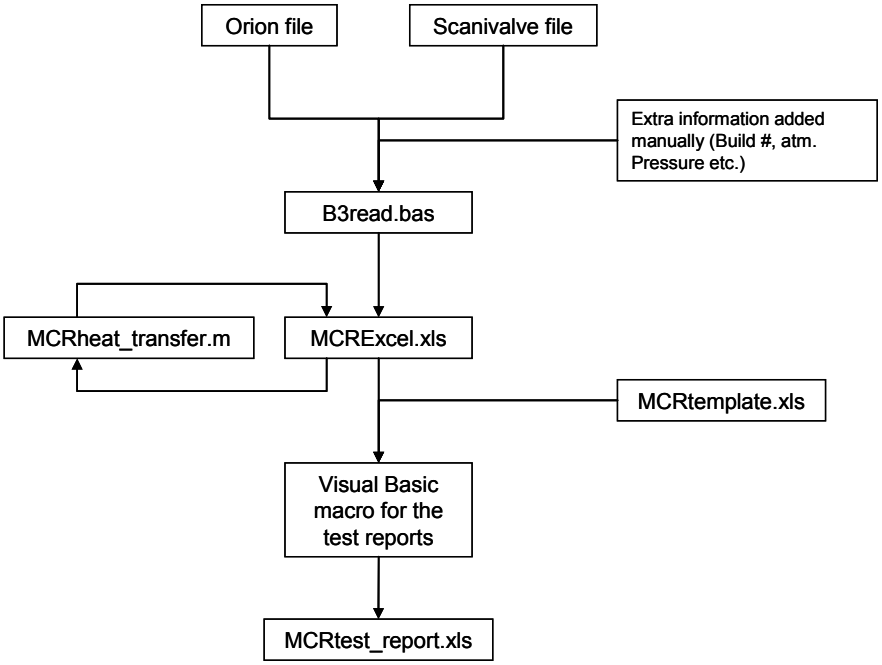

Fig 4. 5 Heat transfer post-processing software overall architecture

The main post processing programme named MCRheat_transfer.m allowed the calculation of the heat transfer parameters described in section 4.2.1, such as local heat fluxes and Nusselt numbers, Reynolds numbers etc. The calculated nominal values were bounded by calculated intervals of uncertainty on each parameters. Fig 4.6 shows a schematic of the structure of the MCRheat_transfer.m programme.

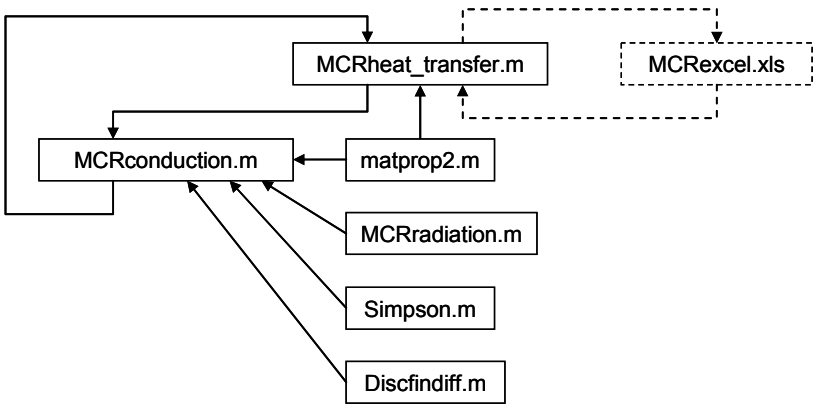

Fig 4. 6 Details of the subroutines of MCRheat_transfer.m

Following is a basic description of the written algorithm when performing a case of analysis (the reader is invited to refer to the programme listings in the appendix for further details and a complete list of the calculated parameters).

Firstly, running MCRheat_transfer.m, an initiation phase is performed where the cavity dimensions are declared and the grid for the conduction solution defined. The data labels for the results file are also declared. The raw data is read from the raw data worksheet in MCRexcel.xls and the tests are separated for each experimental case.

The experimental thermocouple data is then copied into a sub case matrix in the first row: this is the nominal data set for the considered experimental case. The following rows (2 to 101) are filled up with generated temperature variations from the uncertainty analysis on the experimental equipment described in detail in chapter 5. The uncertainty values for the experimental apparatus defined by the analysis are combined together with the calculated uncertainty of the measurement itself (from the 100 recording scans) and used to generate 100 sub cases around the nominal value with a normal distribution defined by the overall standard error deduced by the combined experimental and calculated uncertainties.

This “Monte Carlo” approach to the measured data allows the generation of a realistic set of calculations of uncertainties on the processed results of the experimental case directly, taking into account all experimental error sources, without introducing further uncertainty assumptions in the data processing stages. Standard uncertainties are derived from the results of the 100 generated sub cases for each calculated parameter and the final result of each processed datum is hence the nominal calculated value (first sub case) plus or minus the related uncertainty interval from the generated sub cases.

Once the nominal and randomly generated sub cases for the thermocouples and rotational speed values were generated, calculations for each sub cases are then initiated. The directly calculated values such as Ro, Re_{Φ}, Re_{z}, etc. are obtained. The one-dimensional radial conduction solution for the shroud heat transfer parameters values were calculated from equations 4.18 to 4.21. Then, the relevant thermocouples values for the discs heat transfer finite difference calculations and the thermocouples radial locations are inputted into the MCRconduction.m subroutine (Appendix 4.11). The MCRconduction.m

subroutine allows the disc thermocouple temperature interpolation along the disc surfaces and discretises the interpolated temperatures for each of the outer nodes on the conduction solution grid. The number of thermocouples used in this interpolation and the degree of the polynomial curve fit used can be varied as discussed in chapter 5. Once the temperatures at the corners of the grid have been determined, the axial temperatures at the inner and outer radii of the grid are interpolated linearly. The temperature grid boundary conditions are now defined and the actual finite difference computations to define the temperature values within the grid can be initiated by invoking the discfindiff.m subroutine (Appendix 4.12). This subroutine solves the temperature grid from equation 4.5 and resolves the n_z x n_r system of equations by Gaussian pivot. As mentioned in 4.2.1, the fin conduction solutions use the same resolving method as above, the only difference being that the radially fitted temperatures are defined as the average of the temperature fits on both discs faces, applied to both surfaces. Thus creating a plane of symmetry by mirroring the temperature boundary conditions by the plane at mid-thickness of the disc.

Once the temperature for each grid node has been defined in the discfindiff.m subroutine, the total heat flux on the discs surfaces can be calculated by using the second order backward difference expression in equation 4.6. The radiative heat flux contribution is determined as explained in 4.2.1 by the MCRradiation.m subroutine which calculates the view factors, radiosities, and radiative heat fluxes according to the surfaces enclosure model in figure 4.4 (Appendix 4.13). It is worth mentioning again that the radiative heat fluxes are only calculated for the surfaces within Cavity 3. Therefore, only the surface heat flux for Cavity 3 upstream and Cavity 3 downstream are corrected for radiation.

However, the computations showed that the contribution of radiative heat flux on the discs was typically less than 10% of the measured total heat flux on the disc's faces, and therefore were not deemed to significantly affect the overall results. With the heat fluxes defined and corrected as per equation 4.8, all the remaining results parameters such as Nu_{av}, $\beta \Delta T_{av}$, $T_{s,av}$, etc. can be calculated.

Back in the MCRheat_transfer.m programme, once the nominal and generated sub cases are processed, the output files are then organised by taking the nominal result value of each calculated parameter and by calculating the

associated standard deviation from the sub cases results. The 95% confidence semi-interval is then determined as:

$$U_{95} = \frac{s}{\sqrt{n}} \times 1.96 \qquad \text{Eq. 4.24}$$

Where s is the standard deviation value of the considered parameter and n is the number of generated sub cases (100 in this instance).

Following these processes, the results data is labelled and copied into the MCRexcel.xls file in the format shown by the example in appendix 4.14 and in a separate list of non-dimensional and averaged values for each experimental case in appendix 6.2 and 6.3

An embedded Visual Basic routine into the MCRexcel.xls (listed in Appendix 4.15) file allows the creation of standard test report sheets from the template in MCRtemplate.xlt. For each experimental condition, a worksheet is created from the template model and named according to its test identification.

The template features pre-made plots and spaces for the experimental data results. The Visual Basic macro copies the calculated results of the tests into the right places in the test reports, hence filling the displayed values up and updating the plots with the related data of each experimental test. Examples of heat transfer test reports are shown in appendix 7.1. It should be noted that the data is provided as a nominal value and their 95% uncertainty interval, also reflected on the plots by the error bars.

The first page of the test report features the main operational and average heat transfer related parameters for the discs and shrouds.

The plot represents the measured disc and shroud thermocouple values and the fitted temperatures on the discs' grid nodes. Page 2 features plots of local Nu and heat flux h, along the disc's radius. Page 3 and 4 collect the numerical values related to the local temperatures and heat transfer on the discs faces.

4.3 Air velocity data processing

4.3.1 Data processing method

The post processing of the velocimetry data consisted mainly of the consideration of the measured data under two categories. The ensemble averaged post processing allowed the determination of averaged values over time of the validated bursts. Statistical data such as average velocity, RMS (Root Mean Square) and intervals of confidence were derived from this method. The time dependent post processing looks at the time sequence of the randomly arriving bursts of velocity values in order to characterise the cyclic properties of the flow through a spectral analysis.

The relevant post processing calculations for this study were readily integrated in the LDA post processing software and are briefly described below.

The mean value of each velocity component was defined (in the case of velocity component u):

$$\overline{u} = \sum_{i=0}^{N-1} \eta_i \cdot u_i \qquad \text{Eq. 4.25}$$

Where N is the number of validated bursts collected on the Doppler channel u, and η_i is a statistical weighting factor.

The weighting factor η_i for the determination of ensemble averaged statistics was taken as the transit time weighted expression defined as:

$$\eta_i = \frac{t_i}{\sum_{j=0}^{N-1} t_j} \qquad \text{Eq. 4.26}$$

Where t_i is the transit time of the i'th particle crossing the measuring volume.

Transit time weighting ensures a bias free method of performing statistical averages on potentially statistically dependent samples, as will be explained in Chapter 5.

The transit time weighting bias correction avoids the necessity of having to use a dead time burst recording method that would involve the fastidious determination of the integral time scale of the flow in order to pace of the burst data recording by a period of two times the integral scale of the flow in order to ensure statistical independence between the samples. Moreover, the samples data rate would be largely reduced by the use of dead time recording, which would further add difficulties to the experiments.

The variance of the average velocity sample is defined as:

$$\sigma^2 = \sum_{i=0}^{N-1} \eta_i \left(u_i - \bar{u}\right)^2 \qquad \text{Eq. 4.27}$$

Steady turbulent flows can be treated as a time averaged flow on which is superimposed a turbulent time varying component. The RMS value of the velocity sample is defined as:

$$\sigma = \sqrt{\sigma^2} \qquad \text{Eq. 4.28}$$

And the turbulence intensity of the flow is expressed as:

$$T_u = \frac{\sigma}{\bar{u}} \times 100\% \qquad \text{Eq. 4.29}$$

An angular error between the horizontal marker of the rig beam target and the probe in the V_r/V_φ configuration was found after the measurements had been made. A precise orientation of the beams is important especially when one measured velocity component is considerably greater than another. This was the case with the radial velocity measurement, as explained later in Chapter 5. The angle declination was measured on the rig as α=-1.389°±0.0135° with a precision machining spirit level on the rig according to the coordinate system in Fig 4.7.

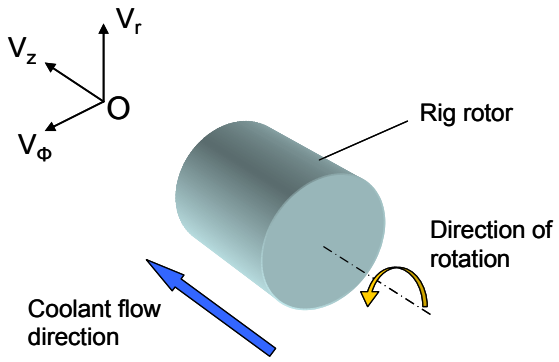

Fig 4. 7 Schematics of the coordinate system employed for the V_r,V_Φ LDA measurements

The correction of the measured data from the probe angular error involved the application of a coordinate transform on the measured velocities. The two velocity channels samples had to be made coincident by filtering samples by arrival times to each other, considering two velocity samples would originate from the same particle if the arrival times would be within a time window set as the probe volume diameter divided by the highest velocity present in the flow as recommended in DANTEC (2004).

The rotation coordinate transform matrix applied to the sampled velocities data was expressed as:

$$\begin{pmatrix} x' \\ y' \\ z' \end{pmatrix} = \begin{bmatrix} \cos\alpha & \sin\alpha & 0 \\ -\sin\alpha & \cos\alpha & 0 \\ 0 & 0 & 1 \end{bmatrix} \cdot \begin{pmatrix} x \\ y \\ z \end{pmatrix} \qquad \text{Eq. 4.30}$$

With α=-1.389° and z=0 as the measurements were two-dimensional.

A spectral analysis was performed in order to highlight multiple flow cores in cavities as previously observed by Farthing et al. (1992a) and Owen and Powell (2004). The tangential component of velocity within the cavities was considered. DANTEC's post processing software integrates a Fast Fourier Transform functionality based on spectral analysis algorithms in order to resolve the time based sampled velocities into the frequency domain. The spectral analysis solver turns the samples discrete velocities into a waveform signal that in turn decomposes into a series of frequencies by the use of Fast Fourier Transforms.

The Fast Fourier Transform algorithm used requires input samples equally spaced in time in order to operate. Because the nature of the LDA sample collecting being inherently random, a conditioning of the measured data is required prior to running the Fourier analysis. A re-sampling technique called "sample and hold" is applied to the raw sampled data. This consists in dividing the time domain into equally spaced bins and assuming the sampled velocity in the bins to remain constant at the latest burst (true) sampled value until another burst is present within the time bin. This is illustrated in Fig. 4.8, showing the randomly arriving burst velocity samples and the generated re-sampled values over time.

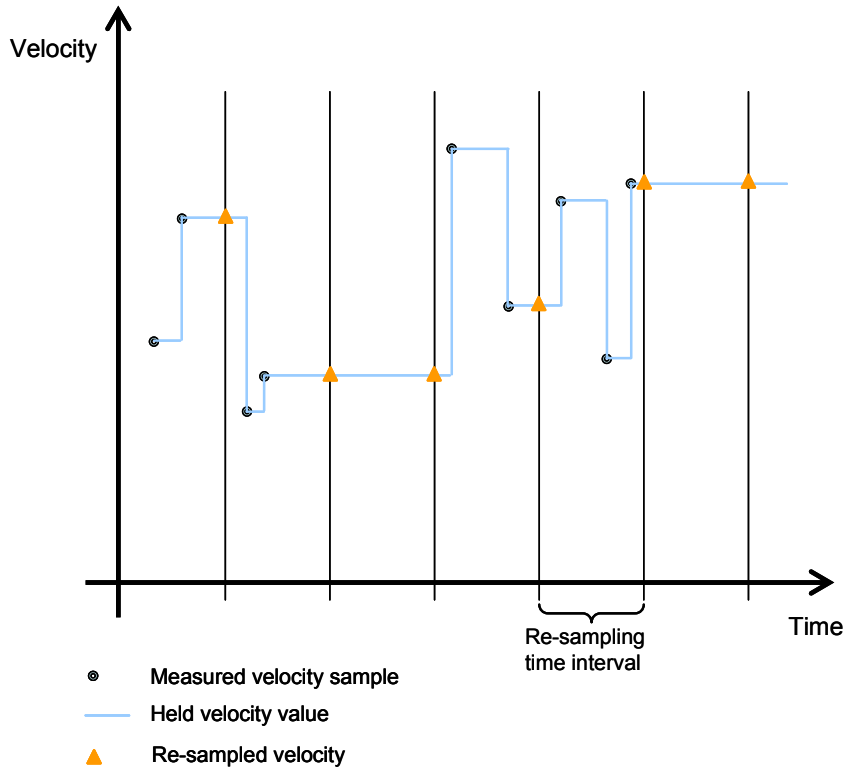

Fig 4. 8 Principles of the Sample and Hold re-sampling method for the LDA processing

It can be noticed from Fig. 4.8 that in the event of discontinuous measurements, re-sampled values will be generated at the last known value until new information about the flow is available. On the other hand, if several bursts are present within a time bin, only the last burst value within the time bin will be kept as the re-sampled value and information about the other bursts will be lost. The duration of the re-sampling interval is an important parameter to be adjusted when post processing the time series data as it will directly affect the rate of rejected data due to re-sampling. The re-sampling rate applied to the calculation process was determined as being twice the desired maximum frequency of the calculated spectrum, chosen as five times the mean data rate (Dantec 2005).

In the instance of flows measured through the shaft (V_z,V_φ configuration), the spectral analysis method described above is immediately applicable as the measurements are continuous.

However, when measuring through the passing rotor windows (V_r,V_φ configuration) the mechanical shuttering provided by the passing windows fools the re-sampling phase of the spectral analysis algorithm by filling up the non-measuring periods (in between windows) with the last measured values data at the re-sampling rate.

The FFT solver therefore picks up the windows passing frequency as dominant and internal filters damp the flow frequency out.
The flow could be re-composed from the measured data of each window added up over time by using the encoder time stamp of the rotor, but knowing that the cavity flow has a slippage from solid body rotation, the superimposed collected data per window would not be relevant as discontinuous in phase.
Moreover, following a discussion on this matter with a DANTEC representative (private conversation with R. Jariczewski 04/08/2005), it was realised that the spectrum analysis software requires a minimum of 1.1 to 1.2 times the flow cycle to be present in a given measurement period in order to be able to be detected and processed by the software. For instance, a window passage, when filtered into a measurement time period, can be for a rotational speed of 2700 rpm found to last about 0.5 ms resulting in a flow frequency of 2 kHz and above that can be processed. This is well beyond the minimal range of ~40 Hz to be expected at this specific operating condition.
Finally, considering a spectral analysis from a single window passage also would not be relevant due to the small amount of samples collected per window passage (between 1 and 15 typically).

Phasing of the collected samples in reference to the flow was attempted in order to improve the samples density over one flow resolution. Adaptive time stamping methods are required in order to re-organise the data collected over hundreds of cycles from the slipping rate of the flow measured on the time-averaged tangential velocity component. This method is considered to present the potential to provide possibly the best sample densities from measured data over a long period of time but could not be applied successfully within the scope and time constraints of the present project.

A practical solution to the spectral analysis from data collected through passing windows was suggested by Long (2004) who wrote a simple averaging programme in order to average the sample data per window passage into one value. Applied to a full LDA measurement, the data set obtained was a regularly sampled (one per window passage) smoothed data series over the whole test duration which was readily usable by the FFT software.

This method helped in obtaining a successful operation of the spectral analysis software in order to derive information on cavity flow structure.

4.3.2 Data processing software

As previously mentioned, most of the post processing related to the Build 2 and 3 LDA measurements was executed directly on the post processing modules of the DANTEC LDA software. The software allowed the production of ensemble averaged velocities and statistics for each measured point of each experiment. The data was then integrated into a specific Excel based test report template for uniformity of display and inclusion of the associated rig operation specific parameter. The non-dimensional speeds were plotted against the relevant rig's non-dimensional location and the 95% interval of confidence was displayed for each data point as an "error bar".

These test reports provided a rational and comparable set of data for archiving and data analysis. An example of an LDA test report can be found in Appendix 4.16.

The spectral analysis performed for several experimental conditions of Build 3 was executed by averaging the data as explained in 4.3.1 using avenoco.bas (reproduced in Appendix 4.17). The obtained data sets were imported back into the LDA software for frequency domain calculations. The resulting spectra were saved as numerical lists and plots, examples of which can be found in Appendix 4.18.

5. Data analysis

This chapter provides an estimation and discussion on the error and uncertainties associated with the measurement and analysis of the heat transfer and flow velocity data.

5.1 Heat transfer data analysis

5.1.1 Heat transfer measurements error

The error on the calculated heat transfer data was assessed by the use of a plain disc inverse fin calculation model, following a method described in the literature, notably Owen (1979), Alexiou (2000), Cooke (2007) and Patounas (2007). The inverse fin solution model employed used a modified algorithm from Patounas (2007) in order to generate the temperature profile on a plain disc that would return from a one-dimensional fin solution a fixed heat transfer coefficient, h_c, along the surface of a plain disc (thsol_MCR1.m in Appendix 5.1). The disc dimensions were taken as the disc's dimensions encountered on the Multiple Cavity Rig. The temperatures of the base and extremity of the modelled fin were inputted from typical experimental values, respectively Tb= 372 K and Te= 320 K. The constant heat transfer coefficient, h_c, was given a value h_c= 30 W/(m^2.K). The generated temperature profile along the modelled plain disc can be seen in Figure 5.1.

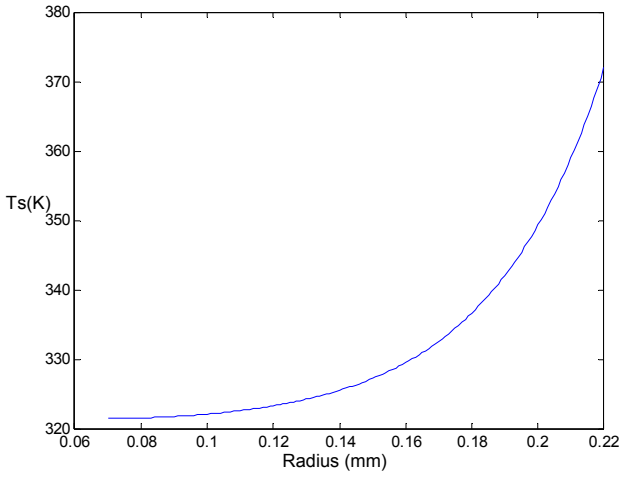

Fig 5. 1 Generated surface temperature profile of plain disc inverse fin solution model

The inverse fin model was checked by inputting the temperature profile back into a fin solution calculation along the length of a plain disc (finsol3_MCR1.m in Appendix 5.1). The temperature profile was also decomposed into discrete temperature values at known radii in order to represent the feed values from thermocouples in an experimental situation. The number and radius locations of the considered simulated thermocouples were chosen to be representative of thermocouples 7, 8, 9, 10, 11 and 12 related to Disc 2 in the Multiple Cavity Rig. Various curve fits were tested on the six simulated thermocouples and the heat transfer coefficient outputs compared in Figure 5.2.

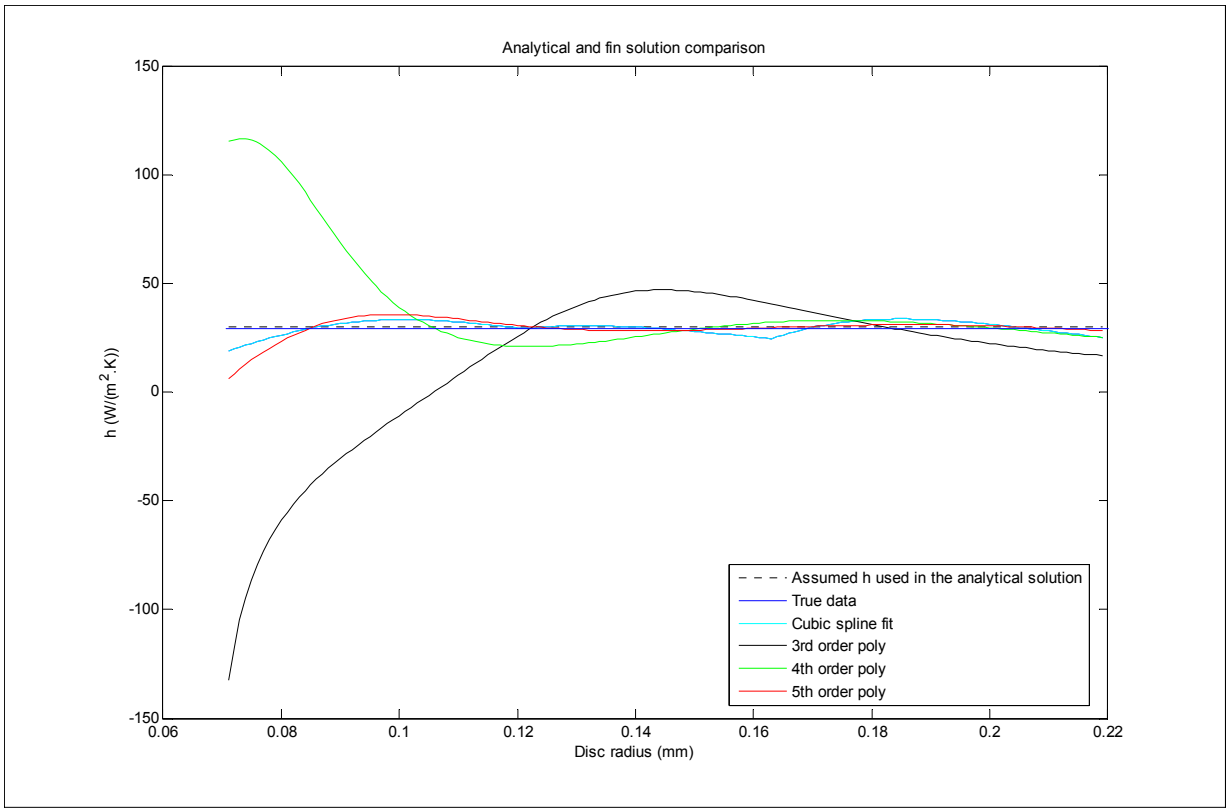

Fig 5. 2 Comparison of plain disc fin solution local heat transfer coefficient outputs from discrete temperature fits

From figure 5.2 it can be noticed that inputting the inverse fin solution 'true' temperature profile back into the fin solution results in the constant expected output values of h_c= 30 W/(m^2.K).

As already noticed by Alexiou (2000), Cooke (2007) and Patounas (2007), the highest order least square polynomial curve fit shows to return the best heat transfer coefficient results when solving from the modelled thermocouple data.

This can simply be explained by the minimisation of temperature bias at the N thermocouple locations resulting in the use of a N-1 order of polynomial which accounts for N pivoting points. Therefore, for the case of least square fitting of 6 thermocouples with a 5^{th} order polynomial, each thermocouple point temperature value will be exact and the interpolated temperatures in between will be expected to be at their closest fit. Table 5.1 compares the resulting average heat transfer coefficient values h_{av} for each type of fitting considered in the present case.

h_c	Analytical		3^{rd} order polynomial		4^{th} order polynomial		5^{th} order polynomial		Cubic spline	
Value $W/(m^2.K)$	h_{av} $W/(m^2.K)$	% delta Vs h_c	h_{av} $W/(m^2.K)$	% delta Vs h_c	h_{av} $W/(m^2.K)$	% delta Vs h_c	h_{av} $W/(m^2.K)$	% delta Vs h_c	h_{av} $W/(m^2.K)$	% delta Vs h_c
30	30.002	7×10^{-3}	23.930	20.23	29.367	2.11	29.808	0.64	29.513	1.62

Table 5. 1 Comparison of average heat transfer coefficients from different temperature curve fittings on the inverse fin solution

The cubic spline fitting returned a close fit of results; however its broken aspect resulting in discontinuous rate variations causes local sudden bias that might not reflect a realistic spread of temperatures. Knowing that the local heat transfer calculations, either by one-dimensional fin analysis or 2D solution might see a small error of temperature fit largely amplified (see Owen 1979), to have sudden changes (however small) into a fit might induce distorted results of local heat transfer that could be misleading to an analyst.

From the previous plain disc fin solution model, a case whereby the number of simulated thermocouples would vary was considered. The thermocouple groups in Table 5.2 were temperature fitted with their highest order polynomial ($N_{T/C}$-1) and the resulting temperature profiles along the plain disc length was used to calculate the local heat transfer coefficients shown in Fig 5.3 (using finsol3_MCR3.m in Appendix 5.1).

Number of T/Cs	Simulated rig thermocouples group	Temperature fit Polynomial order
3	9 – 10 – 11	2nd
4	8 – 9 – 10 – 11	3rd
5	7 – 8 – 9 – 10 – 11	4th
6	7 – 8 – 9 – 10 – 11 – 12	5th

Table 5. 2 Cases of varying thermocouple numbers in the plain disc fin solution model

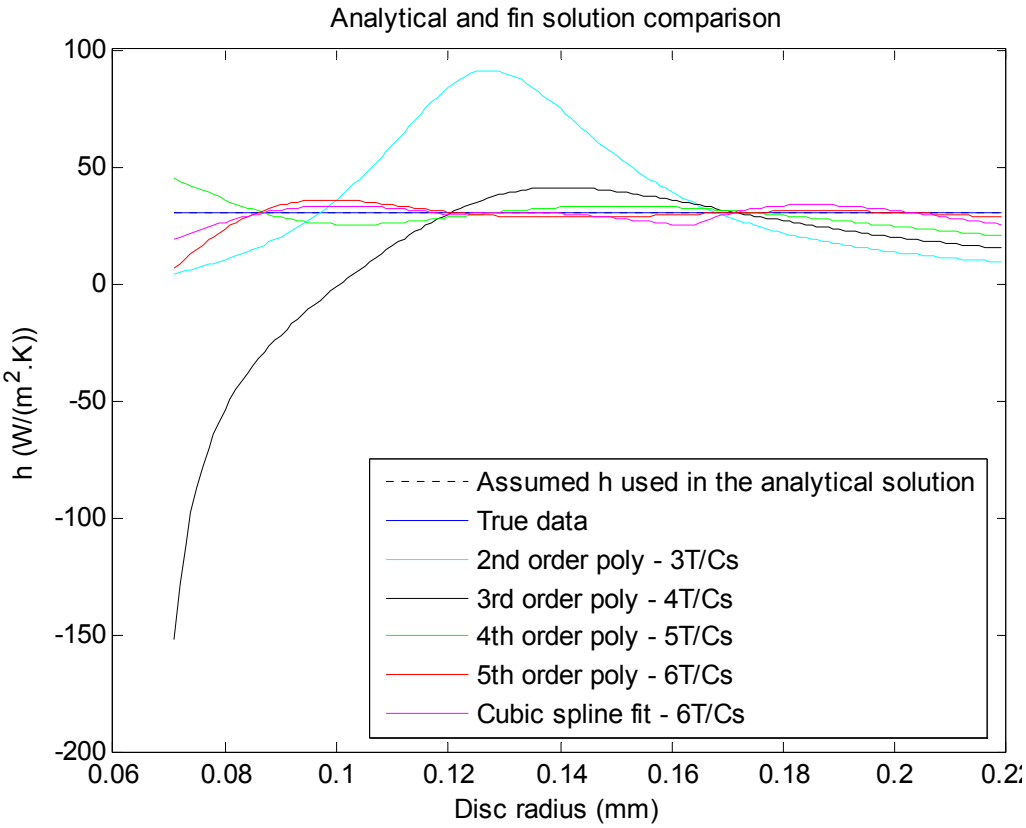

Fig 5. 3 Local heat transfer coefficients on the plain disc fins solution model with varying number of thermocouples

The local heat transfer coefficients shown in Fig 5.3 show better results for the cases including the most thermocouples. When considering cases with less thermocouples involved in the definition of the temperature profile along the disc length, the temperature errors on the extrapolated temperatures outside of the considered disc portion defined by the thermocouple group are amplified and therefore the heat transfer calculations might locally become unstable.

This was seen for the cases with 3 and 4 thermocouples. The average heat transfer coefficient values obtained are compared in Table 5.3.

h_c	Analytical		3 T/C 2^{nd} order poly		4 T/C 3^{rd} order poly		5 T/C 4^{th} order poly		6 T/C 5^{th} order poly	
Value $W/(m^2.K)$	hav $W/(m^2.K)$	% delta Vs h_c	hav $W/(m^2.K)$	% delta Vs h_c	hav $W/(m^2.K)$	% delta Vs h_c	hav $W/(m^2.K)$	% delta Vs h_c	hav $W/(m^2.K)$	% delta Vs h_c
30	30.002	7×10^{-3}	20.515	31.62	21.847	27.18	25.700	14.33	29.808	0.64

Table 5. 3 Comparison of average heat transfer coefficients from the plain disc fin model with varying number of thermocouples

The results in Table 5.3 above were obtained from simulated thermocouple temperatures analytically derived from the inverse fin solution previously described. A typical set of experimental temperatures (from run 2-1 in Build 3 of the Multiple Cavity Rig) was introduced into the plain disc model. The resulting local heat transfer coefficients were plotted in Figure 5.4 (using finsol_MCR4.m listed in Appendix 5.1).

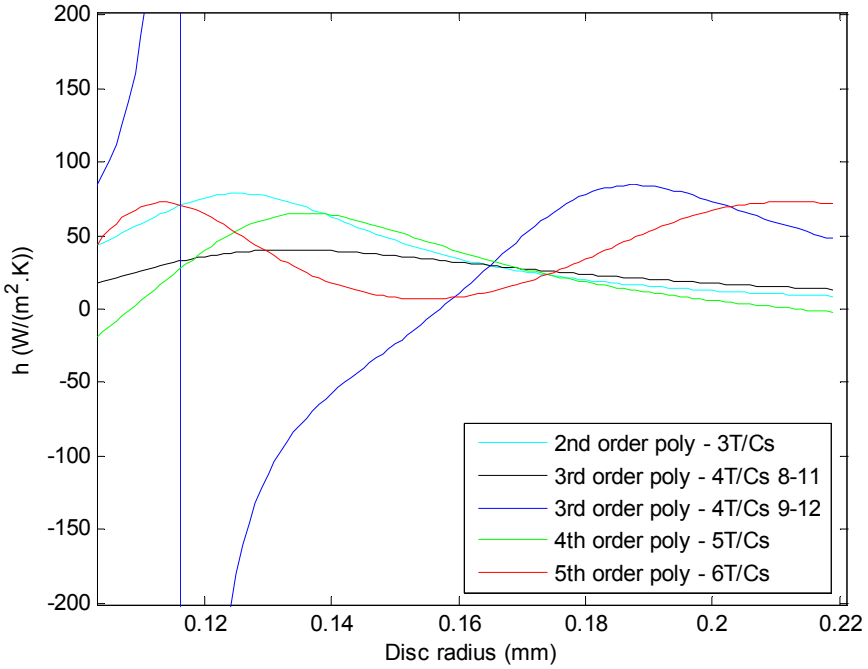

Fig 5. 4 Local heat transfer coefficients with varying number of thermocouples using an experimental temperature distribution

The results of real thermocouples temperatures in the plain disc model show a different behaviour than when inputting the idealised temperatures from the inverse fin solution.

When considering a greater number of thermocouples, the resulting local heat transfer coefficient profiles seem to become unstable on portions of the disc. Important facts to remember are that the experimental temperatures were obtained on a disc of varying dimensions along its radius, most certainly of varying heat transfer coefficient profile and that the temperature measurements could have been biased by experimental noise. A confirmation can be found when comparing the calculated local heat transfer coefficients considering the four-thermocouple set 4a: 8 – 9 – 10 – 11, and the four-thermocouple set 4b: 9 – 10 – 11 – 12. Set 4a is mostly located on a plain disc portion of Disc 2 in the Multiple Cavity Rig (minus a small portion of the disc cob by thermocouple 8), whereas set 4b is including the shroud portion of the disc. The sudden change of thickness and heat transfer characteristics by the disc rim might result in a measured temperature distribution that will cause discrepancies into the plain disc fin calculation model from bias in temperature fitting and also measurement noise as explained by Patounas (2007). It therefore appears that the use of 1D or 2D calculation models should be limited only to plain portions of discs for better accuracy of results. Patounas (2007) demonstrated the unsuitability of analytical 1D and 2D based local heat transfer calculations on a whole disc of variable geometry.

Cooke (2007) and Patounas (2007) used commercial codes such as Rolls Royce's SC03 (used as a solver for 2D heat conduction calculations from separately generated temperature profiles) and Fluent respectively in order to resolve the local heat transfer coefficients along a disc of realistic geometry. Even though an adaptive meshing and finer heat transfer properties definition could be obtained from these packages, the local heat transfer solving along the length of the disc still depended strongly on fitting accurately a radial temperature profile from few and sparse thermocouples data. These resolving methods can therefore still be error prone around the cobs and shrouds where sudden variations of geometries and temperatures would be encountered, which would not be possible to fit accurately as concluded by Cooke (2007).

Following this, and in order to minimise errors on the calculated results, the calculation zone on the Multiple Cavity Rig should therefore be limited to the

plain portions of the discs in order to avoid errors due to the sudden change of heat transfer properties and geometries as explained above.

The comparison of average heat transfer coefficient values along the disc obtained from the plain disc model using experimental temperatures plotted in Figure 5.4 is shown in Table 5.4.

3 T/C 9 – 10 -11 2nd order poly	4 T/C a 8 – 9 – 10 – 11 3rd order poly	4 T/C b 9 – 10 – 11 – 12 4th order poly	5 T/C 7–8–9–10–11 5th order poly	6 T/C 7-8-9-10-11-12 5th order poly
h_{av} W/(m^2.K)	h_{av} W/(m^2.K)	h_{av} W/(m^2.K)	h_{av} W/(m^2.K)	h_{av} W/(m^2.K)
19.231	20.175	41.499	10.369	50.626

Table 5. 4 Comparison of average heat transfer coefficients from the plain disc fin model using experimental temperatures with varying number of modelled thermocouples

The results in Table 5.4 obtained in the cases of temperature fitting from thermocouples located in a plain portion of the disc surface (cases with 3 T/C and 4T/C a) produce close results of average heat transfer with each other. As discussed above, the accuracy of results is to be considered better only by limiting the calculation range of the disc surface to within the plain surface portion of the disc. Therefore the heat transfer calculations for the experiments on the Multiple Cavity Rig were limited to the discs cross sectional areas delimited by thermocouples 3 – 5 – 9 – 11 and 13 – 15 – 19 – 21 for Disc 2 and Disc 3 respectively.

A 4 thermocouple curve fit was employed in order to generate the experimental temperature profiles on the discs faces, using a third order polynomial as a pre-requisite to the heat transfer calculations on the discs following the method described in Chapter 4. This allowed for the best definition of temperatures along the disc portion considered, while minimising errors as discussed above.

An example of temperature curve fit obtained from various considerations of thermocouples inclusion on an experimental case can be seen in Figure 5.5, with a close up of the possible fits inputted into the analysis software shown in Figure 5.6.

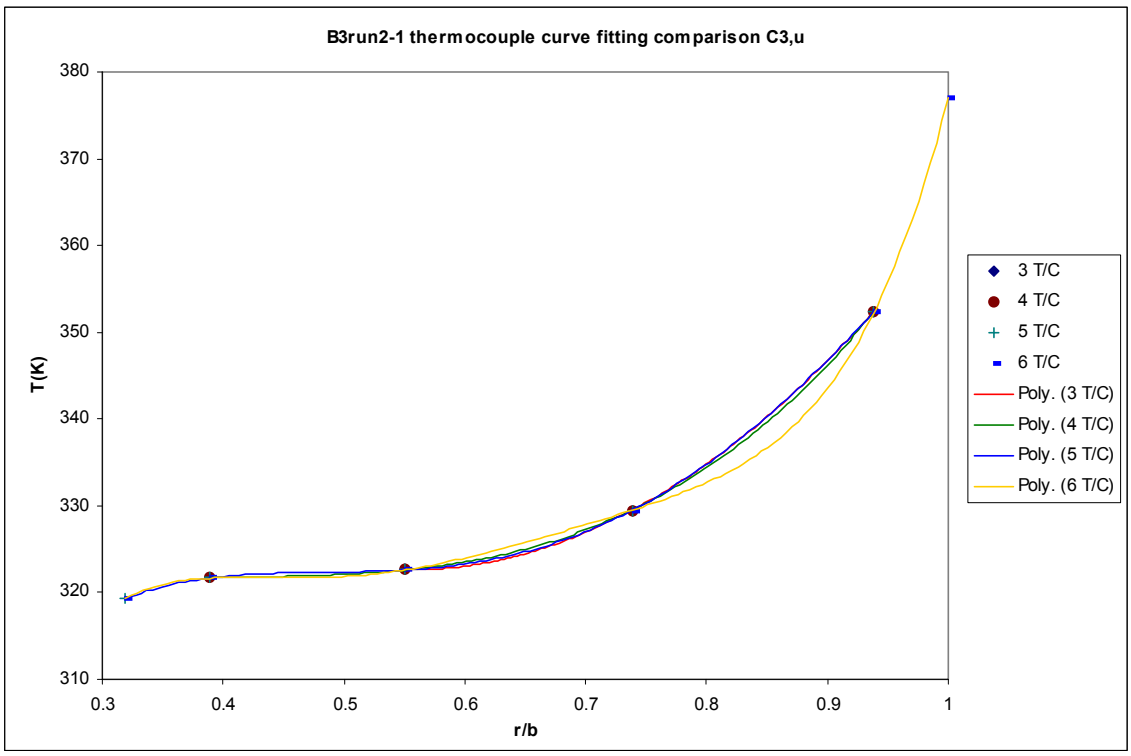

Fig 5. 5 Temperature fit comparison on Disc 2, downstream face from experimental temperature data

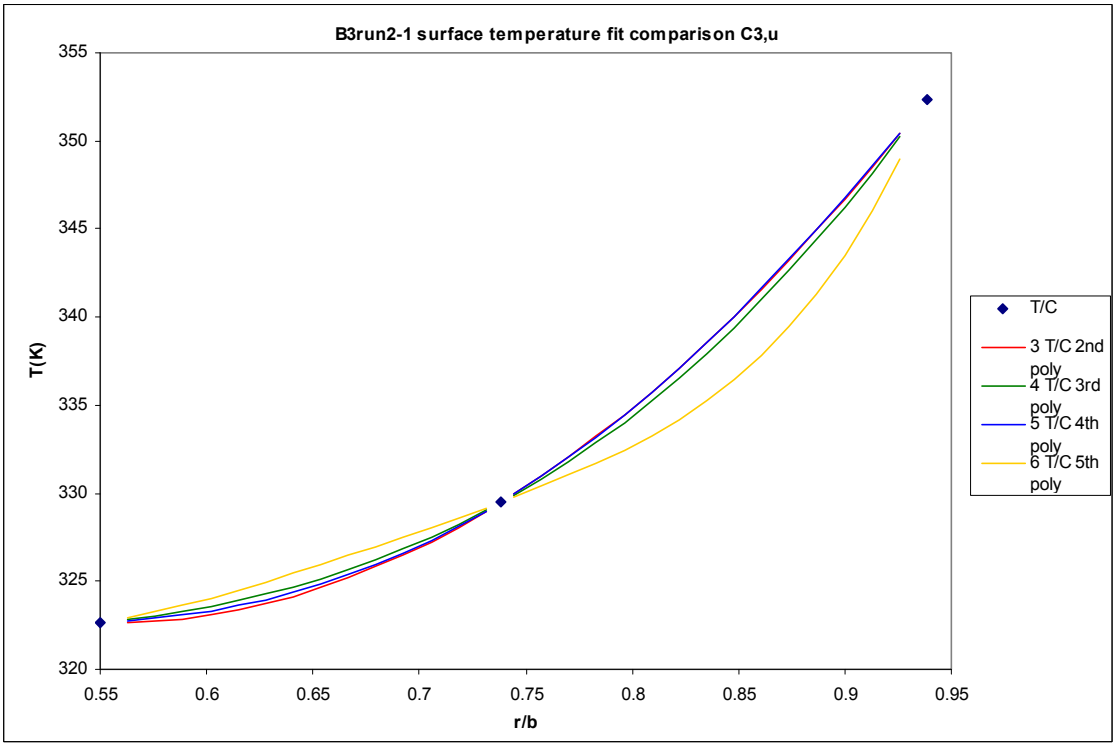

Fig 5. 6 Close up of temperature fits from experimental data on the analysis disc section

An error estimation of the temperature fit was performed on the average surface temperatures of Disc 2 for the fin calculation over the whole range of experiments performed on the Multiple Cavity Rig. The values of Deltas between the three thermocouple and 4 thermocouple fits were found to be within 0.04 % of each other. The derived sensitivity on the average heat transfer coefficient values were found to be typically within 7% of each other.

The effects of grid size on finD2h_{av} were also assessed on the considered 4 T/C case. All the experimental cases were processed in turn with the original finite difference grid of 31 x 21 nodes. Then a 'quadrupled' grid size of 61 x 41 nodes was used and finally an 'octupled' grid of 121 x 41 nodes. The computing time per experimental case (143 in total to be processed) varied greatly between the original grid and the octupled grid by a factor of more than 50. The average relative error on all experimental cases between the finest grid average heat transfer coefficient and the original grid was found to be in the order of 4.2 %.

Therefore the 31 x 21 nodes grid was retained for having a reasonable computing time for an acceptable error on calculated heat transfer parameters. A summary of relative error and computation time against grid size is shown in Figure 5.7.

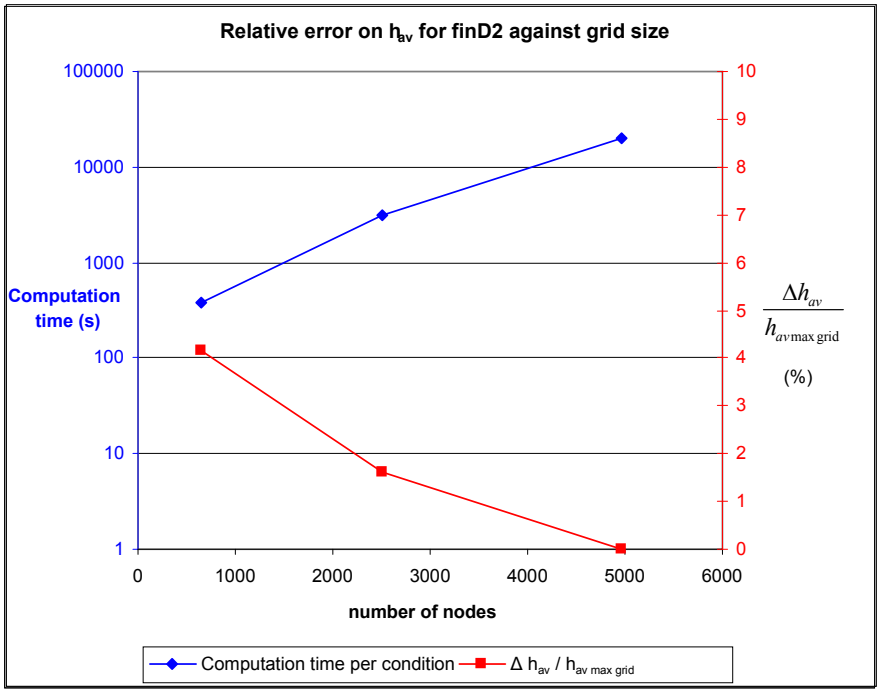

Fig 5. 7 Heat transfer relative error and computation time for different grid sizes against grid size

5.1.2 Heat transfer measurement uncertainties

The heat transfer calculation method used for the Multiple Cavity Rig can be very sensitive to small fluctuations of temperatures as seen in the previous section. The calculations error range due to bias in the way the thermocouple data was used into the finite difference processing was shown from defined, 'perfect' temperature inputs. The reality of experimental measurements however shows that the measured temperature data, even in a thermal steady state process, will show some fluctuations. These small experimental variations will influence the calculated results and small imperfections in temperature measurement could lead to discrepancies as reported by Owen (1979) and more recently by Cooke et al. (2006). The determination of the 'true' value of the measured temperature or calculated datum can only be determined by means of statistics.

This statistical process on a measured value will lead to a determined averaged 'nominal' value bounded within an uncertainty range representing the influence of the different sources of errors on the measuring process. Typical sources of uncertainty on measurements could be accounted for as:

- Noise in the recorded signal (e.g. random electrical interference)
- Sparseness of measurements (e.g. from physical fluctuations due to cyclic variations on flow)
- Resolution of recording instrumentation
- Calibration precision of instruments

Repeating an experimental measurement n number of times represents a statistical process of population n. The standard uncertainty, u, on the measurement is expressed as its Root Mean Square s, divided by the square root of the population:

$$u = \frac{s}{\sqrt{n}} \qquad \text{Eq. 5.1}$$

In the case of data issued from past experience of measurement, calibration certificates, scarce number of measurements or knowledge of the noisy nature of the measurement, the standard uncertainty of the measurement can be estimated as the semi range of the standard spread of the measurement a, divided by $\sqrt{3}$.

$$u = \frac{a}{\sqrt{3}} \qquad \text{Eq. 5.2}$$

The uncertainty in the latter case is said to be issued from a rectangular, or uniform distribution of measurements, in contrast to the former which is issued from a normal distribution.

The combined standard uncertainty in a case whereby the parameters' uncertainties add up to each other is expressed as the square root of the sum of the squares of each uncertainties.

$$u_{combined} = \sqrt{u_1^2 + u_2^2 + u_3^2 + \ldots} \qquad \text{Eq. 5.3}$$

More information on the expression of experimental uncertainties can be found in Bell (1999) and Moffat (1988).

The sources of uncertainties on the measured temperatures of the Multiple Cavity Rig are summarised in Table 5.5 below.

Source of uncertainty	**Value s ± °C**	**Probability distribution**	**Divisor**	**Standard uncertainty u ± °C**	**Source of data**
Thermocouple resolution (half interval)	0.0125	rectangular	$\sqrt{3}$	0.0072	Orion data logger resolution specification
Cold junction resolution (half interval)	0.0005	rectangular	$\sqrt{3}$	0.0003	Orion data logger spec. and Alexiou (2000)
Measurements spread (incl. noise, slip ring unit and cabling)	Calculated from measurements (100 scans)	Rectangular if signal is considered as noise dominated (Normal if considered as statistical process)	$\sqrt{3}$ $\left(\sqrt{100}\right)$	$\frac{s}{\sqrt{3}}$ $\left(\frac{s}{\sqrt{100}}\right)$	Experimental data
Thermocouple calibration bath stability				0.04167	Long et Childs (2007)
Calibration PRT precision				0.015	Alexiou (2000)
Interpolation up to 100 °C				0.05	Lancel (2002)
Repeatability				0.0415	Lancel (2002)

Table 5. 5 Sources of uncertainty on the measured temperatures of the Multiple Cavity Rig

Table 5.5 lists the standard error value of each source of uncertainty, the estimated standard uncertainty and specifies the origin of the estimation, from previous studies, materials specifications, or measured data. The Orion data logger used to measure the signals from the thermocouples had a resolution of ± 1 μV, corresponding to ±0.025 °C. The cold junction reference sensor had a resolution of ± 10 μV corresponding to ±0.001 °C. The uncertainty values related to the thermocouples calibration process were obtained from different separate studies. The set-up and calibration of the thermocouples in the Multiple Cavity Rig followed the method described in Alexiou (2000). The calibration was performed in a water bath at constant temperature against a Platinum Resistance Thermometer.

The standard uncertainty on the stability of the water bath temperature was determined in Long et Childs (2007) as ±0.04167 °C. The Platinum Resistance Thermometer probe calibration uncertainty was estimated by Alexiou (2000) as ±0.015 °C. Lancel (2002) estimated the interpolation and repeatability on the calibration measurements respectively as ±0.05 °C and ±0.0415 °C. The measured thermocouples temperature standard spread over 100 measurements during the experiment was representing the overall variation of the data due to experimental fluctuations, cabling noise and slip ring unit noise. Noise can be considered to have a rectangular probability distribution. Depending on the considered dominance of the temperature measurement variations or the noise in the fluctuations of the experimental thermocouples measurements, a choice of divisor is possible for the determination of the standard uncertainty (respectively $\sqrt{3}$ or $\sqrt{n}$). The experimental measurement spread over all the experiments was typically within a value of 0.2 °C. Considering a normal distribution, an estimate of the standard uncertainty on the spread, u_A, would be:

$$u_A = \frac{s}{\sqrt{n}} = \frac{0.2}{\sqrt{100}} = 0.02 \qquad \text{Eq. 5.4}$$

The overall combined standard uncertainty value on the thermocouples measurements would be:

$$u_{T/C,A} = \sqrt{0.0072^2 + 0.0003^2 + 0.04167^2 + 0.015^2 + 0.05^2 + 0.0415^2 + 0.02^2} = 0.08\,°C \qquad \text{Eq. 5.5}$$

The corresponding 95 % interval of confidence considering a normal distribution of the measured temperatures would therefore be estimated to be:

$$u_{95_{T/C,A}} = 1.96 \times u_{T/C,A} = 0.1568\,°C \qquad \text{Eq. 5.6}$$

Considering a rectangular distribution of the measured temperatures, the estimated standard uncertainty u_B becomes:

$$u_B = \frac{s}{\sqrt{3}} = \frac{0.2}{\sqrt{3}} = 0.11547\,°C \qquad \text{Eq. 5.7}$$

And $u_{T/C,B} = 0.14\,°C$ Eq. 5.8

And hence $u_{95_{T/C,B}} = 0.2744\,°C$ Eq. 5.9

However, considering that the rotating thermocouples on the rig use another thermocouple as the slip ring unit cold junction reference, the corrected standard uncertainties lead to:

For a normal distribution

$$u_{T/C,C} = \sqrt{\left(u_{T/C,A}\right)^2 + \left(u_{T/C,A}\right)^2} = \sqrt{2} \times 0.08 = 0.11°C \qquad \text{Eq. 5.10}$$

$$u_{95_{T/C,C}} = 0.2217\,°C \qquad \text{Eq. 5.11}$$

And for a rectangular distribution

$$u_{T/C,D} = \sqrt{\left(u_{T/C,B}\right)^2 + \left(u_{T/C,B}\right)^2} = \sqrt{2} \times 0.14 = 0.20°C \qquad \text{Eq. 5.12}$$

$$u_{95_{T/C,D}} = 0.3881°C \qquad \text{Eq. 5.13}$$

Previous studies on rotating temperature measurements by Lancel (2002), using a similar experimental set-up of data logger and slip ring unit, evaluated the 95% interval of confidence in the temperature measurements at a value of 0.294 °C. It could be argued that the temperature measurement spread would follow a normal distribution and therefore the thermocouple uncertainty divisors to be used into the heat transfer analysis programme should follow the calculation method of $u_{T/C,A}$ and $u_{T/C,C}$. However, as the participation of noise into the recorded signals cannot be separated from the recorded data of the

physical temperature fluctuations, and in regard to the levels of uncertainty determined by Lancel (2002) in a similar range of temperature, it appears that a rectangular distribution of data should be considered for the determination of thermocouples measurement uncertainties in the Multiple Cavity Rig. Moreover, the measurement uncertainty value to be retained on a conservative basis should be the value associated with the rotating thermocouples, i.e. $u_{95_{T/C,D}}$=0.3881°C (Eq. 5.13).

As described in Chapter 4, the estimated standard uncertainties and average values from the thermocouples temperatures and rotational speed recordings for each experiment were integrated into the heat transfer processing programme.

This generated a hundred and one sub-cases of processing based on the uncertainty spread in order to calculate the nominal results and their respective 95% interval of confidence.
Owen (1979), followed by Cooke (2007) previously studied gas turbine disc heat transfer experimental uncertainty using a calculation method based on a Monte-Carlo simulation. The heat transfer processing programme for the Multiple Cavity Rig operates on similar principles, but uses actual experimental data to be processed with an estimation of uncertainty values. The sensitivity of the results to small variations of surface temperatures was considered as predominant on the heat transfer results as reported by Owen (1979) and Cooke (2007). Therefore the variability of coolant pressure or hardware dimensions were not taken into account in this study.

The uncertainty values produced by the heat transfer processing programme therefore not only included the inputted fluctuating variables such as temperatures and rotational speed, but also any calculated parameter involving one or more of the inputs such as h, Nu, Re_z etc. A list of parameter outputs and their respective intervals of confidence can be seen in the processing examples in Appendix 7.1.

Figure 5.8 shows an example of results of local heat transfer results obtained from the two-dimensional solution method and the fin solution method, as previously described in Chapters 4 and 5, for the experimental conditions of Re_{Φ}= 4.12 x 10^6, Re_z= 1.16 x 10^5, Ro= 0.54 and $\beta\Delta T_{av}$= 0.03.

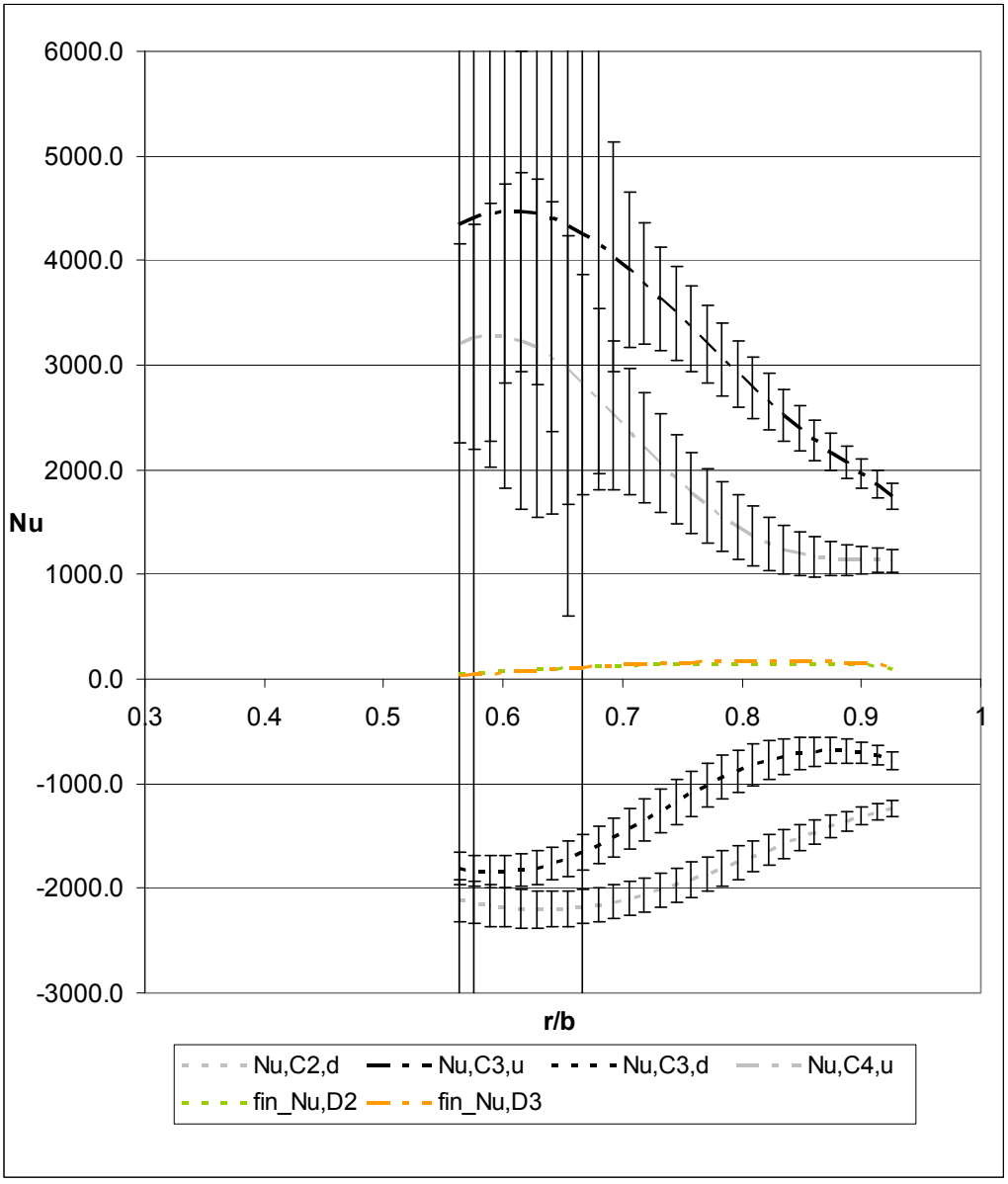

Fig 5. 8 Local Nusselt numbers against r/b for Build 3, run28-1, Re_{Φ}= 4.12 x 10^6, Re_z= 1.16 x 10^5, Ro= 0.54 and $\beta\Delta T_{av}$= 0.03

The plotted Nusselt numbers were determined on the flat surface portion of the discs between 0.55 ≤ r/b ≤ 0.94 as previously described. The local Nusselt number values resulting from the two-dimensional solution are represented in Figure 5.8 with error bars indicating the calculated 95% interval of confidence.

The fin solution plots were not represented with error bars for clarity of display. Their 95% uncertainty intervals were typically in the order of ± 10 %. The calculated average total heat flux from the two-dimensional solution for the downstream face of Disc 2 in this example was found to be $q_{T,av,D2,dn} = 3307$ W/m^2, with a contribution of radiative heat flux of about 1.5%. Similarly, the calculated value for the upstream face of Disc 3 was $q_{T,av,D3,up} = 1665$ W/m^2 with a radiative contribution of 1.2%. The overall contribution of radiative heat flux on the discs across all the experiments was typically found to be less than 10% of the measured total heat flux on the discs faces as already mentioned in section 4.2.2. The results from the two-dimensional solution show a lower overall level of heat transfer from Disc 3 (both upstream and downstream faces) compared to Disc 2. The differences between the upstream and downstream faces of both discs indicate large values of positive heat transfer on the upstream faces (heat flows out of the disc face to the cavity air) whereas the discs' downstream faces show negative values of Nusselt number that would suggest that heat is given into the disc from the cavity air. This described discs heat transfer behaviour does not fit the current understanding of cavity flow and heat transfer from its direction and magnitude in regards to the measured relatively low magnitudes of cavity air velocities previously described. The two-dimensional solution local heat transfer results could only illustrate further the inherent problems of results from this calculation method as explained above. Discrepancies on the calculated local heat transfer values from the two-dimensional solution were seen across the whole test range. Figure 5.9 shows another example of results for Re_Φ= 0.49 x 10^6, Re_z= 0.92 x 10^5, Ro= 3.56 and $\beta\Delta T_{\mathrm{av}}$= 0.09. On this test, the local Nusselt number profiles on Disc 3 indicate both positive and negative heat transfer along the calculated discs surfaces. The variation of average Nusselt number for all tests carried out on Build 2 of the test rig (narrow annular gap, 0.4x10^6 < Re_Φ < 5x10^6, 4.2x10^4 < Re_z < 1.9x10^5, 0.29 < Ro < 8.6) with Rossby number is shown in Figure 5.10 (2-D solution) and Figure 5.11 (fin solution). The behaviour of negative Nusselt numbers noted above is also applicable to average Nusselt numbers as shown in Figure 5.10. This inconsistency is not seen in the results of the fin solution in Figure 5.11.

In this chapter, the instrumentation design of the series of the Multiple Cavity Rigs using a finite number of surface thermocouples on the discs surfaces and relying on 2-D analysis to determine values of disc to air heat fluxes has been demonstrated as inadequate. However the results from the fin analysis are more in agreement with the current consensus in disc heater transfer even though the scale of the bias resulting from the limited number of thermocouples on the rig discs cannot be ascertained. Other methods of determining disc heat fluxes or improved temperature definition should be sought for future studies, as concluded by Cooke (2007) subsequently to the end of the presented experimental programme.

The presented heat transfer results in Chapter 7 therefore should be considered bearing in mind the limitations of the heat transfer calculation method implemented by design on the Multiple Cavity Rig.

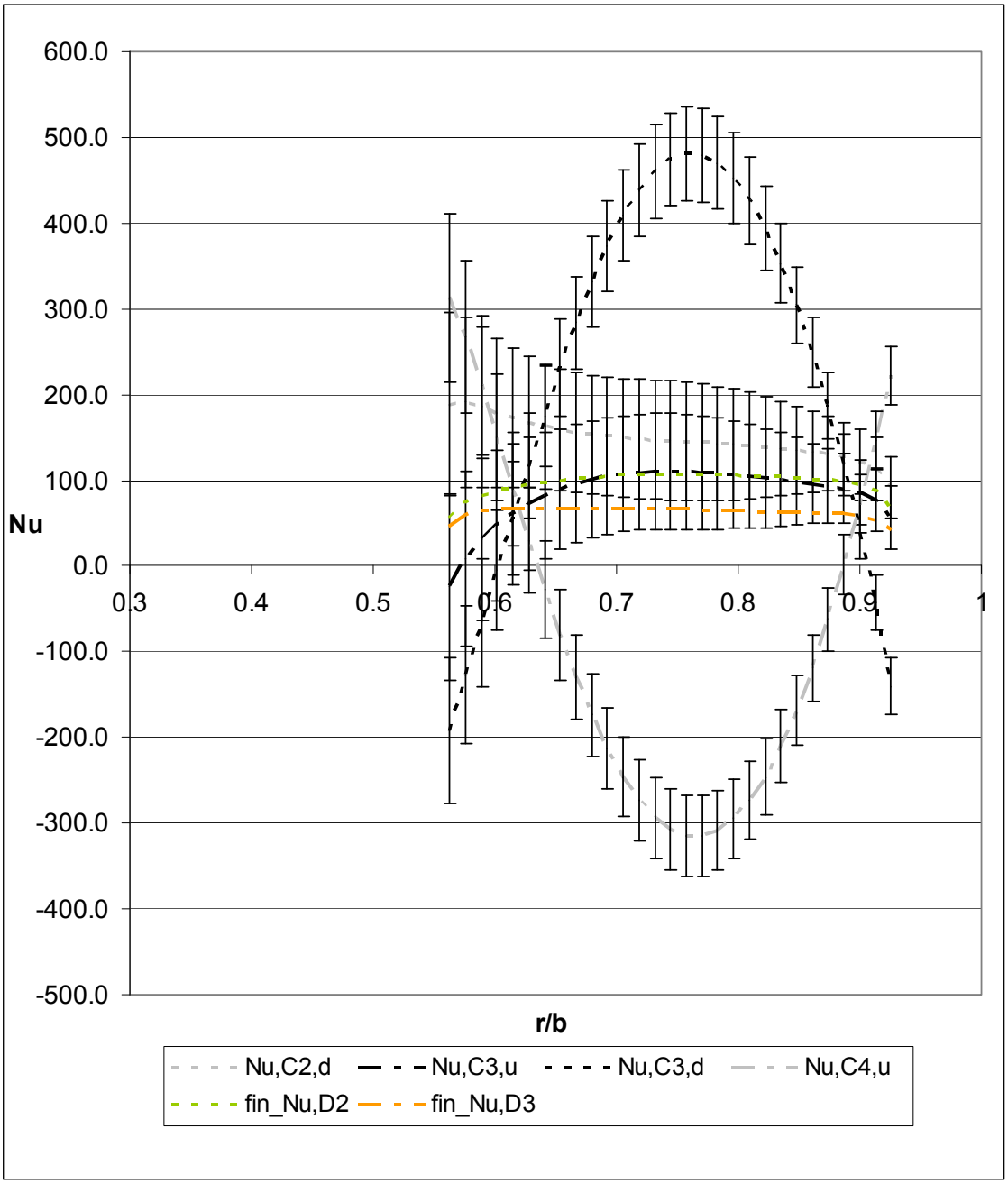

Fig 5. 9 Local Nusselt numbers against r/b for Build3, run32-1, Re_{Φ}= 0.49 x 10^6, Re_z= 0.92 x 10^5, Ro= 3.56 and $\beta\Delta T_{av}$= 0.09

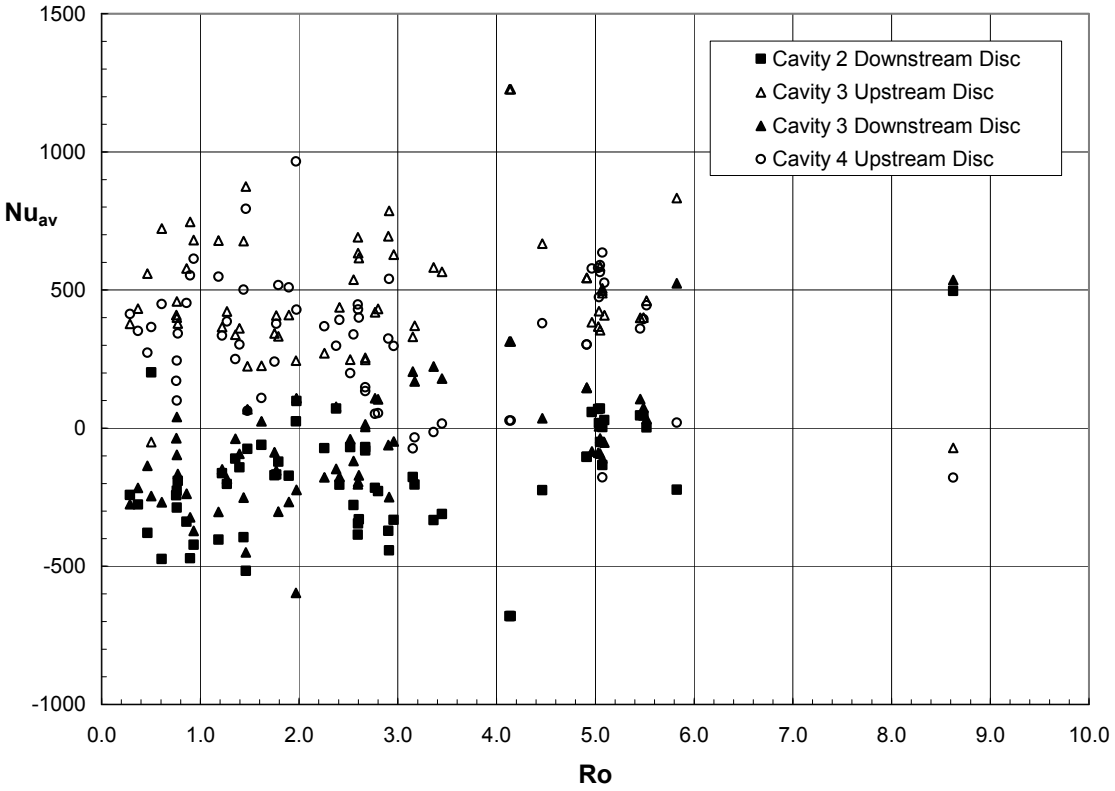

Fig 5. 10 2D solution results for Build 2 (narrow annular gap)
Variation of average Nusselt number with Rossby number

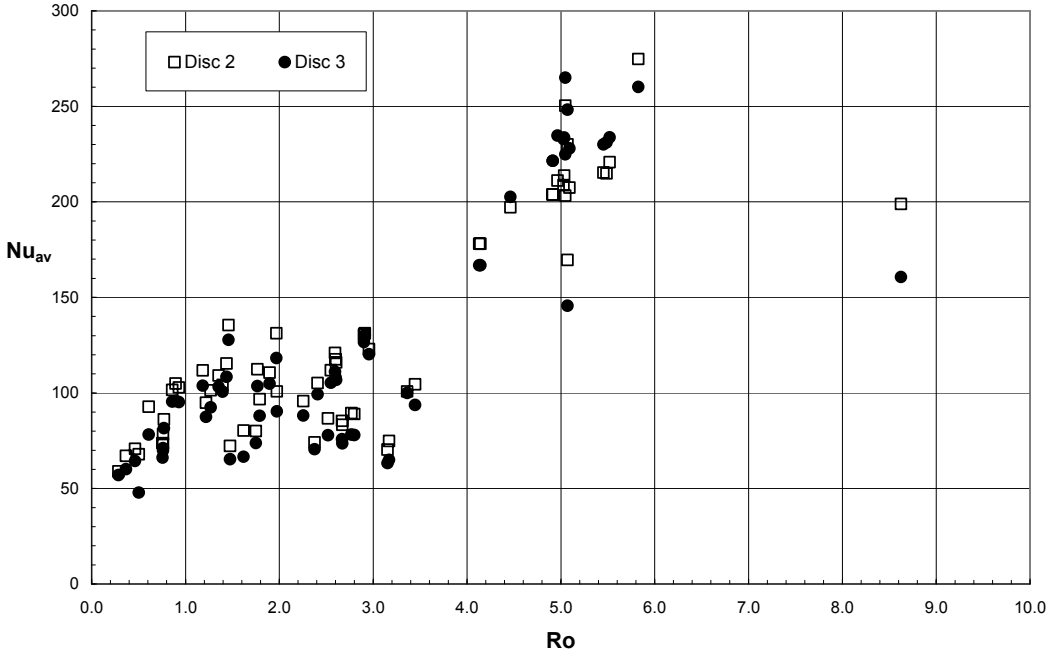

Fig 5. 11 Fin solution results for Build 2 (narrow annular gap)
Variation of average Nusselt number with Rossby number

5.2 Flow velocity measurement uncertainties

As explained in Chapter 4, Laser Doppler Anemometry is a direct measurement technique providing a direct reading of velocity without requiring prior calibration. However, in experimental situations, some bias can be introduced as a result of experimental set-up, flow conditions and data processing. Begg (2003) categorises the sources of uncertainty on the measurements into two groups: The systematic uncertainties introduced from the experiment, instrument and environment; and the statistical uncertainties arising from the estimation of flow quantities through a finite number of samples.

5.2.1 Systematic uncertainties

The principal systematic sources of uncertainties on the flow velocity measurements in the Multiple Cavity Rig were identified as:

- Signal noise
- Laser wavelength stability
- Beam crossing angle
- Seeding
- Velocity bias
- Velocity gradient broadening
- Probe alignment
- Finite transit time broadening
- Fringe bias

Following is a brief description of these sources of uncertainty and how they were addressed in the experimental set-up of the Multiple Cavity Rig.

Signal noise

The signal noise in the Laser Doppler Anemometry signals is considered as the main cause of data rejection in the burst signal processing unit, therefore impairing the validated data collection rate.

This in turn affects the velocity sample size able to be collected in a reasonable time. Signal noise is present electronically from the photomultipliers, amplifier circuits etc.

Noise also presents itself optically from reflections of scattered light onto surfaces, seeding particles and reflections on mirrors and windows. The optical noise was reduced in the test rig by having the discs and shrouds surfaces painted matt black to reduce surface reflections. The optical access windows are made of optical grade glass (BK7) widely used for Laser Doppler applications and their surfaces had an anti-reflective coating applied specifically in tune with the laser beams frequencies in order to minimise reflection losses. The windows and mirrors were also cleaned before each test. The laser power was kept at a working minimum (150 mW to 350 mW at the probe volume) in order to minimise the optical glare and saturation of the photomultipliers. The photomultipliers driving voltage and gain were adjusted in order to produce the best trade off between validation rate and data rate of the collected bursts signals. The signal to noise ratio threshold filter of the signal processor was also adjusted in order to achieve an optimum of this balance.

Seeding

The seeding in Laser Doppler Anemometry experiments is of prime importance in determining the accuracy of the flow measurements. As the measurements result from the tracking of seeding particles velocity, it is therefore of primordial importance that the seeding particles move at an equal velocity to the flow. Particle sizes and mass will affect their ability to follow the flow faithfully. Generally speaking, the smaller and lighter the particles, the better the accuracy. On the other hand, too small particles will increase the chances of multiple occurrences within the probe volume and therefore could be detrimental to the validated data rate of the measurement. Quenching oil was used for the flow measurements on the Multiple Cavity Rig. It was atomised at a size of approximately 1 μm. This is generally accepted as being small enough to faithfully follow the motion of air flow in experimental conditions.

No difference was noted in the measurements validation and data rates by varying the seeding atomisation rates from one jet to the maximum six jets, so one jet was used in order to reduce the fouling of the windows.

Laser wavelength stability

Laser Doppler Anemometry measurements assume a fixed light source frequency in order to derive burst frequencies. Therefore the wavelength stability of the laser source will directly affect the accuracy of the velocity measurements. Argon Ion lasers, as used on the present experiments, are considered as inherently stable in operation. Therefore the uncertainty associated with wavelength stability is considered as negligible.

Velocity bias

Velocity bias originates from the intermittent data collection nature of Laser Doppler Anemometry coming from passing seeding particles rather than from the air velocity itself. In regions of high flow velocity, the probability of a seeding particle to cross the measurement volume at a given time is higher than in a region of low velocity for a considered uniform particles concentration. Hence a disproportionate number of high velocity value samples are obtained when measuring in regions of turbulent flow, biasing the velocity measurement towards a higher value than the 'true' mean of the flow. This phenomenon is well known and a transit time weighted mean velocity flow estimator is generally accepted to give valid results in all conditions (Tropea 2002). It is expressed as:

$$\overline{u} = \frac{\sum \left(u_i \cdot \Delta t_i \right)}{\sum \Delta t_i} \qquad \text{Eq. 5.14}$$

Where u_i is the individual velocity sample and Δt_i is its residence time in the measuring volume.

This corrected method of calculation was already implemented in the Dantec post processing software, therefore the uncertainty associated with velocity bias on the measurements was considered as negligible.

Velocity gradient broadening

When a fluid flow has a significant velocity gradient in the direction normal to the fringes of the measurement volume, the successive passage of particles at different positions into the probe volume will produce different velocity values according to their position in the velocity gradient field.

The measured velocity values will appear to fluctuate even though the flow might be perfectly steady. The extra variance to the measurements resulting from velocity gradient broadening is defined by:

$$V_g^{'} = \left(\sigma_p \cdot \frac{\partial \overline{u}}{\partial y} \right)^2 \qquad \text{Eq. 5.15}$$

Where $\frac{\partial \overline{u}}{\partial y}$ is the mean velocity gradient at the point of measurement and σ_p is the standard deviation of the distribution of particles in the direction parallel to the fringes in the measurement volume.

This variance needs to be subtracted from the measured value in order to obtain the true variance of the flow. In the Multiple Cavity Rig, velocity gradient broadening is unlikely to be a significant source of uncertainty in regions away from the solid surfaces.

Probe alignment

As mentioned in Chapter 4, the accuracy of positioning of the probe volume was considered as ±0.5 mm in the axial and radial directions for both traverse configurations. The accuracy of orientation of the laser probe in respect to the rig was of particular importance as a small error in orientation of the orthogonal beams could be a significant source of uncertainty when one velocity component is greater than another. The angular locating of the laser beam alignment targets was set against a precision machining spirit level giving an accuracy of ±0.015 °. The uncertainty on the radial velocity measurements associated with probe alignment error is therefore:

$$u_{V_r,probe} = \pm V_\phi \cdot \cos(0.015°) \qquad \text{Eq. 5.16}$$

In the case of a velocity measurement at the largest tangential velocity measured (50 m/s), the corresponding uncertainty on the radial velocity measurement due to angular probe alignment was estimated as 0.014 m/s.

Transit time broadening

Transit time broadening occurs as a result of measurement of Doppler burst frequencies being obtained from a limited number of cycles, i.e. fringe passages. The fewer the fringes, the greater is the potential uncertainty in estimation of the frequency content of the signal.
The probe volume of the laser set-up used in this work featured 14 fringes, and therefore the uncertainty introduced considering the large number of samples usually taken is considered to be small.

Fringe bias

Fringe bias (or direction bias) occurs in flows with significant changes of direction, as in recirculation flows for instance, whereby the flow will change direction within the probe volume itself. Particles approaching the probe volume in such flows might arrive at a flat angle to the fringes, or reverse direction, and therefore might not have crossed a sufficient number of fringes for the burst signal processor to accept the sample as valid (thus affecting the data rate of measurement). This might affect the flow statistics, but the effects on the experimental measurements are considered to be marginal in the present case.

5.2.2 Statistical uncertainties

Statistical uncertainties on a Laser Doppler Anemometry measurement are a direct result of it being essentially an averaged technique of measurement based on irregular sample collection of instantaneous velocities over time. Sample sizes of 30 or more are recommended as a very minimum of validity or the calculation of a mean as the expression of the mean velocity $\overline{u}$ in Equation 5.14. The uncertainty calculations on the velocity samples were carried out by the Dantec processing software while acquiring. The 95 % confidence interval on the mean velocity was expressed as:

$$\overline{u}_{95} = 1.96 \times \sqrt{\frac{\overline{u}^2}{N}} \qquad \text{Eq. 5.17}$$

Where N is the number of collected samples, and $\overline{u}$ is the mean of the sample velocities.
The 95 % confidence interval of the Root Mean Square of the collected samples was calculated as:

$$\sigma_{u_{95}} = 1.96 \times \sqrt{\frac{\overline{u}^2}{2 \cdot N}} \qquad \text{Eq. 5.18}$$

Calculated flow measurement uncertainties were integrated in the results and shown on velocity measurement plots with “error bars” representing $\overline{u} \pm \overline{u}_{95}$ in the example of an average velocity plot.

6. Velocity measurements results

This chapter presents the velocity measurement results for Build 2 and Build 3 of the Multiple Cavity Rig. The main difference and measurement capability of Build 2 and Build 3 are recapped in Table 6.1 below.

All the measured velocity data cases were processed into detailed test reports for ease of archiving and analysis. The list of all experiments, with the velocity components measured when applicable and the operating conditions and main non-dimensional results can be found in Appendices 6.2 and 6.3. From these lists, the Reader can select a test of interest and consult the detailed results report in the attached CD-Rom following the instructions in Appendix 6.1. For convenience of reading, the reports of the specifically mentioned tests in this chapter are also included in Appendix 6.4.

	Build 2	**Build 3**
Annular gap	0.092	0.164
Heat transfer measurement	Disc, shroud	Disc, shroud
LDA measurement	VΦ, Vz	VΦ, Vz and VΦ, Vr

Table 6. 1 Principal operational differences between Build 2 and Build 3 of the Multiple Cavity Rig

Table 6.2 summarises the range of experimental conditions performed for the velocity measurements on Build 2 and Build 3 of the Multiple Cavity Rig. By comparison, typical engine values for cruise operation may be taken as Re_{Φ}= $7.7x10^6$ and Re_z= $2.4x10^5$ (Alexiou 2000). The experimental data reported here has been obtained over a range of values overlapping both real engine conditions and also those used by authors of previous research in this field as shown in Fig. 2.17.

Parameter		Build 2 LDA	Build 3 LDA
Rotor speed	Ω (rad/s)	$123 \le \Omega \le 306$	$65 \le \Omega \le 570$
Cooling air flow rate	$\dot{m}$ (kg/s)	$0.184 \le \dot{m} \le 0.618$	$0.2 \le \dot{m} \le 0.72$
Inlet pressure	p_{in} (bar, abs)	$2.25 \le p_{in} \le 3$	$2.3 \le p_{in} \le 3.1$
Inlet temperature	T_{in} (K)	$311 \le T_{in} \le 319$	$302 \le T_{in} \le 339$
Disc average surface temperature	$T_{s,av}$ (K)	$328 \le T_{s,av} \le 339$	$321 \le T_{s,av} \le 353$
Shroud average surface temperature	T_{sh} (K)	$361 \le T_{sh} \le 376$	$353 \le T_{sh} \le 385$
Disc rotational Reynolds number	Re_Φ (Eq. 4.1)	$9.5 \times 10^5 \le Re_\Phi \le 2 \times 10^6$	$4 \times 10^5 \le Re_\Phi \le 4.1 \times 10^6$
Axial Reynolds number	Re_z (Eq. 4.2)	$4.8 \times 10^4 \le Re_z \le 1.5 \times 10^5$	$4.7 \times 10^4 \le Re_z \le 1.8 \times 10^5$
Rossby number	Ro (Eq. 4.3)	$1.27 \le Ro \le 5.1$	$0.27 \le Ro \le 7.5$
Disc buoyancy parameter	$\beta\Delta T_{av}$	$0.04 \le \beta\Delta T_{av} \le 0.08$	$0.02 \le \beta\Delta T_{av} \le 0.09$
Shroud buoyancy parameter	$\beta\Delta T_{sh}$ (Eq. 4.20)	$0.15 \le \beta\Delta T_{sh} \le 0.19$	$0.11 \le \beta\Delta T_{sh} \le 0.238$
Shroud Grashof number	Gr_{sh} (Eq. 4.20)	$1.6 \times 10^8 \le Gr_{sh} \le 6.2 \times 10^8$	$3.3 \times 10^7 \le Gr_{sh} \le 1.4 \times 10^9$

Table 6. 2 Range of LDA experimental conditions for Build 2 and Build 3 of the Multiple Cavity Rig

6.1 Axial and tangential velocity components

Figure 6.1 and Figure 6.2 show the measurements of tangential velocity, V_Φ, in Build 2 and 3 of the Multiple Cavity Rig respectively, normalised with respect of the cavity rotation Ωr against the non dimensional radial location r/b. Owing to a difference in annular gap size, the velocity profiles along the non-dimensional radius from Build 2 and Build 3 differ, in that the tangential velocity profiles of Build 2 would tend to indicate a gradual acceleration to solid body rotation as the radius increases, while Build 3 would tend to indicate an over-spinning of the flow in the region between the shaft and the cavity entrance ($0.236 \leq r/b \leq 0.318$) with a gradual decrease to solid body rotation as progressing radially outwards in the cavity . More details will be provided later in this chapter.

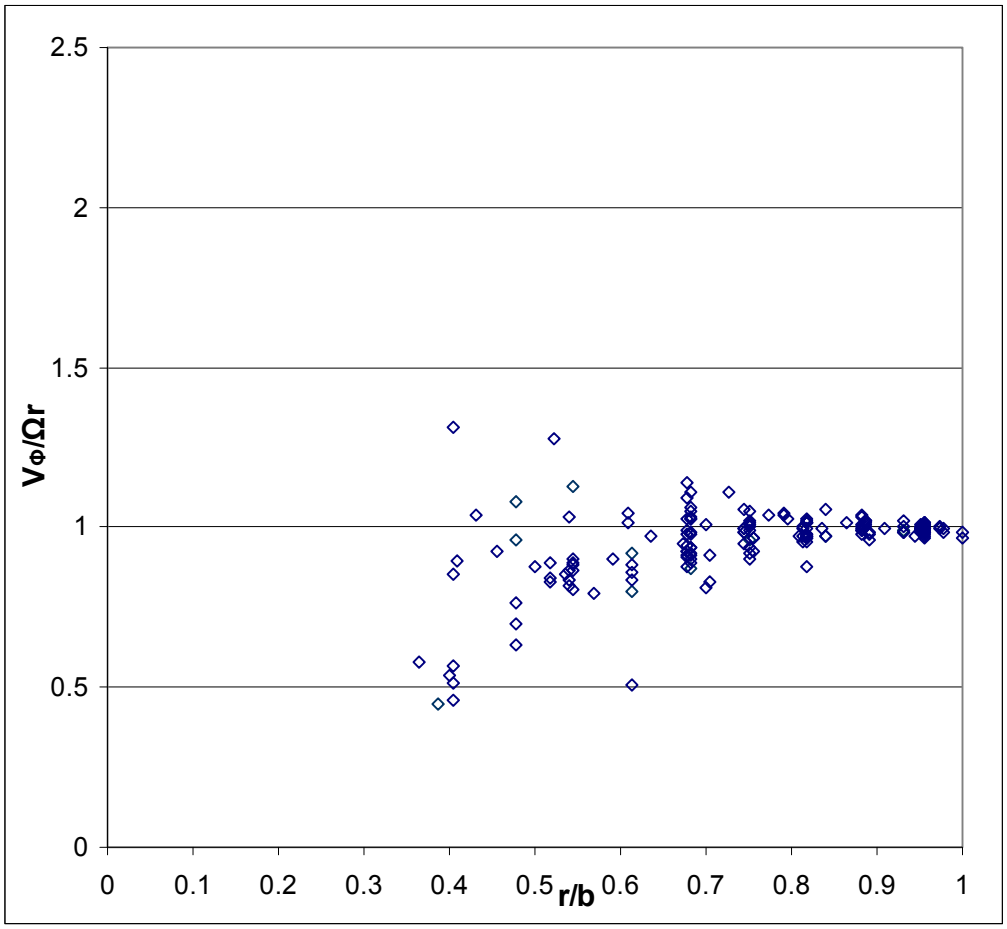

Fig 6. 1 Tangential velocity measurements for Build 2 (all data)

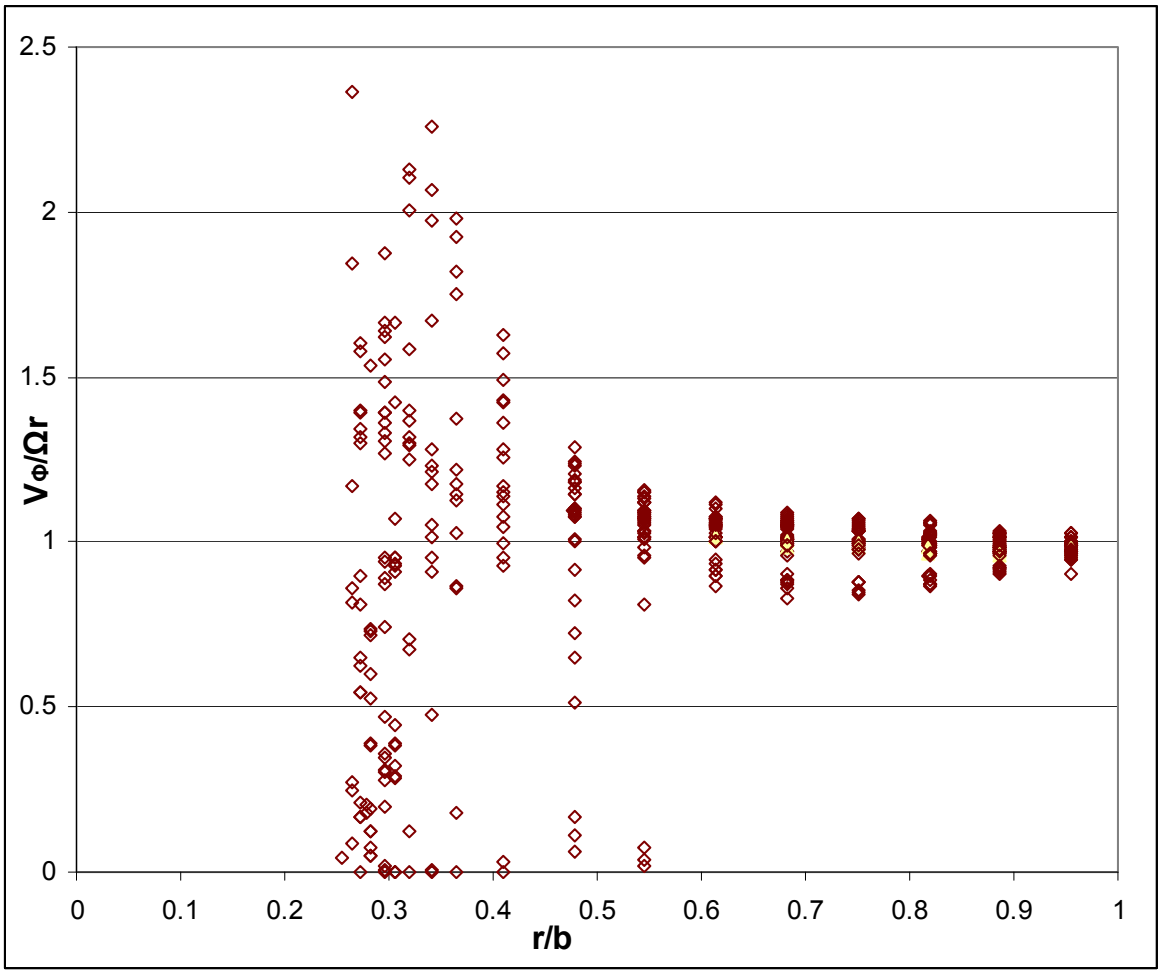

Fig 6. 2 Tangential velocity measurements for Build 3 (all data)

A typical plot of the measured variation of normalised tangential velocity in the Multiple Cavity Rig Build 3 against r/b is shown in Fig 6.3.

The velocity measurements were performed inside Cavity 3 and locations within the throughflow annular gap in axial regions by the cobs of Disc 2 and Disc 3.

The cavity measurement points were positioned along r/b on three different axial locations. The mid axial plane of measurement (z/s= 0.508) consisted of fifteen points in the radial range 0.264 ≤ r/b ≤ 0.955. At the lower radii, the central measurement line at mid Cavity 3 comprised 6 points more closely spaced at a 5mm radius interval in the region between 0.264 ≤ r/b ≤ 0.364 in order to improve the measurement definition in the lower part of the cavity. Measurements in the upstream (z/s= 0.345) and downstream (z/s= 0.671) parts of Cavity 3 comprised of six points each in the radial range 0.614 ≤ r/b ≤ 0.955 for this experimental condition.

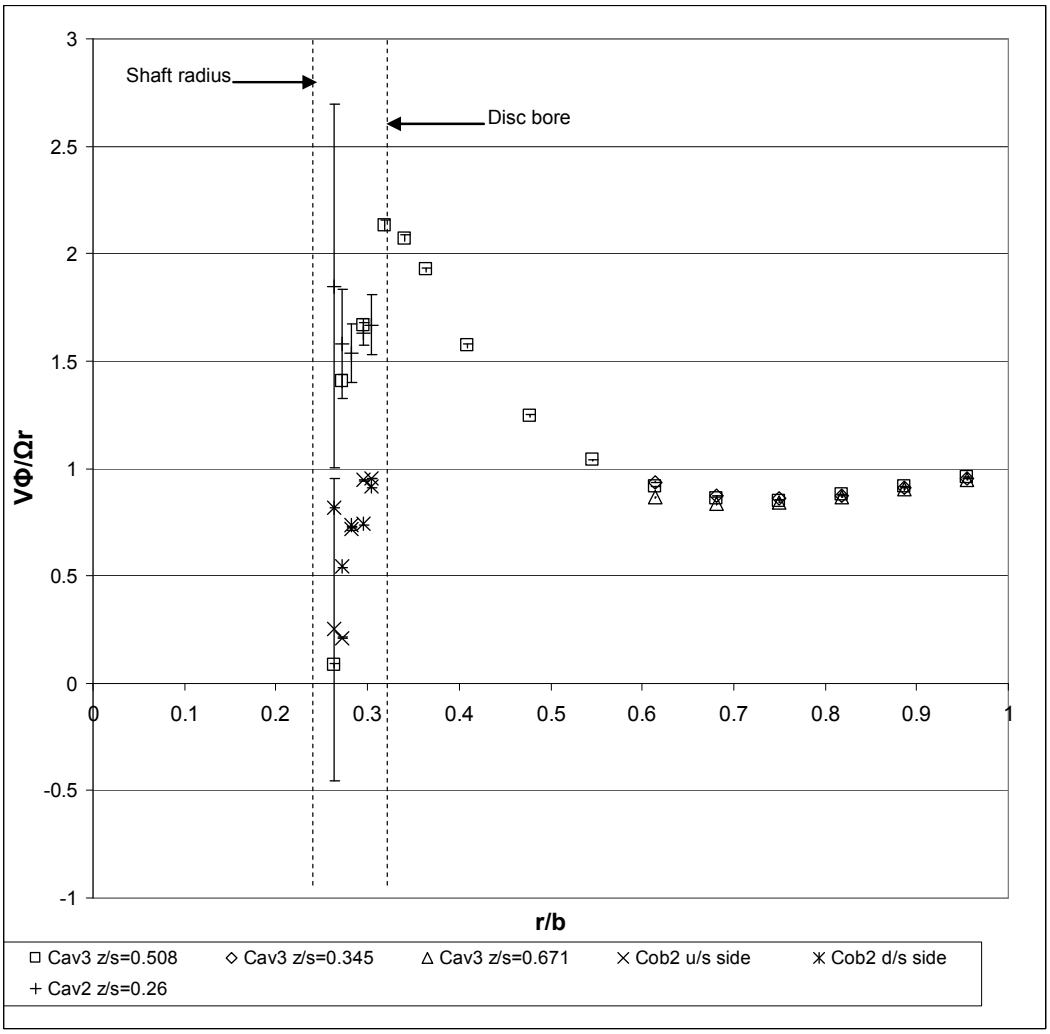

Fig 6. 3 Normalised tangential velocity plot for B3run32-1, Re_Φ= 0.49 x 10^6, Re_z= 0.92 x 10^5, Ro= 3.56, in Build 3 (wide annular gap)

The five measuring points under Cob 2 downstream side, Cob 3 upstream side, and the downstream corner of Cob 1 (z/s= 0.26 in Cavity 2), were close spaced together within the radius region representing the gap space of the central throughflow annulus (between the shaft, r/b= 0.236 and the disc bore, r/b= 0.318) in the range 0.264 ≤ r/b ≤ 0.305.

On some other tests, the number of points and their locations could vary, therefore the measurement points locations shall be mentioned when appropriate in the results presented.

The velocity plots shown in Figure 6.3 were produced for an operating condition of Re_Φ= 0.49 x 10^6, Re_z= 0.92 x 10^5 and Ro=3.56. The error bars associated with each velocity measurement represent the 95% uncertainty confidence interval values on the time averaged velocity samples as explained in Chapter 5. The

velocity measurements under Cob 2 show the tangential velocity varying from $V_\Phi/\Omega r \approx 0.25$ close to the shaft surface to $V_\Phi/\Omega r \approx 0.9$ by the bore of Disc 2.

For the measurements at the lower radii of the upstream part of Cavity 2 (by the axial location of the downstream face of Cob 2, $z/s = 0.26$), the tangential velocities measured show magnitudes of $V_\Phi/\Omega r \geq 1.54$ along the measurement line, with peaks at the extremities of $V_\Phi/\Omega r = 1.85$ at r/b=0.264 and $V_\Phi/\Omega r = 1.67$ at $r/b = 0.305$.

The tangential velocity profile at mid-Cavity 3 on the lower radii show a sharp tangential velocity increase from $V_\Phi/\Omega r = 0.08$ by the shaft at $r/b = 0.264$, culminating at $V_\Phi/\Omega r = 2.13$ at r/b= 0.318, which corresponds approximately to the discs bore radius.

It is believed that the overspinning of the central throughflow at the junction of a cavity is the result of the conversion of axial momentum being redirected tangentially as the flow penetrates within the inner section of the cavity. A radial inflow in the discs boundary layer at the inner radii of the cavity should occur in order to recirculate the flow being 'spun out' into the cavity but this could only be assumed as no velocity measurements were possible in this region of the cavity due to the limited optical access to the discs surfaces posed by the protruding discs cobs.

Progressing further outwards the cavity, the relative tangential velocities show a decrease with radius and tend to reach a value close to solid body rotation by $r/b \approx 0.6$. No significant differences of tangential velocities were found across the axial width of the cavity.

Variations in the instantaneous velocities of the measured flows can be represented in relation with the RMS values of the velocity samples at each position. Figure 6.4 shows the turbulence intensity (defined in Eq.4.25) related to the tangential velocity measurements shown in Figure 6.1 for mid Cavity 3. It can be related that the flow within the throughflow annular gap presents a level of turbulence indicating highly fluctuating tangential velocities. The levels of turbulence intensity sharply reduce up to a radius corresponding to the discs bore and then further reduces, albeit slowly, as progressing radially through the cavity.

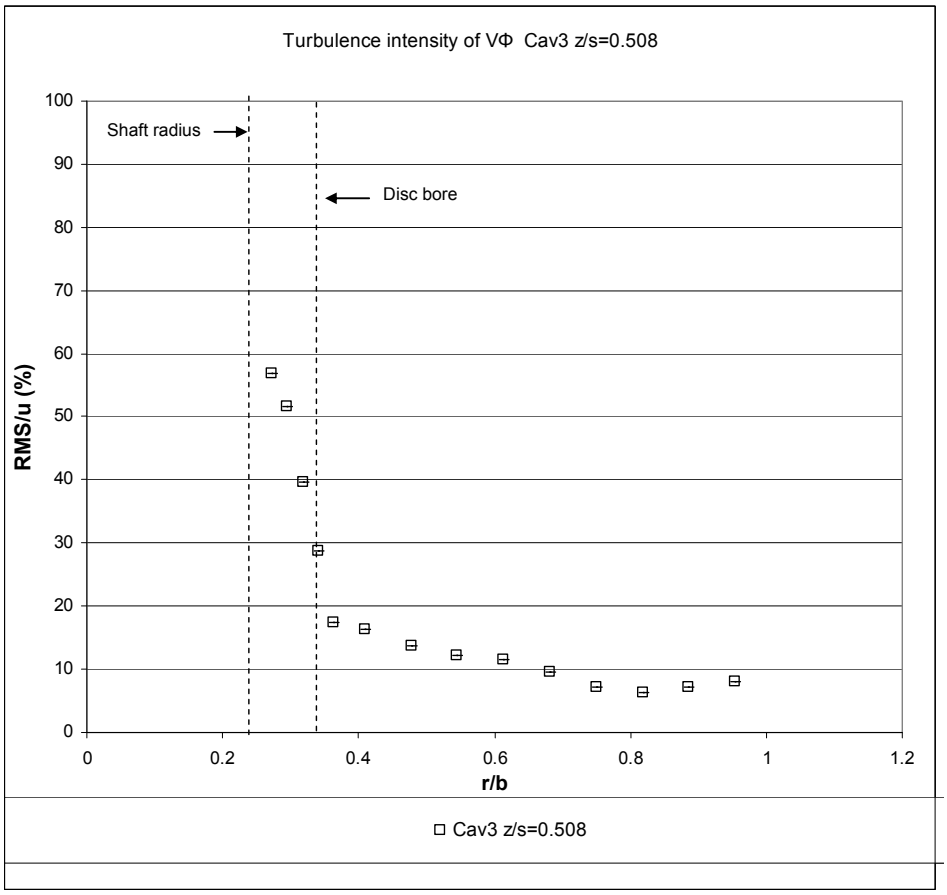

Fig 6. 4 Turbulence intensity of VΦ against r/b in mid Cavity 3 for B3run32-1, Re_Φ= 0.49 x 10^6, Re_z= 0.92 x 10^5 and Ro= 3.56

Figure 6.5 shows a contour plot interpretation of the measured normalised tangential velocities shown in Figure 6.3. The boundaries of this contour plot were attributed a non slip flow condition, $V_\Phi/\Omega r$= 1, except on the (non-rotating) shaft surface where $V_\Phi/\Omega r$= 0. The measurement point locations are materialised by squares on the plot.

The extent of the overspinning region by the entrance of Cavity 3 can clearly be seen from the plot, while a similar pattern can be guessed from the measurements at the entrance of Cavity 2. The swirling profile of the throughflow along the shaft annulus also clearly stabilises in the disc bore passage before being spun up again by interacting with Cavity 3.

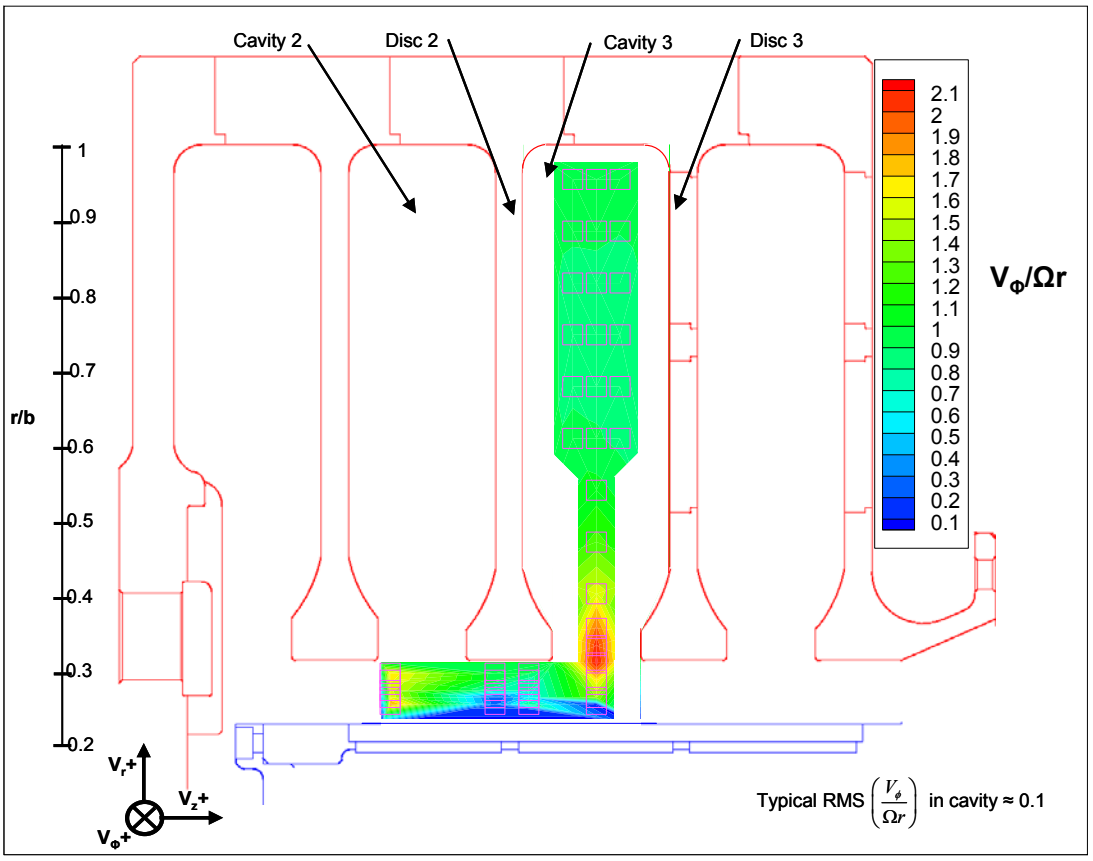

Fig 6. 5 Normalised tangential velocity contour plot for B3run32-1, Re_Φ= 0.49 x 10^6, Re_z= 0.92 x 10^5 and Ro= 3.56

The axial velocity measurements for this test are shown in Figure 6.6, with the error bars on the plot representing the 95% interval of confidence of the average measurements.

In the central annular throughflow region of the rig (0.236 ≤ r/b ≤ 0.318) the measured axial velocities are consistent with the bulk average velocity (W= 17.45 m/s in this instance) ranging within about 0.7 ≤ V_z/W ≤ 1.5. In radial locations within Cavity 3 (r/b ≥ 0.318), the axial velocities tend towards zero. The associated normalised RMS values on the averaged axial velocity measurements shown in Figure 6.7 indicate an increasing level of local velocity fluctuations for 0.236 ≤ r/b ≤ 0.318, then a sharp decrease when entering Cavity 3, followed by a steady decrease as progressing radially through the cavity towards r/b≈ 1. The turbulence intensity (Eq. 4.25) levels achieved in the central throughflow reached values of the order of RMS/$\overline{u}$ = 53% for r/b= 0.38 in the mid-plane of Cavity 3. The normalised axial velocity RMS values (RMS/W) were chosen to be plotted instead of the turbulence intensity in Figure 6.7 as the

excessively high values obtained for measured points where $\bar{u}$ (Eq. 4.21) tended towards zero were not representative of the overall turbulence levels of the flow within the cavity.

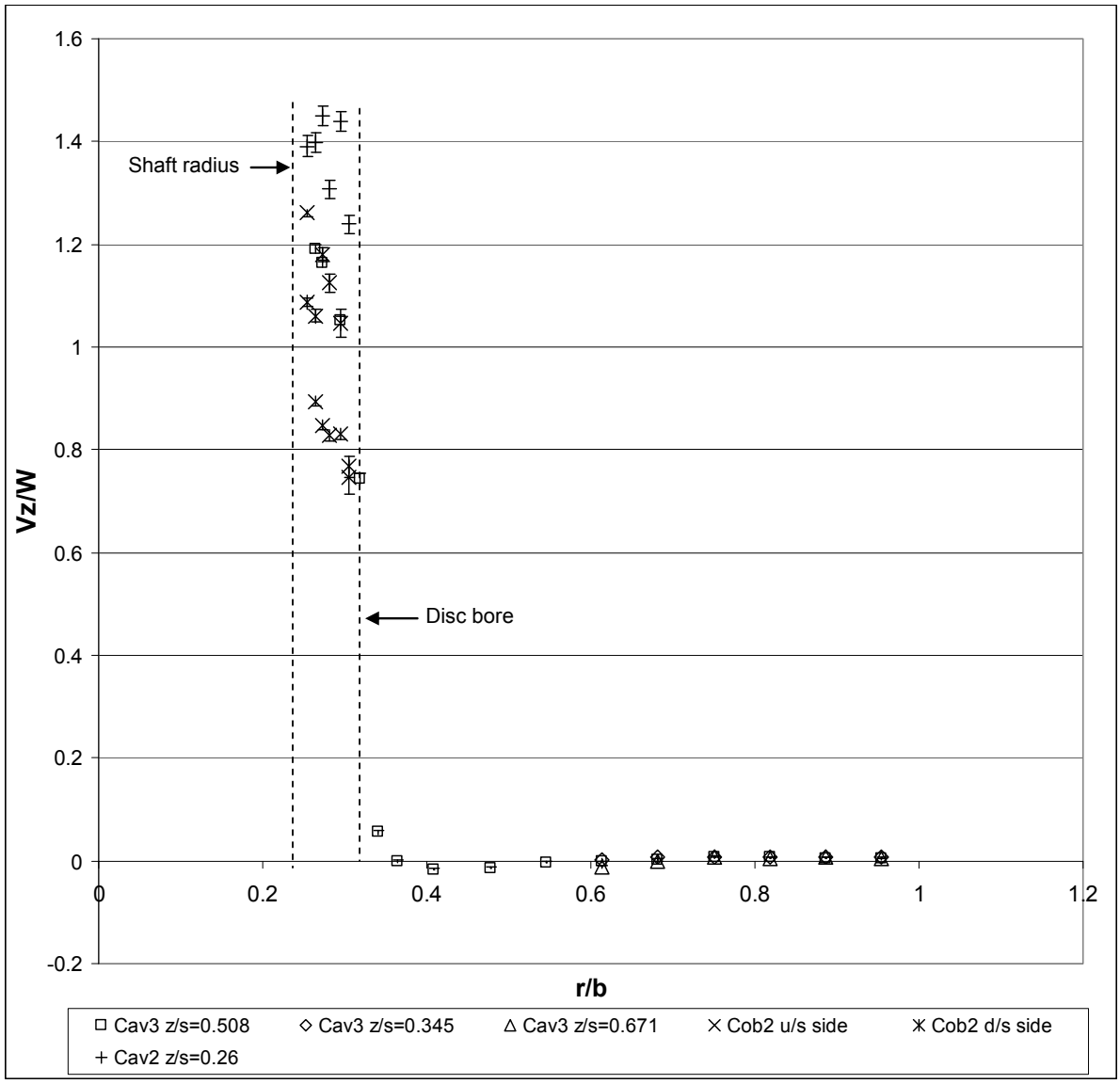

Fig 6. 6 Normalised axial velocity measurements for B3run32-1, Re_Φ= 0.49 x 10^6, Re_z= 0.92 x 10^5 and Ro= 3.56

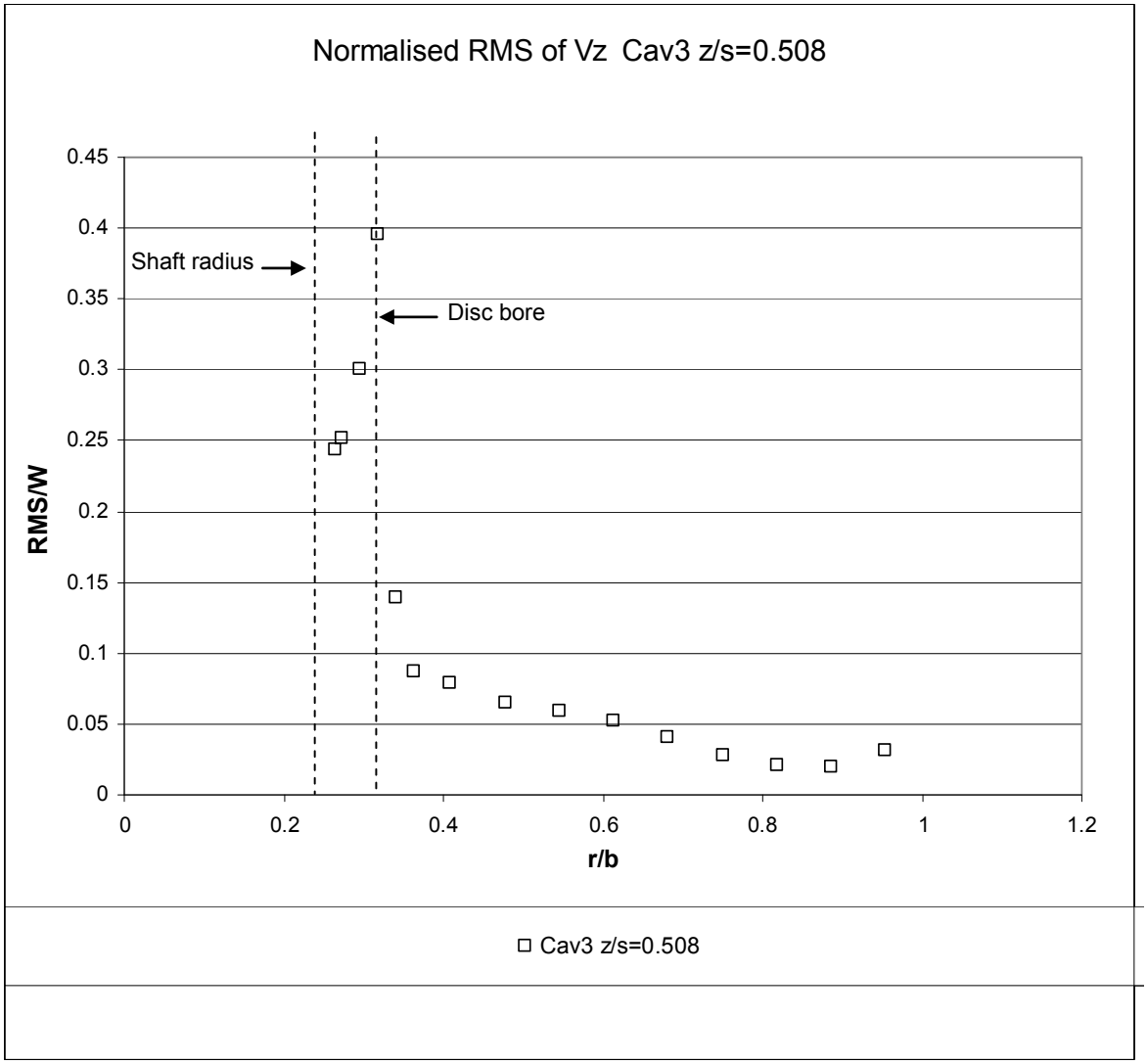

Fig 6. 7 Normalised RMS of V_z in mid-cavity 3 for B3run32-1, Re_Φ= 0.49 x 10^6, Re_z= 0.92 x 10^5 and Ro= 3.56

Figure 6.8 shows the contour plot of V_z/W in the measurement volume of the test rig for the considered test. The boundaries of this contour plot were attributed a non slip condition, Vz=0. A boundary condition had to be attributed on the upstream and downstream boundaries of the central annulus by the plotting software. Therefore the attention of the Reader is drawn to the display anomalies shown on the upstream and downstream regions due to the presence of a zero velocity boundary condition and is invited to bear this in mind when looking at the contour plot.

The interpretation of the plotted axial velocity measurements highlights an accelerated axial throughflow in the central annular gap within the cavities entrance regions (with $V_z/W > 1$) while the flow appears steadier while passing under Disc 2 ($V_z/W \approx 1$). This presents similarities with the tangential velocity measurements shown in Figure 6.3 which indicated a more stable flow under Disc 2.

The acceleration of the axial throughflow in the connecting regions of the cavities could result from an interaction with the cavity flow whereby the bulk of the throughflow might have to 'squeeze by' the interacting zone and therefore accelerate locally in the process as a result of conservation of mass.

The flow at the entrance of Cavity 3 appears to slow down from Vz/W=0.74 at r/b= 0.318 (disc bore radius) to zero at r/b= 0.364. A clockwise recirculation motion also appears to be present in the remaining radially out region of Cavity 3, although of very low magnitudes.

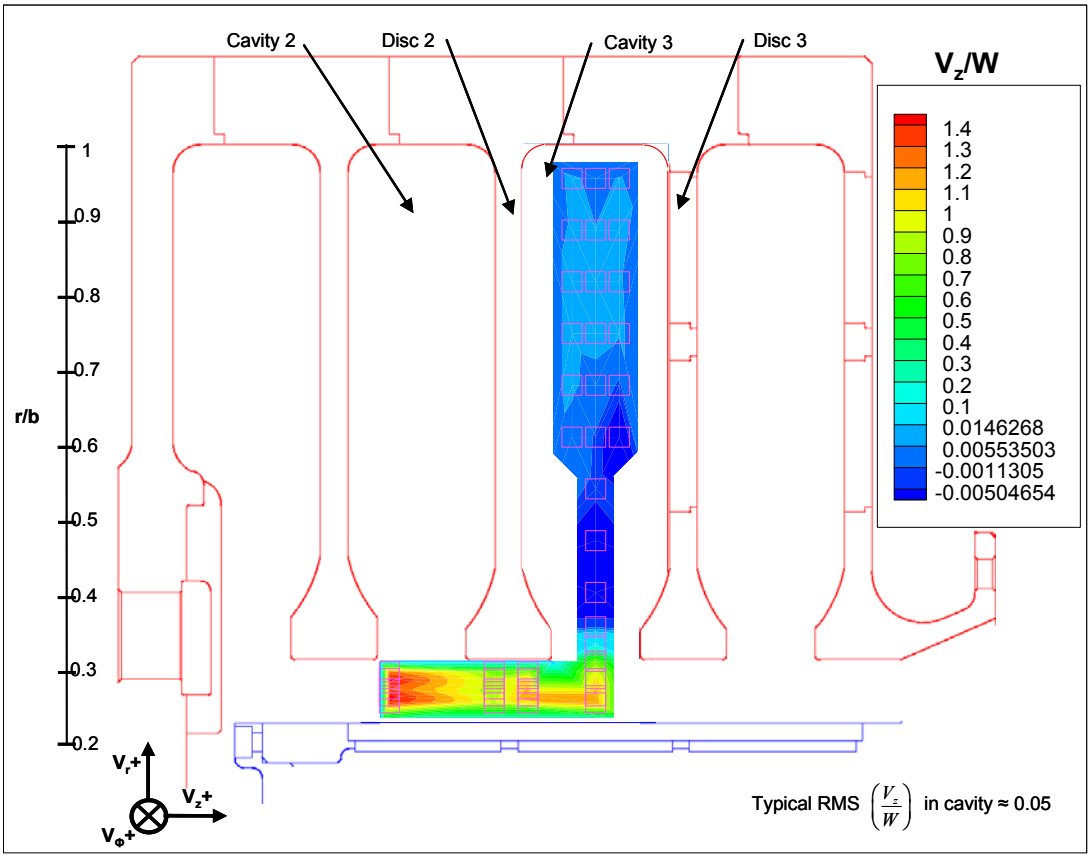

Fig 6. 8 Normalised axial velocity contour plot for B3run32-1, Re_Φ= 0.49 x 10^6, Re_z= 0.92 x 10^5 and Ro= 3.56

Figure 6.9 shows the normalised tangential velocity contour plot for an operating condition of Re_Φ= 4.12 x 10^6, Re_z= 1.16 x 10^5 and Ro= 0.54. This condition represents the other end of the spectrum of operating conditions of the rig with a flow condition expected to be rotationally dominated (Ro= 0.54), compared to the previously described condition in Figures 6.1 to 6.8 which is expected to be axially dominated (Ro= 3.56). The tangential velocity flow behaviour of the latter condition on Figure 6.9 is broadly similar to the previous condition, with an overspinning of the flow in the shaft annular gap region, reaching a maximum by the entrance of Cavity 3, then decreasing sharply as progressing radially through the cavity towards r/b= 0.4, then continuing to slow down progressively, reaching solid body rotation by the outer part of the cavity.

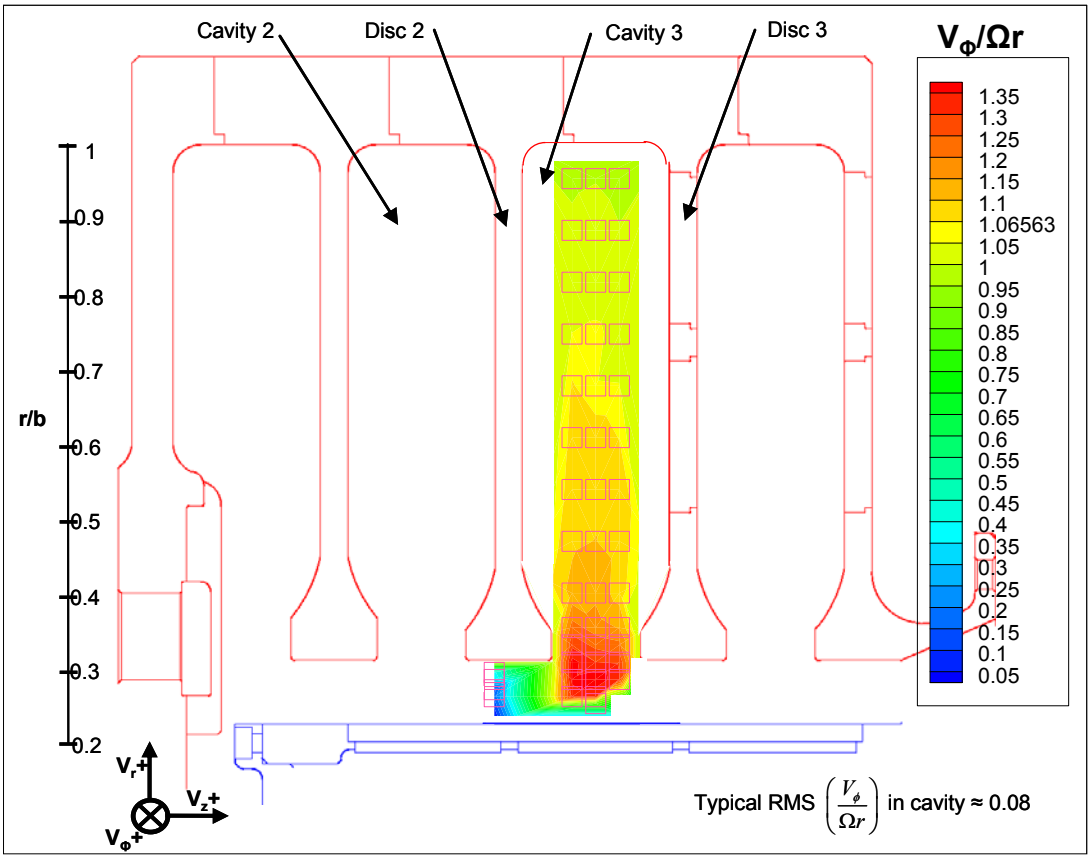

Fig 6. 9 Normalised tangential velocity contour plot for B3run28-1, Re_Φ= 4.12 x 10^6, Re_z= 1.16 x 10^5 and Ro= 0.54

The maximum overall level of swirl achieved was in the order of $V_\Phi/\Omega r \approx$ 1.4, which is less than achieved in the previous test for Ro= 3.56 ($V_\Phi/\Omega r \approx$ 2.1).

Tangential velocity measurements under the bore of Disc 2 returned values of $V_\Phi/\Omega r$= 0.17 for r/b= 0.27 and $V_\Phi/\Omega r$= 0.38 at r/b= 0.30.

Velocity measurements by the shaft proved more difficult to obtain at this operating condition, possibly due to an increase in vibrations from a much higher rotational speed of the rig (4552 rev/min against 666 rev/min for the previously described condition).

The corresponding contour plot of the normalised axial velocities is shown in Figure 6.10.

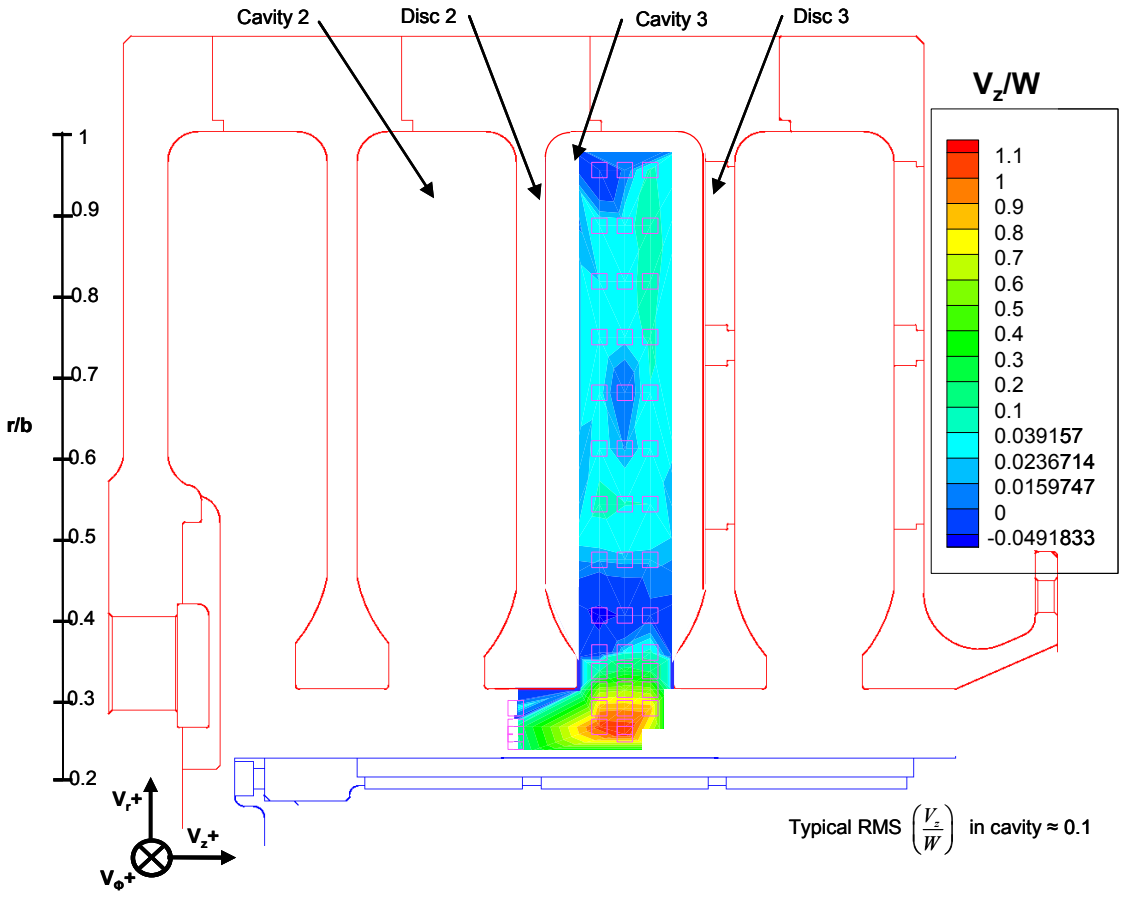

Fig 6. 10 Normalised axial velocity contour plot for B3run28-1, Re_Φ= 4.12 x 10^6, Re_z= 1.16 x 10^5 and Ro= 0.54

Axial velocity measurements under the bore of Disc 2 resulted in values of V_z/W= 1.15 at r/b= 0.255, V_z/W= 1.18 at r/b= 0.264, V_z/W= 0.11 at r/b= 0.273 and Vz/W≈0 for 0.282≤ r/b ≤ 0.305. The contour plot generation unfortunately

failed to show these values on Figure 6.10 for the same reasons of boundary conditions as explained before for the case in Figure 6.8.

The axial flow at the entrance of Cavity 3, mid-plane, shows a decrease in velocity from Vz/W=1.1 at r/b, Vz/W=0.59 at r/b=0.318 (disc bore radius), to Vz/W≈0 for r/b≥0.364. The axial velocity measurements further inside the cavity appear to show a relatively quiescent region of flow with no noticeably clear recirculations present.

From the plots above, differences in flow patterns and magnitudes between the two previously described conditions (high throughflow – low rotation speed and low throughflow – high rotation speed respectively) can be observed. The influence on the tangential velocity within the mid axial plane of Cavity 3 with increasing Re_Φ for a fixed axial Reynolds number of Re_z≈ 1 x 10^5 is shown in Figure 6.11. The test conditions featured in Figure 6.11 are detailed in Table 6.3.

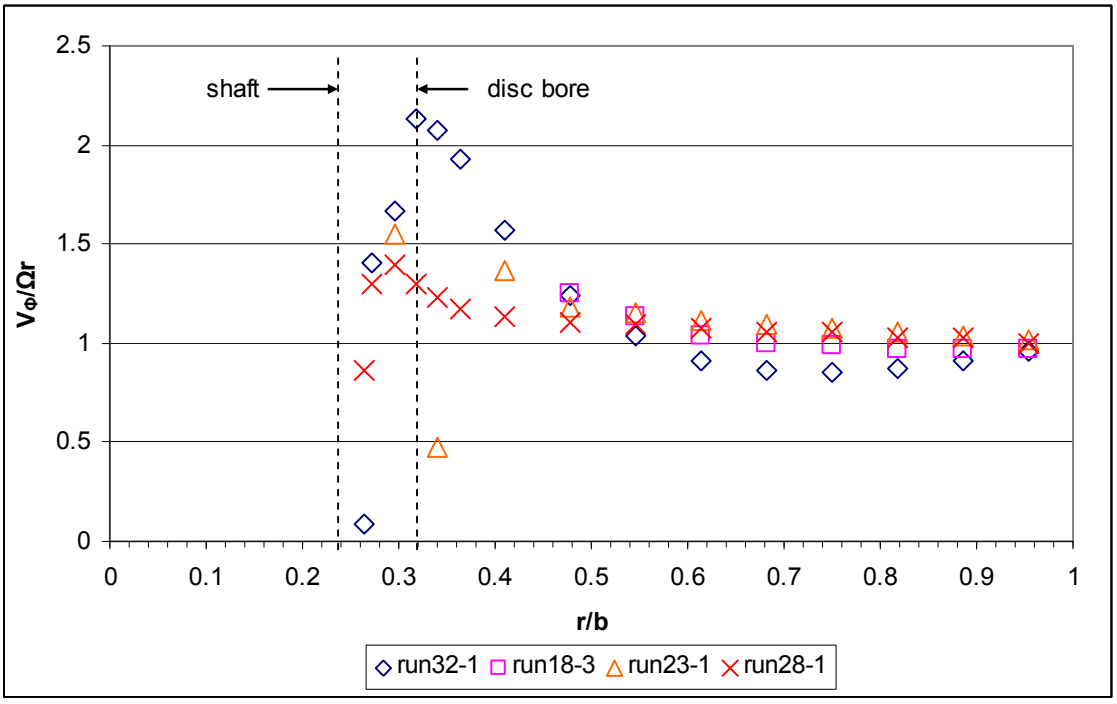

Fig 6. 11 Comparison of normalised tangential velocities in Build 3 at mid Cavity 3 with increasing Re_Φ for fixed Re_z≈ 10^5

Test	$Re_\Phi/10^6$	$Re_z/10^5$	Ro	$\beta\Delta T_{av}$	$\beta\Delta T_{sh,C3}$	$Gr_{sh,C3}/10^7$
Run32-1	0.49	0.92	3.56	0.09	0.23	5.3
Run18-3	1.03	1.01	1.87	0.05	0.18	17.1
Run23-1	2.02	0.99	0.93	0.04	0.13	46.1
Run28-1	4.12	1.16	0.54	0.03	0.11	137

Table 6. 3 Experimental conditions for Figure 6.9 (Build3)

For the lowest value of Re_Φ= 0.49 x 10^6 (Ro= 3.56), the tangential velocity profile in the throughflow annulus possesses the sharpest increase in velocity, reaching a swirl value of $V_\Phi/\Omega r \approx$ 2.3 by the radius corresponding to the disc bore, then decreases with increasing radial location for r/b> 0.32. A value just below solid body rotation is achieved at $r/b \approx$ 0.6, before gradually reaching solid body rotation by r/b=1. With an increase of Re_Φ to 1 x 10^6 (Ro= 1.87), 2 x 10^6 (Ro= 0.93) and 4 x 10^6 (Ro= 0.54), the peak value of relative tangential velocity achieved by the entrance of Cavity 3 decreases, reading values of $V_\Phi/\Omega r \approx$ 1.3 for Re_Φ= 4 x 10^6. The tendency for decelerating swirling flows to reduce to values of normalised tangential velocity below solid body rotation in the cavity could indicate a recirculation flow in the tangential plane. The tangential velocity profiles for conditions with $Re_\Phi \geq$ 2 x 10^6 show the decelerating tangential velocity values in the cavity above solid body rotation up to $r/b \approx$1.

A similar trend can be observed when comparing tests at fixed rotational Reynolds number values and increasing Re_z (hence increasing Ro). Figure 6.12 shows a comparison between the tangential velocity profiles along the mid plane of Cavity 3 for operating conditions of increasing axial Reynolds number values $Re_z \approx$ 0.59 x 10^5, 1 x 10^5 and 1.7 x 10^5 at fixed $Re_\Phi \approx$ 1.1 x 10^6. The details of the operating conditions of the tests plotted in Figure 6.12 are shown in Table 6.4.

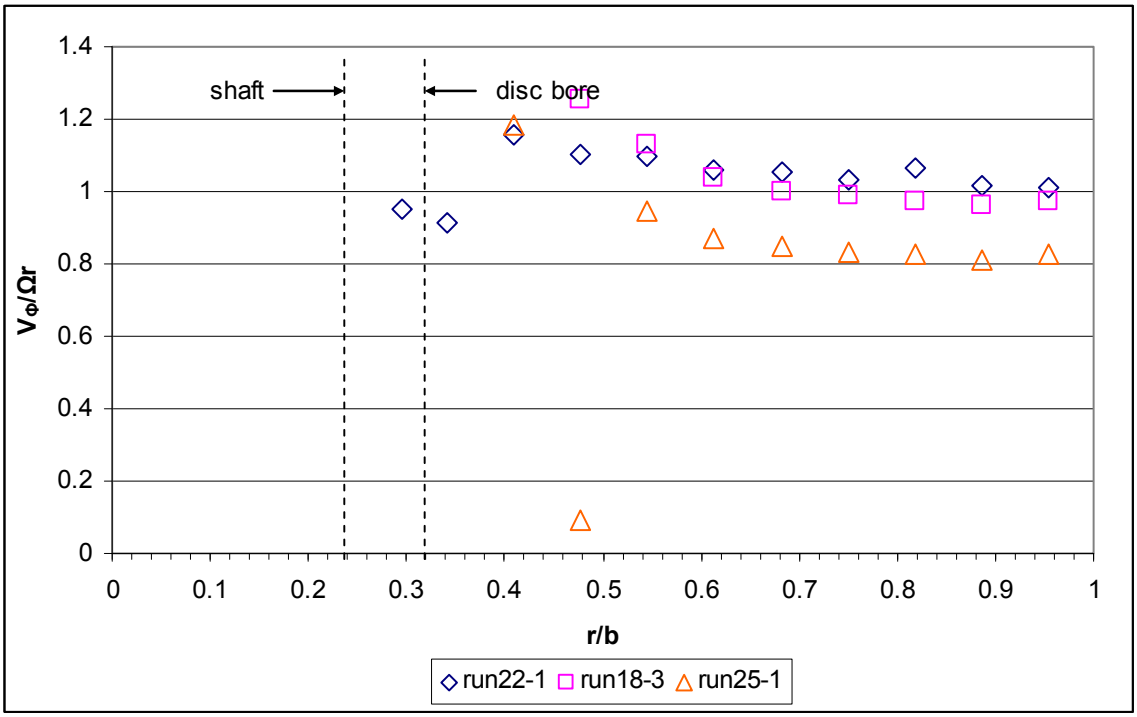

Fig 6. 12 Comparison of normalised tangential velocities in Build 3 at mid Cavity 3 with increasing Re_z for fixed $Re_\Phi \approx 1.1 \times 10^6$

Test	$Re_\Phi/10^6$	$Re_z/10^5$	Ro	$\beta\Delta T_{av}$	$\beta\Delta T_{sh,C3}$	$Gr_{sh,C3}/10^8$
Run22-1	1.24	0.49	0.75	0.06	0.17	2.43
Run18-3	1.03	1.01	1.87	0.05	0.18	1.71
Run25-1	1.15	1.71	2.84	0.05	0.17	1.97

Table 6. 4 Experimental conditions for Figure 6.10 (Build3)

Although the velocity measurements shown in Figure 6.12 are incomplete at the lower radii (r/b<0.4), the velocity profiles shown further inside the cavity (r/b≥0.409) would suggest a similar influence of the increase of Ro on the cavity velocity profiles. It can only be assumed that the influence of Ro on the peak swirl velocity in the inner region of the cavity (r/b<0.4) will be similar to that observed in Figure 6.11.

The results shown in Figure 6.12 and 6.11 therefore suggest that the distribution of tangential velocity in the inner region of the cavity (r/b < 0.5) is governed by the Rossby number, with an increase in the magnitude of $V_\Phi/\Omega r$ as the operating conditions become more dominated by the throughflow (large Ro).

It is interesting to notice some similarities with the observations in an isothermal cavity with throughflow by Farthing et al. (1992a) who described a similar increase of the relative tangential component to above solid body rotation in the central throughflow region of the cavity that was decreasing to solid body rotation as progressing radially out. They also observed an increase of the maximum relative swirl by the disc bore with increasing Rossby number.

Figure 6.13 compares the values of $V_\Phi/\Omega r$ taken from Build 3 and Build 2 of the Multiple Cavity Rig. The principal geometrical difference between Build 2 and Build 3 of the Multiple Cavity Rig, as previously mentioned, lies in a shaft radius decrease between Build 2 and Build 3 from r_s= 60 mm to r_s= 52 mm. The corresponding non-dimensional annular gap sizes are d_h/b= 0.164 for Build 3 (wide annular gap) and d_h/b=0.092 for Build 2 (narrow annular gap).

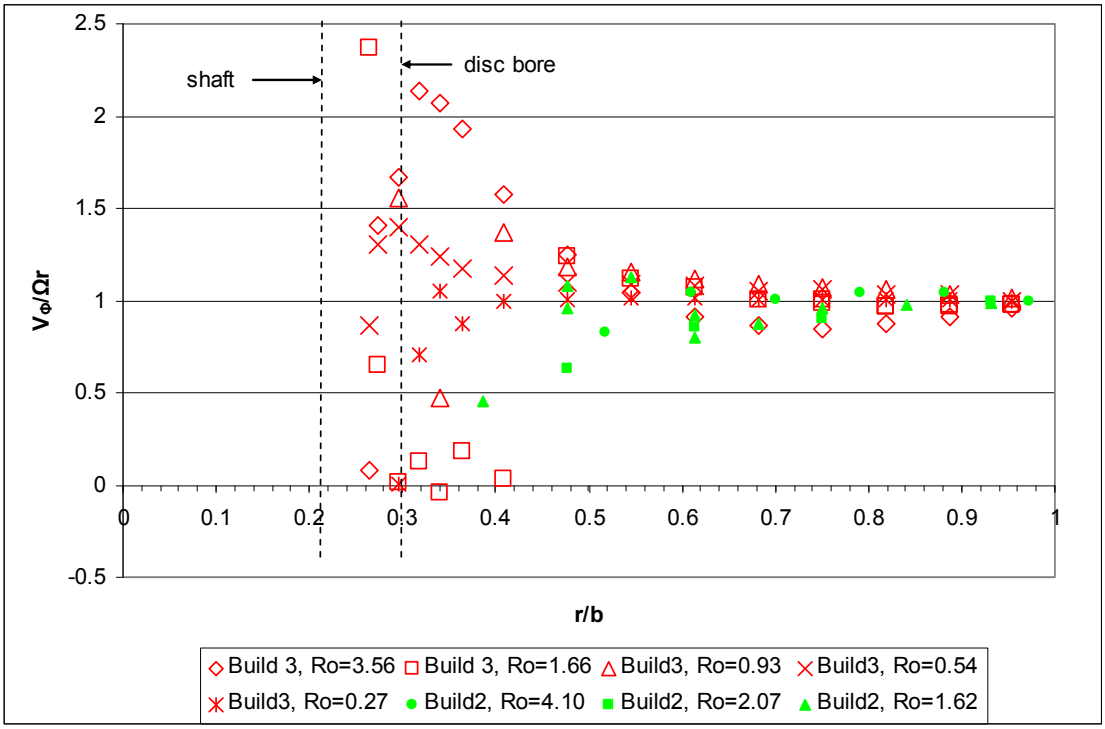

Fig 6. 13 Tangential velocity profiles at mid Cavity 3 for Build 2 and Build 3 with varying Ro

As also seen in Figure 6.1, the velocity measurements along the cavity radius in Build 2 shown in Fig. 6.13 suggest a gradual acceleration of the flow from the shaft region tending to $V_\Phi/\Omega r$=1 towards the outer radii of Cavity 3.

Some support to the tangential velocity observations on Build 2 can be found from the measurements of Owen and Powell (2004) who obtained similar cavity tangential velocity flow profiles behaviour on their rig with a narrower annular gap (d_h/b= 0.026) to Build 2 for a range of experimental conditions. It is worth noting that the low values of tangential velocity recorded for Ro=1.66 between 0.26≤ r/b ≤0.42 do not fit into the explication above and could be the result of a measurement fault or other phenomenon that cannot be explained by the author at present.

It would therefore appear that the tangential velocity profile characteristics in a rotating cavity with axial throughflow are principally governed by the influence of the throughflow interacting with the entrance of the cavity, that a variation in the throughflow dominance (variation in Ro) would affect the cavity tangential velocity profile. However the effects of the throughflow can be largely attenuated by reducing the annular gap ratio of the cavity, d_h/b, and also by reducing the cavity gap ratio, G, as previously demonstrated by Farthing et al (1992a).

Figures 6.14 and 6.15 show a comparison of tangential velocity profiles between Cavities 2, 3 and 4 in Build 3 and Build 2 respectively of the Multiple Cavity Rig.

The differences in measured tangential velocities shown for both builds between Cavities 2, 3 and 4 would suggest some evidence of variations of cavity tangential velocity profile behaviour as progressing through the rigs' cavities along the throughflow direction. From what was described above, the variations of the cavities tangential flow could perhaps suggest an increase of the influence of the throughflow interaction with the cavities as progressing through the rig, similarly to a local increase in Ro. This could suggest a cumulative influence of the exit flow conditions of one cavity onto the next, affecting the mechanism of vortex breakdown which in turn would affect the tangential distribution inside the cavities.

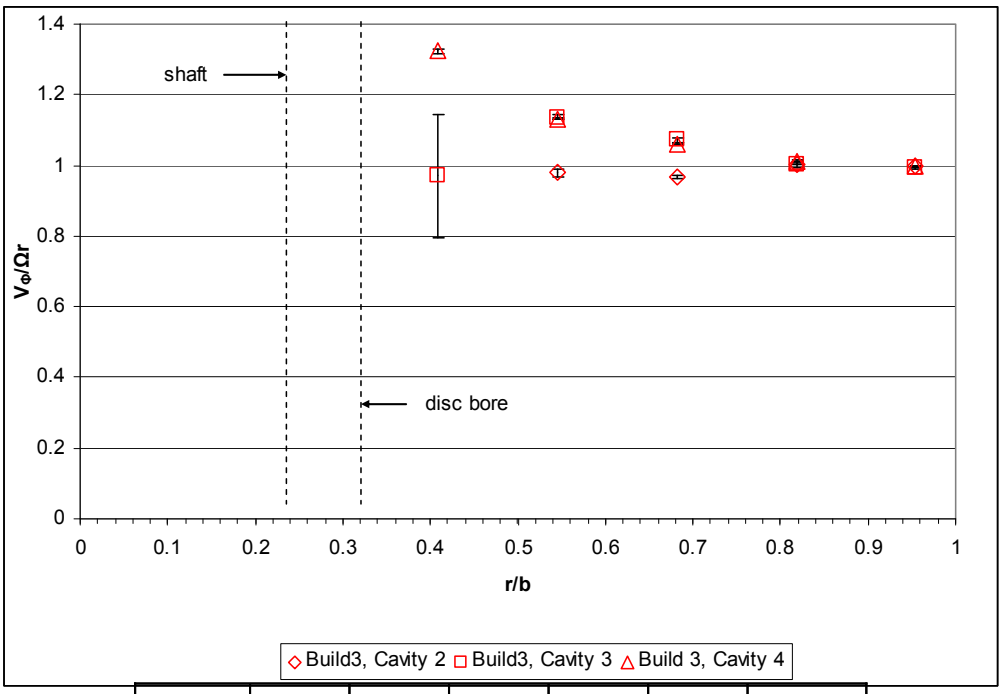

Test	ReΦ/10^6	Rez/10^5	Ro	βΔTav	βΔTsh, C3	Grsh,C3
B3run4-1	1	0.63	1.19	0.06	0.19	1.71E+08

Fig 6. 14 Tangential velocity profile comparison between Cavities 2, 3 and 4 in Build 3

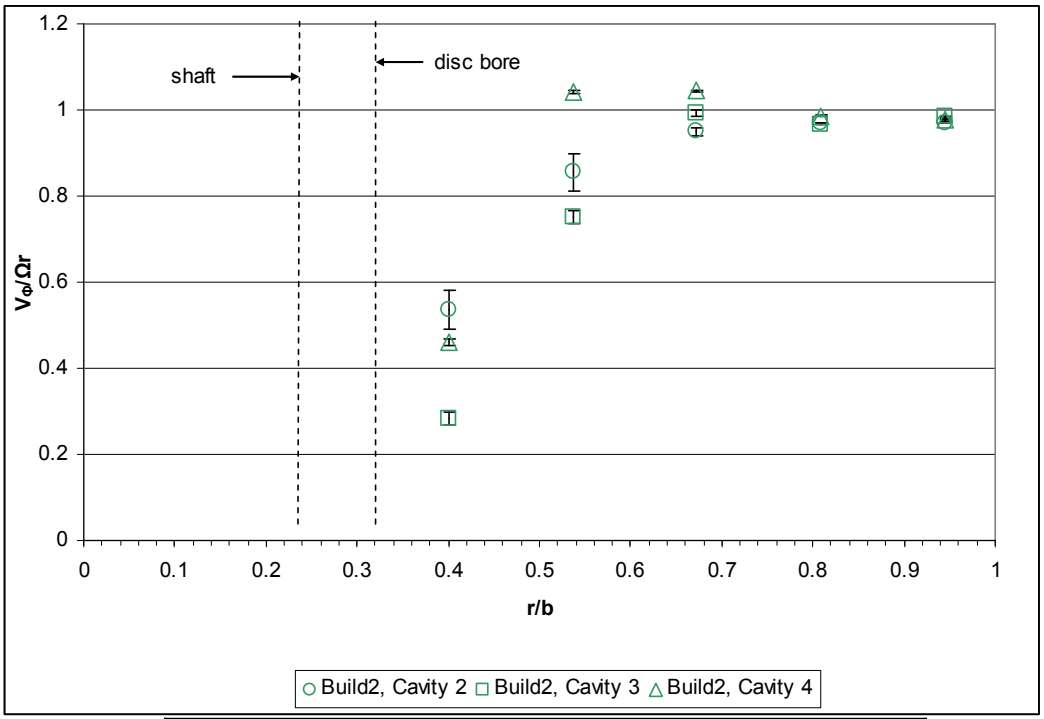

Test	ReΦ/10^6	Rez/10^5	Ro	βΔTav	βΔTsh, C3	Grsh,C3
B2test6	1.09	1.42	3.56	0.04	0.16	1.72E+08

Fig 6. 15 Tangential velocity profile comparison between Cavities 2, 3 and 4 in Build 2

6.2 Radial velocity measurements

Simultaneous radial and tangential velocity measurements were performed in Build 3 of the Multiple Cavity Rig using the optical access of the passing windows of Disc 3 and Disc 4 as described in Chapter 3. The measurement regions in Cavity 3 and 4 were within 0.067 ≤ z/s ≤ 0.946 and 0.565 ≤ r/b ≤ 0.925. Figures 6.14, 6.15 and 6.16 show the time averaged radial velocity measurements at respectively r/b= 0.924, r/b= 0.765, and r/b= 0.566 across the cavities width for a test condition of Re_Φ= 0.4 x 10^6, Re_z= 1.57 x 10^5 and Ro= 7.51 (B3run 38-1).

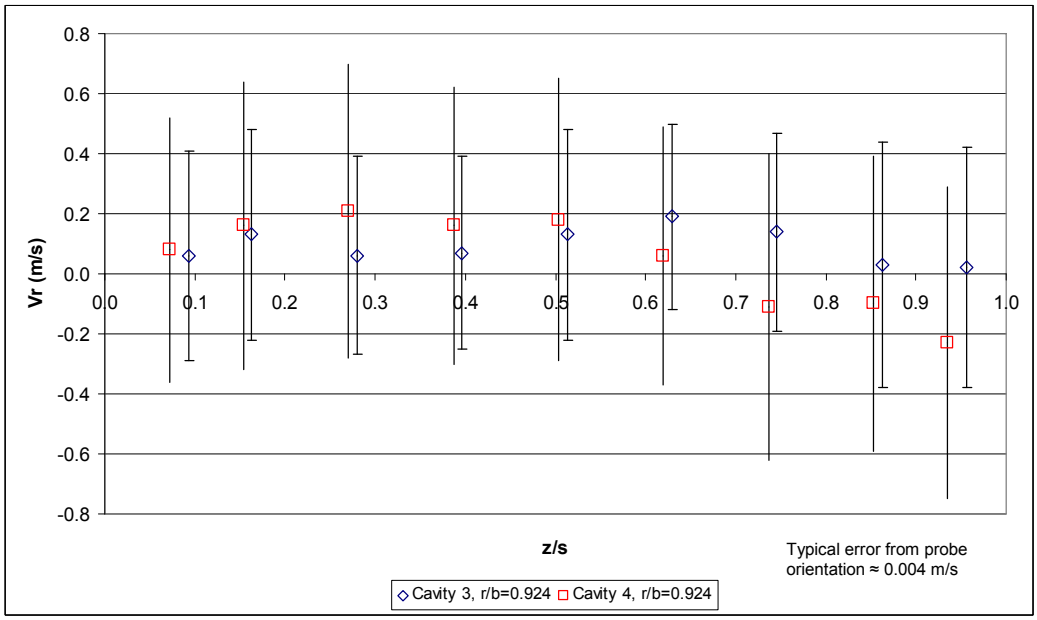

Fig 6. 16 Radial velocity measurements in Cavities 3 and 4 at r/b= 0.924 for Re_Φ= 0.4 x 10^6, Re_z= 1.57 x 10^5 and Ro= 7.51

The error bars on the velocity plot points of Figure 6.16, 6.17 and 6.18 represent the flow measurement spread, comprising the RMS of the measured velocity and the probe orientation error (Eq. 5.16). Positive values of radial velocity correspond to a cavity radial outflow while z/s= 0 corresponds to the upstream side disc wall of the considered cavity. The peak magnitude of the radial velocities in the present case can be seen from the plots to be in the order of Vr ≤ 0.25 m/s at r/b=0.765, which is about 0.7 % of the bulk average velocity (W= 36.10 m/s) and about 1.6% of the solid-body tangential velocity at $r=b$ (Ωb=15.09 m/s).

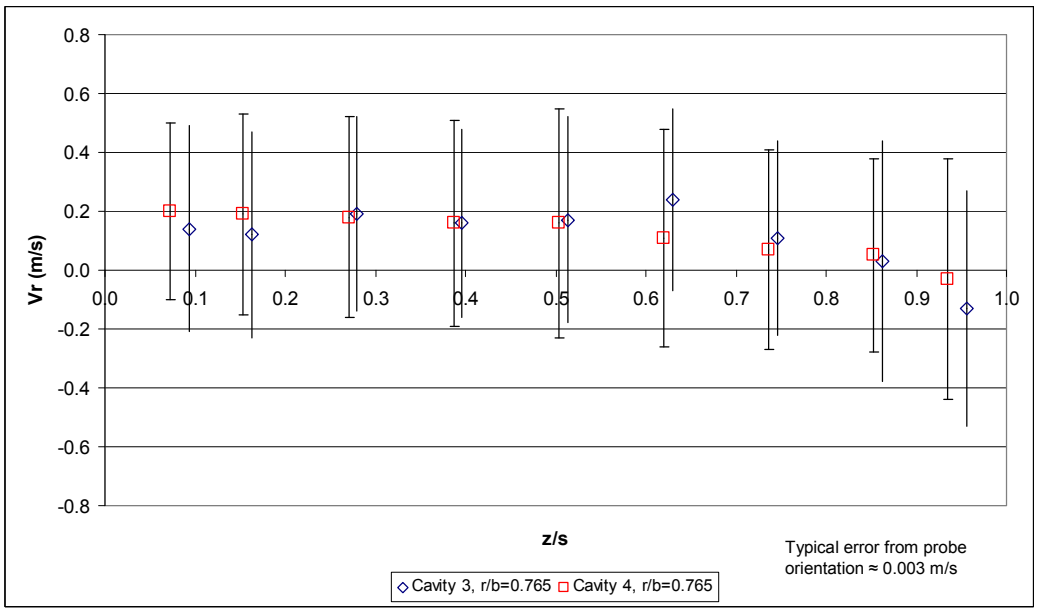

Fig 6. 17 Radial velocity measurements in Cavities 3 and 4 at r/b= 0.765 for Re_{Φ}= 4 x 10^6, Re_z= 1.57 x 10^5 and Ro= 7.54

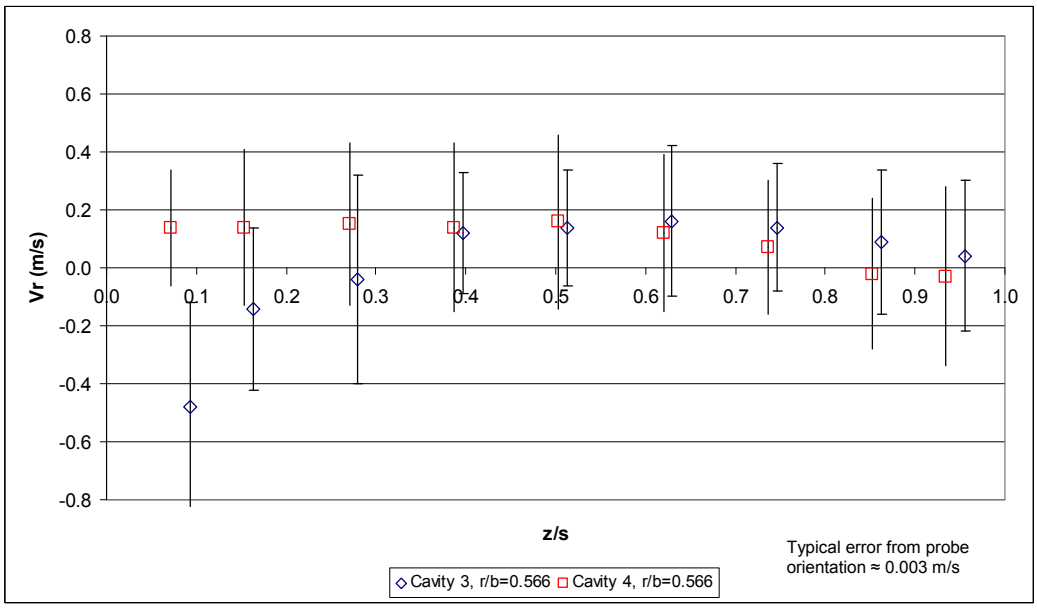

Fig 6. 18 Radial velocity measurements in Cavities 3 and 4 at r/b= 0.566 for Build 3, run38-1, Re_{Φ}= 0.4 x 10^6, Re_z= 1.57 x 10^5 and Ro= 7.51

The measured tangential velocities in this optical access configuration provided similar information than previously measured, i.e. velocities close to solid body rotation considering the location of the measuring region beyond $r/b \approx$ 0.6. The measured tangential velocities were therefore deemed not necessary to be included in the following results for ease of reading.

The magnitude of the RMS values of the sampled radial velocities exceeded the magnitude of the measured radial velocities by a factor of two typically. This level of fluctuations in the radial velocities could be the result of circulation flows within the cavity as characterised by Farthing et al. (1992a), or turbulence resulting from the interaction with the central throughflow. The magnitude of the RMS is seen to increase as Ro decreases, probably suggesting vortex breakdown occurring as the flow conditions become rotationally dominated.
The magnitude of the error due to probe orientation represents about 1% of the magnitude of the RMS of the flow measurement. Typical values are mentioned included in Fig 6.16 to 6.18.
Contour plots of the local measured radial velocities in Cavity 3 and 4 of Build 3 of the Multiple Cavity Rig were generated for easier interpretation of the results. The considered experimental conditions are detailed in Table 6.5, the first condition of which was previously described in Figures 6.16 to 6.18.

Condition	Test	$Re_\Phi/10^6$	$Re_z/10^5$	Ro	$\beta\Delta T_{av}$	$\beta\Delta T_{sh,C3}$	$Gr_{sh,C3}/10^7$
Condition 1	run38-1	0.40	1.57	7.51	0.067	0.22	3.3
Condition 2	Run40-1	0.39	0.61	2.98	0.107	0.24	3.4
Condition 3	Run44-1	1.99	1.65	1.58	0.004	0.11	37
Condition 4	Run39-1	1.93	0.53	0.53	0.001	0.08	25

Table 6. 5 Radial velocity measurements experimental conditions (Build3)

Figure 6.19 shows the radial velocity contour plot for Build 3, run38-1, Re_Φ=0.4x10^6, Re_z=1.57x10^5, Ro=7.51. The measurements points are shown as squares on the plot.

The radial velocity profiles in Cavity 3 show a central outflow region of peak magnitude $V_r \approx$ 0.2 m/s originating from the inner section of the cavity reaching up to r/b≈ 0.9. On the upstream side of Cavity 3 (about z/s= 0.1), a relatively strong radial inflow of velocity $V_r \approx$(-0.2) m/s is showing from r/b= 0.57, extending up to r/b= 0.68. At higher radii, the flow appears relatively quiescent with radial velocities decreasing to close to zero. The downstream side of Cavity 3 (by z/s= 0.95) shows a clear radial inflow region along the radial length of the measurement area, with a magnitude $V_r \approx$ (-0.1) m/s.

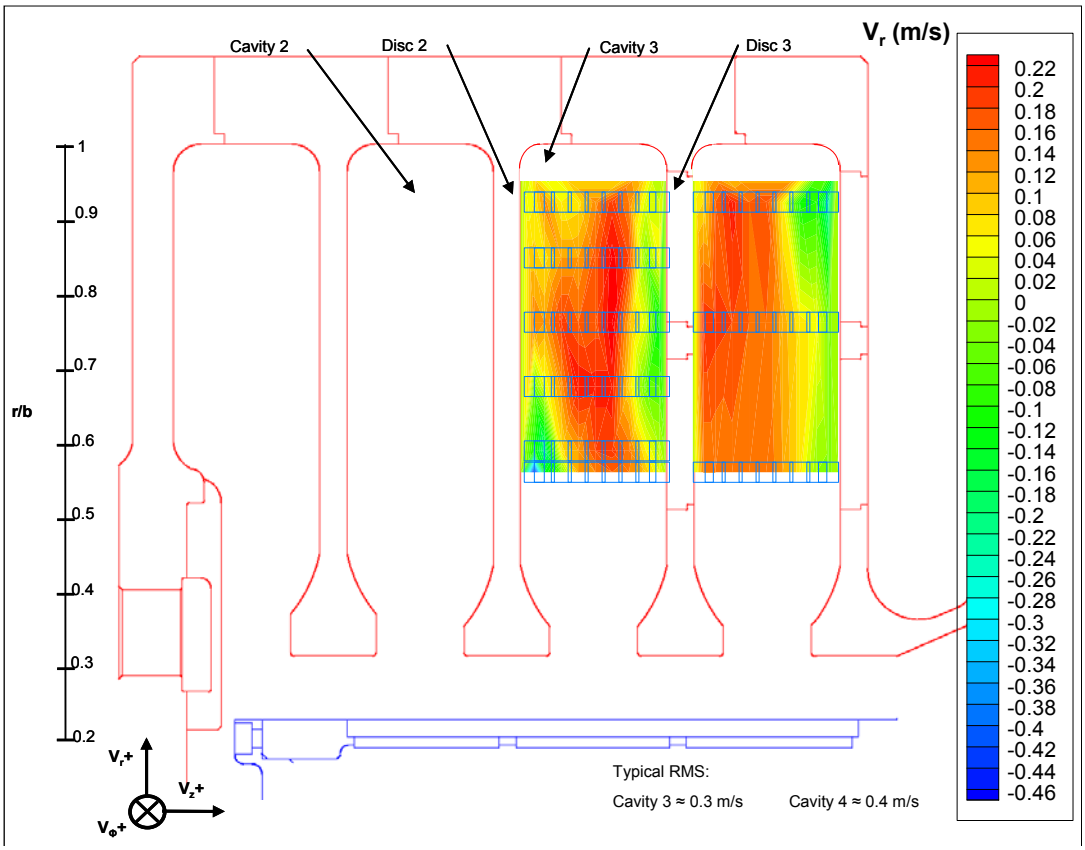

Fig 6. 19 Radial velocity contour plot for Build 3 run38-1, Re_Φ= 0.4 x 10^6, Re_z= 1.57 x 10^5 and Ro= 7.51

The measurements in Cavity 4 indicate a different radial flow pattern to Cavity 3, with a clockwise recirculation zone delimited by a radial outflow of $V_r \geq 0.15$ in the upstream axial portion of Cavity 4, between $0 \leq z/s \leq 0.6$, with the radial inflow region along the whole cavity measurement radii in the axial portion $0.6 \leq z/s \leq 1$, showing a magnitude of about V_r= (-0.1) m/s.

The radial velocity contours shown in Figure 6.20 for run40-1, Re_Φ= 0.39 x 10^6, Re_z= 0.61 x 10^5 and Ro= 2.98, show some clear similarities in their patterns when compared to the previous condition.

The difference between the condition in Figure 6.19 and the condition in Figure 6.20 lies in the axial throughflow being lower in the latter case, with an axial Reynolds number value of Re_z= 0.6 x 10^5 while the former case had a value nearly three times as much.

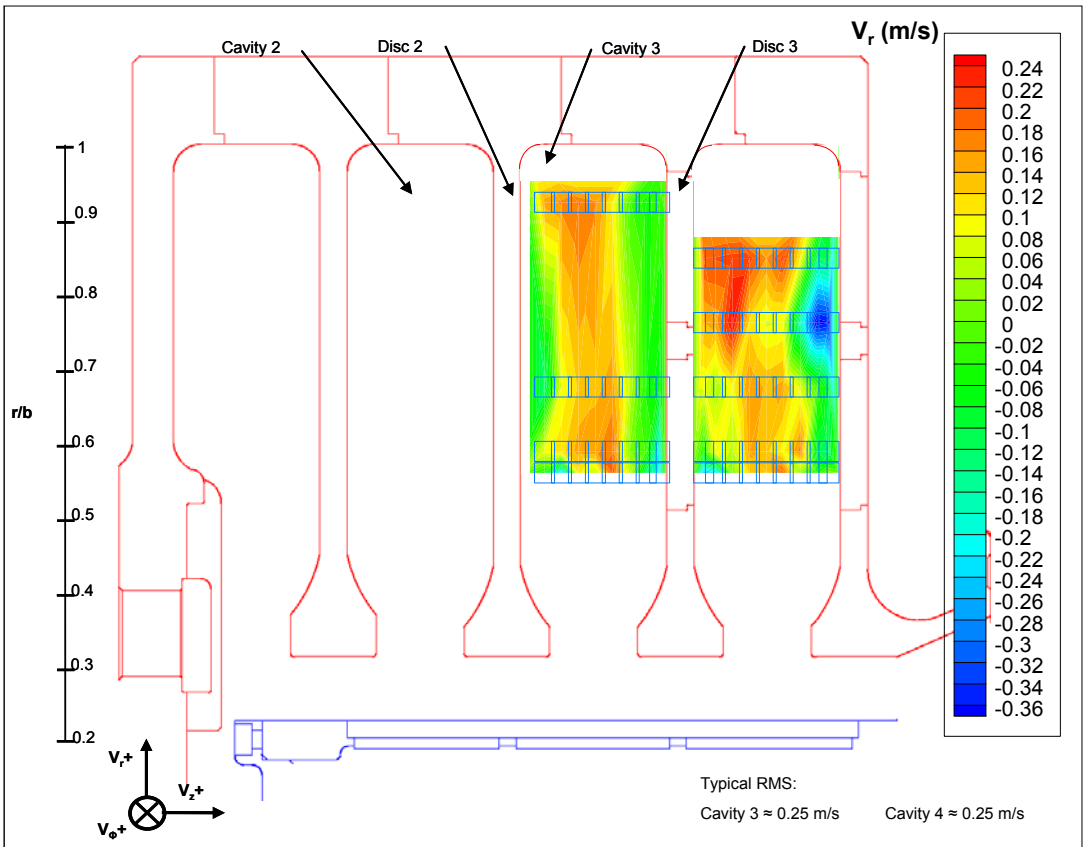

Fig 6. 20 Radial velocity contour plot for B3run40-1, Re_Φ= 0.39 x 10^6, Re_z= 0.61 x 10^5 and Ro= 2.98

The magnitude of the radial velocity component in both cavities in the condition featured in Figure 6.20 remains similar to the previous case, if somewhat slightly increased with a maximum of $V_r \approx$ 0.24 m/s and a minimum of $V_r \approx$ (-0.36) m/s. Cavity 3 shows a radial outflow region located in mid cavity between 0.396 ≤ z/s ≤ 0.629 of peak magnitude $V_r \approx$ 0.15 m/s at r/b=0.68. For W= 13.31 m/s, this corresponds to about 1.1 % of the throughflow velocity and about 1.1% of the solid-body tangential velocity at $r=b$ (Ωb=14.03 m/s). Radial inflow regions can be observed on the upstream and downstream side walls of Cavity 3, with magnitudes ≥ (-0.15) m/s by the inner radial part of the measurement region.

The radial velocity contours in Cavity 4 present a similar recirculation flow pattern to run38-1 (Re_Φ=0.4x10^6, Re_z=1.57x10^5, Ro=7.51). An outflow region is present in the upstream part of the cavity between 0 ≤ z/s ≤ 0.62 with flow velocities reaching values above $V_r \approx$ 0.2 m/s. The downstream part of the cavity features a radial inflow region of magnitude in excess of $V_r \approx$ (-0.2) m/s.

Comparing run38-1 (Fig.6.19) and run40-1 (Fig.6.20), it would appear that a reduction in axial Reynolds number affected the radial flows slightly in making the circulating flow regions somewhat weaker.

The radial velocity contour plots for run44-1, Re_Φ= 1.99 x 10^6, Re_z= 1.65 x 10^5 and Ro= 1.58 are shown in Figure 6.21.

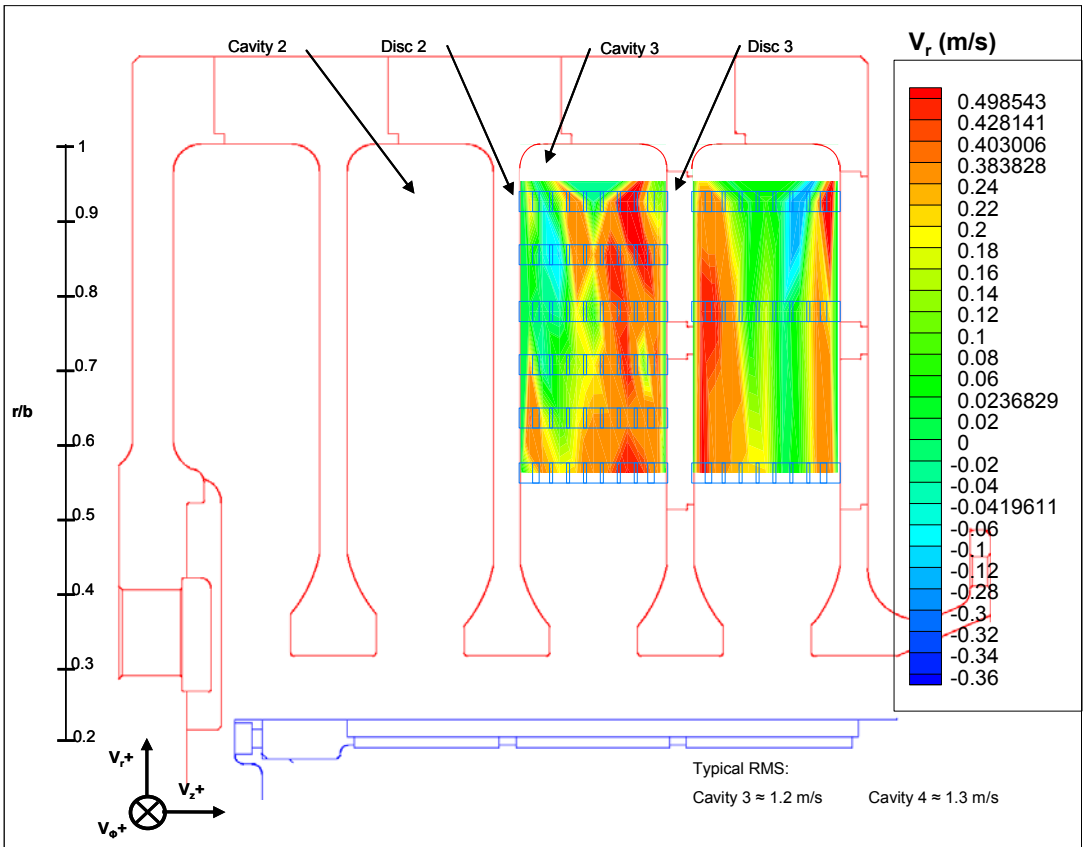

Fig 6. 21 Radial velocity contour plot for Build3, run44-1, Re_Φ= 1.99 x 10^6, Re_z= 1.65 x 10^5 and Ro= 1.58

Run38-1 (in Figure 6.19) and run44-1 (Fig. 6.21) were operated at similar values of Rez ≈1.6x10^5, but with a five-fold increase in rotational Reynolds number (Re_Φ=0.4x10^6 to Re_Φ=1.99x10^6 for run38-1 and run44-1 respectively). This resulted in a near doubling in radial velocity magnitudes from peak values of V_r≈ 0.22 m/s (run38-1) to V_r≈ 0.5 m/s (run44-1). Radial velocity patterns in Cavities 3 and 4 appear radically different from the patterns encountered in Conditions 1 and 2. However, the time averaged radial velocity results presented in Figure 6.19 could be misleading at first sight. A second look would suggest the evidence of axi-symmetric vortex breakdown (possibly of type IIa from the classification of Farthing et al. (1992a)) entering into both cavities. The

signs of direct throughflow impingement along the downstream disc walls of Cavities 3 and 4 can be seen from a radial outflow region of velocity $V_r \approx 0.4$ m/s occupying most of the cavities' radial lengths.

These could effectively offset or superimpose onto the radial inflow regions previously described on the downstream sides of Cavities 3 and 4.

The maximum peak measured radial velocity magnitude at r/b=0.78 in Cavity 3 was 0.42 m/s. This corresponds to 1.3 % of the bulk average throughflow velocity (W= 32.3 m/s) and about 0.7% of the solid-body tangential velocity at $r=b$ (Ωb=63.94 m/s). The radial flow pattern of Cavity 3 for this condition could therefore be described as a central region of radial outflow flanked by regions of radial inflows in the upstream and downstream sides of the cavity, with a downstream throughflow direct impingement resulting from vortex breakdown superimposing onto the cavity flow. Similarly in Cavity 4, the already described radial outflow in the upstream part of the cavity remains, with the vortex breakdown impingement flow superimposed on the downstream inflow region.

Figure 6.20 shows the radial velocity contours for Build 3, Run39-1, Re_Φ= 1.93x10^6, Re_z= 0.53x10^5 and Ro= 0.53, operated with a similar rotational Reynolds number than run44-1 (Re_Φ= 1.93 x 10^6), but with a lower axial throughflow (Re_z= 0.53 x 10^5) equivalent to run40-1. The associated Rossby number with this condition was Ro= 0.53. The magnitude of measured peak radial velocity in Cavity 3 at r/b=0.765 reached a value of 0.9 m/s, equivalent to about 7.4 % of the axial bulk velocity (W= 12.1 m/s), and about 1.2% of the solid-body tangential velocity at $r=b$ (Ωb=72.42 m/s).

The radial velocity profile of Cavity 3 suggests a similar central outflow region as observed on the previous conditions, with some relatively strong inflow regions (of magnitude $V_r \approx$ (-1) m/s) along the lengths of the upstream and downstream discs. The radial measurements in Cavity 4 indicate a clear outflow region in the part of the cavity between approximately $0 \leq z/s \leq 0.5$ along the cavity radius, and an inflow region in the downstream part of the cavity.

Considering the inflow regions in Cavity 3 measured adjacent to the shroud (at r/b=0.924) on figures 6.19 to 6.22, it can be noticed that as the Rossby number of the experimental conditions decreases, the magnitude of the inflow increases. This behaviour is summarised in Table 6.6 below and would be expected from buoyancy driven flow in this part of the cavity.

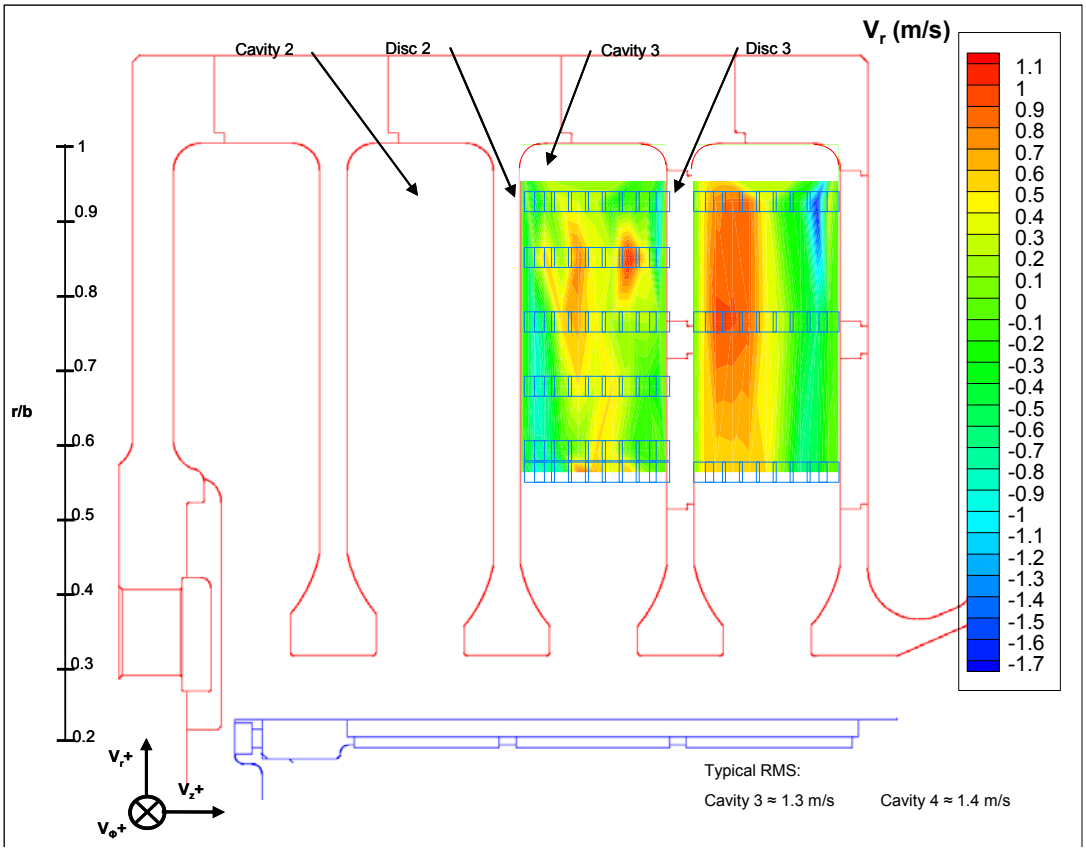

Fig 6. 22 Radial velocity contour plot for Build 3, run39-1, Re_Φ= 1.93 x 10^6, Re_z= 0.53 x 10^5 and Ro= 0.53

Test (Build 3)	$Re_\Phi/10^6$	$Re_z/10^5$	Ro	Cav3 peak radial inflow by shroud (m/s)
Run38-1	0.40	1.57	7.51	-0.02
Run40-1	0.39	0.61	2.98	0.05
Run44-1	1.99	1.65	1.58	0.05
Run39-1	1.93	0.53	0.53	0.89

Table 6. 6 Measured peak radial inflow in Build 3, Cavity 3, at r/b=0.924 for different experimental conditions (a negative value indicates an outflow velocity)

In the outer cavity region (at about r/b=0.75) , the magnitudes of the radial circulation flows appear to be related to the compound influence of the cavity rotation and the throughflow, with the velocity magnitudes generally increasing as Re_Φ increases, but also being impeded by an increasing Re_z. The measured peak radial velocity values in Cavity 3 previously mentioned in the test descriptions are summarised in Table 6.7.

Test (Build 3)	$Re_\Phi/10^6$	$Re_z/10^5$	Ro	Mid-Cav3 peak Vr (m/s)	Meas. at (r/b)	Ω (rad/s)	W (m/s)	Vr/Ωb	Vr/W
Run38-1	0.40	1.57	7.51	0.24	0.765	68.6	36.1	$1.59x10^{-2}$	$6.65x10^{-3}$
Run40-1	0.39	0.61	2.98	0.15	0.68	63.8	13.3	$1.07x10^{-2}$	$1.12x10^{-2}$
Run44-1	1.99	1.65	1.58	0.42	0.78	290.7	32.3	$6.57x10^{-3}$	$1.30x10^{-2}$
Run39-1	1.93	0.53	0.53	0.9	0.765	329.2	12.1	$1.24x10^{-2}$	$7.44x10^{-2}$

Table 6. 7 Cavity radial relative velocity magnitudes

6.3 Spectral analysis of the tangential velocity component

A frequency spectrum analysis was carried out on the tangential velocity component measured data from the experimental configuration measuring simultaneous radial and tangential velocity components in Build 3 of the Multiple Cavity Rig. The experimental conditions were the same as previously described in Table 6.5. The frequency spectrum analysis operates in determining the natural frequencies in the succession of the collected velocity samples values over the measurement time. Following the frequency spectra analysis of Owen and Powell (2004), a Fast Fourier Transform algorithm was employed in the determination of the flow frequency characteristics as described in Chapter 3. The results were displayed in a power spectrum diagram representing the relative dominance of a frequency over the spectrum of analysis.

Figure 6.23 shows a series of power spectra diagrams for the measurement points located mid Cavity 3 (z/s= 0.5) at different radii.

The experimental condition of the results shown in Figure 6.23 was Re_Φ= 0.4 x 10^6, Re_z= 1.57 x 10^5 and Ro= 7.51. The rotational speed of the cavity was 655 rev/min; corresponding to a cavity rotational frequency of 10.92 Hz. Looking at the dominant spikes at the different radii plots, a broad interpretation on the recirculation pattern in view of the current understanding of heated cavity flow behaviour from Farthing et al. (1992a) would indicate the presence of a pair of contra rotating vortices (when a spike is about at the frequency of the cavity rotation assuming the tangential flow is near solid body rotation) between 0.765 ≤ r/b ≤ 0.924, blending into two pairs of contra rotating vortices between 0.566 ≤ r/b ≤ 0.765. Another interpretation could suggest a pair of vortices at higher radii (in the region 0.851≤ r/b ≤ 0.924) and a pair at lower radii (0.56≤ r/b ≤ 0.595) intersecting each other in between (region 0.68≤ r/b ≤ 0.763), resulting in the doubling of frequency seen. The presence of secondary spikes in the power spectrum diagrams at dominant frequencies of roughly multiples of the cavity rotational frequency could be explained from the simulations of Owen et al. (2006) and Sun et al. (2006), observing the ever changing nature over time of the cavity vortex structure in a heated cavity with axial throughflow. The laser

Doppler measurements resulting in the spectrum values shown in Figure 6.23 were, by nature of the measuring technique, taken over a certain length of time, sometimes in tens of seconds, therefore the information provided by the spectra determined for each location might be incomplete and moreover the relation between each location might also be non-representative of the flow as measured at different times from each other. The re-sampling method employed for the spectral analysis of velocimetry data taken across the rotor windows was also inducing a reduced time density of the data (as discussed in Chapter 4) which would undermine the accuracy of the analysis greatly as aliasing of the re-sampled data would be very likely to occur during the Fourier analysis.

Bearing this in mind, the frequency spectra produced over the experimental conditions showed some broadly similar characteristics to as described above and can be seen in Appendix 6.5.

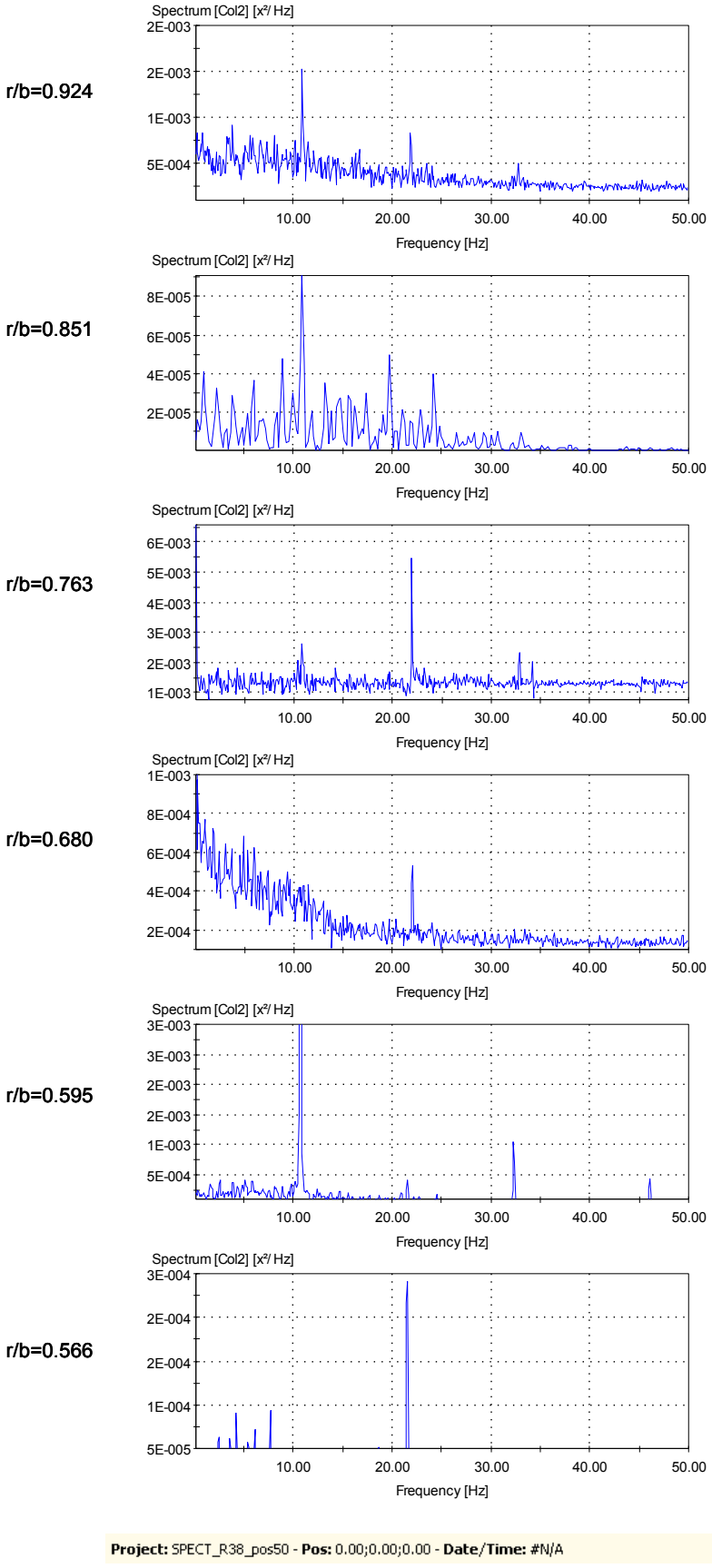

Fig 6. 23 Tangential velocity power spectra on mid-plane of Cavity 3 for Build 3, run38-1, Re_Φ= 0.4 x 10^6, Re_z= 1.57 x 10^5 and Ro= 7.51

7. Heat transfer results

This chapter presents the heat transfer measurement results for Build 2 and Build 3 of the Multiple Cavity Rig. The main difference and measurement capability of Build 2 and Build 3 are recapped in Table 7.1 below.

All the measured heat transfer data cases were processed into detailed test reports for ease of archiving and analysis. The list of all experiments, operating conditions and main non-dimensional results can be found in Appendices 6.2 and 6.3. From this list, the Reader can select a test of interest and consult the detailed results report in the attached CD-Rom following the instructions in Appendix 6.1. For convenience of reading, the reports of the specifically mentioned tests in this chapter are also included in Appendix 7.1.

	Build 2	**Build 3**
Annular gap	0.092	0.164
Heat transfer measurement	Disc, shroud	Disc, shroud
LDA measurement	VΦ, Vz	VΦ, Vz and VΦ, Vr

Table 7. 1 Principal operational differences between Build 2 and Build 3 of the Multiple Cavity Rig

Table 7.2 summarises the range of experimental conditions performed for the velocity measurements on Build 2 and Build 3 of the Multiple Cavity Rig. By comparison, typical engine values for cruise operation may be taken as $Re_\Phi = 7.7x10^6$ and $Re_z = 2.4x10^5$ (Alexiou 2000). The experimental data reported here has been obtained over a range of values overlapping both real engine conditions and also those used by authors of previous research in this field as shown in Fig. 2.17.

Parameter		Build 2 heat transfer	Build 3 heat transfer
Rotor speed	Ω (rad/s)	$57 \le \Omega \le 615$	$65 \le \Omega \le 608$
Cooling air flow rate	$\dot{m}$ (kg/s)	$0.164 \le \dot{m} \le 0.8$	$0.16 \le \dot{m} \le 0.75$
Inlet pressure	p_{in} (bar, abs)	$2.2 \le p_{in} \le 3.16$	$2.3 \le p_{in} \le 3.7$
Inlet temperature	T_{in} (K)	$309 \le T_{in} \le 324$	$302 \le T_{in} \le 339$
Disc average surface temperature	$T_{s,av}$ (K)	$328 \le T_{s,av} \le 351$	$321 \le T_{s,av} \le 353$
Shroud average surface temperature	T_{sh} (K)	$359 \le T_{sh} \le 407$	$353 \le T_{sh} \le 386$
Disc rotational Reynolds number	Re_{Φ} (Eq. 4.1)	$4 \times 10^5 \le Re_{\Phi} \le 5 \times 10^6$	$4.7 \times 10^5 \le Re_{\Phi} \le 5 \times 10^6$
Axial Reynolds number	Re_z (Eq. 4.2)	$4.2 \times 10^4 \le Re_z \le 1.9 \times 10^5$	$4.3 \times 10^4 \le Re_z \le 2 \times 10^5$
Rossby number	Ro (Eq. 4.3)	$0.29 \le \mathrm{Ro} \le 8.6$	$0.53 \le \mathrm{Ro} \le 7.51$
Disc buoyancy parameter	$\beta\Delta T_{av}$	$0.04 \le \beta\Delta T_{av} \le 0.13$	$0.017 \le \beta\Delta T_{av} \le 0.09$
Shroud buoyancy parameter	$\beta\Delta T_{sh}$ (Eq. 4.20)	$0.14 \le \beta\Delta T_{sh} \le 0.302$	$0.086 \le \beta\Delta T_{sh} \le 0.238$
Shroud Grashof number	Gr_{sh} (Eq. 4.20)	$3.8 \times 10^7 \le Gr_{sh} \le 4.5 \times 10^9$	$4 \times 10^7 \le Gr_{sh} \le 3.1 \times 10^9$

Table 7. 2 Range of heat transfer experimental conditions for Build 2 and Build 3 of the Multiple Cavity Rig

7.1 Disc heat transfer

Figures 7.1 and 7.2 show examples of discs temperature measurements in Build 3 of the Multiple Cavity Rig plotted against the non-dimensional radius (r/b) for operating conditions of Re_Φ= 4.12x10^6 , Re_z= 1.16x10^5, Ro=0.54 , $\beta\Delta T_{av}$= 0.03 and Re_Φ= 0.49x10^6 , Re_z= 0.92x10^5, Ro= 3.56 , $\beta\Delta T_{av}$= 0.09 respectively. The thermocouples on the discs and shroud are shown as symbols on the plots, with their respective measurement uncertainty (calculated from the method in 5.1.2) are displayed as “error bars”. A profile of the disc shape is included above the horizontal axis for reference. The fitted temperature profiles used for the disc heat transfer calculations (section 4.2) are displayed as dotted lines. From Figs 7.1 and 7.2 it can be seen that the stability of thermocouples measurement is good and that there is a relatively small temperature difference across the axial thickness of the discs.

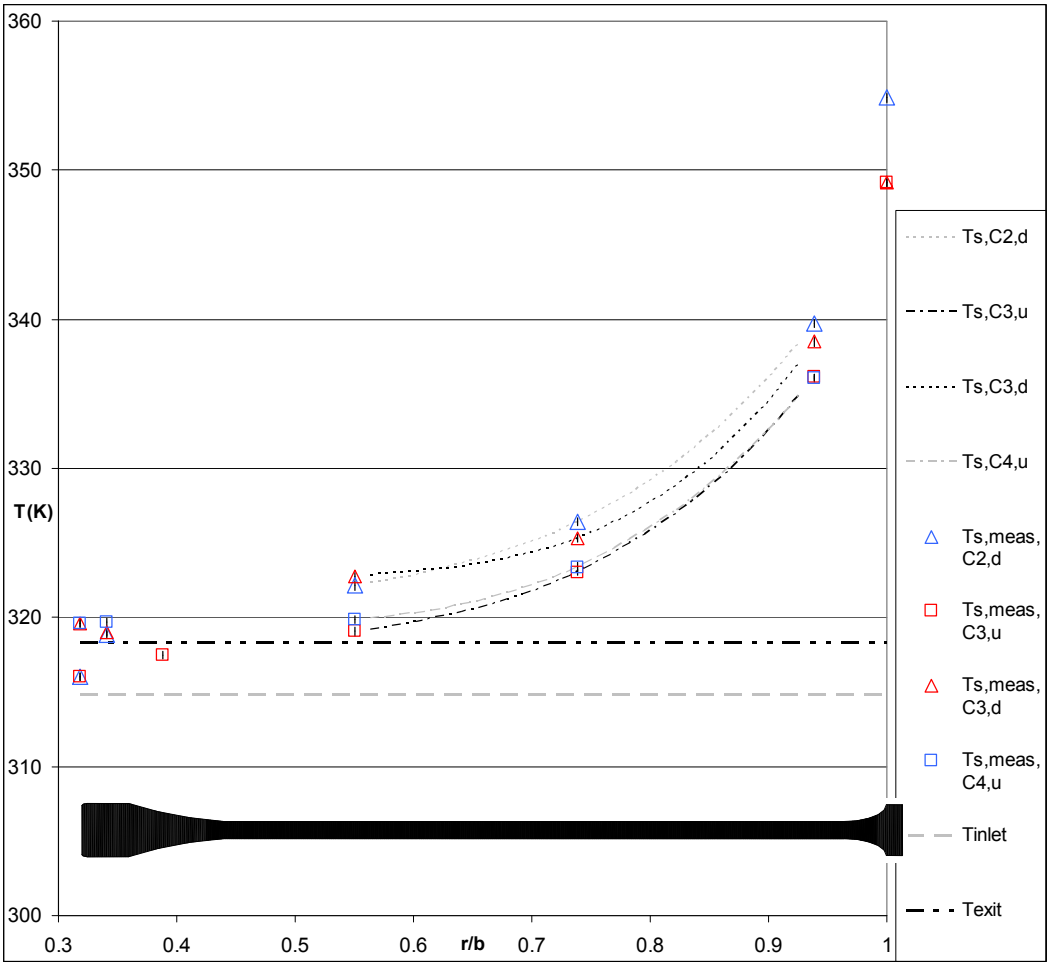

Fig 7. 1 Disc temperature measurements in Build 3 for run28-1, Re_Φ= 4.12x10^6 , Re_z= 1.16x10^5, Ro=0.54 and $\beta\Delta T_{av}$= 0.03

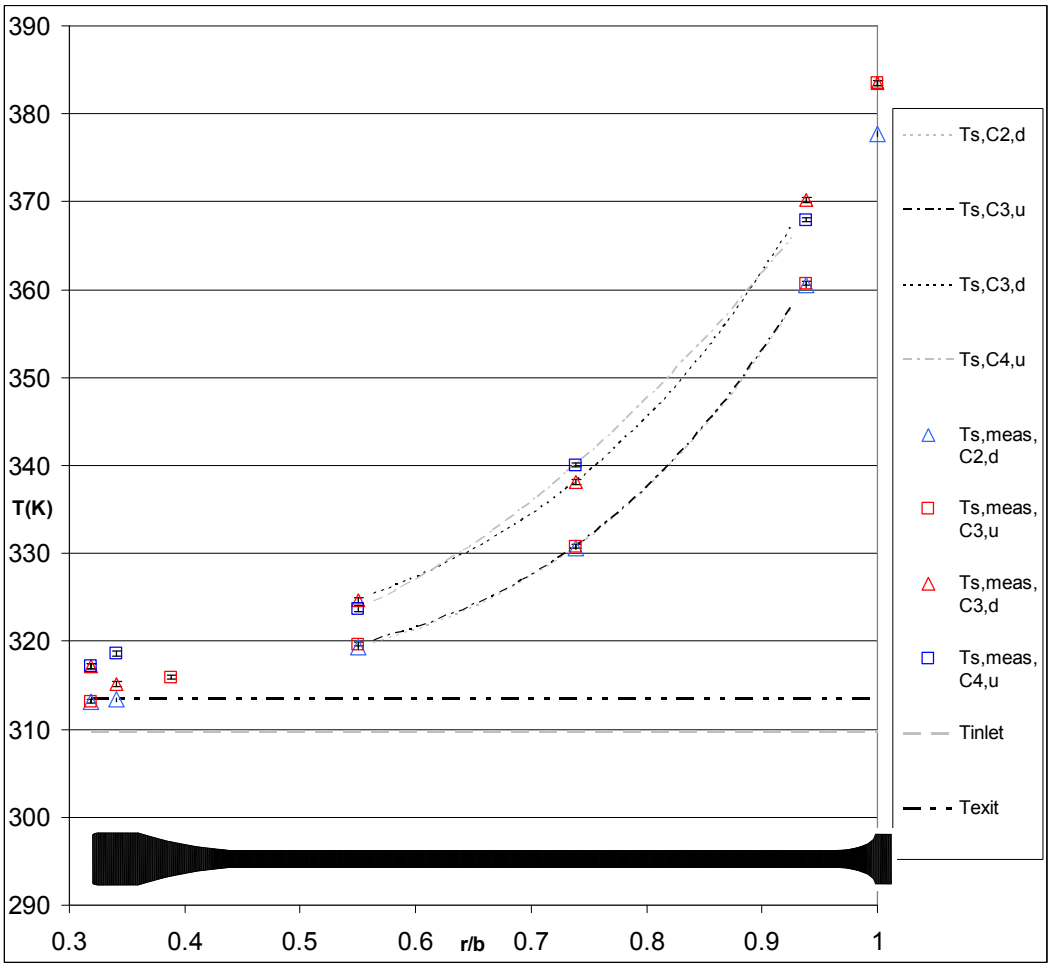

Fig 7. 2 Disc temperature measurements in Build 3 for run32-1, Re_{Φ}= 0.49x10^6 , Re_z= 0.92x10^5, Ro=3.56 and $\beta\Delta T_{av}$= 0.09

As explained in Chapter 5, the heat transfer results from the fin solution appear in better relation with a heat transfer behaviour involving heat conducted out of the discs (although no differentiation from the discs surfaces can be made due to the adiabatic mid-plane assumption) and with magnitude levels more in relation with relatively low cavity air velocities as illustrated in Figure 7.3 for Build 2 and Build 3 when compared to correlations for forced convection flow over a flat plate (from Long, 1999). A comparison with correlations for a free disc rotating in quiescent air from Dorfman (1963) is also included in Fig 7.4.

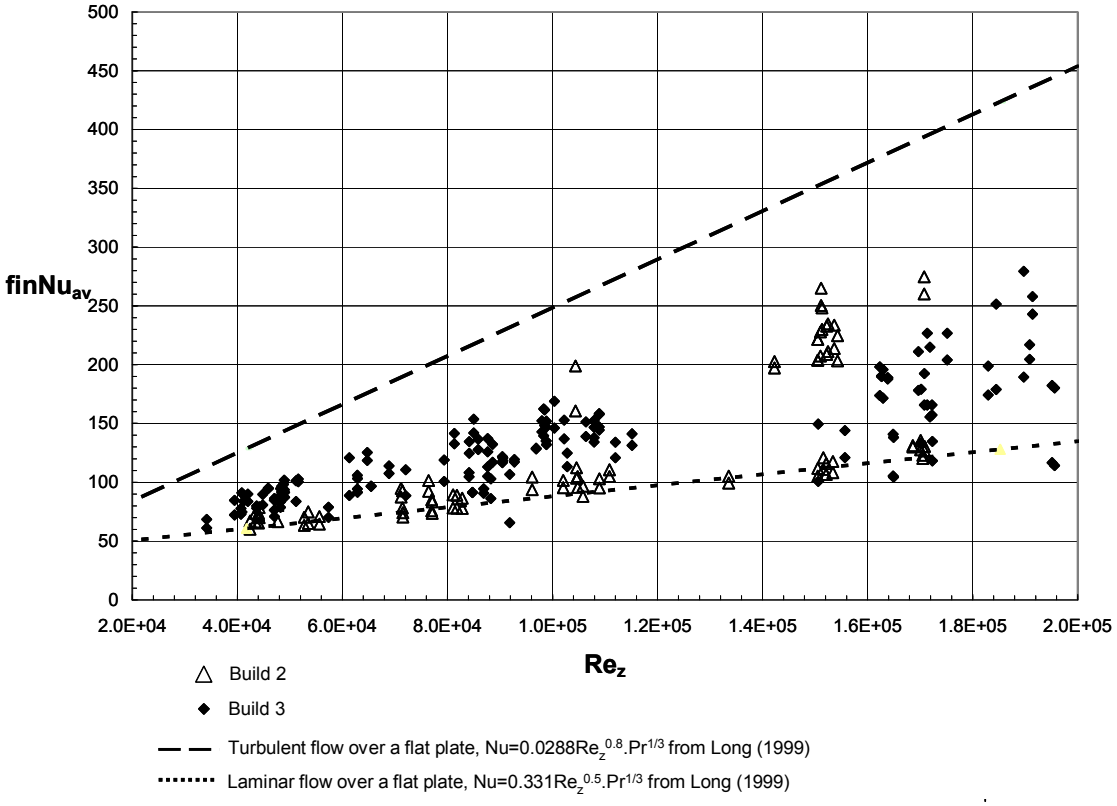

Fig 7. 3 Average disc Nusselt number from the fin solution for Build 2 and Build 3 (all data) compared with correlations of forced convection over a flat plate

An overall check of the estimated values of cavity heat transfer from the fin solution was performed by comparing the measured temperature rise of the cooling air across the rig against a calculated value of temperature rise resulting from the contribution of discs and shrouds heat transfer. The rig's energy balance was expressed on the principle that the total convective heat transfer from the disc and shroud surfaces is equal to the change of enthalpy of the cooling air, neglecting viscous dissipation and heat transfer to/from the shaft:

$$\dot{m}\cdot Cp\left(T_{exit}-T_{inlet}\right)=n_{sh}\cdot Q_{sh}+n_{df}\cdot Q_{df} \qquad \text{Eq.7.1}$$

hence

$$\Delta T=\left(T_{exit}-T_{inlet}\right)=\frac{\pi\cdot k}{\dot{m}\cdot \mathrm{Cp}}\left[\left\{4\cdot b\cdot n_{sh}\left(T_{sh}-T_{in}\right)\cdot Nu_{sh}\right\}+\left\{\frac{\left(b^2-a^2\right)}{b}n_{df}\left(T_{s,av}-T_{in}\right)\cdot Nu_{av}\right\}\right] \qquad \text{Eq.7.2}$$

Where n_{sh} is the number of shroud surfaces in the rig (4), n_{df} is the number of disc faces (8), Nu_{sh} is the mean of the calculated shroud Nusselt numbers (Eq.

4.18) in Cavities 2 and 3, Nu_{av} is the mean of the discs average Nusselt numbers (defined in Eq. 4.13) and $T_{s,av}$ is the mean value of the average disc surface temperatures for Disc 2 and 3.

The temperature differences between the measured and calculated values are plotted in Figure 7.5 for different values of Ro.

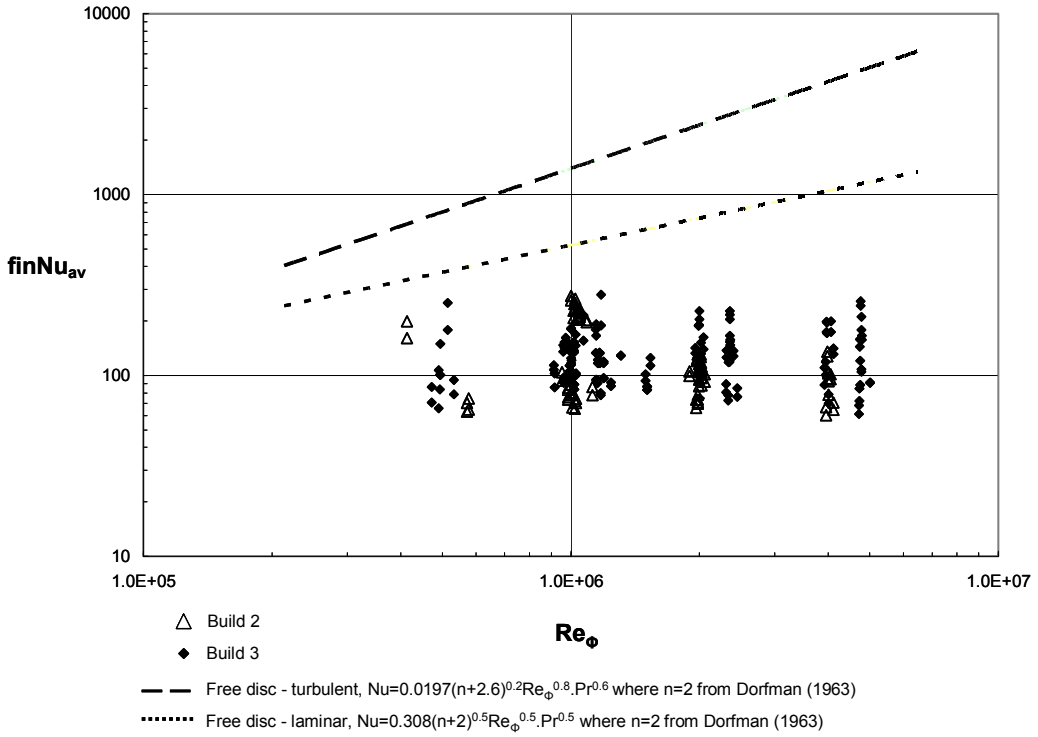

Fig 7. 4 Average disc Nusselt number from the fin solution for Build 2 and Build 3 (all data) compared with correlations for a free disc

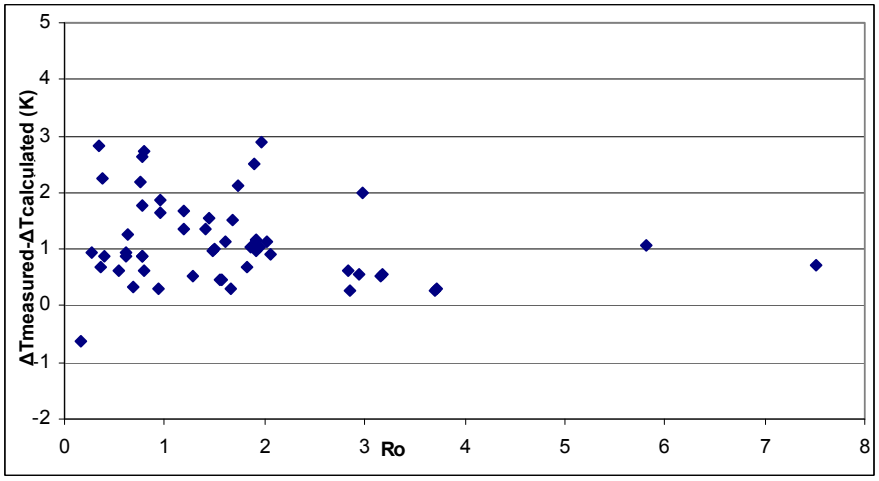

Fig 7. 5 Differences of measured rig temperature rise and calculated temperature rise with Rossby number

Figure 7.5 indicates that the calculated values of temperature difference across the rig are generally less than measured (as not taking into account all of the rig's surfaces participating into the energy balance) and are acceptable with the measured values, giving some level of confidence on the averaged Nusselt numbers of the fin solution to give an acceptably accurate indication of the overall heat transfer behaviour. The heat transfer results to follow will therefore be expressed from the results of the fin solution method and as average values as Discussed in Chapter 5.

The variation of average Nusselt number with axial Reynolds number for Build 2 (narrow annular gap) and for various values of rotational Reynolds number (Re_Φ= 0.5 x 10^6, 10^6, 2 x 10^6 and 4x10^6), is shown in Figure 7.6. Average values of Nusselt number are shown for both Disc 2 and Disc 3 and there appears to be little significant difference between the two discs. There also appears to be a clear trend – increasing the axial Reynolds number increases the average Nusselt number.

For the larger values of axial Reynolds number (Re_z > 10^5) and the lower values of rotational Reynolds number (Re_Φ < 10^6), i.e. the largest values of Rossby number, this increase is more noticeable. There is some evidence, at Re_z < 10^5, to suggest that increasing the rotational Reynolds number increases the average Nusselt number and the results for Re_z > 10^5 suggest the opposite is true as increasing Re_Φ actually decreases the Nusselt number. This is consistent with the findings of Bohn et al. (1994), who also noted a similar attenuating effect due to the Coriolis acceleration.

A corresponding plot, but for Build3 (wide annular gap) is shown in Figure 7.7. The overall impression is that for the same value of Re_z and Re_Φ, the average Nusselt number from the disc surface is increased by increasing the size of the annular gap between the shaft and disc bore.

The behaviour shown in Figure 7.6 for Build 2, where at the larger values of Re_z increasing Re_Φ actually decreases the Nusselt number does not seem to occur with the wide annular gap. This and the higher overall level of heat transfer are caused by the difference in geometry. Equal values of Re_z imply that the average velocity of the throughflow is lower in the wider annular gap.

Consequently there will be a greater tendency for the flow to penetrate the cavity and interact with the disc surfaces. If this is the case, then a greater sensitivity to the rotational Reynolds number may be expected to be shown in Figure 7.7 (Build 3) compared to Figure 7.6 (Build 2). It is possible that this is reflected in the data but the results are far from conclusive. It is worth reminding that the LDA measurements in Chapter 6 made in this test rig show a significant difference in the distribution of tangential velocities between Build 2 and Build 3.

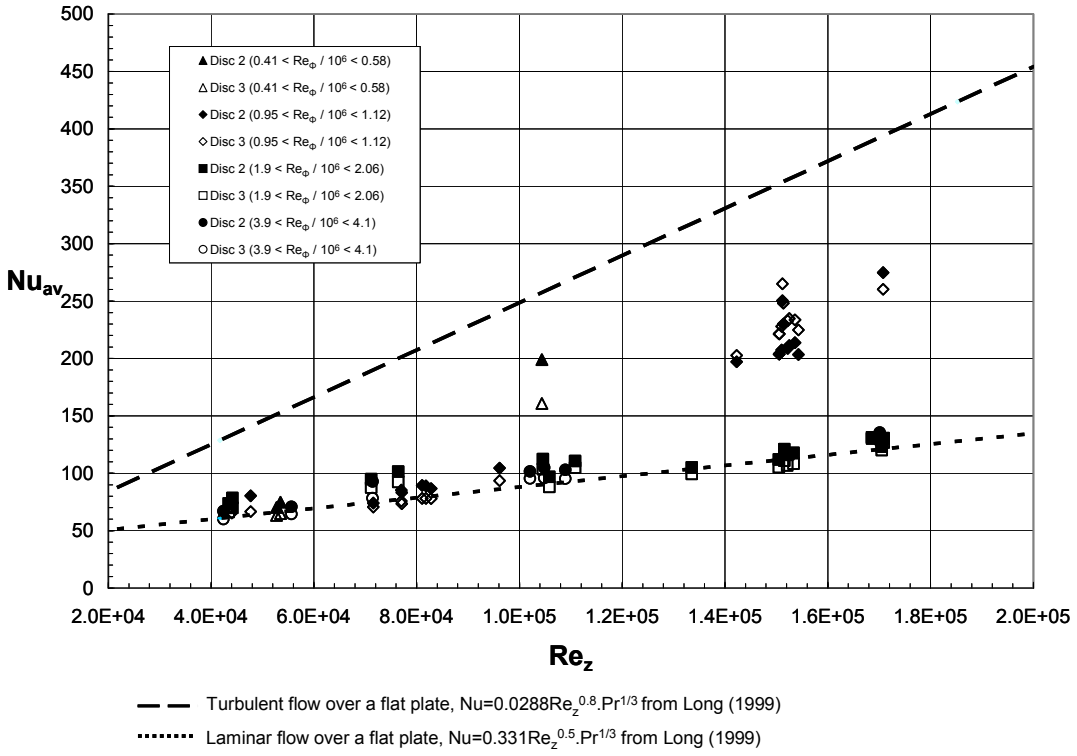

Fig 7. 6 Build 2, variation of Nu_{av} with Re_z for various values of Re_Φ

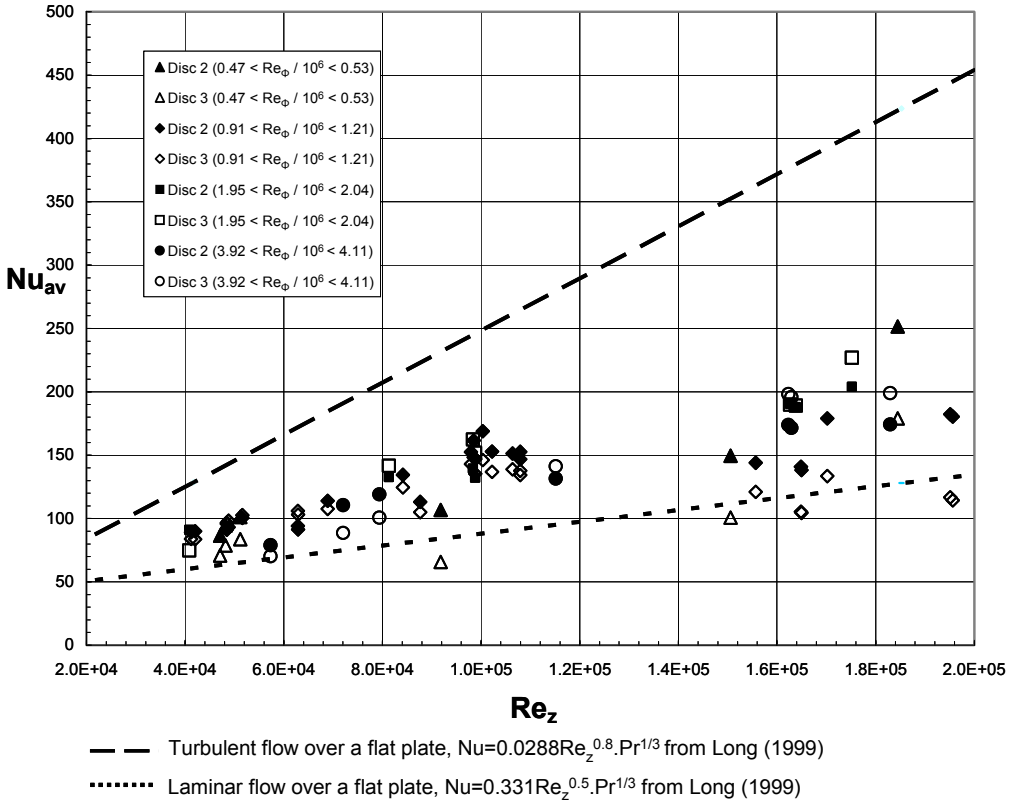

Fig 7. 7 Build 3, variation of Nu_{av} with Re_z for various values of Re_Φ

Figure 7.8 shows a plot of average Nusselt numbers against Rossby number for Build 3, Disc 2 and Disc 3. The heat transfer in Disc 3 tends to be greater than Disc 2 for operating conditions of $Ro \leq 2$, while the trend seems reversed for values of $Ro \geq 2$. This could be attributed to differences in flow structures affecting the discs faces that vary with operating conditions.

From the preceding discussions, it is apparent that a simple plot of average Nusselt number against axial Reynolds number does not adequately represent trends in the heat transfer data. A number of attempts have been made at correlating the average Nusselt numbers and the most promising of these is shown in Figure 7.10 for Build 2 and Figure 7.9 for Build 3. In both cases the parameter $Nu_{av} / Re_{\Phi}^{1/2}$ is plotted against the Rossby number. It is worth noting here that a previously used parameter, the buoyancy number ($Ro/(\beta\Delta T_{av})^{0.5}$ – see Alexiou 2000), had also been used in the past. This differs from the Rossby number through the inclusion of the dimensionless temperature $\beta\Delta T_{av}$ in the

buoyancy number. The Rossby number has been chosen for use here as this was found to give a small reduction in the scatter of the data. The parameter $\beta\Delta T_{av}$ was varied in the presented experiments ($0.04 < \beta\Delta T_{av} < 0.13$ in Build 2 and $0.017 < \beta\Delta T_{av} < 0.09$ in Build 3) but not in any systematic sense. Further work is therefore required to establish the relevance of this parameter in characterising the disc heat transfer results.

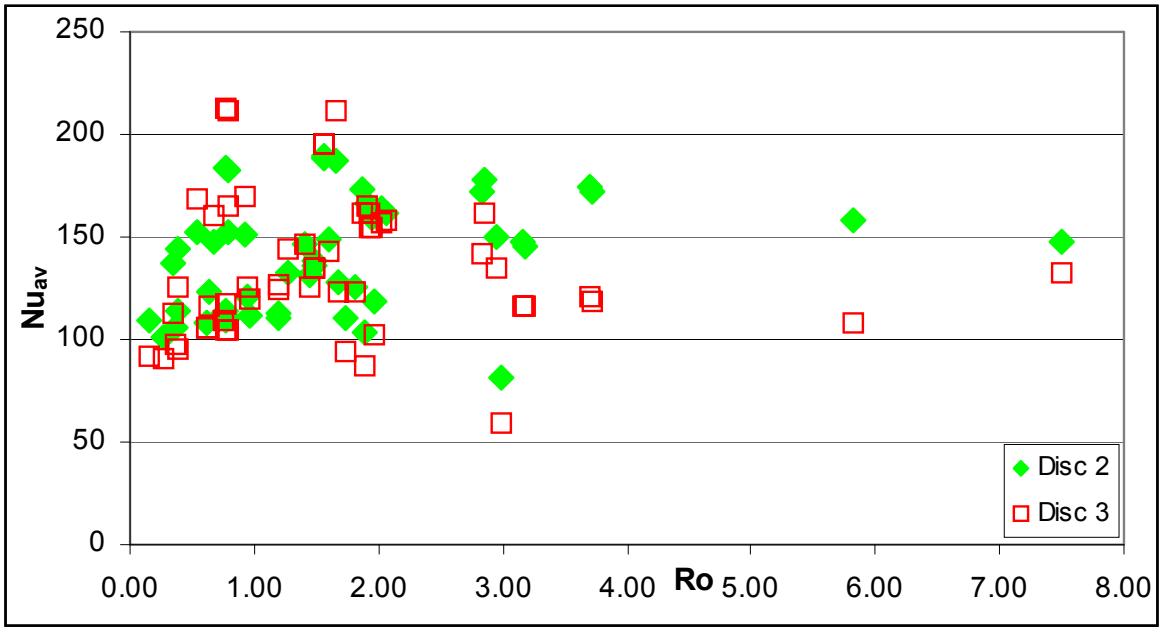

Fig 7. 8 Variations of Nu_{av} in Build 3 for Disc 2 and 3 with Ro

Correlation attempts on the average Nusselt numbers of Build 3 resulted in a good data collapse for $Nu_{av}/Re_{\Phi}^{0.5}$ against Ro as shown in Figure 7.9.

The average Nusselt number values for both discs showed to follow the relationship below for values of $Ro \leq 2$ but appeared more scattered at higher values of Ro.

$$\frac{Nu_{av}}{Re_{\phi}^{0.5}} \approx 0.1 \times Ro^{0.5} \qquad \text{Eq. 7.3}$$

From Eq. 7.3, since $Nu_{av} / Re_{\Phi}^{0.5} \propto Ro^{0.5}$, then $Nu_{av} \propto Re_z^{0.5}$ suggesting laminar forced convection.

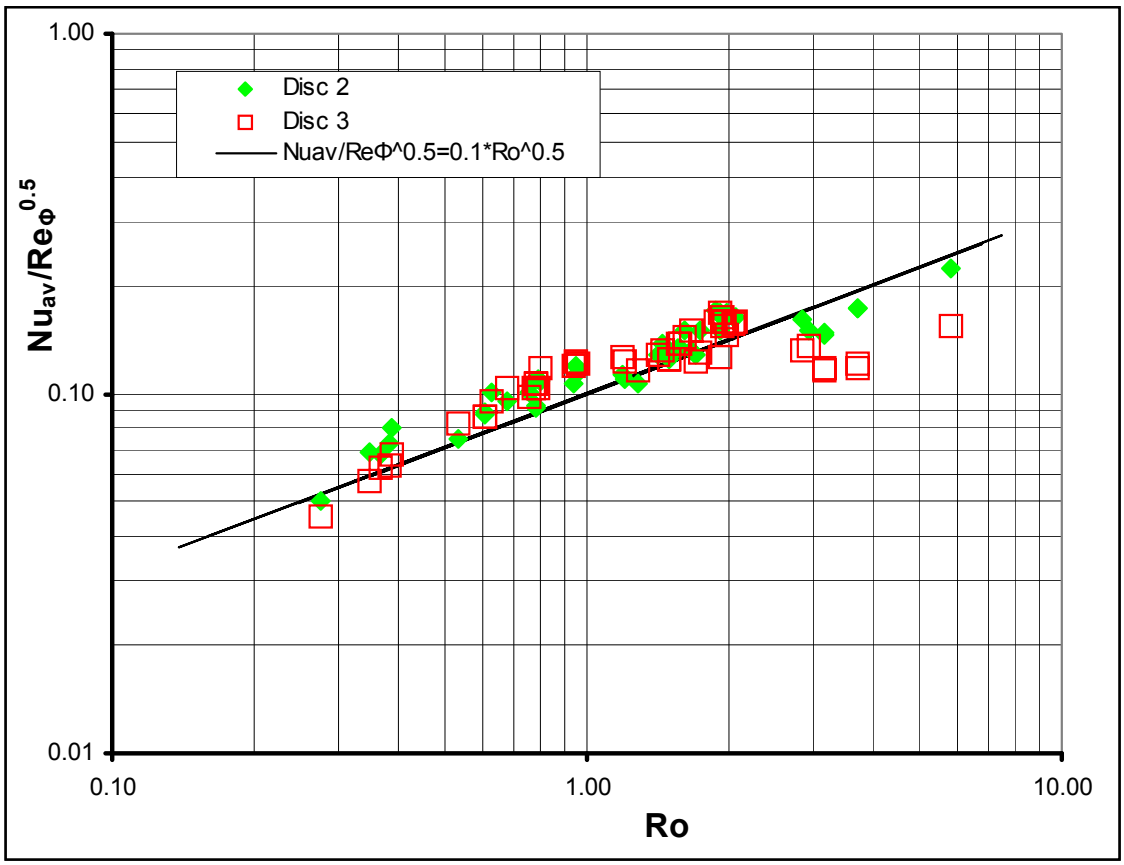

Fig 7. 9 Variations of $Nu_{av}/Re_{\Phi}^{0.5}$ against Ro for Disc 2 and 3 in Build 3 with Ro

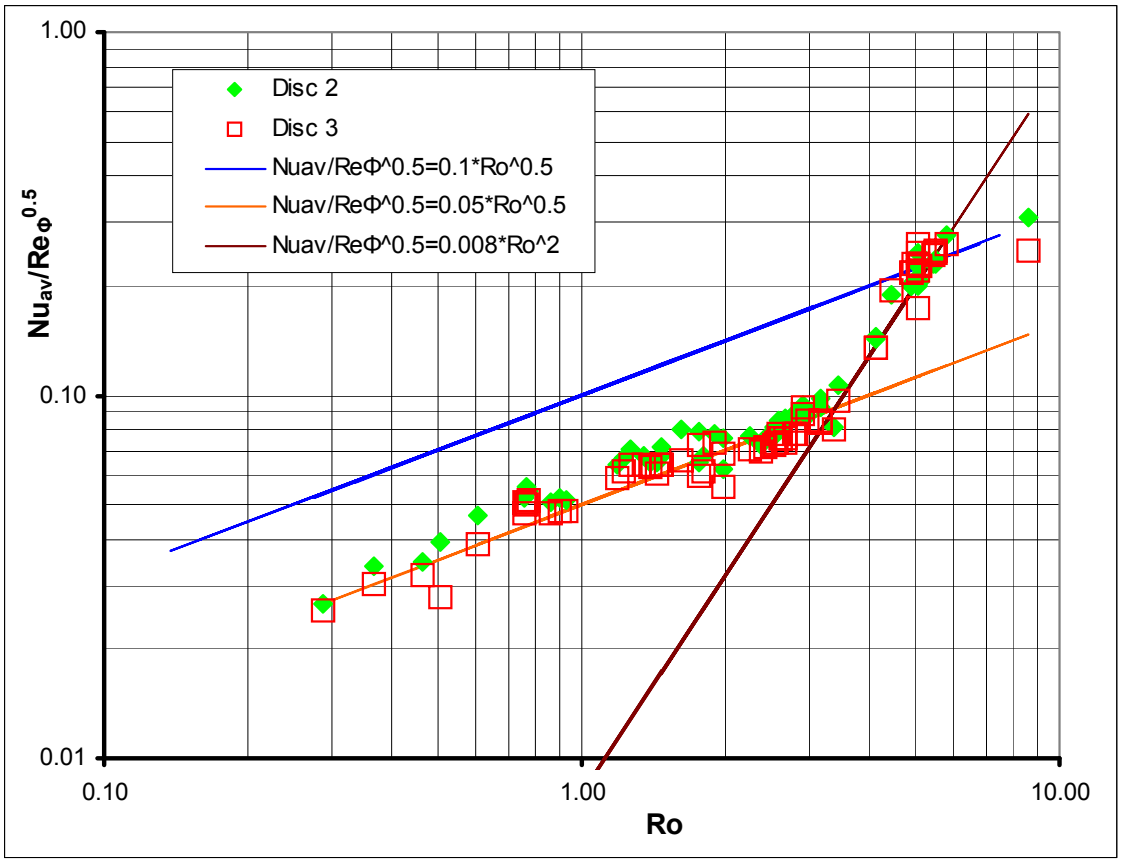

Fig 7. 10 Variations of $Nu_{av}/Re_{\Phi}^{0.5}$ against Ro for Disc 2 and 3 in Build 2 with Ro

On the average Nusselt number plot for Build 2 (Fig 7.10), there appears to be two different 'regimes': 1) 0.3 < Ro < 3, and 2) Ro > 3. In the first of these, since $Nu_{av} / Re_{\Phi}^{0.5} \propto Ro^{0.5}$, then $Nu_{av} \propto Re_z^{0.5}$ suggesting laminar forced convection as for Build 3, following a relationship close to:

$$\frac{Nu_{av}}{Re_{\phi}^{0.5}} \approx 0.05 \times Ro^{0.5} \qquad \text{Eq. 7.4}$$

In the second 'regime', for Ro > 3, an increase in Nu_{av} can be observed, following a relationship close to:

$$\frac{Nu_{av}}{Re_{\phi}^{0.5}} \approx 0.08 \times Ro^{2} \qquad \text{Eq. 7.5}$$

For Build 2, since $Nu_{av} / Re_{\Phi}^{0.5} \propto Ro^2$, then $Nu_{av} \propto Re_z \,.\, Re_{\Phi}^{0.5}$. This is consistent with a flow which is mainly affected by the axial throughflow rate at large values of Rossby number and this sensitivity diminishes as the Rossby number (and inertial effects) is reduced. The differing influence of the rotational Reynolds number previously noted on Figure 7.7 is also evident in these two relationships.

Differences in magnitudes of Nu_{av} for Build 2 and 3 could be explained from the observations of Alexiou et al. (2000) in Build 1 of the Multiple Cavity Rig, which central shaft could be co-rotated or contra-rotated relative to the rotor direction. Co-rotating operation resulted in greater heat transfer values through the rig than contra-rotating conditions. Considering the tangential velocity profile of the throughflow under the discs of Build 2 and 3, Build 3, with its wider annular gap would present a tangential velocity shear profile lower than the narrow annular gap at same flow and rotational conditions. Therefore, making a parallel with the co-rotating condition increase of Nu_{av} on Build 1, it could be justified that Build 3's average Nusselt number values should be greater than Build 2 at similar conditions due to the lower tangential velocity shear profile of the throughflow by the shaft affecting the influence of the axial throughflow on the flow inside the cavity.

It is appropriate here to comment on similarities and differences between the heat transfer results from various test rigs with axial throughflow. The earlier

work on single cavities (G = 0.13, a/b = 0.1 and an unheated shroud) by Farthing et al. (1992b), showed the heat transfer from the discs to be consistent with free convection. Long (1994) found that the disc heat transfer (G = 0.13 and 0.36, a/b = 0.1, heated and unheated shroud) was influenced by both forced and free convection effects. The results presented here seem to contradict these earlier findings. There is little evidence to suggest that the disc heat transfer is affected by buoyancy driven flow and is, in fact, mostly influenced by forced convection effects. This can be reconciled by the following. It is clear that the shroud has an influence on the flow in the cavity. For an unheated shroud and with a narrow cavity and small inlet radius ratio (as in the work of Farthing et al. 1992b), heating the discs creates buoyancy forces which destabilise the throughflow, and the narrow gap suppresses forced convection effects. For a wider gap ratio (as in the work of Long 1994), forced convection does affect the flow in the cavity. In both these cases, the maximum disc surface temperature was comparable to the shroud temperature, with values of the buoyancy parameter based on the average disc surface temperature of $\beta\Delta T_{av}$ ~ 0.25. So, even in the wider gap ratio cavity, buoyancy driven effects occur towards the outer radius of the discs. The disc heating pattern on the Multiple Cavity Rig is quite different to that on the earlier single cavities. The maximum disc temperature is around 25K less than the shroud temperature and typical values of the buoyancy parameter are in the range: $0.02 < \beta\Delta T_{av} < 0.1$. The gap ratio at G ~ 0.2 is also significantly larger than the earlier single cavity work that so clearly indicated free convection on the discs. Taking into consideration all these factors, and the presence of a shaft at a relatively large radius ratio, it is not surprising that there is little evidence of buoyancy driven heat transfer behaviour on the disc surfaces of the Multiple Cavity Rig. It is however suggested that it may well occur. With improved spatial resolution of the surface temperature measurements, and more confidence in the heat transfer data, it may be possible to notice this behaviour towards the outer radius of the cavities in the future.

7.2 Shroud heat transfer

A parallel investigation on the shroud heat transfer in the series of Multiple Cavity Rigs was performed by Long and Childs (2007) from experimental data derived from the current work. A one dimensional radial conduction method was used to determine the heat transfer characteristics of the shroud, which is believed to provide better accuracy of results than from the disc heat transfer methods because of the lack of bias introduced by surface temperature fitting. Therefore in order to help understand the heat transfer in rotating cavities with axial throughflow, Long and Childs' observations ought to be described below.

It was seen that the heat transfer from the shroud was governed by rotationally induced free convection and depended only on the shroud Grashof number. Figure 7.11 illustrates this for the results of Build 2, showing independence of the results on axial Reynolds number.

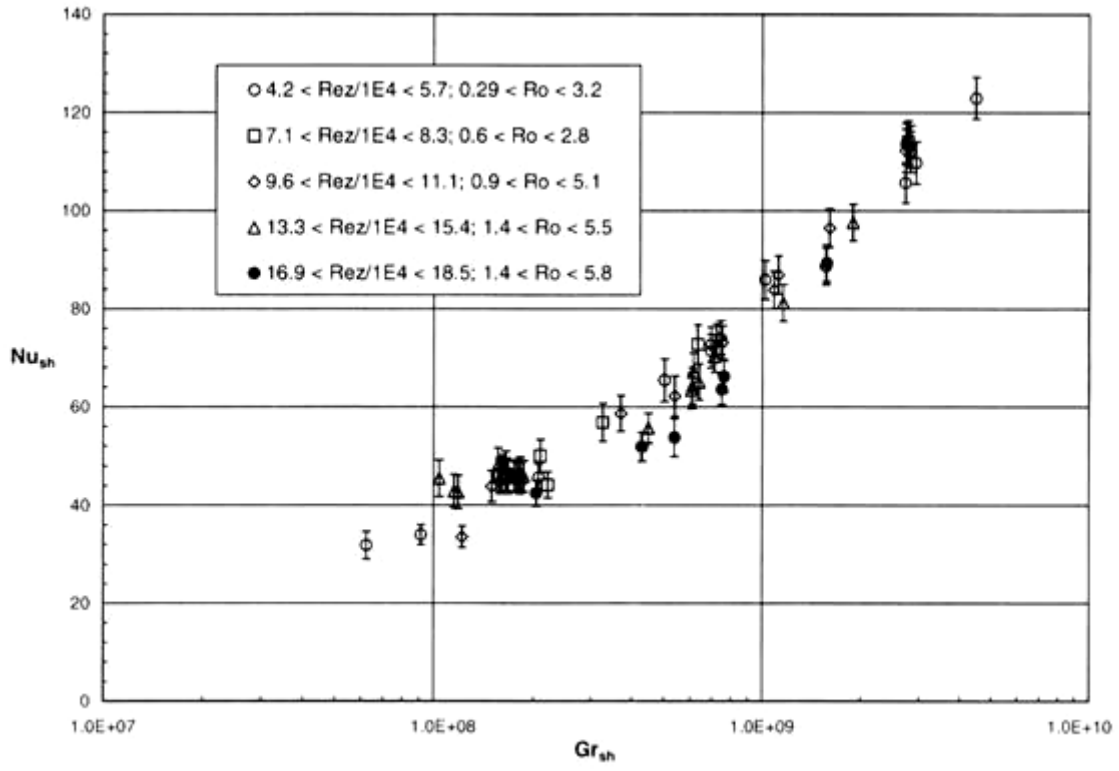

Fig 7. 11 Variation of shroud Nusselt number with Grashof number in Cavity 2 for Build 2 (narrow annular gap) and various values of Re_z (Long and Childs, 2007).

There were also indications that the shroud heat transfer results could be correlated on the characteristics similar to Rayleigh-Bénard convection in a stationary enclosure. Higher shroud heat transfer values were found in Build 3 of the Multiple Cavity Rig compared to Build 2, as was noticed from the discs heat transfer results, also suggesting a greater influence of the throughflow on the cavity heat transfer when the annular gap is increased. Figure 7.12 shows the shroud Nusselt number results for Build 2 (narrow annular gap). The most acceptable fit of the data for Nu_{sh} of Build 2 was determined as:

$$Nu_{sh} = 0.216\left(Gr_{sh} \cdot \mathrm{Pr}\right)^{1/4} + 0.0494\left(Gr_{sh} \cdot \mathrm{Pr}\right)^{1/3} \qquad \text{Eq. 7.5}$$

Figure 7.13 shows the shroud Nusselt number results for Build 3 (wide annular gap). The data collapsed following:

$$Nu_{sh} = 0.25\left(Gr_{sh} \cdot \mathrm{Pr}\right)^{1/4} + 0.057\left(Gr_{sh} \cdot \mathrm{Pr}\right)^{1/3} \qquad \text{Eq. 7.6}$$

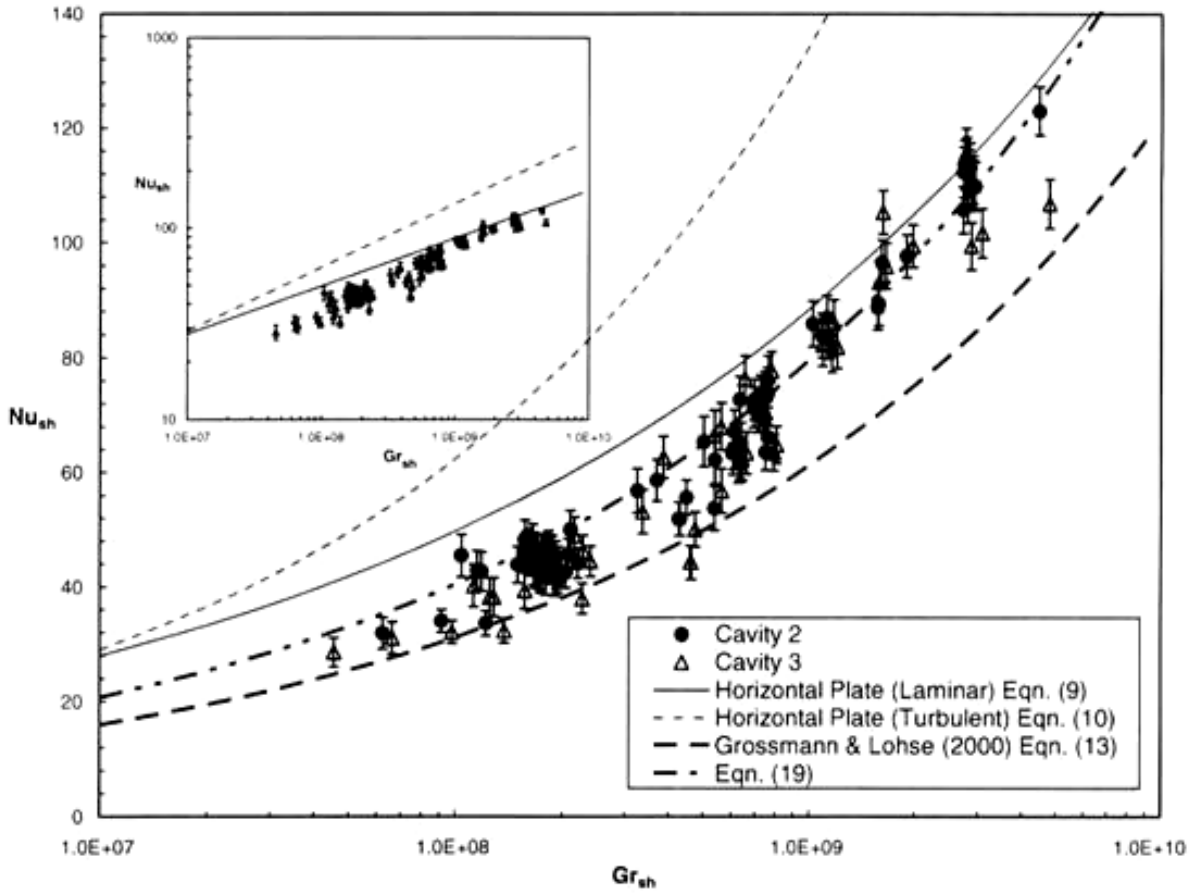

Fig 7. 12 Variation of shroud Nusselt number with Grashof number in both Cavity 2 and Cavity 3 for Build 2 (narrow annular gap); $4x10^4 < Re_z < 1.9x10^5$; $0.29 < Ro < 5.8$. Insert is same data plotted on a logarithmic scale (Long and Childs, 2007)

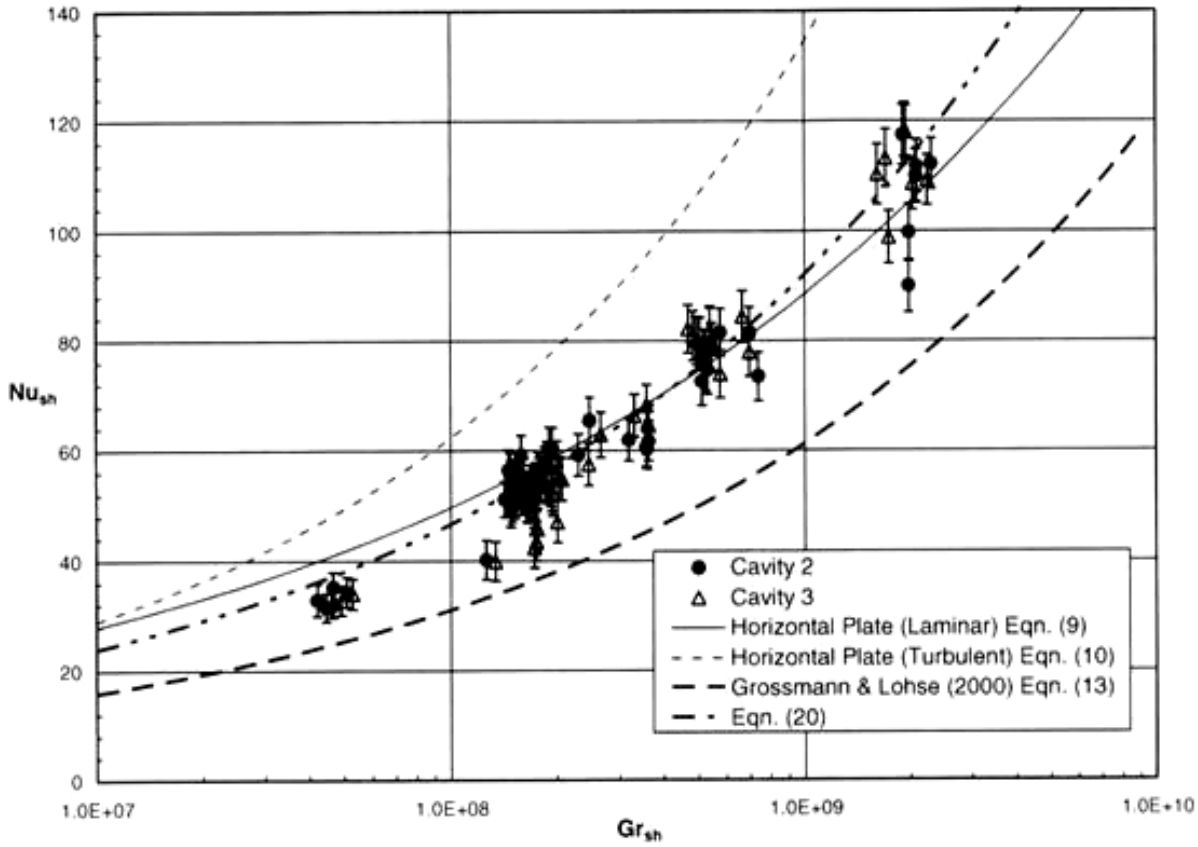

Fig 7. 13 Variation of shroud Nusselt number with Grashof number in both Cavity 2 and Cavity 3 for Build 3 (wide annular gap); $4.1x10^4 < Re_z < 2.0x10^5$; $0.27 < Ro < 5.8$ (Long and Childs, 2007).

7.3 Effect of the Flow Control Feature on cavity heat transfer

The heat transfer results of tests with the Flow Control Feature described in Chapter 3 were plotted for each position: position 1 being located under Disc 2, position 2 is at mid Cavity 3 and position 3 is located under Disc 3.

Figures 7.14 and 7.15 show $Nu_{av}/Re_{\Phi}^{0.5}$ against Ro for tests with and without Flow Control Feature for Disc 2 and Disc 3 respectively.

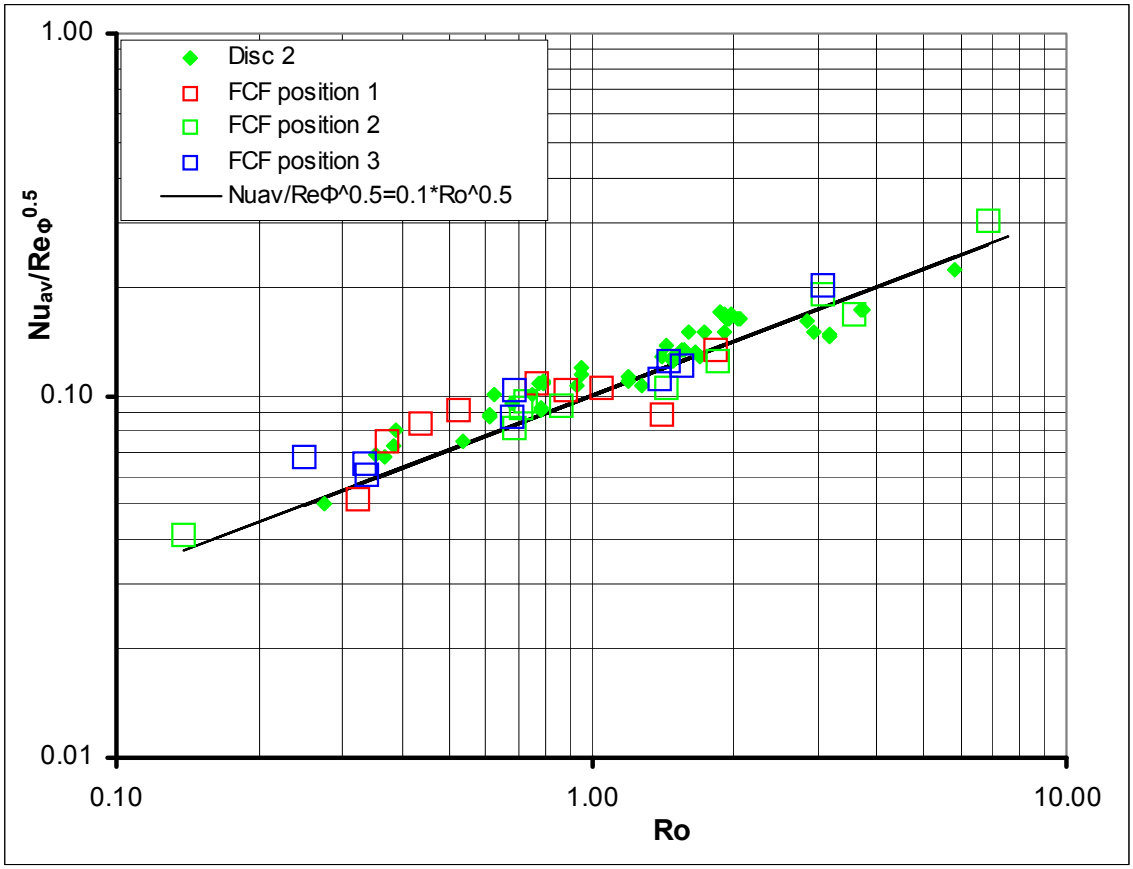

Fig 7. 14 Variations of Disc 2 $Nu_{av}/Re_{\Phi}^{0.5}$ against Ro for tests with and without Flow Control Feature against Ro

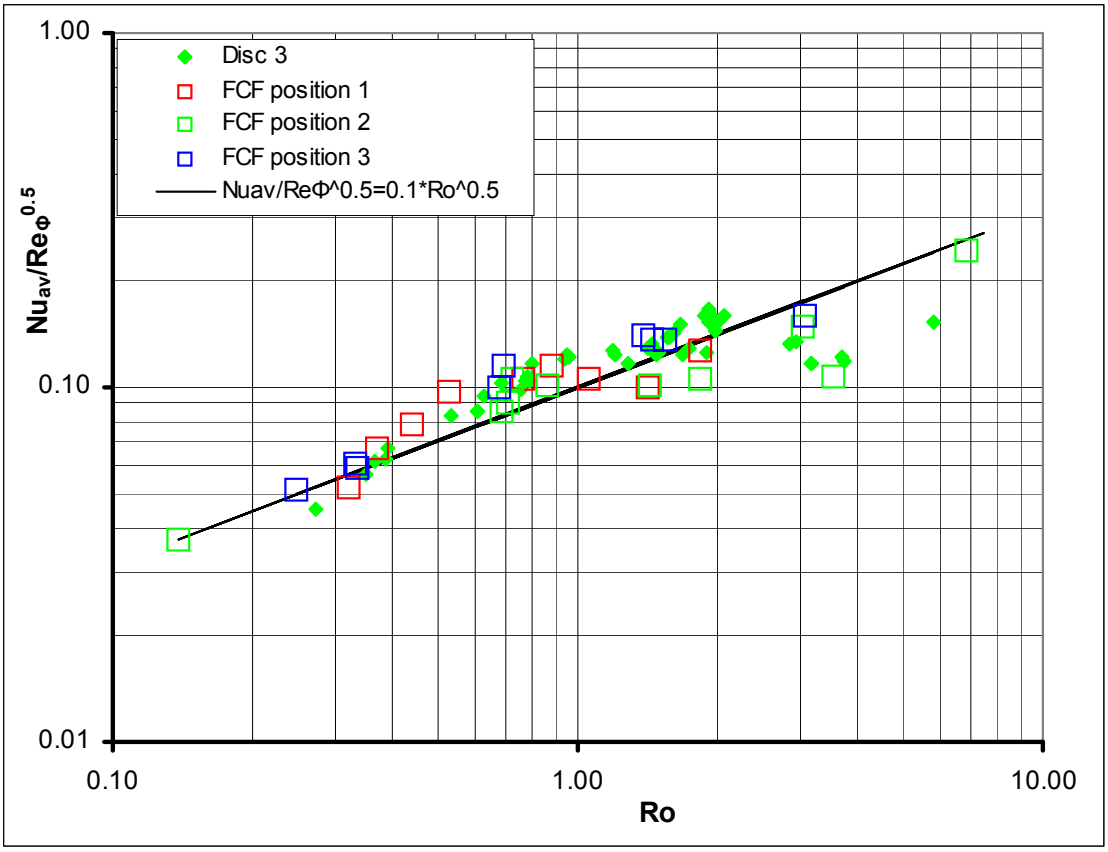

Fig 7. 15 Variations of Disc 3 $Nu_{av}/Re_{\Phi}^{0.5}$ against Ro for tests with and without Flow Control Feature against Ro

Taking into account the overall level of uncertainty on the discs heat transfer results, it would appear from Figures 7.14 and 7.15 that the inclusion of the Flow Control Feature on the shaft (in any position) would not have affected the disc heat transfer in a significant or systematic way. The comparison of shroud heat transfer measurements with and without Flow Control Feature for Shroud 2 and 3 in Figures 7.16 and 7.17 respectively would also indicate that the Flow Control Feature did not affect the cavity flow enough to significantly modify the heat transfer characteristics of the shroud.

There probably is an insufficient amount of data to provide any conclusive remarks at this stage on the effect of this Flow Control Feature on the cavity heat transfer and probably more investigations would be required (possibly also with different geometries of Flow Control Features) in order to offer further conclusions on this matter.

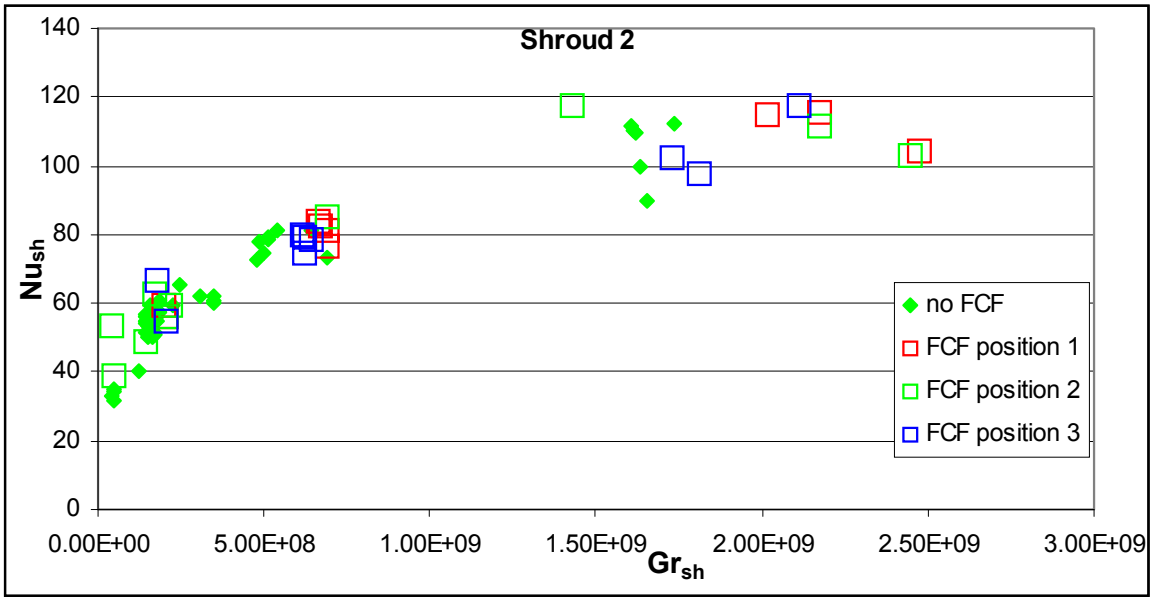

Fig 7. 16 Variations of Shroud 2 Nu_{sh} against Gr_{sh} for tests with and without Flow Control Feature

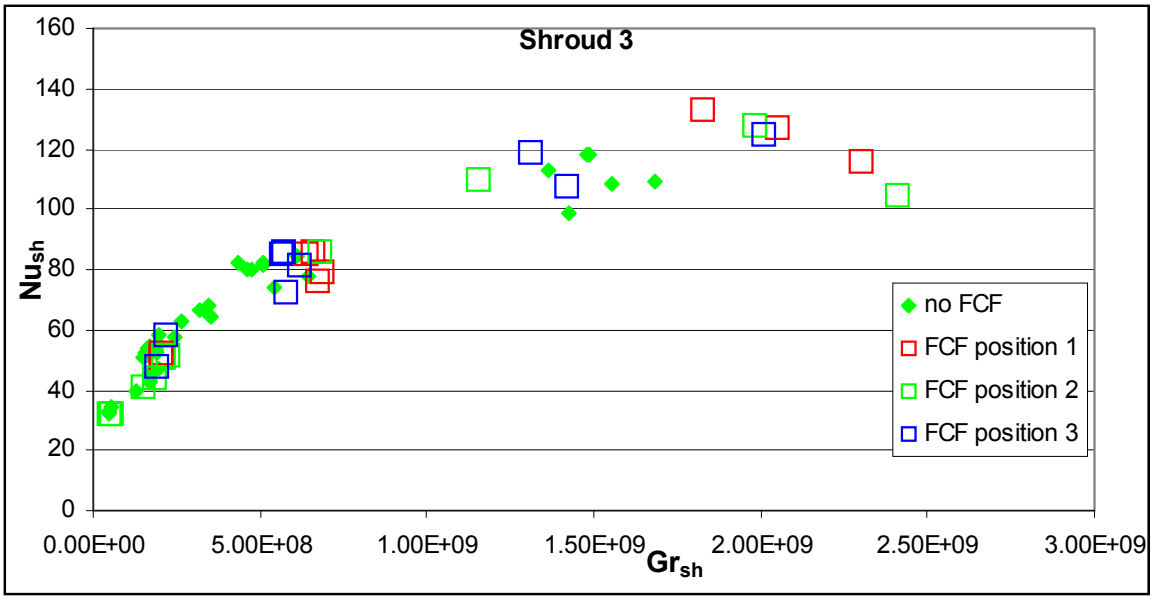

Fig 7. 17 Variations of Shroud 3 Nu_{sh} against Gr_{sh} for tests with and without Flow Control Feature

8. Conclusions

8.1 Experimental apparatus and methodology

This thesis has presented measurements of heat transfer and velocity flow in a heated multiple cavity test rig with axial throughflow.

The experimental test rig was previously designed to be a 70% full scale replica of the internal air system within the high pressure compressor of a gas turbine aero-engine. The rig comprised an encased rotor section reproducing four internal cavities from a typical compressor disc-shroud stack and a central shaft. The cavities had an internal outer diameter b= 220 mm and the axial spacing between discs was s= 42.9 mm, giving a gap ratio G= s/b= 0.195. The discs bore radius on the principal studied rig (Build 3 of the Multiple Cavity Rig) was r_s= 52 mm. In the course of this study, comparisons were made with previous results on a former version of the Multiple Cavity Rig, namely Build 2, which featured similar cavity dimensions but with a bigger shaft diameter of value r_s= 60 mm. Build 2's major geometrical difference therefore lay in a smaller annular gap ratio d_h/b= 0.092 compared to Build 3 (d_h/b= 0.164). In the wider annular gap of Build 3 a Flow Control Feature ring of trapezoidal cross section and outer diameter 60 mm could be sleeved around the shaft at three determined axial positions: under Disc 2, at mid Cavity 3 and under Disc 3. The simulated cooling throughflow of air was provided by a single screw compressor at rates up to 1.1 kg/s at 4 bar absolute and 200 °C. The related throughflow operating capacity of the rig was up to $Re_z \leq 1.8 \times 10^5$. Rotation of the rotor assembly was provided by an electrical motor via a belt drive at speeds up to 570 rad/s, corresponding to a maximum operation rotational condition of $Re_\Phi \leq 4.1 \times 10^6$. The range of experimental steady-state conditions were $4.7 \times 10^4 \leq Re_z \leq 1.8 \times 10^5$, $4.0 \times 10^5 \leq Re_\Phi \leq 4.1 \times 10^6$; giving a corresponding range of Rossby number $0.27 \leq Ro \leq 7.5$.

Heating of the outer rotor surface was provided by hot air impingement from two 10 kW hot air blowers delivering 0.01 kg/s of air at 800 K. This heating configuration provided a realistic, increasing with radius, temperature distribution in the shrouds and discs.

This is representative of the heat generated by the air mainstream in the high pressure compressor stages of a gas turbine. Mass flow and pressure across the rig were measured by orifice plates and pressure tappings linked to a pressure logging unit. Embedded thermocouples provided axi-symmetrical surface measurement temperatures on the surfaces of Shrouds 2 and 3 as well as Discs 2 and 3. The rotating thermocouples were led to a data logger via a slip ring unit and a thermally insulated cold junction box. Additional thermocouples provided information on throughflow air and shaft surface temperatures.

Two-dimensional laser velocimetry was employed for the throughflow and cavity airflow measurements. Two different laser probe mountings were possible, each providing access to different measurement zones and different velocity components. With the laser probe installed in a coaxially translating probe and mirror assembly within the shaft, measurements of axial and tangential velocities were possible in all cavities and the central annular gap regions within the bores of Discs 2 and 3. Optical access to these regions was provided by a longitudinal window on the shaft surface. With the laser probe shooting across windows installed on Discs 3 and 4, measurements of tangential and radial velocity components were made possible in Cavities 3 and 4 for $0.566 \leq r/b \leq 0.924$. Processing of the velocimetry data was executed using the processing software provided with the measuring equipment. The results were collated onto test reports for archiving and analysis, with calculated uncertainty intervals on the results included.

The data from the temperature and pressure measurements were processed into operational parameters and heat transfer local and average values from a purpose written processing piece of software that would handle the raw data, process it and turn the results into lists and standard test reports for each experimental conditions for the purpose of archiving and further analysis. The processing software included one-dimensional shroud heat transfer calculations, two-dimensional disc heat transfer and an adiabatic plane assumption fin solution on Discs 2 and 3. Heat fluxes on the surfaces of Cavity 3 were corrected for radiation by an integrated grey body enclosure radiation model.

A separate error analysis highlighted the sensitivity of the disc heat transfer solutions to the quality of interpolation of the temperature profiles along the discs surfaces from a limited number of thermocouples. This allowed the selection of the appropriate fitting technique to be implemented into the processing software in order to minimise bias on the results. This study also highlighted the sensitivity of the disc heat transfer calculations to the number of thermocouples involved in the surface temperature profiles definition and to the number of nodes of the finite difference grid. A comprehensive uncertainty analysis quantified the influence of different uncertainty sources onto the experimental temperature measurements. The compounded uncertainties were integrated into the processing software as an input into a Monte-Carlo analysis coupled onto the results calculation algorithm in order to provide the resulting values as nominal values bounded by an uncertainty interval for each calculated parameters of each experimental test.

8.2 Experimental results

8.2.1 Flow velocity measurements

Tangential velocity measurements in Build 3 of the Multiple Cavity Rig showed a sharply increasing profile between the shaft and a radius close to the disc bore, at the entrance of the cavity, where it reached a maximum. Then the tangential velocity within the cavity would decrease gradually until reaching solid body rotation at about $r/b \approx 0.6$. The tangential velocities measured in the annular gap showed a quasi linear velocity profile from close to zero by the shaft, tending to solid body rotation by the disc bore. The tangential velocity did not appear to vary significantly across the width of a cavity, although measurements could not be made inside the discs boundary layers. The magnitude of the tangential velocity peak by the cavity entrance appeared related to the dominance of the axial throughflow, with either a decrease of Re_Φ or an increase in Re_z (hence increase in Ro in both cases) increasing the peak tangential velocity value in the inner regions of a cavity ($r/b < 0.5$). Comparing the tangential velocities of Build 3 to Build 2, which featured a smaller axial gap, showed attenuated velocity profiles compared to Build 3, suggesting a lesser influence of the throughflow on the cavity tangential velocities resulting from the smaller annular gap (as also reported by Owen and Powell 2004), similarly to the attenuating effect reported by Farthing et al. (1992a) when reducing the cavity width. Tangential velocity profiles between cavities in Builds 2 and 3 highlighted more acute velocity profiles as progressing from one cavity to the next. This could be attributed to a compounding influence on the exit flow conditions as progressing through the rig, affecting the cavity flows and vortex breakdown into what would appear to be an increase in throughflow dominance. Axial velocity measurements of the annular gap flow showed a relatively homogeneous flow, although highly fluctuating, under the discs bore being constricted (and accelerated) under the interacting region with the cavity entrance. Contra rotating circulations from the cavity entrance interaction with the throughflow to the outer cavity regions were highlighted, with axial velocity magnitudes of these circulations found to be less than $1/10^{th}$ of the axial throughflow bulk velocity.

Time averaged radial velocity measurements in the outer regions (r/b> 0.55) of Cavities 3 and 4 in Build 3 of the Multiple Cavity Rig were performed in the experimental range 0.39x10^6 ≤ Re_Φ ≤ 1.99x10^6, 0.53x10^5 ≤ Re_z ≤ 1.65x10^5, 0.53 ≤ Ro ≤ 7.51. High levels of fluctuation in the measured velocities (higher to the average values by a factor of two typically) suggested an unsteady or circulatory nature of the flow in the cavities. The radial average velocity circulating flow patterns showed to be different for each cavity and similar across the experimental range, consistent with buoyancy driven flows. The direct inclusion of vortex breakdown into the cavity flow was also recorded on an experiment at Ro≈ 1.5. The cavity radial velocities suggested a dominant influence with rotational Reynolds number. Spectral analysis of the tangential velocity measurements across the discs windows showed evidence of periodicity in the flow structure, linked to the current understanding of the flow structure in a heated rotating cavity with axial throughflow.

8.2.2 Heat transfer measurements

The disc heat transfer data were analysed from an adiabatic plane assumption solution. Average disc heat transfer values on Build 3 of the Multiple Cavity Rig showed a good collapse with $Ro.Re_\Phi$ and were correlated as:

$$\frac{Nu_{av}}{\mathrm{Re}_\phi^{0.5}} \approx 0.1 \times Ro^{0.5} \qquad \text{Eq. 8.1}$$

The average disc heat transfer data of Build 2 showed two different regimes, correlated for Ro ≤ 3 by:

$$\frac{Nu_{av}}{\mathrm{Re}_\phi^{0.5}} \approx 0.05 \cdot Ro^{0.5} \qquad \text{Eq. 8.2}$$

For Ro > 3 an increase in average Nusselt number values was observed, consistent with a flow which is mainly affected by the axial throughflow at large values of rossby numbers, with this sensitivity decreasing as the Rossby number decreases and the influence of the rotational Reynolds increases.

The effects of the Flow Control Feature on the cavity heat transfer were assessed and appeared not to affect the cavity flow enough to significantly modify the cavity heat transfer.

This newly reported data which has been obtained at near engine representative conditions extends the understanding of the unsteady flow structures that exist in the rotating cavities commonly found in gas-turbine power plants. In particular, the velocimetry and temperature data provide improved quantification of the complex and often buoyancy driven flows that determine the heat transfer characteristics within multiple cavity engine architecture. This data is necessary for the validation of thermo-fluid models used to predict components temperature and life as part of the engine design process.

8.3 Recommendations for future work

8.3.1 Flow velocity measurements

Important difficulties in taking Laser Doppler Anemometry measurements inside the Multiple Cavity Rig were found in the relatively small validated data rates obtained. The relatively important probe volume due to a narrow crossing angle of the beams involves relatively wide spaced fringes and also fewer of them; hence all working towards a configuration more prone to surface proximity glaring, multiple occurrence sample rejection and poor signal to noise ratio. Improvements on the data measurements density and on the ability to better measure in the central annular gap region could easily be obtained on the current laser system by changing the probe front optics for a reduced focal length. This would induce a bigger crossing angle and therefore a smaller probe volume, more fringes etc. The immediate drawback would be reduced measurement volume range ability. If considering a focal length of 100 mm for instance (compared to 250 mm used in the present experiments), the measurement region range in the configuration with the laser probe installed within the shaft would not allow to measure deep within the cavity radius. On the other hand, the present measurements would indicate relatively quiescent flows in the outer part of cavities beyond $r/b \approx 0.5$, which might be of a lesser interest for further measurements compared to the complex circulatory nature of the flows encountered at the interaction of the annular gap and the cavity entrances and the onset characteristics of vortex breakdown. A more detailed study of these flow regions would therefore be of interest with the benefit of improved spatial and temporal flow definition potential brought by a smaller probe volume. With higher temporal densities also, spectral analysis would increase in confidence of accuracy and perhaps a cellular nature of the swirling throughflow akin to Taylor-Couette type of cells within the central vortex could be identified as the explanation for the very high values of fluctuations on the current time averaged measured flows in this region.

Particle Image Velocimetry could be suitably employed for measurements through the discs windows, with illumination from the shaft optical access.

This would provide a better planar definition than single point measurement and could capture more instantaneous flow characteristics. The difficulties of reconstructing a full cavity flow from discrete window passage measurements would however remain.

The effect of variations of annular gap on the cavity flow could easily be studied by the relatively simple adjunction of varying thickness sleeves with a provision for optical access included onto the existing shaft.

8.3.2 Heat transfer measurements

The presented work has shown that the instrumentation and method used on the Multiple Cavity Rig for the calculation of surface heat transfer is not adequate for the current design. More thermocouples on the disc faces could improve the surface temperature fitting definition but will not remove the fact that the heat transfer solutions are inherently error prone. Statistical error analyses (notably by Cooke 2007) have now demonstrated the extent of bias that such methods could incur. The task remains for future experiments to determine a better type of instrumentation and calculation suitable for inclusion within the intricate confines of a rotating cavity, allowing precise measurement of heat transfer with a good spatial definition, reliability of use and minimal re-calibration requirements. Thin film heat flux sensors, thermochromic paint and thermal imaging have been put forward as possible techniques to allow improved heat transfer measurements within rotating cavities, but each have their pros and cons and none are standing out so far as the best answer to this issue.

Bibliography

Albrecht H.-E., Borys M., Damaschke N., Tropea C. (2003), “Laser Doppler and Phase Doppler Measurement Techniques”, Springer Verlag, Berlin, Germany.

Alexiou, A. (2000), “Flow and Heat Transfer in Gas Turbine H.P. Compressor Internal Air Systems”, D. Phil. Thesis, School of Engineering, University of Sussex.

Alexiou, A. (2001), “ICAS GT Final Report – Task 2.2 Multiple Rotating Cavities”, Internal Report TFMRC, University of Sussex.

Alexiou, A. (2002), “ICAS GT2 Year 1 Progress Report”, Internal Report TFMRC, University of Sussex.

Alexiou A., Hills N.J., Long C.A., Turner A.B. and Millward J.A. (2000), “Heat Transfer in High-Pressure Compressor Gas Turbine Internal Air Systems: A Rotating Disc-Cone Cavity with Axial Throughflow. Experimental Heat Transfer, Vol. 13, pp. 299-328.

Begg S. (2003), “In-Cylinder Airflow and Fuel Spray Characteristics for a Top-Entry, Direct Injection, Gasoline Engine”, PhD. Thesis, School of Engineering, University of Brighton.

Bell, S. (1999), “A Beginner’s Guide to Uncertainty of Measurement”, Measurement Good Practice Guide, No. 11, National Physical Laboratory, Department of Trade and Industry, U.K.

Bohn D., Dibelius G.H., Deuker E. and Edmunds R. (1994), “Flow Pattern and Heat Transfer in a Closed Rotating Annulus”, ASME Journal of Turbomachinery, Vol. 116, pp. 542-547.

Bohn D., Deuker E., Emuns R., Gorzelitz V. (1995), “Experimental and Theoretical Investigations of Heat Transfer in Closed Gas-Filled Rotating Annuli”, ASME Journal of Turbomachinery, Vol. 117, pp. 175-183.

Bohn D. and Gier J. (1998), “The Effect of Turbulence on the Heat Transfer in Closed Gas-Filled Rotating Annuli”, ASME Journal of Turbomachinery, Vol. 120, pp. 824-830.

Burkhardt C., Mayer A. and Reile E. (1992), “Transient Thermal Behaviour of a Compressor Rotor with Axial Cooling Air Flow and Co-Rotating or Contra-Rotating Shaft”, AGARD-CP-527, pp. 21-1 to 21-9.

Cooke, A. (2007), “Turbomachinery Disc Heat Transfer Uncertainty”, D. Phil. Thesis, Department of Engineering and Design, University of Sussex.

Cooke A., Childs P., Long C. (2006), “An Investigation into the Uncertainty of Turbomachinery Disc Heat Transfer Calculations Using Monte Carlo Simulation Methods”, ASME Turbo Expo 2006: Power for Land, Sea and Air, May 8-11 2006, Barcelona, Spain, paper no. GT-2006-90143.

Curzons, S. (1991), “Revised Method for Calculating Flow Through Straight-Through and Stepped Labyrinth Seals”, Rolls-Royce plc., Technical Design Report No. TDR 90294.

Dantec Dynamics (2004), “BSA Flow Software: Version 3 Installation and User’s Guide”, Dantec Dynamics A/S, Skovlunde, Denmark.

Dorfman, L.A. (1963), “Hydrodynamic Resistance and the Heat Loss from Rotating Solids”, Edinburgh: Oliver & Boyd.

Farthing P.R., Long C.A., Owen J.M. and Pincombe J.R. (1992a), “Rotating Cavity with Axial Throughflow of Cooling Air: Flow Structure”, Journal of Turbomachinery, Vol. 114, pp. 237-246.

Farthing P.R., Long C.A., Owen J.M. and Pincombe J.R. (1992b), “Rotating Cavity with Axial Throughflow of Cooling Air: Heat Transfer”, Journal of Turbomachinery Vol. 114, pp. 229-236.

Freeman, C. (1985), “Effect of Tip Clearance Flow on Compressor Stability and Engine Performance”, Von Karman Institute for Flow Dynamics, Lecture Series, 1985-05.

Hjmelfelt A.T., Mockros L.F. (1966), “Motion of Discrete Particles in a Turbulent Fluid”, Appl. Sci. Res., Vol. 16, p. 149

Howell, J.R. (1982), “A Catalog of Radiation Configuration Factors”, McGraw-Hill, New York.

King M.P., Wilson M., Owen J.M. (2005), “Rayleigh-Bénard convection in open and closed rotating cavities”, ASME Turbo-Expo, Reno, Nevada U.S.A, paper GT2005-68948.

Lancel, J. (2002), “Analysis and Test of a Centrifugal Compressor”, D. Phil. Thesis, School of Engineering, University of Sussex.

Long, C.A. (1994), “Disc Heat Transfer in a Rotating Cavity with an Axial Throughflow of Cooling Air”, International Journal of Heat Fluid Flow, Vol. 15, pp. 307-316.

Long, C.A. (1999), “Essential Heat Transfer”, Pearson Education Limited, U.K.

Long C.A., Alexiou A. and Smout P.D. (2003), “Heat Transfer in H.P. Compressor Gas Turbine Internal Air Systems: Measurements from the Peripheral Shroud of a Rotating Cavity with Axial Throughflow”, HEFAT 2003,

2nd International Conference on Heat Transfer, Fluid Mechanics and Thermodynamics, 23-26 June 2003, Victoria Falls, Zambia, paper LC1.

Long C.A. and Childs P.R.N. (2007), "Shroud Heat Transfer Measurements Inside a Heated Multiple Rotating Cavity with Axial Throughflow", International Journal of Heat and Fluid Flow, Vol. 28, pp. 1405-1417.

Long C.A., Miché N.D.D., Childs P.R.N. (2007), "Flow measurements inside a heated multiple rotating cavity with axial Throughflow", International Journal of Heat and Fluid Flow, Vol. 28, pp. 1391-1404.

Long C.A., Morse A.P. and Tucker P.G. (1997), "Measurement and Computation of Heat Transfer in High Pressure Compressor Drum Geometries with Axial Throughflow", Journal of Turbomachinery, Vol. 119, pp. 51-60.

Melling A. (1997), "Tracer Particles and Seeding for Particle Image Velocimetry", Meas. Sci. Technol., Vol. 8, pp. 1406-1416

Minning, C.P. (1979), "Shape Factors between Coaxial Annular Discs Separated by a Solid Cylinder", AIAA J., Vol. 17, pp. 318-320.

Moffat, R.J. (1988), "Describing the Uncertainties in Experimental Results", Experimental Thermal and Fluid Science, Vol. 1, pp. 3-17.

Owen, J.M. (1979), "On the Computation of Heat-Transfer Coefficients from Imperfect Temperature Measurements", Journal Mechanical Engineering Science, Vol. 21 No. 5, pp. 323-334.

Owen J.M., Abrahamsson H., Linblad K. (2006), "Buoyancy induced flow in open rotating cavities. ASME Turbo-Expo, Barcelona, Spain, paper GT2006-91134.

Owen J.M. and Powell J. (2004), "Buoyancy-Induced Flow in a Heated Rotating Cavity", Proceedings of ASME Turbo-Expo 2004, June 14-17, 2004, Vienna, Austria, paper GT2004-53210.

Owen J.M. and Rogers R.H. (1995), "Flow and Heat Transfer in Rotating-Disc Systems: Vol. 2, Rotating Cavities", Research Studies Press, Taunton, U.K.; Wiley, New York, U.S.A.

Patounas, D. (2007), "Disc Heat Transfer in Gas Turbine H.P. Compressor Internal Air Systems", D. Phil. Thesis, Department of Engineering, University of Sussex.

Rea, S.N. (1975), "Rapid Method for Determining Concentric Cylinder Radiation View Factors", AIAA J., Vol. 13, pp. 1122-1123.

Rolls Royce plc. (1983), "Labyrinth Seal – Gas – Rotating Straight Through Type", JDS 641.01

Rolls Royce plc. (2005), “The Jet Engine”, ISBN 0 902121 2 35, Rolls Royce Technical Publications Department, Derby, U.K.

Schlichting H. and Gersten K. (2000), “Boundary Layer Theory”, Springer-Verlag, Berlin, Germany.

Sun Z., Lindblad K., Chew J.W., Young C. (2006), “LES and RANS Investigations into Buoyancy-Affected Convection in a Rotating Cavity with a Central Axial Throughflow”, Proceedings of ASME Turbo-Expo 2006, Barcelona, Spain, paper GT2006-90251.

Sun Z., Kilfoil A., Chew J.W. and Hills N.J. (2004), “Numerical Simulation of Natural Convection in Stationary and Rotating Cavities”, Proceedings of ASME Turbo-Expo, June 14-17, 2004, Vienna, Austria, paper GT2004-53528.

Tian S., Tao Z., Ding S. and Xu G. (2004), “Investigation of Flow and Heat Transfer Instabilities in a Rotating Cavity with Axial Throughflow of Cooling Air”, Proceedings of ASME Turbo-Expo, June 14-17, 2004, Vienna, Austria, paper GT2004-53525.

Touloukian Y.S., Liley P.E., Saxena S.C. (1970), “Thermophysical properties of matterThermal Conductivity of Metallic Elements and Alloys”, Vol. 1, IFI/Plenum, New York.

Tropea C., Yarin A.L., Foss J.F. (2007), “Springer Handbook of Experimental Fluid Mechanics”, Springer.

Appendix 1.1: Reproduction of Long et al. (2007)

Available online at www.sciencedirect.com
ScienceDirect
International Journal of Heat and Fluid Flow 28 (2007) 1391–1404
International Journal of HEAT AND FLUID FLOW
www.elsevier.com/locate/ijhff

Flow measurements inside a heated multiple rotating cavity with axial throughflow

C.A. Long *, N.D.D. Miché, P.R.N. Childs

Thermo-Fluid Mechanics Research Centre, Department of Engineering & Design, University of Sussex, Brighton, Sussex BN1 9QT, UK

Received 27 June 2006; received in revised form 30 March 2007; accepted 2 April 2007
Available online 13 June 2007

Available online at www.sciencedirect.com
ScienceDirect
International Journal of Heat and Fluid Flow 28 (2007) 1391–1404
HEAT AND FLUID FLOW
www.elsevier.com/locate/ijhff

Flow measurements inside a heated multiple rotating cavity with axial throughflow

C.A. Long *, N.D.D. Miché, P.R.N. Childs

Thermo-Fluid Mechanics Research Centre, Department of Engineering & Design, University of Sussex, Brighton, Sussex BN1 9QT, UK

Received 27 June 2006; received in revised form 30 March 2007; accepted 2 April 2007
Available online 13 June 2007

Abstract

This paper discusses experimental results from a multiple cavity test rig representative of a high pressure compressor internal air system. Measurements of the axial, tangential and radial velocity components are presented. These were made using a two component, laser doppler anemometry (LDA) system for a range of non-dimensional parameters representative of engine conditions (Re_ϕ up to 4×10^6 and Re_z up to 1.8×10^5). Tests were carried out for two different sizes of annular gap between the (non-rotating) drive shaft and the disc bores.

The axial and radial velocities inside the cavities are virtually zero. The size of the annular gap between disc bore and shaft has a significant effect on the radial distribution of tangential velocity. For the narrow annular gap ($d_h/b = 0.092$), there is an increase of non-dimensional tangential velocity $V_\phi/\Omega r$ with radial location from $V_\phi/\Omega r < 1$ at the lower radii to solid body rotation $V_\phi/\Omega r = 1$ further into the cavity. For the wider annular gap ($d_h/b = 0.164$), there is a decrease from $V_\phi/\Omega r > 1$ at the lower radii to solid body rotation further into the cavity. An analysis of the frequency spectrum obtained from the tangential velocity measurements is consistent with a flow structure in the r–ϕ plane consisting of pairs of contra rotating vortices.

Keywords: Rotating cavity flow; Gas turbine internal air system; Axial throughflow; LDA measurements

1. Introduction

Contemporary gas turbine aircraft engines operate at the limits of technology. Indeed, the *compressor exit* temperature on a modern civil engine exceeds the *turbine entry* temperature of engines 50 years ago. The combination of high temperatures and high rotational speeds creates significant levels of stress. This can lead to deflections in components and cause a loss in efficiency, or worse, compromise safety. Such engines would not be able to operate without an internal air system. This provides ventilation (mostly cooling, but sometimes components are heated), sealing and purging air to the discs, blades, bearing chambers and various cavities.

A schematic diagram of a typical high pressure (H.P.) compressor internal air system is shown in Fig. 1. Air, extracted from stages of the intermediate pressure compressor and destined for the intermediate pressure turbine blades and seals, flows through the annular passage between the drive shaft and H.P. compressor disc bores. On its route, this throughflow may be heated by both convection and viscous dissipation. Since it is bled from the compressor where work has been done to raise its pressure, use of this air represents a parasitic loss to the main cycle. In fact, the internal air system as a whole may use 20% of the mainstream air flow and cost up to 5% of the specific fuel consumption in a modern turbofan engine (Rolls-Royce, 2005).

This paper is the first of two reporting on experimental measurements of flow and heat transfer in H.P. compressor internal air systems. The work reported here focuses on laser Doppler anemometer (LDA) measurements of the

* Corresponding author. Tel.: +44 0 1273 678945; fax: +44 0 1273 678486.
E-mail address: c.a.long@sussex.ac.uk (C.A. Long).

0142-727X/$ - see front matter © 2007 Elsevier Inc. All rights reserved.
doi:10.1016/j.ijheatfluidflow.2007.04.010

Nomenclature

a, b	inner and outer radii of a disc
d_h	hydraulic diameter
$G = s/b$	gap ratio
$\dot{m}$	mass flow rate of the throughflow
p	pressure
r, z, ϕ	radial, axial and tangential coordinates
r_s	shaft radius
$Re_z = Wd_h/\nu$	axial Reynolds number
$Re_\phi = \Omega b^2/\nu$	rotational Reynolds number
$Ro = W/\Omega a$	Rossby number
s	axial width of cavity
t	time
T	temperature
V_r, V_z, V_ϕ	radial, axial and tangential velocity components
W	bulk mean axial velocity of the throughflow
$\beta = 1/T$	volume expansion coefficient
ΔT	temperature difference
μ	dynamic viscosity
ν	kinematic viscosity
ρ	density
Ω	rotational speed of the cavity

Subscripts and superscripts

av	radially weighted average
in	value at inlet
s	denotes a value at the surface
sh	pertaining to the shroud

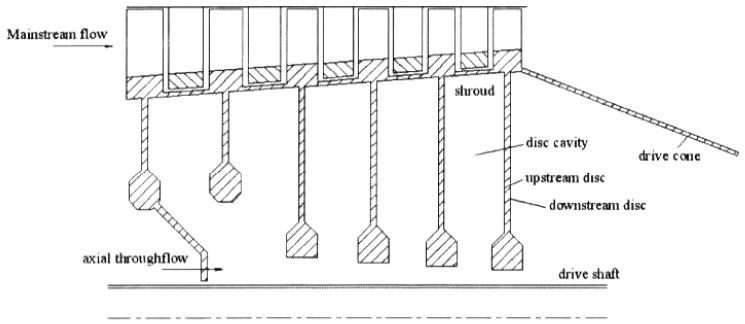

Fig. 1. A schematic diagram of a gas turbine high pressure compressor internal air system.

flow field inside the annular cavities of a test rig which is representative of the design and non-dimensional operating conditions of modern H.P. axial compressors. A background to the flow behaviour including a review of previous relevant work is presented in Section 2. The rig is described in Section 3. The LDA measurements of flow velocities are described in Section 4, and the conclusions to this study are presented in Section 5.

2. Background to the flow behaviour and review of previous work

Previous work, see for example Farthing et al. (1992), on rotating cavities with axial throughflow has mostly concentrated on an idealised single rotating cavity. A simplified model of the compressor cavities depicted in Fig. 1 is shown in Fig. 2. Two discs of outer radius, b, and inner radius, a, are separated by an axial gap, s. The rotational speed of the cavity is Ω and the bulk average velocity of the axial throughflow is W. For a fluid of kinematic viscosity ν, the rotational and axial Reynolds numbers are defined as:

$$Re_\phi = \Omega b^2/\nu \tag{1}$$

$$Re_z = Wd_h/\nu \tag{2}$$

where d_h is the hydraulic diameter of the inlet (for a cavity with an inner shaft of radius, r_s, $d_h = 2(a - r_s)$, for one without an inner shaft, $d_h = 2a$). A further non-dimensional parameter, the Rossby number, Ro links the effects of both rotation and the inertia of the throughflow. This is defined as the ratio of the mean velocity of the throughflow to the tangential velocity at the bore radius:

$$Ro = W/\Omega a \tag{3}$$

This can also be expressed in terms of the rotational and axial Reynolds numbers as:

$$Ro = \left\{\frac{b^2 Re_z}{2a(a - r_s)Re_\phi}\right\} \tag{4}$$

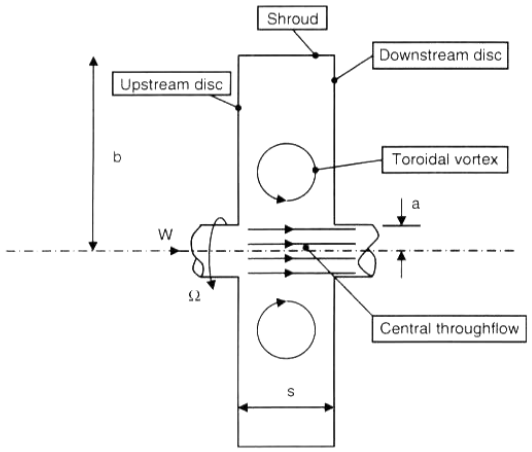

Fig. 2. A schematic diagram in the r–z plane of the isothermal flow structure in a rotating cavity with axial throughflow.

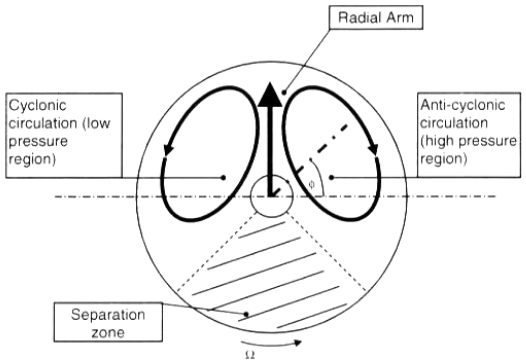

Fig. 3. A schematic diagram in the r–ϕ plane of the heated flow structure in a rotating cavity with axial throughflow.

Laser illuminated flow visualisation and LDA was used by Farthing et al. to study the flow structure in unheated (or isothermal) and heated cavities with $a/b \approx 0.1$. The principal parameters to affect the resulting flow are the Rossby number, Ro, and the gap ratio, $G = s/b$. For no rotation, $Ro = \infty$, the throughflow generates one or more (depending on gap ratio) axisymmetric toroidal vortices. Rotation has the effect of suppressing the toroidal vortex and destabilising the central throughflow, creating a change in the behaviour of the central jet. This is characterised by a number of regimes of axisymmetric and non-axisymmetric vortex breakdown. For turbulent ($Re_z > 2000$) flow and for a constant gap ratio four separate regimes of vortex breakdown were identified as the Rossby number was decreased from around 100 to a value of less than 1. These were given the following names, in order of decreasing Rossby number: Mode 1a, Mode 2a, Mode 1b and Mode 2b. For a gap ratio of $G = 0.533$, the respective boundaries of these regimes occur at $Ro = 20$, 2.6 and 1.5. A full description of these regimes of vortex breakdown can be found in Owen and Rogers (1995). In brief, Mode 1 regimes are associated with a non-axisymmetric behaviour of the central throughflow; Mode 2 behaviour is associated with axisymmetric behaviour. Decreasing the gap ratio suppresses the formation of Mode 1a behaviour.

When heated, significantly more of the throughflow appears to penetrate further into the outer part of the cavity. Most observations of the heated flow structure were made with a cavity ($G = 0.124$ and 0.267) having a surface temperature distribution that decreased with radius. A schematic diagram, in the r–ϕ plane, of the heated flow structure is shown in Fig. 3. Flow enters the cavity through a radial arm, bifurcates near the outer radius and forms a region of cyclonic flow (with the same sense of rotation as the cavity) and anticyclonic flow (having the opposite sense of rotation). It was not possible to obtain such clear visual or photographic evidence of the flow structure in a cavity with a surface temperature distribution that increased with radius. The overall impression was that significantly more of the central throughflow penetrated the cavity, the higher velocities leading to an ill defined flow structure especially in the region adjacent to the peripheral shroud. These differences may be qualitatively explained from consideration of thermal stratification in a rotating flow field. A surface-to-fluid temperature difference that decreases with radius results in stable stratification. For a surface-to-fluid temperature difference that increases with radius there is unstable stratification, resulting in increased radial mixing. This suggests that heating the cavity creates buoyancy forces that act to destabilise the central throughflow. The resulting flow structure may or may not be dominated by buoyancy forces – it depends on cavity geometry as well as physical parameters such as the axial and rotational Reynolds numbers.

The role of buoyancy forces is confirmed in the various studies carried out to measure heat transfer in rotating cavities with axial throughflow. A more detailed review can be found in Alexiou (2000). In brief, measurements appear to indicate a flow that can be either dominated by free convection, by forced convection or a combination of these. The heat transfer behaviour depends not only on the values of rotational and axial Reynolds numbers but also on geometric parameters such as gap ratio, inlet radius ratio, the presence of a shaft, its radius and sense of rotation relative to the cavity surfaces. It is obvious from this list of many variables that to carry out a comprehensive study of their effects on the flow presents a time consuming and daunting task.

Owen and Powell (2004) made velocity and heat transfer measurements in a single cavity research rig with an annular inlet, $a/b = 0.4$, $s/b = 0.2$ with just the downstream disc heated. Tests were carried out for $4 \times 10^5 < Re_\phi < 3.2 \times 10^6$ and $1.4 \times 10^3 < Re_z < 5 \times 10^4$. The time-average LDA measurements of the tangential velocity show that near to solid body rotation occurs ($0.96 < V_\phi/\Omega r < 0.99$ for the range of dimensionless radii $0.67 < r/b < 0.97$) in a cavity where the

downstream disc is heated to 75 K above the inlet air temperature. The radial velocity was found to be approximately two orders of magnitude smaller than the absolute value of tangential velocity. The time-average tangential velocity was also found to increase above $V_\phi/\Omega r = 1$ when the temperature difference between the disc surface and the inlet air was reduced to below approximately 40 K. A spectral analysis of the velocity measurements revealed behaviour that is consistent with one, two or three pairs of cyclonic and anticyclonic vortices in the flow field. In general, (although there are exceptions) for a constant axial Reynolds number, increasing the rotational Reynolds number reduces the number of cyclone–anticyclone vortex pairs. The heat transfer measurements support the existence of two different regimes: a buoyancy induced regime at large rotational speeds and small axial flow, and a throughflow dominated regime at the smaller values of rotational speed and larger values of axial throughflow.

Various numerical studies have been carried out: Long and Tucker (1994), Long et al. (1997), Tucker and Long (1995), Tucker and Long (1996), Wong (2002), Sun et al. (2004) and Tian et al. (2004). In general, the results from these CFD studies are qualitatively similar to experimental observations and give acceptable agreement with heat transfer and LDA measurements. However, massive computational resources are required for CFD simulations of this flow. Owen et al. (2006) report on using a cluster of 16 Linux PCs on a 3-D, time-dependent model with 2.6 million grid nodes. This required one week of CPU time. So, the accuracy of much of the numerical work is expected to be constrained by relatively coarse grid sizes and also inappropriate turbulence models. The recent 3D numerical study by Tian et al. (2004) supports the earlier qualitative flow visualisation work of Farthing et al. The isothermal flow structure is seen to be axisymmetric and stable, rotation decreases the influence of the central toroidal vortex. For a heated cavity, the flow may become unstable due to the influence of rotationally induced buoyancy. An instability that develops close to the shroud was seen to affect the rest of the cavity as the Grashof number was increased. Heat transfer data are also presented and these appear to be consistent with previous experimental measurements and show the different effects of the two regimes of forced and free convective heat transfer.

Johnson et al. (2004) developed a stability analysis and applied this to the case of rotating cavity flow with axial throughflow. This shows that for $Ro < 0.1$ the flow in the cavity may be stabilised by a density gradient that increases with increasing radius, but not for $Ro > 1$. For intermediate values of Ro ($0.1 < Ro < 1$) achieving stability involves a more complex relationship of velocity and temperature profiles.

3. Experimental apparatus

The LDA measurements discussed in this paper were carried out on a multiple cavity test rig. As shown in Fig. 4, the rotor has three internal discs forming four cylindrical cavities and the disc bores are of identical inner radius. To allow optical access along the centreline, the central shaft is stationary. The titanium 318 rotor is bolted together at the periphery, each cylindrical cavity has an inner radius ratio of $a/b = 0.318$, and a gap ratio of $s/b = 0.195$ (dimensions are given in non-dimensional form at the request of the industrial sponsors). The rotor is independently driven by an A.C. motor up to 10,000 rev/min. As in a high pressure compressor, a steel 'drive' shaft runs through the centre of the rig. Two different sizes of shaft were investigated. These will be referred to as the narrow annular gap, with $d_h/b = 0.092$, and the wide annular gap with $d_h/b = 0.164$.

The rotor assembly is housed within a steel pressure casing and supported by a high precision grease lubricated ball bearing on the upstream side and an oil lubricated cylindrical roller bearing on the downstream side. Since the rig is pressurised, a number of labyrinth seals are used in critical locations to reduce the leakage flow. These seals were designed to industrial design codes; the fins are on the rotating part, the static radial clearance is 0.1 mm and the stationary components are coated with an abradable material. Full details are available in Alexiou (2000).

Air is supplied to the rig by a single stage 275 kW Howden compressor which can deliver up to 1.1 kg/s of air at 4 bar (absolute) and 200 °C. Before entry to the rig, the air is cooled to 30–55 °C. To eliminate condensation, the actual value of this temperature is varied depending on the measured relative humidity of the air and its supply pressure. The air flow rate is measured by a single orifice plate at inlet and by another at exit to the rig. These orifice plates are designed to BS 1042, and this particular configuration allows separate determination of the inlet mass flow and by inference (and also calculation) the leakage through the labyrinth seals. Air enters the rig itself through a circumferential array of six 25 mm diameter holes. On the downstream side of this is a thin perforated plate designed to create a uniform velocity profile at inlet to the rig.

The outer surface of the rotor assembly is heated by impingement of hot air obtained from two 10 kW Leister 5000 8D5 heaters. These each supply 0.01 kg/s of air at up to 800 K. Using this system it was possible to obtain a maximum rotor surface temperature of 195 °C at 10,000 rev/min. As in an actual high pressure compressor, the discs are heated by conduction from the outer surface of the rotor. Although the level of surface temperature is lower, this method of heating the test rig achieves similar temperature distributions on the discs and similar values of the surface to air temperature difference to that found in an engine.

The surface temperatures of the rotor assembly and relevant air temperatures are measured using calibrated 0.25 mm wire diameter K-type (NiCr–NiAl) thermocouples. All the rotor instrumentation is led out to a 48-way, Wendon slip ring unit driven from the upstream side of the rig. The signals from all the temperature instrumentation are recorded by a Solartron Orion data logger, with

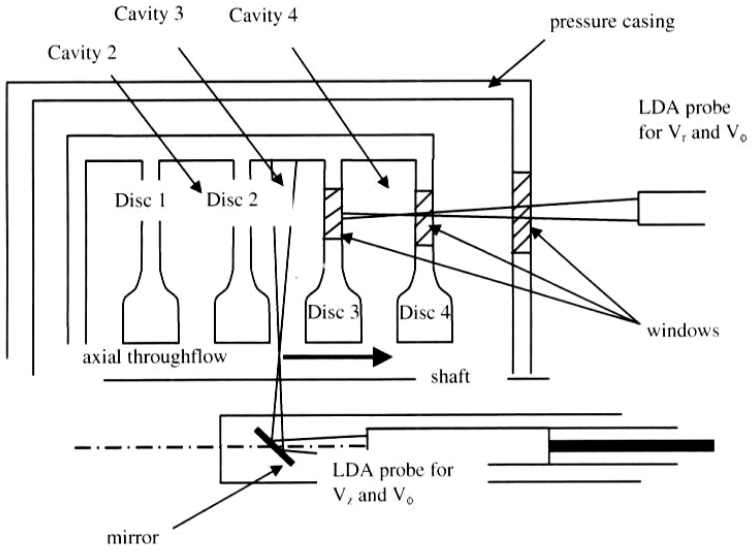

Fig. 4. A schematic diagram of the multiple cavity rig.

a sensitivity of ±1 μV corresponding to ±0.025 °C for the thermocouples used. However, the overall uncertainty in temperature measurement, which includes the effects of measurement and calibration uncertainty, is around an order of magnitude greater than this figure.

Velocity measurements were carried out using a Dantec, two component, LDA system. The discs and inner peripheral surfaces were painted black to reduce reflections and all the windows had an anti-reflection coating. The most important parameters of the LDA system are given in Table 1. The flow was seeded from the upstream part of the shaft with atomised quenching oil (RS 184-7939) using a TSI 9306 six jet oil droplet atomiser, the diameter of the seeding particles is expected to be approximately 1 μm.

Two different configurations of optical access were used for the LDA measurements, depending on which components of velocity were being measured. For the simultaneous measurement of axial and tangential components, the LDA probe was mounted on a traverse aligned with the centreline of the test rig. This allowed optical access into each cavity through a window in the central shaft made from 3 mm thick BK 7, Grade A optical quality glass, 20 mm wide and 150 mm long. Fig. 4 shows part of the traverse system used to move the LDA probe volume in the radial and axial directions. This tube is inserted into the downstream end of the rig inside the hollow non-rotating central drive shaft. The LDA probe, containing transmitting and receiving optics, is carried within the inner tube indicated in Fig. 4, the mirror, which directs the beams into the cavity space is carried inside the outer tube. Both inner and outer tubes can be independently positioned in the axial direction by stepper motors. Radial displacement of the probe volume is obtained by moving the inner tube (carrying the LDA probe) and axial displacement by moving the whole system. For the simultaneous measurement of radial and tangential components, the LDA probe was mounted off-axis in another traverse system and optical access into Cavities 3 and 4 obtained through eight 50 mm diameter windows in the outer casing and in the disc surfaces (four equally spaced at $r/b = 0.638$ and the other four at $r/b = 0.838$). This arrangement is also indicated in Fig. 4.

Table 1
LDA system parameters

Parameter	Value
Transmitting lens focal length	250 mm
Beam spacing	15 mm
Wavelengths	
Tangential velocity (green)	514.5 nm
Axial velocity (blue)	488 nm
Laser beam diameter	1.35 mm
Beam half angle	1.718°
Expansion factor	1
Probe volume diameter	0.121 mm (514.5 nm wavelength)
Probe volume length	4.046 mm (514.5 nm wavelength)
Number of fringes	14
Fringe spacing	8.579 μm
Frequency shift	40 MHz

4. LDA velocity measurements

4.1. Experimental procedure and data analysis

The data from LDA tests discussed in this paper were acquired under thermal steady state conditions. This was

confirmed by monitoring a change in surface temperature of less than 0.2 °C in a period of 5 min. The variables investigated, their range, the corresponding range of the relevant non-dimensional groups, together with typical values from an engine, are given in Table 2.

For all the measurements presented here, the mean value of velocity is estimated from a minimum sample size of 100, although usually the sample size was 5000. Also shown in some graphs is the root-mean-square (RMS) variation in the sample. It should be emphasised that this is not an 'error' bar, even though it is presented in a similar form. The RMS variation in the velocity measurement represents true physical fluctuations in the measured velocity in addition to various sources of experimental uncertainty.

Uncertainties in LDA measurements can arise from several sources:

- signal noise
- seeding
- velocity bias
- velocity gradient broadening
- probe alignment
- transit time broadening
- fringe bias.

It is perhaps worthwhile to briefly explain how these have been addressed and their effect on the measurements. Signal noise is reduced in the test rig by painting all the interior surfaces matt black. The windows are made from a high quality glass (BK7) that is recommended for LDA work. The windows and mirrors were cleaned regularly, usually before a test. The trade off between validation and data rate was investigated and the signal to noise ratio of the signal processor adjusted to achieve an optimum of this balance. The laser power was maintained at the lowest working value (usually around 150–350 mW), to reduce the effects of saturating the photomultipliers.

Quenching oil was used for the seeding medium and this can be atomised to a mean particle size of approximately 1 μm. This is generally accepted as being small enough to faithfully follow the motion of air flows with or without rotation. No difference was noted in the validation and data rates of using either one jet or all six jets in the atomiser, so one jet was used to reduce the fouling of the window.

Velocity bias originates from the fact that LDA signals are obtained from intermittent data. So a disproportionate number of signals are obtained when the velocity is high, since more of these particles pass through the probe volume in a given time. This results in a value of mean velocity that is biased towards a higher value than the 'true' mean. There are well known data processing algorithms to correct for this and these are implemented in the Dantec software and so no further correction was considered necessary.

Velocity gradient broadening occurs in regions where there is a significant velocity gradient in a direction normal to the fringes of the probe volume. This is unlikely to be a significant source of uncertainty in regions away from the solid surfaces. For the measurements of tangential velocity inside the cavity, at the highest rotational speed, there will be a velocity difference of about 2 m/s across the probe volume and this is less than 3% of the tangential velocity.

Transit time broadening occurs as a result of a measurement of Doppler burst frequency being obtained from a finite number of fringes – the fewer the fringes the greater is the potential uncertainty. The LDA apparatus uses 14 fringes and the uncertainty introduced by this considering the large number of samples usually taken is considered to be small.

Fringe bias occurs in flows with significant changes of direction, e.g., in highly recirculating flows, where the flow will change direction inside the probe volume itself. This causes the measurement to be rejected as insufficient fringes have been traversed. This will affect the flow statistics, but

Table 2
Range of experimental conditions

Parameter	Symbol (units)	Narrow annular gap $d_h/b = 0.092$	Wide annular gap $d_h/b = 0.164$	Uncertainty/[ ][a]
Rotor speed	Ω (rad/s)	$123 \leqslant \Omega \leqslant 306$	$65 \leqslant \Omega \leqslant 570$	±1 rad/s
Cooling air flow rate	$\dot{m}$ (kg/s)	$0.184 \leqslant \dot{m} \leqslant 0.618$	$0.2 \leqslant \dot{m} \leqslant 0.72$	±3%
Inlet pressure	p_{in} (bar, abs.)	$2.25 \leqslant p_{in} \leqslant 3.0$	$2.3 \leqslant p_{in} \leqslant 3.1$	±0.1%
Inlet temperature	T_{in} (K)	$311 \leqslant T_{in} \leqslant 319$	$302 \leqslant T_{in} \leqslant 339$	±0.2 K
Disc average surface temperature	$T_{s,av}$ (K)	$328 \leqslant T_{s,av} \leqslant 339$	$321 \leqslant T_{s,av} \leqslant 353$	±0.4 K
Shroud average surface temperature	T_{sh} (K)	$361 \leqslant T_{sh} \leqslant 376$	$353 \leqslant T_{sh} \leqslant 385$	±0.4 K
Disc rotational Reynolds number	Re_ϕ, Eq. (1)	$9.5 \times 10^5 \leqslant Re_\phi \leqslant 2 \times 10^6$	$4.0 \times 10^5 \leqslant Re_\phi \leqslant 4.1 \times 10^6$	$[8 \times 10^6]$
Axial Reynolds number	Re_z, Eq. (2)	$4.8 \times 10^4 \leqslant Re_z \leqslant 1.5 \times 10^5$	$4.7 \times 10^4 \leqslant Re_z \leqslant 1.8 \times 10^5$	$[2 \times 10^5]$
Rossby number	Ro, Eq. (3)	$1.27 \leqslant Ro \leqslant 5.1$	$0.27 \leqslant Ro \leqslant 7.5$	[1.5]
Shroud buoyancy parameter	$\beta\Delta T_{sh} = \beta(T_{sh} - T_{in})$	$0.15 \leqslant \beta\Delta T_{sh} \leqslant 0.19$	$0.11 \leqslant \beta\Delta T_{sh} \leqslant 0.238$	[0.35]
Disc buoyancy parameter	$\beta\Delta T_{av} = \beta(T_{s,av} - T_{in})$	$0.04 \leqslant \beta\Delta T_{av} \leqslant 0.08$	$0.02 \leqslant \beta\Delta T_{av} \leqslant 0.09$	[0.15]
Grashof number	$Re_\phi^2(\beta\Delta T)_{sh}$	$1.7 \times 10^{11} \leqslant Re_\phi^2(\beta\Delta T)_{sh} \leqslant 6 \times 10^{11}$	$1.8 \times 10^{10} \leqslant Re_\phi^2(\beta\Delta T)_{sh} \leqslant 2.5 \times 10^{12}$	$[2 \times 10^{13}]$

[a] Values indicated in square brackets '[ ]' are typical of engine conditions.

its effect on the measurements in this particular flow is considered to be marginal.

The accuracy of the location of the probe with respect to the test rig and maintaining that accuracy over successive tests can be a significant source of uncertainty when one velocity component is considerably greater than another. This is the case in the measurements of radial velocity and as will be explained later in this section, great care was taken to achieve accurate alignment.

4.2. Axial and tangential velocity components

Fig. 5 shows the variation of tangential velocity, V_ϕ, with non-dimensional radial location, r/b, for a wide annular gap ($d_h/b = 0.164$) test with $Re_\phi = 0.49 \times 10^6$, $Re_z = 0.92 \times 0^5$ and $Ro = 3.57$. The velocity measurements are mostly made inside Cavity 3 (see Fig. 4), with others made directly under the bore of Disc 2 (3 mm from the upstream face and 3 mm from the downstream face) and a further set of measurements made at the entrance to Cavity 2 (approximately 3 mm downstream of the bore of Disc 1). The measurements at $z/s = 0.33$ are made in the same plane as are the measurements at $z/s = 0.5$ and 0.67 and the axial width of the cavity at $r/b = 0.9$ is used as a reference value for s. The outer radius of the shaft is located at $r/b = 0.236$ and the bore of the discs at $r/b = 0.318$. The velocity measurements show that the tangential velocity is below disc speed in the annular gap between shaft and disc bores, varying from around 1 m/s (corresponding to $V_\phi/\Omega r \approx 0.25$) just above the shaft to 5 m /s ($V_\phi/\Omega r = 0.9$), just radially inward of the bore of Disc 2. Within the cavity itself, the flow is spun up to above disc speed in the small radial distance between the shaft and the equivalent radius to the disc bore and a maximum tangential velocity of 12 m/s ($V_\phi/\Omega r = 2.2$) is obtained inside Cavity 3 at $r/b = 0.34$. A value of $V_\phi/\Omega r > 1$ suggests that radial inflow should occur in the disc boundary layers. However, due to the shape of the disc cobs it was not possible to measure velocities close to the disc surface. Further into the cavity, the tangential velocity reduces and tends toward disc speed or solid body rotation ($V_\phi/\Omega r = 1$). There appears to be little significant difference between the tangential velocities measured at the different planes inside Cavity 3. The RMS values are much larger in the inlet region than in the cavity itself indicating the presence of widely fluctuating velocities and a region of mixing between the cavity flow and the axial throughflow. It is interesting to compare the velocity measurements shown in Fig. 5 with those presented by Farthing et al., for *isothermal flow*. These show similar behaviour: an increase in the normalised tangential velocity to above solid body rotation in the inlet region and a decrease to solid body rotation further into the cavity.

The radial variation of the *axial* component of velocity for the test shown in Fig. 5 (with $Re_\phi = 0.49 \times 10^6$, $Re_z = 0.92 \times 10^5$, $Ro = 3.57$) is presented in Fig. 6. For $r/b > 0.318$, which is inside the cavity, the axial velocity is virtually zero irrespective of the axial location of the measurement plane. For $0.236 < r/b < 0.318$, which is in the inlet region, the values of axial velocity are comparable with the bulk average velocity ($W = 17.45$ m/s). As was noted for the tangential component of velocity, the RMS values are much larger in the inlet region indicating large local fluctuations in velocity, considerable turbulence and mixing between the throughflow and the cavity flow. An

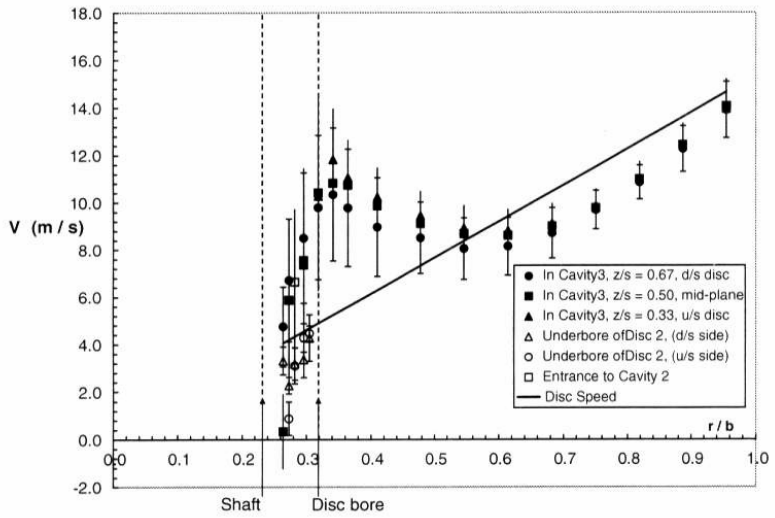

Fig. 5. Radial variation of tangential velocity at different measurement planes: $d_h/b = 0.164$, $Re_\phi = 0.49 \times 10^6$, $Re_z = 0.92 \times 10^5$, $\beta\Delta T_{av} = 0.09$, $\beta\Delta T_{sh} = 0.23$ and $Ro = 3.57$. Bars show RMS variation in velocity.

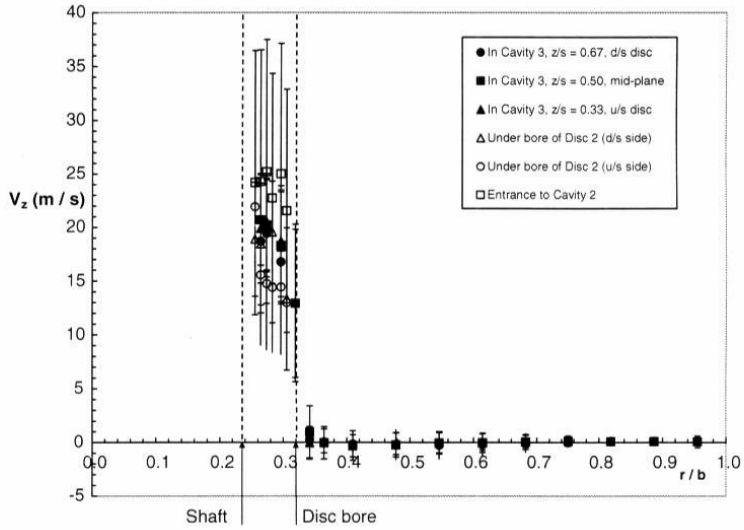

Fig. 6. Radial variation of axial velocity at different measurement planes: $d_h/b = 0.164$, $Re_\phi = 0.49 \times 10^6$, $Re_z = 0.92 \times 10^5$, $\beta\Delta T_{av} = 0.09$, $\beta\Delta T_{sh} = 0.23$ and $Ro = 3.57$. Bars show RMS variation in velocity.

estimate of the turbulence intensity can be made directly from the RMS values. For the data shown here, a value of ± 0.4 W is representative of the flow in the region between the shaft and the disc bore. For the flow in the outer part of the cavity, a value of $\pm 0.05\Omega r$ is representative of the data at $r/b = 0.89$.

Fig. 7 shows the variation of non dimensional tangential velocity $V_\phi/\Omega r$ with radius ratio, r/b, for a number of tests at $Re_z \approx 10^5$ and different values of rotational Reynolds number Re_ϕ with the wide annular gap ($d_h/b = 0.164$). The measurements are made in the mid-plane, $z/s = 0.5$, of Cavity 3. At the lowest value of Re_ϕ ($Re_\phi = 4.9 \times 10^5$), the normalised tangential velocity increases from just above zero near to the stationary shaft and reaches a maximum value of $V_\phi/\Omega r = 2.3$ at $r/b = 0.35$ which approximately corresponds to the radial location of the disc bores. Further into the cavity, $r/b > 0.35$, $V_\phi/\Omega r$ decreases and a value just below solid body rotation occurs at $r/b = 0.6$. The effect of increasing the rotational Reynolds number is seen by comparing these results with those for $Re_\phi = 10^6$, $2 \times 10^6$and 4.1×10^6. An increase in Re_ϕ (that is, a decrease in Ro) reduces the peak dimensionless tangential velocity in the region between the shaft and the disc bore. Further into the cavity there is little difference between the values of $V_\phi/\Omega r$.

A similar trend occurs when the axial Reynolds number is varied and the rotational Reynolds number held constant. This is illustrated in Fig. 8 which shows the variation of $V_\phi/\Omega r$ with r/b for tests with $Re_\phi \approx 10^6$ and $Re_z = 4.9 \times 10^4$, 9.7×10^4 and 1.7×10^5. Decreasing the Rossby number by decreasing the axial Reynolds number reduces the peak dimensionless tangential velocity in the region between the shaft and the disc bore.

The results shown in Figs. 7 and 8 suggest that the distribution of tangential velocity close to the shaft ($r/b < 0.5$) is controlled by the Rossby number (Eq. (4)) since this is a ratio of axial to rotational Reynolds numbers. A larger value of Rossby number implies an increase in the relative strength of the axial to tangential velocities which is expected to have more of an influence on the flow inside the cavity. This is also consistent with the findings of Farthing et al. who found that increasing the Rossby number increased the value of maximum normalised tangential velocity near the disc bore.

It is possible to use the results shown in Figs. 7 and 8 to comment on the role of buoyancy in this flow. For a buoyancy induced flow, the relative surface to freestream velocity outside the boundary layers is expected to be close to zero. Although the velocity inside the boundary layers will depend on the value of the Grashof number. The Grashof number may be thought of as the product Re_ϕ and $\beta\Delta T$. The sensitivity to Re_ϕ, as shown in Fig. 7, would therefore tend to suggest that the flow *outside* the boundary layers is governed by buoyancy forces. However, the results shown in Fig. 8 would appear to contradict this as such a flow regime would not be expected to show a variation with a Reynolds number based on the axial flow. The evidence presented by Long and Childs (2007) clearly demonstrates that the heat transfer from the peripheral shroud of this test rig is governed by the Grashof number. These conflicting observations may be resolved in the following way. As noted above, in the inner part of the cavity (say $r/b < 0.6$)

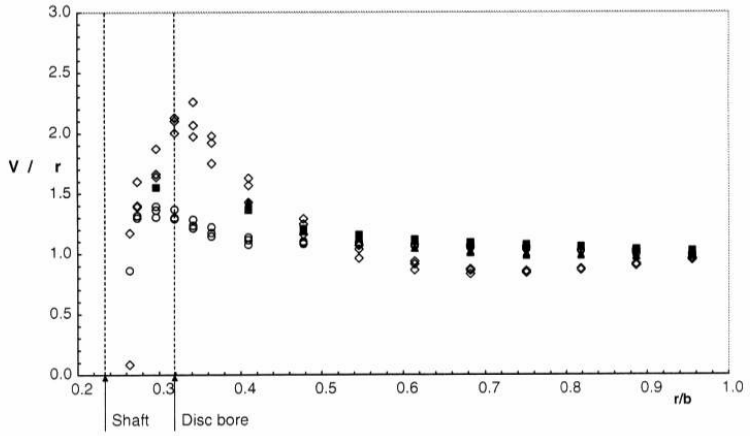

Fig. 7. Radial variation of normalised tangential velocity, $V_\phi/\Omega r$, with rotational Reynolds number for tests with the wide annular gap ($d_h/b = 0.164$) and $Re_z \approx 10^5$.

	$Re_\phi/10^6$	$Re_z/10^5$	Ro	$\beta\Delta T_{av}$	$\beta\Delta T_{sh}$
◊	0.49	0.92	3.57	0.09	0.23
▲	1.31	0.97	1.41	0.05	0.16
■	2.0	0.99	0.94	0.04	0.14
○	4.1	1.15	0.53	0.03	0.12

the flow is controlled by the ratio of axial to rotational Reynolds numbers as expressed by the Rossby number, Ro. In the outer part of the cavity ($r/b > 0.6$) solid body rotation occurs for all values of Ro tested. Since the relative velocity between surface and freestream is close to zero, buoyancy forces will be significant. Hence the heat transfer

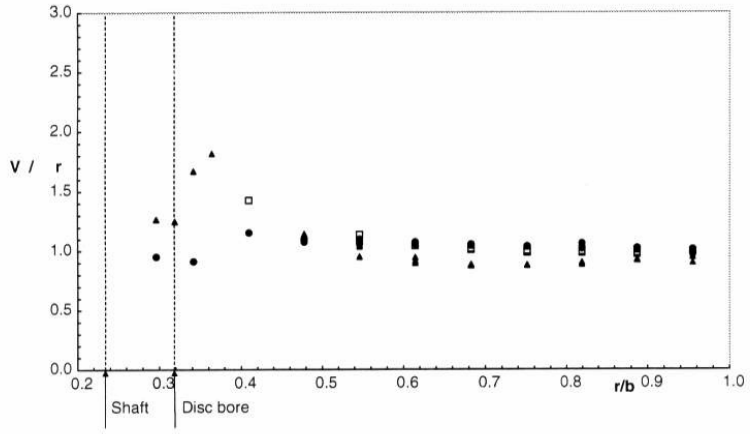

Fig. 8. Radial variation of normalised tangential velocity, $V_\phi/\Omega r$, with axial Reynolds number for tests with the wide annular gap ($d_h/b = 0.164$) and $Re_\phi \approx 10^6$.

	$Re_\phi/10^6$	$Re_z/10^5$	Ro	$\beta\Delta T_{av}$	$\beta\Delta T_{sh}$
●	1.24	0.49	0.75	0.06	0.17
□	1.31	0.97	1.41	0.05	0.16
▲	1.14	1.75	2.84	0.05	0.16

from the shroud can show a behaviour that is consistent with free convection and at the same time the flow structure in the inner part of the cavity can show a behaviour that is consistent with forced convection.

The dependence noted above, of the dimensionless tangential velocity on the Rossby number, is qualified in Fig. 9. This shows measured values of $V_\phi/\Omega r$ with r/b for a number of tests with the wide annular gap ($d_h/b = 0.164$) and also for the narrow annular gap ($d_h/b = 0.092$) between the disc bore and shaft. For $d_h/b = 0.164$, the tests were carried out at $Re_\phi = 0.49 \times 10^6$, 2×10^6 and 4×10^6 with $Re_z = 0.6 \times 10^5$, 10^5 and 1.8×10^5. For $d_h/b = 0.092$, the tests were carried out at $Re_\phi = 10^6$, 1.5×10^6 and 2×10^6 with $Re_z = 0.8 \times 10^5$, 10^5 and 1.5×10^5. For the wide annular gap, the comments made above can be observed – increasing the Rossby number increases the peak value of $V_\phi/\Omega r$ in the inlet region. Further into the cavity, the Rossby number has little influence on the values of $V_\phi/\Omega r$ and solid body rotation occurs. There certainly appears to be a marked difference between the two sets of results for the different annular gaps between shaft and disc bore. For the narrow annular gap ($d_h/b = 0.092$) the values of $V_\phi/\Omega r$ are seen to be lower than solid body rotation and increase to $V_\phi/\Omega r \approx 1$, further into the cavity. Since the annular gap between shaft and disc bore differs by a factor of almost two, it is not unreasonable to expect that this does have an influence on the flow inside the cavity. In this case reducing the annular gap between the shaft and disc bore attenuates the influence of the throughflow on the tangential velocity for $r/b < 0.6$.

Some support for this can be found in the measurements of Owen and Powell (2004) in a rig with an annular gap of $d_h/b = 0.026$ ($r_s = 145.2$ mm, $a = 150$ mm, $b = 371$ mm, $s = 75.2$ mm). These also show the behaviour noted here in the narrow gap data. The detailed measurements of Pincombe (1983) display two different types of behaviour (free and forced vortex flow). For $G = 0.53$, these differences were attributed to a change from Mode 1a to Mode 2a (non-axisymmetric to axisymmetric as reported by Farthing et al.) vortex breakdown. This could be of direct relevance to the present measurements where it is suggested that the geometry of the cavity affects the mechanism of vortex breakdown which in turn affects the tangential velocity distribution inside the cavity.

4.3. Radial velocity component

Simultaneous measurements of the radial and tangential components of velocity were obtained from the test rig with the wider annular gap between shaft and disc bore ($d_h/b = 0.164$). Optical access was gained through windows in Discs 3 and 4 and the stationary outer casing. Since the tangential component of velocity can be two orders of magnitude greater than the radial component, any misalignment of the LDA beams would result in a portion of the tangential velocity biasing the measurement of radial velocity. The angle of the plane of the pair of beams used to measure the radial component of velocity was measured with respect to a vertical line passing through the centreline of the test rig. This angle was measured using a precision spirit level and the uncertainty in this measurement is estimated to be $\pm 0.015°$. For the largest value of tangential velocity measured (50 m/s), this is equivalent to introducing an uncertainty of 0.014 m/s in the measured value of radial velocity. Typically several thousand simultaneous measurements of radial and tangential velocities were made at each location in the test rig. These locations covered the inside of Cavities 3 and 4, over the range ($0.067 \leqslant z/s \leqslant 0.946$) and ($0.565 \leqslant r/b \leqslant 0.925$).

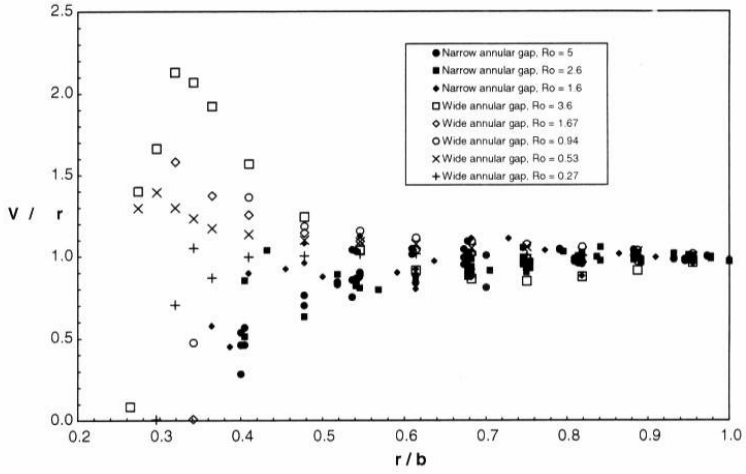

Fig. 9. Radial variation of normalised tangential velocity, $V_\phi/\Omega r$, with Rossby number – comparison between results for $d_h/b = 0.164$ and $d_h/b = 0.092$.

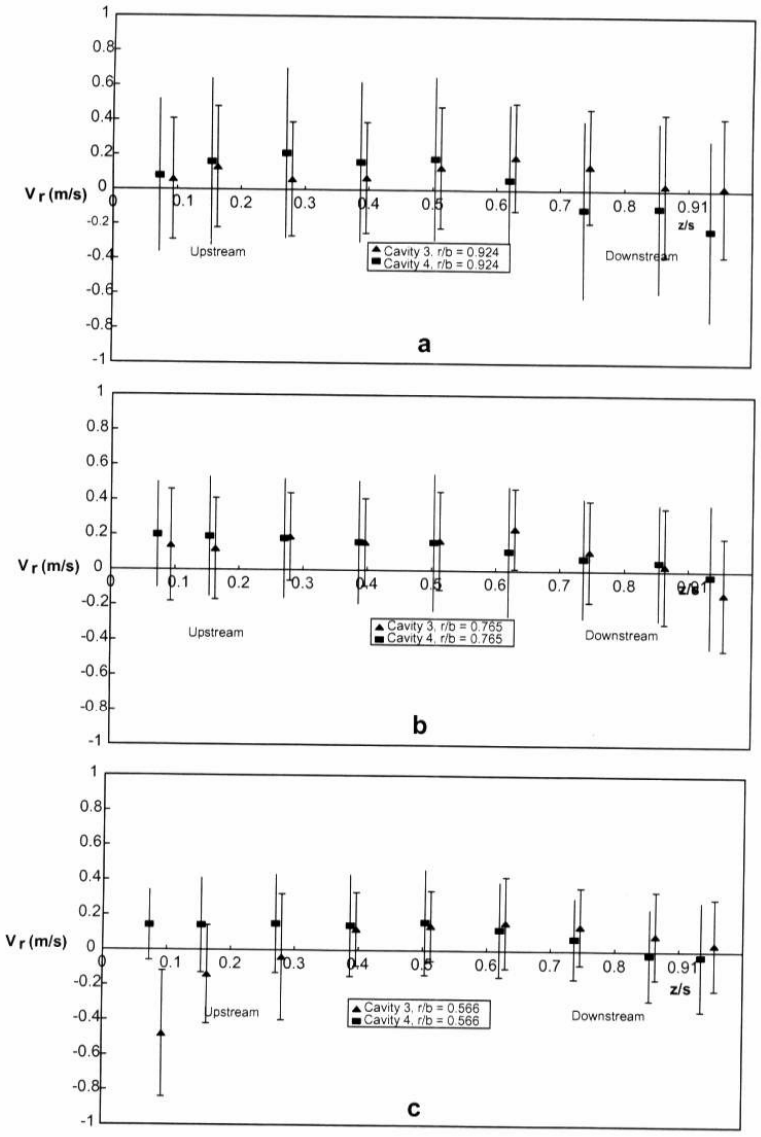

Fig. 10. Axial and radial variations of radial velocity for: $d_h/b = 0.164$, $Re_\phi = 0.4 \times 10^6$, $Re_z = 1.57 \times 10^5$, $\beta\Delta T_{av} = 0.07$, $\beta\Delta T_{sh} = 0.20$ and $Ro = 7.54$. Bars show RMS variation in velocity. (a) $r/b = 0.924$; (b) $r/b = 0.765$; (c) $r/b = 0.566$.

Fig. 10 shows the variation of the average values (each point is obtained from an average of all the measured instantaneous values at each radial and axial location) of radial velocity component with radial and axial locations in both Cavity 3 and Cavity 4. The flow conditions are $Re_\phi = 4 \times 10^5$, $Re_z = 1.57 \times 10^5$, $Ro = 7.54$, which is the largest value of Rossby number tested. A positive value of radial velocity indicates a radial outflow and a negative value, radial inflow. As can be seen, the magnitude of the velocities is generally low, <0.3 m/s, which is less than 1% of the bulk average axial velocity and about 2% of the tangential velocity at $r = b$. For these conditions, the uncertainty in radial velocity due to uncertainty in probe angle is estimated to be less than 0.01 m/s and the size of the data points is chosen to reflect this. Also shown are the RMS values obtained for each measurement. The magnitude of all the RMS values exceeds the magnitude of the measured value of radial velocity. This is in part due to the

periodic variations in radial velocity referred to above and in part due to turbulent fluctuations in the radial velocity.

In Cavity 3 the measurements show evidence of a circulation generated by the throughflow. This is seen by radial outflow at $r/b = 0.566$ (Fig. 10c) in the central region of Cavity 3 and radial inflow close to the upstream disc surface. At $r/b = 0.765$ (Fig. 10b), there appears to be outflow close to the upstream disc surface and in the central region, with inflow adjacent to the downstream disc. This reversal could be a secondary contra-rotating circulation generated by the circulation formed at the inner radius. At the outer radius (Fig. 10a) of Cavity 3 the magnitude of radial velocity is reduced and what motion there is appears to be restricted to the central part ($0.15 < z/s < 0.8$) of the cavity. In the main there appears to be no significant difference between the measurements in Cavities 3 and 4. One exception is at $r/b = 0.566$, where the measurements in Cavity 4 show radial outflow adjacent to the upstream disc. It is quite likely that exit conditions do influence the flow in the cavity (see Tucker and Long (1996), for example), so this difference may be due to a difference in exit geometry. The axial length of the passage between disc bore and shaft is considerably shorter at the exit of Cavity 3 compared with the exit of Cavity 4. The flow leaving Cavity 4 also does not experience a further cavity downstream and this too may affect the flow in the inner region of that cavity. Away from the disc surfaces, in the centre of each cavity, there is little variation of radial velocity with radius. The value of bulk average velocity for this test is $W = 36.2$ m/s using a value of $V_r = \pm 0.2$ m/s as being characteristic of the results shown here gives a non-dimensional velocity of $V_r/W = \pm 0.005$. Although the value of Rossby number tested here ($Ro = 7.54$) is significantly lower than the data of Farthing et al., their data for $G = 0.267$ and $Ro = 80$ give $V_r/W \approx \pm 0.01$. It should be noted that application of mass continuity would imply that at any radial location the outflow should balance the inflow. This does not appear to be the case when looking at the individual data points. However, when the range of the RMS values is taken into consideration, then continuity does appear to be satisfied. Although not shown here, the values of radial velocity obtained from other test conditions ($Re_\phi = 1.9 \times 10^6$, $Re_z = 0.52 \times 10^5$; $Re_\phi = 0.39 \times 10^6$, $Re_z = 0.6 \times 10^5$ and $Re_\phi = 2 \times 10^6$, $Re_z = 1.65 \times 10^5$) show similar behaviour to those in Fig. 10. Decreasing the axial Reynolds number has very little effect on the magnitude of V_r whereas increasing the rotational Reynolds number appears to increase the magnitude of V_r. The magnitude of the radial velocity component remains about two orders of magnitude less than the tangential component.

4.4. Spectral analysis of the tangential component of velocity

As was noted in Section 2, the current model for the flow in a heated rotating cavity with axial throughflow comprises pairs of counter-rotating vortices in the r–ϕ plane (Fig. 3). There is direct experimental evidence of this (see Farthing et al.) and also indirect evidence from the frequency spectrum obtained from velocity measurements (see Owen and Powell). It is therefore of some interest to carry out a similar frequency-spectrum analysis of the present data to see if this is consistent with this model of the heated flow structure.

This was achieved by obtaining a fast Fourier transform of a set of measured values of tangential velocity. Each measured value was obtained by averaging the appropriate number of instantaneous measurements over each pass of one of the windows. Fig. 11 shows the frequency spectrum obtained from the tangential velocity measurements for $Re_\phi = 4 \times 10^5$, $Re_z = 16 \times 10^4$, $Ro = 7.4$ in the mid-plane ($z/s = 0.5$) of Cavity 3 at a radial location of $r/b = 0.765$. There is a clear dominant spike in the spectrum at 22 Hz. The rotational speed of the cavity in this test is 655 rev/min, so the spike occurs at just over twice the rotational speed. It is possible to explain this behaviour in the context of the current model of the heated flow structure. For a uniform flow rotating at a constant speed of $V_\phi = \Omega r$, there is no cyclic variation of velocity in the absence of any vortex pairs. So this would produce a spectrum without any clearly defined peaks. The presence of white noise in this flow, generated by turbulence for example, would be shown as a background of closely spaced peaks and this is also evident in Fig. 11 either side of the main peak at 22 Hz. The velocity measurements from a *single* pair of contra-rotating vortices in a flow rotating at $V_\phi = \Omega r$ would produce, if the measurement point were located towards the outer part of the vortex structure, a velocity signal that increased above Ωr as the cyclonic vortex passed over the measurement point and then decreased below Ωr as the anti-cyclonic vortex passed over the measurement point. Each rotation of the whole flow would produce a signal with the frequency of approximately the rotational speed of the flow. For two vortex pairs, the dominant frequency would be twice the rotational speed; three pairs, three times etc. Naturally this simple explanation assumes the vortices are of identical shape and size and have identical magnitudes of rotational speed. A real flow with variations in these variables will create differences in the spectrum which at this stage are difficult to interpret. It would therefore

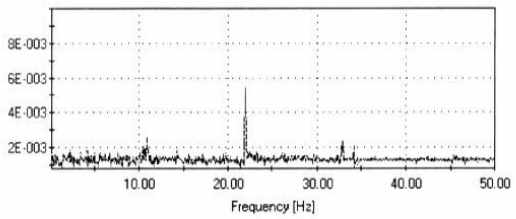

Fig. 11. Frequency Spectrum obtained from tangential velocity measurements: $d_h/b = 0.164$, $Re_\phi = 0.4 \times 10^6$, $Re_z = 1.57 \times 10^5$, $\beta\Delta T_{av} = 0.07$, $\beta\Delta T_{sh} = 0.20$ and $Ro = 7.4$ in the mid-plane ($z/s = 0.5$) of Cavity 3 at a radial location of $r/b = 0.765$ (rotational speed of cavity = 10.92 Hz).

appear that the spectrum shown in Fig. 11 is consistent with two pairs of contra-rotating vortices.

Although not shown here analysis of the frequency spectra obtained at other axial and radial locations and other values of rotational and axial Reynolds numbers is broadly in agreement with these observations. In some cases there is not one single dominant spike in the spectra but two or even three. These occur at frequencies that are harmonics of a fundamental. Recent experimental work and CFD simulation (Bohn et al., 2006 and Owen et al., 2006) has shown that it is possible for the cellular structure to change with time: one pair of vortices can evolve into two pairs of vortices and then into three. So, it may be possible that the appearance of multiple spikes in the frequency spectra indicates this behaviour. An alternative explanation is that the flow behaviour is not adequately represented by a single harmonic. In principle it should be possible to examine the spectral data to see if and when a spike at one frequency changes to a multiple of that frequency, indicating a transition from say two to three pairs of vortices. However, in order to build up a frequency spectrum tens of thousands of data points are required. To investigate how this changes over time would require data sets much larger than those collected from this experiment.

5. Conclusions

This paper has presented measurements of axial, radial and tangential velocities carried out in a heated multiple cavity test rig with axial throughflow. This test rig is designed to be a 70% full scale replica of a high pressure compressor internal air system. The main interest is the flow in the cavities formed between the adjacent heated disc surfaces and the interaction of this flow with the central throughflow of cooling air. Two different variants of the test rig have been investigated, these differ by the size of the annular gap between the central shaft and the disc bores. For the narrow annular gap $d_h/b = 0.092$ and for the wide annular gap $d_h/b = 0.164$.

Measurements were made inside the rig for a range of non-dimensional conditions that are representative of those found inside an engine (values of rotational Reynolds number up to $Re_\phi = 4 \times 10^6$ and axial Reynolds numbers up to $Re_z = 1.8 \times 10^5$). However, the Grashof number based on the shroud conditions (Re_ϕ^2 $(\beta \Delta T)_{sh}$) is at least an order of magnitude lower. Measurements of the tangential and axial velocities inside the cavities were made using a two component LDA system, with optical access being provided through the shaft. Additional measurements of the tangential and radial components of velocity were obtained in for the wide annular gap with optical access being gained via windows in the outer casing and the disc surfaces.

The main conclusions from this work are summarised below:

Although it was not possible to make measurements inside the disc boundary layers, the tangential velocity does not appear to vary across the axial width of a cavity. The axial velocities inside the cavity are close to zero. For the wider annular gap between shaft and disc bore ($d_h/b = 0.164$), the maximum value of $V_\phi/\Omega r$ occurs close to the inner radius of the cavity and its magnitude increases with increasing Rossby number. The non-dimensional tangential velocity decreases from this maximum value to solid body rotation, $V_\phi/\Omega r = 1$, as $r/b > 0.6$. For $d_h/b = 0.092$, the non-dimensional tangential velocities do not show a maximum until solid body rotation is achieved near the outer radius. This difference in radial variation of tangential velocity is attributed to a difference in the influence of the central throughflow on the flow inside the rotating cavities; and a narrow annular gap attenuates this interaction. It appears likely that the behaviour of the jet and hence the mode of vortex breakdown is affected by this change in geometry.

The values of radial velocity are typically two orders of magnitude lower than the tangential component and comparable to the relative tangential velocity. It is difficult to interpret the overall behaviour of the flow from these measurements because the flow is unsteady and an average is misleading. However there is evidence to suggest the existence of circulating flow within the cavities. There also appears to be a difference in the flow structure between Cavity 3 and Cavity 4 which could be attributed to a difference in exit conditions. An analysis of the frequency spectrum obtained from the tangential velocity measurements shows clear evidence of periodicity in the flow structure. This is linked to the existence of pairs of contra-rotating vortices which is consistent with the current understanding of the heated flow structure.

Acknowledgements

The authors express their thanks to the following organisations which have supported this research work: The Engineering and Physical Sciences Research Council, Rolls-Royce Plc, the European Union and participating companies in the 5th Framework of the BRITE-Euram scheme of the European Union. We are indebted to Dr. Alex Alexiou, now at the Technical University of Athens, for his help with the experimental work. The authors are also grateful to our colleague, Dr. Lionel Ripley, in the Department of Engineering & Design, for help with the interpretation of the spectral analysis.

References

Alexiou, A., 2000. Flow and heat transfer in gas turbine H.P. compressor internal air systems. D.Phil. Thesis, School of Engineering, University of Sussex, UK.

Bohn, D., Ren, J., Tuemmers, C., 2006. Investigation of the unstable flow structure in a rotating cavity. Paper No. GT2006-90494, Presented at the ASME Turbo Expo, Barcelona, Spain.

Farthing, P.R., Long, C.A., Owen, J.M., Pincombe, J.R., 1992. Rotating cavity with axial throughflow of cooling air: flow structure. ASME, J. Turbomachinery 114, 237–246.

Johnson, B.V., Lin, J.D., Daniels, W.A., Paolillo, R., 2004. Flow characteristics and stability analysis of variable density rotating flows in compressor disk cavities. Paper No. GT2004-54279, Presented at the ASME Turbo Expo, Vienna, Austria.

Long, C.A., Childs, P.R.N., 2007. Shroud heat transfer measurements inside a heated multiple rotating cavity with axial throughflow. Int. J. Heat Fluid Flow, in press. doi:10.1016/j.ijheatfluidflow.2007.04.009.

Long, C.A., Tucker, P.G., 1994. Numerical computation of laminar flow in a heated rotating cavity with an axial throughflow of air. Int. J. Numer. Meth. Heat Fluid Flow 4, 347–365.

Long, C.A., Morse, A.P., Tucker, P.G., 1997. Measurement and computation of heat transfer in high pressure compressor drum geometries with axial throughflow. ASME, J. Turbomachinery 119, 51–60.

Owen, J.M., Powell, J., 2004. Buoyancy induced flow in a heated rotating cavity. Paper No. GT2004-53210, Presented at the ASME Turbo Expo, Vienna, Austria.

Owen, J.M., Rogers, R.H., 1995. Flow and heat transfer in rotating disc systemsRotating Cavities, vol. 2. Research Studies Press Ltd, UK.

Owen, J.M., Abrahamsson, H., Linblad, K., 2006. Buoyancy induced flow in open rotating cavities. Paper No. GT2006-91134, Presented at the ASME Turbo Expo, Barcelona, Spain.

Pincombe, J.R., 1983. Optical measurements of the flow inside a rotating cylinder. D.Phil Thesis, School of Engineering and Applied Science, University of Sussex, UK.

Rolls-Royce, 2005. The Jet Engine. Rolls-Royce Publications.

Sun, Z., Kilfoil, A., Chew, J.W., Hills, N.J., 2004. Numerical simulation of natural convection in stationary and rotating cavities. Paper No. GT2004-53528, Presented at the ASME Turbo Expo, Vienna, Austria.

Tian, S., Tao, Z., Ding, S., Xu, G., 2004. Investigation of flow and heat transfer instabilities in a rotating cavity with axial throughflow of cooling air. Paper No. GT2004-53525, Presented at the ASME Turbo Expo, Vienna, Austria.

Tucker, P.G., Long, C.A., 1995. CFD prediction of vortex breakdown in a rotating cavity with an axial throughflow of air. Int. Commun. Heat Mass Transfer 22 (5), 639–648.

Tucker, P.G., Long, C.A., 1996. Numerical investigation into influence of geometry on flow in a rotating cavity with an axial throughflow. Int. Commun. Heat Mass Transfer 23 (3), 335–344.

Wong, L.S., 2002. Flow and heat transfer in rotationally induced buoyancy flow. D.Phil. Thesis, School of Engineering and Information Technology, University of Sussex, UK.

Appendix 3.1: ORION data logger channels connections

Thermocouple or Data logger channel number	Location	Thermocouple or Data logger channel number	Location
1	Rotor	38	Annulus (Air)
2	Rotor	39	Annulus (Air)
3	Rotor	40	Annulus (Air)
4	Rotor	41	Annulus (Air)
5	Rotor	42	Annulus (Air)
6	Rotor	43	Annulus (Air)
7	Rotor	44	Casing (inner surface)
8	Rotor	45	Casing (inner surface)
9	Rotor	46	Casing (inner surface)
10	Rotor	47	Casing (inner surface)
11	Rotor	48	Casing (inner surface)
12	Rotor	49	Casing (inner surface)
13	Rotor	50	Casing (outer surface)
14	Rotor	51	Casing (outer surface)
15	Rotor	52	Casing (outer surface)
16	Rotor	53	Casing (outer surface)
17	Rotor	54	Casing (outer surface)
18	Rotor	55	Casing (outer surface)
19	Rotor	56	Orifice (inlet)
20	Rotor	57	Orifice (outlet)
21	Rotor	58	Heater 1
22	Rotor	59	Heater 2
23	Rotor	60	Rotor SRU
24	Rotor	61	Ambient
25	Shaft	62	Sensor 1
26	Shaft	63	Sensor 2
27	Shaft	64	Rotor speed (rev/min)
28	Shaft	65	Pressure Trsdcr 1 (V)
29	Shaft	66	Pressure Trsdcr 2 (V)
30	Shaft	67	Pressure Trsdcr 3 (V)
31	Shaft	68	Mass flow rate (kg/s)
32	Inlet (Air)	69	Re_{Φ}
33	Inlet (Air)	70	Re_z
34	Outlet (Air)	71	Ro
35	Outlet (Air)		
36	Annulus (Air)		
37	Annulus (Air)		

Appendix 3.2: Scanivalve data logger channels connections

Channel number	Location
0	Reference
3	Air IN O/P upstream
4	Air IN O/P downstream
5	Air OUT O/P upstream
6	Air OUT O/P downstream
10	Shaft upstream
11	Shaft downstream
12	Inlet pressure
13	Outlet pressure
15	Heater 1
16	Heater 2

Appendix 3.3: Encoder driver connections

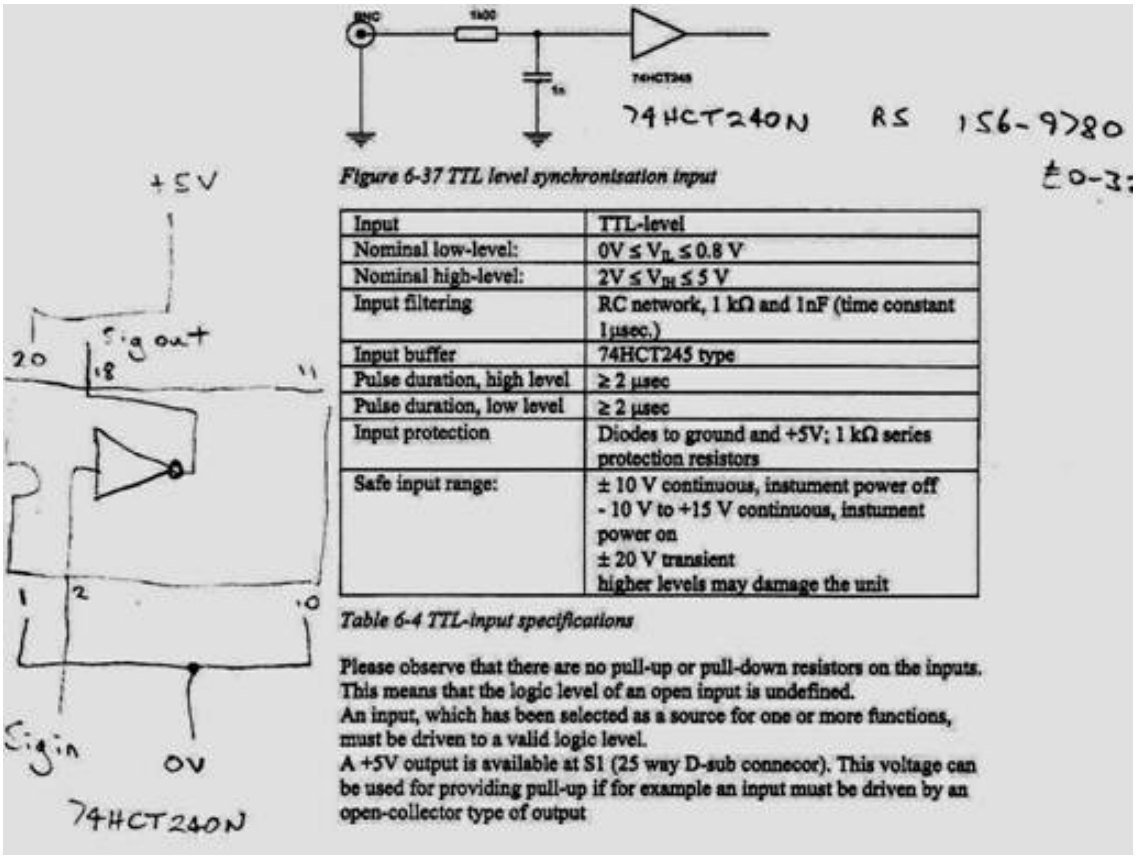

Figure 6-37 TTL level synchronisation input

Input	TTL-level
Nominal low-level:	$0V \leq V_{IL} \leq 0.8$ V
Nominal high-level:	$2V \leq V_{IH} \leq 5$ V
Input filtering	RC network, 1 kΩ and 1nF (time constant 1 µsec.)
Input buffer	74HCT245 type
Pulse duration, high level	≥ 2 µsec
Pulse duration, low level	≥ 2 µsec
Input protection	Diodes to ground and +5V; 1 kΩ series protection resistors
Safe input range:	± 10 V continuous, instument power off - 10 V to +15 V continuous, instument power on ± 20 V transient higher levels may damage the unit

Table 6-4 TTL-input specifications

Please observe that there are no pull-up or pull-down resistors on the inputs. This means that the logic level of an open input is undefined.
An input, which has been selected as a source for one or more functions, must be driven to a valid logic level.
A +5V output is available at S1 (25 way D-sub connecor). This voltage can be used for providing pull-up if for example an input must be driven by an open-collector type of output

Annotated connections diagram from Dantec (2004)

Appendix 3.4: LDA traverse alignment checklist

TRAVERSE SET-UP:
Start laser at low power (0.25W) according to Procedure.
Bring control computer (+ signal and control cables) closer for convenience
Connect and set-up control boxes + computer
Run BSA Flow Software on control computer
New project, F/P BSA application, connect (check connection with on-line LED on processor)
The laser probe is fitted in the traverse tube from the back and slotted in the support ring 1cm out to allow cleaning.
Blow surface of probe optics with dry air canister. !!Hold can UP to avoid blowing liquid.
Clean optic by applying special cloth. Press uniformly and very gently, move in steady and slow motion out. Turn pad on clean area and start again. REMARK: There is 1 scratch in the optic that was already there.
Align optic with tube surface then lock with circumferential screws.
Unlock upper stepper motor to allow access of probe tube in its holding support. Align probe tube with surface of back bracket (rough axial position). Re-screw stepper motor.

Optics cleaning:
Optical surfaces are coated with a non-reflective film that is really thin and fragile. DO NOT touch with hands directly, or scratch in any way.
Blow surface with dry air canister (keep canister up to avoid blowing liquid)
Take optical wash pad and scrape lightly with light pressure in a slow steady motion
Turn pad over and do again
For access and cleaning of disc windows inside the rig, a pad support is employed. The cleaning is monitored visually through the opening of the external casing window (removed).

Mirror cleaning (NOTE: Mirror Extremely Fragile!!):
One of the last thing to be installed. An extremely clean mirror is essential for measurement, scratches are easy to obtain. Same method of cleaning as optics is required, with even more care (sit at table to avoid accidental drops).
Remove little fixating screws.
Without touching it, insert mirror in tube (peg for orientation), and screw the mirror in tube.
Insert mirror tube a bit in shaft after having pulled traverse at max back.
Insert mirror tube in front bracket and align with peg and back surface of bracket.

Orientation of the beams:
The pairs of beams need to be referenced perpendicularly to the geometry of the rig.
Pull back totally the traverse system, cover mirror with piece of paper to avoid accidental contamination.
Install special alignment support on casing.
Sit on rig's ground frame, Goggles ON.
Open probe beams shutters.
Look (with goggles) to target and turn mirror tube to make coincide laser dots and perpendicular lines (precision: as much as it gets).
Fix the mirror tube in support.

Axial and Radial position calibration:
Launch BSA F/P Software.
In properties window (for LDA1 or LDA2), adjust High Voltage at low value first and gradually increase not to overload the photomultiplier.
Set Data collection Type to Continuous instead of burst when calibrating the traverse system.
In Project Explorer, add histogram + 2D plot + list (raw data) objects
Right-click main window to access system monitor, allowing setting the signals according to the beam position for the traverse set-up.
Remove the traverse blocker before operating the traverse
Radial location: Adjust traverse radial position to get maximum signal on the reference plane. If Anode Current indicator gets>1, reduce High Voltage on LDA settings.

The validation indicators get to ~100% when the surface is reached. The radial location is therefore known. Redo with another radial reference to confirm radial calibration.
Axial location: Move along X from surface, reading OK of radial position, until one of the beam pair gets crossed (getting near). Once the first signal is lost, try to get exact location of when second signal is lost (axial location found). Redo with another reference plane to confirm axial calibration.
When the axial and radial locations are calibrated, check repeatability of positioning on different cavity features from design dimensions of the rig.
The stepper motors positions value indicator can be zeroed and a blocker can be put on the axial traverse at max X position. **(Remember to remove the traverse blocker if traverse manipulations are to be done later)**

Re-calibration/Check:
Put traverse in position+ remove blocker
Get control computer closer to rig (convenience)
Log in Bungalow (not to forget the capital B)
Run BSA, open B3setup.lda
Connect to processor (right-click processor)
Connect to traverse
Right-click traverse system to open traverse dialog box (allows manual operation of stepper motors)
Switch transmitter to through position + open fibre shutters
Open AutoCad drawing
Run system monitor to check whereabout the beams are
Re-twitch to adjust origin position + reset axis (precision ±0.5mm)
Check X position accuracy by reaching next cob
Optimise Y position + move on shroud to check
On exit save changes
Turn off computer + control boxes
Shut fibres
Transmitter half-way

Appendix 4.1: Laser operation checklist

LASER OPERATION:

LASER STARTUP:

●WATER: ON (Open water valve to black mark). Check Water Filter ~6Months

●POWER MAINS: Isolator ON

●DOOR: Locked

●LASER POWER: Minimum, Power controls in Current mode set at 15-20 Amps

●LASER SHUTTER: SHUT, Diaphragm Minimum

●PLASMA: Key switch ON (15s wait until laser emits)

●FIBRE SHUTTERS: 4xShut

●TRANSMITTER: Half-way position, Beam way CLEAR

●LASER SHUTTER: OPEN

●WARM UP: Power increased to setting (W), log start time, Warm-up time 30 min

●COMPUTER: ON, Check connection signal cables (Ethernet in LDA slot, COM in top COM plug on computer)

●PROCESSOR: ON, (Ready lamp ON)

●TRAVERSE: Position OK, traverse controller ON

●BSA F/P: Connected (Processor On-line)

LASER SWITCH OFF:

●COMPUTER: OFF

●PROCESSOR: OFF

●TRAVERSE: OFF

●LASER POWER: Minimum

●FIBRE SHUTTERS: 4*shut

●TRANSMITTER: Half-way position

●LASER SHUTTER: Shut

●PLASMA: OFF

●DUST COVER: On transmitter

●COOLING: Wait for cooling (check with water pipes)

●POWER MAINS: Isolator OFF

●WATER: OFF

●LOG: Functioning duration and power used

Laser power change:

: When changing power of laser, turn fibres OFF and allow 10 Minutes stabilisation

Appendix 4.2: Air supply checklist and air cooling diagram

HOWDEN and Water Recirculation:

Single stage, screw type compressor driven by a 275kW electric motor via a 3.95:1 gearbox. Can supply up to 1.1kg/s of air at 4 bar absolute and 200°C.
When the Howden hasn't been run for ~3 or more weeks, the water temperature between the roof and underground tanks needs to be circulated to avoid too important discrepancies of temperature that would produce some irregularities of the cooling (mixing difficult from the baffles inside underground tank especially, resulting in discrepancies of temperatures during run as the cooling flow uniformises). To avoid, turn on recirculation pump for 3-4 hours the afternoon before running tests.

WATER RECIRCULATION:

●VALVES: 1.Roof Tank Main Valve, 2.Heat Exchanger Inlet FULL OPEN, 3.Flow Control valves OPEN TO MARK

●PUMP: ON (A or B)

SAFETY AIR SUPPLY VALVE:

●AIR SUPPLY: ON

●OPERATIVE: CHECK

HOWDEN START-UP:

●HOWDEN WATER COOLING PUMP: ON (on control panel), CHECK Water Pressure (Downstairs) – 5Psi

●MAIN POWER ISOLATOR: ON (Downstairs), Howden double-doors semi locked

●OIL PUMP: ON (control panel), CHECK Oil pressure 12-14 Psi

●PRESSURE CONTROL VALVE: Check OFF-LOAD

●CONTROL PANEL RESET: All Lights ON

●HOWDEN START: Switch ON, Check started

DURING RUN: LOGBOOK
AT START: Time of Start + Finish
Initials of operators
EACH HOUR: Pressure + Temperature

HOWDEN SHUT DOWN:

●PRESSURE CONTROL VALVE: Turn hand wheel OFF-LOAD

●HOWDEN STOP: Switch OFF

●COOLING: Leave Oil Pump, Water Recirculation, Water cooling pumps, ON, WAIT AN HOUR

●OIL PUMP: OFF

●HOWDEN WATER COOLING PUMP: OFF

●CONTROL PANEL: Switch OFF

●MAIN POWER ISOLATOR: OFF, Leave doors open

●WATER RECIRCULATION VALVES: 1.Flow Control, 2.Heat Exchanger Inlet, 3.Roof Tank Main Valve FULL SHUT

RIG AIR WATER COOLING SYSTEM:

ARRANGEMENT DIAGRAM:

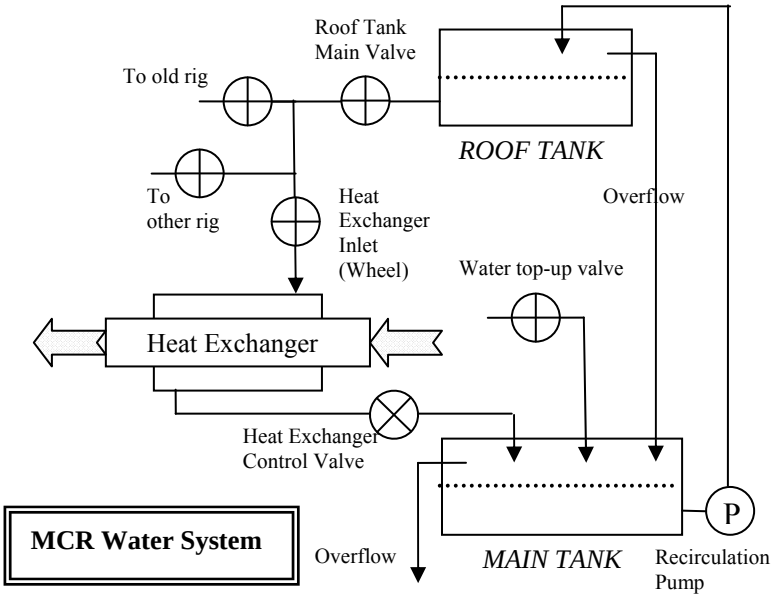

Appendix 4.3: Rig air supply checklist

RIG AIR SUPPLY:

ARRANGEMENT DIAGRAM:

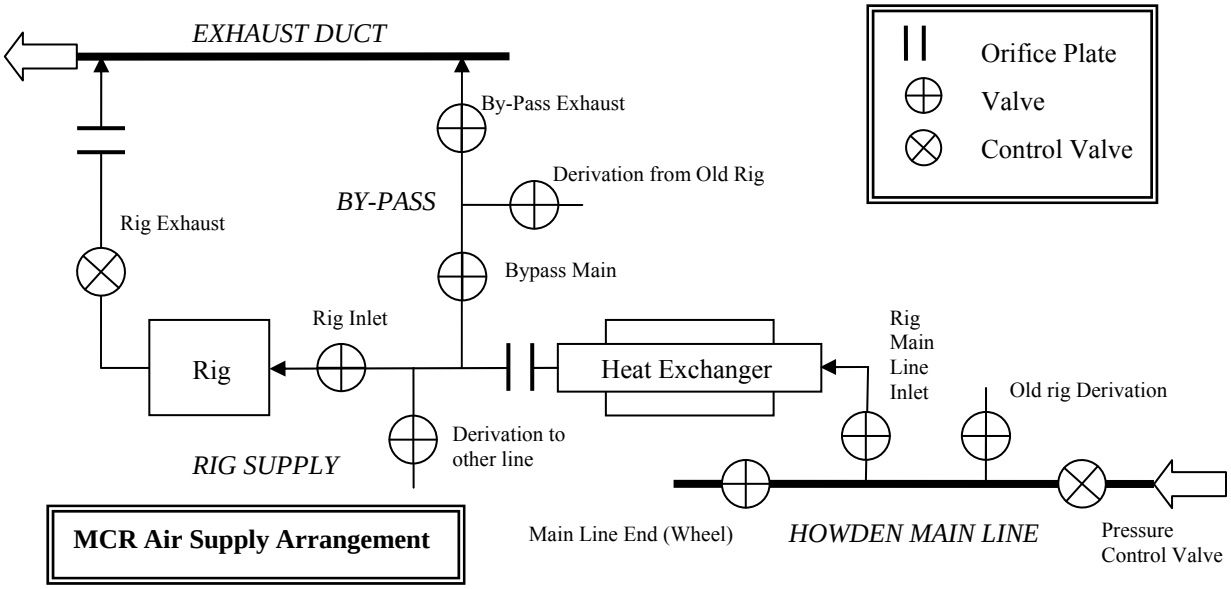

PRE-RUN LINE CHECK:

HOWDEN MAIN LINE:
●OLD RIG DERIVATION: Always OFF

●RIG MAIN LINE INLET: Always ON

●MAIN LINE END (Wheel): Always OFF

RIG SUPPLY:
●DERIVATION TO OTHER LINE: Always OFF

●RIG INLET: OFF

●RIG EXHAUST: Full OPEN

BYPASS:
●BY-PASS MAIN: ON

●DERIVATION FROM OLD RIG: Always OFF

●BY-PASS EXHAUST: ON

HOWDEN SAFETY VALVE:

●AIR SUPPLY: ON

●OPERATION: CHECK

Appendix 4.4: Rig pre-start checklist

MULTI-CAVITY RIG

PRE START CHECK LIST

1 Water valves (roof tank / heat exchanger) - water pump (re-circulating)
2 Compressed air valves (sru, window cleaning)
3 Water for laser, laser 3-phase on, plasma on, set laser power
4 Air inlet valves (howden, by-pass, rig)
5 Oil tank valve & oil level
6 Power supplies, isolators, panel switches & pcs (laser, orion-scani) on
7 Signal processor, traverse controller on
8 Lab ventilation, main fans, oil tank centrifuge, hot air extractor valve
9 Howden water pump, howden isolator, howden oil pump → reset → start howden
10 Hydrovane on, atomiser pressurised (min 25 psi above rig working pressure)

Appendix 4.5: Air supply condition setting checklist

AIR SUPPLY RUN CONDITIONS SETTING:

●RIG BY-PASS: Double Check OPEN (Pre-Run checklist)

●START HOWDEN: (Howden checklist)

●PRESSURE CONTROL VALVE: Apply 10Psi, wait 10 minutes

●RIG EXHAUST VALVE: Double Check FULL OPEN

●RIG INLET VALVE: OPEN

●RIG BY-PASS: SHUT

●CONDENSATION: Check

●FLOW CONDITIONS SETTING: Increase pressure from Pressure Control Valve, Modify opening of Rig Exhaust Valve, until desired value of Rez obtained.

Appendix 4.6: Rig start checklist

MULTI-CAVITY RIG

STARTING PROCEDURE

1 Adjust water flow rate to achieve the required cooling air temperature (1st through by-pass and then in the rig)

2 Using downstream control valve & howden bypass valve pre-set internal rig pressure (min 10 psi)

3 Switch on - oil pump & tasc motor

4 Set rotor speed and rig pressure as required

5 Start blower and switch on heaters

6 Monitor vibration levels & fill in log sheet

7 Wait for thermal steady state

Appendix 4.7: Rig shut down checklist

MULTI-CAVITY RIG

SHUT DOWN PROCEDURE

1 Switch off heaters

2 Reduce rotor speed to 2000 rpm

3 Fully open air flow control valve (min 15 psi)

4 Let rotor rotate for 15 min after switching off heaters to aid cooling

5 Turn off tasc motor

6 When rotor speed falls below 500 rpm stop oil pump

7 When rotor has completely stopped shut down howden

8 Switch off blower

9 Reverse all pre-start conditions

Appendix 4.8: Read.bas listing

```
REM ****PROGRAM MCRread.bas***
REM written by A. Alexiou
REM program last modified 30/04/05 by N. Miché
REM This program reads the data files from the ORION and
SCANIVALVE
REM and writes them to files so that they can be used for further
processing
REM This program requires the modified scanivalve with added
parameters
REM data from build 2 or build 3 is automatically recognised and
processed
DECLARE SUB labyrinth (pup!, pdn!, tup!, r1!, cl!, lk!)
REM SUB "labyrinth" calculates the leakage through the various labyrith
seals
REM in the rig according to Curzons (1991) RR TDR 90294
DECLARE SUB orifice (no, pin!, pout!, cin!, d1!, d!, mn!)
REM SUB "orifice" calculates the mass flow rate in & out of the rig
REM according to BS 1042 for orifice plates
np = 71     'number of parameters supplied by the data logger program
sn = 100     'number of data logger scans
nc = 8      'number of pressures measured by Scanivalve
nsc = 3     'number of Scanivalve scans
DIM scan(sn)
DIM tm(sn)
DIM ChNo(np)
DIM frnm(sn)
DIM dlpr(3, sn)
DIM total(np), row$(28), aval(np), sq(np), valsd(np), header$(20)
DIM PR(nc, nsc), prtot(nc), avpr(nc), ptot(3), pav(3)
DIM value(71, sn)
REM pr?(psi for calculations, Pa for display and reading), temp?(C),
dor?(m), Dpipe?(m), rd?(m)
REM Read Orifice & Pipe Diameter
REM ****************************
READ dor1, Dpipe1, dor2, Dpipe2
DATA 0.055,0.075,0.055,0.075
REM Read Seal Radius and No of Fins
REM *******************************
READ rd1, cl1, rd2, cl2, rd3, cl3, rd4, cl4, rd5, cl5
DATA
0.1265,0.00005,0.0515,0.00005,0.108,0.0001,0.051,0.0001,0.029,0.000
1
CLS
REM Output File
REM ***********
fileout$ = "G:\MCRread\test8.dat"
OPEN fileout$ FOR OUTPUT AS #4
REM INPUT FILES
REM ***********
orion$ = "G:\MCRread\or36-1.dat"
scani$ = "G:\MCRread\testsc36.dat"
OPEN orion$ FOR INPUT AS #2
OPEN scani$ FOR INPUT AS #3
REM *********************
REM Read Data from Orion
REM *********************
c = 273.15
FOR k = 1 TO sn
LINE INPUT #2, ScanNo$
LINE INPUT #2, Times$
scan(k) = VAL(MID$(ScanNo$, 9))
tm(k) = VAL(MID$(Times$, 6, 6))
FOR j = 1 TO 64
INPUT #2, ChNo(j), value(j, k)
NEXT j
FOR j = 65 TO 67
INPUT #2, ChNo(j), value(j, k), dlpr(j - 64, k)
NEXT j
INPUT #2, ChNo(j), value(j, k), frnm(k)
FOR j = 69 TO 71
INPUT #2, ChNo(j), value(j, k)
NEXT j
LINE INPUT #2, emptyline$
NEXT k
ntms = sn
REM *** transient printing ***
            'FOR k = 1 TO ntms
            'PRINT #4, USING "######.##"; tm(k);

            'FOR j = 1 TO np - 1
            'PRINT #4, USING "######.##"; value(j, k);
            'NEXT j
            'PRINT #4, USING "######.##"; value(np, k);
            'PRINT #4, USING "###.##"; dlpr(1, k); dlpr(2, k); dlpr(3, k)
            'NEXT k
REM ***********************************************
REM Calculate Average Values & Standard Deviation
REM ***********************************************
FOR k = 1 TO ntms
FOR i = 1 TO np
            total(i) = total(i) + value(i, k)
NEXT i
NEXT k
REM ************ delete
FOR k = 1 TO ntms
  FOR i = 1 TO 3
            ptot(i) = ptot(i) + dlpr(i, k)
  NEXT i
NEXT k
REM ************
FOR i = 1 TO np
  aval(i) = total(i) / ntms
NEXT i
REM ********** delete
FOR i = 1 TO 3
  pav(i) = ptot(i) / ntms
NEXT i
REM **********
FOR k = 1 TO ntms
   FOR i = 1 TO np
            sq(i) = sq(i) + (value(i, k) - aval(i)) ^ 2
  NEXT i
NEXT k
      FOR i = 1 TO np
    valsd(i) = (sq(i) / (ntms - 1)) ^ .5
    PRINT #4, i;
    PRINT #4, USING "####.#####"; aval(i); valsd(i)
  NEXT i
REM ******** delete
  'FOR i = 1 TO 3
  'PRINT #4, USING "###.###"; pav(i)
'   PRINT USING "###.###"; pav(i)
'   NEXT i
REM ***********************************************
REM *************************
REM Read Data from Scanivalve
REM *************************
FOR i = 1 TO 20
LINE INPUT #3, header$(i)
NEXT i
REM buildn = VAL(MID$(header$(1), 1))   'rig build number
REM prec = VAL(MID$(header$(6), 8))     'weather station recorded
pressure in mbar
buildn = VAL(header$(1))     'rig build number
prec = VAL(header$(6))       'weather station recorded pressure in mbar
nn = 1
DO WHILE NOT EOF(3)
FOR i = 1 TO 13
LINE INPUT #3, row$(i)
NEXT i
PR(1, nn) = VAL(MID$(row$(2), 45, 11))     'inlet orifice upstream
PR(2, nn) = VAL(MID$(row$(3), 9, 11))      'inlet orifice downstream
PR(3, nn) = VAL(MID$(row$(3), 21, 11))     'outlet orifice upstream
PR(4, nn) = VAL(MID$(row$(3), 33, 11))     'outlet orifice downstream
PR(5, nn) = VAL(MID$(row$(5), 9, 11))      'inlet pressure
PR(6, nn) = VAL(MID$(row$(5), 21, 11))     'outlet pressure
REM *** Currently there is NO pressure tapping at the rig OUTLET !!!***
```

```
PR(7, nn) = VAL(MID$(row$(4), 33, 11))     'upstream cavity pressure
PR(8, nn) = VAL(MID$(row$(4), 45, 11))     'downstream cavity pressure
nn = nn + 1
LOOP
isc = nn - 1
IF isc > nsc OR isc < nsc THEN
PRINT "Number of Scanivalve Scans is not Correct"
END IF
FOR k = 1 TO nsc
   FOR i = 1 TO 8
            prtot(i) = prtot(i) + PR(i, k)
   NEXT i
NEXT k
FOR i = 1 TO 8
   avpr(i) = prtot(i) / nsc
   PRINT #4, USING "###.###"; avpr(i)
NEXT i
REM Atmospheric pressure
REM --------------------
g = 9.80665     '(m/s^2)
aws = 252.6     'altitude of weather station in ft
afl = 242.5     'altitude of fluids lab if ft
rhoa = (prec * 100) / (287 * (aval(61) + 273.15))
patm = -rhoa * g * (afl - aws) * .3048 + (prec * 100)   'patm in Pa
REM Orifice Plate Temperatures
REM -------------------------
temp1 = aval(56)
temp2 = aval(57)
REM Mass Flow Rate in & Out of the Rig
REM ----------------------------------
CALL orifice(1, avpr(1), avpr(2), temp1, dor1, Dpipe1, min)
IF avpr(3) > avpr(4) THEN
CALL orifice(2, avpr(3), avpr(4), temp2, dor2, Dpipe2, mout)
END IF
REM     Inlet & Outlet Air Temperatures in C
REM     ------------------------------------
tin = (aval(32) + aval(33)) / 2
tout = (aval(34) + aval(35)) / 2
REM     Find (1/rho)
REM     ------------
inrho = 287 * (tin + c) / (avpr(5) * 6896.55 + patm)
REM     find pressure drop thru the casing holes
(Dp=(m/(CD*A))^2*(1/(2*rho))
REM     ------------------------------------------------------------------------
prdrop = ((min / .001508) ^ 2) * (.5 * inrho) * .000145
pupin = avpr(5) - prdrop    'pressure upstream of lab seals at rotor inlet
pcav = avpr(7)              'Cavity Pressure
pgauge = 0                  'gauge
CALL labyrinth(pupin, pgauge, tin, rd1, cl1, lk1)
CALL labyrinth(pupin, pgauge, tin, rd2, cl2, lk2)
CALL labyrinth(avpr(6), pgauge, tout, rd3, cl3, lk3)
CALL labyrinth(avpr(6), pgauge, tout, rd4, cl4, lk4)
CALL labyrinth(pcav, pgauge, aval(31), rd5, cl5, lk5)
leak = lk1 + lk2 + lk3 + lk4 + lk5
diff = mout + leak - min
m1 = (min - (lk1 + lk2))
m2 = mout + lk3 + lk4 + lk5
PRINT USING "##.###"; m1; m2; (lk1 + lk2)
PRINT USING "#.###"; diff
PRINT USING "##.###"; lk1; lk2; lk3; lk4; lk5
PRINT #4, USING "#.###"; m1
PRINT #4, USING "#.###"; m2
PRINT #4, USING "#.###"; lk1 + lk2
PRINT #4, "-----"
REM    CALCULATE REz and REf
REM    ---------------------
IF buildn = 3 THEN
REM data for build 3
rb = .22
ra = .0701
rs = .052
END IF
IF buildn = 2 THEN
REM data for build 2
rb = .22
ra = .0701
rs = .06
END IF
PI = 3.141592654#
speed = aval(64) * PI / 30
te = tin + c
mi = (1.46E-06 * te ^ 1.5) / (110.33 + te)
pcv = avpr(7) * 6894.8 + patm
rho = pcv / (287 * te)
ni = mi / rho
Ref = speed * rb ^ 2 / (ni * 1000000!)
 v = m1 / (rho * (ra ^ 2 - rs ^ 2) * PI)
PRINT pcv, rho, v, speed
                'Rez = 2 * (ra - rs) * v / (ni * 100000!)
Rez = 2 * m1 / (PI * (ra + rs) * mi * 100000!)
Ro = v / (speed * ra)
PRINT #4, buildn
PRINT #4, header$(2)
PRINT #4, header$(3)
PRINT #4, header$(4)
PRINT #4, header$(5)
PRINT #4, patm
PRINT #4, header$(7)
PRINT #4, header$(8)
PRINT #4, header$(9)
PRINT #4, header$(10)
PRINT #4, "***---***---***"
PRINT
PRINT "Rotational Speed = "; USING "#####"; aval(64);
PRINT " rev/min"
PRINT "Mass Flow Rate In = "; USING "#.###"; m1;
PRINT " kg/s"
PRINT "Cavity Pressure = "; USING "#.##"; pcv / 100000!;
PRINT " bar"
PRINT "Inlet Temperature = "; USING "###.#"; te;
PRINT " K"
PRINT "Max Hot Air Temperature = "; USING "###.#"; (aval(40) +
aval(41)) / 2 + c;
PRINT " K"
PRINT "Axial Reynolds No = "; USING "##.##"; Rez;
PRINT " E5"
PRINT "Rotational Reynolds No = "; USING "##.##"; Ref;
PRINT " E6"
PRINT "Rossby No = "; USING "##.##"; Ro
PRINT "Max Buoyancy = "; USING "##.###"; (aval(12) - tin) / te
PRINT "Axial Velocity = "; USING "###.###"; v
PRINT "Tangential Velocity = "; USING "###.###"; speed * .0701
PRINT
PRINT USING "###.######"; avpr(1); pav(1)
PRINT USING "###.######"; avpr(2); pav(2)
PRINT USING "###.######"; avpr(7); pav(3)
PRINT
'PRINT aval(65), aval(66), aval(67)
CLOSE #2
CLOSE #3
CLOSE #1
CLOSE #4
END
SUB labyrinth (pup, pdn, tup, r1, cl, lk)
PI = 3.141592654#

ptc = .002
ht = .002
nf = 7
REM patm = 14.7                 'check from barometer
Pu = pup + patm / 6894.8
pd = pdn + patm / 6894.8
PR = pd / Pu
Tt = tup + 273.15
area = PI * ((r1 + cl) ^ 2 - r1 ^ 2) * 1550
gam = 1.4
lam = 1.2
r = 2.984                   '(lbf/lb)^2/K - Gas Constant
k = (1 - EXP(-.054 * (ptc / cl))) * (nf - 1) + 1
'X1 = 1.1844 - .0242 * LOG(GAM)
X1 = 1.1808637#
X2 = .2491 - .1562 * ((gam - 1) ^ .937)
X3 = .588 + .3046 * ((gam - 1) ^ 1.153)
X4 = .719 + .1229 * ((gam - 1) ^ 4.178)
X5 = .0218 + .002317 * ((gam - 1) ^ .725)
a = (X1 - X2 * EXP(-X3 * (k - 1) ^ X4)) / k ^ X5
N = k / a
b = SQR(1 + 2 * gam * (1 + gam) * N)
```

```
F1 = 1 - (.0553 * (SIN((3 * PI) / (2 + (ptc / ht))) ^ 2))
F2 = 1
Cd = .92 * F1 * F2
Qc = Cd * SQR((b - 1) / (r * N * (b + 1)))
alpha = (1 - lam * a) / Qc ^ 2
beta = lam * a / 2
delta = ((1 - PR) * (PR * (b + 1) + b - 3) * Cd ^ 2) / (N * r * (b - 1))
q = SQR((SQR(beta ^ 2 + alpha * delta) - beta) / alpha)
lk = area * Pu * q / SQR(Tt) * .454
END SUB
SUB orifice (no, pin, pout, cin, d1, d, mn)
REM     pin (psi), pout (psi), cin (C), d1 (m), D (m)
REM     Flange taps
            PI = 3.141592654#
            k = 1.4
REM       patm = 14.7     'check from barometer
REM     k=isentropic index (cp/cv)=1.4 for air
REM     mu=dynamic viscocity
REM     Converting psi to Pa & gauge pressure to absolute
            p1 = pin * 6894.8 + patm
            p2 = pout * 6894.8 + patm
REM     Converting t1 to Kelvin
            t1 = cin + 273
REM     p1=upstream orifice pressure
REM     p2=downstream orifice pressure
REM     t1=upstream fluid temperature
REM     d1=orifice plate diameter
REM     D=pipe diameter
            b = d1 / d
            a = PI * (d ^ 2) / 4!
            E = (1! - (b ^ 4)) ^ (-.5)
            dp = p1 - p2
            ex = 1! - ((.41 + (.35 * (b ^ 4))) * (dp / (k * p1)))
            rho = p1 / (287! * t1)
REM     b=diameter ratio
REM     A=pipe diameter
REM     E=velocity approach factor
REM     dp=pressure differential
REM     ex=expansion factor
REM     rho=density (p=rho*R*T) (ideal gas equation)
REM     mu calculated from Sutherlands law
            mu = (1.46E-06 * (t1 ^ 1.5)) / (t1 + 110.33)
REM     Guess a value for the pipe velocity u (m/s)
            u = 1!
REM     m=mass flow rate (kg/s)
REM     Red=pipe Reynolds number.
REM     C=discharge coefficient
REM     l1=0.0254/D, l2d=0.0254/D for flange tappings.
            l1 = .0254 / d
            l2d = .0254 / d
REM     mn=recalculated mass flow rate.
REM     tol=tolerance for convergence
            TOL = .00001
REM     Iterative loop for mass flow rate
            i = 0
TARGET1:
            IF i > 0 THEN u = mn / (rho * a)
            m = rho * u * a
            Red = rho * u * d / mu
            x = .5959 + (.0312 * (b ^ 2.1)) - (.184 * (b ^ 8))
            z = .0029 * (b ^ 2.5) * ((1000000! / Red) ^ .75)
            y = (.09 * l1 * (b ^ 4) * (1! / (1 - (b ^ 4)))) - (.0337 * l2d * (b
^ 3))
            c = x + y + z
            mn = c * E * ex * (PI / 4!) * (d1 ^ 2) * ((2! * ABS(dp) * rho) ^
.5)
            i = i + 1
            v = ABS(mn - m)
            IF v > TOL THEN GOTO TARGET1
REM     Check for limits of use of BS1042:1.1. See section 7.3.1
    IF d1 < (.0125) THEN PRINT "WARNING:d1<12.5E-3"
    IF (d < .05 OR d > .76) THEN PRINT "WARNING:D<0.05 OR
D>0.76 for orifice"; no;
    IF (b < .2 OR b > .75) THEN PRINT "WARNING:b<0.2 OR b>0.75
for orifice"; no
    bdre = 1260000! * (b ^ 2) * d1
    IF (Red < bdre OR Red > 1E+08) THEN PRINT "WARNING:RED<";
bdre; "or RED>1E8 for orifice"; no; Red
    IF ((p2 / p1) < .75) THEN PRINT "WARNING: p2 / p1 < .75 for
orifice"; no; "(="; p2 / p1; ")"
END SUB
```

Appendix 4.9: Example of raw data file from READ.bas

File B3R2-1.DAT

```
1   50.36618   0.14552
 2   95.02438   0.24085
 3   80.08801   0.16213
 4   57.25042   0.16239
 5   50.08289   0.15133
 6   47.21490   0.12951
 7   46.16839   0.13801
 8   48.51921   0.14983
 9   49.45892   0.16272
 10   56.35631   0.22404
 11   79.20781   0.18610
 12  103.84522   0.22606
 13   87.45613   0.23742
 14   60.61670   0.23733
 15   52.56359   0.15676
 16   47.75462   0.13398
 17   48.85879   0.14269
 18   50.31999   0.15326
 19   52.18708   0.15876
 20   62.47570   0.19171
 21   85.96541   0.20870
 22   98.32199   0.21945
 23  106.19989   0.20109
 24  114.06989   0.22333
 25   43.33789   0.13578
 26   43.52032   0.13759
 27   43.71591   0.13931
 28   43.92071   0.14623
 29   44.15640   0.14358
 30   44.58379   0.14504
 31   44.67130   0.15036
 32   43.39379   0.12572
 33   44.05550   0.13180
 34   45.35569   0.14248
 35   45.94619   0.15837
 36   88.81811   0.29171
 37  112.20763   0.60255
 38  103.95870   0.51640
 39  205.20535   0.61638
 40  142.92012   0.43456
 41  219.11324   0.92805
 42  118.75108   0.52458
 43  165.40338   1.02676
 44  121.21970   0.36338
 45   77.32111   0.37520
 46  141.33212   0.32820
 47   87.55138   0.40145
 48  136.35988   0.33489
 49   88.78379   0.41649
 50  120.53569   0.37170
 51   77.12339   0.37712
 52  140.26653   0.32937
 53   86.97269   0.39985
 54  137.02914   0.33352
 55   88.23521   0.41377
 56   42.33789   0.10563
 57   43.21550   0.12943
 58  404.23419   0.24925
 59  393.02402   0.24024
 60   36.85699   0.11593
 61   26.32000   0.20099
 62   25.98370   0.02299
 63   25.61559   0.03688
 64 1417.51001   0.90448
 65    0.03346   0.00003
 66    0.02994   0.00003
 67    0.01362   0.00001
 68    0.60030   0.00171
 69    0.98050   0.00219
 70    1.48630   0.00691
 71    5.16950   0.02096
29.675
26.658
 4.118
-2.763
26.578
 0.006
20.510
20.460
0.610
0.550
0.015
-----
 3
B3run2-1
3S---------
10/10/2002
000
 14.64081
run OK
0
-
-
***---***---***
```

Appendix 4.10: Listing of MCRheat_transfer.m

```
%program to process the Multiple Cavity Rig heat transfer data
%requires MATLAB7, MCRconduction.m, discfindiff.m, simpson.m,
matprop2.m,
%MCRradiation.m, reas.m, Minning.m
%Data from and to mcrexcel.xls
%by N.Miche
%last modified 27/03/08
%
%initialisation
%--------------
echo off;
close all;
clear all;
global drd nd dr zl dz nr cti nz tc rsp Cp r rdb rcl kair ctk...
   c_Cp c_k c_mu c_rho c_alfa c_beta c_musu c_krel ro rl zl m rotc phi
nc rdb rsh rs axd qrad;

%load raw data file N:numerical data matrix T:text data matrix
[NUM,TEXT]=xlsread('mcrexcel.xls','rawdata');
endtest=NUM(1,2);      %reads the number of tests to process

%constants
ctk=273.15;  %Celsius to Kelvin

%MESH
%Parameters of disc meshed area
%------------------------------
ro=0.121;       %radius of inside thermocouple
rl=0.0855;      %length of radius distance between inner and outer disc
thermocouples
zl=0.008;       %disc thickness
%   axdtc=[0,zl]    %relative axial positions of discs thermocouples
%nd=int8(3)       %number of thermocouples on each disc side
nd=3;
%nr=int8(31)      %number of radial nodes
nr=31;
%nz=int8(21)      %number of axial nodes
nz=21;
m=nr*nz;
rotc=206.5e-3;  %radius of outside thermocouple
phi=pi/2;

%Dimensions of mesh elements
%---------------------------
dr=rl/(nr-1);
dz=zl/(nz-1);

%Radial position of all the nodes
%--------------------------------
for j=1:nr
   for i=1:nz
%       r(i,j)=ro+dz*(i-1)*cos(phi)+dr*(j-1)*sin(phi)
      r(i,j)=ro+dr*(j-1);  %node radius for calculation
   end
   rcl(j)=r(1,j);   %node radii for results display
end

%Results parameters matrice templates
param1_t=cell(21,6);
param1_t(:,1)={'Build:','ExpCode:','Rez:','Ro:','MassFlow(kg/s):','Bo*:','Tinl
et(K):','Tcav2(K):',...

'DTmeas(K):','BDTav:','Ø:','Ts,C2,d,av(K):','Ts,C3,d,av(K):','finTs,D2,av(K
):','Nu,C2,d,av:',...

'Nu,C3,d,av:','finNu,D2,av:','Tsh,C2(K):','Nush,C2:','Grsh,C2:','Theta2:'};
param1_t(3:21,3)={'±'};

param1_t(:,5)={'ExpDate:','Run:','Refi:','RotSpeed(rpm):','Pcav(abs
Pa):','Pr:','Texit(K):','Tcav3(K):',...

'DTcalc(K):','finBDTav:','finØ:','Ts,C3,u,av(K):','Ts,C4,u,av(K):','finTs,D3,a
v(K):','Nu,C3,u,av:',...
   'Nu,C4,u,av:','finNu,D3,av:','Tsh,C3(K)','Nush,C3','Grsh,C3:','Theta3:'};
param1_t(3:21,7)={'±'};

param2_t=cell(38,50);
param2_t(1,:)={'radius(m)','non-dim radius','shroud/cob C2','+/-
','shroud/cob C3','+/-','T/C C2,d (K)','+/-',...
   'T/C C3,u (K)','+/-','T/C C3,d (K)','+/-','T/C C4,u (K)','+/-','Ts,C2,d
(K)','+/-','Ts,C3,u (K)','+/-','Ts,C3,d (K)','+/-',...
   'Ts,C4,u (K)','+/-','finTs,D2 (K)','+/-','finTs,D3 (K)','+/-','Nu,C2,d','+/-
','Nu,C3,u','+/-','Nu,C3,d','+/-','Nu,C4,u','+/-',...
   'finNu,D2','+/-','finNuD3','+/-','h,C2,d','+/-','h,C3,u','+/-','h,C3,d','+/-
','h,C4,u','+/-','finh,D2','+/-','finh,D3','+/-'};
param2_t(2:5,1)={0.0701,0.0750,0.0855,0.1210}; %thermocouple radii
param2_t(20,1)={0.1625};
param2_t(36:38,1)={0.2065,0.220,0.24565};

param3=cell(endtest+1,88);
param3(1,:)={'Build','ExpCode','Run','ExpDate','LDA code','FCF pos','Lab
atm press (Pa)','Comments','Refi','+/-','Rez','+/-','BDTav','+/-
','finBDTav','+/-','Ro','+/-','Bo*','+/-','Grsh,C2','+/-',...
      'Grsh,C3','+/-','Pr','+/-','RotSpeed(rpm)','+/-','MassFlow(kg/s)','+/-
','Ø','+/-','finØ','+/-','Tcav2(K)','+/-','Tcav3(K)','+/-','Tinlet(K)','+/-',...
      'Texit(K)','+/-','DTmeas(K)','+/-','DTcalc(K)','+/-','Tsh,C2(K)','+/-
','Tsh,C3(K)','+/-','Pcav(abs Pa)','+/-','Ts,C2,d,av(K)','+/-',...
      'Ts,C3,u,av(K)','+/-','TS,C3,d,av(K)','+/-','Ts,C4,u,av(K)','+/-
','finTs,D2,av(K)','+/-','finTs,D3,av(K)','+/-','Nu,C2,d,av','+/-',...
      'Nu,C3,u,av','+/-','Nu,C3,d,av','+/-','Nu,C4,u,av','+/-','Nush,C2','+/-
','Nush,C3','+/-','finNu,D2,av','+/-','finNu,D3,av','+/-','Tsh,C2,out(K)','+/-',...
      'Tsh,C3,out(K)','+/-','k_air(Tin)','+/-','V (m/s)','+/-'};

param4_t=cell(4,2);
param4_t(:,1)={'LDA code:','FCF pos:','Lab Patm (Pa):','Comments:'};

%initialise results arrays
param1=cell(endtest,1);
param2=cell(endtest,1);
results=cell(40*endtest,50);

%ERROR ESTIMATION
   %ALL PRESSURES ARE ASSUMED CONSTANT
   %ALL LENGTHS ARE ASSUMED CONSTANT
%   index raw data numerical and text matrix per test
Traw=cell(endtest,1);
Nraw=cell(endtest,1);
for i=1:endtest
   Traw{i}=TEXT(2+(94*(i-1)):1+(94*i),:);
   Nraw{i}=NUM(2+(94*(i-1)):1+(94*i),:);
   Nraw{i}(1:63,3)=Nraw{i}(1:63,3)+ctk;    %convert temperatures to
Kelvin
end

%Thermocouples error intervals and uncertainties
for i=1:endtest
   for j=1:63
      %u1(j)=Nraw{i}(j,4)/sqrt(100);   %measurement standard uncertainty
on 100 measurements
      u1(j)=Nraw{i}(j,4)/sqrt(3);     %measurement standard uncertainty
considering rectangular distribution
      u2=0.0072;                %thermocouple resolution standard
uncertainty
      u3=0.0003;                %cold junction standard uncertainty
      u4=0.04167;               %calibration water bath stability standard
uncertainty
      u5=0.015;                 %calibration PRT precision standard
uncertainty
      u6=0.05;                  %Interpolation up to 100C standard
uncertainty
      u7=0.0415;                %Repeatability standard uncertainty
      Ucomb_TC{i}(j)=sqrt(u1(j)^2+u2^2+u3^2+u4^2+u5^2+u6^2+u7^2);
%thermocouple combined standard uncertainty
      U_TC{i}(j)=Ucomb_TC{i}(j)*1.96;    %T/C 95% uncertainty
      sig_TC{i}(j)=Ucomb_TC{i}(j)*sqrt(100);  %thermocouple standard
deviation from 100 measurements
   end
%    sig_TC{i}(64)=Nraw{i}(64,4);        %standard deviation for rpm
%    U_TC{i}(64)=sig_TC{i}(64)/(sqrt(100))*1.96;      %95% uncertainty for
rpm from 100 measurements
end

%calculation for each test
%-------------------------
tic
for nrun=1:endtest;        %counter nrun: run number
   nrun
   %Rig parameters
   %testing which rig build
   if Nraw{nrun}(84,1)==3
      %data for build 3
      rsh=0.220;       %shroud radius
      rdb=70.1e-3;     %disc bore radius
      rs=52e-3;        %shaft radius
   end
   if Nraw{nrun}(84,1)==2
      %data for build 2
      rsh=0.220;
      rdb=70.1e-3;
      rs=0.06;
   end
   rout=0.24565;    %rotor outer radius
   axd=42.9e-3;     %axial distance between discs
   aan=pi*(rdb^2-rs^2); %annulus area between disc bore and shaft
   cti=7.72;        %conductivity of titanium 318 (W/mK)
   drd=[0.121,0.1625,0.2065];   %radii of the three outer radius
thermocouples for each side of the discs in m

   %discs measured temperature distribution
   %---------------------------------------
   %Discs measured temperature
   raw_meastemp=[Nraw{nrun}(5,3),Nraw{nrun}(4,3),Nraw{nrun}(3,3);...
         Nraw{nrun}(9,3),Nraw{nrun}(10,3),Nraw{nrun}(11,3);...
         Nraw{nrun}(15,3),Nraw{nrun}(14,3),Nraw{nrun}(13,3);...
         Nraw{nrun}(19,3),Nraw{nrun}(20,3),Nraw{nrun}(21,3)];

raw_fintemp=[mean(raw_meastemp(1:2,1)),mean(raw_meastemp(1:2,2))
,mean(raw_meastemp(1:2,3));...

mean(raw_meastemp(3:4,1)),mean(raw_meastemp(3:4,2)),mean(raw_m
eastemp(3:4,3))];
```

```
    %standard deviation on the discs measured temperatures
    raw_sig_TC=[sig_TC{nrun}(5),sig_TC{nrun}(4),sig_TC{nrun}(3);...
        sig_TC{nrun}(9),sig_TC{nrun}(10),sig_TC{nrun}(11);...
        sig_TC{nrun}(15),sig_TC{nrun}(14),sig_TC{nrun}(13);...
        sig_TC{nrun}(19),sig_TC{nrun}(20),sig_TC{nrun}(21)];
    raw_sig_fintemp=[sqrt(raw_sig_TC(1,1)^2+raw_sig_TC(2,1)^2),...

sqrt(raw_sig_TC(1,2)^2+raw_sig_TC(2,2)^2),sqrt(raw_sig_TC(1,3)^2+ra
w_sig_TC(2,3)^2);...

sqrt(raw_sig_TC(3,1)^2+raw_sig_TC(4,1)^2),sqrt(raw_sig_TC(3,2)^2+ra
w_sig_TC(4,2)^2),...
        sqrt(raw_sig_TC(3,3)^2+raw_sig_TC(4,3)^2)];

    %discs measured temperature cases generation
    %   first row is the nominal measured value, following rows are
    %   the generated temperatures including the normally distributed error
of the
    %   thermocouple around its nominal value
    meastemp_d2up(1,:)=raw_meastemp(1,:);
    meastemp_d2dn(1,:)=raw_meastemp(2,:);
    meastemp_d3up(1,:)=raw_meastemp(3,:);
    meastemp_d3dn(1,:)=raw_meastemp(4,:);
    meastemp_find2(1,:)=raw_fintemp(1,:);
    meastemp_find3(1,:)=raw_fintemp(2,:);
    sig_meastemp_d2up(1,:)=raw_sig_TC(1,:);
    sig_meastemp_d2dn(1,:)=raw_sig_TC(2,:);
    sig_meastemp_d3up(1,:)=raw_sig_TC(3,:);
    sig_meastemp_d3dn(1,:)=raw_sig_TC(4,:);
    sig_meastemp_find2(1,:)=raw_sig_fintemp(1,:);
    sig_meastemp_find3(1,:)=raw_sig_fintemp(2,:);

    for i=2:101
        for j=1:3

meastemp_d2up(i,j)=meastemp_d2up(1,j)+sig_meastemp_d2up(1,j)*ran
dn;

meastemp_d2dn(i,j)=meastemp_d2dn(1,j)+sig_meastemp_d2dn(1,j)*ran
dn;

meastemp_d3up(i,j)=meastemp_d3up(1,j)+sig_meastemp_d3up(1,j)*ran
dn;

meastemp_d3dn(i,j)=meastemp_d3dn(1,j)+sig_meastemp_d3dn(1,j)*ran
dn;

meastemp_find2(i,j)=meastemp_find2(1,j)+sig_meastemp_find2(1,j)*rand
n;

meastemp_find3(i,j)=meastemp_find3(1,j)+sig_meastemp_find3(1,j)*rand
n;
        end
    end

    %other fluctuating parameters
    rsp(1)=Nraw{nrun}(64,3)*pi/30;      %nominal value of rotational speed
(rad/s)
    sig_rsp=Nraw{nrun}(64,4)*pi/30;
    tc(1)=(Nraw{nrun}(32,3)+Nraw{nrun}(33,3))/2;        %nominal value of
inlet temp
    sig_tc=sqrt(U_TC{nrun}(32)^2+U_TC{nrun}(33)^2)/1.96*sqrt(100);
    te(1)=(Nraw{nrun}(34,3)+Nraw{nrun}(35,3))/2;        %nominal value of
exit temp
    sig_te=sqrt(U_TC{nrun}(34)^2+U_TC{nrun}(35)^2)/1.96*sqrt(100);
    TC23(1)=Nraw{nrun}(23,3);               %T/C 23 (rim cav2)
    sig_TC23=sig_TC{nrun}(23);
    TC2(1)=Nraw{nrun}(2,3);         %T/C 2  (shroud cav2)
    sig_TC2=sig_TC{nrun}(2);
    TC24(1)=Nraw{nrun}(24,3);       %T/C 24 (rim cav3)
    sig_TC24=sig_TC{nrun}(24);
    TC12(1)=Nraw{nrun}(12,3);         %T/C 12 (shroud cav3)
    sig_TC12=sig_TC{nrun}(24);
    TC26(1)=Nraw{nrun}(26,3);       %T/C 26 (shaft temp under cav2)
    sig_TC26=sig_TC{nrun}(26);
    TC28(1)=Nraw{nrun}(28,3);       %T/C 28 (shaft temp under cav3)
    sig_TC28=sig_TC{nrun}(28);
    TC27(1)=Nraw{nrun}(27,3);       %T/C 27 (shaft under cob2)
    sig_TC27=sig_TC{nrun}(27);
    TC29(1)=Nraw{nrun}(29,3);       %T/C 29 (shaft under cob3)
    sig_TC29=sig_TC{nrun}(29);
    TC8(1)=Nraw{nrun}(8,3);         %T/C 8 (cob2 downstream face)
    sig_TC8=sig_TC{nrun}(8);
    TC16(1)=Nraw{nrun}(16,3);       %T/C 16 (cob3 upstream face)
    sig_TC16=sig_TC{nrun}(16);
    TC6(1)=Nraw{nrun}(6,3);         %T/C 6 (cob2 upstream face)
                sig_TC6=sig_TC{nrun}(6);
    TC7(1)=Nraw{nrun}(7,3);         %T/C 7 (bore 2)
    sig_TC7=sig_TC{nrun}(7);
    TC17(1)=Nraw{nrun}(17,3);       %T/C 17 (bore 3)
    sig_TC17=sig_TC{nrun}(17);
    TC18(1)=Nraw{nrun}(18,3);       %T/C 18 (cob 3 downstream face)
    sig_TC18=sig_TC{nrun}(18);

    for i=2:101
        rsp(i)=rsp(1)+sig_rsp*randn;        %normally distributed
        tc(i)=tc(1)+sig_tc*randn;
        te(i)=tc(1)+sig_tc*randn;
        TC23(i)=TC23(1)+sig_TC23*randn;
        TC2(i)=TC2(1)+sig_TC2*randn;
        TC24(i)=TC24(1)+sig_TC24*randn;
        TC12(i)=TC12(1)+sig_TC12*randn;
        TC26(i)=TC26(1)+sig_TC26*randn;
        TC28(i)=TC28(1)+sig_TC28*randn;
        TC27(i)=TC27(1)+sig_TC27*randn;
        TC29(i)=TC29(1)+sig_TC29*randn;
        TC8(i)=TC8(1)+sig_TC8*randn;
        TC16(i)=TC16(1)+sig_TC16*randn;
        TC6(i)=TC6(1)+sig_TC6*randn;
        TC7(i)=TC7(1)+sig_TC7*randn;
        TC17(i)=TC17(1)+sig_TC17*randn;
        TC18(i)=TC18(1)+sig_TC18*randn;
    end

    Tfluct.TC23=TC23;       %Multiple Array Tfluct comprising
temperatures
    Tfluct.TC2=TC2;         %to be used for the radiation correction
    Tfluct.TC24=TC24;
    Tfluct.TC12=TC12;
    Tfluct.TC26=TC26;
    Tfluct.TC28=TC28;
    Tfluct.TC27=TC27;
    Tfluct.TC29=TC29;
    Tfluct.TC8=TC8;
    Tfluct.TC16=TC16;
    Tfluct.TC7=TC7;
    Tfluct.TC17=TC17;

%%%%%%%%%%%%%%%%%%%%%%%%%%%%%%%%%%%%%%%%%%%%%%%%%%%%%%%%%%%%%%%%%%%%%%%
%%%
    %CALCULATIONS FOR EACH TEMPERATURE CASE

    for nc=1:101        %nc: temperature case counter

        %OPERATIONAL PARAMETERS
        expdate=Traw{nrun}{87,1};       %date of experiment
        expcode=Traw{nrun}{86,1};       %experiment code
        runid=Traw{nrun}{85,1};         %experiment name
        patm=Nraw{nrun}(89,1)*6894.757;   %Atm press in lab (Pa)
        pc=Nraw{nrun}(78,1)*6894.757+patm;  %abs cavity pressure from
upstream tap in shaft (Pa)
        fl=Nraw{nrun}(80,1);                %mass flow IN (kg/s)

        [Cp,kair,visc,rho,alfa,beta]=matprop2(tc(nc),pc);    %air properties
for tc, pc

        n_kair(nc)=kair;
        V(nc)=fl/(rho*aan);                 %flow velocity in annulus
        Rez(nc)=2*rho*V(nc)*(rdb-rs)/visc;          %Rez
        Ro(nc)=V(nc)/(rsp(nc)*rdb);                 %Ro
        Rephi(nc)=(rho*rsp(nc)*rsh^2)/visc;         %Ref
        Pr(nc)=visc*Cp/kair;                    %Pr


        %SHROUD HEAT TRANSFER (1-D radial conduction)
        ta2(nc)=tc(nc)+(rsp(nc)^2*(rsh^2-rdb^2))/(2*Cp);      %relative total
temperature at rsh in cavity2
        ca2(nc)=0.741e-4*ta2(nc)+4.01e-3;           %conductivity of air for
cavity2
        da2(nc)=pc/(ta2(nc)*287);                   %density in cavity2
        va2(nc)=1.46e-6*ta2(nc)^1.5/(ta2(nc)+110);          %viscosity in
cavity2
        shq2(nc)=cti*(TC23(nc)-TC2(nc))/(rsh*log(rout/rsh));    %shroud
heat flux in cavity2
        shnu2(nc)=shq2(nc)*(axd/2)/(ca2(nc)*(TC2(nc)-ta2(nc)));
%shroud nusselt number in cavity2
        shbdt2(nc)=(TC2(nc)-ta2(nc))/ta2(nc);               %shroud bDT,
cavity2

gr2(nc)=(da2(nc)^2*rsp(nc)^2*rsh*shbdt2(nc)*(axd/2)^3)/(va2(nc)^2);
%shroud grashof number in cavity2
        bostarsh2(nc)=sqrt(shbdt2(nc))/Ro(nc);              %shroud Bo* in
cavity2

        %ta3(nc)=TC28(nc)+(rsp(nc)^2*(rsh^2-rdb^2))/(2*Cp);
        ta3(nc)=ta2(nc);                            %relative total temperature at
rsh in cavity3
        ca3(nc)=0.741e-4*ta3(nc)+4.01e-3;           %conductivity of air for
cavity3
        da3(nc)=pc/(ta3(nc)*287);                   %density in cavity3
        va3(nc)=1.46e-6*ta3(nc)^1.5/(ta3(nc)+110);          %viscosity in
cavity3
        shq3(nc)=cti*(TC24(nc)-TC12(nc))/(rsh*log(rout/rsh));       %shroud
heat flux in cavity3
        shnu3(nc)=shq3(nc)*(axd/2)/(ca3(nc)*(TC12(nc)-ta3(nc)));
%shroud nusselt number in cavity3
        shbdt3(nc)=(TC12(nc)-ta3(nc))/ta3(nc);          %shroud bDT, cavity3

gr3(nc)=(da3(nc)^2*rsp(nc)^2*rsh*shbdt3(nc)*(axd/2)^3)/(va3(nc)^2);
%shroud grashof number in cavity3
        bostarsh3(nc)=sqrt(shbdt3(nc))/Ro(nc);              %shroud Bo*
in cavity3

        %calculations for Tcav2
        if gr2(nc)*Pr(nc) > 1e7
            shroud2C=0.14;
            shroud2n=1/3;
        else
            shroud2C=0.54;
            shroud2n=1/4;
        end
```

```
        TshC2(nc)=TC2(nc);
        Tcav2(nc)=TshC2(nc)-(TshC2(nc)-
tc(nc))/(shroud2C*(gr2(nc)*Pr(nc))^shroud2n/shnu2(nc))^(1/(shroud2n+1)
);
        Theta2(nc)=(TshC2(nc)-tc(nc))/(TshC2(nc)-Tcav2(nc));

        %calculations for Tcav3
        if gr3(nc)*Pr(nc) > 1e7
           shroud3C=0.14;
           shroud3n=1/3;
        else
           shroud3C=0.54;
           shroud3n=1/4;
        end
        TshC3(nc)=TC12(nc);
        Tcav3(nc)=TshC3(nc)-(TshC3(nc)-
tc(nc))/(shroud3C*(gr3(nc)*Pr(nc))^shroud3n/shnu3(nc))^(1/(shroud3n+1)
);
        Theta3(nc)=(TshC3(nc)-tc(nc))/(TshC3(nc)-Tcav3(nc));

        %DISCS CONDUCTION
        %building meastemp matrix for discs surfaces
        meastemp(1,:)=meastemp_d2up(nc,:);
        meastemp(2,:)=meastemp_d2dn(nc,:);
        meastemp(3,:)=meastemp_d3up(nc,:);
        meastemp(4,:)=meastemp_d3dn(nc,:);
        meastemp(5,:)=meastemp_find2(nc,:);
        meastemp(6,:)=meastemp_find2(nc,:);
        meastemp(7,:)=meastemp_find3(nc,:);
        meastemp(8,:)=meastemp_find3(nc,:);
        %
        %Building temperature matrix for radial temp fit and thermocouples
location
        % NOT used for fin calculations

fittemp(1,:)=[TC7(nc),TC6(nc),meastemp(1,1),meastemp(1,2),meastemp(
1,3),TC2(nc)];        %d2_up

fittemp(2,:)=[TC7(nc),TC8(nc),meastemp(2,1),meastemp(2,2),meastemp(
2,3),TC12(nc)];      %d2_dn

fittemp(3,:)=[TC17(nc),TC16(nc),meastemp(3,1),meastemp(3,2),measte
mp(3,3),TC12(nc)];   %d3_up

fittemp(4,:)=[TC17(nc),TC18(nc),meastemp(4,1),meastemp(4,2),measte
mp(4,3),meastemp(4,3)];   %d3_dn shroud T/C n/a
        fitradius(1,:)=[0.0701,0.0750,0.1210,0.1625,0.2065,0.2200];
%d2_up
        fitradius(2,:)=[0.0701,0.0855,0.1210,0.1625,0.2065,0.2200];
%d2_dn
        fitradius(3,:)=[0.0701,0.0750,0.1210,0.1625,0.2065,0.2200];
%d3_up
        fitradius(4,:)=[0.0701,0.0750,0.1210,0.1625,0.2065,0.2065];
%d3_dn (5 thermocouples max on rig)
        %
        %call MCR conduction subroutine

[tradial,q,qrad,DT,Nur,Nu_av,BDT_av,q_av,DT_av]=MCRconduction(me
astemp,Tfluct,fittemp,fitradius);
        %
        %
        i=nc;       %temperature case index
        tradial_d2up(i,:)=tradial(1,:);
        tradial_d2dn(i,:)=tradial(2,:);
        tradial_d3up(i,:)=tradial(3,:);
        tradial_d3dn(i,:)=tradial(4,:);
        tradial_find2(i,:)=tradial(5,:);
        tradial_find3(i,:)=tradial(7,:);
        q_d2up(i,:)=q(1,:);
        q_d2dn(i,:)=q(2,:);
        q_d3up(i,:)=q(3,:);
        q_d3dn(i,:)=q(4,:);
        q_find2(i,:)=q(5,:);
        q_find3(i,:)=q(7,:);
%       qrad_d2up(i,:)=qrad(1,:);
%       qrad_d2dn(i,:)=qrad(2,:);
%       qrad_d3up(i,:)=qrad(3,:);
%       qrad_d3dn(i,:)=qrad(4,:);
%       qrad_find2(i,:)=qrad(5,:);
%       qrad_find3(i,:)=qrad(7,:);
        Nur_d2up(i,:)=Nur(1,:);
        Nur_d2dn(i,:)=Nur(2,:);
        Nur_d3up(i,:)=Nur(3,:);
        Nur_d3dn(i,:)=Nur(4,:);
        Nur_find2(i,:)=Nur(5,:);
        Nur_find3(i,:)=Nur(7,:);
        q_av_d2up(i)=q_av(1);
        q_av_d2dn(i)=q_av(2);
        q_av_d3up(i)=q_av(3);
        q_av_d3dn(i)=q_av(4);
        q_av_find2(i)=q_av(5);
        q_av_find3(i)=q_av(7);
        DT_av_d2up(i)=DT_av(1);
        DT_av_d2dn(i)=DT_av(2);
        DT_av_d3up(i)=DT_av(3);
        DT_av_d3dn(i)=DT_av(4);
        DT_av_find2(i)=DT_av(5);
        DT_av_find3(i)=DT_av(7);
        Nu_av_d2up(i)=Nu_av(1);
        Nu_av_d2dn(i)=Nu_av(2);
        Nu_av_d3up(i)=Nu_av(3);
        Nu_av_d3dn(i)=Nu_av(4);
        Nu_av_find2(i)=Nu_av(5);
        Nu_av_find3(i)=Nu_av(7);
        BDT_av_d2up(i)=BDT_av(1);
        BDT_av_d2dn(i)=BDT_av(2);
        BDT_av_d3up(i)=BDT_av(3);
        BDT_av_d3dn(i)=BDT_av(4);
        BDT_av_find2(i)=BDT_av(5);
        BDT_av_find3(i)=BDT_av(7);

        %Ts_av
        TsC2dav(nc)=(BDT_av_d2up(nc)*tc(nc))+tc(nc);
        TsC3uav(nc)=(BDT_av_d2dn(nc)*tc(nc))+tc(nc);
        TsC3dav(nc)=(BDT_av_d3up(nc)*tc(nc))+tc(nc);
        TsC4uav(nc)=(BDT_av_d3dn(nc)*tc(nc))+tc(nc);
        finTsD2av(nc)=(BDT_av_find2(nc)*tc(nc))+tc(nc);
        finTsD3av(nc)=(BDT_av_find3(nc)*tc(nc))+tc(nc);

        %DT measured
        DTmeas(nc)=te(nc)-tc(nc);

        %DT calculated
        DTcalc(nc)=pi*rsh*kair/(fl*Cp)*(4*4*((TshC3(nc)+TshC2(nc))/2-
tc(nc))*(shnu2(nc)+shnu3(nc))/2+...
        8*((finTsD2av(nc)+finTsD3av(nc))/2-
tc(nc))*(Nu_av_find2(nc)+Nu_av_find3(nc))/2);

        %BDTavav

BDTavav(nc)=(BDT_av_d2up(nc)+BDT_av_d2dn(nc)+BDT_av_d3up(nc)
+BDT_av_d3dn(nc))/4;
        finBDTavav(nc)=(BDT_av_find2(nc)+BDT_av_find3(nc))/2;

        %Bo*
        Bostar(nc)=sqrt(BDTavav(nc))/Ro(nc);

       %O stroke
        Ostroke(nc)=4*Theta3(nc)/(Rez(nc)*(Theta3(nc)-1)*Pr(nc)*2*(rdb-
rs)*(TshC3(nc)-tc(nc)))...
           *((shnu3(nc)*(TshC3(nc)-tc(nc))*4*rsh)...
           +(Nu_av_d2dn(nc)*(TsC3uav(nc)-tc(nc))/rsh*(rsh^2-rdb^2))...
           +(Nu_av_d3up(nc)*(TsC3dav(nc)-tc(nc))/rsh*(rsh^2-rdb^2)));
        finOstroke(nc)=4*Theta3(nc)/(Rez(nc)*(Theta3(nc)-1)*Pr(nc)*2*(rdb-
rs)*(TshC3(nc)-tc(nc)))...
           *((shnu3(nc)*(TshC3(nc)-tc(nc))*4*rsh)...
           +(Nu_av_find2(nc)*(finTsD2av(nc)-tc(nc))/rsh*(rsh^2-rdb^2))...
           +(Nu_av_find3(nc)*(finTsD3av(nc)-tc(nc))/rsh*(rsh^2-rdb^2)));

    end
%%%
```

```
    sd_NuC3dav=std(Nu_av_d3up(2:101));
    n_NuC4uav=Nu_av_d3dn(1);
    sd_NuC4uav=std(Nu_av_d3dn(2:101));
    n_finNuD2av=Nu_av_find2(1);
    sd_finNuD2av=std(Nu_av_find2(2:101));
    n_finNuD3av=Nu_av_find3(1);
    sd_finNuD3av=std(Nu_av_find3(2:101));

    %interpolated values
    for i=1:nr
%
        %n_Ts, sd_Ts
        n_Ts_d2up(i)=tradial_d2up(1,i);
        sd_Ts_d2up(i)=std(tradial_d2up(2:101,i));
        n_Ts_d2dn(i)=tradial_d2dn(1,i);
        sd_Ts_d2dn(i)=std(tradial_d2dn(2:101,i));
        n_Ts_d3up(i)=tradial_d3up(1,i);
        sd_Ts_d3up(i)=std(tradial_d3up(2:101,i));
        n_Ts_d3dn(i)=tradial_d3dn(1,i);
        sd_Ts_d3dn(i)=std(tradial_d3dn(2:101,i));
        n_Ts_find2(i)=tradial_find2(1,i);
        sd_Ts_find2(i)=std(tradial_find2(2:101,i));
        n_Ts_find3(i)=tradial_find3(1,i);
        sd_Ts_find3(i)=std(tradial_find3(2:101,i));

        %n_Nu, sd_Nu
        n_Nu_d2up(i)=Nur_d2up(1,i);
        sd_Nu_d2up(i)=std(Nur_d2up(2:101,i));
        n_Nu_d2dn(i)=Nur_d2dn(1,i);
        sd_Nu_d2dn(i)=std(Nur_d2dn(2:101,i));
        n_Nu_d3up(i)=Nur_d3up(1,i);
        sd_Nu_d3up(i)=std(Nur_d3up(2:101,i));
        n_Nu_d3dn(i)=Nur_d3dn(1,i);
        sd_Nu_d3dn(i)=std(Nur_d3dn(2:101,i));
        n_Nu_find2(i)=Nur_find2(1,i);
        sd_Nu_find2(i)=std(Nur_find2(2:101,i));
        n_Nu_find3(i)=Nur_find3(1,i);
        sd_Nu_find3(i)=std(Nur_find3(2:101,i));

        %h
        for j=1:101
            [c_Cp, c_k, c_mu, c_rho, c_a,
c_b]=matprop2(tradial_d2up(j,i),pc);
            h_d2up(j,i)=c_k*Nur_d2up(j,i)/rcl(i);
            [c_Cp, c_k, c_mu, c_rho, c_a,
c_b]=matprop2(tradial_d2dn(j,i),pc);
            h_d2dn(j,i)=c_k*Nur_d2dn(j,i)/rcl(i);
            [c_Cp, c_k, c_mu, c_rho, c_a,
c_b]=matprop2(tradial_d3up(j,i),pc);
            h_d3up(j,i)=c_k*Nur_d3up(j,i)/rcl(i);
            [c_Cp, c_k, c_mu, c_rho, c_a,
c_b]=matprop2(tradial_d3dn(j,i),pc);
            h_d3dn(j,i)=c_k*Nur_d3dn(j,i)/rcl(i);
            [c_Cp, c_k, c_mu, c_rho, c_a,
c_b]=matprop2(tradial_find2(j,i),pc);
            h_find2(j,i)=c_k*Nur_find2(j,i)/rcl(i);
            [c_Cp, c_k, c_mu, c_rho, c_a,
c_b]=matprop2(tradial_find3(j,i),pc);
            h_find3(j,i)=c_k*Nur_find3(j,i)/rcl(i);
        end
        n_h_d2up(i)=h_d2up(1,i);
        sd_h_d2up(i)=std(h_d2up(2:101,i));
        n_h_d2dn(i)=h_d2dn(1,i);
        sd_h_d2dn(i)=std(h_d2dn(2:101,i));
        n_h_d3up(i)=h_d3up(1,i);
        sd_h_d3up(i)=std(h_d3up(2:101,i));
        n_h_d3dn(i)=h_d3dn(1,i);
        sd_h_d3dn(i)=std(h_d3dn(2:101,i));
        n_h_find2(i)=h_find2(1,i);
        sd_h_find2(i)=std(h_find2(2:101,i));
        n_h_find3(i)=h_find3(1,i);
        sd_h_find3(i)=std(h_find3(2:101,i));

    end

    %CALCULATED OPERATIONAL PARAMETERS NOMINAL VALUES
AND S.D.
    n_V=V(1);
    sd_V=std(V(2:101));
    n_tc=tc(1);
    sd_tc=std(tc(2:101));
    n_te=te(1);
    sd_te=std(te(2:101));
    n_Rez=Rez(1);                % n_ nominal value
    sd_Rez=std(Rez(2:101));      % sd_ Standard deviation
    n_Rephi=Rephi(1);
    sd_Rephi=std(Rephi(2:101));
    n_Ro=Ro(1);
    sd_Ro=std(Ro(2:101));
    n_Pr=Pr(1);
    sd_Pr=std(Pr(2:101));
    n_shnu2=shnu2(1);
    sd_shnu2=std(shnu2(2:101));
    n_shbdt2=shbdt2(1);
    sd_shbdt2=std(shbdt2(2:101));
    n_gr2=gr2(1);
    sd_gr2=std(gr2(2:101));
    n_bostarsh2=bostarsh2(1);
    sd_bostarsh2=std(bostarsh2(2:101));
    n_shnu3=shnu3(1);
    sd_shnu3=std(shnu3(2:101));
    n_shbdt3=shbdt3(1);
    sd_shbdt3=std(shbdt3(2:101));
    n_gr3=gr3(1);
    sd_gr3=std(gr3(2:101));
    n_bostarsh3=bostarsh3(1);
    sd_bostarsh3=std(bostarsh3(2:101));
    n_TshC2=TshC2(1);
    sd_TshC2=std(TshC2(2:101));
    n_Tcav2=Tcav2(1);
    sd_Tcav2=std(Tcav2(2:101));
    n_Theta2=Theta2(1);
    sd_Theta2=std(Theta2(2:101));
    n_TshC3=TshC3(1);
    sd_TshC3=std(TshC3(2:101));
    n_Tcav3=Tcav3(1);
    sd_Tcav3=std(Tcav3(2:101));
    n_Theta3=Theta3(1);
    sd_Theta3=std(Theta3(2:101));
    n_Ostroke=Ostroke(1);
    sd_Ostroke=std(Ostroke(2:101));
    n_finOstroke=finOstroke(1);
    sd_finOstroke=std(finOstroke(2:101));
    n_DTmeas=DTmeas(1);
    sd_DTmeas=std(DTmeas(2:101));
    n_DTcalc=DTcalc(1);
    sd_DTcalc=std(DTcalc(2:101));
    n_TsC2dav=TsC2dav(1);
    sd_TsC2dav=std(TsC2dav(2:101));
    n_TsC3uav=TsC3uav(1);
    sd_TsC3uav=std(TsC3uav(2:101));
    n_TsC3dav=TsC3dav(1);
    sd_TsC3dav=std(TsC3dav(2:101));
    n_TsC4uav=TsC4uav(1);
    sd_TsC4uav=std(TsC4uav(2:101));
    n_finTsD2av=finTsD2av(1);
    sd_finTsD2av=std(finTsD2av(2:101));
    n_finTsD3av=finTsD3av(1);
    sd_finTsD3av=std(finTsD3av(2:101));
    n_BDTavav=BDTavav(1);
    sd_BDTavav=std(BDTavav(2:101));
    n_finBDTavav=finBDTavav(1);
    sd_finBDTavav=std(finBDTavav(2:101));
    n_Bostar=Bostar(1);
    sd_Bostar=std(Bostar(2:101));

    %fill results arrays
    %param1
    param1{nrun}=param1_t;              %labels from param1 template
    param1{nrun}{1,2}=Nraw{nrun}(84,1);     %Build
    param1{nrun}{1,6}=expdate;     %Date of experiment
    param1{nrun}{2,2}=expcode;     %Exp code
    param1{nrun}{2,6}=runid;       %Run

    param1{nrun}{3,2}=n_Rez;                %Rez
    param1{nrun}{3,4}=sd_Rez/sqrt(100)*1.96;            %u_Rez 95%
confidence standard uncertainty
    param1{nrun}{3,6}=n_Rephi;              %Ref
    param1{nrun}{3,8}=sd_Rephi/sqrt(100)*1.96;          %u_Rephi
    param1{nrun}{4,2}=n_Ro;                 %Ro
    param1{nrun}{4,4}=sd_Ro/sqrt(100)*1.96;             %u_Ro
    param1{nrun}{4,6}=rsp(1)*30/pi;         %rot speed
    param1{nrun}{4,8}=sig_rsp/sqrt(100)*1.96;           %u_rsp
    param1{nrun}{5,2}=fl;                   %Mass flow
    %param1{nrun}{5,4}=                     %u_fl
    param1{nrun}{5,6}=pc;                   %Pcav
    %param1{nrun}{5,8}=                     %u_pc
    param1{nrun}{6,2}=n_Bostar;             %Bo*
    param1{nrun}{6,4}=sd_Bostar/sqrt(100)*1.96;         %u_Bo*
    param1{nrun}{6,6}=n_Pr;                 %Pr
    param1{nrun}{6,8}=sd_Pr/sqrt(100)*1.96;             %u_Pr
    param1{nrun}{7,2}=tc(1);                %Tinlet
    param1{nrun}{7,4}=sig_tc/sqrt(100)*1.96;            %u_tc
    param1{nrun}{7,6}=te(1);                %Texit
    param1{nrun}{7,8}=sig_te/sqrt(100)*1.96;            %u_te
    param1{nrun}{8,2}=n_Tcav2;              %Tcav2
    param1{nrun}{8,4}=sd_Tcav2/sqrt(100)*1.96;          %u_Tcav2
    param1{nrun}{8,6}=n_Tcav3;              %Tcav3
    param1{nrun}{8,8}=sd_Tcav3/sqrt(100)*1.96;          %u_Tcav3
    param1{nrun}{9,2}=n_DTmeas;             %DTmeas
    param1{nrun}{9,4}=sd_DTmeas/sqrt(100)*1.96;         %u_DTmeas
    param1{nrun}{9,6}=n_DTcalc;             %DTcalc
    param1{nrun}{9,8}=sd_DTcalc/sqrt(100)*1.96;         %u_DTcalc
    param1{nrun}{10,2}=n_BDTavav;           %BDTavav
    param1{nrun}{10,4}=sd_BDTavav/sqrt(100)*1.96;       %u_BDTavav
    param1{nrun}{10,6}=n_finBDTavav;        %finBDTav
    param1{nrun}{10,8}=sd_finBDTavav/sqrt(100)*1.96;    %u_finBDTav
    param1{nrun}{11,2}=n_Ostroke;           %Ø
    param1{nrun}{11,4}=sd_Ostroke/sqrt(100)*1.96;       %u_Ostroke
    param1{nrun}{11,6}=n_finOstroke;        %finØ
    param1{nrun}{11,8}=sd_finOstroke/sqrt(100)*1.96;    %u_finOstroke
    param1{nrun}{12,2}=n_TsC2dav;           %Ts,C2,d,av
    param1{nrun}{12,4}=sd_TsC2dav/sqrt(100)*1.96;       %u_TsC2dav
    param1{nrun}{12,6}=n_TsC3uav;           %Ts,C3,u,av
    param1{nrun}{12,8}=sd_TsC3uav/sqrt(100)*1.96;       %u_TsC3uav
    param1{nrun}{13,2}=n_TsC3dav;           %Ts,C3,d,av
    param1{nrun}{13,4}=sd_TsC3dav/sqrt(100)*1.96;       %u_TsC3dav
    param1{nrun}{13,6}=n_TsC4uav;           %Ts,C4,u,av
    param1{nrun}{13,8}=sd_TsC4uav/sqrt(100)*1.96;       %u_TsC4uav
    param1{nrun}{14,2}=n_finTsD2av;         %finTs,D2,av
    param1{nrun}{14,4}=sd_finTsD2av/sqrt(100)*1.96;     %u_finTsD2av
    param1{nrun}{14,6}=n_finTsD3av;         %finTs,D3,av
```

```
    param1{nrun}{14,8}=sd_finTsD3av/sqrt(100)*1.96;       %u_finTsD3av
    param1{nrun}{15,2}=n_NuC2dav;              %Nu,C2,d,av
    param1{nrun}{15,4}=sd_NuC2dav/sqrt(100)*1.96;         %u_NuC2dav
    param1{nrun}{15,6}=n_NuC3uav;              %Nu,C3,u,av
    param1{nrun}{15,8}=sd_NuC3uav/sqrt(100)*1.96;         %u_NuC3uav
    param1{nrun}{16,2}=n_NuC3dav;              %Nu,C3,d,av
    param1{nrun}{16,4}=sd_NuC3dav/sqrt(100)*1.96;         %u_NuC3dav
    param1{nrun}{16,6}=n_NuC4uav;              %Nu,C4,u,av
    param1{nrun}{16,8}=sd_NuC4uav/sqrt(100)*1.96;         %u_NuC4uav
    param1{nrun}{17,2}=n_finNuD2av;            %finNu,D2,av
    param1{nrun}{17,4}=sd_finNuD2av/sqrt(100)*1.96;
%u_finNuD2av
    param1{nrun}{17,6}=n_finNuD3av;            %finNu,D3,av
    param1{nrun}{17,8}=sd_finNuD3av/sqrt(100)*1.96;
%u_finNuD3av
    param1{nrun}{18,2}=n_TshC2;                %Tsh,C2
    param1{nrun}{18,4}=sd_TshC2/sqrt(100)*1.96;           %u_TshC2
    param1{nrun}{18,6}=n_TshC3;                %Tsh,C3
    param1{nrun}{18,8}=sd_TshC3/sqrt(100)*1.96;           %u_TshC3
    param1{nrun}{19,2}=n_shnu2;                %Nush,C2
    param1{nrun}{19,4}=sd_shnu2/sqrt(100)*1.96;           %u_shnu2
    param1{nrun}{19,6}=n_shnu3;                %Nush,C3
    param1{nrun}{19,8}=sd_shnu3/sqrt(100)*1.96;           %u_shnu3
    param1{nrun}{20,2}=n_gr2;                  %Grsh,C2
    param1{nrun}{20,4}=sd_gr2/sqrt(100)*1.96;             %u_gr2
    param1{nrun}{20,6}=n_gr3;                  %Grsh,C3
    param1{nrun}{20,8}=sd_gr3/sqrt(100)*1.96;             %u_gr3
    param1{nrun}{21,2}=n_Theta2;               %Theta2
    param1{nrun}{21,4}=sd_Theta2/sqrt(100)*1.96;          %u_Theta2
    param1{nrun}{21,6}=n_Theta3;               %Theta3
    param1{nrun}{21,8}=sd_Theta3/sqrt(100)*1.96;          %u_Theta3

    %fill interpolated results array average and standard deviation
    %param2
    param2{nrun}=param2_t;                 %labels
    for i=1:14
       param2{nrun}{i+5,1}=rcl(i+1);       %node radii
    end
    for i=1:15
       param2{nrun}{i+20,1}=rcl(i+15);
    end
    for i=2:37
       param2{nrun}{i,2}=param2{nrun}{i,1}/rsh;   %non-dim radius
    end
    param2{nrun}{2,3}=Nraw{nrun}(7,3);                    %T/C 7
    param2{nrun}{2,4}=U_TC{nrun}(7);                      %u T/C 7
    param2{nrun}{37,3}=Nraw{nrun}(2,3);                    %T/C 2
    param2{nrun}{37,4}=U_TC{nrun}(2);                      %u T/C 2
    param2{nrun}{38,3}=Nraw{nrun}(23,3);                   %T/C 23
    param2{nrun}{38,4}=U_TC{nrun}(23);                     %u T/C 23
    param2{nrun}{2,5}=Nraw{nrun}(17,3);                    %T/C 17
    param2{nrun}{2,6}=U_TC{nrun}(17);                      %u T/C 17
    param2{nrun}{37,5}=Nraw{nrun}(12,3);                   %T/C 12
    param2{nrun}{37,6}=U_TC{nrun}(12);                     %u T/C 12
    param2{nrun}{38,5}=Nraw{nrun}(24,3);                   %T/C 24
    param2{nrun}{38,6}=U_TC{nrun}(24);                     %u T/C 24
    param2{nrun}{3,7}=Nraw{nrun}(6,3);                    %T/C 6
    param2{nrun}{3,8}=U_TC{nrun}(6);                      %u T/C 6
    param2{nrun}{5,7}=meastemp_d2up(1,1);                  %T/C 5
    param2{nrun}{5,8}=std(meastemp_d2up(2:101,1))/sqrt(100)*1.96;
%u T/C 5
    param2{nrun}{20,7}=meastemp_d2up(1,2);                 %T/C 4
    param2{nrun}{20,8}=std(meastemp_d2up(2:101,2))/sqrt(100)*1.96;
%u T/C 5
    param2{nrun}{36,7}=meastemp_d2up(1,3);                 %T/C 3
    param2{nrun}{36,8}=std(meastemp_d2up(2:101,3))/sqrt(100)*1.96;
%u T/C 3
    param2{nrun}{4,9}=Nraw{nrun}(8,3);                    %T/C 8
    param2{nrun}{4,10}=U_TC{nrun}(8);                      %u T/C 8
    param2{nrun}{5,9}=meastemp_d2dn(1,1);                  %T/C 9
    param2{nrun}{5,10}=std(meastemp_d2dn(2:101,1))/sqrt(100)*1.96;
%u T/C 9
    param2{nrun}{20,9}=meastemp_d2dn(1,2);                 %T/C 10
    param2{nrun}{20,10}=std(meastemp_d2dn(2:101,2))/sqrt(100)*1.96;
%u T/C 10
    param2{nrun}{36,9}=meastemp_d2dn(1,3);                 %T/C 11
    param2{nrun}{36,10}=std(meastemp_d2dn(2:101,3))/sqrt(100)*1.96;
%u T/C 11
    param2{nrun}{3,11}=Nraw{nrun}(16,3);                  %T/C 16
    param2{nrun}{3,12}=U_TC{nrun}(16);                     %u T/C 16
    param2{nrun}{5,11}=meastemp_d3up(1,1);                 %T/C 15
    param2{nrun}{5,12}=std(meastemp_d3up(2:101,1))/sqrt(100)*1.96;
%u T/C 15
    param2{nrun}{20,11}=meastemp_d3up(1,2);                %T/C 14
    param2{nrun}{20,12}=std(meastemp_d3up(2:101,2))/sqrt(100)*1.96;
%u T/C 14
    param2{nrun}{36,11}=meastemp_d3up(1,3);                %T/C 13
    param2{nrun}{36,12}=std(meastemp_d3up(2:101,3))/sqrt(100)*1.96;
%u T/C 13
    param2{nrun}{3,13}=Nraw{nrun}(18,3);                  %T/C 18
    param2{nrun}{3,14}=U_TC{nrun}(18);                     %u T/C 18
    param2{nrun}{5,13}=meastemp_d3dn(1,1);                 %T/C 19
    param2{nrun}{5,14}=std(meastemp_d3dn(2:101,1))/sqrt(100)*1.96;
%u T/C 19
    param2{nrun}{20,13}=meastemp_d3dn(1,2);                %T/C 20
    param2{nrun}{20,14}=std(meastemp_d3dn(2:101,2))/sqrt(100)*1.96;
%u T/C 20
    param2{nrun}{36,13}=meastemp_d3dn(1,3);                %T/C 21
    param2{nrun}{36,14}=std(meastemp_d3dn(2:101,3))/sqrt(100)*1.96;
%u T/C 21

for i=1:14
    param2{nrun}{i+5,15}=n_Ts_d2up(i+1);      %interpolated line6:19
    param2{nrun}{i+5,16}=sd_Ts_d2up(i+1)/sqrt(100)*1.96;
    param2{nrun}{i+5,17}=n_Ts_d2dn(i+1);
    param2{nrun}{i+5,18}=sd_Ts_d2dn(i+1)/sqrt(100)*1.96;
    param2{nrun}{i+5,19}=n_Ts_d3up(i+1);
    param2{nrun}{i+5,20}=sd_Ts_d3up(i+1)/sqrt(100)*1.96;
    param2{nrun}{i+5,21}=n_Ts_d3dn(i+1);
    param2{nrun}{i+5,22}=sd_Ts_d3dn(i+1)/sqrt(100)*1.96;
    param2{nrun}{i+5,23}=n_Ts_find2(i+1);
    param2{nrun}{i+5,24}=sd_Ts_find2(i+1)/sqrt(100)*1.96;
    param2{nrun}{i+5,25}=n_Ts_find3(i+1);
    param2{nrun}{i+5,26}=sd_Ts_find3(i+1)/sqrt(100)*1.96;
    param2{nrun}{i+5,27}=n_Nu_d2up(i+1);
    param2{nrun}{i+5,28}=sd_Nu_d2up(i+1)/sqrt(100)*1.96;
    param2{nrun}{i+5,29}=n_Nu_d2dn(i+1);
    param2{nrun}{i+5,30}=sd_Nu_d2dn(i+1)/sqrt(100)*1.96;
    param2{nrun}{i+5,31}=n_Nu_d3up(i+1);
    param2{nrun}{i+5,32}=sd_Nu_d3up(i+1)/sqrt(100)*1.96;
    param2{nrun}{i+5,33}=n_Nu_d3dn(i+1);
    param2{nrun}{i+5,34}=sd_Nu_d3dn(i+1)/sqrt(100)*1.96;
    param2{nrun}{i+5,35}=n_Nu_find2(i+1);
    param2{nrun}{i+5,36}=sd_Nu_find2(i+1)/sqrt(100)*1.96;
    param2{nrun}{i+5,37}=n_Nu_find3(i+1);
    param2{nrun}{i+5,38}=sd_Nu_find3(i+1)/sqrt(100)*1.96;
    param2{nrun}{i+5,39}=n_h_d2up(i+1);
    param2{nrun}{i+5,40}=sd_h_d2up(i+1)/sqrt(100)*1.96;
    param2{nrun}{i+5,41}=n_h_d2dn(i+1);
    param2{nrun}{i+5,42}=sd_h_d2dn(i+1)/sqrt(100)*1.96;
    param2{nrun}{i+5,43}=n_h_d3up(i+1);
    param2{nrun}{i+5,44}=sd_h_d3up(i+1)/sqrt(100)*1.96;
    param2{nrun}{i+5,45}=n_h_d3dn(i+1);
    param2{nrun}{i+5,46}=sd_h_d3dn(i+1)/sqrt(100)*1.96;
    param2{nrun}{i+5,47}=n_h_find2(i+1);
    param2{nrun}{i+5,48}=sd_h_find2(i+1)/sqrt(100)*1.96;
    param2{nrun}{i+5,49}=n_h_find3(i+1);
    param2{nrun}{i+5,50}=sd_h_find3(i+1)/sqrt(100)*1.96;
end
for i=1:15
    param2{nrun}{i+20,15}=n_Ts_d2up(i+15);  %interpolated line21:35
    param2{nrun}{i+20,16}=sd_Ts_d2up(i+15)/sqrt(100)*1.96;
    param2{nrun}{i+20,17}=n_Ts_d2dn(i+15);
    param2{nrun}{i+20,18}=sd_Ts_d2dn(i+15)/sqrt(100)*1.96;
    param2{nrun}{i+20,19}=n_Ts_d3up(i+15);
    param2{nrun}{i+20,20}=sd_Ts_d3up(i+15)/sqrt(100)*1.96;
    param2{nrun}{i+20,21}=n_Ts_d3dn(i+15);
    param2{nrun}{i+20,22}=sd_Ts_d3dn(i+15)/sqrt(100)*1.96;
    param2{nrun}{i+20,23}=n_Ts_find2(i+15);
    param2{nrun}{i+20,24}=sd_Ts_find2(i+15)/sqrt(100)*1.96;
    param2{nrun}{i+20,25}=n_Ts_find3(i+15);
    param2{nrun}{i+20,26}=sd_Ts_find3(i+15)/sqrt(100)*1.96;
    param2{nrun}{i+20,27}=n_Nu_d2up(i+15);
    param2{nrun}{i+20,28}=sd_Nu_d2up(i+15)/sqrt(100)*1.96;
    param2{nrun}{i+20,29}=n_Nu_d2dn(i+15);
    param2{nrun}{i+20,30}=sd_Nu_d2dn(i+15)/sqrt(100)*1.96;
    param2{nrun}{i+20,31}=n_Nu_d3up(i+15);
    param2{nrun}{i+20,32}=sd_Nu_d3up(i+15)/sqrt(100)*1.96;
    param2{nrun}{i+20,33}=n_Nu_d3dn(i+15);
    param2{nrun}{i+20,34}=sd_Nu_d3dn(i+15)/sqrt(100)*1.96;
    param2{nrun}{i+20,35}=n_Nu_find2(i+15);
    param2{nrun}{i+20,36}=sd_Nu_find2(i+15)/sqrt(100)*1.96;
    param2{nrun}{i+20,37}=n_Nu_find3(i+15);
    param2{nrun}{i+20,38}=sd_Nu_find3(i+15)/sqrt(100)*1.96;
    param2{nrun}{i+20,39}=n_h_d2up(i+15);
    param2{nrun}{i+20,40}=sd_h_d2up(i+15)/sqrt(100)*1.96;
    param2{nrun}{i+20,41}=n_h_d2dn(i+15);
    param2{nrun}{i+20,42}=sd_h_d2dn(i+15)/sqrt(100)*1.96;
    param2{nrun}{i+20,43}=n_h_d3up(i+15);
    param2{nrun}{i+20,44}=sd_h_d3up(i+15)/sqrt(100)*1.96;
    param2{nrun}{i+20,45}=n_h_d3dn(i+15);
    param2{nrun}{i+20,46}=sd_h_d3dn(i+15)/sqrt(100)*1.96;
    param2{nrun}{i+20,47}=n_h_find2(i+15);
    param2{nrun}{i+20,48}=sd_h_find2(i+15)/sqrt(100)*1.96;
    param2{nrun}{i+20,49}=n_h_find3(i+15);
    param2{nrun}{i+20,50}=sd_h_find3(i+15)/sqrt(100)*1.96;
end

%non-dim line matrix param3
%param3{1,1:84}=param3_t(1,1:84)
param3{nrun+1,1}=Nraw{nrun}(84,1);          %Build
param3{nrun+1,2}=expcode;                   %Exp code
param3{nrun+1,3}=runid;                     %Run
param3{nrun+1,4}=expdate;                   %Date of experiment
param3{nrun+1,5}=Nraw{nrun}(88,1);          %LDA code
param3{nrun+1,6}=Nraw{nrun}(91,1);          %FCF position
param3{nrun+1,7}=Nraw{nrun}(89,1)*6894.757; %Lab atm press (Pa)
param3{nrun+1,8}=Traw{nrun}{90,1};          %Comments of experiment
param3{nrun+1,9}=n_Rephi;                   %Ref
param3{nrun+1,10}=sd_Rephi/sqrt(100)*1.96;
param3{nrun+1,11}=n_Rez;                    %Rez
param3{nrun+1,12}=sd_Rez/sqrt(100)*1.96;
param3{nrun+1,13}=n_BDTavav;                %BDTavav
param3{nrun+1,14}=sd_BDTavav/sqrt(100)*1.96;
param3{nrun+1,15}=n_finBDTavav;             %finBDTavav
param3{nrun+1,16}=sd_finBDTavav/sqrt(100)*1.96;
param3{nrun+1,17}=n_Ro;                     %Ro
param3{nrun+1,18}=sd_Ro/sqrt(100)*1.96;
param3{nrun+1,19}=n_Bostar;                 %Bo*
param3{nrun+1,20}=sd_Bostar/sqrt(100)*1.96;
param3{nrun+1,21}=n_gr2;                    %Grsh,C2
param3{nrun+1,22}=sd_gr2/sqrt(100)*1.96;
```

```
param3{nrun+1,23}=n_gr3;                %Grsh,C3
param3{nrun+1,24}=sd_gr3/sqrt(100)*1.96;
param3{nrun+1,25}=n_Pr;                 %Pr
param3{nrun+1,26}=sd_Pr/sqrt(100)*1.96;
param3{nrun+1,27}=rsp(1)*30/pi;         %rot speed (rpm)
param3{nrun+1,28}=sig_rsp/sqrt(100)*1.96*30/pi;
param3{nrun+1,29}=fl;                   %Mass flow
%param3{nrun+1,30}=
param3{nrun+1,31}=n_Ostroke;            %Ø
param3{nrun+1,32}=sd_Ostroke/sqrt(100)*1.96;
param3{nrun+1,33}=n_finOstroke;         %finØ
param3{nrun+1,34}=sd_finOstroke/sqrt(100)*1.96;
param3{nrun+1,35}=n_Tcav2;              %Tcav2
param3{nrun+1,36}=sd_Tcav2/sqrt(100)*1.96;
param3{nrun+1,37}=n_Tcav3;              %Tcav3
param3{nrun+1,38}=sd_Tcav3/sqrt(100)*1.96;
param3{nrun+1,39}=n_tc;                 %Tinlet
param3{nrun+1,40}=sd_tc/sqrt(100)*1.96;
param3{nrun+1,41}=n_te;                 %Texit
param3{nrun+1,42}=sd_te/sqrt(100)*1.96;
param3{nrun+1,43}=n_DTmeas;             %DTmeas
param3{nrun+1,44}=sd_DTmeas/sqrt(100)*1.96;
param3{nrun+1,45}=n_DTcalc;             %DTcalc
param3{nrun+1,46}=sd_DTcalc/sqrt(100)*1.96;
param3{nrun+1,47}=n_TshC2;              %Tsh,C2
param3{nrun+1,48}=sd_TshC2/sqrt(100)*1.96;
param3{nrun+1,49}=n_TshC3;              %Tsh,C3
param3{nrun+1,50}=sd_TshC3/sqrt(100)*1.96;
param3{nrun+1,51}=pc;                   %Pcav
%param3{nrun+1,52}=
param3{nrun+1,53}=n_TsC2dav;            %Ts,C2,d,av
param3{nrun+1,54}=sd_TsC2dav/sqrt(100)*1.96;
param3{nrun+1,55}=n_TsC3uav;            %Ts,C3,u,av
param3{nrun+1,56}=sd_TsC3uav/sqrt(100)*1.96;
param3{nrun+1,57}=n_TsC3dav;            %Ts,C3,d,av
param3{nrun+1,58}=sd_TsC3dav/sqrt(100)*1.96;
param3{nrun+1,59}=n_TsC4uav;            %Ts,C4,u,av
param3{nrun+1,60}=sd_TsC4uav/sqrt(100)*1.96;
param3{nrun+1,61}=n_finTsD2av;          %finTs,D2,av
param3{nrun+1,62}=sd_finTsD2av/sqrt(100)*1.96;
param3{nrun+1,63}=n_finTsD3av;          %finTs,D3,av
param3{nrun+1,64}=sd_finTsD3av/sqrt(100)*1.96;
param3{nrun+1,65}=n_NuC2dav;            %Nu,C2,d,av
param3{nrun+1,66}=sd_NuC2dav/sqrt(100)*1.96;
param3{nrun+1,67}=n_NuC3uav;            %Nu,C3,u,av
param3{nrun+1,68}=sd_NuC3uav/sqrt(100)*1.96;
param3{nrun+1,69}=n_NuC3dav;            %Nu,C3,d,av
param3{nrun+1,70}=sd_NuC3dav/sqrt(100)*1.96;
param3{nrun+1,71}=n_NuC4uav;            %Nu,C4,u,av
param3{nrun+1,72}=sd_NuC4uav/sqrt(100)*1.96;
param3{nrun+1,73}=n_shnu2;              %Nush,C2
param3{nrun+1,74}=sd_shnu2/sqrt(100)*1.96;
param3{nrun+1,75}=n_shnu3;              %Nush,C3
param3{nrun+1,76}=sd_shnu3/sqrt(100)*1.96;
param3{nrun+1,77}=n_finNuD2av;          %finNu,D2,av
param3{nrun+1,78}=sd_finNuD2av/sqrt(100)*1.96;
param3{nrun+1,79}=n_finNuD3av;          %finNu,D3,av
param3{nrun+1,80}=sd_finNuD3av/sqrt(100)*1.96;
param3{nrun+1,81}=Nraw{nrun}(23,3);     %T/C 23
param3{nrun+1,82}=U_TC{nrun}(23);
param3{nrun+1,83}=Nraw{nrun}(24,3);     %T/C 24
param3{nrun+1,84}=U_TC{nrun}(24);
param3{nrun+1,85}=n_kair(1);            %k(Tinlet)
param3{nrun+1,86}=std(n_kair(2:101))/sqrt(100)*1.96;
param3{nrun+1,87}=n_V;                  %Flow annulus velocity (m/s)
param3{nrun+1,88}=sd_V/sqrt(100)*1.96;

%param4
param4{nrun}=param4_t;
param4{nrun}{1,2}=Nraw{nrun}(88,1);     %LDA code
param4{nrun}{2,2}=Nraw{nrun}(91,1);     %FCF position
param4{nrun}{3,2}=Nraw{nrun}(89,1)*6894.757; %Lab atm press (Pa)
param4{nrun}{4,2}=Traw{nrun}{90,1};     %Comments of
experiment
 toc
end

%Build results matrix
for i=1:endtest
   for j=1:21
      for k=1:8
         results{j+(i-1)*40,k}=param1{i}{j,k};
      end
   end
   for j=1:38
      for k=10:59
         results{j+(i-1)*40,k}=param2{i}{j,k-9};
      end
   end
   for j=23:26
      for k=1:2
         results{j+(i-1)*40,k}=param4{i}{j-22,k};
      end
   end
end

%copy result matrix worksheet
xlswrite('MCRexcel.xls',results,'results')

%copy to non-dim worksheet
xlswrite('MCRexcel.xls',param3,'non-dims')
```

Appendix 4.11: Listing of MCRconduction.m

```
function[tradial,q,qrad,DT,Nur,Nu_av,BDT_av,q_av,DT_av]=MCRconduction(meastemp,Tfluct,fittemp,fitradius)
%subroutine calculating the conduction solution of the Multiple Cavity Rig's discs surfaces
%by N.Miche
%last modified 22/03/08
%requires
%
%input: meastemp
%output: tradial,q,qrad,DT,Nur,Nu_av,BDT_av
global drd nd dr zl dz nr cti nz tc rsp Cp r rdb rcl kair ro rl zl m rotc phi nc rdb rsh rs axd qrad;
%radial temperature curve fitting
%--------------------------------
%
%fitting on 3 thermocouples per disc face: 2nd order polynomial
%for i=1:4
%    fitradial=polyfit(drd,meastemp(i,1:nd),2);
%    tradial(i,:)=polyval(fitradial,drd(1):dr:drd(nd));
%end
%
%fitting on 4 thermocouples per disc face: 3rd order poly, cob and disc
for i=1:4
   fitradial=polyfit(fitradius(i,2:5),fittemp(i,2:5),3);
   tradial(i,:)=polyval(fitradial,drd(1):dr:drd(nd));
end
%
%fitting on 5 thermocouples per disc face, bore,cob and disc, 4th order
%poly
%for i=1:4
%    fitradial=polyfit(fitradius(i,1:5),fittemp(i,1:5),4);
%    tradial(i,:)=polyval(fitradial,drd(1):dr:drd(nd));
%end
%
%fitting on 6 thermocouples per disc face, bore, cob, disc, shroud, 5th
%order polynomial (d3_dn fitted on 5 thermocouples)
%for i=1:3
%    fitradial=polyfit(fitradius(i,:),fittemp(i,:),5);
%    tradial(i,:)=polyval(fitradial,drd(1):dr:drd(nd));
%end
%fitradial=polyfit(fitradius(4,1:5),fittemp(4,1:5),5);  %d3_dn has only 5 thermocouples max
%tradial(4,:)=polyval(fitradial,drd(1):dr:drd(nd));
%
%for i=5:8   %fits on 3 thermocouple per face for findisks
   %fitradial=polyfit(drd,meastemp(i,1:nd),2);       %2nd order polynomial
   %apply fitted temperatures at nodes
   %tradial(i,:)=polyval(fitradial,drd(1):dr:drd(nd));  %interpolation between the three thermocouples on discs faces
%       if i== 2 | 4 | 6 | 8 %if i=2 or 4 or 6 or 8
%          axq(i/2,j)=(cti/zl)*(tradial(i-1,j)-tradial(i,j)) %1-D axial
%          heat flux calculation
%end
tradial(5,:)=(tradial(1,:)+tradial(2,:))/2;   %average temperature profile for finTs,D2,u
tradial(6,:)=tradial(5,:);                    %fin,Ts,D2,d
tradial(7,:)=(tradial(3,:)+tradial(4,:))/2;   %fin,Ts,D3,u
tradial(8,:)=tradial(7,:);                    %fin,Ts,D3,d
%temperatures at the inner and outer radii by linear interpolation
%-----------------------------------------------------------------------
for j=2:2:8
   infitaxial=polyfit([0,zl],[meastemp((j-1):j,1)]',1);       %linear interpolation
   outfitaxial=polyfit([0,zl],[meastemp((j-1):j,3)]',1);
   taxial_inner(j/2,:)=polyval(infitaxial,0:dz:zl);
   taxial_outer(j/2,:)=polyval(outfitaxial,0:dz:zl);
end
%1-D axial heat flux calculation
%------------------------------
for i=2:2:8
   for j=1:nr
   axq(i/2,j)=(cti/zl)*(tradial(i-1,j)-tradial(i,j));
   end
end
%FINITE DIFFERENCE
[Tdisc2]=discfindiff(tradial(1:2,:),[taxial_inner(1,:);taxial_outer(1,:)]);
%conditions for disc2
[Tdisc3]=discfindiff(tradial(3:4,:),[taxial_inner(2,:);taxial_outer(2,:)]);
%conditions for disc3
[Tfindisc2]=discfindiff(tradial(5:6,:),[taxial_inner(3,:);taxial_outer(3,:)]);
%conditions for findisc2
[Tfindisc3]=discfindiff(tradial(7:8,:),[taxial_inner(4,:);taxial_outer(4,:)]);
%conditions for findisc3
%total heat flux using backward difference formula
T=[Tdisc2;Tdisc3;Tfindisc2;Tfindisc3];
for i=2:2:8
   for j=1:nr
   qt((i-1),j)=cti*(-3*T((i/2),((j-1)*nz+1))+4*T((i/2),((j-1)*nz+2))-T((i/2),((j-1)*nz+3)))/(2*dz);
   qt(i,j)=cti*(-3*T((i/2),(j*nz))+4*T((i/2),(j*nz-1))-T((i/2),(j*nz-2)))/(2*dz);
end
end
%RADIATION HEAT FLUX
%Temperatures for the radiation calculations
Trad(1)=(Tfluct.TC27(nc)+Tfluct.TC28(nc)+Tfluct.TC29(nc))/3; %Tsurf1 (shaft)
Trad(2)=tc(nc);                              %Tsurf2
Trad(3)=(Tfluct.TC8(nc)+meastemp(2,1)+Tfluct.TC7(nc))/3;
%Tsurf3
for i=4:nr+3
   Trad(i)=tradial(2,i-3);    %Interpolated surf temp upstream
end
Trad(nr+4)=(meastemp(2,nd)+Tfluct.TC12(nc))/2;         %Tsurf35
Trad(nr+5)=Tfluct.TC12(nc);         %Tsurf36 (shroud)
Trad(nr+6)=(Tfluct.TC12(nc)+meastemp(3,nd))/2;         %Tsurf37
for i=nr+7:2*nr+6
   Trad(i)=tradial(3,(2*nr+7)-i);     %Intepolated surf temp downstream
end
Trad(2*nr+7)=(meastemp(3,1)+Tfluct.TC16(nc)+Tfluct.TC17(nc))/3;
%Tsurf69
Trad(2*nr+8)=tc(nc);       %Tsurf70
%qrad=zeros(8,nr);
[qrad]=MCRradiation(Trad);
%corrected heat flux
q(1,:)=qt(1,:);                          %D2up
q(2,:)=qt(2,1:nr)-qrad(4:nr+3);          %D2dn  corrected between T/C9 and T/C11
for i=1:nr
q(3,i)=qt(3,i)-qrad(2*nr+7-i);     %D3up  corrected between T/C15 and T/C13
end
q(4,:)=qt(4,:);                          %D3dn
q(5:8,:)=qt(5:8,:);                       %finD2 and finD3
%LOCAL NON-DIMENSIONAL NUMBERS
for i=2:2:8
   for j=1:nr
      Tref(j)=tc(nc)+rsp(nc)^2*(r(1,j)^2-rdb^2)/(2*Cp);  %adiabatic wall fluid temperature
      DT((i-1),j)=T((i/2),((j-1)*nz+1))-Tref(j);   %surface to fluid Delta T (upstream disc face)
      DT(i,j)=T((i/2),(j*nz))-Tref(j);             %(downstream)
      Nur((i-1),j)=q((i-1),j)*rcl(j)/(kair*DT((i-1),j));   %local Nu
      Nur(i,j)=q(i,j)*rcl(j)/(kair*DT(i,j));
   end
end
%average nusselt number and average BetaDeltaT
for i=1:8
   for j=1:nr-2
      y1(j)=q(i,j+1)*r(1,j+1);
      y2(j)=DT(i,j+1)*r(1,j+1);
   end
   q_av(i)=simpson(y1,nr-2,dr);
   DT_av(i)=simpson(y2,nr-2,dr);
   Nu_av(i)=(q_av(i)*rotc)/(DT_av(i)*kair);
   BDT_av(i)=(1/tc(nc))*(2/(rotc^2-ro^2))*DT_av(i);
End
```

Function matprop2.m

```
function [c_Cp, c_krel, c_musu, c_rho, c_alfa, c_beta] = matprop2(T,P)
% function [Cp, k, mu, rho, alfa, beta] = matprop2(T,P)
% return material properties value for given temperature
% 10/8/99
% L.S.Wong, TFMRC, University of Sussex
%modified by N. Miché 05/05/2005
b0=0.1034009e4;
b1=-0.2848870;
b2=0.7816818e-3;
b3=-0.4970786e-6;
b4=0.1077024e-9;
c0=-2.276501e-3;
c1=1.2598485e-4;
c2=-1.4815235e-7;
c3=1.73550646e-10;
c4=-1.066657e-13;
c5=2.47663035e-17;
d0=-9.8601e-7;
d1=9.080125e-8;
d2=-1.17635575e-10;
d3=1.2349703e-13;
d4=-5.7971299e-17;
R=287; % Specific gas constant
```

Appendix 4.12: Listing of discfindiff.m

```
function [T]=discfindiff(Tempradial,Tempaxial)
%Finite difference for a disc in the multiple cavity rig
%-----------------
%----- AT=B to be solved-----
%A: temperature dependant coefficient matrix
%T: node temperature vector
%B: vectore containing the temperature independant boundary condition
information
%clear all
global nr nz dr dz r;
%dnr=int16(nr)
%dnz=int16(nz)
%nr=31
%nz=21
%dr=0.00285
%dz=0.0004
%load tempaxial1
%load tempradial1
%load r1
%Build matrix A and B
A=zeros(nr*nz);      %A: empty matrix (nr*nz)X(nr*nz)
B=zeros(1,nr*nz);    %B: empty matrix 1X(nr*nz)
T=zeros(1,nr*nz);
for j=1:nr
%     if j==nr
%         l=nz-1
%     else
%         l=nz
%     end
   for i=1:nz
      k=(j-1)*nz+i;
      if i==1     %assign left wall boundary temperature
         A(k,k)=1;
         B(k)=Tempradial(1,j);  %upstream disc radial temperature
      elseif i==nz    %assign right wall boundary temperature
         A(k,k)=1;
         B(k)=Tempradial(2,j);    %downstream disc radial temperature
      elseif j==1 & i~=(1 | nz)   %assign inner radius boundary
temperature
         A(k,k)=1;
         B(k)=Tempaxial(1,i);        %inner radius temperature
      elseif j==nr & i~=(1 | nz)  %assign outer radius boundary
temperature
         A(k,k)=1;
         B(k)=Tempaxial(2,i);     %outer radius temperature
      else                    %assign coefficients for inside boundaries point
         A(k,k+nz)=(1/dr^2+1/(2*r(i,j)*dr));      %north node
         A(k,k-nz)=(1/dr^2-1/(2*r(i,j)*dr));      %south node
         A(k,k)=(-2/dr^2-2/dz^2);                 %point node
         A(k,k+1)=1/dz^2;                         %east node
         A(k,k-1)=1/dz^2;                         %west node
      end
   end
end

%solve system of simultaneous linear equations AT=B
%T'=minres(A,B')     %minimal residual method (iterative)
%T=B/A
T=A\B';     %Gaussian pivot
T=T';
```

Function simpson.m

```
function [area]=simpson(y,n,h)
%   SEE ICASGT1 REPORT
%   y:function
%   n:number of points (must be odd)
%   h:strip width (=(b-a)/m where m=n-1:number of strips)
%   a & b:lower and upper limits of integration
%
area=0;
for i=1:2:n-2
   y0=y(i);
   y1=y(i+1);
   y2=y(i+2);
   area=area+((h/3)*(y0+(4*y1)+y2));
end
```

Function minning.m

```
function [VFdtd]=minning(ri,ro,rc,rho1,rho2,s)
%Calculates the View Factors between coaxial annular discs separated
by a solid cylinder
%based on Mining (1978) Eq. (9)
%
%The input values are [ri, ro] disc radius (A2)
% [rho1, rho2] differential area radius (dA1)
% [rc] cylinder outer radius
% [s] disc spacing
% A. Alexiou (28/11/00)

step=(rho2-rho1)/1000;
r=rho1:step:rho2;
omg=acos(rc./r)+acos(rc/ro);
phi=acos(rc./r)+acos(rc/ri);

f = r .* ((omg - phi) ./ (2*pi) + (ro.^2 - r.^2 - s.^2) ./...
   (pi * sqrt((ro^2 + r.^2 + s^2).^2 - (4 * r.^2 * ro^2))).*...
   atan(sqrt((ro^2 + r.^2 + s^2 + (2.*r*ro)).*...
   (ro^2 + r.^2 + s^2 - (2.* r * ro))) .* tan(omg/2)) - (ri^2 - r.^2 - s^2) ./...
   (pi*sqrt((ri^2 + r.^2 + s^2).^2 - (4.* r.^2 * ri^2))).*...
                atan(sqrt((ri^2 + r.^2 + s^2 + (2 .* r * ri)) ./...
     (ri^2 + r.^2 + s^2 - (2 .* r * ri))) .* tan(phi/2)));


 area=trapz(r,f);

 VFdtd=2*area/(rho2^2 - rho1^2);
```

Appendix 4.13: Listing of MCRradiation.m

```
function[qrad]=MCRradiation(Trad)
%Funtion to calculate the black and grey body radiation of the Multiple
Cavity Rig
%in cavity 3. Assumes Isothermal surfaces.
%requires, MATLAB7, MCRheat_transfer.m main program, Rea.m
subroutine,
%minning.m subroutine
global rs rdb rcl dr nr rsh axd

F=zeros(2*nr+8);

%radiation surfaces nodes RADII
%---------------------------
rrd(1)=rs;
rrd(2)=rdb;
rrd(3)=rcl(1)-dr;
for j=1:nr
   rrd(3+j)=rcl(j)+dr;
end
rrd(4+nr)=rsh;


%AREA calculation
%---------------
A(1)=2*pi*rrd(1)*axd;              %shaft
A(2)=pi*(rrd(2)^2-rrd(1)^2);     %Disc2,downstream
A(3)=pi*(rrd(3)^2-rrd(2)^2);
for i=1:nr
   A(3+i)=pi*(rrd(3+i)^2-rrd(2+i)^2);
end
A(nr+4)=pi*(rrd(nr+4)^2-rrd(nr+3)^2);
A(nr+5)=2*pi*rrd(nr+4)*axd;        %shroud
for i=1:(nr+3)
   A(nr+5+i)=A(nr+5-i);         %Disc3,upstream
end


%VIEW FACTORS
%------------
%Flat or convex surfaces: F(i,i)=0
F(1,1)=0;
F(2:nr+4,2:nr+4)=0;
F(nr+6:2*nr+8,nr+6:2*nr+8)=0;

%Shaft-Disc View Factors using Rea (1975) Eq.(2)
F(1,2)=reas(axd,rrd(2),rrd(1));       %shaft to Disc2,downstream
for j=3:nr+4
   F(1,j)=reas(axd,rrd(j),rrd(1))-reas(axd,rrd(j-1),rrd(1));
end
for i=1:nr+3
   F(1,nr+5+i)=F(1,nr+5-i);         %shaft to Disc3,upstream
end
F(1,nr+5)=1-sum(F(1,:));                %shaft to shroud by summation rule:
sum(F)=1

%Disc-Shaft View Factors from Reciprocity r/ship: A(i).F(i,j)=A(j).F(j,i)
for i=2:2*nr+8
   F(i,1)=A(1).*F(1,i)./A(i);
end

%UpDisc-DwnDisc View Factors from Minning (1979) Eq (9)
for i=1:nr+3
               for j=1:nr+3
     F(i+1,2*nr+9-j)=minning(rrd(j),rrd(j+1),rrd(1),rrd(i),rrd(i+1),axd);
   end
end

%DwnDisc-UpDisc View Factors (by reciprocity)
for i=0:nr+2
               for j=0:nr+2
     F(2*nr+8-j,2+i)=A(2+i).*F(2+i,2*nr+8-j)./A(2*nr+8-j);
   end
end

%Disc-Shroud View Factors (by summation rule)
for i=0:nr+2
   F(2+i,nr+5)=1-sum(F(2+i,:));
   F(nr+6+i,nr+5)=1-sum(F(nr+6+i,:));
end

%Shroud-Disc View Factors (by reciprocity)
for i=0:nr+2
   F(nr+5,2+i)=A(2+i).*F(2+i,nr+5)./A(nr+5);
   F(nr+5,nr+6+i)=A(nr+6+i).*F(nr+6+i,nr+5)./A(nr+5);
end

%Shroud-Shroud View Factor (by summation)
F(nr+5,nr+5)=1-sum(F(nr+5,:));


%TEMPERATURES on radiation surfaces
%---------------------------------
%Use of array Trad, defined in MCRconduction.m

%RADIATIVE HEAT FLUX
%------------------
sigma=56.7e-9;      %Stefan-Boltzman constant (W/m^2K^4)

%Black bodies
%qradb(0)=0
for i=1:2*nr+8
   qj=0;
   for j=1:2*nr+8
   %qradb(i)=sig.*(Trad(i).^4-(F(i,j)*Trad(j).^4))
   qj=qj+sigma.*F(i,j).*A(j).*(Trad(i).^4-Trad(j).^4); %(From C.Long, p250)
   end
   qradb(i)=qj;
end

%Grey bodies
e1=0.2;     %emissivity value for shaft (not painted)
e2=0.95;    %emissivity value for rotor surfaces (painted black)
e3=1;       %emissivity value for cooling annulus gap (black body)
Eps(1)=e1;          %shaft
Eps(2)=e3;          %upstream gap
Eps(3:2*nr+7)=e2;   %rotor
Eps(2*nr+8)=e3;     %downstream gap
Phi=zeros(1,2*nr+8);
for i=1:2*nr+8
   Phi(i)=(1-Eps(i))/Eps(i);
end


Eb=sigma*Trad.^4;

%solve [B]*(J)=(Eb) for finding (J)
B=zeros(2*nr+8);
for i=1:2*nr+8
   for j=1:2*nr+8
      B(i,j)=-Phi(i)*F(i,j);
   end
   B(i,i)=Phi(i)*(sum(F(i,:))-F(i,i))+1;
end
J=inv(B)*Eb';

qrad=(Eb-J')./Phi;
```

Function Reas.m

```
function [VFctd]=reas(ls,R,rs)
%Calculates the cylinder-disc View Factors
%based on Rea (1975) Eq. (2)
%The input values are [ls] cylinder length
% [R] Disc outer radius
% [rs] cylinder outer radius
% A. Alexiou (28/11/00)

VFctd=(acos((ls^2 - R^2 + rs^2) / (ls^2 + R^2 - rs^2)) - (rs / (2*ls) * ...
  (((((ls^2 + R^2 + rs^2)^2 / rs^4) - (4 * (R / rs)^2))^0.5) * ...
  acos(rs * (ls^2 - R^2 + rs^2) / (R * (ls^2 + R^2 - rs^2))) + ...
  ((ls^2 - R^2 + rs^2) / rs^2) * asin(rs / R) - ...
  (pi * (ls^2 + R^2 - rs^2) / (2 * rs^2))))) / (2*pi);
```

Appendix 4.14: Example of raw results output from the heat transfer processing software

Build:	3			ExpDate:	10/10/2002		
ExpCode:	3S---------			Run:	B3run2-1		
Rez:	165239.0376	±	127.4045483	Refi:	994725.8213	±	1747.92541
Ro:	3.168312702	±	0.003119535	RotSpeed(rpm):	1417.51001	±	0.018564517
MassFlow(kg/s):	0.61	±		Pcav(abs Pa):	242356.2933	±	
Bo*:	0.074591357	±	0.00073897	Pr:	0.70541207	±	5.15656E-05
Tinlet(K):	316.874645	±	0.3006544	Texit(K):	318.80094	±	0.325609864
Tcav2(K):	323.4873662	±	1.486228649	Tcav3(K):	335.2485335	±	1.322226369
DTmeas(K):	1.926295	±	0.427102029	DTcalc(K):	1.916532512	±	0.049249949
BDTav:	0.055851275	±	0.001014786	finBDTav:	0.055851273	±	0.001014786
Ø:	0.309718793	±	0.056327455	finØ:	0.163084407	±	0.035363792
Ts,C2,d,av(K):	332.6420843	±	0.169165908	Ts,C3,u,av(K):	331.8430508	±	0.221672842
Ts,C3,d,av(K):	336.3923706	±	0.22221217	Ts,C4,u,av(K):	337.4124858	±	0.202030464
finTs,D2,av(K):	332.2425669	±	0.146426366	finTs,D3,av(K):	336.9024278	±	0.149754908
Nu,C2,d,av:	-223.3319762	±	118.0043467	Nu,C3,u,av:	590.4948835	±	140.6639831
Nu,C3,d,av:	520.243974	±	115.9289847	Nu,C4,u,av:	-252.2868387	±	105.5465394
finNu,D2,av:	147.983547	±	12.74509059	finNu,D3,av:	116.8387643	±	11.81800361
Tsh,C2(K):	368.17438	±	0.320184871	Tsh,C3(K)	376.99522	±	0.304000388
Nush,C2:	54.52348377	±	2.295260988	Nush,C3	42.50712749	±	1.681067738
Grsh,C2:	145431656.3	±	1829398.146	Grsh,C3:	170672181.1	±	1971165.54
Theta2:	1.147978589	±	0.042482679	Theta3:	1.440128068	±	0.049213152

LDA code:	0
FCF pos:	0
Lab Patm (Pa):	100944.8272
Comments:	run OK

radius(m)	non-dim radius	shroud/cob C2	+/-	shroud/cob C3	+/-	T/C C2,d (K)	+/-	T/C C3,u (K)	+/-	T/C C3,d (K)	+/-	T/C C4,u (K)	+/-
0.0701	0.318636364	319.31839	0.219873993	322.00879	0.223666668								
0.075	0.340909091					320.3649	0.213149577			320.90462	0.216658614	323.46999	0.232448988
0.0855	0.388636364							321.66921	0.229567618				
0.121	0.55					323.23289	0.216698825	322.60892	0.223286466	325.71359	0.227324962	325.33708	0.234116562
0.12385	0.562954545												
0.1267	0.575909091												
0.12955	0.588863636												
0.1324	0.601818182												
0.13525	0.614772727												
0.1381	0.627727273												
0.14095	0.640681818												
0.1438	0.653636364												
0.14665	0.666590909												
0.1495	0.679545455												
0.15235	0.6925												
0.1552	0.705454545												
0.15805	0.718409091												
0.1609	0.731363636												
0.1625	0.738636364					330.40042	0.226654131	329.50631	0.30930212	333.7667	0.296427294	335.6257	0.272780285
0.16375	0.744318182												
0.1666	0.757272727												
0.16945	0.770227273												
0.1723	0.783181818												
0.17515	0.796136364												
0.178	0.809090909												
0.18085	0.822045455												
0.1837	0.835												
0.18655	0.847954545												
0.1894	0.860909091												
0.19225	0.873863636												
0.1951	0.886818182												
0.19795	0.899772727												
0.2008	0.912727273												
0.20365	0.925681818												
0.2065	0.938636364					353.23801	0.254401911	352.35781	0.272102752	360.60613	0.286195571	359.11541	0.264547647
0.22	1	368.17438	0.313427287	376.99522	0.298987984								
0.24565		379.34989	0.275201251	387.21989	0.296349139								

radius(m)	non-dim radius	Ts,C2,d (K)	+/-	Ts,C3,u (K)	+/-	Ts,C3,d (K)	+/-	Ts,C4,u (K)	+/-	finTs,D2 (K)	+/-	finTs,D3 (K)	+/-
0.0701	0.318636364												
0.075	0.340909091												
0.0855	0.388636364												
0.121	0.55												
0.12385	0.562954545	323.4720458	0.207080424	322.8018568	0.216488607	325.9967489	0.220394035	325.7427538	0.227374947	323.1369513	0.154549478	325.8697513	0.159041589
0.1267	0.575909091	323.7361881	0.197325748	323.0250662	0.210051996	326.3027191	0.214228124	326.1884914	0.221039369	323.3806272	0.14781909	326.2456053	0.154211234
0.12955	0.588863636	324.0282632	0.188018904	323.2812062	0.2047996	326.6355585	0.209466301	326.6753225	0.215631584	323.6547347	0.141860654	326.6554405	0.150096462
0.1324	0.601818182	324.3512171	0.179790852	323.5729352	0.201535796	326.999325	0.206690022	327.2042766	0.211648082	323.9620761	0.137323663	327.1018008	0.147095482
0.13525	0.614772727	324.7079959	0.173282214	323.9029111	0.20094458	327.3980763	0.20634969	327.7763835	0.209509779	324.3054535	0.13481009	327.5872299	0.145546716
0.1381	0.627727273	325.1015459	0.169075304	324.2737924	0.203475135	327.8358704	0.208694907	328.3926727	0.209507742	324.6876691	0.134770574	328.1142715	0.145682253
0.14095	0.640681818	325.5348131	0.167601293	324.6882371	0.209258274	328.316765	0.21373449	329.054174	0.211759744	325.1115251	0.137404918	328.6854695	0.147590703
0.1438	0.653636364	326.0107436	0.169051102	325.1489034	0.218093813	328.844818	0.221243497	329.7619169	0.216192892	325.5798235	0.142618536	329.3033675	0.151203881
0.14665	0.666590909	326.5322837	0.173331931	325.6584496	0.229512524	329.4240872	0.230812655	330.5169312	0.222558728	326.0953666	0.150060189	329.9705092	0.156312714
0.1495	0.679545455	327.1023793	0.180093748	326.2195337	0.242877571	330.0586306	0.241917826	331.3202464	0.230473965	326.6609565	0.159215179	330.6894385	0.162604771
0.15235	0.6925	327.7239767	0.188810308	326.8348141	0.257482014	330.7525058	0.253985481	332.1728923	0.239471632	327.2793954	0.169503692	331.4626991	0.169708593
0.1552	0.705454545	328.4000219	0.198874086	327.5069488	0.272617881	331.5097708	0.266440708	333.0758984	0.24904822	327.9534854	0.180350776	332.2928346	0.177232136
0.15805	0.718409091	329.1334612	0.209671653	328.2385962	0.287614272	332.3344834	0.278735923	334.0302944	0.25869905	328.6860287	0.191222487	333.1823889	0.184789637
0.1609	0.731363636	329.9272406	0.220628585	329.0324143	0.301853061	333.2307015	0.290364839	335.03711	0.267940866	329.4798274	0.201637969	334.1339058	0.1920173
0.1625	0.738636364												
0.16375	0.744318182	330.7843062	0.231229284	329.8910613	0.314772158	334.2024829	0.300867619	336.0973748	0.276324497	330.3376838	0.21116902	335.1499288	0.19858101
0.1666	0.757272727	331.7076043	0.241021962	330.8171955	0.325863704	335.2538854	0.30983209	337.2121184	0.2834415	331.2623999	0.219435156	336.2330019	0.20417966
0.16945	0.770227273	332.7000808	0.249617353	331.813475	0.334671718	336.3889668	0.316894465	338.3823705	0.28892831	332.2567779	0.22609854	337.3856687	0.208546949
0.1723	0.783181818	333.764682	0.25668666	332.8825581	0.340791878	337.6117851	0.32174172	339.6091608	0.292470755	333.3236201	0.230860958	338.6104729	0.211453796
0.17515	0.796136364	334.904354	0.261961955	334.0271028	0.343875371	338.926398	0.324117806	340.8935188	0.29381136	334.4657284	0.233464091	339.9098584	0.212713085
0.178	0.809090909	336.1220429	0.265241205	335.2497675	0.343638928	340.3368634	0.32383552	342.2364743	0.292762	335.6859052	0.233694289	341.2866688	0.212188553
0.18085	0.822045455	337.4206948	0.266399971	336.5532103	0.339884238	341.8472392	0.320797166	343.6390568	0.289225325	336.9869525	0.231393782	342.743148	0.209810231
0.1837	0.835	338.8032559	0.26541251	337.9400893	0.332532273	343.4615831	0.315028596	345.1022961	0.283230044	338.3716726	0.22648184	344.2819396	0.205600173
0.18655	0.847954545	340.2726723	0.262386244	339.4130628	0.321682269	345.1839531	0.306733937	346.6272217	0.274988064	339.8428675	0.218992369	345.9055874	0.1997143
0.1894	0.860909091	341.8318901	0.257615156	340.9747889	0.307712383	347.0184069	0.296381835	348.2148634	0.264985089	341.4033395	0.2091398	347.6166351	0.19250897
0.19225	0.873863636	343.4838554	0.251658472	342.6279259	0.291449894	348.9690024	0.284836582	349.8662507	0.254118447	343.0558907	0.197433976	349.4176266	0.184642527
0.1951	0.886818182	345.2315145	0.245447572	344.3751319	0.274447751	351.0397975	0.273541267	351.5824134	0.243886239	344.8033232	0.184875376	351.3111054	0.177215137
0.19795	0.899772727	347.0778133	0.240407807	346.2190651	0.259379524	353.2348499	0.264723076	353.364381	0.236583523	346.6484392	0.173255692	353.2996154	0.171914481
0.2008	0.912727273	349.0256981	0.238539319	348.1623837	0.250404102	355.5582176	0.261486944	355.2131832	0.235337171	348.5940409	0.165489113	355.3857004	0.17104252
0.20365	0.925681818	351.078115	0.242334801	350.207746	0.252938591	358.0139583	0.26751771	357.1298496	0.243676538	350.6429305	0.16556819	357.571904	0.177197642
0.2065	0.938636364												
0.22	1												
0.24565													

radius(m)	non-dim radius	Nu,C2,d	+/-	Nu,C3,u	+/-	Nu,C3,d	+/-	Nu,C4,u	+/-	finNu,D2	+/-	finNuD3	+/-
0.0701	0.318636364												
0.075	0.340909091												
0.0855	0.388636364												
0.121	0.55												
0.12385	0.562954545	-386.4389253	224.6602032	638.5979603	1713.732784	-53.4293632	174.3295462	189.1393214	176.2181015	68.15229852	553.0957487	56.39908479	369.8276235
0.1267	0.575909091	-383.9278925	209.7840934	688.6635565	8248.652663	33.93561481	163.6225735	135.7584882	163.3473807	91.94624041	135.0191111	74.61542129	89.91813571
0.12955	0.588863636	-386.5181144	195.7733041	719.3449654	1049.219355	117.8749196	154.7622848	68.8161546	151.7491451	104.3848076	45.18341548	83.21380129	29.15096879
0.1324	0.601818182	-387.7114828	183.2308706	738.7665877	566.3111343	201.8723173	148.2004123	-2.369944508	142.0662335	112.7290853	18.33355649	88.48899005	10.75889531
0.13525	0.614772727	-385.6896566	172.5115075	749.6978048	396.3687718	285.5781058	144.0553722	-73.6729272	134.5260707	119.2392917	10.36333837	92.41142067	5.363722993
0.1381	0.627727273	-380.17475	163.8346212	753.5385025	312.678231	367.5022717	142.2142372	-142.6480719	129.1149488	124.6723064	7.908061256	95.62941093	3.919520156
0.14095	0.640681818	-371.4266014	157.2709484	751.1668682	264.9955202	445.7890685	142.3485657	-207.58477	125.6319996	129.2047972	6.885431957	98.34697774	3.4018817
0.1438	0.653636364	-359.8539147	152.7209174	743.4375087	235.8561968	518.6675198	143.9630902	-267.1816516	123.7448056	132.9733612	6.327818484	100.6463872	3.115730892
0.14665	0.666590909	-345.9617544	149.9168463	731.1260059	217.5189042	584.5130077	146.4760325	-320.4484883	123.0496987	135.992385	6.014087517	102.5671275	2.944600841
0.1495	0.679545455	-330.2291937	148.4631975	715.0638579	205.8643659	641.9617633	149.3047276	-366.5999626	123.1314396	138.3189308	5.872398372	104.1151507	2.866182086
0.15235	0.6925	-313.1438499	147.896385	695.9810976	198.3394862	689.909654	151.928818	-405.0944061	123.606161	139.9836333	5.855739564	105.3254339	2.864869892
0.1552	0.705454545	-295.1386794	147.749649	674.6004779	193.2006465	727.5563179	153.9261336	-435.53403	124.146005	141.0515473	5.92217416	106.2137053	2.922321503
0.15805	0.718409091	-276.6234232	147.6012598	651.5798761	189.2133342	754.3730907	154.983756	-457.6752764	124.4872751	141.5579828	6.034571581	106.8027676	3.018836185
0.1609	0.731363636	-257.9428714	147.1046578	627.468448	185.5179357	770.0950158	154.8958413	-471.3833734	124.4276506	141.5788486	6.163647438	107.1201496	3.137096306
0.1625	0.738636364												
0.16375	0.744318182	-239.4030507	145.9980359	602.7888817	181.5454069	774.7008077	153.5506179	-476.6286075	123.8194564	141.1592464	6.287538407	107.1851421	3.262587317
0.1666	0.757272727	-221.2679703	144.1039736	577.9391849	176.952363	768.3667032	150.9158839	-473.4713205	122.5612588	140.3604301	6.393107137	107.0286626	3.385751678
0.16945	0.770227273	-203.7244425	141.3210329	553.2627232	171.5642847	751.4429562	147.023136	-462.0085145	120.5901877	139.2409453	6.472070297	106.6683335	3.499547884
0.1723	0.783181818	-186.9632253	137.6130913	529.0523379	165.3276107	724.4059876	141.9525484	-442.4072063	117.87601	137.8400484	6.521140759	106.1312259	3.599889914
0.17515	0.796136364	-171.0976307	132.9997494	505.5084491	158.2723329	687.8392741	135.8223269	-414.8565072	114.4174295	136.2102512	6.539608122	105.4336669	3.684451661
0.178	0.809090909	-156.2180941	127.5479533	482.8065983	150.4850832	642.3887849	128.7788704	-379.584375	110.2398652	134.3964713	6.528727229	104.6077613	3.752137012
0.18085	0.822045455	-142.4021446	121.3669307	461.0478584	142.0917645	588.7333974	120.9924672	-336.8249409	105.3975889	132.4179758	6.49055385	103.6541559	3.802355268
0.1837	0.835	-129.6776593	114.6070644	440.3183386	133.2497281	527.5759087	112.6572785	-286.8381669	99.97856744	130.3158712	6.426681096	102.5941448	3.834509275
0.18655	0.847954545	-118.1017823	107.4638504	420.6493645	124.1486648	459.5872049	103.9951338	-229.882559	94.11431711	128.0904361	6.338255051	101.4256836	3.849774217
0.1894	0.860909091	-107.7129312	100.1865849	401.990654	115.0172167	385.4156934	95.26752262	-166.2813662	87.99729365	125.7150667	6.236115787	100.1200592	3.875399624
0.19225	0.873863636	-98.65171453	93.09343515	384.2043691	106.1410607	305.5801469	86.79239618	-96.39354558	81.90729365	123.0599163	6.248115199	98.56912961	4.170972126
0.1951	0.886818182	-91.30549304	86.58743876	366.8548399	97.88229253	220.3689022	78.96786875	-20.81548523	76.24629091	119.7262286	7.38735854	96.44737264	6.290826524
0.19795	0.899772727	-86.7606116	81.1622907	348.7571385	90.69927594	129.4174321	72.28875332	59.28276703	71.57199625	114.5978189	14.12140763	92.84214275	14.98290554
0.2008	0.912727273	-88.1340647	77.36590829	326.6616594	85.14582862	30.59593284	67.32667447	141.0912677	68.59513394	104.4999958	38.5127326	85.14210589	42.99037959
0.20365	0.925681818	-104.7552632	75.67571985	290.9827238	81.83051175	-83.8634228	64.61894563	217.0095872	68.08763929	79.98714093	145.6235303	65.54355956	164.3013774
0.2065	0.938636364												
0.22	1												
0.24565													

radius(m)	non-dim radius	h,C2,d	+/-	h,C3,u	+/-	h,C3,d	+/-	h,C4,u	+/-	finh,D2	+/-	finh,D3	+/-
0.0701	0.318636364												
0.075	0.340909091												
0.0855	0.388636364												
0.121	0.55												
0.12385	0.562954545	-87.30143197	50.741925	144.0112784	383.9705868	-12.1510749	39.59301007	42.98592044	39.9872122	15.3828	124.7031	12.82217	84.06206
0.1267	0.575909091	-84.84246302	46.36166076	151.8981859	1807.583588	7.550214004	36.36368017	30.1953528	36.28244746	20.29966	29.77965	16.59843	19.99761
0.12955	0.588863636	-83.60037532	42.35697708	155.2804383	225.1304223	25.67106921	33.67238299	14.98850449	33.01433174	22.55519	9.75225	18.12344	6.345771
0.1324	0.601818182	-82.12345675	38.83118386	156.1607184	119.0720544	43.05895358	31.58101838	-0.505776174	30.29121302	23.85326	3.872681	18.8796	2.292273
0.13525	0.614772727	-80.04910401	35.82845031	155.2675744	81.71197407	59.69204761	30.07785618	-15.41451711	28.12725368	24.72158	2.143168	19.32558	1.118171
0.1381	0.627727273	-77.35640702	33.36228148	152.9922591	63.2279911	75.31704387	29.10555697	-29.27735166	26.48677569	25.34013	1.602622	19.61287	0.800508
0.14095	0.640681818	-74.13282232	31.41574286	149.5906496	52.58331167	89.6267613	28.56866936	-41.81579697	25.2996081	25.75916	1.368237	19.79191	0.68142
0.1438	0.653636364	-70.48781471	29.94007901	145.29361	45.94319702	102.3535202	28.34657463	-52.85172284	24.47506967	26.01716	1.23334	19.88528	0.612286
0.14665	0.666590909	-66.54082408	28.85804784	140.2988733	41.61052647	113.2768467	28.311018	-62.27889516	23.91536191	26.12618	1.150005	19.90552	0.567783
0.1495	0.679545455	-62.39738335	28.07401597	134.7996651	38.68931572	122.2404461	28.34275282	-70.03611575	23.52743366	26.10534	1.10199	19.85785	0.542405
0.15235	0.6925	-58.15687987	27.48657611	128.9561824	36.63536879	129.1458373	28.34232055	-76.11044875	23.23051505	25.9674	1.078848	19.7525	0.532329
0.1552	0.705454545	-53.90168215	27.00075665	122.9157927	35.08877431	133.955091	28.23477424	-80.51465069	22.95953459	25.73041	1.071791	19.5954	0.5335
0.15805	0.718409091	-49.70433634	26.53600731	116.8040101	33.80462256	136.6796373	27.96951549	-83.28689492	22.66524303	25.40577	1.073474	19.39331	0.541877
0.1609	0.731363636	-45.62111409	26.03022419	110.7187454	32.6197195	137.3745887	27.5178353	-84.48060118	22.31239482	25.0112	1.07839	19.15335	0.554085
0.1625	0.738636364												
0.16375	0.744318182	-41.6979691	25.43984478	104.7469558	31.43122678	136.1316275	26.86885662	-84.16261516	21.87743146	24.55785	1.082651	18.88069	0.567434
0.1666	0.757272727	-37.97087662	24.738265	98.94885749	30.18074119	133.0681666	26.02563545	-82.40963852	21.34610886	24.05888	1.084083	18.58217	0.58025
0.16945	0.770227273	-34.46072102	23.91308318	93.3718708	28.84131677	128.3214566	25.00142872	-79.29842068	20.71147868	23.52611	1.081445	18.26189	0.591377
0.1723	0.783181818	-31.1879866	22.96325222	88.05235623	27.40721304	122.0392148	23.81647483	-74.91147658	19.97235836	22.96743	1.074385	17.9253	0.600217
0.17515	0.796136364	-28.15946847	21.8966859	83.00961984	25.88632026	114.3758941	22.49579761	-69.32878664	19.13231702	22.39238	1.062983	17.57569	0.606492
0.178	0.809090909	-25.37810627	20.7282977	78.25808835	24.29495377	105.4851523	21.0673556	-62.63083063	18.19900105	21.80872	1.04762	17.21876	0.610135
0.18085	0.822045455	-22.84487368	19.47875798	73.79976085	22.65462538	95.51537857	19.56125474	-54.89334699	17.18423471	21.21963	1.028772	16.85477	0.611159
0.1837	0.835	-20.5531122	18.17399549	69.63444116	20.99058179	84.60888298	18.00972503	-46.19090714	16.10456212	20.63158	1.006806	16.48727	0.609563
0.18655	0.847954545	-18.50137067	16.84556326	65.75368072	19.3318248	72.89373567	16.44773461	-36.59276505	14.98255923	20.04429	0.981978	16.11589	0.605618
0.1894	0.860909091	-16.68569021	15.53173516	62.13712562	17.71202644	60.48638182	14.91487271	-26.17370666	13.84925491	19.4533	0.955999	15.73608	0.60368
0.19225	0.873863636	-15.11829376	14.27954402	58.75225095	16.17212967	47.47595379	13.45791168	-15.0093596	12.74780096	18.83853	0.948433	15.33107	0.64421
0.1951	0.886818182	-13.84869641	13.14687409	55.52312703	14.76299818	33.91043556	12.1343338	-3.207383203	11.73823415	18.13992	1.112617	14.85129	0.965689
0.19795	0.899772727	-13.02985546	12.20297967	52.26482534	13.54797706	19.73441107	11.01465518	9.042696085	10.90179568	17.19207	2.113823	14.15942	2.283254
0.2008	0.912727273	-13.11161186	11.52284961	48.4930415	12.60227651	4.625480926	10.17922997	21.31215701	10.33964193	15.62975	5.718883	12.86633	6.494932
0.20365	0.925681818	-15.44446392	11.16917986	42.80852956	12.00676247	-12.5759449	9.701794077	32.4723938	10.15860268	11.78014	21.43754	9.818203	24.60926
0.2065	0.938636364												
0.22	1												
0.24565													

Appendix 4.15: Listing of the Visual Basic routine arranging the heat transfer results data into test reports from the layout template MCRtemplate.xlt

```
Public Sub MCR_test_reports()
'Macro processing the raw data into test reports from a template
'Created by N. Miché on 06/06/05
'Last modified by N. Miché on 06/06/2005

Dim i As Integer
Dim wbd As Workbook  'workbook containing the raw data (present
workbook)
Dim wbt As Workbook  'template workbook
Dim wslabel(1 To 250) As String   'worksheet labels
Dim n As Integer
Dim rng As Range
Dim j As Integer
Dim k As Integer


'open template file
Workbooks.Open Filename:="C:\Documents and
Settings\nicolas\Desktop\Matlab_conduction\MCRtemplate.xlt",
editable:=True
'initialisation
Set wbd = Workbooks("mcrexcel.xls")
Set wbt = Workbooks("MCRtemplate.xlt")
n = wbd.Sheets("rawdata").Cells(1, 2).Value


'program core

'For i = 1 To 25
'   j = i
'For i = 26 To 50
'   j = i - 25
'For i = 51 To 75
'   j = i - 50
'For i = 76 To 100
'   j = i - 75
'For i = 101 To 125
'   j = i - 100
For i = 126 To n
  j = i - 125


   'create test report sheet
      'copy template sheet at end of book
      wbt.Activate
      wbt.Worksheets("template").Copy
after:=wbt.Worksheets(Worksheets.Count)
      'read worksheet label
      wslabel(i) = wbd.Sheets("results").Cells(2 + (i - 1) * 40, 6).Value
      'rename added worksheet with label
      wbt.Sheets(j + 1).Name = wslabel(i)


   'COPY TEST RESULTS TO TEMPLATE
   wbt.Sheets(j + 1).Activate

   'PARAM1
      'build
      wbd.Worksheets("results").Cells((i - 1) * 40 + 1, 2).Copy
      wbt.Sheets(j + 1).Cells(2, 3).PasteSpecial Paste:=xlPasteValues,
Operation:=xlNone, SkipBlanks _
      :=False, Transpose:=False

      'exp code
      wbd.Worksheets("results").Cells((i - 1) * 40 + 2, 2).Copy
      wbt.Sheets(j + 1).Activate
      Range("C3:F3").Select
      ActiveSheet.Paste

      'exp date
      wbd.Worksheets("results").Cells((i - 1) * 40 + 1, 6).Copy
      wbt.Sheets(j + 1).Activate
      Range("J2:M2").Select
      ActiveSheet.Paste

      'run
      wbd.Worksheets("results").Cells((i - 1) * 40 + 2, 6).Copy
      wbt.Sheets(j + 1).Activate
      Range("J3:M3").Select
      ActiveSheet.Paste

      'Rez
      wbd.Worksheets("results").Cells((i - 1) * 40 + 3, 2).Copy
      wbt.Sheets(j + 1).Activate
      Range("C5:D5").Select
      ActiveSheet.Paste
      wbd.Worksheets("results").Cells((i - 1) * 40 + 3, 4).Copy
      wbt.Sheets(j + 1).Activate
      Range("F5:G5").Select
      ActiveSheet.Paste

      'Ref
      wbd.Worksheets("results").Cells((i - 1) * 40 + 3, 6).Copy
      wbt.Sheets(j + 1).Activate
      Range("J5:K5").Select
      ActiveSheet.Paste
      wbd.Worksheets("results").Cells((i - 1) * 40 + 3, 8).Copy
      wbt.Sheets(j + 1).Activate
      Range("M5:N5").Select
      ActiveSheet.Paste

      'Ro
      wbd.Worksheets("results").Cells((i - 1) * 40 + 4, 2).Copy
      wbt.Sheets(j + 1).Activate
      Range("C6:D6").Select
      ActiveSheet.Paste
      wbd.Worksheets("results").Cells((i - 1) * 40 + 4, 4).Copy
      wbt.Sheets(j + 1).Activate
      Range("F6:G6").Select
      ActiveSheet.Paste

      'Rot speed
      wbd.Worksheets("results").Cells((i - 1) * 40 + 4, 6).Copy
      wbt.Sheets(j + 1).Activate
      Range("J6:K6").Select
      ActiveSheet.Paste
      wbd.Worksheets("results").Cells((i - 1) * 40 + 4, 8).Copy
      wbt.Sheets(j + 1).Activate
      Range("M6:N6").Select
      ActiveSheet.Paste

      'Mflow
      wbd.Worksheets("results").Cells((i - 1) * 40 + 5, 2).Copy
      wbt.Sheets(j + 1).Activate
      Range("C7:D7").Select
      ActiveSheet.Paste
      wbd.Worksheets("results").Cells((i - 1) * 40 + 5, 4).Copy
      wbt.Sheets(j + 1).Activate
      Range("F7:G7").Select
      ActiveSheet.Paste

      'Pcav
      wbd.Worksheets("results").Cells((i - 1) * 40 + 5, 6).Copy
      wbt.Sheets(j + 1).Activate
      Range("J7:K7").Select
      ActiveSheet.Paste
      wbd.Worksheets("results").Cells((i - 1) * 40 + 5, 8).Copy
      wbt.Sheets(j + 1).Activate
      Range("M7:N7").Select
      ActiveSheet.Paste

      'Bo*
      wbd.Worksheets("results").Cells((i - 1) * 40 + 6, 2).Copy
      wbt.Sheets(j + 1).Activate
      Range("C8:D8").Select
      ActiveSheet.Paste
      wbd.Worksheets("results").Cells((i - 1) * 40 + 6, 4).Copy
      wbt.Sheets(j + 1).Activate
      Range("F8:G8").Select
      ActiveSheet.Paste

      'Pr
      wbd.Worksheets("results").Cells((i - 1) * 40 + 6, 6).Copy
      wbt.Sheets(j + 1).Activate
      Range("J8:K8").Select
      ActiveSheet.Paste
      wbd.Worksheets("results").Cells((i - 1) * 40 + 6, 8).Copy
      wbt.Sheets(j + 1).Activate
      Range("M8:N8").Select
      ActiveSheet.Paste

      'Tinlet
      wbd.Worksheets("results").Cells((i - 1) * 40 + 7, 2).Copy
      wbt.Sheets(j + 1).Activate
      Range("C9:D9").Select
      ActiveSheet.Paste
      wbd.Worksheets("results").Cells((i - 1) * 40 + 7, 4).Copy
      wbt.Sheets(j + 1).Activate
      Range("F9:G9").Select
      ActiveSheet.Paste

      'Texit
      wbd.Worksheets("results").Cells((i - 1) * 40 + 7, 6).Copy
      wbt.Sheets(j + 1).Activate
      Range("J9:K9").Select
      ActiveSheet.Paste
      wbd.Worksheets("results").Cells((i - 1) * 40 + 7, 8).Copy
      wbt.Sheets(j + 1).Activate
      Range("M9:N9").Select
      ActiveSheet.Paste

      'Tcav2
      wbd.Worksheets("results").Cells((i - 1) * 40 + 8, 2).Copy
      wbt.Sheets(j + 1).Activate
      Range("C10:D10").Select
      ActiveSheet.Paste
```

```
wbd.Worksheets("results").Cells((i - 1) * 40 + 8, 4).Copy
wbt.Sheets(j + 1).Activate
Range("F10:G10").Select
ActiveSheet.Paste

'Tcav3
wbd.Worksheets("results").Cells((i - 1) * 40 + 8, 6).Copy
wbt.Sheets(j + 1).Activate
Range("J10:K10").Select
ActiveSheet.Paste
wbd.Worksheets("results").Cells((i - 1) * 40 + 8, 8).Copy
wbt.Sheets(j + 1).Activate
Range("M10:N10").Select
ActiveSheet.Paste

'DTmeas
wbd.Worksheets("results").Cells((i - 1) * 40 + 9, 2).Copy
wbt.Sheets(j + 1).Activate
Range("C11:D11").Select
ActiveSheet.Paste
wbd.Worksheets("results").Cells((i - 1) * 40 + 9, 4).Copy
wbt.Sheets(j + 1).Activate
Range("F11:G11").Select
ActiveSheet.Paste

'DTcalc
wbd.Worksheets("results").Cells((i - 1) * 40 + 9, 6).Copy
wbt.Sheets(j + 1).Activate
Range("J11:K11").Select
ActiveSheet.Paste
wbd.Worksheets("results").Cells((i - 1) * 40 + 9, 8).Copy
wbt.Sheets(j + 1).Activate
Range("M11:N11").Select
ActiveSheet.Paste

'BDTav
wbd.Worksheets("results").Cells((i - 1) * 40 + 10, 2).Copy
wbt.Sheets(j + 1).Activate
Range("C12:D12").Select
ActiveSheet.Paste
wbd.Worksheets("results").Cells((i - 1) * 40 + 10, 4).Copy
wbt.Sheets(j + 1).Activate
Range("F12:G12").Select
ActiveSheet.Paste

'finBDTav
wbd.Worksheets("results").Cells((i - 1) * 40 + 10, 6).Copy
wbt.Sheets(j + 1).Activate
Range("J12:K12").Select
ActiveSheet.Paste
wbd.Worksheets("results").Cells((i - 1) * 40 + 10, 8).Copy
wbt.Sheets(j + 1).Activate
Range("M12:N12").Select
ActiveSheet.Paste

'Ostroke
wbd.Worksheets("results").Cells((i - 1) * 40 + 11, 2).Copy
wbt.Sheets(j + 1).Activate
Range("C13:D13").Select
ActiveSheet.Paste
wbd.Worksheets("results").Cells((i - 1) * 40 + 11, 4).Copy
wbt.Sheets(j + 1).Activate
Range("F13:G13").Select
ActiveSheet.Paste

'finOstroke
wbd.Worksheets("results").Cells((i - 1) * 40 + 11, 6).Copy
wbt.Sheets(j + 1).Activate
Range("J13:K13").Select
ActiveSheet.Paste
wbd.Worksheets("results").Cells((i - 1) * 40 + 11, 8).Copy
wbt.Sheets(j + 1).Activate
Range("M13:N13").Select
ActiveSheet.Paste

'TsC2dav
wbd.Worksheets("results").Cells((i - 1) * 40 + 12, 2).Copy
wbt.Sheets(j + 1).Activate
Range("C14:D14").Select
ActiveSheet.Paste
wbd.Worksheets("results").Cells((i - 1) * 40 + 12, 4).Copy
wbt.Sheets(j + 1).Activate
Range("F14:G14").Select
ActiveSheet.Paste

'TsC3uav
wbd.Worksheets("results").Cells((i - 1) * 40 + 12, 6).Copy
wbt.Sheets(j + 1).Activate
Range("J14:K14").Select
ActiveSheet.Paste
wbd.Worksheets("results").Cells((i - 1) * 40 + 12, 8).Copy
wbt.Sheets(j + 1).Activate
Range("M14:N14").Select
ActiveSheet.Paste

'TsC3dav
wbd.Worksheets("results").Cells((i - 1) * 40 + 13, 2).Copy
wbt.Sheets(j + 1).Activate
Range("C15:D15").Select
ActiveSheet.Paste
wbd.Worksheets("results").Cells((i - 1) * 40 + 13, 4).Copy
wbt.Sheets(j + 1).Activate
Range("F15:G15").Select
ActiveSheet.Paste

'TsC4uav
wbd.Worksheets("results").Cells((i - 1) * 40 + 13, 6).Copy
wbt.Sheets(j + 1).Activate
Range("J15:K15").Select
ActiveSheet.Paste
wbd.Worksheets("results").Cells((i - 1) * 40 + 13, 8).Copy
wbt.Sheets(j + 1).Activate
Range("M15:N15").Select
ActiveSheet.Paste

'finTsD2av
wbd.Worksheets("results").Cells((i - 1) * 40 + 14, 2).Copy
wbt.Sheets(j + 1).Activate
Range("C16:D16").Select
ActiveSheet.Paste
wbd.Worksheets("results").Cells((i - 1) * 40 + 14, 4).Copy
wbt.Sheets(j + 1).Activate
Range("F16:G16").Select
ActiveSheet.Paste

'finTsD3av
wbd.Worksheets("results").Cells((i - 1) * 40 + 14, 6).Copy
wbt.Sheets(j + 1).Activate
Range("J16:K16").Select
ActiveSheet.Paste
wbd.Worksheets("results").Cells((i - 1) * 40 + 14, 8).Copy
wbt.Sheets(j + 1).Activate
Range("M16:N16").Select
ActiveSheet.Paste

'NuC2dav
wbd.Worksheets("results").Cells((i - 1) * 40 + 15, 2).Copy
wbt.Sheets(j + 1).Activate
Range("C17:D17").Select
ActiveSheet.Paste
wbd.Worksheets("results").Cells((i - 1) * 40 + 15, 4).Copy
wbt.Sheets(j + 1).Activate
Range("F17:G17").Select
ActiveSheet.Paste

'NuC3uav
wbd.Worksheets("results").Cells((i - 1) * 40 + 15, 6).Copy
wbt.Sheets(j + 1).Activate
Range("J17:K17").Select
ActiveSheet.Paste
wbd.Worksheets("results").Cells((i - 1) * 40 + 15, 8).Copy
wbt.Sheets(j + 1).Activate
Range("M17:N17").Select
ActiveSheet.Paste

'NuC3dav
wbd.Worksheets("results").Cells((i - 1) * 40 + 16, 2).Copy
wbt.Sheets(j + 1).Activate
Range("C18:D18").Select
ActiveSheet.Paste
wbd.Worksheets("results").Cells((i - 1) * 40 + 16, 4).Copy
wbt.Sheets(j + 1).Activate
Range("F18:G18").Select
ActiveSheet.Paste

'NuC4uav
wbd.Worksheets("results").Cells((i - 1) * 40 + 16, 6).Copy
wbt.Sheets(j + 1).Activate
Range("J18:K18").Select
ActiveSheet.Paste
wbd.Worksheets("results").Cells((i - 1) * 40 + 16, 8).Copy
wbt.Sheets(j + 1).Activate
Range("M18:N18").Select
ActiveSheet.Paste

'finNuD2av
wbd.Worksheets("results").Cells((i - 1) * 40 + 17, 2).Copy
wbt.Sheets(j + 1).Activate
Range("C19:D19").Select
ActiveSheet.Paste
wbd.Worksheets("results").Cells((i - 1) * 40 + 17, 4).Copy
wbt.Sheets(j + 1).Activate
Range("F19:G19").Select
ActiveSheet.Paste

'finNuD3av
wbd.Worksheets("results").Cells((i - 1) * 40 + 17, 6).Copy
wbt.Sheets(j + 1).Activate
Range("J19:K19").Select
ActiveSheet.Paste
wbd.Worksheets("results").Cells((i - 1) * 40 + 17, 8).Copy
wbt.Sheets(j + 1).Activate
Range("M19:N19").Select
ActiveSheet.Paste

'TshC2
wbd.Worksheets("results").Cells((i - 1) * 40 + 18, 2).Copy
wbt.Sheets(j + 1).Activate
Range("C20:D20").Select
ActiveSheet.Paste
wbd.Worksheets("results").Cells((i - 1) * 40 + 18, 4).Copy
wbt.Sheets(j + 1).Activate
```

```
        Range("F20:G20").Select
        ActiveSheet.Paste

        'TshC3
        wbd.Worksheets("results").Cells((i - 1) * 40 + 18, 6).Copy
        wbt.Sheets(j + 1).Activate
        Range("J20:K20").Select
        ActiveSheet.Paste
        wbd.Worksheets("results").Cells((i - 1) * 40 + 18, 8).Copy
        wbt.Sheets(j + 1).Activate
        Range("M20:N20").Select
        ActiveSheet.Paste

        'NushC2
        wbd.Worksheets("results").Cells((i - 1) * 40 + 19, 2).Copy
        wbt.Sheets(j + 1).Activate
        Range("C21:D21").Select
        ActiveSheet.Paste
        wbd.Worksheets("results").Cells((i - 1) * 40 + 19, 4).Copy
        wbt.Sheets(j + 1).Activate
        Range("F21:G21").Select
        ActiveSheet.Paste

        'NushC3
        wbd.Worksheets("results").Cells((i - 1) * 40 + 19, 6).Copy
        wbt.Sheets(j + 1).Activate
        Range("J21:K21").Select
        ActiveSheet.Paste
        wbd.Worksheets("results").Cells((i - 1) * 40 + 19, 8).Copy
        wbt.Sheets(j + 1).Activate
        Range("M21:N21").Select
        ActiveSheet.Paste

        'GrshC2
        wbd.Worksheets("results").Cells((i - 1) * 40 + 20, 2).Copy
        wbt.Sheets(j + 1).Activate
        Range("C22:D22").Select
        ActiveSheet.Paste
        wbd.Worksheets("results").Cells((i - 1) * 40 + 20, 4).Copy
        wbt.Sheets(j + 1).Activate
        Range("F22:G22").Select
        ActiveSheet.Paste

        'GrshC3
        wbd.Worksheets("results").Cells((i - 1) * 40 + 20, 6).Copy
        wbt.Sheets(j + 1).Activate
        Range("J22:K22").Select
        ActiveSheet.Paste
        wbd.Worksheets("results").Cells((i - 1) * 40 + 20, 8).Copy
        wbt.Sheets(j + 1).Activate
        Range("M22:N22").Select
        ActiveSheet.Paste

        'Theta 2
        wbd.Worksheets("results").Cells((i - 1) * 40 + 21, 2).Copy
        wbt.Sheets(j + 1).Activate
        Range("C23:D23").Select
        ActiveSheet.Paste
        wbd.Worksheets("results").Cells((i - 1) * 40 + 21, 4).Copy
        wbt.Sheets(j + 1).Activate
        Range("F23:G23").Select
        ActiveSheet.Paste

        'Theta 3
        wbd.Worksheets("results").Cells((i - 1) * 40 + 21, 6).Copy
        wbt.Sheets(j + 1).Activate
        Range("J23:K23").Select
        ActiveSheet.Paste
        wbd.Worksheets("results").Cells((i - 1) * 40 + 21, 8).Copy
        wbt.Sheets(j + 1).Activate
        Range("M23:N23").Select
        ActiveSheet.Paste



    'PARAM2

        'page 3 report

        wbd.Worksheets("results").Activate
        With ActiveSheet
        Set rng = .Range(Cells(((i - 1) * 40 + 2), 12), Cells(((i - 1) * 40 + 2),
13))
        rng.Copy
        wbt.Sheets(j + 1).Range("C58").PasteSpecial
Paste:=xlPasteValues, Operation:=xlNone, SkipBlanks _
        :=False, Transpose:=False
        End With

        wbd.Worksheets("results").Activate
        With ActiveSheet
        Set rng = .Range(Cells(((i - 1) * 40 + 37), 12), Cells(((i - 1) * 40 +
38), 13))
        rng.Copy
        wbt.Sheets(j + 1).Range("C93").PasteSpecial
Paste:=xlPasteValues, Operation:=xlNone, SkipBlanks _
        :=False, Transpose:=False
        End With

        wbd.Worksheets("results").Cells((i - 1) * 40 + 2, 14).Copy
        wbt.Sheets(j + 1).Activate
        Range("E58:F58").Select
        ActiveSheet.Paste

        wbd.Worksheets("results").Cells((i - 1) * 40 + 37, 14).Copy
        wbt.Sheets(j + 1).Activate
        Range("E93:F93").Select
        ActiveSheet.Paste

        wbd.Worksheets("results").Cells((i - 1) * 40 + 38, 14).Copy
        wbt.Sheets(j + 1).Activate
        Range("E94:F94").Select
        ActiveSheet.Paste

        wbd.Worksheets("results").Cells((i - 1) * 40 + 2, 15).Copy
        wbt.Sheets(j + 1).Cells(58, 7).PasteSpecial Paste:=xlPasteValues,
Operation:=xlNone, SkipBlanks _
        :=False, Transpose:=False

        wbd.Worksheets("results").Cells((i - 1) * 40 + 37, 15).Copy
        wbt.Sheets(j + 1).Cells(93, 7).PasteSpecial Paste:=xlPasteValues,
Operation:=xlNone, SkipBlanks _
        :=False, Transpose:=False

        wbd.Worksheets("results").Cells((i - 1) * 40 + 38, 15).Copy
        wbt.Sheets(j + 1).Cells(94, 7).PasteSpecial Paste:=xlPasteValues,
Operation:=xlNone, SkipBlanks _
        :=False, Transpose:=False

        wbd.Worksheets("results").Activate
        With ActiveSheet
        Set rng = .Range(Cells(((i - 1) * 40 + 3), 16), Cells(((i - 1) * 40 + 3),
17))
        rng.Copy
        wbt.Sheets(j + 1).Range("H59").PasteSpecial
Paste:=xlPasteValues, Operation:=xlNone, SkipBlanks _
        :=False, Transpose:=False
        End With

        wbd.Worksheets("results").Activate
        With ActiveSheet
        Set rng = .Range(Cells(((i - 1) * 40 + 5), 16), Cells(((i - 1) * 40 + 5),
19))
        rng.Copy
        wbt.Sheets(j + 1).Range("H61").PasteSpecial
Paste:=xlPasteValues, Operation:=xlNone, SkipBlanks _
        :=False, Transpose:=False
        End With

        wbd.Worksheets("results").Activate
        With ActiveSheet
        Set rng = .Range(Cells(((i - 1) * 40 + 20), 16), Cells(((i - 1) * 40 +
20), 19))
        rng.Copy
        wbt.Sheets(j + 1).Range("H76").PasteSpecial
Paste:=xlPasteValues, Operation:=xlNone, SkipBlanks _
        :=False, Transpose:=False
        End With

        wbd.Worksheets("results").Activate
        With ActiveSheet
        Set rng = .Range(Cells(((i - 1) * 40 + 36), 16), Cells(((i - 1) * 40 +
36), 19))
        rng.Copy
        wbt.Sheets(j + 1).Range("H92").PasteSpecial
Paste:=xlPasteValues, Operation:=xlNone, SkipBlanks _
        :=False, Transpose:=False
        End With

        wbd.Worksheets("results").Activate
        With ActiveSheet
        Set rng = .Range(Cells(((i - 1) * 40 + 4), 18), Cells(((i - 1) * 40 + 4),
19))
        rng.Copy
        wbt.Sheets(j + 1).Range("J60").PasteSpecial Paste:=xlPasteValues,
Operation:=xlNone, SkipBlanks _
        :=False, Transpose:=False
        End With

        wbd.Worksheets("results").Cells((i - 1) * 40 + 3, 20).Copy
        wbt.Sheets(j + 1).Activate
        Range("L59:M59").Select
        ActiveSheet.Paste

        wbd.Worksheets("results").Cells((i - 1) * 40 + 5, 20).Copy
        wbt.Sheets(j + 1).Activate
        Range("L61:M61").Select
        ActiveSheet.Paste

        wbd.Worksheets("results").Cells((i - 1) * 40 + 20, 20).Copy
        wbt.Sheets(j + 1).Activate
        Range("L76:M76").Select
        ActiveSheet.Paste

        wbd.Worksheets("results").Cells((i - 1) * 40 + 36, 20).Copy
        wbt.Sheets(j + 1).Activate
        Range("L92:M92").Select
        ActiveSheet.Paste

        wbd.Worksheets("results").Activate
```

```
        With ActiveSheet
        Set rng = .Range(Cells(((i - 1) * 40 + 3), 21), Cells(((i - 1) * 40 + 3),
23))
        rng.Copy
        wbt.Sheets(j + 1).Range("N59").PasteSpecial
Paste:=xlPasteValues, Operation:=xlNone, SkipBlanks _
        :=False, Transpose:=False
        End With

        wbd.Worksheets("results").Activate
        With ActiveSheet
        Set rng = .Range(Cells(((i - 1) * 40 + 5), 21), Cells(((i - 1) * 40 + 5),
23))
        rng.Copy
        wbt.Sheets(j + 1).Range("N61").PasteSpecial
Paste:=xlPasteValues, Operation:=xlNone, SkipBlanks _
        :=False, Transpose:=False
        End With

        wbd.Worksheets("results").Activate
        With ActiveSheet
        Set rng = .Range(Cells(((i - 1) * 40 + 20), 21), Cells(((i - 1) * 40 +
20), 23))
        rng.Copy
        wbt.Sheets(j + 1).Range("N76").PasteSpecial
Paste:=xlPasteValues, Operation:=xlNone, SkipBlanks _
        :=False, Transpose:=False
        End With

        wbd.Worksheets("results").Activate
        With ActiveSheet
        Set rng = .Range(Cells(((i - 1) * 40 + 36), 21), Cells(((i - 1) * 40 +
36), 23))
        rng.Copy
        wbt.Sheets(j + 1).Range("N92").PasteSpecial
Paste:=xlPasteValues, Operation:=xlNone, SkipBlanks _
        :=False, Transpose:=False
        End With

        wbd.Worksheets("results").Activate
        With ActiveSheet
        Set rng = .Range(Cells(((i - 1) * 40 + 6), 24), Cells(((i - 1) * 40 + 19),
35))
        rng.Copy
        wbt.Sheets(j + 1).Range("Q62").PasteSpecial
Paste:=xlPasteValues, Operation:=xlNone, SkipBlanks _
        :=False, Transpose:=False
        End With

        wbd.Worksheets("results").Activate
        With ActiveSheet
        Set rng = .Range(Cells(((i - 1) * 40 + 21), 24), Cells(((i - 1) * 40 +
35), 35))
        rng.Copy
        wbt.Sheets(j + 1).Range("Q77").PasteSpecial
Paste:=xlPasteValues, Operation:=xlNone, SkipBlanks _
        :=False, Transpose:=False
        End With


        'page4 report

        wbd.Worksheets("results").Activate
        With ActiveSheet
        Set rng = .Range(Cells(((i - 1) * 40 + 6), 36), Cells(((i - 1) * 40 + 19),
37))
        rng.Copy
        wbt.Sheets(j + 1).Range("C103").PasteSpecial
Paste:=xlPasteValues, Operation:=xlNone, SkipBlanks _
        :=False, Transpose:=False
        End With

        wbd.Worksheets("results").Activate
        With ActiveSheet
        Set rng = .Range(Cells(((i - 1) * 40 + 21), 36), Cells(((i - 1) * 40 +
35), 37))
        rng.Copy
        wbt.Sheets(j + 1).Range("C118").PasteSpecial
Paste:=xlPasteValues, Operation:=xlNone, SkipBlanks _
        :=False, Transpose:=False
        End With

        wbd.Worksheets("results").Cells((i - 1) * 40 + 6, 38).Copy
        wbt.Sheets(j + 1).Activate
        Range("E103:F103").Select
        ActiveSheet.Paste

        wbd.Worksheets("results").Cells((i - 1) * 40 + 7, 38).Copy
        wbt.Sheets(j + 1).Activate
        Range("E104:F104").Select
        ActiveSheet.Paste

        wbd.Worksheets("results").Cells((i - 1) * 40 + 8, 38).Copy
        wbt.Sheets(j + 1).Activate
        Range("E105:F105").Select
        ActiveSheet.Paste

        wbd.Worksheets("results").Cells((i - 1) * 40 + 9, 38).Copy
        wbt.Sheets(j + 1).Activate
        Range("E106:F106").Select
        ActiveSheet.Paste

        wbd.Worksheets("results").Cells((i - 1) * 40 + 10, 38).Copy
        wbt.Sheets(j + 1).Activate
        Range("E107:F107").Select
        ActiveSheet.Paste

        wbd.Worksheets("results").Cells((i - 1) * 40 + 11, 38).Copy
        wbt.Sheets(j + 1).Activate
        Range("E108:F108").Select
        ActiveSheet.Paste

        wbd.Worksheets("results").Cells((i - 1) * 40 + 12, 38).Copy
        wbt.Sheets(j + 1).Activate
        Range("E109:F109").Select
        ActiveSheet.Paste

        wbd.Worksheets("results").Cells((i - 1) * 40 + 13, 38).Copy
        wbt.Sheets(j + 1).Activate
        Range("E110:F110").Select
        ActiveSheet.Paste

        wbd.Worksheets("results").Cells((i - 1) * 40 + 14, 38).Copy
        wbt.Sheets(j + 1).Activate
        Range("E111:F111").Select
        ActiveSheet.Paste

        wbd.Worksheets("results").Cells((i - 1) * 40 + 15, 38).Copy
        wbt.Sheets(j + 1).Activate
        Range("E112:F112").Select
        ActiveSheet.Paste

        wbd.Worksheets("results").Cells((i - 1) * 40 + 16, 38).Copy
        wbt.Sheets(j + 1).Activate
        Range("E113:F113").Select
        ActiveSheet.Paste

        wbd.Worksheets("results").Cells((i - 1) * 40 + 17, 38).Copy
        wbt.Sheets(j + 1).Activate
        Range("E114:F114").Select
        ActiveSheet.Paste

        wbd.Worksheets("results").Cells((i - 1) * 40 + 18, 38).Copy
        wbt.Sheets(j + 1).Activate
        Range("E115:F115").Select
        ActiveSheet.Paste

        wbd.Worksheets("results").Cells((i - 1) * 40 + 19, 38).Copy
        wbt.Sheets(j + 1).Activate
        Range("E116:F116").Select
        ActiveSheet.Paste

        wbd.Worksheets("results").Cells((i - 1) * 40 + 21, 38).Copy
        wbt.Sheets(j + 1).Activate
        Range("E118:F118").Select
        ActiveSheet.Paste

        wbd.Worksheets("results").Cells((i - 1) * 40 + 22, 38).Copy
        wbt.Sheets(j + 1).Activate
        Range("E119:F119").Select
        ActiveSheet.Paste

        wbd.Worksheets("results").Cells((i - 1) * 40 + 23, 38).Copy
        wbt.Sheets(j + 1).Activate
        Range("E120:F120").Select
        ActiveSheet.Paste

        wbd.Worksheets("results").Cells((i - 1) * 40 + 24, 38).Copy
        wbt.Sheets(j + 1).Activate
        Range("E121:F121").Select
        ActiveSheet.Paste

        wbd.Worksheets("results").Cells((i - 1) * 40 + 25, 38).Copy
        wbt.Sheets(j + 1).Activate
        Range("E122:F122").Select
        ActiveSheet.Paste

        wbd.Worksheets("results").Cells((i - 1) * 40 + 26, 38).Copy
        wbt.Sheets(j + 1).Activate
        Range("E123:F123").Select
        ActiveSheet.Paste

        wbd.Worksheets("results").Cells((i - 1) * 40 + 27, 38).Copy
        wbt.Sheets(j + 1).Activate
        Range("E124:F124").Select
        ActiveSheet.Paste

        wbd.Worksheets("results").Cells((i - 1) * 40 + 28, 38).Copy
        wbt.Sheets(j + 1).Activate
        Range("E125:F125").Select
        ActiveSheet.Paste

        wbd.Worksheets("results").Cells((i - 1) * 40 + 29, 38).Copy
        wbt.Sheets(j + 1).Activate
        Range("E126:F126").Select
        ActiveSheet.Paste

        wbd.Worksheets("results").Cells((i - 1) * 40 + 30, 38).Copy
        wbt.Sheets(j + 1).Activate
        Range("E127:F127").Select
        ActiveSheet.Paste
```

```
        wbd.Worksheets("results").Cells((i - 1) * 40 + 31, 38).Copy
        wbt.Sheets(j + 1).Activate
        Range("E128:F128").Select
        ActiveSheet.Paste

        wbd.Worksheets("results").Cells((i - 1) * 40 + 32, 38).Copy
        wbt.Sheets(j + 1).Activate
        Range("E129:F129").Select
        ActiveSheet.Paste

        wbd.Worksheets("results").Cells((i - 1) * 40 + 33, 38).Copy
        wbt.Sheets(j + 1).Activate
        Range("E130:F130").Select
        ActiveSheet.Paste

        wbd.Worksheets("results").Cells((i - 1) * 40 + 34, 38).Copy
        wbt.Sheets(j + 1).Activate
        Range("E131:F131").Select
        ActiveSheet.Paste

        wbd.Worksheets("results").Cells((i - 1) * 40 + 35, 38).Copy
        wbt.Sheets(j + 1).Activate
        Range("E132:F132").Select
        ActiveSheet.Paste

        wbd.Worksheets("results").Activate
        With ActiveSheet
        Set rng = .Range(Cells(((i - 1) * 40 + 6), 39), Cells(((i - 1) * 40 + 19),
43))
        rng.Copy
        wbt.Sheets(j + 1).Range("G103").PasteSpecial
Paste:=xlPasteValues, Operation:=xlNone, SkipBlanks _
        :=False, Transpose:=False
        End With

        wbd.Worksheets("results").Activate
        With ActiveSheet
        Set rng = .Range(Cells(((i - 1) * 40 + 21), 39), Cells(((i - 1) * 40 +
35), 43))
        rng.Copy
        wbt.Sheets(j + 1).Range("G118").PasteSpecial
Paste:=xlPasteValues, Operation:=xlNone, SkipBlanks _
        :=False, Transpose:=False
        End With

        wbd.Worksheets("results").Cells((i - 1) * 40 + 6, 44).Copy
        wbt.Sheets(j + 1).Activate
        Range("L103:M103").Select
        ActiveSheet.Paste

        wbd.Worksheets("results").Cells((i - 1) * 40 + 7, 44).Copy
        wbt.Sheets(j + 1).Activate
        Range("L104:M104").Select
        ActiveSheet.Paste

        wbd.Worksheets("results").Cells((i - 1) * 40 + 8, 44).Copy
        wbt.Sheets(j + 1).Activate
        Range("L105:M105").Select
        ActiveSheet.Paste

        wbd.Worksheets("results").Cells((i - 1) * 40 + 9, 44).Copy
        wbt.Sheets(j + 1).Activate
        Range("L106:M106").Select
        ActiveSheet.Paste

        wbd.Worksheets("results").Cells((i - 1) * 40 + 10, 44).Copy
        wbt.Sheets(j + 1).Activate
        Range("L107:M107").Select
        ActiveSheet.Paste

        wbd.Worksheets("results").Cells((i - 1) * 40 + 11, 44).Copy
        wbt.Sheets(j + 1).Activate
        Range("L108:M108").Select
        ActiveSheet.Paste

        wbd.Worksheets("results").Cells((i - 1) * 40 + 12, 44).Copy
        wbt.Sheets(j + 1).Activate
        Range("L109:M109").Select
        ActiveSheet.Paste

        wbd.Worksheets("results").Cells((i - 1) * 40 + 13, 44).Copy
        wbt.Sheets(j + 1).Activate
        Range("L110:M110").Select
        ActiveSheet.Paste

        wbd.Worksheets("results").Cells((i - 1) * 40 + 14, 44).Copy
        wbt.Sheets(j + 1).Activate
        Range("L111:M111").Select
        ActiveSheet.Paste

        wbd.Worksheets("results").Cells((i - 1) * 40 + 15, 44).Copy
        wbt.Sheets(j + 1).Activate
        Range("L112:M112").Select
        ActiveSheet.Paste

        wbd.Worksheets("results").Cells((i - 1) * 40 + 16, 44).Copy
        wbt.Sheets(j + 1).Activate
        Range("L113:M113").Select
        ActiveSheet.Paste

        wbd.Worksheets("results").Cells((i - 1) * 40 + 17, 44).Copy
        wbt.Sheets(j + 1).Activate
        Range("L114:M114").Select
        ActiveSheet.Paste

        wbd.Worksheets("results").Cells((i - 1) * 40 + 18, 44).Copy
        wbt.Sheets(j + 1).Activate
        Range("L115:M115").Select
        ActiveSheet.Paste

        wbd.Worksheets("results").Cells((i - 1) * 40 + 19, 44).Copy
        wbt.Sheets(j + 1).Activate
        Range("L116:M116").Select
        ActiveSheet.Paste

        wbd.Worksheets("results").Cells((i - 1) * 40 + 21, 44).Copy
        wbt.Sheets(j + 1).Activate
        Range("L118:M118").Select
        ActiveSheet.Paste

        wbd.Worksheets("results").Cells((i - 1) * 40 + 22, 44).Copy
        wbt.Sheets(j + 1).Activate
        Range("L119:M119").Select
        ActiveSheet.Paste

        wbd.Worksheets("results").Cells((i - 1) * 40 + 23, 44).Copy
        wbt.Sheets(j + 1).Activate
        Range("L120:M120").Select
        ActiveSheet.Paste

        wbd.Worksheets("results").Cells((i - 1) * 40 + 24, 44).Copy
        wbt.Sheets(j + 1).Activate
        Range("L121:M121").Select
        ActiveSheet.Paste

        wbd.Worksheets("results").Cells((i - 1) * 40 + 25, 44).Copy
        wbt.Sheets(j + 1).Activate
        Range("L122:M122").Select
        ActiveSheet.Paste

        wbd.Worksheets("results").Cells((i - 1) * 40 + 26, 44).Copy
        wbt.Sheets(j + 1).Activate
        Range("L123:M123").Select
        ActiveSheet.Paste

        wbd.Worksheets("results").Cells((i - 1) * 40 + 27, 44).Copy
        wbt.Sheets(j + 1).Activate
        Range("L124:M124").Select
        ActiveSheet.Paste

        wbd.Worksheets("results").Cells((i - 1) * 40 + 28, 44).Copy
        wbt.Sheets(j + 1).Activate
        Range("L125:M125").Select
        ActiveSheet.Paste

        wbd.Worksheets("results").Cells((i - 1) * 40 + 29, 44).Copy
        wbt.Sheets(j + 1).Activate
        Range("L126:M126").Select
        ActiveSheet.Paste

        wbd.Worksheets("results").Cells((i - 1) * 40 + 30, 44).Copy
        wbt.Sheets(j + 1).Activate
        Range("L127:M127").Select
        ActiveSheet.Paste

        wbd.Worksheets("results").Cells((i - 1) * 40 + 31, 44).Copy
        wbt.Sheets(j + 1).Activate
        Range("L128:M128").Select
        ActiveSheet.Paste

        wbd.Worksheets("results").Cells((i - 1) * 40 + 32, 44).Copy
        wbt.Sheets(j + 1).Activate
        Range("L129:M129").Select
        ActiveSheet.Paste

        wbd.Worksheets("results").Cells((i - 1) * 40 + 33, 44).Copy
        wbt.Sheets(j + 1).Activate
        Range("L130:M130").Select
        ActiveSheet.Paste

        wbd.Worksheets("results").Cells((i - 1) * 40 + 34, 44).Copy
        wbt.Sheets(j + 1).Activate
        Range("L131:M131").Select
        ActiveSheet.Paste

        wbd.Worksheets("results").Cells((i - 1) * 40 + 35, 44).Copy
        wbt.Sheets(j + 1).Activate
        Range("L132:M132").Select
        ActiveSheet.Paste

        wbd.Worksheets("results").Activate
        With ActiveSheet
        Set rng = .Range(Cells(((i - 1) * 40 + 6), 45), Cells(((i - 1) * 40 + 19),
59))
        rng.Copy
        wbt.Sheets(j + 1).Range("N103").PasteSpecial
Paste:=xlPasteValues, Operation:=xlNone, SkipBlanks _
        :=False, Transpose:=False
        End With

        wbd.Worksheets("results").Activate
        With ActiveSheet
```

```
        Set rng = .Range(Cells(((i - 1) * 40 + 21), 45), Cells(((i - 1) * 40 +
35), 59))
        rng.Copy
        wbt.Sheets(j + 1).Range("N118").PasteSpecial
Paste:=xlPasteValues, Operation:=xlNone, SkipBlanks _
        :=False, Transpose:=False
        End With

Next i
```

```
'Create results workbook
wbt.SaveAs Filename:="C:\Documents and
Settings\nicolas\Desktop\Matlab_conduction\MCR_HT-reports6.xls",
FileFormat:=xlNormal, Password:="", WriteResPassword:="",
ReadOnlyRecommended:=False, CreateBackup:=False


End Sub
```

Appendix 4.16: Example of LDA test report

LDA measurement		**LDA code:**	101	**rpm:**	4552.2	**Perfd by:**	NM	Printed: 16/09/2008	Page 1/3
Build:	3	**ReΦ:**	4.12E+06	**Date:**	12/11/2003	**LDA1:**	VΦ	**Comments:**	run OK
LDA test # :	B3run28-1	**Rez:**	1.16E+05	**raw LDA file:**	\MCRLDA\Build3\B3run28-1.lda	**LDA2:**	Vz	**Traverse ref:**	
Heat Transfer run:	B3run28-1	**Ro:**	0.54	**LDA list file:**	\MCRLDA\Build3\B3run28-1.xls	**W (m/s):**	17.88		

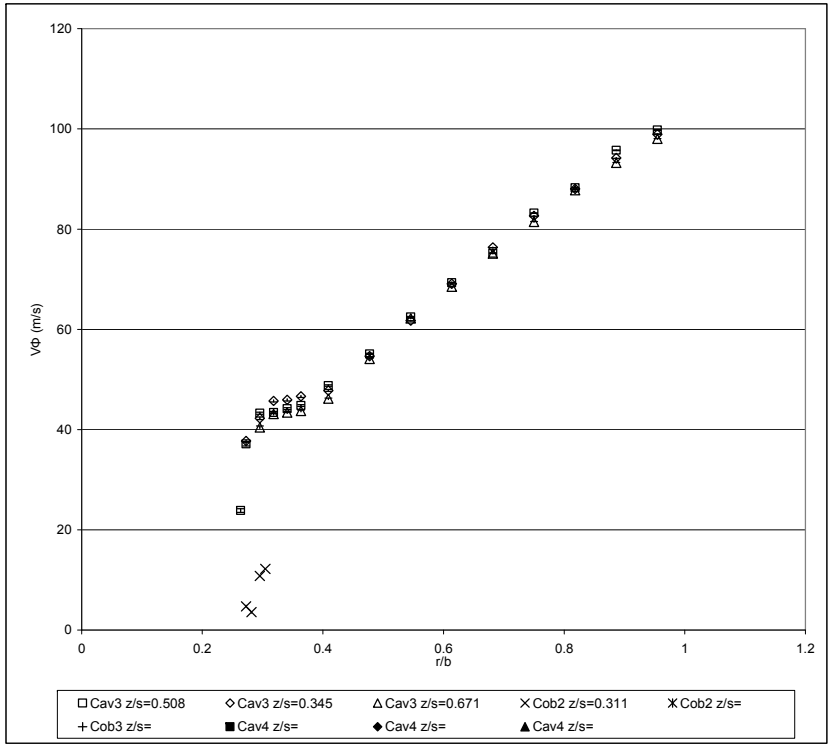

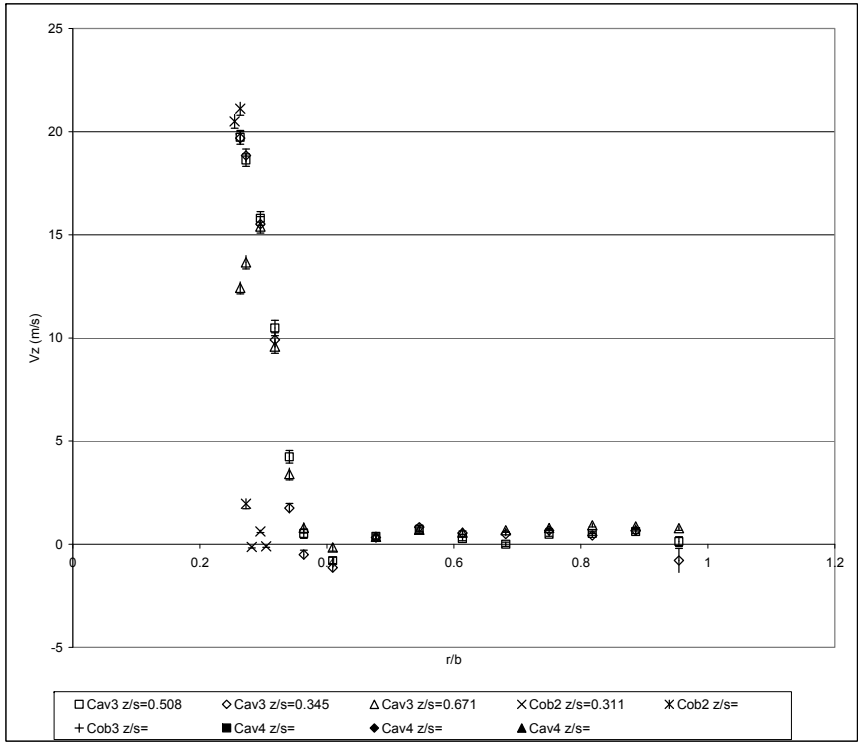

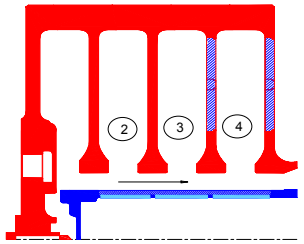

LDA measurement		**LDA code:**	101	**rpm:**	4552.2	**Perfd by:**	NM	Printed: 16/09/2008	Page 2/3
Build:	3	**Re_Φ:**	4.12E+06	**Date:**	12/11/2003	**LDA1:**	VΦ	**Comments:**	run OK
LDA test # :	B3run28-1	**Re_z:**	1.16E+05	**raw LDA file:**	\MCRLDA\Build3\B3run28-1.lda	**LDA2:**	Vz	**Traverse corresp:**	0
Heat Transfer run:	B3run28-1	**Ro:**	0.54	**LDA list file:**	\MCRLDA\Build3\B3run28-1.xls	**W (m/s):**	17.88		

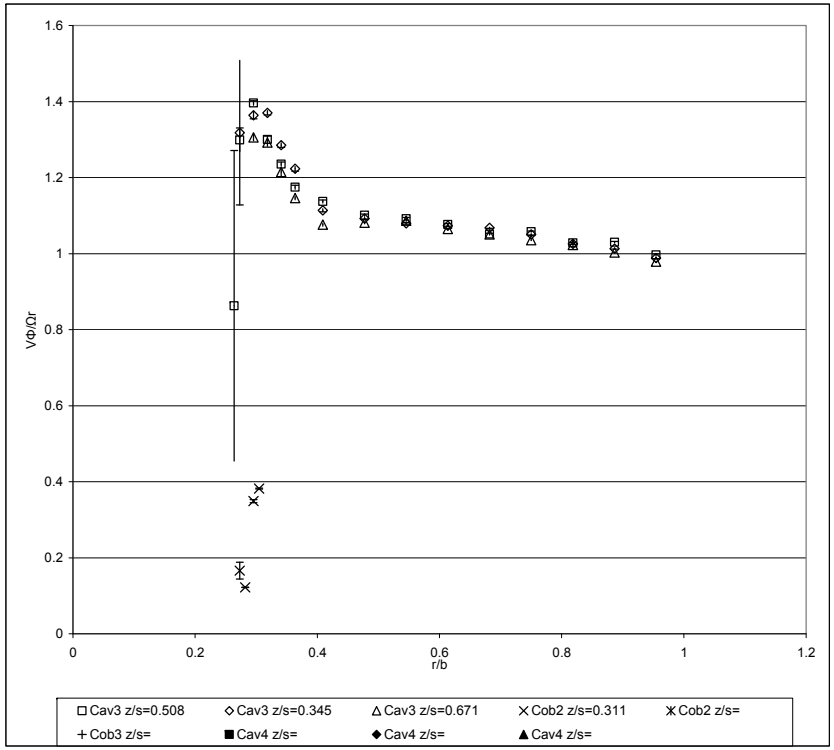

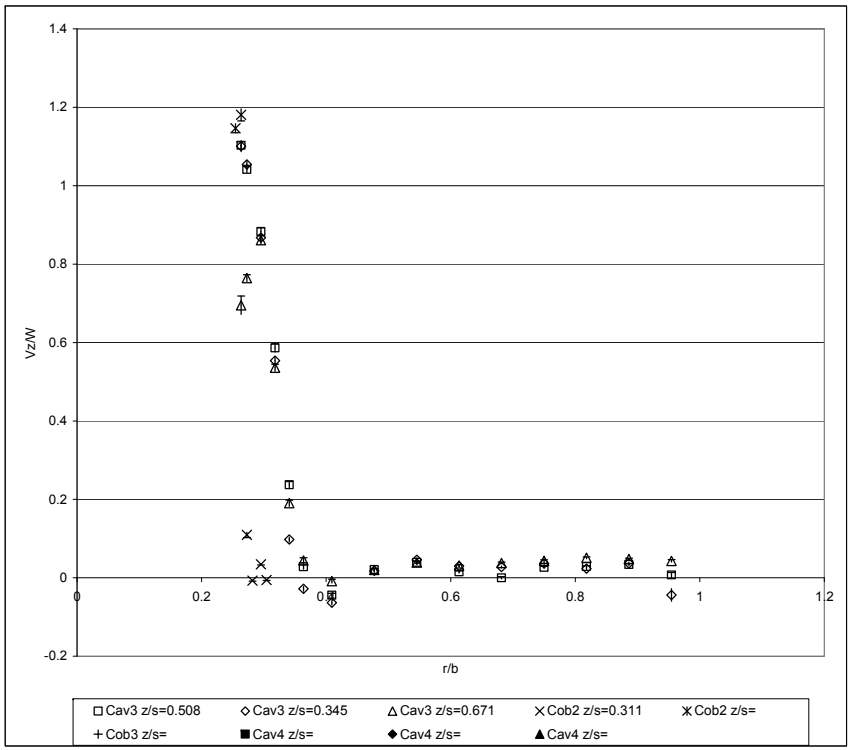

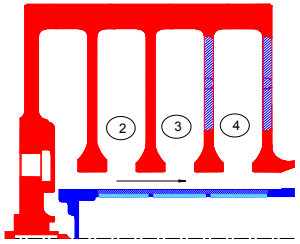

LDA measurement | **LDA code:** 101 | **rpm:** 4552.2 | **Perfd by:** NM | Printed: 16/09/2008 | Page 3/3

Build: 3 | **ReΦ:** 4.12E+06 | **Date:** 12/11/2003 | **LDA1:** VΦ | **Comments:** run OK

LDA test # : B3run28-1 | **Rez:** 1.16E+05 | **raw LDA file:** \MCRLDA\Build3\B3run28-1.lda | **LDA2:** Vz | **Traverse corresp:** 0

Heat Transfer run: B3run28-1 | **Ro:** 0.54 | **LDA list file:** \MCRLDA\Build3\B3run28-1.xls | **W (m/s):** 17.88

X [mm]	corrected X	Y [mm]	corrected Y / Radius (mm)	Count{1}	Count{2}	Data Rate{1} [#/s]	Data Rate{2} [#/s]	Validation{1} [%]	Validation{2} [%]	LDA1 Mean [m/s]	LDA2 Mean [m/s]	LDA1 RMS [m/s]	LDA2 RMS [m/s]	LDA1 MeanConf [m/s]	LDA2 MeanConf [m/s]	LDA1 RMSConf [m/s]	LDA2 RMSConf [m/s]	Cavity	r/b	z/s	Ωr (m/s)	$V_\Phi/\Omega r$	$V_{\Phi U95\%}/\Omega r$	$V_{\Phi(RMS)}/\Omega r$	Vz/W	$Vz_{(RMS)}/W$	$Vz_{U95\%}/W$
64	140	210	5000	5000	10221.0	3203.8			99.79	0.13	9.62	4.21	0.27	0.12	0.19	0.08	3	0.955	0.508	100.11	1.00	2.66E-03	0.10	0.01	0.24	6.53E-03
64	125	195	5000	5000	12325.4	4253.1			95.76	0.61	6.38	1.65	0.18	0.05	0.13	0.03	3	0.886	0.508	92.96	1.03	1.90E-03	0.07	0.03	0.09	2.57E-03
64	110	180	5000	5000	13403.7	5287.8			88.24	0.51	4.52	1.51	0.13	0.04	0.09	0.03	3	0.818	0.508	85.81	1.03	1.46E-03	0.05	0.03	0.08	2.34E-03
64	95	165	5000	5000	13316.7	5092.9			83.22	0.48	4.29	1.65	0.12	0.05	0.08	0.03	3	0.750	0.508	78.66	1.06	1.51E-03	0.05	0.03	0.09	2.56E-03
64	80	150	5000	4941	28626.4	82.4			75.20	0.00	5.08	1.78	0.14	0.05	0.10	0.04	3	0.682	0.508	71.51	1.05	1.97E-03	0.07	0.00	0.10	2.77E-03
64	65	135	5000	5000	28517.4	234.1			69.30	0.26	5.45	1.76	0.15	0.05	0.11	0.03	3	0.614	0.508	64.36	1.08	2.35E-03	0.08	0.01	0.10	2.72E-03
64	50	120	5000	5000	12005.9	596.4			62.47	0.71	6.98	2.02	0.19	0.06	0.14	0.04	3	0.545	0.508	57.20	1.09	3.38E-03	0.12	0.04	0.11	3.13E-03
64	35	105	5000	5000	396.0	1118.5			55.12	0.38	5.09	2.21	0.14	0.06	0.10	0.04	3	0.477	0.508	50.05	1.10	2.82E-03	0.10	0.02	0.12	3.43E-03
71	140	210	5000	5000	3371.3	7047.3			98.93	-0.79	5.22	10.37	0.14	0.29	0.10	0.20	3	0.955	0.345	100.11	0.99	1.44E-03	0.05	-0.04	0.58	1.61E-02
71	125	195	5000	5000	3076.8	6422.7			94.19	0.66	4.98	1.66	0.14	0.05	0.10	0.03	3	0.886	0.345	92.96	1.01	1.48E-03	0.05	0.04	0.09	2.57E-03
71	110	180	5000	5000	2985.2	5562.2			88.02	0.42	5.04	1.69	0.14	0.05	0.10	0.03	3	0.818	0.345	85.81	1.03	1.63E-03	0.06	0.02	0.09	2.62E-03
71	95	165	5000	5000	3270.3	7008.6			82.64	0.66	4.27	1.79	0.12	0.05	0.08	0.04	3	0.750	0.345	78.66	1.05	1.50E-03	0.05	0.04	0.10	2.77E-03
71	80	150	5000	5000	3670.7	8791.2			76.35	0.49	3.34	1.56	0.09	0.04	0.07	0.03	3	0.682	0.345	71.51	1.07	1.30E-03	0.05	0.03	0.09	2.42E-03
71	65	135	5000	5000	3320.9	8138.1			69.08	0.54	2.91	1.74	0.08	0.05	0.06	0.03	3	0.614	0.345	64.36	1.07	1.25E-03	0.05	0.03	0.10	2.70E-03
57	140	210	5000	5000	1064.4	1723.1			98.02	0.77	5.25	1.92	0.15	0.05	0.10	0.04	3	0.955	0.671	100.11	0.98	1.45E-03	0.05	0.04	0.11	2.97E-03
57	125	195	5000	5000	1465.3	2380.8			93.26	0.86	5.01	1.40	0.14	0.04	0.10	0.03	3	0.886	0.671	92.96	1.00	1.50E-03	0.05	0.05	0.08	2.18E-03
57	110	180	5000	5000	1861.4	2430.6			87.78	0.91	4.74	1.50	0.13	0.04	0.09	0.03	3	0.818	0.671	85.81	1.02	1.53E-03	0.06	0.05	0.08	2.33E-03
57	95	165	5000	5000	2097.1	2880.4			81.47	0.78	3.68	1.49	0.10	0.04	0.07	0.03	3	0.750	0.671	78.66	1.04	1.30E-03	0.05	0.04	0.08	2.31E-03
57	80	150	5000	5000	1958.9	3122.6			75.14	0.68	3.20	1.52	0.09	0.04	0.06	0.03	3	0.682	0.671	71.51	1.05	1.24E-03	0.04	0.04	0.08	2.36E-03
57	65	135	5000	5000	2950.1	3139.6			68.53	0.56	2.88	1.47	0.08	0.04	0.06	0.03	3	0.614	0.671	64.36	1.06	1.24E-03	0.04	0.03	0.08	2.28E-03
94	-3	67	5000	5000	54.3	1694.6			12.20	-0.10	1.46	0.80	0.04	0.02	0.03	0.02	cob2	0.305	0.311	31.94	0.38	1.27E-03	0.05	-0.01	0.04	1.24E-03
94	-5	65	5000	5000	43.8	521.3			10.81	0.62	4.42	1.00	0.12	0.03	0.09	0.02	cob2	0.295	0.311	30.99	0.35	3.95E-03	0.14	0.03	0.06	1.55E-03
94	-8	62	5000	5000	328.6	288.2			3.60	-0.13	0.48	0.79	0.01	0.02	0.01	0.02	cob2	0.282	0.311	29.56	0.12	4.50E-04	0.02	-0.01	0.04	1.22E-03
94	-10	60	352	5000	2.0	288.1			4.75	1.96	6.08	4.28	0.64	0.12	0.45	0.08	cob2	0.273	0.311	28.60	0.17	2.22E-02	0.21	0.11	0.24	6.63E-03
94	-12	58	0	1613	#N/A	13.5			#N/A	21.11	#N/A	5.57	#N/A	0.27	#N/A	0.19	cob2	0.264	0.311	27.65	#N/A	#N/A	#N/A	1.18	0.31	1.52E-02
94	-14	56	0	3321	#N/A	27.7			#N/A	20.50	#N/A	6.01	#N/A	0.20	#N/A	0.14	cob2	0.255	0.311	26.70	#N/A	#N/A	#N/A	1.15	0.34	1.14E-02
64	20	90	5000	5000	290.5	215.8			48.79	-0.80	6.10	3.02	0.17	0.08	0.12	0.06	3	0.409	0.508	42.90	1.14	3.94E-03	0.14	-0.04	0.17	4.68E-03
64	10	80	4277	5000	42.8	222.7			44.80	0.51	6.75	4.07	0.20	0.11	0.14	0.08	3	0.364	0.508	38.14	1.17	5.30E-03	0.18	0.03	0.23	6.32E-03
64	5	75	5000	5000	70.1	263.8			44.17	4.24	7.06	5.41	0.20	0.15	0.14	0.11	3	0.341	0.508	35.75	1.24	5.47E-03	0.20	0.24	0.30	8.39E-03
64	0	70	2508	5000	25.1	115.2			43.40	10.48	7.39	6.65	0.29	0.18	0.20	0.13	3	0.318	0.508	33.37	1.30	8.67E-03	0.22	0.59	0.37	1.03E-02
64	-5	65	5000	5000	62.3	104.1			43.27	15.79	6.56	6.06	0.18	0.17	0.13	0.12	3	0.295	0.508	30.99	1.40	5.87E-03	0.21	0.88	0.34	9.39E-03
64	-10	60	681	5000	4.5	187.3			37.17	18.62	11.96	5.38	0.90	0.15	0.64	0.11	3	0.273	0.508	28.60	1.30	3.14E-02	0.42	1.04	0.30	8.33E-03
64	-12	58	4	5000	0.1	142.1			23.85	19.72	9.98	5.96	11.29	0.17	7.98	0.12	3	0.264	0.508	27.65	0.86	4.08E-01	0.36	1.10	0.33	9.24E-03
71	50	120	5000	5000	1474.2	652.3			61.75	0.82	3.81	1.94	0.11	0.05	0.07	0.04	3	0.545	0.345	57.20	1.08	1.85E-03	0.07	0.05	0.11	3.01E-03
71	35	105	5000	5000	1860.7	930.4			54.67	0.32	5.05	2.30	0.14	0.06	0.10	0.05	3	0.477	0.345	50.05	1.09	2.80E-03	0.10	0.02	0.13	3.57E-03
57	50	120	5000	5000	1343.4	664.6			62.18	0.70	3.76	1.91	0.10	0.05	0.07	0.04	3	0.545	0.671	57.20	1.09	1.82E-03	0.07	0.04	0.11	2.96E-03
57	35	105	5000	5000	133.8	1185.8			54.13	0.36	5.19	2.14	0.14	0.06	0.10	0.04	3	0.477	0.671	50.05	1.08	2.88E-03	0.10	0.02	0.12	3.32E-03
71	20	90	5000	5000	86.6	102.0			47.79	-1.14	6.40	3.54	0.18	0.10	0.13	0.07	3	0.409	0.345	42.90	1.11	4.14E-03	0.15	-0.06	0.20	5.50E-03
71	10	80	4081	5000	68.0	93.3			46.64	-0.51	7.59	3.94	0.23	0.11	0.16	0.08	3	0.364	0.345	38.14	1.22	6.11E-03	0.20	-0.03	0.22	6.11E-03
71	5	75	5000	5000	88.4	119.6			45.95	1.75	8.14	4.10	0.23	0.11	0.16	0.08	3	0.341	0.345	35.75	1.29	6.31E-03	0.23	0.10	0.23	6.36E-03
71	0	70	5000	4902	106.3	81.7			45.73	9.90	6.98	6.32	0.19	0.18	0.14	0.13	3	0.318	0.345	33.37	1.37	5.80E-03	0.21	0.55	0.35	9.90E-03
71	-5	65	3050	5000	17.0	45.0			42.26	15.52	7.79	6.46	0.28	0.18	0.20	0.13	3	0.295	0.345	30.99	1.36	8.92E-03	0.25	0.87	0.36	1.00E-02
71	-10	60	7	4447	0.1	24.7			37.71	18.84	6.80	5.70	5.44	0.17	3.85	0.12	3	0.273	0.345	28.60	1.32	1.90E-01	0.24	1.05	0.32	9.38E-03
71	-12	58	0	1797	#N/A	10.0			#N/A	19.68	#N/A	5.55	#N/A	0.26	#N/A	0.18	3	0.264	0.345	27.65	#N/A	#N/A	#N/A	1.10	0.31	1.43E-02
57	20	90	5000	5000	99.3	73.2			46.17	-0.16	6.31	3.11	0.17	0.09	0.12	0.06	3	0.409	0.671	42.90	1.08	4.07E-03	0.15	-0.01	0.17	4.82E-03
57	10	80	5000	5000	115.3	80.6			43.71	0.79	6.55	4.48	0.18	0.12	0.13	0.09	3	0.364	0.671	38.14	1.15	4.76E-03	0.17	0.04	0.25	6.94E-03
57	5	75	1429	5000	7.9	71.2			43.42	3.40	7.18	5.13	0.37	0.14	0.26	0.10	3	0.341	0.671	35.75	1.21	1.04E-02	0.20	0.19	0.29	7.96E-03
57	0	70	1789	5000	10.0	66.3			43.12	9.58	7.11	5.78	0.33	0.16	0.23	0.11	3	0.318	0.671	33.37	1.29	9.87E-03	0.21	0.54	0.32	8.95E-03
57	-5	65	3017	3070	16.8	25.6			40.47	15.40	8.03	5.56	0.29	0.20	0.20	0.14	3	0.295	0.671	30.99	1.31	9.25E-03	0.26	0.86	0.31	1.10E-02
57	-10	60	0	5000	#N/A	94.3			#N/A	13.67	#N/A	5.71	#N/A	0.16	#N/A	0.11	3	0.273	0.671	28.60	#N/A	#N/A	#N/A	0.76	0.32	8.86E-03
57	-12	58	0	586	#N/A	4.9			#N/A	12.43	#N/A	5.17	#N/A	0.42	#N/A	0.30	3	0.264	0.671	27.65	#N/A	#N/A	#N/A	0.69	0.29	2.35E-02

Appendix 4.17: Listing of avenoco.bas

```
100 REM Program to average tangential velocity
measurements over each pass of a window
101 REM Christopher Long   8th December 2004
102 REM Modified on 8th July to read from new files
(corrected for probe misallignment)
103 REM Also does batch processing of up to 100
different files
104 REM Modified to read from non-coincident data
files 23rd August 2005
200 DIM at(500), lda1(500), lda2(500), pt(10), sp(10)
205 DIM xval4(500), xval6(500)
210 DIM infile$(100), outfile$(100), xprobe(100),
yprobe(100)

211 infile$(1) = "E:\SPECTRA\R44\R44_5.TXT"
212 infile$(2) = "E:\SPECTRA\R44\R44_14.TXT"
213 infile$(3) = "E:\SPECTRA\R44\R44_23.TXT"
214 infile$(4) = "E:\SPECTRA\R44\R44_32.TXT"
215 infile$(5) = "E:\SPECTRA\R44\R44_41.TXT"
216 infile$(6) = "E:\SPECTRA\R44\R44_50.TXT"
REM 217 infile$(7) = "D:\CAL\MCAV\VR\Run38-
1\007.TXT"
REM 218 infile$(8) = "D:\CAL\MCAV\VR\Run38-
1\008.TXT"
REM 219 infile$(9) = "D:\CAL\MCAV\VR\Run38-
1\009.TXT"
REM 220 infile$(10) = "D:\CAL\MCAV\VR\Run38-
1\00a.TXT"
REM 221 infile$(11) = "D:\CAL\MCAV\VR\Run38-
1\00b.TXT"

251 outfile$(1) = "E:\SPECTRA\R44\P44_5.TXT"
252 outfile$(2) = "E:\SPECTRA\R44\P44_14.TXT"
253 outfile$(3) = "E:\SPECTRA\R44\P44_23.TXT"
254 outfile$(4) = "E:\SPECTRA\R44\P44_32.TXT"
255 outfile$(5) = "E:\SPECTRA\R44\P44_41.TXT"
256 outfile$(6) = "E:\SPECTRA\R44\P44_50.TXT"
REM 257 outfile$(7) = "D:\CAL\MCAV\VR\Run38-
1\007.DAT"
REM 258 outfile$(8) = "D:\CAL\MCAV\VR\Run38-
1\008.DAT"
REM 259 outfile$(9) = "D:\CAL\MCAV\VR\Run38-
1\009.DAT"
REM 260 outfile$(10) = "D:\CAL\MCAV\VR\Run38-
1\00a.DAT"
REM 261 outfile$(11) = "D:\CAL\MCAV\VR\Run38-
1\00b.DAT"

270 nfiles = 6

1300 PRINT "Enter the rotational speed for this series
of tests"
1310 INPUT revmin
1305 REM tau is the time period between window
passes [in ms]
1320 tau = (60! / (revmin * 4!)) * 1000!

1345 REM **** NOTE ****
1346 REM Program requires correct filepath name
1347 FOR ifile = 1 TO nfiles
1350 OPEN infile$(ifile) FOR INPUT AS #1
1360 OPEN outfile$(ifile) FOR OUTPUT AS #2
1370 PRINT #2, "Time (ms)", " ", "Vphi(m / s)", " ",
"Npts"
1400 LINE INPUT #1, line1$
3400 a$ = before$ + after$
3500 x4 = VAL(a$)
3999 RETURN

4000 REM Get sixth variable (tangential velocity)
4050 c$ = " "
4100 blen = pt(6) - sp(5) - 1
1410 LINE INPUT #1, line2$
1420 LINE INPUT #1, line3$
1430 LINE INPUT #1, line4$
1440 LINE INPUT #1, line5$

1500 kline = 0: irec = 0: fileline = 0

1502 IF EOF(1) THEN
1503 CLOSE 1: GOTO 1995
1504 END IF

1505 fileline = fileline + 1
1506 irec = irec + 1
1510 LINE INPUT #1, in$
1550 GOSUB 2000
1560 GOSUB 3000
1570 GOSUB 4000

1590 xval4(irec) = x4
1595 xval6(irec) = x6
1600 IF fileline <> 1 THEN
1605 tdiff = xval4(irec) - xval4(irec - 1)
1609 END IF
1620 IF tdiff > tau / 4! THEN
1625 Npts = irec - 1
1630 GOSUB 5000
1632 PRINT #2, tave / 1000, CHR$(9), vphiave,
CHR$(9), Npts
1635 irec = 1
1660 END IF

1990 GOTO 1502
1995 CLOSE #2: NEXT ifile
1999 STOP

2000 REM Does character handling bit
2001 lenin = LEN(in$)
2100 ipt = 0: isp = 0

2150 FOR i = 1 TO 10
2170 pt(i) = 0
2180 sp(i) = 0
2190 NEXT i

2200 FOR i = 1 TO lenin
2300 IF MID$(in$, i, 1) = "." THEN
2450 ipt = ipt + 1: pt(ipt) = i
2570 END IF
2600 IF MID$(in$, i, 1) = CHR$(9) THEN
2620 isp = isp + 1: sp(isp) = i
2650 END IF

2700 NEXT i

2800 REM PRINT pt(1), pt(2), pt(3), pt(4), pt(5), pt(6)
2950 REM PRINT sp(1), sp(2), sp(3), sp(4), sp(5),
sp(6)
2999 RETURN

3000 REM Get fourth variable (arrival time 2)
3050 blen = pt(4) - sp(3) - 1
3100 before$ = MID$(in$, sp(3) + 1, blen)
3200 after$ = MID$(in$, pt(4), 4)
3300 a$ = " "
```

```
4200 before$ = MID$(in$, sp(5) + 1, blen)
4300 after$ = MID$(in$, pt(6), 3)
4400 c$ = before$ + after$
4500 x6 = VAL(c$)
4999 RETURN
5000 REM Do averaging on npts of data, transfer last point into new data aray
5005 sumt = 0!: sumvphi = 0!
5010 FOR idata = 1 TO Npts
5020 sumt = sumt + xval4(idata)
5026 sumvphi = sumvphi + xval6(idata)
5030 tave = sumt / Npts: vphiave = sumvphi / Npts
5050 NEXT idata
5070 xval4(1) = xval4(Npts + 1)
5072 xval6(1) = xval6(Npts + 1)
5999 RETURN


9001 RETURN
```

Appendix 4.18: Example of tangential velocity power spectrum plot and output file

Plot

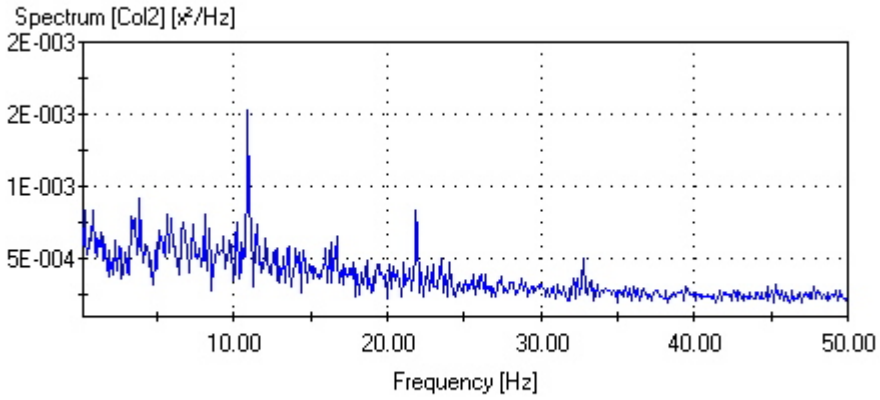

Project: SPECT_R38_pos05 - **Pos:** 0.00;0.00;0.00 - **Date/Time:** #N/A

List

DXEX v1
Untitled
No date/time available.
0.00 mm;0.00 mm;0.00 mm
"Row#""Frequency [Hz]" "Spectrum [Col3] [x2/Hz]"

1	0.10	0.001	36	3.52	0.0008	78	7.62	0.0005
2	0.20	0.0006	37	3.61	0.0008	79	7.71	0.0006
3	0.29	0.0008	38	3.71	0.0005	80	7.81	0.0006
4	0.39	0.0006	39	3.81	0.0006	81	7.91	0.0004
5	0.49	0.0005	40	3.91	0.0009	82	8.01	0.0005
6	0.59	0.0006	41	4.00	0.0006	83	8.11	0.0008
7	0.68	0.0007	42	4.10	0.0005	84	8.20	0.0005
8	0.78	0.0006	43	4.20	0.0006	85	8.30	0.0004
9	0.88	0.0008	44	4.30	0.0005	86	8.40	0.0007
10	0.98	0.0006	45	4.39	0.0006	87	8.50	0.0004
11	1.07	0.0005	46	4.49	0.0005	88	8.59	0.0003
12	1.17	0.0006	47	4.59	0.0004	89	8.69	0.0005
13	1.27	0.0006	48	4.69	0.0005	90	8.79	0.0005
14	1.37	0.0007	49	4.79	0.0003	91	8.89	0.0006
15	1.46	0.0005	50	4.88	0.0005	92	8.98	0.0005
16	1.56	0.0007	51	4.98	0.0006	93	9.08	0.0005
17	1.66	0.0006	52	5.08	0.0004	94	9.18	0.0006
18	1.76	0.0004	53	5.18	0.0007	95	9.28	0.0005
19	1.86	0.0006	54	5.27	0.0006	96	9.38	0.0007
20	1.95	0.0004	55	5.37	0.0006	97	9.47	0.0004
21	2.05	0.0005	56	5.47	0.0006	98	9.57	0.0005
22	2.15	0.0004	57	5.57	0.0005	99	9.67	0.0005
23	2.25	0.0006	58	5.66	0.0008	100	9.77	0.0006
24	2.34	0.0006	59	5.76	0.0006	101	9.86	0.0006
25	2.44	0.0004	60	5.86	0.0006	102	9.96	0.0003
26	2.54	0.0006	61	5.96	0.0008	103	10.06	0.0004
27	2.64	0.0006	62	6.05	0.0006	104	10.16	0.0006
28	2.73	0.0004	63	6.15	0.0006	105	10.25	0.0007
29	2.83	0.0004	64	6.25	0.0005	106	10.35	0.0004
30	2.93	0.0006	65	6.35	0.0005	107	10.45	0.0006
31	3.03	0.0005	66	6.45	0.0004	108	10.55	0.0004
32	3.13	0.0004	67	6.54	0.0006	109	10.64	0.0006
33	3.22	0.0004	68	6.64	0.0007	110	10.74	0.0005
34	3.32	0.0008	69	6.74	0.0007	111	10.84	0.001
35	3.42	0.0007	70	6.84	0.0007	112	10.94	0.002
			71	6.93	0.0006	113	11.04	0.0009
			72	7.03	0.0006	114	11.13	0.0007
			73	7.13	0.0004	115	11.23	0.0005
			74	7.23	0.0006	116	11.33	0.0003
			75	7.32	0.0007	117	11.43	0.0006
			76	7.42	0.0007	118	11.52	0.0007
			77	7.52	0.0005	119	11.62	0.0005

120	11.72	0.0006	196	19.14	0.0003	272	26.56	0.0003
121	11.82	0.0004	197	19.24	0.0004	273	26.66	0.0003
122	11.91	0.0005	198	19.34	0.0005	274	26.76	0.0002
123	12.01	0.0005	199	19.43	0.0005	275	26.86	0.0003
124	12.11	0.0006	200	19.53	0.0004	276	26.95	0.0003
125	12.21	0.0005	201	19.63	0.0004	277	27.05	0.0002
126	12.30	0.0004	202	19.73	0.0004	278	27.15	0.0003
127	12.40	0.0004	203	19.82	0.0004	279	27.25	0.0003
128	12.50	0.0004	204	19.92	0.0004	280	27.34	0.0003
129	12.60	0.0005	205	20.02	0.0002	281	27.44	0.0004
130	12.70	0.0006	206	20.12	0.0005	282	27.54	0.0003
131	12.79	0.0004	207	20.21	0.0004	283	27.64	0.0003
132	12.89	0.0006	208	20.31	0.0003	284	27.73	0.0003
133	12.99	0.0003	209	20.41	0.0004	285	27.83	0.0003
134	13.09	0.0004	210	20.51	0.0003	286	27.93	0.0003
135	13.18	0.0004	211	20.61	0.0004	287	28.03	0.0003
136	13.28	0.0005	212	20.70	0.0004	288	28.13	0.0003
137	13.38	0.0003	213	20.80	0.0004	289	28.22	0.0003
138	13.48	0.0006	214	20.90	0.0002	290	28.32	0.0003
139	13.57	0.0006	215	21.00	0.0004	291	28.42	0.0003
140	13.67	0.0004	216	21.09	0.0005	292	28.52	0.0003
141	13.77	0.0003	217	21.19	0.0003	293	28.61	0.0003
142	13.87	0.0004	218	21.29	0.0003	294	28.71	0.0004
143	13.96	0.0005	219	21.39	0.0004	295	28.81	0.0004
144	14.06	0.0006	220	21.48	0.0004	296	28.91	0.0003
145	14.16	0.0005	221	21.58	0.0003	297	29.00	0.0003
146	14.26	0.0005	222	21.68	0.0004	298	29.10	0.0003
147	14.36	0.0003	223	21.78	0.0005	299	29.20	0.0002
148	14.45	0.0004	224	21.88	0.0008	300	29.30	0.0003
149	14.55	0.0006	225	21.97	0.0007	301	29.39	0.0003
150	14.65	0.0005	226	22.07	0.0003	302	29.49	0.0003
151	14.75	0.0003	227	22.17	0.0004	303	29.59	0.0003
152	14.84	0.0004	228	22.27	0.0004	304	29.69	0.0003
153	14.94	0.0005	229	22.36	0.0002	305	29.79	0.0003
154	15.04	0.0004	230	22.46	0.0004	306	29.88	0.0003
155	15.14	0.0004	231	22.56	0.0004	307	29.98	0.0003
156	15.23	0.0004	232	22.66	0.0004	308	30.08	0.0003
157	15.33	0.0004	233	22.75	0.0003	309	30.18	0.0003
158	15.43	0.0004	234	22.85	0.0004	310	30.27	0.0003
159	15.53	0.0004	235	22.95	0.0005	311	30.37	0.0002
160	15.63	0.0004	236	23.05	0.0003	312	30.47	0.0003
161	15.72	0.0004	237	23.14	0.0003	313	30.57	0.0002
162	15.82	0.0005	238	23.24	0.0003	314	30.66	0.0003
163	15.92	0.0005	239	23.34	0.0004	315	30.76	0.0003
164	16.02	0.0006	240	23.44	0.0004	316	30.86	0.0003
165	16.11	0.0003	241	23.54	0.0005	317	30.96	0.0002
166	16.21	0.0005	242	23.63	0.0003	318	31.05	0.0003
167	16.31	0.0006	243	23.73	0.0004	319	31.15	0.0003
168	16.41	0.0003	244	23.83	0.0004	320	31.25	0.0003
169	16.50	0.0005	245	23.93	0.0002	321	31.35	0.0003
170	16.60	0.0005	246	24.02	0.0005	322	31.45	0.0003
171	16.70	0.0007	247	24.12	0.0003	323	31.54	0.0003
172	16.80	0.0005	248	24.22	0.0004	324	31.64	0.0003
173	16.89	0.0003	249	24.32	0.0003	325	31.74	0.0002
174	16.99	0.0004	250	24.41	0.0002	326	31.84	0.0002
175	17.09	0.0005	251	24.51	0.0003	327	31.93	0.0003
176	17.19	0.0003	252	24.61	0.0003	328	32.03	0.0003
177	17.29	0.0004	253	24.71	0.0003	329	32.13	0.0004
178	17.38	0.0004	254	24.80	0.0003	330	32.23	0.0003
179	17.48	0.0004	255	24.90	0.0003	331	32.32	0.0002
180	17.58	0.0004	256	25.00	0.0003	332	32.42	0.0004
181	17.68	0.0004	257	25.10	0.0004	333	32.52	0.0003
182	17.77	0.0005	258	25.20	0.0003	334	32.62	0.0003
183	17.87	0.0002	259	25.29	0.0003	335	32.71	0.0003
184	17.97	0.0004	260	25.39	0.0003	336	32.81	0.0005
185	18.07	0.0004	261	25.49	0.0003	337	32.91	0.0003
186	18.16	0.0003	262	25.59	0.0003	338	33.01	0.0003
187	18.26	0.0004	263	25.68	0.0004	339	33.11	0.0003
188	18.36	0.0004	264	25.78	0.0003	340	33.20	0.0003
189	18.46	0.0003	265	25.88	0.0003	341	33.30	0.0004
190	18.55	0.0004	266	25.98	0.0004	342	33.40	0.0002
191	18.65	0.0005	267	26.07	0.0003	343	33.50	0.0003
192	18.75	0.0003	268	26.17	0.0004	344	33.59	0.0002
193	18.85	0.0004	269	26.27	0.0003	345	33.69	0.0003
194	18.95	0.0003	270	26.37	0.0004	346	33.79	0.0002
195	19.04	0.0004	271	26.46	0.0003	347	33.89	0.0003

348	33.98	0.0003	424	41.41	0.0002	500	48.83	0.0002
349	34.08	0.0003	425	41.50	0.0002	501	48.93	0.0002
350	34.18	0.0003	426	41.60	0.0003	502	49.02	0.0003
351	34.28	0.0003	427	41.70	0.0003	503	49.12	0.0002
352	34.38	0.0003	428	41.80	0.0002	504	49.22	0.0003
353	34.47	0.0003	429	41.89	0.0003	505	49.32	0.0002
354	34.57	0.0003	430	41.99	0.0003	506	49.41	0.0002
355	34.67	0.0003	431	42.09	0.0003	507	49.51	0.0003
356	34.77	0.0003	432	42.19	0.0002	508	49.61	0.0002
357	34.86	0.0003	433	42.29	0.0003	509	49.71	0.0002
358	34.96	0.0002	434	42.38	0.0002	510	49.80	0.0002
359	35.06	0.0003	435	42.48	0.0002	511	49.90	0.0002
360	35.16	0.0003	436	42.58	0.0003	512	50.00	#N/A
361	35.25	0.0002	437	42.68	0.0003			
362	35.35	0.0003	438	42.77	0.0002			
363	35.45	0.0002	439	42.87	0.0003			
364	35.55	0.0003	440	42.97	0.0003			
365	35.64	0.0002	441	43.07	0.0002			
366	35.74	0.0003	442	43.16	0.0002			
367	35.84	0.0003	443	43.26	0.0003			
368	35.94	0.0002	444	43.36	0.0002			
369	36.04	0.0003	445	43.46	0.0002			
370	36.13	0.0003	446	43.55	0.0003			
371	36.23	0.0002	447	43.65	0.0002			
372	36.33	0.0003	448	43.75	0.0002			
373	36.43	0.0002	449	43.85	0.0002			
374	36.52	0.0002	450	43.95	0.0002			
375	36.62	0.0003	451	44.04	0.0003			
376	36.72	0.0003	452	44.14	0.0003			
377	36.82	0.0003	453	44.24	0.0002			
378	36.91	0.0003	454	44.34	0.0003			
379	37.01	0.0002	455	44.43	0.0002			
380	37.11	0.0003	456	44.53	0.0002			
381	37.21	0.0002	457	44.63	0.0002			
382	37.30	0.0003	458	44.73	0.0003			
383	37.40	0.0003	459	44.82	0.0002			
384	37.50	0.0003	460	44.92	0.0002			
385	37.60	0.0003	461	45.02	0.0003			
386	37.70	0.0002	462	45.12	0.0003			
387	37.79	0.0002	463	45.21	0.0002			
388	37.89	0.0002	464	45.31	0.0003			
389	37.99	0.0002	465	45.41	0.0003			
390	38.09	0.0002	466	45.51	0.0002			
391	38.18	0.0003	467	45.61	0.0002			
392	38.28	0.0002	468	45.70	0.0003			
393	38.38	0.0002	469	45.80	0.0002			
394	38.48	0.0003	470	45.90	0.0003			
395	38.57	0.0002	471	46.00	0.0003			
396	38.67	0.0003	472	46.09	0.0002			
397	38.77	0.0002	473	46.19	0.0002			
398	38.87	0.0003	474	46.29	0.0002			
399	38.96	0.0003	475	46.39	0.0003			
400	39.06	0.0003	476	46.48	0.0002			
401	39.16	0.0003	477	46.58	0.0002			
402	39.26	0.0003	478	46.68	0.0002			
403	39.36	0.0002	479	46.78	0.0003			
404	39.45	0.0003	480	46.88	0.0003			
405	39.55	0.0003	481	46.97	0.0002			
406	39.65	0.0002	482	47.07	0.0002			
407	39.75	0.0003	483	47.17	0.0002			
408	39.84	0.0002	484	47.27	0.0003			
409	39.94	0.0003	485	47.36	0.0002			
410	40.04	0.0002	486	47.46	0.0003			
411	40.14	0.0003	487	47.56	0.0002			
412	40.23	0.0002	488	47.66	0.0002			
413	40.33	0.0003	489	47.75	0.0003			
414	40.43	0.0002	490	47.85	0.0002			
415	40.53	0.0002	491	47.95	0.0002			
416	40.63	0.0002	492	48.05	0.0003			
417	40.72	0.0002	493	48.14	0.0003			
418	40.82	0.0003	494	48.24	0.0002			
419	40.92	0.0002	495	48.34	0.0002			
420	41.02	0.0002	496	48.44	0.0003			
421	41.11	0.0002	497	48.54	0.0002			
422	41.21	0.0002	498	48.63	0.0002			
423	41.31	0.0002	499	48.73	0.0003			

Appendix 5.1: Programme listings

thsol_MCR1.m

```
%program THSOL
%analytical inverse fin solution for a fin with
constant heat transfer
%adapted from Patounas (2007)

%uses MCR related parameters

%input parameters
hc=30;
t=0.004;
K=7.72;
r1=0.22;
r2=0.07;
Tb=372;
Te=320;
dr=0.001;

%calculated parameters
bita=sqrt(hc/(t*K));
z1=bita*r1;
z2=bita*r2;

%calculate Bessel values
I0z1=besseli(0,z1);
I1z1=besseli(1,z1);
K0z1=besselk(0,z1);
K1z1=besselk(1,z1);
I0z2=besseli(0,z2);
I1z2=besseli(1,z2);
K0z2=besselk(0,z2);
K1z2=besselk(1,z2);

%calculate thita argument
arg1=K1z2/(I0z1*K1z2+I1z2*K0z1);
arg2=I1z2/(I0z1*K1z2+I1z2*K0z1);

%establish r grid
r=r2:dr:r1;
nopoints=(r1-r2)/dr+1;

%loop for all points in the grid
for c=1:nopoints
   %calculate thita using analytical solution
   z=bita*r(c);
   I0z=besseli(0,z);
   K0z=besselk(0,z);
   thita=arg1*I0z+arg2*K0z;
   %calculate T from thita
   T(c)=thita*(Tb-Te)+Te;
end
plot(r,T)
```

finsol3_MCR1.m

```
%program finsol3_MCR1
%m-file to apply to fit various curves
%and apply the fin solution on whole length
of disc
%
%adapted from Patounas (2007)
%
%input is the measurements of several t/cs

%define basic parameters
%T has already been defined from ansol
dr=0.001;
L=0.004;
K=7.72;
r=0.07:dr:0.22;
nopoints=(0.22-0.07)/0.001+1;
Te=320;
Tb=372;

%set-up thermocouple temperatures and
locations
%6 T/C case
x6=r([1 11 52 94 138 151]);
y6=T([1 11 52 94 138 151]);

%use analytical solution
Tan=T;

%fit third order polynomial on temperatures
pol3=polyfit(x6,y6,3);
Tpol3=polyval(pol3,r);

%fit 4th order polynomial on temperatures
pol4=polyfit(x6,y6,4);
Tpol4=polyval(pol4,r);

%fit 5th order polynomial on temperatures
pol5=polyfit(x6,y6,5);
Tpol5=polyval(pol5,r);

%fit cubic spline on temperatures
s=spline(x6,y6);
Tspline=ppval(s,r);

%calculation loop
for times=1:5
   if times==1;
      T=Tan;
   elseif times==2;
      T=Tpol3;
   elseif times==3;
      T=Tpol4;
   elseif times==4;
      T=Tpol5;
   elseif times==5;
      T=Tspline;
   end
   for c=1:(nopoints-2)
      p=c+1;
      dev2=(T(p+1)-2*T(p)+T(p-1))/dr^2;
      rdev=(T(p+1)-T(p-1))/(2*r(p)*dr);
      q(c)=K*L*(dev2+rdev);
      h(c)=q(c)/((T(p)-Te));
   end
   %create reduced 149 points matrices
   r149=r(2:150);
   T149=T(2:150);

   %calculate average values
   qr=q.*r149;
   rDT=(T149-Te).*r149;
   hav=(trapz(r149,qr)/trapz(r149,rDT));

   %save output for each type of fitting
   if times==1;
      han=h;
      hanav=hav;
   elseif times==2;
      hpol3=h;
      hpol3av=hav;
   elseif times==3;
      hpol4=h;
      hpol4av=hav;
   elseif times==4;
      hpol5=h;
      hpol5av=hav;
   elseif times==5;
      hspline=h;
      hsplineav=hav;
   end
end

%plot the results
sampleh=hc*ones(1,149);
plot(r149,sampleh,':k')
hold on
plot(r149,han)
plot(r149,hspline,'c')
plot(r149,hpol3,'k')
plot(r149,hpol4,'g')
plot(r149,hpol5,'r')
legend('Assumed h used in the analytical
solution','True data','Cubic spline fit','3rd
order poly','4th order poly','5th order poly',4)
title('Analytical and fin solution comparison')
xlabel('Disc radius (mm)')
ylabel('h (W/(m^2.K))')
```

finsol3_MCR3.m

```
%program finsol3_MCR3
%m-file to apply to fit various curves
%and apply the fin solution on whole length of disc
%
%adapted from Patounas (2007)
%
%input is the measurements of several combinations of T/Cs and
%polynomial interpolation orders

%define basic parameters
%T has already been defined from ansol
dr=0.001;   %grid increment 1mm
L=0.004;    %half thickness of disc
K=7.72;     %thermal conductivity titanium 318
r=0.07:dr:0.22;
nopoints=(0.22-0.07)/0.001+1;
Te=320;
Tb=372;

%set-up thermocouple temperatures and locations
%6 T/C case
x6=r([1 11 52 94 138 151]);
y6=T([1 11 52 94 138 151]);
%5 T/C case
x5=r([1 11 52 94 138]);
y5=T([1 11 52 94 138]);
%4 T/C case
x4=r([11 52 94 138]);
y4=T([11 52 94 138]);
%3 T/C case
x3=r([52 94 138]);
y3=T([52 94 138]);

%use analytical solution
Tan=T;

%fit second order polynomial using T/Cs 9-10-11
pol2=polyfit(x3,y3,2);
Tpol2=polyval(pol2,r);

%fit third order polynomial using T/Cs 8-9-10-11
pol3=polyfit(x4,y4,3);
Tpol3=polyval(pol3,r);

%fit 4th order polynomial using T/Cs 7-8-9-10-11
pol4=polyfit(x5,y5,4);
Tpol4=polyval(pol4,r);

%fit 5th order polynomial using T/Cs 7-8-9-10-11-12
pol5=polyfit(x6,y6,5);
Tpol5=polyval(pol5,r);

%fit cubic spline on temperatures
s=spline(x6,y6);
Tspline=ppval(s,r);

%calculation loop
for times=1:6
   if times==1;
      Tt=Tan;
   elseif times==2;
      Tt=Tpol2;
   elseif times==3;
      Tt=Tpol3;
   elseif times==4;
      Tt=Tpol4;
   elseif times==5;
      Tt=Tpol5;
   elseif times==6;
      Tt=Tspline;
   end
   for c=1:(nopoints-2)
      p=c+1;
      dev2=(Tt(p+1)-2*Tt(p)+Tt(p-1))/dr^2;
      rdev=(Tt(p+1)-Tt(p-1))/(2*r(p)*dr);
```

```
    q(c)=K*L*(dev2+rdev);
    h(c)=q(c)/((Tt(p)-Te));
  end
  %create reduced 149 points matrices
  r149=r(2:150);
  T149=Tt(2:150);

  %calculate average values
  qr=q.*r149;
  rDT=(T149-Te).*r149;
  hav=(trapz(r149,qr)/trapz(r149,rDT));

  %save output for each type of fitting
  if times==1;
    han=h;
    hanav=hav;
  elseif times==2;
    hpol2=h;
    hpol2av=hav;
  elseif times==3;
    hpol3=h;
    hpol3av=hav;
  elseif times==4;
    hpol4=h;
    hpol4av=hav;
  elseif times==5;
    hpol5=h;
    hpol5av=hav;
  elseif times==6;
    hspline=h;
    hsplineav=hav;
  end
end

%plot the results
sampleh=hc*ones(1,149);
plot(r149,sampleh,':k')
hold on
plot(r149,han)
plot(r149,hpol2,'c')
plot(r149,hpol3,'k')
plot(r149,hpol4,'g')
plot(r149,hpol5,'r')
%plot(r149,hspline,'m')
legend('Assumed h used in the analytical solution','True data','2nd order
poly - 3T/Cs','3rd order poly - 4T/Cs','4th order poly - 5T/Cs','5th order
poly - 6T/Cs',4)
title('Plain disc fin solution')
xlabel('Disc radius (mm)')
ylabel('h (W/(m^2.K))')
```

finsol_MCR4.m

```
%program finsol3_MCR4
%m-file to apply to fit various curves
%and apply the fin solution on whole length of plain disc
%
%adapted from Patounas (2007)
%
%input is the experimental temperature measurements of several
combinations of T/Cs and
%polynomial interpolation orders - using thermocouples values from
B3run2-1

%define basic parameters
%
dr=0.001;   %grid increment 1mm
L=0.004;    %half thickness of disc
K=7.72;     %thermal conductivity titanium 318
r=0.07:dr:0.22;
nopoints=(0.22-0.07)/0.001+1;
Te=319.3;
Tb=377;

%set-up thermocouple temperatures and locations
%6 T/C case
x6=[0.070 0.080 0.121 0.163 0.207 0.22];
y6=[319.3 321.7 322.6 329.5 352.4 377.0];
%5 T/C case 7-11
x5=[0.070 0.080 0.121 0.163 0.207];
y5=[319.3 321.7 322.6 329.5 352.4];
%4 T/C case T/Cs 8-11
x4a=[0.080 0.121 0.163 0.207];
y4a=[321.7 322.6 329.5 352.4];
%4 T/C case T/Cs 9-12
x4b=[0.121 0.163 0.207 0.22];
y4b=[322.6 329.5 352.4 377.0];
%3 T/C case
x3=[0.121 0.163 0.207];
y3=[322.6 329.5 352.4];

%use analytical solution
%Tan=T;

%fit second order polynomial using T/Cs 9-10-11
pol2=polyfit(x3,y3,2);
Tpol2=polyval(pol2,r);

%fit third order polynomial using T/Cs 8-9-10-11
pol3a=polyfit(x4a,y4a,3);
Tpol3a=polyval(pol3a,r);

%fit third order polynomial using T/Cs 9-10-11-12
pol3b=polyfit(x4b,y4b,3);
Tpol3b=polyval(pol3b,r);

%fit 4th order polynomial using T/Cs 7-8-9-10-11
pol4=polyfit(x5,y5,4);
Tpol4=polyval(pol4,r);

%fit 5th order polynomial using T/Cs 7-8-9-10-11-12
pol5=polyfit(x6,y6,5);
Tpol5=polyval(pol5,r);

%fit cubic spline on temperatures
s=spline(x6,y6);
Tspline=ppval(s,r);

%calculation loop
for times=1:6
  if times==1;
    Tt=Tpol3b;
  elseif times==2;
    Tt=Tpol2;
  elseif times==3;
    Tt=Tpol3a;
  elseif times==4;
    Tt=Tpol4;
  elseif times==5;
    Tt=Tpol5;
  elseif times==6;
    Tt=Tspline;
  end
  for c=1:(nopoints-2)
    p=c+1;
    dev2=(Tt(p+1)-2*Tt(p)+Tt(p-1))/dr^2;
    rdev=(Tt(p+1)-Tt(p-1))/(2*r(p)*dr);
    q(c)=K*L*(dev2+rdev);
    h(c)=q(c)/((Tt(p)-Te));
  end
  %create reduced 149 points matrices
  r149=r(2:150);
  T149=Tt(2:150);

  %calculate average values
  qr=q.*r149;
  rDT=(T149-Te).*r149;
  hav=(trapz(r149,qr)/trapz(r149,rDT));

  %save output for each type of fitting
  if times==1;
    hpol3b=h;
    hpol3bav=hav;
  elseif times==2;
    hpol2=h;
    hpol2av=hav;
  elseif times==3;
    hpol3a=h;
    hpol3aav=hav;
  elseif times==4;
    hpol4=h;
    hpol4av=hav;
  elseif times==5;
    hpol5=h;
    hpol5av=hav;
  elseif times==6;
    hspline=h;
    hsplineav=hav;
  end
end

%plot the results
%sampleh=hc*ones(1,149);
%plot(r149,sampleh,':k')
%hold on
%plot(r149,han)
plot(r149,hpol2,'c')
hold on
plot(r149,hpol3a,'k')
plot(r149,hpol3b,'b')
plot(r149,hpol4,'g')
plot(r149,hpol5,'r')
%plot(r149,hspline,'m')
legend('2nd order poly - 3T/Cs','3rd order poly - 4T/Cs 8-11','3rd order
poly - 4T/Cs 9-12','4th order poly - 5T/Cs','5th order poly - 6T/Cs',4)
title('Comparison of different experimental configurations on a plain disc
fin solution')
xlabel('Disc radius (mm)')
ylabel('h (W/(m^2.K))')
```

Appendix 6.1: Instructions for the selection and access to the experimental data

The experimental data comes in a separate CD-Rom included with this thesis.

The list of all experimental conditions for Build 2 and Build 3 can be found in the file **MCR_non_dim_results.xls** or in Appendix 6.2 and 6.3. For each test the information provided in the columns are explained in the table below.

Build	Which Build (2 or 3)
ExpCode	Not used
Run	Test identification
ExpDate	Date of testing
LDA code	000: No LDA included, 100: LDA V_Φ, 101: LDA V_Φ and V_z, 110: LDA V_Φ and V_r
FCF pos	0: Flow Control Feature not installed, 1: FCF in upstream position, 2: FCF in mid-position, 3: FCF in downstream position
Lab atm press (Pa)	Measured atmospheric pressure
Comments	Note on test
Refi	Value of Re_Φ for test
+/-	95% confidence interval of calculated Re_Φ
Rez	Value of Re_z for test
+/-	95% confidence interval of calculated Re_z
BDTav	Calculated value of $\beta\Delta T_{av}$ for test
+/-	95% confidence interval of calculated $\beta\Delta T_{av}$
finBDTav	Calculated value of $fin\beta\Delta T_{av}$ for test
+/-	95% confidence interval of calculated $fin\beta\Delta T_{av}$
Ro	Value of Ro for test
+/-	95% confidence interval of calculated Ro
etc.	…

Having selected a test of interest from this list, the corresponding test reports can be found in the Directories **\Heat Transfer Test Reports** and **\LDA Test Reports**, the contents of which are described below. Please note that the test reports of the tests specifically mentioned in Chapter 6 and 7 are also included in Appendix 6.4 for LDA and Appendix 7.1 for heat transfer for convenience of reading.

CD-Rom contents:

\Heat Transfer Test Reports

MCR_HT-reports1.xls	B3run2-1 to B3run16-1
MCR_HT-reports2.xls	B3run16-2 to B3run31-1
MCR_HT-reports3.xls	B3run32-1 to B3run35-5
MCR_HT-reports4.xls	B3run35-6 to B2run08-1
MCR_HT-reports5.xls	B2run08-2 to B2t13-a
MCR_HT-reports6.xls	B2t13-b to B2t19-d

\LDA Test Reports

B2_LDA_test-reports1.xls	All Build 2 LDA data
B3_LDA_test-reports1.xls	B3run3-1 to B3run28-1
B3_LDA_test-reports2.xls	B3run28-2 to B3run45-1

\LDA Test Reports\SPECTRA

This contains the output files for the spectral analysis in Chapter 6 and plots. The positions are taken in the mid plane of Cavity 3 with non-dimensional radius included in the file name.

e.g:	SPECT_R38_rb-0566_list.txt	output file for B3run38-1, r/b=0.566
	SPECT_R38_rb-0566.jpg	plot image for B3run38-1, r/b=0.566

Appendix 6.2: Test conditions and main non-dimensional results for Build 2

Build	Exp Code	Run	ExpDate	LDA code	FCF pos	Lab atm press (Pa)	Comments	Refi	+/-	Rez	+/-	BDTav	+/-	finBDTav	+/-	Ro	+/-
2	2S----	B2run02-1	6/30/2000	0	0	1.016E+05		3.20E+04	4.8E+04	1.05E+05	2.2E+02	0.086	4.4E-03	0.086	4.4E-03	112.08	1.9E+01
2	2S----	B2run02-2	6/30/2000	0	0	1.016E+05		4.72E+04	5.2E+04	1.28E+05	8.2E+01	0.018	1.4E-03	0.018	1.4E-03	92.52	2.9E+01
2	2S----	B2run02-3	6/30/2000	0	0	1.016E+05		3.16E+04	6.5E+04	1.04E+05	2.4E+02	0.081	3.9E-03	0.081	3.9E-03	112.47	1.3E+01
2	2S----	B2run03-1	07/04/2000	0	0	1.007E+05		2.59E+04	3.4E+04	1.58E+05	1.5E+02	0.077	3.5E-03	0.077	3.5E-03	208.98	1.3E+02
2	2S----	B2run04-1	7/19/2000	0	0	1.022E+05		2.62E+04	5.0E+04	1.26E+05	1.8E+02	0.077	2.7E-03	0.077	2.7E-03	165.17	4.1E+01
2	2S----	B2run04-2	7/19/2000	0	0	1.022E+05		1.56E+04	2.8E+04	1.28E+05	1.8E+02	0.085	2.7E-03	0.085	2.7E-03	280.80	5.8E+01
2	2S----	B2run04-3	7/19/2000	0	0	1.022E+05		4.03E+04	7.8E+04	8.42E+04	2.2E+02	0.070	3.7E-03	0.070	3.7E-03	71.41	1.3E+02
2	2S----	B2run04-4	7/19/2000	0	0	1.022E+05		2.57E+04	4.9E+04	8.44E+04	1.9E+02	0.073	3.6E-03	0.073	3.6E-03	112.27	1.9E+01
2	2S----	B2run04-7	7/19/2000	0	0	1.022E+05		2.52E+04	4.9E+04	8.53E+04	1.6E+02	0.075	3.0E-03	0.075	3.0E-03	115.66	4.9E+01
2	2S----	B2run06-1	10/03/2000	0	0	1.020E+05		4.15E+05	5.9E+02	8.49E+04	4.9E+01	0.070	7.9E-04	0.070	7.9E-04	7.00	6.2E-03
2	2S----	B2run06-2	10/03/2000	0	0	1.020E+05		7.05E+05	9.3E+02	8.49E+04	4.7E+01	0.086	7.8E-04	0.086	7.8E-04	4.12	3.2E-03
2	2S----	B2run08-1	10/05/2000	0	0	1.017E+05		1.03E+06	1.5E+03	5.92E+04	3.7E+01	0.095	8.6E-04	0.095	8.6E-04	1.96	1.6E-03
2	2S----	B2run08-2	10/05/2000	0	0	1.017E+05		2.00E+06	3.0E+03	5.89E+04	3.9E+01	0.070	8.9E-04	0.070	8.9E-04	1.01	8.7E-04
2	2S----	B2run08-3	10/05/2000	0	0	1.017E+05		4.02E+06	5.0E+03	5.91E+04	3.2E+01	0.061	7.3E-04	0.061	7.3E-04	0.50	3.5E-04
2	2S----	B2run08-4	10/05/2000	0	0	1.017E+05		4.01E+06	5.6E+03	8.61E+04	5.2E+01	0.056	8.1E-04	0.056	8.1E-04	0.73	5.8E-04
2	2S----	B2run08-5	10/05/2000	0	0	1.017E+05		3.05E+06	4.0E+03	8.65E+04	4.8E+01	0.056	7.4E-04	0.056	7.4E-04	0.97	7.4E-04
2	2S----	B2run08-6	10/05/2000	0	0	1.017E+05		2.03E+06	2.4E+03	8.58E+04	4.5E+01	0.062	7.3E-04	0.062	7.3E-04	1.45	1.0E-03
2	2S----	B2run08-7	10/05/2000	0	0	1.017E+05		2.03E+06	2.4E+03	8.68E+04	4.3E+01	0.048	7.0E-04	0.048	7.0E-04	1.46	1.0E-03
2	2S----	B2run09-1	10/09/2000	0	0	9.881E+04		2.02E+06	3.0E+03	1.43E+05	9.3E+01	0.060	9.1E-04	0.060	9.1E-04	2.43	2.1E-03
2	2S----	B2run09-2	10/09/2000	0	0	9.881E+04		3.99E+06	6.8E+03	1.43E+05	1.1E+02	0.046	9.8E-04	0.046	9.8E-04	1.22	1.2E-03
2	2S----	B2run09-3	10/09/2000	0	0	9.881E+04		2.97E+06	4.4E+03	1.43E+05	9.2E+01	0.052	8.3E-04	0.052	8.3E-04	1.64	1.4E-03
2	2S----	B2run09-5a	10/09/2000	0	0	9.881E+04		1.01E+06	1.6E+03	1.43E+05	9.6E+01	0.055	9.1E-04	0.054504	9.1E-04	4.87	4.3E-03
2	2S----	B2run09-5b	10/09/2000	0	0	9.881E+04		1.98E+06	3.0E+03	1.43E+05	9.4E+01	0.062	8.8E-04	0.062393	8.8E-04	2.47	2.1E-03

Build	Exp Code	Run	ExpDate	LDA code	FCF pos	Lab atm press (Pa)	Comments	Refi	+/-	Rez	+/-	BDTav	+/-	finBDTav	+/-	Ro	+/-
2	2S----	B2run09-6	10/09/2000	0	0	9.881E+04		1.99E+06	2.9E+03	1.41E+05	8.8E+01	0.044	8.0E-04	0.04407	8.0E-04	2.43	2.0E-03
2	2S----	B2run12-1	10/24/2000	0	0	1.021E+05		2.00E+06	3.0E+03	9.15E+04	6.0E+01	0.063	9.0E-04	0.062996	9.0E-04	1.56	1.3E-03
2	2S----	B2run12-2	10/24/2000	0	0	1.021E+05		4.01E+06	5.6E+03	9.04E+04	5.5E+01	0.057	8.4E-04	0.057225	8.4E-04	0.77	6.2E-04
2	2S----	B2t05	08/04/2001	101	0	1.017E+05		1.56E+06	2.1E+03	8.16E+04	4.7E+01	0.057	7.6E-04	0.057178	7.6E-04	1.79	1.4E-03
2	2S----	B2t06	08/07/2001	101	0	1.007E+05		1.09E+06	1.4E+03	1.14E+05	6.5E+01	0.041	7.4E-04	0.041394	7.4E-04	3.56	2.6E-03
2	2S----	B2t07-a	8/13/2001	101	0	1.016E+05		1.05E+06	1.4E+03	1.23E+05	6.9E+01	0.049	7.5E-04	0.048657	7.5E-04	3.99	3.1E-03
2	2S----	B2t07-b	8/13/2001	101	0	1.016E+05		2.02E+06	3.0E+03	1.23E+05	7.7E+01	0.051	8.5E-04	0.050863	8.5E-04	2.07	1.7E-03
2	2S----	B2t09a	09/03/2001	0	0	1.014E+05		8.70E+05	1.2E+03	1.12E+05	6.4E+01	0.040	7.8E-04	0.039554	7.8E-04	4.39	3.4E-03
2	2S----	B2t09b	09/03/2001	0	0	1.014E+05		8.80E+05	1.2E+03	1.12E+05	6.9E+01	0.044	8.0E-04	0.043624	8.0E-04	4.37	3.5E-03
2	2S----	B2t09-c	09/03/2001	0	0	1.014E+05		8.87E+05	1.1E+03	1.13E+05	6.2E+01	0.044	7.5E-04	0.044162	7.5E-04	4.35	3.1E-03
2	2S----	B2t10	09/05/2001	101	0	1.023E+05		1.50E+06	1.6E+03	6.40E+04	2.9E+01	0.062	6.5E-04	0.061683	6.5E-04	1.45	9.0E-04
2	2S----	B2t11	09/06/2001	101	0	1.018E+05		9.56E+05	1.9E+03	7.60E+04	6.3E+01	0.062	1.1E-03	0.061815	1.1E-03	2.72	3.0E-03
2	2S----	B2t12	09/06/2001	100	0	1.018E+05		1.13E+06	1.7E+03	6.63E+04	4.3E+01	0.067	8.3E-04	0.066697	8.3E-04	2.01	1.7E-03
2	2s----	B2t13-a	10/17/2001	0	0	1.015E+05		1.03E+06	6.5E+03	1.23E+05	3.3E+02	0.041	3.6E-03	0.040952	3.6E-03	4.10	1.5E-02
2	2S----	B2t13-b	10/17/2001	100	0	1.015E+05		1.05E+06	1.6E+03	1.25E+05	8.1E+01	0.047	8.6E-04	0.047233	8.6E-04	4.10	3.5E-03
2	2S----	B2t14	10/19/2001	101	0	1.008E+05		1.02E+06	1.7E+03	1.23E+05	8.6E+01	0.048	9.5E-04	0.047568	9.5E-04	4.13	4.0E-03
2	2S----	B2t15-a	10/23/2001	0	0	1.012E+05		1.05E+06	1.6E+03	1.26E+05	7.8E+01	0.049	8.5E-04	0.048812	8.5E-04	4.10	3.6E-03
2	2S----	B2t15-b	10/23/2001	101	0	1.012E+05		2.00E+06	3.0E+03	1.24E+05	8.0E+01	0.050	8.4E-04	0.049629	8.4E-04	2.12	1.8E-03
2	2S----	B2t16-a	11/20/2001	101	0	1.032E+05		1.02E+06	3.3E+03	1.23E+05	1.3E+02	0.044	1.4E-03	0.044454	1.4E-03	4.12	1.0E-02
2	2S----	B2t16-b	11/20/2001	101	0	1.032E+05		1.04E+06	1.4E+03	1.24E+05	7.4E+01	0.049	7.8E-04	0.049024	7.8E-04	4.08	3.2E-03
2	2S----	B2t16-c	11/20/2001	0	0	1.032E+05		1.05E+06	2.3E+03	1.24E+05	1.2E+02	0.049	1.2E-03	0.048797	1.2E-03	4.03	5.0E-03
2	2S----	B2t17-a	11/21/2001	101	0	1.031E+05		2.00E+06	2.9E+03	1.24E+05	7.7E+01	0.049	8.6E-04	0.049293	8.6E-04	2.11	1.7E-03
2	2S----	B2t17-b	11/21/2001	101	0	1.031E+05		2.02E+06	2.7E+03	1.25E+05	7.2E+01	0.051	8.0E-04	0.050684	8.0E-04	2.12	1.6E-03
2	2S----	B2t17-c	11/21/2001	0	0	1.022E+05		2.00E+06	2.3E+03	1.25E+05	6.1E+01	0.050	6.7E-04	0.050421	6.7E-04	2.13	1.4E-03
2	2S----	B2t18-a	11/22/2001	101	0	1.022E+05		9.89E+05	1.3E+03	6.22E+04	3.6E+01	0.068	8.1E-04	0.067906	8.1E-04	2.15	1.7E-03
2	2S----	B2t18-b	11/22/2001	101	0	1.022E+05		9.89E+05	1.3E+03	6.23E+04	3.5E+01	0.069	7.4E-04	0.068677	7.4E-04	2.15	1.7E-03
2	2S----	B2t18-c	11/22/2001	101	0	1.022E+05		2.06E+06	2.7E+03	6.17E+04	3.5E+01	0.054	8.1E-04	0.054443	8.1E-04	1.02	7.7E-04

Build	Exp Code	Run	ExpDate	LDA code	FCF pos	Lab atm press (Pa)	Comments	Refi	+/-	Rez	+/-	BDTav	+/-	finBDTav	+/-	Ro	+/-
2	2S----	B2t18-d	11/22/2001	0	0	1.022E+05		2.06E+06	2.9E+03	6.21E+04	3.8E+01	0.055	8.1E-04	0.054533	8.1E-04	1.03	8.2E-04
2	2S----	B2t19-a	11/23/2001	101	0	1.030E+05		1.00E+06	1.4E+03	6.55E+04	3.9E+01	0.067	8.0E-04	0.067237	8.0E-04	2.23	1.7E-03
2	2S----	B2t19-b	11/23/2001	101	0	1.030E+05		1.00E+06	1.5E+03	6.60E+04	4.2E+01	0.067	8.5E-04	0.067338	8.5E-04	2.25	1.9E-03
2	2S----	B2t19-c	11/23/2001	0	0	1.030E+05		2.03E+06	2.2E+03	6.47E+04	3.1E+01	0.055	6.5E-04	0.055157	6.5E-04	1.09	6.8E-04
2	2S----	B2t19-d	11/23/2001	0	0	1.030E+05		2.03E+06	2.9E+03	6.51E+04	4.0E+01	0.055	8.1E-04	0.055017	8.1E-04	1.10	8.8E-04

Build	Exp Code	Run	Bo*	+/-	Grsh,C2	+/-	Grsh,C3	+/-	Pr	+/-	Rot Speed (rpm)	+/-	Mass Flow (kg/s)	Ø	+/-	finØ	+/-
2	2S----	B2run02-1	0.003	3.8E-03	1.30E+05	1.8E+06	1.40E+05	6.5E+06	0.705	1.5E-04	51.3	7.7E+01	0.418	-0.008	1.1E-01	-0.033	1.7E-02
2	2S----	B2run02-2	0.001	1.7E-03	6.81E+04	8.0E+05	7.21E+04	1.0E+06	0.705	4.3E-05	65.9	6.9E+01	0.503	-0.024	4.1E-01	-0.025	2.8E-01
2	2S----	B2run02-3	0.003	5.3E-03	1.13E+05	3.8E+06	1.24E+05	6.7E+06	0.704	1.7E-04	50.9	9.9E+01	0.415	-0.011	7.4E-02	-0.032	2.0E-02
2	2S----	B2run03-1	0.001	1.7E-03	8.45E+04	9.7E+05	9.06E+04	1.9E+06	0.704	7.1E-05	31.4	4.7E+01	0.634	-0.011	1.3E-01	-0.020	1.4E-02
2	2S----	B2run04-1	0.002	3.2E-03	7.27E+04	1.9E+06	7.96E+04	2.3E+06	0.705	9.8E-05	29.9	5.8E+01	0.499	-0.013	8.8E-01	-0.024	1.4E-01
2	2S----	B2run04-2	0.001	1.9E-03	3.07E+04	6.7E+05	3.31E+04	1.6E+06	0.705	9.2E-05	17.7	3.4E+01	0.504	-0.010	2.8E-02	-0.021	1.1E-02
2	2S----	B2run04-3	0.004	7.3E-03	1.58E+05	4.2E+06	1.69E+05	7.3E+06	0.705	1.8E-04	45.1	8.8E+01	0.333	-0.016	4.9E-01	-0.042	3.9E-02
2	2S----	B2run04-4	0.002	4.7E-03	6.76E+04	2.1E+06	7.32E+04	3.0E+06	0.705	1.5E-04	28.7	5.6E+01	0.333	-0.019	2.0E-01	-0.036	1.0E-01
2	2S----	B2run04-7	0.002	4.7E-03	6.64E+04	2.3E+06	7.19E+04	3.5E+06	0.705	1.3E-04	28.2	5.5E+01	0.337	-0.019	6.5E-02	-0.036	1.7E-02
2	2S----	B2run06-1	0.038	2.4E-04	3.84E+07	2.5E+05	4.55E+07	2.9E+05	0.706	3.8E-05	539.5	2.2E-01	0.332	0.633	8.9E-02	0.506	8.0E-02
2	2S----	B2run06-2	0.071	3.8E-04	1.22E+08	7.9E+05	1.37E+08	8.3E+05	0.706	3.7E-05	921.6	1.9E-01	0.333	0.658	4.1E-02	0.384	1.7E-02
2	2S----	B2run08-1	0.157	8.4E-04	2.19E+08	1.8E+06	2.38E+08	1.9E+06	0.706	4.2E-05	1239.7	1.7E-01	0.232	0.447	1.2E-01	0.745	5.8E-02
2	2S----	B2run08-2	0.262	1.9E-03	6.96E+08	6.1E+06	7.31E+08	6.3E+06	0.706	4.4E-05	2402.5	1.4E-01	0.231	1.546	1.5E-01	1.475	8.0E-02
2	2S----	B2run08-3	0.491	3.3E-03	2.32E+09	2.0E+07	2.41E+09	2.3E+07	0.705	3.6E-05	4914.2	2.1E-01	0.233	2.241	2.3E-01	1.952	1.5E-01
2	2S----	B2run08-4	0.322	2.6E-03	2.32E+09	2.1E+07	2.38E+09	2.1E+07	0.705	4.1E-05	5177.6	2.6E-01	0.340	1.554	1.3E-01	1.392	9.0E-02
2	2S----	B2run08-5	0.244	1.8E-03	1.44E+09	1.1E+07	1.48E+09	1.2E+07	0.705	3.8E-05	3945.4	3.6E-01	0.342	1.400	1.1E-01	1.270	6.8E-02
2	2S----	B2run08-6	0.172	1.1E-03	7.19E+08	5.6E+06	7.44E+08	4.9E+06	0.705	3.6E-05	2623.6	4.0E-01	0.339	1.224	1.0E-01	1.124	5.7E-02
2	2S----	B2run08-7	0.149	1.2E-03	5.10E+08	4.8E+06	5.31E+08	4.6E+06	0.705	3.4E-05	2621.5	5.7E-01	0.343	0.781	1.5E-01	0.937	1.2E-01
2	2S----	B2run09-1	0.101	8.6E-04	7.27E+08	6.8E+06	7.71E+08	7.7E+06	0.706	4.3E-05	2595.9	2.9E-01	0.560	0.500	8.3E-02	0.410	4.7E-02
2	2S----	B2run09-2	0.176	2.0E-03	2.24E+09	2.6E+07	2.27E+09	2.8E+07	0.706	4.9E-05	5143.9	2.2E-01	0.560	1.080	2.3E-01	1.004	2.0E-01
2	2S----	B2run09-3	0.138	1.2E-03	1.42E+09	1.3E+07	1.43E+09	1.3E+07	0.706	4.3E-05	3824.4	2.0E-01	0.560	0.485	6.0E-02	0.722	3.8E-02
2	2S----	B2run09-5a	0.048	4.5E-04	2.02E+08	1.7E+06	2.26E+08	1.9E+06	0.706	4.5E-05	1288.0	2.6E-01	0.561	0.400	3.8E-02	0.262	2.0E-02
2	2S----	B2run09-5b	0.101	8.0E-04	7.18E+08	6.0E+06	7.59E+08	6.5E+06	0.706	4.4E-05	2538.2	1.3E-01	0.560	0.472	3.7E-02	0.393	1.4E-02
2	2S----	B2run09-6	0.086	8.6E-04	5.10E+08	5.1E+06	5.35E+08	5.1E+06	0.705	4.2E-05	2585.7	3.3E-01	0.557	0.421	4.1E-02	0.371	2.6E-02
2	2S----	B2run12-1	0.161	1.3E-03	7.16E+08	6.8E+06	7.33E+08	6.7E+06	0.706	4.2E-05	2409.4	3.3E-01	0.355	1.000	1.5E-01	1.030	8.4E-02
2	2S----	B2run12-2	0.310	2.5E-03	2.38E+09	2.1E+07	2.43E+09	2.0E+07	0.706	3.9E-05	4813.9	4.0E-01	0.352	1.361	8.4E-02	1.278	5.6E-02
2	2S----	B2t05	0.134	9.9E-04	3.57E+08	3.3E+06	3.72E+08	3.4E+06	0.705	3.9E-05	2257.3	8.9E-02	0.321	0.917	9.8E-01	1.021	8.4E-01
2	2S----	B2t06	0.057	5.5E-04	1.58E+08	1.5E+06	1.69E+08	1.4E+06	0.706	3.7E-05	1655.2	2.6E-01	0.446	0.563	9.8E-02	0.495	7.3E-02
2	2S----	B2t07-a	0.055	4.7E-04	1.80E+08	1.5E+06	1.92E+08	1.6E+06	0.705	3.8E-05	1514.9	2.6E-01	0.483	0.482	6.3E-02	0.436	3.4E-02

Build	Exp Code	Run	Bo*	+/-	Grsh,C2	+/-	Grsh,C3	+/-	Pr	+/-	Rot Speed (rpm)	+/-	Mass Flow (kg/s)	Ø	+/-	finØ	+/-
2	2S----	B2t07-b	0.109	9.9E-04	5.73E+08	5.5E+06	6.03E+08	5.9E+06	0.705	4.2E-05	2924.8	2.8E-01	0.483	0.562	5.8E-02	0.490	2.8E-02
2	2S----	B2t09a	0.045	4.8E-04	1.03E+08	1.1E+06	1.11E+08	1.1E+06	0.705	4.0E-05	1353.0	1.4E-01	0.442	0.521	6.5E+00	0.543	1.0E+01
2	2S----	B2t09b	0.048	4.8E-04	1.14E+08	9.9E+05	1.24E+08	1.1E+06	0.705	4.2E-05	1353.2	1.9E-01	0.443	0.425	8.0E-02	0.443	4.2E-02
2	2S----	B2t09-c	0.048	4.4E-04	1.17E+08	9.8E+05	1.27E+08	1.0E+06	0.705	3.7E-05	1359.0	0.0E+00	0.444	0.423	6.5E-02	0.433	4.1E-02
2	2S----	B2t10	0.171	1.0E-03	3.18E+08	2.4E+06	3.30E+08	2.5E+06	0.706	3.0E-05	1745.6	1.5E-01	0.250	1.049	2.5E-01	0.888	2.6E-01
2	2S----	B2t11	0.092	9.1E-04	1.48E+08	2.0E+06	1.55E+08	1.8E+06	0.706	5.5E-05	1384.9	6.2E-02	0.298	0.870	2.5E-01	0.554	2.2E-01
2	2S----	B2t12	0.128	9.0E-04	2.07E+08	1.9E+06	2.13E+08	1.9E+06	0.706	4.2E-05	1524.7	9.4E-02	0.259	0.924	1.9E-01	0.897	1.3E-01
2	2s----	B2t13-a	0.049	2.6E-03	1.55E+08	6.1E+06	1.66E+08	6.4E+06	0.705	1.9E-04	1487.8	8.3E-02	0.488	0.470	5.1E-01	0.475	2.1E+00
2	2S----	B2t13-b	0.053	5.3E-04	1.76E+08	1.7E+06	1.87E+08	1.5E+06	0.705	4.3E-05	1484.5	2.8E-01	0.493	0.377	4.7E-02	0.387	2.4E-02
2	2S----	B2t14	0.053	5.8E-04	1.66E+08	1.7E+06	1.77E+08	1.8E+06	0.705	4.7E-05	1469.8	4.2E-01	0.484	0.336	5.3E-02	0.408	2.9E-02
2	2S----	B2t15-a	0.054	5.1E-04	1.80E+08	1.7E+06	1.91E+08	1.6E+06	0.706	4.2E-05	1485.3	3.8E-01	0.494	0.298	4.4E-02	0.390	2.1E-02
2	2S----	B2t15-b	0.105	9.8E-04	5.68E+08	5.7E+06	5.91E+08	5.7E+06	0.705	4.4E-05	2876.6	4.3E-01	0.491	0.542	6.7E-02	0.480	3.1E-02
2	2S----	B2t16-a	0.051	9.0E-04	1.63E+08	3.0E+06	1.74E+08	2.8E+06	0.705	7.3E-05	1476.0	2.9E+00	0.486	0.396	2.4E-01	0.471	1.8E-01
2	2S----	B2t16-b	0.054	4.7E-04	1.79E+08	1.5E+06	1.90E+08	1.6E+06	0.706	4.0E-05	1482.4	2.4E-01	0.486	0.327	4.9E-02	0.413	2.8E-02
2	2S----	B2t16-c	0.055	7.5E-04	1.84E+08	2.4E+06	1.96E+08	2.4E+06	0.705	6.3E-05	1503.1	5.0E-02	0.488	0.334	4.9E-02	0.410	2.9E-02
2	2S----	B2t17-a	0.105	1.0E-03	5.72E+08	5.7E+06	5.96E+08	6.0E+06	0.705	4.3E-05	2874.9	2.8E-01	0.489	0.576	7.9E-02	0.493	5.2E-02
2	2S----	B2t17-b	0.106	9.2E-04	5.99E+08	5.3E+06	6.22E+08	5.1E+06	0.705	3.9E-05	2871.1	9.6E-02	0.493	0.560	5.1E-02	0.491	2.3E-02
2	2S----	B2t17-c	0.105	7.7E-04	5.85E+08	4.4E+06	6.08E+08	4.7E+06	0.705	3.4E-05	2866.0	0.0E+00	0.493	0.555	6.6E-02	0.483	3.0E-02
2	2S----	B2t18-a	0.121	8.1E-04	1.56E+08	1.3E+06	1.65E+08	1.4E+06	0.706	3.7E-05	1270.7	3.0E-01	0.241	0.893	2.5E-01	0.832	1.7E-01
2	2S----	B2t18-b	0.122	7.4E-04	1.57E+08	1.3E+06	1.65E+08	1.3E+06	0.706	3.5E-05	1274.6	2.3E-01	0.242	0.899	1.3E-01	0.800	7.1E-02
2	2S----	B2t18-c	0.228	1.9E-03	5.99E+08	5.0E+06	6.18E+08	5.6E+06	0.706	3.7E-05	2671.3	1.5E-01	0.240	1.828	2.3E-01	1.714	2.1E-01
2	2S----	B2t18-d	0.227	1.8E-03	5.97E+08	5.6E+06	6.17E+08	5.9E+06	0.706	3.9E-05	2674.6	2.8E-01	0.242	1.734	6.0E-01	1.632	5.6E-01
2	2S----	B2t19-a	0.116	7.8E-04	1.65E+08	1.4E+06	1.73E+08	1.4E+06	0.706	3.8E-05	1292.9	5.1E-02	0.254	1.022	1.6E-01	0.720	1.5E-01
2	2S----	B2t19-b	0.115	8.2E-04	1.64E+08	1.5E+06	1.72E+08	1.4E+06	0.706	4.0E-05	1293.0	3.9E-02	0.256	1.011	1.5E-01	0.703	6.5E-02
2	2S----	B2t19-c	0.216	1.4E-03	5.95E+08	4.7E+06	6.15E+08	4.6E+06	0.706	3.0E-05	2622.5	2.1E-01	0.251	1.724	2.3E-01	1.611	1.4E-01
2	2S----	B2t19-d	0.214	1.7E-03	5.91E+08	5.6E+06	6.10E+08	5.6E+06	0.706	3.9E-05	2622.1	4.7E-02	0.253	1.702	2.0E-01	1.585	1.6E-01

Build	Exp Code	Run	Tcav2 (K)	+/-	Tcav3 (K)	+/-	Tinlet (K)	+/-	Texit (K)	+/-	Dtmeas (K)	+/-	Dtcalc (K)	+/-	Tsh,C2 (K)	+/-	Tsh,C3 (K)	+/-
2	2S----	B2run02-2	301.81	9.2E+00	458.42	3.5E+01	317.04	2.7E-01	320.42	2.4E-01	3.38	3.8E-01	-0.71	1.4E+00	327.53	5.9E-01	328.15	2.6E+00
2	2S----	B2run02-3	315.63	4.6E+01	840.36	1.1E+02	323.06	9.9E-01	369.58	1.0E+00	46.53	1.4E+00	1.46	5.5E+00	362.81	2.7E+00	366.44	1.2E+01
2	2S----	B2run03-1	187.55	4.7E+01	922.32	1.6E+02	324.73	4.2E-01	355.12	3.9E-01	30.40	5.9E-01	-0.38	1.4E+00	369.13	2.6E+00	372.33	1.2E+01
2	2S----	B2run04-1	281.49	4.0E+01	846.67	1.2E+02	318.15	6.0E-01	355.50	5.8E-01	37.35	7.8E-01	0.68	1.6E+00	354.76	2.3E+00	358.20	8.4E+00
2	2S----	B2run04-2	345.35	6.6E+01	1049.07	1.3E+02	317.41	5.7E-01	351.90	5.4E-01	34.49	8.1E-01	-0.35	1.5E+01	360.89	2.6E+00	364.40	9.9E+00
2	2S----	B2run04-3	201.63	6.3E+01	739.68	1.4E+02	318.90	1.1E+00	359.20	1.2E+00	40.30	1.6E+00	1.55	2.2E+00	352.43	2.6E+00	354.81	9.2E+00
2	2S----	B2run04-4	295.48	4.2E+01	838.52	1.0E+02	318.18	9.4E-01	356.97	1.0E+00	38.80	1.4E+00	1.13	2.2E+00	353.51	2.3E+00	356.41	9.7E+00
2	2S----	B2run04-7	292.57	5.8E+01	852.65	1.0E+02	318.92	7.8E-01	357.28	8.4E-01	38.36	1.1E+00	0.96	2.1E+00	355.06	2.5E+00	358.07	8.8E+00
2	2S----	B2run06-1	310.51	1.1E+00	339.82	1.4E+00	314.28	2.4E-01	320.70	2.2E-01	6.42	3.4E-01	4.66	6.2E-02	390.40	1.6E-01	404.48	1.7E-01
2	2S----	B2run06-2	346.59	1.0E+00	353.96	1.0E+00	315.73	2.3E-01	320.80	2.4E-01	5.07	3.6E-01	4.66	6.4E-02	399.95	1.7E-01	410.63	1.7E-01
2	2S----	B2run08-1	338.74	1.3E+00	341.42	1.2E+00	315.35	2.6E-01	322.09	2.4E-01	6.74	3.8E-01	6.02	1.3E-01	386.50	2.8E-01	392.45	2.6E-01
2	2S----	B2run08-2	332.29	5.9E-01	333.02	5.3E-01	315.92	2.7E-01	323.71	2.3E-01	7.79	3.5E-01	7.80	8.0E-02	378.06	1.8E-01	381.12	1.6E-01
2	2S----	B2run08-3	331.83	6.4E-01	334.00	8.1E-01	317.52	2.2E-01	328.94	2.2E-01	11.42	3.2E-01	10.15	1.3E-01	376.74	2.4E-01	378.80	3.1E-01
2	2S----	B2run08-4	333.91	5.7E-01	334.97	5.5E-01	318.64	2.5E-01	327.42	2.7E-01	8.78	3.5E-01	7.11	6.3E-02	379.31	2.1E-01	380.90	2.0E-01
2	2S----	B2run08-5	333.72	5.8E-01	334.65	4.9E-01	318.95	2.4E-01	325.96	2.3E-01	7.00	3.4E-01	6.25	6.3E-02	378.98	1.8E-01	380.58	1.9E-01
2	2S----	B2run08-6	335.87	6.2E-01	334.64	6.1E-01	318.62	2.2E-01	324.03	2.5E-01	5.40	3.2E-01	5.50	6.2E-02	382.05	1.8E-01	384.15	1.7E-01
2	2S----	B2run08-7	332.17	8.6E-01	330.74	7.4E-01	318.63	2.1E-01	322.06	2.1E-01	3.43	3.1E-01	3.43	7.1E-02	364.14	2.5E-01	365.97	2.0E-01
2	2S----	B2run09-1	335.44	1.1E+00	338.04	1.3E+00	314.58	2.7E-01	317.12	2.9E-01	2.54	4.1E-01	3.02	6.6E-02	378.49	3.3E-01	382.26	3.7E-01
2	2S----	B2run09-2	329.78	8.8E-01	329.46	1.2E+00	315.82	3.1E-01	320.89	3.1E-01	5.07	4.5E-01	4.26	6.6E-02	374.62	2.8E-01	375.30	3.8E-01
2	2S----	B2run09-3	333.28	6.0E-01	331.98	5.4E-01	315.66	2.7E-01	319.25	2.7E-01	3.59	3.6E-01	3.66	4.7E-02	377.14	2.1E-01	377.32	1.9E-01
2	2S----	B2run09-5a	338.61	7.7E-01	346.71	1.3E+00	315.43	2.8E-01	317.72	2.6E-01	2.29	3.8E-01	2.67	4.5E-02	384.73	1.5E-01	392.64	2.5E-01
2	2S----	B2run09-5b	338.10	6.2E-01	340.06	5.4E-01	315.47	2.7E-01	318.10	2.8E-01	2.64	3.9E-01	3.02	3.8E-02	381.19	1.8E-01	384.87	1.5E-01
2	2S----	B2run09-6	335.01	5.8E-01	334.90	6.7E-01	317.59	2.6E-01	319.10	2.7E-01	1.51	3.5E-01	1.98	3.6E-02	364.68	1.5E-01	366.91	1.8E-01
2	2S----	B2run12-1	327.64	9.2E-01	326.98	6.5E-01	311.07	2.7E-01	315.87	2.7E-01	4.80	3.8E-01	5.08	6.9E-02	373.83	2.9E-01	375.22	2.1E-01
2	2S----	B2run12-2	327.60	5.5E-01	329.05	4.8E-01	312.57	2.5E-01	320.75	2.4E-01	8.18	3.7E-01	6.66	7.1E-02	372.34	1.9E-01	373.51	1.8E-01
2	2S----	B2t05	330.56	9.8E-01	329.56	1.1E+00	316.73	2.4E-01	319.97	2.5E-01	3.24	3.6E-01	4.00	8.1E-02	369.02	2.3E-01	371.24	2.7E-01

Build	Exp Code	Run	Tcav2 (K)	+/-	Tcav3 (K)	+/-	Tinlet (K)	+/-	Texit (K)	+/-	Dtmeas (K)	+/-	Dtcalc (K)	+/-	Tsh,C2 (K)	+/-	Tsh,C3 (K)	+/-
2	2S----	B2t06	326.08	1.0E+00	329.06	1.1E+00	314.76	2.3E-01	315.71	2.4E-01	0.95	3.5E-01	2.28	4.9E-02	360.98	1.9E-01	364.00	1.9E-01
2	2S----	B2t07-a	332.41	8.4E-01	336.00	8.2E-01	317.25	2.4E-01	318.77	2.3E-01	1.52	3.5E-01	2.64	3.7E-02	374.40	1.6E-01	377.96	1.8E-01
2	2S----	B2t07-b	331.64	6.2E-01	334.94	6.1E-01	317.33	2.6E-01	319.37	2.5E-01	2.05	3.7E-01	2.77	4.3E-02	368.94	1.8E-01	371.52	1.6E-01
2	2S----	B2t09a	326.84	1.7E+00	332.12	2.1E+00	318.77	2.4E-01	319.82	2.3E-01	1.05	3.2E-01	2.37	7.6E-02	366.26	2.7E-01	370.32	3.6E-01
2	2S----	B2t09b	329.16	8.4E-01	334.50	8.6E-01	317.49	2.6E-01	318.78	2.6E-01	1.29	3.9E-01	2.47	4.3E-02	368.91	1.5E-01	373.20	1.6E-01
2	2S----	B2t09-c	329.10	8.3E-01	334.39	8.0E-01	316.90	2.3E-01	318.23	2.2E-01	1.33	3.0E-01	2.48	4.1E-02	368.91	1.6E-01	373.23	1.6E-01
2	2S----	B2t10	326.82	8.5E-01	329.40	8.0E-01	313.98	1.9E-01	318.24	2.2E-01	4.26	3.0E-01	4.42	9.9E-02	363.07	2.2E-01	364.78	1.8E-01
2	2S----	B2t11	330.55	1.9E+00	335.17	1.7E+00	315.77	3.5E-01	318.70	3.1E-01	2.93	4.5E-01	3.53	1.2E-01	371.99	4.0E-01	374.72	3.3E-01
2	2S----	B2t12	327.98	7.4E-01	329.37	8.3E-01	313.71	2.7E-01	317.90	2.7E-01	4.19	3.8E-01	4.48	8.7E-02	370.17	1.6E-01	371.73	1.7E-01
2	2s----	B2t13-a	330.95	2.6E+00	335.47	2.6E+00	319.67	1.1E+00	320.55	1.2E+00	0.88	1.5E+00	2.45	2.1E-01	371.45	5.3E-01	375.05	5.2E-01
2	2S----	B2t13-b	331.45	8.7E-01	336.14	8.6E-01	316.40	2.7E-01	317.72	3.0E-01	1.33	4.1E-01	2.50	4.4E-02	372.51	1.8E-01	376.06	1.7E-01
2	2S----	B2t14	331.97	8.8E-01	336.46	7.8E-01	317.31	2.9E-01	318.75	2.5E-01	1.44	3.6E-01	2.54	3.9E-02	373.34	1.7E-01	377.16	1.5E-01
2	2S----	B2t15-a	331.82	8.1E-01	335.83	6.6E-01	315.96	2.6E-01	317.37	2.4E-01	1.41	3.5E-01	2.52	3.8E-02	372.95	1.6E-01	376.47	1.3E-01
2	2S----	B2t15-b	334.49	6.6E-01	336.08	6.8E-01	318.45	2.7E-01	320.55	2.7E-01	2.10	3.8E-01	2.68	5.0E-02	370.78	1.8E-01	372.77	1.7E-01
2	2S----	B2t16-a	330.61	2.5E+00	334.50	1.9E+00	317.81	4.5E-01	318.98	3.8E-01	1.17	6.3E-01	2.55	8.9E-02	372.33	5.5E-01	375.86	3.9E-01
2	2S----	B2t16-b	331.86	8.3E-01	335.75	8.0E-01	316.11	2.5E-01	317.55	2.5E-01	1.44	3.6E-01	2.63	4.1E-02	374.08	1.7E-01	377.62	1.5E-01
2	2S----	B2t16-c	332.92	8.2E-01	336.54	7.7E-01	316.75	3.9E-01	318.17	3.7E-01	1.42	5.8E-01	2.62	4.1E-02	374.83	1.6E-01	378.33	1.7E-01
2	2S----	B2t17-a	334.34	8.2E-01	336.14	9.6E-01	318.55	2.6E-01	320.64	2.6E-01	2.08	3.9E-01	2.74	5.6E-02	371.13	2.2E-01	373.26	2.7E-01
2	2S----	B2t17-b	333.30	6.4E-01	334.97	5.6E-01	317.09	2.4E-01	319.29	2.4E-01	2.20	3.4E-01	2.78	4.0E-02	370.76	1.6E-01	372.74	1.7E-01
2	2S----	B2t17-c	334.77	7.0E-01	336.32	6.3E-01	318.24	2.1E-01	320.42	2.5E-01	2.17	3.3E-01	2.76	3.8E-02	371.83	1.8E-01	373.90	1.8E-01
2	2S----	B2t18-a	323.92	1.1E+00	327.02	1.2E+00	310.64	2.4E-01	314.90	2.6E-01	4.26	3.3E-01	4.37	9.3E-02	365.19	2.0E-01	368.12	2.0E-01
2	2S----	B2t18-b	325.29	8.4E-01	328.38	8.6E-01	311.50	2.3E-01	315.82	2.4E-01	4.31	3.5E-01	4.34	8.1E-02	366.41	1.7E-01	369.29	1.7E-01
2	2S----	B2t18-c	324.60	6.7E-01	323.85	5.5E-01	312.43	2.3E-01	318.00	2.6E-01	5.56	3.6E-01	6.02	8.5E-02	362.91	1.7E-01	364.50	1.5E-01
2	2S----	B2t18-d	325.43	5.3E-01	324.94	6.7E-01	313.12	2.5E-01	318.70	2.4E-01	5.58	3.6E-01	5.95	8.9E-02	363.72	1.6E-01	365.38	1.9E-01
2	2S----	B2t19-a	324.89	9.2E-01	328.66	1.0E+00	310.77	2.4E-01	314.86	2.6E-01	4.09	3.9E-01	4.19	8.0E-02	366.49	1.8E-01	369.19	2.0E-01
2	2S----	B2t19-b	325.46	8.6E-01	329.29	7.8E-01	311.18	2.6E-01	315.28	2.2E-01	4.11	3.4E-01	4.14	8.6E-02	366.95	1.7E-01	369.68	1.6E-01
2	2S----	B2t19-c	323.53	6.7E-01	322.91	6.1E-01	311.15	1.9E-01	316.54	2.2E-01	5.39	3.0E-01	5.83	8.5E-02	362.59	1.9E-01	364.23	1.8E-01
2	2S----	B2t19-d	324.41	5.7E-01	323.72	6.2E-01	311.91	2.5E-01	317.31	2.3E-01	5.40	3.8E-01	5.77	7.3E-02	363.36	1.6E-01	364.94	1.8E-01

Build	Exp Code	Run	Tcav2 (K)	+/-	Tcav3 (K)	+/-	Tinlet (K)	+/-	Texit (K)	+/-	Dtmeas (K)	+/-	Dtcalc (K)	+/-	Tsh,C2 (K)	+/-	Tsh,C3 (K)	+/-
2	2S----	B2run02-2	301.81	9.2E+00	458.42	3.5E+01	317.04	2.7E-01	320.42	2.4E-01	3.38	3.8E-01	-0.71	1.4E+00	327.53	5.9E-01	328.15	2.6E+00
2	2S----	B2run02-3	315.63	4.6E+01	840.36	1.1E+02	323.06	9.9E-01	369.58	1.0E+00	46.53	1.4E+00	1.46	5.5E+00	362.81	2.7E+00	366.44	1.2E+01
2	2S----	B2run03-1	187.55	4.7E+01	922.32	1.6E+02	324.73	4.2E-01	355.12	3.9E-01	30.40	5.9E-01	-0.38	1.4E+00	369.13	2.6E+00	372.33	1.2E+01
2	2S----	B2run04-1	281.49	4.0E+01	846.67	1.2E+02	318.15	6.0E-01	355.50	5.8E-01	37.35	7.8E-01	0.68	1.6E+00	354.76	2.3E+00	358.20	8.4E+00
2	2S----	B2run04-2	345.35	6.6E+01	1049.07	1.3E+02	317.41	5.7E-01	351.90	5.4E-01	34.49	8.1E-01	-0.35	1.5E+01	360.89	2.6E+00	364.40	9.9E+00
2	2S----	B2run04-3	201.63	6.3E+01	739.68	1.4E+02	318.90	1.1E+00	359.20	1.2E+00	40.30	1.6E+00	1.55	2.2E+00	352.43	2.6E+00	354.81	9.2E+00
2	2S----	B2run04-4	295.48	4.2E+01	838.52	1.0E+02	318.18	9.4E-01	356.97	1.0E+00	38.80	1.4E+00	1.13	2.2E+00	353.51	2.3E+00	356.41	9.7E+00
2	2S----	B2run04-7	292.57	5.8E+01	852.65	1.0E+02	318.92	7.8E-01	357.28	8.4E-01	38.36	1.1E+00	0.96	2.1E+00	355.06	2.5E+00	358.07	8.8E+00
2	2S----	B2run06-1	310.51	1.1E+00	339.82	1.4E+00	314.28	2.4E-01	320.70	2.2E-01	6.42	3.4E-01	4.66	6.2E-02	390.40	1.6E-01	404.48	1.7E-01
2	2S----	B2run06-2	346.59	1.0E+00	353.96	1.0E+00	315.73	2.3E-01	320.80	2.4E-01	5.07	3.6E-01	4.66	6.4E-02	399.95	1.7E-01	410.63	1.7E-01
2	2S----	B2run08-1	338.74	1.3E+00	341.42	1.2E+00	315.35	2.6E-01	322.09	2.4E-01	6.74	3.8E-01	6.02	1.3E-01	386.50	2.8E-01	392.45	2.6E-01
2	2S----	B2run08-2	332.29	5.9E-01	333.02	5.3E-01	315.92	2.7E-01	323.71	2.3E-01	7.79	3.5E-01	7.80	8.0E-02	378.06	1.8E-01	381.12	1.6E-01
2	2S----	B2run08-3	331.83	6.4E-01	334.00	8.1E-01	317.52	2.2E-01	328.94	2.2E-01	11.42	3.2E-01	10.15	1.3E-01	376.74	2.4E-01	378.80	3.1E-01
2	2S----	B2run08-4	333.91	5.7E-01	334.97	5.5E-01	318.64	2.5E-01	327.42	2.7E-01	8.78	3.5E-01	7.11	6.3E-02	379.31	2.1E-01	380.90	2.0E-01
2	2S----	B2run08-5	333.72	5.8E-01	334.65	4.9E-01	318.95	2.4E-01	325.96	2.3E-01	7.00	3.4E-01	6.25	6.3E-02	378.98	1.8E-01	380.58	1.9E-01
2	2S----	B2run08-6	335.87	6.2E-01	334.64	6.1E-01	318.62	2.2E-01	324.03	2.5E-01	5.40	3.2E-01	5.50	6.2E-02	382.05	1.8E-01	384.15	1.7E-01
2	2S----	B2run08-7	332.17	8.6E-01	330.74	7.4E-01	318.63	2.1E-01	322.06	2.1E-01	3.43	3.1E-01	3.43	7.1E-02	364.14	2.5E-01	365.97	2.0E-01
2	2S----	B2run09-1	335.44	1.1E+00	338.04	1.3E+00	314.58	2.7E-01	317.12	2.9E-01	2.54	4.1E-01	3.02	6.6E-02	378.49	3.3E-01	382.26	3.7E-01
2	2S----	B2run09-2	329.78	8.8E-01	329.46	1.2E+00	315.82	3.1E-01	320.89	3.1E-01	5.07	4.5E-01	4.26	6.6E-02	374.62	2.8E-01	375.30	3.8E-01
2	2S----	B2run09-3	333.28	6.0E-01	331.98	5.4E-01	315.66	2.7E-01	319.25	2.7E-01	3.59	3.6E-01	3.66	4.7E-02	377.14	2.1E-01	377.32	1.9E-01
2	2S----	B2run09-5a	338.61	7.7E-01	346.71	1.3E+00	315.43	2.8E-01	317.72	2.6E-01	2.29	3.8E-01	2.67	4.5E-02	384.73	1.5E-01	392.64	2.5E-01
2	2S----	B2run09-5b	338.10	6.2E-01	340.06	5.4E-01	315.47	2.7E-01	318.10	2.8E-01	2.64	3.9E-01	3.02	3.8E-02	381.19	1.8E-01	384.87	1.5E-01
2	2S----	B2run09-6	335.01	5.8E-01	334.90	6.7E-01	317.59	2.6E-01	319.10	2.7E-01	1.51	3.5E-01	1.98	3.6E-02	364.68	1.5E-01	366.91	1.8E-01
2	2S----	B2run12-1	327.64	9.2E-01	326.98	6.5E-01	311.07	2.7E-01	315.87	2.7E-01	4.80	3.8E-01	5.08	6.9E-02	373.83	2.9E-01	375.22	2.1E-01
2	2S----	B2run12-2	327.60	5.5E-01	329.05	4.8E-01	312.57	2.5E-01	320.75	2.4E-01	8.18	3.7E-01	6.66	7.1E-02	372.34	1.9E-01	373.51	1.8E-01
2	2S----	B2t05	330.56	9.8E-01	329.56	1.1E+00	316.73	2.4E-01	319.97	2.5E-01	3.24	3.6E-01	4.00	8.1E-02	369.02	2.3E-01	371.24	2.7E-01

Build	Exp Code	Run	Tcav2 (K)	+/-	Tcav3 (K)	+/-	Tinlet (K)	+/-	Texit (K)	+/-	Dtmeas (K)	+/-	Dtcalc (K)	+/-	Tsh,C2 (K)	+/-	Tsh,C3 (K)	+/-
2	2S----	B2t06	326.08	1.0E+00	329.06	1.1E+00	314.76	2.3E-01	315.71	2.4E-01	0.95	3.5E-01	2.28	4.9E-02	360.98	1.9E-01	364.00	1.9E-01
2	2S----	B2t07-a	332.41	8.4E-01	336.00	8.2E-01	317.25	2.4E-01	318.77	2.3E-01	1.52	3.5E-01	2.64	3.7E-02	374.40	1.6E-01	377.96	1.8E-01
2	2S----	B2t07-b	331.64	6.2E-01	334.94	6.1E-01	317.33	2.6E-01	319.37	2.5E-01	2.05	3.7E-01	2.77	4.3E-02	368.94	1.8E-01	371.52	1.6E-01
2	2S----	B2t09a	326.84	1.7E+00	332.12	2.1E+00	318.77	2.4E-01	319.82	2.3E-01	1.05	3.2E-01	2.37	7.6E-02	366.26	2.7E-01	370.32	3.6E-01
2	2S----	B2t09b	329.16	8.4E-01	334.50	8.6E-01	317.49	2.6E-01	318.78	2.6E-01	1.29	3.9E-01	2.47	4.3E-02	368.91	1.5E-01	373.20	1.6E-01
2	2S----	B2t09-c	329.10	8.3E-01	334.39	8.0E-01	316.90	2.3E-01	318.23	2.2E-01	1.33	3.0E-01	2.48	4.1E-02	368.91	1.6E-01	373.23	1.6E-01
2	2S----	B2t10	326.82	8.5E-01	329.40	8.0E-01	313.98	1.9E-01	318.24	2.2E-01	4.26	3.0E-01	4.42	9.9E-02	363.07	2.2E-01	364.78	1.8E-01
2	2S----	B2t11	330.55	1.9E+00	335.17	1.7E+00	315.77	3.5E-01	318.70	3.1E-01	2.93	4.5E-01	3.53	1.2E-01	371.99	4.0E-01	374.72	3.3E-01
2	2S----	B2t12	327.98	7.4E-01	329.37	8.3E-01	313.71	2.7E-01	317.90	2.7E-01	4.19	3.8E-01	4.48	8.7E-02	370.17	1.6E-01	371.73	1.7E-01
2	2s----	B2t13-a	330.95	2.6E+00	335.47	2.6E+00	319.67	1.1E+00	320.55	1.2E+00	0.88	1.5E+00	2.45	2.1E-01	371.45	5.3E-01	375.05	5.2E-01
2	2S----	B2t13-b	331.45	8.7E-01	336.14	8.6E-01	316.40	2.7E-01	317.72	3.0E-01	1.33	4.1E-01	2.50	4.4E-02	372.51	1.8E-01	376.06	1.7E-01
2	2S----	B2t14	331.97	8.8E-01	336.46	7.8E-01	317.31	2.9E-01	318.75	2.5E-01	1.44	3.6E-01	2.54	3.9E-02	373.34	1.7E-01	377.16	1.5E-01
2	2S----	B2t15-a	331.82	8.1E-01	335.83	6.6E-01	315.96	2.6E-01	317.37	2.4E-01	1.41	3.5E-01	2.52	3.8E-02	372.95	1.6E-01	376.47	1.3E-01
2	2S----	B2t15-b	334.49	6.6E-01	336.08	6.8E-01	318.45	2.7E-01	320.55	2.7E-01	2.10	3.8E-01	2.68	5.0E-02	370.78	1.8E-01	372.77	1.7E-01
2	2S----	B2t16-a	330.61	2.5E+00	334.50	1.9E+00	317.81	4.5E-01	318.98	3.8E-01	1.17	6.3E-01	2.55	8.9E-02	372.33	5.5E-01	375.86	3.9E-01
2	2S----	B2t16-b	331.86	8.3E-01	335.75	8.0E-01	316.11	2.5E-01	317.55	2.5E-01	1.44	3.6E-01	2.63	4.1E-02	374.08	1.7E-01	377.62	1.5E-01
2	2S----	B2t16-c	332.92	8.2E-01	336.54	7.7E-01	316.75	3.9E-01	318.17	3.7E-01	1.42	5.8E-01	2.62	4.1E-02	374.83	1.6E-01	378.33	1.7E-01
2	2S----	B2t17-a	334.34	8.2E-01	336.14	9.6E-01	318.55	2.6E-01	320.64	2.6E-01	2.08	3.9E-01	2.74	5.6E-02	371.13	2.2E-01	373.26	2.7E-01
2	2S----	B2t17-b	333.30	6.4E-01	334.97	5.6E-01	317.09	2.4E-01	319.29	2.4E-01	2.20	3.4E-01	2.78	4.0E-02	370.76	1.6E-01	372.74	1.7E-01
2	2S----	B2t17-c	334.77	7.0E-01	336.32	6.3E-01	318.24	2.1E-01	320.42	2.5E-01	2.17	3.3E-01	2.76	3.8E-02	371.83	1.8E-01	373.90	1.8E-01
2	2S----	B2t18-a	323.92	1.1E+00	327.02	1.2E+00	310.64	2.4E-01	314.90	2.6E-01	4.26	3.3E-01	4.37	9.3E-02	365.19	2.0E-01	368.12	2.0E-01
2	2S----	B2t18-b	325.29	8.4E-01	328.38	8.6E-01	311.50	2.3E-01	315.82	2.4E-01	4.31	3.5E-01	4.34	8.1E-02	366.41	1.7E-01	369.29	1.7E-01
2	2S----	B2t18-c	324.60	6.7E-01	323.85	5.5E-01	312.43	2.3E-01	318.00	2.6E-01	5.56	3.6E-01	6.02	8.5E-02	362.91	1.7E-01	364.50	1.5E-01
2	2S----	B2t18-d	325.43	5.3E-01	324.94	6.7E-01	313.12	2.5E-01	318.70	2.4E-01	5.58	3.6E-01	5.95	8.9E-02	363.72	1.6E-01	365.38	1.9E-01
2	2S----	B2t19-a	324.89	9.2E-01	328.66	1.0E+00	310.77	2.4E-01	314.86	2.6E-01	4.09	3.9E-01	4.19	8.0E-02	366.49	1.8E-01	369.19	2.0E-01
2	2S----	B2t19-b	325.46	8.6E-01	329.29	7.8E-01	311.18	2.6E-01	315.28	2.2E-01	4.11	3.4E-01	4.14	8.6E-02	366.95	1.7E-01	369.68	1.6E-01
2	2S----	B2t19-c	323.53	6.7E-01	322.91	6.1E-01	311.15	1.9E-01	316.54	2.2E-01	5.39	3.0E-01	5.83	8.5E-02	362.59	1.9E-01	364.23	1.8E-01
2	2S----	B2t19-d	324.41	5.7E-01	323.72	6.2E-01	311.91	2.5E-01	317.31	2.3E-01	5.40	3.8E-01	5.77	7.3E-02	363.36	1.6E-01	364.94	1.8E-01

Build	Exp Code	Run	Pcav (abs Pa)	Ts,C2,d,av (K)	+/-	Ts,C3,u,av (K)	+/-	TS,C3,d,av (K)	+/-	Ts,C4,u,av (K)	+/-	finTs,D2,av (K)	+/-	finTs,D3,av (K)	+/-
2	2S----	B2run02-2	2.479E+05	319.54	4.4E-01	325.69	8.3E-01	319.76	5.0E-01	325.97	9.7E-01	322.62	4.9E-01	322.87	5.5E-01
2	2S----	B2run02-3	2.219E+05	333.10	6.3E-01	360.69	1.6E+00	335.65	6.5E-01	367.27	2.0E+00	346.89	8.7E-01	351.46	1.0E+00
2	2S----	B2run03-1	2.974E+05	332.06	1.1E+00	365.30	3.0E+00	332.56	1.0E+00	368.95	3.0E+00	348.68	1.6E+00	350.75	1.5E+00
2	2S----	B2run04-1	3.049E+05	328.15	5.5E-01	353.21	1.7E+00	330.50	5.6E-01	358.39	1.7E+00	340.68	8.7E-01	344.44	9.2E-01
2	2S----	B2run04-2	3.050E+05	327.48	8.5E-01	358.75	1.8E+00	327.97	8.9E-01	362.87	2.2E+00	343.12	9.7E-01	345.42	1.3E+00
2	2S----	B2run04-3	3.122E+05	328.36	5.0E-01	350.47	1.4E+00	330.56	5.1E-01	356.08	2.0E+00	339.41	7.7E-01	343.32	1.1E+00
2	2S----	B2run04-4	3.109E+05	327.08	5.7E-01	352.36	1.8E+00	329.32	6.1E-01	357.30	1.8E+00	339.72	9.6E-01	343.31	9.3E-01
2	2S----	B2run04-7	3.117E+05	328.35	6.1E-01	353.54	1.6E+00	330.68	5.2E-01	358.62	1.9E+00	340.94	8.7E-01	344.65	9.6E-01
2	2S----	B2run06-1	2.618E+05	332.99	1.2E-01	333.58	1.1E-01	339.06	1.1E-01	340.05	1.2E-01	333.29	7.8E-02	339.56	8.4E-02
2	2S----	B2run06-2	2.625E+05	340.58	1.2E-01	339.70	1.2E-01	345.10	1.3E-01	346.14	1.3E-01	340.14	8.6E-02	345.62	9.0E-02
2	2S----	B2run08-1	2.851E+05	342.55	1.5E-01	342.60	2.0E-01	348.53	1.7E-01	347.28	2.2E-01	342.57	1.4E-01	347.90	1.4E-01
2	2S----	B2run08-2	2.859E+05	336.85	1.2E-01	335.97	1.3E-01	339.87	1.2E-01	339.02	1.2E-01	336.41	9.0E-02	339.44	8.5E-02
2	2S----	B2run08-3	2.835E+05	335.90	1.6E-01	334.15	1.6E-01	339.34	1.5E-01	338.15	1.3E-01	335.03	1.2E-01	338.75	9.5E-02
2	2S----	B2run08-4	2.702E+05	335.99	1.3E-01	334.34	1.3E-01	338.24	1.4E-01	337.00	1.4E-01	335.17	1.0E-01	337.62	8.5E-02
2	2S----	B2run08-5	2.700E+05	336.38	1.1E-01	334.92	1.1E-01	338.49	1.2E-01	337.33	1.2E-01	335.65	7.8E-02	337.91	8.5E-02
2	2S----	B2run08-6	2.695E+05	337.59	1.4E-01	336.69	1.1E-01	340.08	1.0E-01	339.36	1.2E-01	337.14	8.5E-02	339.72	7.8E-02
2	2S----	B2run08-7	2.695E+05	332.90	1.5E-01	332.49	1.3E-01	335.31	1.6E-01	334.40	1.5E-01	332.69	9.9E-02	334.85	1.1E-01
2	2S----	B2run09-1	2.650E+05	333.03	1.7E-01	331.76	1.5E-01	334.57	1.7E-01	333.90	1.7E-01	332.40	1.0E-01	334.23	1.2E-01
2	2S----	B2run09-2	2.666E+05	330.26	1.5E-01	328.77	1.4E-01	331.82	1.6E-01	330.55	1.5E-01	329.52	1.0E-01	331.18	1.1E-01
2	2S----	B2run09-3	2.662E+05	331.16	1.4E-01	330.84	1.8E-01	333.93	1.7E-01	332.11	1.3E-01	331.00	1.3E-01	333.02	1.0E-01
2	2S----	B2run09-5a	2.673E+05	331.89	1.6E-01	330.90	1.4E-01	333.70	1.5E-01	334.01	1.7E-01	331.39	1.1E-01	333.85	1.1E-01
2	2S----	B2run09-5b	2.669E+05	334.79	1.3E-01	333.58	1.4E-01	336.46	1.2E-01	335.77	1.3E-01	334.19	9.8E-02	336.11	9.3E-02
2	2S----	B2run09-6	2.663E+05	331.56	1.3E-01	330.45	1.2E-01	332.62	1.2E-01	331.70	1.1E-01	331.00	9.7E-02	332.16	9.0E-02
2	2S----	B2run12-1	2.780E+05	329.99	1.7E-01	329.15	1.3E-01	332.31	1.5E-01	331.22	1.5E-01	329.57	1.1E-01	331.77	9.7E-02
2	2S----	B2run12-2	2.809E+05	330.13	1.4E-01	328.61	1.2E-01	332.21	1.2E-01	330.86	1.4E-01	329.37	9.7E-02	331.54	9.0E-02
2	2S----	B2t05	2.387E+05	333.91	1.7E-01	333.45	1.6E-01	336.42	1.4E-01	335.58	1.5E-01	333.68	1.2E-01	336.00	1.1E-01
2	2S----	B2t06	2.254E+05	327.60	1.1E-01	326.97	1.2E-01	328.52	1.2E-01	328.05	1.1E-01	327.28	9.0E-02	328.29	8.5E-02

Build	Exp Code	Run	Pcav (abs Pa)	Ts,C2,d,av (K)	+/-	Ts,C3,u,av (K)	+/-	TS,C3,d,av (K)	+/-	Ts,C4,u,av (K)	+/-	finTs,D2,av (K)	+/-	finTs,D3,av (K)	+/-
2	2S----	B2t07-a	2.400E+05	332.34	1.1E-01	331.89	1.3E-01	333.42	1.2E-01	333.08	1.1E-01	332.11	7.9E-02	333.25	7.7E-02
2	2S----	B2t07-b	2.395E+05	333.00	1.2E-01	332.11	1.2E-01	334.68	1.3E-01	334.07	1.3E-01	332.55	8.2E-02	334.38	9.6E-02
2	2S----	B2t09a	2.245E+05	330.83	1.4E-01	330.62	1.4E-01	332.24	1.4E-01	331.82	1.2E-01	330.73	1.0E-01	332.03	9.2E-02
2	2S----	B2t09b	2.253E+05	330.78	1.2E-01	330.63	1.1E-01	332.16	9.8E-02	331.79	1.2E-01	330.71	8.5E-02	331.97	7.4E-02
2	2S----	B2t09-c	2.253E+05	330.33	1.1E-01	330.18	1.1E-01	331.71	1.1E-01	331.37	1.1E-01	330.26	7.5E-02	331.54	7.6E-02
2	2S----	B2t10	2.929E+05	332.45	1.6E-01	331.64	1.2E-01	334.92	1.3E-01	334.40	1.1E-01	332.04	9.9E-02	334.66	8.8E-02
2	2S----	B2t11	2.370E+05	334.60	2.4E-01	333.59	1.9E-01	336.47	2.4E-01	336.49	2.3E-01	334.09	1.4E-01	336.48	1.8E-01
2	2S----	B2t12	2.509E+05	333.56	1.3E-01	333.11	1.6E-01	336.17	1.4E-01	335.68	1.5E-01	333.33	1.1E-01	335.93	9.6E-02
2	2s----	B2t13-a	2.420E+05	332.40	4.7E-01	332.03	4.4E-01	333.58	5.0E-01	333.05	4.4E-01	332.21	3.4E-01	333.32	3.6E-01
2	2S----	B2t13-b	2.426E+05	330.96	1.4E-01	330.68	1.2E-01	332.10	1.2E-01	331.61	1.3E-01	330.82	9.5E-02	331.86	9.5E-02
2	2S----	B2t14	2.395E+05	331.88	1.4E-01	331.75	1.2E-01	333.34	1.1E-01	332.64	1.2E-01	331.82	9.1E-02	332.99	8.2E-02
2	2S----	B2t15-a	2.425E+05	330.86	1.0E-01	330.81	1.3E-01	332.32	9.8E-02	331.55	1.0E-01	330.84	8.9E-02	331.93	6.5E-02
2	2S----	B2t15-b	2.423E+05	333.83	1.6E-01	332.90	1.4E-01	335.49	1.5E-01	334.78	1.3E-01	333.36	1.1E-01	335.14	1.1E-01
2	2S----	B2t16-a	2.407E+05	331.48	2.4E-01	331.29	2.2E-01	332.86	2.2E-01	332.14	2.5E-01	331.38	1.7E-01	332.50	1.8E-01
2	2S----	B2t16-b	2.408E+05	331.10	1.2E-01	331.05	1.1E-01	332.50	9.9E-02	331.77	1.1E-01	331.08	9.0E-02	332.14	7.5E-02
2	2S----	B2t16-c	2.417E+05	331.73	1.3E-01	331.63	1.3E-01	333.08	1.2E-01	332.38	1.3E-01	331.68	9.6E-02	332.73	8.6E-02
2	2S----	B2t17-a	2.428E+05	333.91	1.4E-01	332.80	1.4E-01	335.55	1.5E-01	334.77	1.4E-01	333.35	9.6E-02	335.16	1.0E-01
2	2S----	B2t17-b	2.437E+05	332.77	1.2E-01	331.75	1.4E-01	334.45	1.2E-01	333.69	1.2E-01	332.26	9.6E-02	334.07	8.4E-02
2	2S----	B2t17-c	2.433E+05	333.91	1.4E-01	332.85	1.4E-01	335.59	1.2E-01	334.81	1.3E-01	333.38	1.0E-01	335.20	9.3E-02
2	2S----	B2t18-a	2.595E+05	330.28	1.2E-01	329.89	1.3E-01	333.56	1.4E-01	333.22	1.3E-01	330.08	8.7E-02	333.39	9.8E-02
2	2S----	B2t18-b	2.601E+05	331.46	1.1E-01	331.03	1.3E-01	334.70	1.4E-01	334.41	1.4E-01	331.24	9.3E-02	334.55	1.0E-01
2	2S----	B2t18-c	2.603E+05	328.78	1.2E-01	327.98	1.2E-01	330.86	9.8E-02	330.15	1.1E-01	328.38	8.9E-02	330.50	7.6E-02
2	2S----	B2t18-d	2.604E+05	329.54	1.4E-01	328.74	1.3E-01	331.62	1.4E-01	330.89	1.2E-01	329.14	9.3E-02	331.26	9.8E-02
2	2S----	B2t19-a	2.592E+05	330.49	1.2E-01	329.70	1.3E-01	333.24	1.2E-01	333.21	1.1E-01	330.10	9.4E-02	333.22	8.5E-02
2	2S----	B2t19-b	2.592E+05	330.98	1.2E-01	330.15	1.3E-01	333.72	1.3E-01	333.68	1.4E-01	330.56	8.5E-02	333.70	9.2E-02
2	2S----	B2t19-c	2.591E+05	327.65	1.1E-01	326.80	1.1E-01	329.78	1.5E-01	329.03	1.2E-01	327.23	8.3E-02	329.40	9.4E-02
2	2S----	B2t19-d	2.597E+05	328.40	1.1E-01	327.52	1.3E-01	330.56	1.1E-01	329.79	1.3E-01	327.96	8.4E-02	330.18	8.9E-02

Build	Exp Code	Run	Nu,C2,d,av	+/-	Nu,C3,u,av	+/-	Nu,C3,d,av	+/-	Nu,C4,u,av	+/-	Nush,C2	+/-	Nush,C3	+/-	finNu,D2,av	+/-	finNu,D3,av	+/-
2	2S----	B2run02-2	17905.7	2.9E+04	-5187.7	1.0E+03	16564.5	3.7E+05	-5.1E+03	2515.3	2.5E+01	26	-229.4	9.0E+02	5.5	5.0E+02	-56.4	2.9E+02
2	2S----	B2run02-3	19628.1	2.0E+05	-5243.2	2.3E+02	18085.7	1.0E+04	-5.1E+03	198.5	3.1E+02	61	-240.2	6.9E+02	23.9	1.1E+02	40.8	1.2E+02
2	2S----	B2run03-1	32249.4	2.3E+05	-5847.9	3.1E+02	33245.0	5.5E+04	-5.8E+03	297.5	2.0E+02	50	-238.2	1.9E+02	20.9	1.9E+02	-2.3	1.4E+02
2	2S----	B2run04-1	18126.2	7.3E+03	-5177.5	1.9E+02	16465.6	9.7E+03	-5.0E+03	186.1	2.9E+02	59	-246.9	3.0E+02	20.7	9.1E+01	32.6	1.1E+02
2	2S----	B2run04-2	22513.1	1.5E+04	-5502.5	1.8E+02	24137.8	1.2E+04	-5.6E+03	190.2	2.1E+02	48	-247.8	2.4E+03	17.2	8.3E+01	12.2	8.0E+01
2	2S----	B2run04-3	16886.4	1.8E+04	-5061.1	2.9E+02	15932.0	5.3E+03	-4.9E+03	226.5	3.3E+02	65	-253.5	2.4E+02	23.1	1.1E+02	48.9	1.3E+02
2	2S----	B2run04-4	20525.8	6.3E+04	-5360.1	2.5E+02	18298.9	1.7E+04	-5.1E+03	234.8	3.0E+02	211	-252.1	1.8E+02	18.8	1.4E+02	32.9	1.2E+02
2	2S----	B2run04-7	19274.1	1.9E+04	-5262.1	1.9E+02	17274.3	7.0E+03	-5.0E+03	183.0	2.9E+02	82	-251.5	1.4E+02	19.6	9.0E+01	28.9	8.9E+01
2	2S----	B2run06-1	441.7	6.7E+01	45.4	6.4E+01	500.5	4.7E+01	-1.1E+02	43.1	4.5E+01	1	28.6	7.6E-01	205.5	7.3E+00	175.0	6.5E+00
2	2S----	B2run06-2	-90.1	5.1E+01	498.1	5.6E+01	439.5	4.9E+01	-9.7E+01	45.1	3.4E+01	1	32.3	7.3E-01	170.9	6.1E+00	154.2	5.3E+00
2	2S----	B2run08-1	106.5	6.3E+01	113.5	6.4E+01	-179.3	6.1E+01	3.8E+02	66.5	4.4E+01	2	44.5	1.2E+00	92.4	9.2E+00	89.5	8.8E+00
2	2S----	B2run08-2	-188.8	5.9E+01	477.6	6.4E+01	-135.8	5.4E+01	3.8E+02	58.9	7.3E+01	1	74.8	1.0E+00	118.6	6.8E+00	111.1	5.1E+00
2	2S----	B2run08-3	-571.3	8.3E+01	931.8	1.0E+02	-281.6	6.6E+01	5.2E+02	74.5	1.1E+02	2	110.0	2.3E+00	120.4	1.1E+01	102.3	9.0E+00
2	2S----	B2run08-4	-562.6	7.2E+01	947.1	8.9E+01	-319.1	8.2E+01	6.1E+02	90.7	1.1E+02	2	110.9	1.6E+00	131.8	9.2E+00	122.3	7.6E+00
2	2S----	B2run08-5	-469.2	6.9E+01	844.7	8.5E+01	-284.0	6.3E+01	5.9E+02	70.4	9.7E+01	1	95.9	1.3E+00	137.1	9.8E+00	129.7	7.6E+00
2	2S----	B2run08-6	-211.4	7.1E+01	541.4	7.8E+01	-99.5	5.7E+01	3.8E+02	59.9	7.3E+01	1	77.7	1.1E+00	134.8	9.1E+00	126.3	6.9E+00
2	2S----	B2run08-7	-88.8	1.0E+02	364.8	1.0E+02	-276.3	9.5E+01	5.3E+02	105.2	6.2E+01	2	68.1	1.7E+00	116.7	1.1E+01	108.8	1.2E+01
2	2S----	B2run09-1	-361.4	9.8E+01	730.6	1.1E+02	-89.4	8.9E+01	4.0E+02	95.3	6.6E+01	2	64.8	2.2E+00	143.6	1.3E+01	139.0	1.3E+01
2	2S----	B2run09-2	-593.4	1.0E+02	1056.7	1.3E+02	-401.5	9.2E+01	7.8E+02	108.8	1.1E+02	3	115.7	3.5E+00	161.9	1.6E+01	154.9	1.6E+01
2	2S----	B2run09-3	7.7	9.5E+01	351.0	1.1E+02	-575.0	8.7E+01	9.5E+02	109.1	8.9E+01	1	93.1	1.3E+00	154.7	1.4E+01	138.4	1.2E+01
2	2S----	B2run09-5a	-207.3	9.4E+01	775.2	1.1E+02	398.3	9.5E+01	1.1E+02	93.8	4.3E+01	1	38.0	1.4E+00	237.2	1.3E+01	234.3	1.1E+01
2	2S----	B2run09-5b	-320.8	6.9E+01	668.7	8.1E+01	-85.8	6.1E+01	3.8E+02	63.2	6.4E+01	1	63.4	9.2E-01	136.9	9.6E+00	133.7	8.9E+00
2	2S----	B2run09-6	-440.3	8.1E+01	808.1	9.8E+01	-287.4	7.1E+01	6.1E+02	77.7	5.4E+01	1	56.8	1.4E+00	139.0	1.2E+01	139.5	9.9E+00
2	2S----	B2run12-1	-196.8	8.5E+01	517.0	9.1E+01	-236.7	7.8E+01	5.3E+02	89.2	7.4E+01	2	76.9	1.3E+00	132.8	9.0E+00	128.4	9.9E+00
2	2S----	B2run12-2	-510.1	7.0E+01	873.9	8.6E+01	-370.6	6.6E+01	6.7E+02	75.2	1.1E+02	2	110.1	1.4E+00	130.0	1.1E+01	121.7	1.0E+01
2	2S----	B2t05	-75.7	1.0E+02	347.6	1.0E+02	-189.2	7.3E+01	4.3E+02	79.4	5.9E+01	2	62.7	2.1E+00	116.1	1.1E+01	108.1	9.4E+00

Build	Exp Code	Run	Nu,C2,d,av	+/-	Nu,C3,u,av	+/-	Nu,C3,d,av	+/-	Nu,C4,u,av	+/-	Nush,C2	+/-	Nush,C3	+/-	finNu,D2,av	+/-	finNu,D3,av	+/-
2	2S----	B2t06	-171.5	8.5E+01	605.9	9.8E+01	-30.0	8.9E+01	4.5E+02	95.7	4.6E+01	2	43.6	1.6E+00	187.6	1.2E+01	195.1	1.1E+01
2	2S----	B2t07-a	-25.5	8.8E+01	462.2	9.9E+01	82.0	7.8E+01	3.7E+02	81.0	4.7E+01	1	43.9	1.1E+00	192.5	1.0E+01	208.4	8.9E+00
2	2S----	B2t07-b	-280.0	8.2E+01	602.2	9.6E+01	-118.2	6.9E+01	3.9E+02	75.1	6.7E+01	1	62.3	1.3E+00	129.5	9.4E+00	121.2	9.3E+00
2	2S----	B2t09a	79.5	1.2E+02	381.7	1.2E+02	18.9	1.0E+02	4.6E+02	99.8	4.6E+01	2	40.2	2.6E+00	205.8	1.7E+01	218.8	1.9E+01
2	2S----	B2t09b	122.3	9.4E+01	328.1	9.8E+01	58.3	8.0E+01	4.1E+02	80.9	4.3E+01	1	38.2	1.1E+00	201.9	1.3E+01	216.8	9.8E+00
2	2S----	B2t09-c	119.7	9.2E+01	329.9	9.9E+01	73.9	7.7E+01	3.9E+02	83.8	4.3E+01	1	38.2	9.9E-01	201.4	1.1E+01	215.7	9.8E+00
2	2S----	B2t10	-224.4	8.1E+01	468.8	8.6E+01	-78.3	5.7E+01	2.8E+02	59.3	5.7E+01	2	53.2	1.5E+00	100.0	8.8E+00	95.3	8.7E+00
2	2S----	B2t11	-275.2	1.2E+02	566.7	1.4E+02	129.5	1.0E+02	1.0E+02	101.3	4.4E+01	3	39.3	2.1E+00	117.2	1.4E+01	108.0	1.4E+01
2	2S----	B2t12	-61.3	7.4E+01	303.5	7.9E+01	-54.3	7.2E+01	2.6E+02	76.3	5.0E+01	1	48.9	1.2E+00	104.0	8.6E+00	95.2	8.3E+00
2	2s----	B2t13-a	4.9	1.1E+03	484.1	7.9E+02	-18.9	6.1E+02	5.2E+02	710.0	4.8E+01	4	43.7	3.8E+00	216.4	2.5E+02	230.9	6.6E+01
2	2S----	B2t13-b	60.2	9.0E+01	384.3	9.4E+01	17.3	7.7E+01	4.5E+02	82.0	4.6E+01	1	41.7	1.1E+00	198.5	1.1E+01	216.4	1.2E+01
2	2S----	B2t14	131.1	9.0E+01	303.5	9.4E+01	-78.9	7.6E+01	5.5E+02	86.3	4.6E+01	1	41.8	1.0E+00	194.5	1.1E+01	212.7	9.2E+00
2	2S----	B2t15-a	168.7	7.4E+01	258.6	7.5E+01	-107.6	7.0E+01	5.8E+02	75.9	4.6E+01	1	42.2	8.6E-01	191.9	1.2E+01	210.9	8.6E+00
2	2S----	B2t15-b	-308.1	9.8E+01	641.6	1.1E+02	-167.2	8.1E+01	4.4E+02	86.8	6.3E+01	1	62.0	1.4E+00	132.2	1.2E+01	120.5	1.0E+01
2	2S----	B2t16-a	105.5	1.8E+02	353.1	1.9E+02	-99.9	1.5E+02	5.9E+02	180.8	4.8E+01	4	44.2	2.5E+00	205.0	2.8E+01	221.8	2.8E+01
2	2S----	B2t16-b	168.1	7.2E+01	262.6	7.3E+01	-81.4	6.7E+01	5.6E+02	73.1	4.6E+01	1	42.9	1.0E+00	193.2	9.5E+00	214.5	9.0E+00
2	2S----	B2t16-c	147.9	8.7E+01	283.6	9.1E+01	-76.1	8.5E+01	5.5E+02	97.2	4.6E+01	1	43.1	9.8E-01	193.4	1.3E+01	213.7	9.4E+00
2	2S----	B2t17-a	-386.0	9.9E+01	742.7	1.2E+02	-189.5	8.4E+01	4.7E+02	92.5	6.4E+01	2	62.5	1.9E+00	136.9	1.3E+01	124.2	1.1E+01
2	2S----	B2t17-b	-340.0	8.2E+01	682.3	9.8E+01	-179.0	7.1E+01	4.6E+02	77.5	6.5E+01	1	63.5	1.1E+00	134.1	1.0E+01	121.6	9.8E+00
2	2S----	B2t17-c	-356.1	9.1E+01	704.1	1.1E+02	-185.9	6.8E+01	4.7E+02	75.9	6.4E+01	1	62.6	1.3E+00	135.2	1.2E+01	123.2	9.3E+00
2	2S----	B2t18-a	-42.6	6.8E+01	281.9	7.2E+01	-8.1	6.3E+01	2.0E+02	64.4	4.6E+01	2	43.7	1.5E+00	102.6	7.2E+00	92.7	8.0E+00
2	2S----	B2t18-b	-59.9	5.6E+01	295.3	6.0E+01	7.9	6.0E+01	1.8E+02	60.5	4.6E+01	1	43.2	1.1E+00	100.5	8.0E+00	90.2	6.3E+00
2	2S----	B2t18-c	-236.9	6.6E+01	539.5	7.5E+01	-155.8	5.4E+01	4.1E+02	58.7	7.3E+01	2	76.4	1.3E+00	124.5	1.0E+01	115.3	7.9E+00
2	2S----	B2t18-d	-235.8	8.9E+01	536.7	9.6E+01	-160.9	6.9E+01	4.2E+02	75.0	7.2E+01	1	75.4	1.5E+00	123.7	8.6E+00	114.5	1.0E+01
2	2S----	B2t19-a	-189.9	6.1E+01	445.5	6.7E+01	93.6	5.1E+01	1.1E+02	50.2	4.6E+01	1	42.6	1.3E+00	105.6	7.9E+00	94.2	6.6E+00
2	2S----	B2t19-b	-205.5	6.9E+01	461.5	7.7E+01	90.6	6.6E+01	1.1E+02	66.6	4.6E+01	1	42.3	1.0E+00	105.0	7.7E+00	94.0	7.4E+00
2	2S----	B2t19-c	-255.5	6.6E+01	563.8	7.5E+01	-166.9	7.7E+01	4.3E+02	84.2	7.3E+01	2	75.9	1.4E+00	126.0	9.8E+00	117.0	8.8E+00
2	2S----	B2t19-d	-269.9	7.5E+01	581.2	8.6E+01	-175.7	6.5E+01	4.4E+02	72.9	7.2E+01	1	75.6	1.4E+00	126.4	8.4E+00	116.5	8.1E+00

Build	Exp Code	Run	Tsh,C2,out(K)	+/-	Tsh,C3,out(K)	+/-	k_air(Tin)	+/-	V (m/s)	+/-
2	2S----	B2run02-2	329	0.3	3.2E+02	2.46	2.8E-02	1.98E-05	44.73	3.8E-02
2	2S----	B2run02-3	414	0.6	3.2E+02	10.35	2.8E-02	7.37E-05	42.00	1.3E-01
2	2S----	B2run03-1	405	0.7	3.3E+02	11.98	2.8E-02	3.11E-05	48.12	6.2E-02
2	2S----	B2run04-1	397	0.4	3.2E+02	9.09	2.8E-02	4.44E-05	36.19	6.8E-02
2	2S----	B2run04-2	398	0.4	3.2E+02	9.33	2.8E-02	4.25E-05	36.46	6.6E-02
2	2S----	B2run04-3	397	0.2	3.2E+02	9.08	2.8E-02	8.21E-05	23.65	8.2E-02
2	2S----	B2run04-4	397	0.4	3.2E+02	9.15	2.8E-02	7.00E-05	23.69	7.0E-02
2	2S----	B2run04-7	398	0.5	3.2E+02	9.20	2.8E-02	5.80E-05	23.97	5.9E-02
2	2S----	B2run06-1	404	0.2	4.1E+02	0.17	2.7E-02	1.78E-05	27.70	2.1E-02
2	2S----	B2run06-2	411	0.2	4.2E+02	0.17	2.7E-02	1.70E-05	27.85	2.0E-02
2	2S----	B2run08-1	399	0.3	4.1E+02	0.31	2.7E-02	1.94E-05	17.84	1.5E-02
2	2S----	B2run08-2	396	0.2	4.0E+02	0.16	2.7E-02	2.03E-05	17.75	1.5E-02
2	2S----	B2run08-3	402	0.3	4.0E+02	0.30	2.8E-02	1.66E-05	18.14	1.3E-02
2	2S----	B2run08-4	404	0.2	4.1E+02	0.21	2.8E-02	1.88E-05	27.88	2.2E-02
2	2S----	B2run08-5	401	0.2	4.0E+02	0.20	2.8E-02	1.75E-05	28.09	2.1E-02
2	2S----	B2run08-6	400	0.2	4.0E+02	0.17	2.8E-02	1.62E-05	27.86	1.9E-02
2	2S----	B2run08-7	375	0.2	3.8E+02	0.21	2.8E-02	1.54E-05	28.19	1.8E-02
2	2S----	B2run09-1	395	0.3	4.0E+02	0.38	2.7E-02	2.01E-05	46.21	4.0E-02
2	2S----	B2run09-2	399	0.3	4.0E+02	0.33	2.7E-02	2.27E-05	46.13	4.5E-02
2	2S----	B2run09-3	398	0.2	4.0E+02	0.16	2.7E-02	1.99E-05	46.17	3.9E-02
2	2S----	B2run09-5a	396	0.2	4.0E+02	0.30	2.7E-02	2.07E-05	46.02	4.1E-02
2	2S----	B2run09-5b	398	0.2	4.0E+02	0.17	2.7E-02	2.02E-05	46.02	4.0E-02
2	2S----	B2run09-6	375	0.2	3.8E+02	0.17	2.8E-02	1.94E-05	46.19	3.8E-02
2	2S----	B2run12-1	392	0.2	3.9E+02	0.20	2.7E-02	1.98E-05	27.62	2.4E-02
2	2S----	B2run12-2	397	0.2	4.0E+02	0.19	2.7E-02	1.85E-05	27.24	2.2E-02
2	2S----	B2t05	381	0.3	3.8E+02	0.27	2.7E-02	1.79E-05	29.62	2.3E-02

Build	Exp Code	Run	Tsh,C2,out(K)	+/-	Tsh,C3,out(K)	+/-	k_air(Tin)	+/-	V (m/s)	+/-
2	2S----	B2t06	369	0.2	3.7E+02	0.19	2.7E-02	1.74E-05	43.30	3.2E-02
2	2S----	B2t07-a	385	0.2	3.9E+02	0.18	2.8E-02	1.74E-05	44.38	3.3E-02
2	2S----	B2t07-b	382	0.2	3.8E+02	0.17	2.8E-02	1.94E-05	44.50	3.7E-02
2	2S----	B2t09a	375	0.3	3.8E+02	0.34	2.8E-02	1.80E-05	43.63	3.3E-02
2	2S----	B2t09b	378	0.2	3.8E+02	0.16	2.8E-02	1.90E-05	43.39	3.5E-02
2	2S----	B2t09-c	378	0.2	3.8E+02	0.16	2.7E-02	1.70E-05	43.41	3.1E-02
2	2S----	B2t10	374	0.2	3.8E+02	0.17	2.7E-02	1.40E-05	18.63	1.1E-02
2	2S----	B2t11	382	0.4	3.8E+02	0.32	2.7E-02	2.57E-05	27.60	3.0E-02
2	2S----	B2t12	381	0.2	3.8E+02	0.16	2.7E-02	1.99E-05	22.52	1.9E-02
2	2s----	B2t13-a	381	0.5	3.8E+02	0.47	2.8E-02	8.51E-05	44.81	1.6E-01
2	2S----	B2t13-b	383	0.2	3.9E+02	0.16	2.7E-02	2.00E-05	44.70	3.8E-02
2	2S----	B2t14	384	0.2	3.9E+02	0.16	2.8E-02	2.17E-05	44.58	4.1E-02
2	2S----	B2t15-a	383	0.2	3.9E+02	0.16	2.7E-02	1.92E-05	44.75	3.7E-02
2	2S----	B2t15-b	384	0.2	3.9E+02	0.16	2.8E-02	2.00E-05	44.86	3.8E-02
2	2S----	B2t16-a	383	0.4	3.9E+02	0.37	2.8E-02	3.34E-05	44.62	6.3E-02
2	2S----	B2t16-b	385	0.2	3.9E+02	0.16	2.7E-02	1.86E-05	44.36	3.5E-02
2	2S----	B2t16-c	385	0.2	3.9E+02	0.16	2.7E-02	2.88E-05	44.45	5.5E-02
2	2S----	B2t17-a	384	0.2	3.9E+02	0.26	2.8E-02	1.95E-05	44.60	3.7E-02
2	2S----	B2t17-b	384	0.2	3.9E+02	0.17	2.8E-02	1.79E-05	44.59	3.4E-02
2	2S----	B2t17-c	385	0.2	3.9E+02	0.17	2.8E-02	1.53E-05	44.83	2.9E-02
2	2S----	B2t18-a	375	0.2	3.8E+02	0.20	2.7E-02	1.76E-05	20.06	1.5E-02
2	2S----	B2t18-b	376	0.2	3.8E+02	0.17	2.7E-02	1.68E-05	20.15	1.5E-02
2	2S----	B2t18-c	377	0.2	3.8E+02	0.17	2.7E-02	1.74E-05	20.03	1.5E-02
2	2S----	B2t18-d	378	0.2	3.8E+02	0.17	2.7E-02	1.86E-05	20.23	1.6E-02
2	2S----	B2t19-a	377	0.2	3.8E+02	0.19	2.7E-02	1.80E-05	21.17	1.7E-02
2	2S----	B2t19-b	377	0.2	3.8E+02	0.17	2.7E-02	1.91E-05	21.37	1.8E-02
2	2S----	B2t19-c	377	0.2	3.8E+02	0.17	2.7E-02	1.43E-05	20.95	1.3E-02
2	2S----	B2t19-d	378	0.2	3.8E+02	0.16	2.7E-02	1.86E-05	21.13	1.7E-02

Appendix 6.3: Test conditions and main non-dimensional results for Build 3

Build	Exp Code	Run	ExpDate	LDA code	FCF pos	Lab atm press (Pa)	Comments	Refi	+/-	Rez	+/-	BDTav	+/-	finBDTav	+/-	Ro	+/-
3	3S---- -----	B3run2-1	10/10/2002	0	0	1.009E+05	run OK	9.95E+05	1.7E+03	1.65E+05	1.3E+02	0.056	1.0E-03	0.056	1.0E-03	3.17	3.1E-03
3	3S---- -----	B3run2-2	10/10/2002	0	0	1.009E+05	run OK	9.92E+05	1.3E+03	1.65E+05	9.4E+01	0.056	7.8E-04	0.056	7.8E-04	3.17	2.4E-03
3	3S---- -----	B3run3-1	10/21/2002	101	0	9.962E+04	run OK	1.01E+06	1.6E+03	1.56E+05	1.1E+02	0.054	9.2E-04	0.054	9.2E-04	2.94	2.7E-03
3	3S---- -----	B3run4-1	10/23/2002	101	0	1.006E+05	run OK	1.00E+06	2.0E+03	6.27E+04	5.5E+01	0.062	1.1E-03	0.062	1.1E-03	1.19	1.4E-03
3	3S---- -----	B3run4-2	10/23/2002	0	0	1.006E+05	run OK	1.00E+06	2.4E+03	6.30E+04	6.5E+01	0.063	1.4E-03	0.063	1.4E-03	1.20	1.6E-03
3	3S---- -----	B3run5-1	10/29/2002	101	0	1.012E+05	run OK	9.90E+05	1.8E+03	1.07E+05	8.2E+01	0.054	1.1E-03	0.054	1.1E-03	2.05	2.1E-03
3	3S---- -----	B3run5-3	10/29/2002	0	0	1.012E+05	run OK	1.02E+06	1.3E+03	1.08E+05	5.8E+01	0.059	6.9E-04	0.059	6.9E-04	2.03	1.4E-03
3	3S---- -----	B3run6-1	11/14/2002	101	0	9.806E+04	run OK	9.63E+05	1.5E+03	9.85E+04	6.3E+01	0.058	8.8E-04	0.058	8.8E-04	1.95	1.7E-03
3	3S---- -----	B3run6-2	11/14/2002	0	0	9.806E+04	run OK	9.76E+05	5.1E+03	9.79E+04	2.2E+02	0.054	3.1E-03	0.054	3.1E-03	1.91	5.6E-03
3	3S---- -----	B3run6-3	11/14/2002	0	0	9.806E+04	run OK	9.69E+05	1.4E+03	9.77E+04	6.2E+01	0.055	8.8E-04	0.055	8.8E-04	1.92	1.6E-03
3	3S---- -----	B3run7-1	11/28/2002	101	0	1.007E+05	run OK	1.03E+06	1.7E+03	5.14E+04	3.7E+01	0.068	1.2E-03	0.068	1.2E-03	0.95	9.2E-04
3	3S---- -----	B3run7-2	11/28/2002	0	0	1.007E+05	run OK	9.70E+05	2.2E+03	4.87E+04	4.7E+01	0.063	1.3E-03	0.063	1.3E-03	0.96	1.2E-03
3	3S---- -----	B3run7-4	11/28/2002	0	0	1.007E+05	run OK	5.34E+05	1.5E+03	4.83E+04	5.9E+01	0.074	1.7E-03	0.074	1.7E-03	1.73	2.8E-03
3	3S---- -----	B3run8-1	12/03/2002	101	0	1.011E+05	run OK	4.74E+05	8.3E+02	4.72E+04	3.4E+01	0.087	1.0E-03	0.087	1.0E-03	1.90	2.1E-03
3	3S---- -----	B3run9-1	12/05/2002	101	0	1.025E+05	run OK	4.96E+05	7.1E+02	1.51E+05	9.3E+01	0.066	8.3E-04	0.066	8.3E-04	5.81	4.7E-03
3	3S---- -----	B3run9-2	12/05/2002	0	0	1.025E+05	run OK	1.51E+06	2.2E+03	4.83E+04	3.0E+01	0.061	8.4E-04	0.061	8.4E-04	0.61	5.0E-04
3	3S---- -----	B3run9-3	12/05/2002	0	0	1.025E+05	run OK	1.51E+06	2.1E+03	4.83E+04	2.9E+01	0.060	7.9E-04	0.060	7.9E-04	0.61	4.8E-04
3	3S---- -----	B3run9-4	12/05/2002	0	0	1.025E+05	run OK	1.54E+06	2.4E+03	1.03E+05	7.0E+01	0.049	9.0E-04	0.049	9.0E-04	1.28	1.2E-03
3	3S---- -----	B3run12-1	3/18/2003	0	0	1.033E+05	run OK	9.15E+05	1.1E+03	6.93E+04	3.6E+01	0.064	7.3E-04	0.064	7.3E-04	1.44	1.0E-03
3	3S---- -----	B3run13-1	04/10/2003	0	0	1.010E+05	not fully steady state	1.00E+06	1.8E+03	1.95E+05	1.5E+02	0.053	1.0E-03	0.053	1.0E-03	3.71	4.0E-03
3	3S---- -----	B3run13-2	04/10/2003	0	0	1.010E+05	measurement OK	1.00E+06	2.5E+03	1.96E+05	2.1E+02	0.054	1.4E-03	0.054	1.4E-03	3.72	5.2E-03
3	3S---- -----	B3run13-3	04/10/2003	0	0	1.010E+05	measurement OK	3.93E+06	5.3E+03	7.22E+04	4.2E+01	0.044	7.7E-04	0.044	7.7E-04	0.35	2.7E-04

Build	Exp Code	Run	ExpDate	LDA code	FCF pos	Lab atm press (Pa)	Comments	Refi	+/-	Rez	+/-	BDTav	+/-	finBDTav	+/-	Ro	+/-
3	3S---- -----	B3run15-1	4/15/2003	0	0	1.019E+05	run OK	1.00E+06	1.5E+03	8.44E+04	5.4E+01	0.056	8.5E-04	0.056	8.5E-04	1.60	1.5E-03
3	3S---- -----	B3run15-2	4/15/2003	0	0	1.019E+05	run OK	2.01E+06	2.7E+03	4.10E+04	2.3E+01	0.054	7.6E-04	0.054	7.6E-04	0.39	3.0E-04
3	3S---- -----	B3run16-1	4/16/2003	0	0	1.024E+05	run OK	1.96E+06	2.7E+03	8.18E+04	4.8E+01	0.038	7.3E-04	0.038	7.3E-04	0.80	6.3E-04
3	3S---- -----	B3run16-2	4/16/2003	0	0	1.024E+05	run OK	3.95E+06	5.3E+03	7.98E+04	4.6E+01	0.037	7.5E-04	0.037	7.5E-04	0.39	3.0E-04
3	3S---- -----	B3run17-1	4/24/2003	0	0	1.016E+05	run OK	2.00E+06	2.5E+03	1.64E+05	8.8E+01	0.035	6.8E-04	0.035	6.8E-04	1.57	1.1E-03
3	3S---- -----	B3run17-2	4/24/2003	0	0	1.016E+05	run OK	2.00E+06	2.8E+03	1.63E+05	1.0E+02	0.035	8.0E-04	0.035	8.0E-04	1.56	1.3E-03
3	3S---- -----	B3run17-3	4/24/2003	0	0	1.016E+05	run OK	3.98E+06	5.5E+03	1.63E+05	9.7E+01	0.027	7.3E-04	0.027	7.3E-04	0.78	6.1E-04
3	3S---- -----	B3run17-4	4/24/2003	0	0	1.016E+05	run OK	3.98E+06	5.4E+03	1.63E+05	9.5E+01	0.027	7.4E-04	0.027	7.4E-04	0.78	6.0E-04
3	3S---- -----	B3run17-5	4/24/2003	0	0	1.016E+05	run OK	1.02E+06	1.2E+03	4.21E+04	2.2E+01	0.069	7.0E-04	0.069	7.0E-04	0.79	5.5E-04
3	3S---- -----	B3run17-6	4/24/2003	0	0	1.016E+05	run OK	1.02E+06	1.5E+03	4.13E+04	2.5E+01	0.070	8.3E-04	0.070	8.3E-04	0.77	6.3E-04
3	3S---- -----	B3run18-1	6/21/2003	101	0	1.021E+05	run OK	4.96E+05	6.8E+02	5.13E+04	3.1E+01	0.081	8.4E-04	0.081	8.4E-04	1.97	1.5E-03
3	3S---- -----	B3run18-2	6/21/2003	101	0	1.021E+05	run OK	1.50E+06	2.0E+03	4.93E+04	2.8E+01	0.052	7.9E-04	0.052	7.9E-04	0.63	4.8E-04
3	3S---- -----	B3run18-3	6/21/2003	101	0	1.021E+05	run OK	1.03E+06	1.3E+03	1.01E+05	5.3E+01	0.050	6.8E-04	0.050	6.8E-04	1.87	1.3E-03
3	3S---- -----	B3run19-1	6/24/2003	101	0	1.021E+05	run OK	1.02E+06	1.9E+03	1.03E+05	8.0E+01	0.051	1.2E-03	0.051	1.2E-03	1.92	2.1E-03
3	3S---- -----	B3run20-1	6/30/2003	101	0	9.993E+04	run OK	1.16E+06	3.8E+03	9.06E+04	1.3E+02	0.050	1.8E-03	0.050	1.8E-03	1.49	2.8E-03
3	3S---- -----	B3run21-1	07/01/2003	101	0	9.993E+04	run OK	1.20E+06	1.6E+03	9.29E+04	5.4E+01	0.046	7.7E-04	0.046	7.7E-04	1.48	1.1E-03
3	3S---- -----	B3run22-1	07/07/2003	101	0	1.024E+05	run OK	1.24E+06	1.7E+03	4.91E+04	3.0E+01	0.061	8.1E-04	0.061	8.1E-04	0.75	6.1E-04
3	3S---- -----	B3run22-2	07/07/2003	101	0	1.024E+05	run OK	2.41E+06	3.4E+03	8.60E+04	5.2E+01	0.033	8.5E-04	0.033	8.5E-04	0.68	5.4E-04
3	3S---- -----	B3run23-1	07/09/2003	101	0	1.022E+05	run OK	2.02E+06	2.4E+03	9.91E+04	5.1E+01	0.035	6.8E-04	0.035	6.8E-04	0.93	6.2E-04
3	3S---- -----	B3run24-1	7/29/2003	101	0	1.022E+05	run OK	1.31E+06	1.9E+03	9.74E+04	5.9E+01	0.050	7.9E-04	0.050	7.9E-04	1.41	1.2E-03
3	3S---- -----	B3run24-2	7/29/2003	0	0	1.022E+05	run OK	9.94E+05	1.7E+03	8.79E+04	6.3E+01	0.047	9.9E-04	0.047	9.9E-04	1.69	1.6E-03
3	3S---- ----	B3run25-1	8/27/2003	101	0	1.015E+05	run OK	1.15E+06	1.4E+03	1.71E+05	8.7E+01	0.045	6.6E-04	0.045	6.6E-04	2.84	1.9E-03
3	3S---- -----	B3run26-1	10/17/2003	101	0	1.014E+05	run OK	2.46E+06	2.9E+03	4.71E+04	2.3E+01	0.043	6.5E-04	0.043	6.5E-04	0.37	2.5E-04
3	3S---- -----	B3run27-1	10/31/2003	101	0	9.778E+04	LDA file is identified as run27-2	2.00E+06	2.7E+03	1.75E+05	1.0E+02	0.029	8.0E-04	0.029	8.0E-04	1.66	1.3E-03
3	3S---- -----	B3run28-1	11/12/2003	101	0	1.017E+05	run OK	4.12E+06	5.7E+03	1.16E+05	6.9E+01	0.027	7.7E-04	0.027	7.7E-04	0.54	4.4E-04
3	3S---- -----	B3run28-2	11/12/2003	101	0	1.017E+05	run OK	4.02E+06	5.7E+03	5.77E+04	3.5E+01	0.040	7.8E-04	0.040	7.8E-04	0.27	2.2E-04
3	3S---- -----	B3run30-1	12/10/2003	101	0	1.016E+05	run OK	4.07E+06	5.3E+03	1.84E+05	1.0E+02	0.021	7.2E-04	0.021	7.2E-04	0.86	6.3E-04

Build	Exp Code	Run	ExpDate	LDA code	FCF pos	Lab atm press (Pa)	Comments	Refi	+/-	Rez	+/-	BDTav	+/-	finBDTav	+/-	Ro	+/-
3	3S---- -----	B3run31-1	12/12/2003	101	0	1.018E+05	run OK	5.17E+05	7.7E+02	1.85E+05	1.2E+02	0.050	8.2E-04	0.050	8.2E-04	6.82	5.9E-03
3	3S---- -----	B3run32-1	1/16/2004	101	0	9.956E+04	run OK	4.92E+05	6.9E+02	9.18E+04	5.5E+01	0.089	8.3E-04	0.089	8.3E-04	3.56	2.9E-03
3	3S---- -----	B3run33-1	04/07/2004	0	2	1.014E+05	FCF	9.18E+05	1.5E+03	8.85E+04	6.4E+01	0.067	9.3E-04	0.067	9.3E-04	1.84	1.8E-03
3	3S---- -----	B3run33-2	04/07/2004	0	2	1.014E+05	FCF	2.32E+06	3.0E+03	8.79E+04	4.9E+01	0.040	7.4E-04	0.040	7.4E-04	0.72	5.3E-04
3	3S---- -----	B3run33-3	04/07/2004	0	2	1.014E+05	FCF	1.18E+06	1.5E+03	4.38E+04	2.4E+01	0.067	7.4E-04	0.067	7.4E-04	0.71	5.1E-04
3	3S---- -----	B3run33-4	04/07/2004	0	2	1.014E+05	FCF	1.07E+06	1.5E+03	1.72E+05	1.0E+02	0.046	8.1E-04	0.046	8.1E-04	3.06	2.4E-03
3	3S---- -----	B3run33-5	04/07/2004	0	2	1.014E+05	FCF	4.81E+06	7.1E+03	1.73E+05	1.1E+02	0.026	8.5E-04	0.026	8.5E-04	0.69	5.8E-04
3	3S---- -----	B3run33-6	04/07/2004	0	2	1.014E+05	FCF	4.74E+06	6.0E+03	3.43E+04	1.9E+01	0.053	7.4E-04	0.053	7.4E-04	0.14	1.0E-04
3	3S---- -----	B3run33-7	04/07/2004	0	2	1.014E+05	FCF	1.16E+06	1.4E+03	8.71E+04	4.4E+01	0.060	6.9E-04	0.060	6.9E-04	1.43	9.6E-04
3	3S---- -----	B3run33-8	04/07/2004	0	2	1.014E+05	FCF	2.34E+06	3.0E+03	1.73E+05	9.6E+01	0.040	7.3E-04	0.040	7.3E-04	1.41	1.0E-03
3	3S---- -----	B3run33-9	04/07/2004	0	2	1.014E+05	FCF	2.31E+06	2.7E+03	4.49E+04	2.2E+01	0.052	6.7E-04	0.052	6.7E-04	0.37	2.4E-04
3	3S---- -----	B3run33-10	04/07/2004	0	2	1.014E+05	FCF	5.02E+06	5.7E+03	8.50E+04	4.1E+01	0.036	6.1E-04	0.036	6.1E-04	0.32	2.1E-04
3	3S---- -----	B3run34-1	4/13/2004	0	1	1.026E+05	FCF	1.17E+06	1.7E+03	1.13E+05	6.8E+01	0.050	8.0E-04	0.050	8.0E-04	1.83	1.5E-03
3	3S---- -----	B3run34-2	4/13/2004	0	1	1.026E+05	FCF	4.76E+06	5.7E+03	1.09E+05	5.7E+01	0.028	7.1E-04	0.028	7.1E-04	0.44	3.0E-04
3	3S---- -----	B3run34-3	4/13/2004	0	1	1.026E+05	FCF	2.36E+06	3.3E+03	6.52E+04	3.9E+01	0.039	8.1E-04	0.039	8.1E-04	0.53	4.2E-04
3	3S---- -----	B3run34-4	4/13/2004	0	1	1.026E+05	FCF	1.19E+06	1.5E+03	6.59E+04	3.4E+01	0.052	6.9E-04	0.052	6.9E-04	1.05	7.6E-04
3	3S---- -----	B3run34-5	4/13/2004	0	1	1.026E+05	FCF	2.37E+06	3.0E+03	1.09E+05	6.1E+01	0.034	7.0E-04	0.034	7.0E-04	0.88	6.4E-04
3	3S---- -----	B3run34-6	4/13/2004	0	1	1.026E+05	FCF	4.77E+06	5.0E+03	1.92E+05	8.6E+01	0.020	5.8E-04	0.020	5.8E-04	0.77	4.5E-04
3	3S---- -----	B3run34-7	4/13/2004	0	1	1.026E+05	FCF	4.76E+06	5.8E+03	6.17E+04	3.2E+01	0.034	7.0E-04	0.034	7.0E-04	0.25	1.7E-04
3	3S---- -----	B3run34-8	4/13/2004	0	1	1.026E+05	FCF	2.36E+06	2.9E+03	1.92E+05	1.0E+02	0.029	7.0E-04	0.029	7.0E-04	1.55	1.1E-03
3	3S---- -----	B3run34-9	4/13/2004	0	1	1.026E+05	FCF	1.18E+06	1.7E+03	1.90E+05	1.1E+02	0.037	7.8E-04	0.037	7.8E-04	3.08	2.5E-03
3	3S---- -----	B3run35-1	4/15/2004	0	3	1.017E+05	FCF	1.17E+06	1.4E+03	8.91E+04	4.7E+01	0.053	7.1E-04	0.053	7.1E-04	1.45	1.0E-03
3	3S---- -----	B3run35-2	4/15/2004	0	3	1.017E+05	FCF	2.36E+06	3.2E+03	1.72E+05	1.0E+02	0.027	7.6E-04	0.027	7.6E-04	1.39	1.1E-03
3	3S---- -----	B3run35-3	4/15/2004	0	3	1.017E+05	FCF	2.36E+06	2.8E+03	8.55E+04	4.4E+01	0.031	6.9E-04	0.031	6.9E-04	0.69	4.7E-04
3	3S---- -----	B3run35-4	4/15/2004	0	3	1.017E+05	FCF	4.79E+06	7.9E+03	1.70E+05	1.2E+02	0.017	8.9E-04	0.017	8.9E-04	0.68	6.9E-04
3	3S---- -----	B3run35-5	4/15/2004	0	3	1.017E+05	FCF	2.34E+06	2.8E+03	4.08E+04	2.1E+01	0.045	6.7E-04	0.045	6.7E-04	0.33	2.3E-04
3	3S---- -----	B3run35-6	4/15/2004	0	3	1.017E+05	FCF	4.79E+06	6.2E+03	8.43E+04	4.4E+01	0.024	6.9E-04	0.024	6.9E-04	0.34	2.7E-04

Build	Exp Code	Run	ExpDate	LDA code	FCF pos	Lab atm press (Pa)	Comments	Refi	+/-	Rez	+/-	BDTav	+/-	finBDTav	+/-	Ro	+/-
3	3S---- -----	B3run35-7	4/15/2004	0	3	1.017E+05	FCF	1.15E+06	1.3E+03	4.62E+04	2.3E+01	0.058	6.6E-04	0.058	6.6E-04	0.77	5.0E-04
3	3S---- -----	B3run35-8	4/15/2004	0	3	1.017E+05	FCF	1.15E+06	1.6E+03	1.71E+05	1.0E+02	0.041	7.9E-04	0.041	7.9E-04	2.84	2.3E-03
3	3S---- -----	B3run35-9	4/15/2004	0	3	1.017E+05	FCF	4.75E+06	6.1E+03	3.95E+04	2.2E+01	0.029	7.1E-04	0.029	7.1E-04	0.16	1.2E-04
3	3S---- -----	B3run36-1	9/20/2004	110	0	1.012E+05	run OK	1.15E+06	1.6E+03	1.10E+05	6.7E+01	0.057	8.1E-04	0.057	8.1E-04	1.82	1.5E-03
3	3S---- -----	B3run37-1	9/24/2004	0	0	1.021E+05	LDA Vr Vf unsuccesful	1.88E+06	8.6E+03	5.47E+04	1.1E+02	0.001	3.0E-03	0.001	3.0E-03	0.56	1.5E-03
3	3S---- -----	B3run38-1	9/27/2004	110	0	1.024E+05	Run OK	3.99E+05	5.8E+02	1.57E+05	9.7E+01	0.067	8.3E-04	0.067	8.3E-04	7.51	6.2E-03
3	3S---- -----	B3run39-1	9/28/2004	110	0	1.021E+05	run OK	1.93E+06	2.5E+03	5.31E+04	2.9E+01	-0.001	7.0E-04	-0.001	7.0E-04	0.53	4.0E-04
3	3S---- -----	B3run40-1	10/05/2004	110	0	1.011E+05	run OK	3.88E+05	4.9E+02	6.07E+04	3.3E+01	0.107	7.9E-04	0.107	7.9E-04	2.98	2.2E-03
3	3S---- -----	B3run44-1	12/20/2004	0	0	1.022E+05	run OK	1.99E+06	1.1E+04	1.65E+05	3.8E+02	0.004	3.4E-03	0.004	3.4E-03	1.58	4.8E-03
3	3S---- -----	B3run44-2	12/20/2004	0	0	1.022E+05	run OK	1.97E+06	1.2E+04	1.64E+05	4.2E+02	0.012	3.6E-03	0.012	3.6E-03	1.59	5.4E-03
3	3S---- -----	B3run44-3	12/20/2004	110	0	1.022E+05	run OK	1.93E+06	2.7E+03	1.63E+05	1.0E+02	0.016	7.7E-04	0.016	7.7E-04	1.61	1.3E-03
3	3S---- -----	B3run45-1	12/22/2004	110	0	1.015E+05	no rotation of rotor	6.86E+02	1.2E+00	5.09E+04	3.8E+01	-0.010	9.2E-04	-0.010	9.2E-04	1415.40	1.4E+00

Build	Exp Code	Run	Bo*	+/-	Grsh,C2	+/-	Grsh,C3	+/-	Pr	+/-	Rot Speed (rpm)	+/-	Mass Flow (kg/s)	Ø	+/-	finØ	+/-
3	3S--------	B3run2-1	0.075	7.4E-04	1.45E+08	1.8E+06	1.71E+08	2.0E+06	0.705	5.2E-05	1417.5	1.8E-01	0.610	0.310	5.6E-02	0.163	3.5E-02
3	3S--------	B3run2-2	0.075	5.7E-04	1.45E+08	1.4E+06	1.70E+08	1.3E+06	0.705	3.9E-05	1415.3	1.4E-01	0.610	0.296	2.9E-02	0.162	1.3E-02
3	3S--------	B3run3-1	0.079	7.5E-04	1.50E+08	1.6E+06	1.73E+08	1.7E+06	0.705	4.7E-05	1480.7	1.0E-01	0.578	0.357	4.7E-02	0.187	1.9E-02
3	3S--------	B3run4-1	0.209	2.1E-03	1.62E+08	2.1E+06	1.71E+08	2.1E+06	0.706	5.8E-05	1311.8	2.4E-01	0.230	1.540	1.3E+00	0.858	8.0E-01
3	3S--------	B3run4-2	0.211	2.6E-03	1.65E+08	2.6E+06	1.73E+08	2.7E+06	0.706	6.7E-05	1309.1	1.2E-01	0.231	1.419	5.3E+00	0.803	3.2E+00
3	3S--------	B3run5-1	0.113	1.2E-03	1.53E+08	1.8E+06	1.66E+08	1.8E+06	0.706	5.0E-05	1328.9	2.0E-01	0.391	1.010	1.6E+00	0.530	9.0E-01
3	3S--------	B3run5-3	0.120	7.8E-04	1.76E+08	1.3E+06	1.90E+08	1.5E+06	0.707	3.3E-05	1324.0	0.0E+00	0.391	0.857	7.4E-01	0.477	3.4E-01
3	3S--------	B3run6-1	0.123	1.0E-03	1.51E+08	1.5E+06	1.65E+08	1.4E+06	0.706	4.0E-05	1390.5	2.4E-01	0.359	1.136	9.2E-01	0.581	4.5E-01
3	3S--------	B3run6-2	0.121	3.8E-03	1.51E+08	6.3E+06	1.66E+08	6.5E+06	0.706	1.4E-04	1410.5	3.5E-01	0.357	1.095	1.2E+00	0.637	4.2E-01
3	3S--------	B3run6-3	0.122	1.1E-03	1.50E+08	1.4E+06	1.65E+08	1.4E+06	0.706	4.1E-05	1409.5	2.6E-01	0.357	1.037	1.5E+00	0.569	8.8E-01
3	3S--------	B3run7-1	0.274	2.7E-03	1.82E+08	2.7E+06	1.97E+08	2.5E+06	0.708	4.1E-05	1342.1	2.6E-01	0.183	2.175	6.0E+00	1.351	3.2E+00
3	3S--------	B3run7-2	0.262	3.1E-03	1.47E+08	2.1E+06	1.58E+08	2.2E+06	0.705	6.6E-05	1366.2	1.9E-01	0.180	2.096	2.6E+00	1.173	1.5E+00
3	3S--------	B3run7-4	0.157	2.1E-03	5.08E+07	8.4E+05	5.26E+07	8.4E+05	0.705	8.5E-05	766.2	1.2E-01	0.180	1.517	1.2E+01	0.689	5.3E+00
3	3S--------	B3run8-1	0.155	1.1E-03	4.44E+07	4.0E+05	4.60E+07	4.2E+05	0.705	4.8E-05	656.0	2.8E-01	0.174	1.638	1.8E+00	0.659	5.9E-01
3	3S--------	B3run9-1	0.044	3.1E-04	4.19E+07	3.4E+05	4.66E+07	3.9E+05	0.706	4.1E-05	623.0	3.4E-02	0.556	-0.174	1.2E-01	0.224	1.7E-01
3	3S--------	B3run9-2	0.404	3.1E-03	3.47E+08	3.2E+06	3.51E+08	3.0E+06	0.706	4.2E-05	2177.8	8.2E-02	0.178	1.711	3.2E-01	1.126	2.3E-01
3	3S--------	B3run9-3	0.403	3.0E-03	3.45E+08	3.1E+06	3.49E+08	3.1E+06	0.705	4.0E-05	2178.1	1.9E-01	0.178	1.760	3.3E-01	1.162	1.8E-01
3	3S--------	B3run9-4	0.173	1.8E-03	3.51E+08	3.6E+06	3.45E+08	3.4E+06	0.705	4.6E-05	2171.6	2.3E-01	0.382	1.047	1.3E+00	0.686	8.0E-01
3	3S--------	B3run12-1	0.175	1.1E-03	1.40E+08	1.0E+06	1.50E+08	1.1E+06	0.705	3.5E-05	1403.0	2.0E-02	0.256	1.160	1.6E-01	0.779	1.3E-01
3	3S--------	B3run13-1	0.062	6.8E-04	1.43E+08	1.8E+06	1.72E+08	1.8E+06	0.705	5.3E-05	1521.4	3.3E-01	0.726	0.123	3.0E-02	0.169	2.0E-02
3	3S--------	B3run13-2	0.062	8.9E-04	1.45E+08	2.4E+06	1.74E+08	2.5E+06	0.705	7.3E-05	1516.2	1.2E-01	0.727	0.107	2.5E-02	0.167	1.7E-02
3	3S--------	B3run13-3	0.599	5.7E-03	1.74E+09	1.7E+07	1.68E+09	1.7E+07	0.706	3.7E-05	5804.2	2.2E-01	0.263	1.475	1.6E-01	1.161	1.0E-01
3	3S--------	B3run15-1	0.147	1.3E-03	1.57E+08	1.6E+06	1.68E+08	1.4E+06	0.706	4.2E-05	1335.3	3.5E-01	0.310	1.154	3.1E-01	0.717	1.7E-01
3	3S--------	B3run15-2	0.599	4.6E-03	5.42E+08	5.0E+06	5.42E+08	4.8E+06	0.706	3.6E-05	2783.3	1.9E-01	0.149	2.036	6.2E+00	1.425	3.0E+00
3	3S--------	B3run16-1	0.246	2.5E-03	4.87E+08	4.6E+06	4.75E+08	4.8E+06	0.706	3.9E-05	2688.5	2.0E-01	0.301	1.829	3.3E+00	1.210	1.9E+00

Build	Exp Code	Run	Bo*	+/-	Grsh,C2	+/-	Grsh,C3	+/-	Pr	+/-	Rot Speed (rpm)	+/-	Mass Flow (kg/s)	Ø	+/-	finØ	+/-
3	3S--------	B3run16-2	0.500	5.5E-03	1.60E+09	1.7E+07	1.55E+09	1.6E+07	0.705	4.0E-05	5507.7	1.6E-01	0.296	1.481	3.1E-01	1.116	2.0E-01
3	3S--------	B3run17-1	0.119	1.2E-03	5.14E+08	4.4E+06	5.09E+08	4.4E+06	0.706	3.5E-05	2653.6	2.7E-01	0.604	0.929	9.1E-01	0.633	7.0E-01
3	3S--------	B3run17-2	0.119	1.5E-03	5.13E+08	5.2E+06	5.09E+08	4.9E+06	0.706	4.1E-05	2656.7	1.3E-01	0.601	0.925	4.1E-01	0.623	2.9E-01
3	3S--------	B3run17-3	0.210	3.0E-03	1.62E+09	1.8E+07	1.49E+09	1.6E+07	0.705	4.0E-05	5342.8	2.5E-01	0.603	1.150	3.4E-01	0.875	2.9E-01
3	3S--------	B3run17-4	0.210	3.0E-03	1.62E+09	1.8E+07	1.48E+09	1.8E+07	0.705	3.9E-05	5344.0	7.3E-02	0.601	1.188	3.1E+00	0.904	2.3E+00
3	3S--------	B3run17-5	0.334	1.9E-03	1.69E+08	1.3E+06	1.84E+08	1.3E+06	0.706	3.3E-05	1474.4	1.8E-01	0.154	2.145	7.1E-01	1.270	4.9E-01
3	3S--------	B3run17-6	0.342	2.3E-03	1.70E+08	1.5E+06	1.85E+08	1.6E+06	0.706	4.0E-05	1474.4	2.2E-01	0.151	2.104	1.0E+00	1.267	6.3E-01
3	3S--------	B3run18-1	0.144	8.6E-04	4.65E+07	3.7E+05	4.90E+07	3.8E+05	0.706	3.9E-05	662.9	7.9E-02	0.188	1.556	4.7E+00	0.633	2.5E+00
3	3S--------	B3run18-2	0.363	3.0E-03	3.09E+08	3.1E+06	3.20E+08	2.8E+06	0.705	4.0E-05	2085.5	1.7E-01	0.184	2.110	1.1E+00	1.376	8.1E-01
3	3S--------	B3run18-3	0.119	8.9E-04	1.59E+08	1.4E+06	1.71E+08	1.3E+06	0.705	3.6E-05	1497.8	7.4E-02	0.373	1.183	6.3E-01	0.620	3.8E-01
3	3S--------	B3run19-1	0.118	1.5E-03	1.54E+08	3.1E+06	1.66E+08	2.9E+06	0.705	5.4E-05	1369.6	2.5E-01	0.382	1.065	2.4E+00	0.501	9.8E-01
3	3S--------	B3run20-1	0.151	3.0E-03	1.88E+08	3.9E+06	2.00E+08	4.1E+06	0.705	9.6E-05	1426.0	3.4E-02	0.336	0.880	3.6E-01	0.592	2.0E-01
3	3S--------	B3run21-1	0.144	1.3E-03	1.85E+08	1.8E+06	1.92E+08	1.7E+06	0.705	3.9E-05	1430.2	1.1E-01	0.343	0.793	7.1E-01	0.501	4.6E-01
3	3S--------	B3run22-1	0.327	2.5E-03	2.27E+08	2.0E+06	2.43E+08	2.2E+06	0.706	3.8E-05	1452.2	1.9E-01	0.179	1.690	3.6E-01	1.042	2.1E-01
3	3S--------	B3run22-2	0.266	3.6E-03	6.45E+08	7.9E+06	6.14E+08	7.2E+06	0.705	4.3E-05	2983.4	3.2E-01	0.321	1.555	1.0E+00	1.052	6.9E-01
3	3S--------	B3run23-1	0.200	2.1E-03	4.98E+08	4.8E+06	4.61E+08	4.5E+06	0.705	3.5E-05	2787.3	2.1E-01	0.367	1.522	1.7E+00	1.069	1.2E+00
3	3S--------	B3run24-1	0.158	1.4E-03	2.43E+08	2.4E+06	2.62E+08	2.5E+06	0.707	3.7E-05	1459.3	5.4E-01	0.351	1.001	6.6E-01	0.715	3.9E-01
3	3S--------	B3run24-2	0.129	1.5E-03	1.24E+08	1.7E+06	1.32E+08	1.6E+06	0.702	5.8E-05	1285.6	1.6E-01	0.341	0.638	3.5E-01	0.314	1.7E-01
3	3S--------	B3run25-1	0.075	6.0E-04	1.75E+08	1.6E+06	1.97E+08	1.5E+06	0.704	3.8E-05	1546.8	2.2E-01	0.646	0.319	4.7E-02	0.194	3.7E-02
3	3S--------	B3run26-1	0.570	4.6E-03	6.88E+08	5.7E+06	6.47E+08	6.1E+06	0.704	3.6E-05	2864.5	2.5E-01	0.177	1.905	5.0E-01	1.273	2.8E-01
3	3S--------	B3run27-1	0.102	1.5E-03	4.77E+08	4.9E+06	4.35E+08	4.5E+06	0.705	4.0E-05	2892.0	2.8E-01	0.648	1.267	6.7E+00	0.817	3.5E+00
3	3S--------	B3run28-1	0.308	4.7E-03	1.63E+09	1.9E+07	1.37E+09	1.7E+07	0.706	3.9E-05	4552.2	9.7E-01	0.425	1.646	4.8E+00	1.119	5.1E+00
3	3S--------	B3run28-2	0.727	7.7E-03	1.66E+09	1.9E+07	1.43E+09	1.7E+07	0.705	4.1E-05	4453.7	2.1E-01	0.213	1.716	4.0E-01	1.171	2.1E-01
3	3S--------	B3run30-1	0.170	3.0E-03	1.43E+09	2.1E+07	1.16E+09	1.8E+07	0.706	3.6E-05	5436.5	2.7E-01	0.673	0.929	1.2E+00	0.797	1.4E+00
3	3S--------	B3run31-1	0.033	3.0E-04	4.01E+07	4.0E+05	4.79E+07	4.1E+05	0.705	4.4E-05	698.5	1.8E-01	0.688	0.212	7.6E-02	0.182	9.3E-02
3	3S--------	B3run32-1	0.084	4.5E-04	4.89E+07	3.8E+05	5.30E+07	3.8E+05	0.707	3.7E-05	665.6	1.6E-01	0.333	0.404	5.5E-02	0.283	3.3E-02
3	3S--------	B3run33-1	0.140	1.1E-03	1.45E+08	1.4E+06	1.47E+08	1.5E+06	0.707	4.3E-05	1186.9	1.8E-01	0.318	0.521	1.0E-01	0.306	7.1E-02

Build	Exp Code	Run	Bo*	+/-	Grsh,C2	+/-	Grsh,C3	+/-	Pr	+/-	Rot Speed (rpm)	+/-	Mass Flow (kg/s)	Ø	+/-	finØ	+/-
3	3S---------	B3run33-2	0.278	2.8E-03	6.91E+08	6.4E+06	6.79E+08	6.5E+06	0.707	3.5E-05	3028.8	3.1E-01	0.318	1.414	1.6E+00	0.997	9.1E-01
3	3S---------	B3run33-3	0.364	2.3E-03	2.18E+08	1.8E+06	2.25E+08	1.8E+06	0.707	3.3E-05	1480.7	1.6E-01	0.158	1.492	1.5E-01	0.859	7.0E-02
3	3S---------	B3run33-4	0.070	6.7E-04	1.67E+08	1.5E+06	1.82E+08	1.6E+06	0.706	4.0E-05	1477.4	2.1E-01	0.635	0.305	3.3E-02	0.177	1.7E-02
3	3S---------	B3run33-5	0.234	4.1E-03	2.17E+09	2.5E+07	1.98E+09	2.5E+07	0.705	4.3E-05	4915.7	9.3E-02	0.639	1.126	6.1E-01	0.837	4.3E-01
3	3S---------	B3run33-6	1.667	1.3E-02	2.44E+09	2.5E+07	2.41E+09	2.4E+07	0.706	3.6E-05	5060.8	1.8E-01	0.126	2.176	2.4E-01	1.619	1.2E-01
3	3S---------	B3run33-7	0.170	1.1E-03	2.08E+08	1.6E+06	2.12E+08	1.5E+06	0.706	3.3E-05	1575.8	2.6E-01	0.320	0.749	1.2E-01	0.435	5.8E-02
3	3S---------	B3run33-8	0.142	1.4E-03	6.88E+08	6.4E+06	6.75E+08	6.4E+06	0.705	3.8E-05	3177.2	1.3E-01	0.640	0.496	5.9E-02	0.314	2.9E-02
3	3S---------	B3run33-9	0.615	4.4E-03	6.88E+08	5.9E+06	6.87E+08	5.9E+06	0.705	3.3E-05	3317.8	8.3E-02	0.166	1.880	2.5E-01	1.354	1.6E-01
3	3S---------	B3run33-10	0.590	5.3E-03	2.47E+09	2.6E+07	2.30E+09	2.4E+07	0.705	3.3E-05	4748.1	2.3E-01	0.315	1.306	1.7E-01	0.925	1.0E-01
3	3S---------	B3run34-1	0.122	1.1E-03	2.00E+08	1.7E+06	2.03E+08	1.9E+06	0.706	4.0E-05	1506.3	2.1E-01	0.413	0.664	3.2E-01	0.388	2.5E-01
3	3S---------	B3run34-2	0.384	5.2E-03	2.17E+09	2.3E+07	2.05E+09	2.2E+07	0.705	3.5E-05	5366.8	2.1E-01	0.403	1.636	1.7E+00	1.221	1.6E+00
3	3S---------	B3run34-3	0.373	4.2E-03	6.70E+08	7.0E+06	6.55E+08	7.1E+06	0.706	3.9E-05	2715.3	2.2E-01	0.239	2.083	4.7E+01	1.380	3.4E+01
3	3S---------	B3run34-4	0.217	1.6E-03	2.03E+08	1.6E+06	2.01E+08	1.8E+06	0.706	3.4E-05	1381.6	2.6E-01	0.242	1.005	1.4E-01	0.590	6.9E-02
3	3S---------	B3run34-5	0.209	2.3E-03	6.62E+08	6.3E+06	6.38E+08	6.4E+06	0.705	3.8E-05	3008.9	2.0E-01	0.405	1.317	3.4E+00	0.846	2.5E+00
3	3S---------	B3run34-6	0.184	2.8E-03	2.02E+09	2.1E+07	1.82E+09	1.9E+07	0.704	3.2E-05	5495.9	1.0E-01	0.721	1.587	1.3E+00	1.153	1.1E+00
3	3S---------	B3run34-7	0.740	8.3E-03	2.11E+09	2.3E+07	2.01E+09	2.3E+07	0.705	3.6E-05	5270.8	2.0E-01	0.230	2.505	1.0E+02	1.992	1.0E+02
3	3S---------	B3run34-8	0.109	1.4E-03	6.39E+08	6.2E+06	6.15E+08	5.8E+06	0.704	3.8E-05	3071.6	1.1E-01	0.719	0.652	3.0E-01	0.403	1.9E-01
3	3S---------	B3run34-9	0.063	7.1E-04	1.78E+08	1.9E+06	1.93E+08	1.9E+06	0.704	4.4E-05	1546.8	2.1E-01	0.716	0.366	1.3E-01	0.187	8.7E-02
3	3S---------	B3run35-1	0.158	1.2E-03	2.04E+08	1.7E+06	2.19E+08	1.7E+06	0.705	3.6E-05	1559.0	3.9E-02	0.329	1.093	7.5E-01	0.690	6.4E-01
3	3S---------	B3run35-2	0.119	1.8E-03	6.21E+08	6.6E+06	5.64E+08	6.5E+06	0.705	4.1E-05	2969.4	1.8E-01	0.641	0.922	6.9E-01	0.647	3.7E-01
3	3S---------	B3run35-3	0.255	3.0E-03	6.17E+08	5.9E+06	5.69E+08	5.8E+06	0.705	3.6E-05	2952.9	3.3E-01	0.319	2.153	1.6E+00	1.316	8.4E-01
3	3S---------	B3run35-4	0.191	5.6E-03	1.73E+09	2.6E+07	1.31E+09	2.6E+07	0.704	5.0E-05	5078.7	2.4E+00	0.643	1.730	2.7E+00	1.156	1.7E+00
3	3S---------	B3run35-5	0.638	5.2E-03	6.19E+08	5.9E+06	5.76E+08	5.7E+06	0.704	3.7E-05	3183.8	2.9E-01	0.153	1.793	3.0E-01	1.258	2.0E-01
3	3S---------	B3run35-6	0.466	7.0E-03	1.81E+09	2.0E+07	1.42E+09	2.0E+07	0.704	3.8E-05	5173.5	1.4E+00	0.318	1.674	7.6E+00	1.126	3.7E+00
3	3S---------	B3run35-7	0.313	2.0E-03	1.96E+08	1.5E+06	2.04E+08	1.6E+06	0.704	3.6E-05	1842.0	3.9E-02	0.174	2.356	2.4E+00	1.232	1.3E+00
3	3S---------	B3run35-8	0.072	7.3E-04	1.80E+08	1.7E+06	1.94E+08	1.8E+06	0.703	4.5E-05	1861.1	6.6E-02	0.651	0.367	6.2E-02	0.224	3.0E-02
3	3S---------	B3run35-9	1.068	1.4E-02	1.71E+09	2.3E+07	1.33E+09	2.2E+07	0.703	4.1E-05	5542.1	2.4E-01	0.150	2.566	1.7E+00	1.928	1.8E+00

Build	Exp Code	Run	Bo*	+/-	Grsh,C2	+/-	Grsh,C3	+/-	Pr	+/-	Rot Speed (rpm)	+/-	Mass Flow (kg/s)	Ø	+/-	finØ	+/-
3	3S--------	B3run36-1	0.131	1.0E-03	1.96E+08	1.9E+06	2.12E+08	1.9E+06	0.704	4.3E-05	1611.3	3.2E-01	0.412	0.711	1.0E+00	0.420	5.3E-01
3	3S--------	B3run37-1	0.065	2.9E-02	3.02E+08	2.1E+07	2.70E+08	2.2E+07	0.705	1.4E-04	2964.1	3.6E-01	0.203	-1.622	1.6E+00	-1.314	8.9E-01
3	3S--------	B3run38-1	0.034	2.4E-04	2.65E+07	2.2E+05	3.25E+07	2.5E+05	0.704	4.6E-05	655.0	0.0E+00	0.595	0.146	1.5E-02	0.069	7.1E-03
3	3S--------	B3run39-1	0.000	1.5E-02	2.85E+08	3.7E+06	2.49E+08	3.7E+06	0.704	4.0E-05	3143.4	3.0E-01	0.200	-1.712	4.6E-01	-1.193	2.8E-01
3	3S--------	B3run40-1	0.110	4.8E-04	3.18E+07	2.0E+05	3.37E+07	2.1E+05	0.704	3.9E-05	608.8	1.9E-01	0.227	0.399	5.5E-02	0.310	2.7E-02
3	3S--------	B3run44-1	0.040	1.1E-02	4.05E+08	3.1E+07	3.70E+08	3.1E+07	0.707	1.4E-04	2780.1	9.8E-02	0.596	-0.759	4.1E+01	-0.712	7.8E-01
3	3S--------	B3run44-2	0.068	1.1E-02	4.17E+08	2.6E+07	3.84E+08	2.6E+07	0.707	1.6E-04	2775.5	1.7E-01	0.596	-1.657	2.1E+00	-1.449	1.3E-01
3	3S--------	B3run44-3	0.078	1.9E-03	4.12E+08	4.8E+06	3.81E+08	4.5E+06	0.706	3.9E-05	2768.6	2.7E-01	0.595	-5.395	1.3E+01	-4.043	7.4E+00
3	3S--------	B3run45-1	0.000	3.9E-06	-5.47E+00	4.6E-01	-6.08E+00	5.0E-01	0.707	4.4E-05	1.0	0.0E+00	0.183	0.069	3.0E-02	0.001	3.2E-03

Build	Exp Code	Run	Tcav2 (K)	+/-	Tcav3 (K)	+/-	Tinlet (K)	+/-	Texit (K)	+/-	Dtmeas (K)	+/-	Dtcalc (K)	+/-	Tsh,C2 (K)	+/-	Tsh,C3 (K)	+/-
3	3S---- -----	B3run2-1	323.49	1.5E+00	335.25	1.3E+00	316.87	3.2E-01	318.80	3.0E-01	1.93	4.3E-01	1.92	4.9E-02	368.17	3.2E-01	377.00	3.0E-01
3	3S---- -----	B3run2-2	324.31	1.1E+00	335.86	8.6E-01	317.32	2.4E-01	319.27	2.4E-01	1.95	3.2E-01	1.91	3.6E-02	368.92	2.3E-01	377.76	1.9E-01
3	3S---- -----	B3run3-1	326.92	1.2E+00	337.38	8.3E-01	319.73	2.9E-01	321.79	2.9E-01	2.06	4.0E-01	2.09	4.6E-02	371.77	2.4E-01	379.69	1.9E-01
3	3S---- -----	B3run4-1	325.12	1.3E+00	324.68	1.3E+00	314.06	3.6E-01	319.43	3.4E-01	5.36	4.8E-01	5.36	1.2E-01	369.53	2.8E-01	372.49	2.5E-01
3	3S---- -----	B3run4-2	325.39	2.9E+00	325.08	2.8E+00	313.83	4.2E-01	319.49	3.7E-01	5.67	5.6E-01	5.34	2.9E-01	369.99	5.1E-01	372.80	5.0E-01
3	3S---- -----	B3run5-1	321.39	1.4E+00	324.62	1.3E+00	314.14	3.2E-01	317.48	3.4E-01	3.34	5.0E-01	3.35	8.6E-02	367.95	2.7E-01	372.65	2.7E-01
3	3S---- -----	B3run5-3	316.66	1.0E+00	320.43	1.1E+00	308.14	2.2E-01	311.87	2.5E-01	3.73	3.6E-01	3.56	6.9E-02	365.43	1.9E-01	370.08	2.1E-01
3	3S---- -----	B3run6-1	319.87	9.8E-01	322.46	1.1E+00	311.65	2.6E-01	315.41	2.6E-01	3.75	3.4E-01	3.74	7.7E-02	367.34	1.9E-01	372.73	2.0E-01
3	3S---- -----	B3run6-2	318.94	7.8E+00	321.56	7.6E+00	311.73	9.1E-01	315.61	1.0E+00	3.88	1.4E+00	3.74	6.1E-01	366.01	1.6E+00	371.39	1.5E+00
3	3S---- -----	B3run6-3	320.56	1.2E+00	323.76	1.2E+00	312.84	2.6E-01	316.69	2.6E-01	3.85	3.5E-01	3.73	7.4E-02	367.74	2.8E-01	373.12	2.2E-01
3	3S---- -----	B3run7-1	310.31	3.4E+00	311.38	2.7E+00	302.03	2.8E-01	309.55	2.2E-01	7.52	3.8E-01	7.42	4.1E-01	358.82	6.5E-01	363.56	5.7E-01
3	3S---- -----	B3run7-2	327.62	1.6E+00	327.72	1.3E+00	317.74	4.1E-01	324.53	3.6E-01	6.79	5.1E-01	6.85	1.9E-01	372.40	3.4E-01	376.50	2.8E-01
3	3S---- -----	B3run7-4	333.15	2.5E+00	334.42	2.3E+00	320.84	5.2E-01	326.87	4.9E-01	6.03	7.6E-01	5.72	2.5E-01	383.08	3.5E-01	385.33	3.2E-01
3	3S---- -----	B3run8-1	331.45	1.5E+00	331.56	1.4E+00	316.35	3.0E-01	322.94	2.6E-01	6.59	4.0E-01	6.08	1.5E-01	384.32	2.2E-01	386.74	2.0E-01
3	3S---- -----	B3run9-1	326.00	1.5E+00	328.75	1.5E+00	315.21	2.6E-01	317.45	3.1E-01	2.24	4.1E-01	1.84	4.8E-02	373.59	1.8E-01	380.10	2.0E-01
3	3S---- -----	B3run9-2	329.37	7.3E-01	327.47	7.3E-01	316.22	2.6E-01	323.07	2.5E-01	6.85	3.5E-01	7.46	1.2E-01	370.11	1.7E-01	370.75	1.8E-01
3	3S---- -----	B3run9-3	329.35	7.6E-01	327.42	6.1E-01	316.48	2.5E-01	323.32	2.3E-01	6.84	3.5E-01	7.48	1.0E-01	370.26	1.7E-01	370.80	1.5E-01
3	3S---- -----	B3run9-4	329.81	8.2E-01	326.35	7.2E-01	317.57	2.8E-01	320.90	2.8E-01	3.32	4.0E-01	3.55	5.7E-02	370.29	1.8E-01	369.48	1.6E-01
3	3S---- -----	B3run12-1	326.48	9.8E-01	328.18	8.4E-01	317.07	2.2E-01	322.42	2.3E-01	5.35	3.1E-01	5.17	8.5E-02	375.45	1.8E-01	379.54	1.5E-01
3	3S---- -----	B3run13-1	324.84	1.1E+00	335.77	9.6E-01	319.73	3.2E-01	321.25	3.6E-01	1.52	4.5E-01	1.71	3.7E-02	369.90	2.5E-01	379.94	2.0E-01
3	3S---- -----	B3run13-2	324.95	9.6E-01	335.60	7.7E-01	319.29	4.5E-01	320.82	3.8E-01	1.54	5.1E-01	1.70	3.0E-02	369.96	2.0E-01	380.01	1.6E-01
3	3S---- -----	B3run13-3	321.14	5.4E-01	321.38	4.9E-01	311.31	2.4E-01	320.49	2.0E-01	9.18	2.9E-01	7.20	8.1E-02	361.74	1.6E-01	360.46	1.5E-01
3	3S---- -----	B3run15-1	319.85	1.0E+00	324.67	7.1E-01	314.98	2.7E-01	319.32	2.5E-01	4.34	3.7E-01	4.29	6.9E-02	368.78	2.1E-01	372.76	1.4E-01
3	3S---- -----	B3run15-2	318.24	5.9E-01	321.17	6.5E-01	310.88	2.3E-01	319.44	2.6E-01	8.57	3.4E-01	9.25	1.3E-01	359.18	1.7E-01	359.20	1.8E-01
3	3S---- -----	B3run16-1	322.98	5.6E-01	321.75	6.2E-01	315.54	2.5E-01	319.84	2.2E-01	4.31	3.1E-01	4.55	6.4E-02	361.74	1.3E-01	360.65	1.6E-01

Build	Exp Code	Run	Tcav2 (K)	+/-	Tcav3 (K)	+/-	Tinlet (K)	+/-	Texit (K)	+/-	Dtmeas (K)	+/-	Dtcalc (K)	+/-	Tsh,C2 (K)	+/-	Tsh,C3 (K)	+/-
3	3S---- -----	B3run16-2	327.05	5.1E-01	327.33	5.5E-01	318.66	2.4E-01	326.17	2.5E-01	7.51	3.3E-01	5.97	7.6E-02	364.98	1.6E-01	363.75	1.7E-01
3	3S---- -----	B3run17-1	322.88	5.8E-01	321.59	5.4E-01	315.31	2.2E-01	317.69	2.7E-01	2.38	3.5E-01	2.39	3.1E-02	362.11	1.5E-01	361.67	1.5E-01
3	3S---- -----	B3run17-2	323.18	6.1E-01	321.94	6.9E-01	315.54	2.6E-01	317.91	2.6E-01	2.37	4.0E-01	2.39	3.5E-02	362.26	1.7E-01	361.87	1.7E-01
3	3S---- -----	B3run17-3	325.70	5.2E-01	322.46	5.2E-01	316.92	2.5E-01	320.35	2.2E-01	3.43	3.5E-01	2.92	3.6E-02	362.31	1.6E-01	359.14	1.7E-01
3	3S---- -----	B3run17-4	325.81	5.0E-01	322.50	5.5E-01	317.11	2.4E-01	320.53	2.4E-01	3.43	3.0E-01	2.94	3.8E-02	362.48	1.6E-01	359.28	1.7E-01
3	3S---- -----	B3run17-5	324.25	9.1E-01	324.27	7.2E-01	313.07	2.1E-01	322.04	2.1E-01	8.97	2.8E-01	8.27	1.1E-01	369.36	2.1E-01	374.09	1.5E-01
3	3S---- -----	B3run17-6	324.49	9.9E-01	324.49	8.8E-01	313.06	2.5E-01	322.05	2.1E-01	8.99	3.4E-01	8.41	1.4E-01	369.41	1.7E-01	374.17	1.8E-01
3	3S---- -----	B3run18-1	324.58	1.4E+00	328.74	1.4E+00	313.93	2.5E-01	320.68	2.3E-01	6.74	3.3E-01	5.84	1.3E-01	378.60	2.0E-01	382.03	2.0E-01
3	3S---- -----	B3run18-2	331.58	7.8E-01	330.17	7.0E-01	321.42	2.4E-01	328.22	2.4E-01	6.80	3.3E-01	7.02	1.3E-01	370.90	1.9E-01	372.70	1.7E-01
3	3S---- -----	B3run18-3	326.31	8.5E-01	328.25	9.5E-01	318.78	2.2E-01	322.39	2.4E-01	3.61	3.5E-01	3.52	5.7E-02	371.64	1.7E-01	375.72	1.9E-01
3	3S---- -----	B3run19-1	327.11	3.8E+00	330.83	4.0E+00	319.99	3.3E-01	323.37	3.2E-01	3.38	4.4E-01	3.33	2.2E-01	372.16	8.1E-01	376.00	7.9E-01
3	3S---- -----	B3run20-1	324.28	9.0E-01	328.48	8.3E-01	318.57	5.9E-01	322.33	5.8E-01	3.76	8.9E-01	3.62	8.3E-02	367.51	1.9E-01	370.73	1.7E-01
3	3S---- -----	B3run21-1	323.29	1.0E+00	326.62	8.3E-01	316.75	2.4E-01	320.03	2.4E-01	3.29	3.5E-01	3.09	6.7E-02	361.92	2.1E-01	363.63	1.7E-01
3	3S---- -----	B3run22-1	320.09	6.5E-01	322.38	7.5E-01	311.53	2.5E-01	318.97	2.8E-01	7.45	3.9E-01	6.79	1.1E-01	361.80	1.7E-01	365.30	1.6E-01
3	3S---- -----	B3run22-2	329.31	8.7E-01	327.62	7.8E-01	321.35	2.6E-01	325.00	2.2E-01	3.65	3.5E-01	4.01	8.8E-02	363.34	2.4E-01	361.42	2.3E-01
3	3S---- -----	B3run23-1	326.87	6.7E-01	323.72	7.1E-01	318.33	2.1E-01	321.49	2.2E-01	3.16	2.9E-01	3.51	5.0E-02	363.33	1.9E-01	360.06	1.8E-01
3	3S---- -----	B3run24-1	312.77	1.0E+00	315.35	8.5E-01	306.98	2.4E-01	311.10	2.8E-01	4.12	3.9E-01	3.60	6.8E-02	354.74	2.4E-01	358.35	2.1E-01
3	3S---- -----	B3run24-2	351.69	1.5E+00	353.24	1.3E+00	338.71	3.2E-01	342.13	2.9E-01	3.42	4.6E-01	2.75	7.6E-02	385.45	3.0E-01	388.43	2.5E-01
3	3S---- ----	B3run25-1	335.67	1.2E+00	342.81	9.2E-01	327.80	2.2E-01	329.73	2.3E-01	1.93	3.3E-01	1.81	3.7E-02	376.05	2.5E-01	382.24	1.9E-01
3	3S---- -----	B3run26-1	335.43	5.5E-01	332.95	5.9E-01	324.18	2.1E-01	330.50	2.3E-01	6.32	3.0E-01	6.75	1.1E-01	367.27	1.6E-01	364.86	1.5E-01
3	3S---- -----	B3run27-1	328.08	6.5E-01	323.32	6.4E-01	319.31	2.5E-01	321.20	2.4E-01	1.90	3.7E-01	1.97	3.0E-02	363.61	1.7E-01	359.84	1.8E-01
3	3S---- -----	B3run28-1	324.92	6.7E-01	319.62	6.7E-01	314.83	2.5E-01	318.29	2.3E-01	3.45	3.3E-01	3.28	5.5E-02	354.86	2.4E-01	349.15	2.3E-01
3	3S---- -----	B3run28-2	329.67	5.9E-01	325.17	4.5E-01	316.59	2.5E-01	322.92	2.4E-01	6.33	3.3E-01	6.15	9.8E-02	358.84	1.9E-01	353.69	1.3E-01
3	3S---- -----	B3run30-1	318.73	9.8E-01	317.80	9.9E-01	313.79	2.3E-01	316.00	2.5E-01	2.21	3.5E-01	2.13	4.3E-02	353.22	3.2E-01	347.02	2.8E-01
3	3S---- -----	B3run31-1	310.28	1.2E+00	334.08	1.0E+00	320.16	2.7E-01	321.89	2.7E-01	1.74	3.8E-01	1.78	2.6E-02	372.45	1.8E-01	382.58	1.5E-01
3	3S---- -----	B3run32-1	317.27	1.3E+00	328.33	1.0E+00	309.75	2.4E-01	313.60	2.4E-01	3.85	3.3E-01	3.42	6.3E-02	377.70	2.0E-01	383.50	1.5E-01
3	3S---- -----	B3run33-1	317.52	1.1E+00	323.38	1.3E+00	306.02	2.9E-01	309.49	2.6E-01	3.47	3.9E-01	3.46	7.0E-02	363.88	2.1E-01	364.53	2.3E-01

Build	Exp Code	Run	Tcav2 (K)	+/-	Tcav3 (K)	+/-	Tinlet (K)	+/-	Texit (K)	+/-	Dtmeas (K)	+/-	Dtcalc (K)	+/-	Tsh,C2 (K)	+/-	Tsh,C3 (K)	+/-
3	3S---- -----	B3run33-2	316.77	6.2E-01	316.24	5.9E-01	308.68	2.3E-01	313.18	2.4E-01	4.50	3.3E-01	4.58	6.1E-02	355.25	1.7E-01	354.47	1.7E-01
3	3S---- -----	B3run33-3	315.73	7.4E-01	321.08	7.1E-01	307.36	2.2E-01	314.91	2.2E-01	7.55	3.5E-01	7.51	1.3E-01	360.54	1.8E-01	362.30	1.5E-01
3	3S---- -----	B3run33-4	319.72	8.9E-01	332.34	7.9E-01	316.21	2.5E-01	317.87	2.1E-01	1.67	3.4E-01	1.95	3.4E-02	366.89	1.8E-01	371.15	1.5E-01
3	3S---- -----	B3run33-5	327.20	5.0E-01	322.54	5.4E-01	317.30	2.7E-01	320.45	3.0E-01	3.15	3.7E-01	2.57	3.4E-02	358.03	1.7E-01	354.98	1.8E-01
3	3S---- -----	B3run33-6	329.50	6.9E-01	328.83	5.5E-01	315.24	2.3E-01	329.05	2.6E-01	13.81	3.5E-01	13.20	1.8E-01	361.88	2.6E-01	361.34	1.8E-01
3	3S---- -----	B3run33-7	324.85	7.9E-01	328.37	7.5E-01	314.78	2.1E-01	318.41	2.5E-01	3.63	3.2E-01	3.71	6.7E-02	368.60	1.7E-01	369.77	1.4E-01
3	3S---- -----	B3run33-8	329.54	6.1E-01	329.37	6.3E-01	318.37	2.3E-01	320.65	2.4E-01	2.28	3.3E-01	2.12	3.1E-02	365.44	1.8E-01	364.60	1.7E-01
3	3S---- -----	B3run33-9	327.03	6.8E-01	327.59	5.7E-01	317.09	2.1E-01	326.21	2.2E-01	9.13	3.2E-01	8.67	1.3E-01	365.51	2.0E-01	365.44	1.6E-01
3	3S---- -----	B3run33-10	331.38	6.4E-01	327.76	5.3E-01	318.72	2.0E-01	324.84	2.1E-01	6.12	3.0E-01	4.94	6.7E-02	360.54	2.3E-01	357.94	1.7E-01
3	3S---- -----	B3run34-1	321.50	7.6E-01	326.03	7.5E-01	314.44	2.5E-01	317.19	2.3E-01	2.76	3.5E-01	2.87	4.7E-02	365.05	1.6E-01	365.90	1.5E-01
3	3S---- -----	B3run34-2	326.39	5.1E-01	323.02	5.1E-01	316.88	2.2E-01	322.73	2.2E-01	5.86	3.0E-01	4.42	6.0E-02	359.97	1.7E-01	357.92	1.7E-01
3	3S---- -----	B3run34-3	322.47	6.2E-01	320.99	6.7E-01	314.14	2.5E-01	319.43	2.3E-01	5.29	3.5E-01	5.68	8.5E-02	357.96	1.9E-01	357.01	1.8E-01
3	3S---- -----	B3run34-4	323.57	7.4E-01	326.36	7.0E-01	314.62	2.2E-01	319.16	2.4E-01	4.54	3.3E-01	4.41	8.5E-02	363.88	1.8E-01	363.36	1.7E-01
3	3S---- -----	B3run34-5	325.75	6.2E-01	324.54	6.0E-01	317.89	2.3E-01	321.24	2.5E-01	3.34	3.3E-01	3.42	5.1E-02	362.06	1.8E-01	360.50	1.7E-01
3	3S---- -----	B3run34-6	332.64	5.4E-01	327.48	4.9E-01	323.89	1.9E-01	327.09	2.2E-01	3.20	3.2E-01	2.43	3.2E-02	365.30	1.7E-01	362.01	1.5E-01
3	3S---- -----	B3run34-7	329.28	6.1E-01	327.01	5.1E-01	320.65	2.2E-01	329.29	2.1E-01	8.64	2.9E-01	7.55	1.0E-01	362.68	2.2E-01	360.99	1.7E-01
3	3S---- -----	B3run34-8	332.94	6.6E-01	331.47	5.6E-01	323.86	2.3E-01	325.77	2.5E-01	1.90	3.5E-01	1.86	3.1E-02	367.67	1.9E-01	366.10	1.6E-01
3	3S---- -----	B3run34-9	326.29	8.5E-01	337.93	7.7E-01	324.68	2.6E-01	326.02	2.3E-01	1.34	3.3E-01	1.68	3.0E-02	370.50	2.0E-01	374.46	1.7E-01
3	3S---- -----	B3run35-1	327.25	7.8E-01	326.77	8.3E-01	317.09	2.2E-01	321.19	2.4E-01	4.10	3.5E-01	3.88	5.9E-02	369.14	1.6E-01	372.92	1.8E-01
3	3S---- -----	B3run35-2	329.68	5.5E-01	326.44	6.2E-01	321.44	2.5E-01	323.31	2.5E-01	1.87	3.4E-01	1.98	3.3E-02	363.45	1.6E-01	359.77	1.6E-01
3	3S---- -----	B3run35-3	329.46	5.6E-01	326.52	5.4E-01	321.51	2.2E-01	325.06	2.3E-01	3.55	3.2E-01	4.00	5.7E-02	363.28	1.7E-01	360.21	1.4E-01
3	3S---- -----	B3run35-4	335.04	4.9E-01	329.06	5.5E-01	326.36	2.9E-01	328.45	2.9E-01	2.09	4.2E-01	1.95	3.4E-02	361.39	1.5E-01	354.40	1.5E-01
3	3S---- -----	B3run35-5	333.80	6.2E-01	333.38	6.0E-01	323.81	2.2E-01	330.65	2.2E-01	6.83	3.5E-01	7.60	1.5E-01	367.14	1.9E-01	364.29	1.5E-01
3	3S---- -----	B3run35-6	336.38	4.9E-01	331.51	5.4E-01	326.11	2.2E-01	330.21	2.5E-01	4.10	3.4E-01	3.85	7.0E-02	362.83	1.4E-01	356.24	1.5E-01
3	3S---- -----	B3run35-7	337.40	8.5E-01	334.92	7.4E-01	324.92	2.1E-01	332.10	2.6E-01	7.19	3.4E-01	7.12	1.0E-01	378.49	1.7E-01	380.72	1.7E-01
3	3S---- -----	B3run35-8	336.97	9.4E-01	342.21	7.8E-01	328.91	2.6E-01	330.55	2.6E-01	1.64	3.5E-01	1.86	3.4E-02	378.94	1.9E-01	382.74	1.5E-01
3	3S---- -----	B3run35-9	338.10	6.4E-01	334.90	6.6E-01	328.60	2.4E-01	335.08	2.4E-01	6.48	3.5E-01	7.99	1.7E-01	365.64	2.0E-01	358.98	1.9E-01

Build	Exp Code	Run	Tcav2 (K)	+/-	Tcav3 (K)	+/-	Tinlet (K)	+/-	Texit (K)	+/-	Dtmeas (K)	+/-	Dtcalc (K)	+/-	Tsh,C2 (K)	+/-	Tsh,C3 (K)	+/-
3	3S---- -----	B3run36-1	333.08	8.3E-01	335.08	8.3E-01	322.86	2.6E-01	325.83	2.7E-01	2.96	3.6E-01	3.05	5.7E-02	375.40	1.9E-01	379.71	1.8E-01
3	3S---- -----	B3run37-1	312.94	1.3E+01	311.58	3.2E+01	319.16	8.4E-01	324.02	9.3E-01	4.86	1.4E+00	6.48	7.4E+00	351.77	1.9E+00	348.46	1.8E+00
3	3S---- -----	B3run38-1	319.08	1.3E+00	361.17	1.7E+00	327.51	2.7E-01	329.38	2.6E-01	1.87	3.6E-01	1.86	3.6E-02	386.76	1.5E-01	400.04	1.7E-01
3	3S---- -----	B3run39-1	318.42	5.7E-01	317.72	5.5E-01	325.74	2.4E-01	330.37	2.2E-01	4.63	3.2E-01	6.16	8.9E-01	356.11	1.5E-01	352.56	1.4E-01
3	3S---- -----	B3run40-1	337.34	1.4E+00	345.19	1.1E+00	322.63	2.3E-01	327.62	2.5E-01	4.99	3.6E-01	4.45	8.5E-02	396.52	1.7E-01	400.95	1.5E-01
3	3S---- -----	B3run44-1	301.98	8.4E+00	301.51	8.6E+00	306.80	9.3E-01	308.84	1.0E+00	2.03	1.4E+00	2.45	1.0E+00	343.45	2.2E+00	340.42	2.1E+00
3	3S---- -----	B3run44-2	306.96	6.2E+00	306.62	8.7E+00	309.18	1.0E+00	311.14	1.0E+00	1.97	1.5E+00	2.34	1.9E+01	347.91	1.6E+00	344.97	2.0E+00
3	3S---- -----	B3run44-3	311.32	7.2E-01	311.06	7.3E-01	311.96	2.5E-01	313.86	2.5E-01	1.90	3.3E-01	2.31	3.9E-02	352.03	2.1E-01	349.16	1.8E-01
3	3S---- -----	B3run45-1	358.76	3.3E+01	299.35	3.2E+01	306.17	3.0E-01	305.75	2.6E-01	-0.43	4.0E-01	-0.11	1.5E-01	302.31	2.0E-01	301.88	1.9E-01

Build	Exp Code	Run	Pcav (abs Pa)	Ts,C2,d,av (K)	+/-	Ts,C3,u,av (K)	+/-	TS,C3,d,av (K)	+/-	Ts,C4,u,av (K)	+/-	finTs,D2,av (K)	+/-	finTs,D3,av (K)	+/-
3	3S---- -----	B3run2-1	2.424E+05	332.64	1.7E-01	331.84	2.2E-01	336.39	2.2E-01	337.41	2.0E-01	332.24	1.5E-01	336.90	1.5E-01
3	3S---- -----	B3run2-2	2.427E+05	333.22	1.3E-01	332.46	1.2E-01	337.05	1.3E-01	337.95	1.3E-01	332.84	9.1E-02	337.50	9.1E-02
3	3S---- -----	B3run3-1	2.387E+05	335.71	1.8E-01	334.49	1.7E-01	338.56	1.7E-01	339.26	1.7E-01	335.10	1.3E-01	338.91	1.2E-01
3	3S---- -----	B3run4-1	2.605E+05	333.74	2.1E-01	332.18	1.9E-01	334.04	1.6E-01	334.36	1.9E-01	332.96	1.4E-01	334.20	1.3E-01
3	3S---- -----	B3run4-2	2.606E+05	333.86	3.7E-01	332.38	4.4E-01	334.19	3.9E-01	334.50	3.6E-01	333.12	2.9E-01	334.34	2.6E-01
3	3S---- -----	B3run5-1	2.535E+05	330.49	1.7E-01	328.59	2.0E-01	332.55	2.1E-01	332.85	1.6E-01	329.54	1.4E-01	332.70	1.3E-01
3	3S---- -----	B3run5-3	2.529E+05	325.49	1.4E-01	323.70	1.5E-01	327.70	1.3E-01	327.97	1.3E-01	324.59	1.1E-01	327.84	8.8E-02
3	3S---- -----	B3run6-1	2.324E+05	329.08	1.3E-01	326.98	1.2E-01	331.07	1.5E-01	331.40	1.3E-01	328.03	9.3E-02	331.23	1.1E-01
3	3S---- -----	B3run6-2	2.322E+05	327.73	1.0E+00	326.18	1.2E+00	329.84	1.2E+00	330.07	1.2E+00	326.95	7.7E-01	329.96	8.5E-01
3	3S---- -----	B3run6-3	2.322E+05	329.56	2.1E-01	327.74	1.7E-01	331.49	2.1E-01	331.71	2.1E-01	328.65	1.5E-01	331.60	1.5E-01
3	3S---- -----	B3run7-1	2.440E+05	321.94	4.4E-01	320.88	2.3E-01	323.45	4.2E-01	323.97	4.9E-01	321.41	2.3E-01	323.71	3.2E-01
3	3S---- -----	B3run7-2	2.464E+05	337.47	2.2E-01	335.88	2.2E-01	338.57	2.0E-01	338.84	2.2E-01	336.67	1.7E-01	338.71	1.4E-01
3	3S---- -----	B3run7-4	2.459E+05	343.25	3.3E-01	341.53	2.2E-01	346.25	2.4E-01	346.81	3.1E-01	342.39	2.1E-01	346.53	2.1E-01
3	3S---- -----	B3run8-1	2.489E+05	342.55	1.1E-01	340.33	1.4E-01	345.67	1.4E-01	346.40	1.7E-01	341.44	9.0E-02	346.03	1.0E-01
3	3S---- -----	B3run9-1	2.725E+05	330.94	1.5E-01	333.59	1.5E-01	340.41	1.5E-01	339.30	1.5E-01	332.26	1.1E-01	339.86	9.8E-02
3	3S---- -----	B3run9-2	2.390E+05	335.48	1.2E-01	333.85	1.0E-01	336.26	1.1E-01	335.92	1.1E-01	334.67	8.2E-02	336.09	8.2E-02
3	3S---- -----	B3run9-3	2.392E+05	335.67	1.1E-01	334.05	9.2E-02	336.39	1.3E-01	336.06	1.1E-01	334.86	7.4E-02	336.22	8.3E-02
3	3S---- -----	B3run9-4	2.461E+05	334.14	1.4E-01	332.50	1.3E-01	333.12	1.1E-01	332.81	1.5E-01	333.32	9.9E-02	332.96	9.3E-02
3	3S---- -----	B3run12-1	2.256E+05	336.53	1.1E-01	335.47	1.3E-01	338.44	1.2E-01	338.53	1.2E-01	336.00	9.0E-02	338.49	8.3E-02
3	3S---- -----	B3run13-1	2.316E+05	333.58	1.6E-01	333.90	1.6E-01	339.75	1.4E-01	339.26	1.9E-01	333.74	1.2E-01	339.51	1.2E-01
3	3S---- -----	B3run13-2	2.318E+05	333.29	1.2E-01	333.70	1.2E-01	339.66	1.2E-01	339.07	1.3E-01	333.50	8.4E-02	339.36	8.3E-02
3	3S---- -----	B3run13-3	2.269E+05	324.95	1.2E-01	322.77	1.1E-01	326.77	1.0E-01	325.49	1.2E-01	323.86	7.3E-02	326.13	7.1E-02
3	3S---- -----	B3run15-1	2.569E+05	331.73	1.2E-01	330.49	1.1E-01	333.71	1.3E-01	333.92	1.3E-01	331.11	8.1E-02	333.81	9.6E-02
3	3S---- -----	B3run15-2	2.410E+05	327.24	1.1E-01	325.95	1.0E-01	329.05	1.1E-01	328.80	1.2E-01	326.59	7.7E-02	328.92	8.7E-02
3	3S---- -----	B3run16-1	2.498E+05	328.54	1.1E-01	327.01	1.3E-01	327.67	1.2E-01	327.43	1.2E-01	327.77	8.6E-02	327.55	8.6E-02

Build	Exp Code	Run	Pcav (abs Pa)	Ts,C2,d,av (K)	+/-	Ts,C3,u,av (K)	+/-	TS,C3,d,av (K)	+/-	Ts,C4,u,av (K)	+/-	finTs,D2,av (K)	+/-	finTs,D3,av (K)	+/-
3	3S---- -----	B3run16-2	2.504E+05	330.70	1.2E-01	328.48	1.4E-01	331.93	1.1E-01	330.75	1.4E-01	329.59	1.0E-01	331.34	9.7E-02
3	3S---- -----	B3run17-1	2.576E+05	326.92	1.3E-01	325.20	1.3E-01	326.77	1.1E-01	326.29	1.4E-01	326.06	9.9E-02	326.53	8.7E-02
3	3S---- -----	B3run17-2	2.578E+05	327.06	1.2E-01	325.34	1.4E-01	326.93	1.3E-01	326.50	1.3E-01	326.20	9.0E-02	326.71	9.7E-02
3	3S---- -----	B3run17-3	2.574E+05	327.01	1.3E-01	324.52	1.5E-01	325.99	1.2E-01	324.50	1.5E-01	325.77	1.0E-01	325.24	9.7E-02
3	3S---- -----	B3run17-4	2.573E+05	327.14	1.3E-01	324.65	1.3E-01	326.14	1.1E-01	324.65	1.2E-01	325.90	8.6E-02	325.39	9.0E-02
3	3S---- -----	B3run17-5	2.335E+05	333.88	1.1E-01	332.57	1.2E-01	336.19	1.3E-01	336.56	1.1E-01	333.22	8.7E-02	336.37	7.6E-02
3	3S---- -----	B3run17-6	2.341E+05	333.95	1.2E-01	332.67	1.3E-01	336.23	1.2E-01	336.56	1.3E-01	333.31	9.2E-02	336.39	8.4E-02
3	3S---- -----	B3run18-1	2.540E+05	337.91	1.4E-01	335.88	1.6E-01	341.41	1.6E-01	342.31	1.4E-01	336.90	1.1E-01	341.86	1.1E-01
3	3S---- -----	B3run18-2	2.548E+05	337.78	1.3E-01	336.44	1.4E-01	339.06	1.3E-01	339.03	1.5E-01	337.11	9.5E-02	339.05	1.0E-01
3	3S---- -----	B3run18-3	2.396E+05	334.11	1.2E-01	332.28	1.1E-01	335.84	1.2E-01	336.27	1.2E-01	333.20	8.3E-02	336.05	9.0E-02
3	3S---- -----	B3run19-1	2.618E+05	335.90	5.8E-01	333.81	3.4E-01	337.52	5.3E-01	338.09	5.0E-01	334.86	3.4E-01	337.80	3.2E-01
3	3S---- -----	B3run20-1	2.836E+05	334.06	2.0E-01	333.03	2.1E-01	335.67	2.0E-01	335.68	1.9E-01	333.55	1.5E-01	335.67	1.3E-01
3	3S---- -----	B3run21-1	2.884E+05	331.05	1.3E-01	329.91	1.3E-01	331.96	1.4E-01	331.91	1.4E-01	330.48	9.7E-02	331.94	1.0E-01
3	3S---- -----	B3run22-1	2.872E+05	329.65	1.0E-01	328.55	1.1E-01	331.54	1.1E-01	331.84	1.2E-01	329.10	7.8E-02	331.69	8.8E-02
3	3S---- -----	B3run22-2	2.857E+05	333.04	1.9E-01	331.29	1.9E-01	332.04	1.9E-01	331.41	1.9E-01	332.16	1.3E-01	331.73	1.2E-01
3	3S---- -----	B3run23-1	2.526E+05	330.79	1.1E-01	329.26	1.2E-01	329.22	1.2E-01	328.68	1.1E-01	330.03	8.1E-02	328.95	7.8E-02
3	3S---- -----	B3run24-1	2.940E+05	321.77	1.3E-01	320.91	1.3E-01	323.13	1.4E-01	323.17	1.3E-01	321.34	9.1E-02	323.15	9.2E-02
3	3S---- -----	B3run24-2	3.002E+05	354.15	1.8E-01	352.29	1.6E-01	356.28	1.8E-01	356.22	1.7E-01	353.22	1.2E-01	356.25	1.3E-01
3	3S---- ----	B3run25-1	2.714E+05	341.23	1.3E-01	340.18	1.2E-01	344.21	1.2E-01	344.48	1.2E-01	340.70	9.6E-02	344.35	8.6E-02
3	3S---- -----	B3run26-1	3.082E+05	338.82	1.3E-01	336.49	1.3E-01	339.52	1.2E-01	338.29	1.1E-01	337.65	8.6E-02	338.91	8.5E-02
3	3S---- -----	B3run27-1	2.425E+05	329.90	1.1E-01	327.47	1.2E-01	328.82	1.2E-01	327.71	9.9E-02	328.69	8.8E-02	328.26	8.3E-02
3	3S---- -----	B3run28-1	3.094E+05	325.12	1.4E-01	321.97	1.2E-01	324.19	1.4E-01	322.26	1.6E-01	323.54	8.9E-02	323.22	1.1E-01
3	3S---- -----	B3run28-2	3.113E+05	330.20	1.2E-01	327.11	1.1E-01	330.64	1.1E-01	328.68	1.2E-01	328.65	8.5E-02	329.66	7.7E-02
3	3S---- -----	B3run30-1	2.540E+05	321.84	1.5E-01	320.42	1.3E-01	320.38	1.3E-01	319.32	1.4E-01	321.13	1.0E-01	319.85	9.5E-02
3	3S---- -----	B3run31-1	2.603E+05	333.26	1.4E-01	332.79	1.5E-01	339.21	1.4E-01	338.94	1.4E-01	333.02	1.1E-01	339.08	1.0E-01
3	3S---- -----	B3run32-1	2.453E+05	333.50	1.3E-01	333.65	1.3E-01	340.66	1.4E-01	341.55	1.2E-01	333.57	9.3E-02	341.11	9.2E-02
3	3S---- -----	B3run33-1	2.512E+05	325.59	1.3E-01	324.59	1.4E-01	327.53	1.3E-01	327.84	1.5E-01	325.09	9.8E-02	327.69	1.0E-01

Build	Exp Code	Run	Pcav (abs Pa)	Ts,C2,d,av (K)	+/-	Ts,C3,u,av (K)	+/-	TS,C3,d,av (K)	+/-	Ts,C4,u,av (K)	+/-	finTs,D2,av (K)	+/-	finTs,D3,av (K)	+/-
3	3S---- -----	B3run33-2	2.524E+05	322.27	1.3E-01	320.34	1.1E-01	321.45	1.2E-01	320.63	1.3E-01	321.30	8.8E-02	321.04	8.7E-02
3	3S---- -----	B3run33-3	2.606E+05	327.85	1.4E-01	326.31	1.2E-01	328.56	1.2E-01	328.56	1.4E-01	327.08	9.5E-02	328.56	9.4E-02
3	3S---- -----	B3run33-4	2.501E+05	329.98	1.1E-01	328.34	1.2E-01	332.68	1.2E-01	332.48	1.2E-01	329.16	8.0E-02	332.58	9.1E-02
3	3S---- -----	B3run33-5	3.385E+05	326.94	1.3E-01	323.91	1.4E-01	326.49	1.3E-01	324.54	1.1E-01	325.43	1.1E-01	325.51	8.9E-02
3	3S---- -----	B3run33-6	3.203E+05	331.80	1.3E-01	329.16	1.8E-01	334.14	1.4E-01	332.57	1.4E-01	330.48	1.1E-01	333.36	1.1E-01
3	3S---- -----	B3run33-7	2.509E+05	333.62	1.2E-01	332.32	1.3E-01	334.04	1.6E-01	334.27	1.3E-01	332.97	9.0E-02	334.16	1.2E-01
3	3S---- -----	B3run33-8	2.569E+05	332.29	1.1E-01	330.16	1.2E-01	331.15	1.3E-01	330.45	1.3E-01	331.23	8.4E-02	330.80	9.5E-02
3	3S---- -----	B3run33-9	2.412E+05	333.58	1.2E-01	331.72	1.2E-01	334.88	1.2E-01	334.03	1.2E-01	332.65	8.0E-02	334.45	8.4E-02
3	3S---- -----	B3run33-10	3.692E+05	331.38	1.4E-01	328.35	1.4E-01	331.57	1.3E-01	329.76	1.3E-01	329.86	1.0E-01	330.66	8.6E-02
3	3S---- -----	B3run34-1	2.648E+05	330.02	1.2E-01	328.50	1.5E-01	330.86	1.3E-01	330.82	1.5E-01	329.26	1.0E-01	330.84	9.6E-02
3	3S---- -----	B3run34-2	3.061E+05	326.72	1.2E-01	323.84	1.3E-01	327.22	1.3E-01	325.50	1.6E-01	325.28	8.4E-02	326.36	1.0E-01
3	3S---- -----	B3run34-3	2.954E+05	327.23	1.2E-01	325.26	1.2E-01	326.71	1.1E-01	326.02	1.1E-01	326.24	8.8E-02	326.37	8.1E-02
3	3S---- -----	B3run34-4	2.950E+05	331.23	1.0E-01	329.93	1.3E-01	331.38	1.4E-01	331.39	1.3E-01	330.58	9.2E-02	331.38	9.6E-02
3	3S---- -----	B3run34-5	2.731E+05	329.82	1.2E-01	327.71	1.2E-01	329.00	1.0E-01	328.32	1.2E-01	328.76	8.5E-02	328.66	8.2E-02
3	3S---- -----	B3run34-6	3.118E+05	331.69	1.1E-01	328.77	1.1E-01	331.33	1.1E-01	329.68	1.2E-01	330.23	8.0E-02	330.51	8.8E-02
3	3S---- -----	B3run34-7	3.184E+05	331.23	1.3E-01	328.91	1.4E-01	333.50	1.1E-01	332.01	1.1E-01	330.07	9.5E-02	332.76	7.4E-02
3	3S---- -----	B3run34-8	2.757E+05	334.36	1.2E-01	332.11	1.6E-01	333.42	1.3E-01	332.69	1.5E-01	333.23	1.1E-01	333.06	9.8E-02
3	3S---- -----	B3run34-9	2.750E+05	336.02	1.6E-01	334.21	1.8E-01	338.27	1.8E-01	338.36	1.5E-01	335.12	1.2E-01	338.32	1.2E-01
3	3S---- -----	B3run35-1	2.599E+05	333.87	1.2E-01	332.58	1.3E-01	334.24	1.1E-01	334.37	1.6E-01	333.22	8.5E-02	334.30	9.3E-02
3	3S---- -----	B3run35-2	2.818E+05	331.83	9.9E-02	329.97	1.2E-01	329.97	1.2E-01	329.09	1.3E-01	330.90	7.7E-02	329.53	9.7E-02
3	3S---- -----	B3run35-3	2.832E+05	332.73	1.2E-01	330.56	1.1E-01	331.69	1.1E-01	331.04	1.1E-01	331.65	8.7E-02	331.37	7.8E-02
3	3S---- -----	B3run35-4	3.433E+05	333.77	1.0E-01	330.76	1.2E-01	332.30	1.3E-01	330.42	1.2E-01	332.27	8.3E-02	331.36	8.7E-02
3	3S---- -----	B3run35-5	2.640E+05	339.03	1.1E-01	337.03	1.1E-01	339.20	1.5E-01	338.07	1.3E-01	338.03	8.3E-02	338.63	9.5E-02
3	3S---- -----	B3run35-6	3.365E+05	335.72	1.2E-01	332.85	1.3E-01	334.77	1.1E-01	332.98	1.2E-01	334.29	7.9E-02	333.87	7.9E-02
3	3S---- -----	B3run35-7	2.251E+05	343.68	1.2E-01	341.76	1.3E-01	344.56	1.3E-01	344.86	1.3E-01	342.72	9.2E-02	344.71	9.6E-02
3	3S---- -----	B3run35-8	2.278E+05	342.54	1.1E-01	340.86	1.4E-01	343.55	1.2E-01	343.20	1.3E-01	341.70	9.1E-02	343.37	9.0E-02
3	3S---- -----	B3run35-9	3.154E+05	339.25	1.4E-01	336.96	1.5E-01	338.81	1.3E-01	337.19	1.0E-01	338.10	1.0E-01	338.00	8.6E-02

Build	Exp Code	Run	Pcav (abs Pa)	Ts,C2,d,av (K)	+/-	Ts,C3,u,av (K)	+/-	TS,C3,d,av (K)	+/-	Ts,C4,u,av (K)	+/-	finTs,D2,av (K)	+/-	finTs,D3,av (K)	+/-
3	3S---- -----	B3run36-1	2.554E+05	340.73	1.3E-01	339.70	1.3E-01	342.19	1.3E-01	342.79	1.4E-01	340.22	9.1E-02	342.49	9.7E-02
3	3S---- -----	B3run37-1	2.216E+05	320.28	1.3E+00	319.22	9.5E-01	319.69	1.4E+00	319.12	1.2E+00	319.75	8.2E-01	319.40	9.1E-01
3	3S---- -----	B3run38-1	2.232E+05	346.72	1.4E-01	345.94	1.5E-01	352.02	1.3E-01	352.92	1.3E-01	346.33	1.0E-01	352.47	9.6E-02
3	3S---- -----	B3run39-1	2.220E+05	326.22	1.1E-01	324.74	1.1E-01	325.57	1.0E-01	325.01	1.1E-01	325.48	7.8E-02	325.29	8.3E-02
3	3S---- -----	B3run40-1	2.274E+05	353.32	1.3E-01	354.01	1.5E-01	359.91	1.4E-01	360.99	1.4E-01	353.67	9.5E-02	360.45	9.7E-02
3	3S---- -----	B3run44-1	2.340E+05	308.79	1.5E+00	308.25	1.1E+00	307.79	1.6E+00	307.34	1.4E+00	308.52	9.4E-01	307.57	1.0E+00
3	3S---- -----	B3run44-2	2.351E+05	313.69	1.5E+00	313.02	1.1E+00	312.41	1.4E+00	312.04	1.3E+00	313.36	9.2E-01	312.23	9.5E-01
3	3S---- -----	B3run44-3	2.347E+05	317.90	1.4E-01	316.79	1.5E-01	316.65	1.6E-01	316.33	1.1E-01	317.35	1.1E-01	316.49	9.4E-02
3	3S---- -----	B3run45-1	2.229E+05	303.21	1.4E-01	303.18	1.3E-01	302.98	1.2E-01	302.72	1.3E-01	303.20	9.3E-02	302.85	8.7E-02

Build	Exp Code	Run	Nu,C2,d,av	+/-	Nu,C3,u,av	+/-	Nu,C3,d,av	+/-	Nu,C4,u,av	+/-	Nush,C2	+/-	Nush,C3	+/-	finNu,D2,av	+/-	finNu,D3,av	+/-
3	3S---------	B3run2-1	-223.3	1.2E+02	590.5	1.4E+02	520.2	1.2E+02	-2.5E+02	105.5	5.5E+01	2	42.5	1.7E+00	148.0	1.3E+01	116.8	1.2E+01
3	3S---------	B3run2-2	-204.2	8.2E+01	563.7	9.1E+01	471.1	7.1E+01	-2.1E+02	64.2	5.4E+01	2	42.4	1.1E+00	145.4	1.1E+01	115.7	7.7E+00
3	3S---------	B3run3-1	-409.4	1.1E+02	807.3	1.3E+02	429.0	9.3E+01	-1.3E+02	86.1	5.4E+01	2	43.6	1.1E+00	149.8	1.4E+01	135.2	9.8E+00
3	3S---------	B3run4-1	-469.2	1.1E+02	776.7	1.4E+02	266.5	9.4E+01	8.2E+00	88.2	5.1E+01	2	53.0	1.8E+00	112.9	1.1E+01	127.0	1.2E+01
3	3S---------	B3run4-2	-437.5	2.1E+02	732.4	2.5E+02	254.2	2.1E+02	1.4E+01	199.0	5.0E+01	4	52.4	3.9E+00	110.0	2.6E+01	123.9	2.0E+01
3	3S---------	B3run5-1	-703.5	1.1E+02	1191.0	1.4E+02	300.1	1.2E+02	3.4E+01	104.7	5.5E+01	2	52.7	1.8E+00	161.7	1.3E+01	157.6	1.4E+01
3	3S---------	B3run5-3	-613.1	7.8E+01	1076.9	1.0E+02	276.8	7.6E+01	5.6E+01	73.9	5.6E+01	1	53.4	1.5E+00	163.7	1.3E+01	157.1	1.0E+01
3	3S---------	B3run6-1	-742.6	6.9E+01	1233.4	8.9E+01	301.3	7.6E+01	2.8E+01	71.7	5.4E+01	1	52.8	1.4E+00	159.1	1.0E+01	154.8	8.8E+00
3	3S---------	B3run6-2	-557.0	1.2E+04	1017.0	3.4E+03	282.0	1.3E+03	6.7E+01	2185.0	5.5E+01	10	53.9	1.1E+01	166.5	2.3E+02	164.6	6.9E+01
3	3S---------	B3run6-3	-648.5	1.1E+02	1118.3	1.4E+02	271.4	1.2E+02	7.0E+01	112.6	5.4E+01	2	52.3	1.6E+00	161.1	1.6E+01	161.1	1.2E+01
3	3S---------	B3run7-1	-281.8	2.3E+02	577.9	2.2E+02	326.4	2.4E+02	-5.5E+01	239.6	5.7E+01	5	58.3	3.7E+00	120.7	2.9E+01	125.3	2.5E+01
3	3S---------	B3run7-2	-477.1	1.0E+02	788.2	1.3E+02	231.6	1.1E+02	2.6E+01	103.1	5.0E+01	2	52.6	1.9E+00	112.2	1.3E+01	120.0	1.2E+01
3	3S---------	B3run7-4	-449.2	1.2E+02	754.1	1.4E+02	264.8	1.1E+02	-6.2E+01	103.5	3.4E+01	2	34.1	1.9E+00	110.0	1.6E+01	94.4	1.4E+01
3	3S---------	B3run8-1	-519.2	4.9E+01	818.5	6.0E+01	281.5	5.9E+01	-9.5E+01	57.3	3.2E+01	1	32.3	1.1E+00	103.0	8.0E+00	86.7	7.5E+00
3	3S---------	B3run9-1	1400.8	1.1E+02	-857.6	7.8E+01	-208.0	6.9E+01	4.5E+02	74.1	3.3E+01	1	32.8	1.2E+00	157.7	1.2E+01	108.1	8.5E+00
3	3S---------	B3run9-2	-510.2	5.8E+01	815.2	7.2E+01	-0.6	5.6E+01	2.3E+02	58.4	6.0E+01	1	64.6	1.3E+00	108.2	7.4E+00	105.6	7.8E+00
3	3S---------	B3run9-3	-506.3	5.3E+01	811.1	6.5E+01	1.0	6.7E+01	2.3E+02	67.8	6.1E+01	1	65.0	1.2E+00	108.5	7.4E+00	105.7	7.2E+00
3	3S---------	B3run9-4	-590.4	7.6E+01	967.6	9.8E+01	29.1	8.8E+01	2.9E+02	93.4	6.2E+01	2	68.3	1.5E+00	133.1	1.2E+01	144.1	1.0E+01
3	3S---------	B3run12-1	-267.1	6.4E+01	590.6	7.5E+01	177.8	6.0E+01	9.2E+01	59.5	5.1E+01	1	51.0	1.0E+00	131.4	8.2E+00	126.1	7.8E+00
3	3S---------	B3run13-1	343.0	1.3E+02	68.4	1.1E+02	-43.8	8.2E+01	3.0E+02	84.8	5.6E+01	2	45.9	1.2E+00	174.0	1.5E+01	121.3	9.9E+00
3	3S---------	B3run13-2	388.7	1.0E+02	20.6	8.9E+01	-79.9	6.7E+01	3.3E+02	69.6	5.6E+01	2	45.8	1.0E+00	172.0	1.2E+01	118.6	7.8E+00
3	3S---------	B3run13-3	-1051.5	9.6E+01	1599.5	1.4E+02	-487.8	8.2E+01	7.8E+02	94.2	1.1E+02	2	109.3	1.7E+00	136.6	1.3E+01	112.9	9.4E+00
3	3S---------	B3run15-1	-393.4	7.4E+01	777.2	8.7E+01	244.3	6.6E+01	6.1E+01	64.3	5.9E+01	2	53.9	9.9E-01	149.0	9.1E+00	143.4	8.6E+00
3	3S---------	B3run15-2	-470.1	6.7E+01	781.0	8.0E+01	4.7	6.7E+01	2.0E+02	67.7	8.2E+01	1	73.9	1.5E+00	113.9	8.6E+00	95.9	8.0E+00
3	3S---------	B3run16-1	-711.9	9.2E+01	1166.8	1.2E+02	51.2	9.8E+01	3.1E+02	103.1	7.8E+01	1	79.8	1.6E+00	152.1	1.2E+01	164.6	1.2E+01

Build	Exp Code	Run	Nu,C2,d,av	+/-	Nu,C3,u,av	+/-	Nu,C3,d,av	+/-	Nu,C4,u,av	+/-	Nush,C2	+/-	Nush,C3	+/-	finNu,D2,av	+/-	finNu,D3,av	+/-
3	3S---------	B3run16-2	-1196.3	9.7E+01	1838.4	1.6E+02	-508.7	9.2E+01	8.3E+02	115.1	1.1E+02	2	108.6	2.0E+00	143.6	1.4E+01	125.1	1.3E+01
3	3S---------	B3run17-1	-907.4	9.9E+01	1524.9	1.4E+02	-88.4	1.2E+02	5.2E+02	125.6	7.9E+01	1	81.9	1.4E+00	188.6	1.3E+01	194.9	1.2E+01
3	3S---------	B3run17-2	-912.1	1.2E+02	1534.9	1.8E+02	-55.8	1.2E+02	4.9E+02	133.6	7.9E+01	2	81.6	1.8E+00	189.8	1.4E+01	194.8	1.3E+01
3	3S---------	B3run17-3	-1634.5	1.3E+02	2651.4	2.4E+02	-960.3	1.5E+02	1.6E+03	227.3	1.1E+02	2	118.0	2.0E+00	182.1	1.8E+01	211.4	2.1E+01
3	3S---------	B3run17-4	-1639.7	1.4E+02	2666.8	2.8E+02	-964.6	1.1E+02	1.7E+03	180.6	1.1E+02	2	118.4	2.3E+00	184.1	1.8E+01	212.7	2.1E+01
3	3S---------	B3run17-5	-353.0	5.3E+01	639.7	6.1E+01	239.1	6.0E+01	-1.5E+01	56.5	5.1E+01	1	54.1	9.9E-01	110.5	6.8E+00	104.9	6.7E+00
3	3S---------	B3run17-6	-342.0	6.0E+01	625.3	6.7E+01	223.6	6.0E+01	7.4E-01	58.3	5.1E+01	1	53.9	1.2E+00	109.7	7.1E+00	105.1	7.1E+00
3	3S---------	B3run18-1	-509.0	6.0E+01	841.5	7.4E+01	354.1	5.4E+01	-1.3E+02	50.4	3.5E+01	1	32.9	1.1E+00	118.1	7.7E+00	102.3	6.8E+00
3	3S---------	B3run18-2	-467.1	8.0E+01	804.1	1.0E+02	120.4	8.1E+01	1.3E+02	82.7	6.2E+01	2	66.4	1.4E+00	123.4	1.1E+01	116.3	8.2E+00
3	3S---------	B3run18-3	-698.3	7.0E+01	1215.5	9.1E+01	364.5	7.6E+01	-1.8E+01	71.7	5.5E+01	1	54.3	1.4E+00	173.6	1.0E+01	161.4	1.0E+01
3	3S---------	B3run19-1	-797.6	3.5E+02	1322.2	3.8E+02	410.7	3.6E+02	-7.6E+01	394.9	5.5E+01	6	51.4	5.5E+00	164.2	4.9E+01	154.9	4.0E+01
3	3S---------	B3run20-1	-343.7	1.4E+02	694.5	1.7E+02	157.5	1.2E+02	1.3E+02	119.0	6.0E+01	2	55.0	1.5E+00	138.5	1.6E+01	134.7	1.4E+01
3	3S---------	B3run21-1	-445.4	8.7E+01	803.1	1.1E+02	129.9	9.6E+01	1.6E+02	95.9	5.8E+01	2	52.4	1.5E+00	135.6	1.2E+01	135.2	1.1E+01
3	3S---------	B3run22-1	-336.2	5.9E+01	623.7	6.9E+01	237.6	6.3E+01	-3.7E+00	60.0	5.9E+01	1	57.6	1.3E+00	112.7	8.9E+00	109.7	7.5E+00
3	3S---------	B3run22-2	-937.2	1.6E+02	1462.7	2.4E+02	-236.5	2.0E+02	6.1E+02	230.9	8.1E+01	3	84.4	2.4E+00	148.2	2.4E+01	160.2	2.3E+01
3	3S---------	B3run23-1	-741.3	9.0E+01	1198.8	1.2E+02	-157.9	1.2E+02	5.5E+02	128.9	7.5E+01	2	80.0	2.0E+00	151.0	1.2E+01	170.2	1.5E+01
3	3S---------	B3run24-1	-289.1	9.7E+01	645.2	1.2E+02	187.3	9.3E+01	1.2E+02	91.7	6.6E+01	2	62.9	1.6E+00	146.3	1.3E+01	147.0	1.3E+01
3	3S---------	B3run24-2	-708.3	1.1E+02	1129.4	1.4E+02	113.0	9.6E+01	1.5E+02	95.1	4.0E+01	2	40.0	1.9E+00	128.1	1.4E+01	123.2	1.3E+01
3	3S--------	B3run25-1	-381.6	8.5E+01	831.4	1.0E+02	278.4	7.7E+01	2.5E+01	72.2	5.5E+01	2	47.2	1.4E+00	172.1	1.2E+01	141.8	1.1E+01
3	3S---------	B3run26-1	-1034.9	8.9E+01	1500.3	1.3E+02	-467.8	6.7E+01	7.2E+02	80.0	7.3E+01	1	77.9	1.8E+00	105.9	1.0E+01	97.5	1.0E+01
3	3S---------	B3run27-1	-1483.0	9.6E+01	2403.4	1.9E+02	-609.2	1.1E+02	1.2E+03	139.8	7.3E+01	2	82.1	1.8E+00	186.7	1.8E+01	211.9	1.9E+01
3	3S---------	B3run28-1	-2103.6	1.3E+02	3453.3	2.8E+02	-1331.1	1.5E+02	2.1E+03	257.2	1.0E+02	3	113.2	3.0E+00	152.0	1.9E+01	168.5	1.9E+01
3	3S---------	B3run28-2	-1557.5	8.0E+01	2286.4	1.3E+02	-919.4	8.9E+01	1.3E+03	126.5	9.0E+01	2	98.8	1.9E+00	101.0	1.4E+01	90.9	1.1E+01
3	3S---------	B3run30-1	-1114.4	1.6E+02	1808.6	2.8E+02	-943.6	2.3E+02	1.6E+03	333.3	1.2E+02	4	110.2	4.7E+00	189.9	2.3E+01	205.2	2.6E+01
3	3S---------	B3run31-1	-34.8	1.0E+02	556.7	1.1E+02	85.0	7.5E+01	2.8E+02	75.6	5.4E+01	1	32.3	8.7E-01	218.7	1.1E+01	175.0	8.0E+00
3	3S---------	B3run32-1	166.7	5.6E+01	108.7	5.5E+01	299.5	4.5E+01	-1.4E+02	42.3	3.9E+01	1	31.8	7.5E-01	117.8	7.4E+00	75.6	5.8E+00
3	3S---------	B3run33-1	-265.7	7.3E+01	557.4	8.4E+01	224.9	6.6E+01	-6.0E+00	62.6	4.9E+01	1	41.2	1.6E+00	120.0	8.6E+00	102.1	8.1E+00

Build	Exp Code	Run	Nu,C2,d,av	+/-	Nu,C3,u,av	+/-	Nu,C3,d,av	+/-	Nu,C4,u,av	+/-	Nush,C2	+/-	Nush,C3	+/-	finNu,D2,av	+/-	finNu,D3,av	+/-
3	3S---------	B3run33-2	-913.9	8.8E+01	1419.7	1.3E+02	-290.9	1.0E+02	6.7E+02	122.8	8.5E+01	2	86.1	1.7E+00	147.6	1.2E+01	162.0	1.3E+01
3	3S---------	B3run33-3	-463.9	6.4E+01	736.4	7.5E+01	114.3	6.4E+01	9.7E+01	65.0	6.0E+01	1	51.7	1.1E+00	100.0	7.5E+00	99.0	7.4E+00
3	3S---------	B3run33-4	-683.9	8.6E+01	1256.3	1.2E+02	79.3	7.2E+01	2.4E+02	72.8	6.2E+01	2	44.4	1.1E+00	197.5	1.4E+01	152.9	9.5E+00
3	3S---------	B3run33-5	-2124.1	1.2E+02	3596.0	3.4E+02	-1344.7	1.4E+02	2.2E+03	269.6	1.1E+02	2	128.2	2.7E+00	177.5	2.2E+01	188.3	2.3E+01
3	3S---------	B3run33-6	-1076.4	9.6E+01	1516.4	1.5E+02	-523.8	7.5E+01	7.4E+02	89.1	1.0E+02	2	104.9	2.1E+00	89.7	1.1E+01	80.8	8.8E+00
3	3S---------	B3run33-7	-391.4	6.7E+01	684.7	7.9E+01	217.6	7.4E+01	1.9E+01	69.7	5.6E+01	1	50.9	1.2E+00	113.3	7.6E+00	109.1	8.3E+00
3	3S---------	B3run33-8	-981.0	8.3E+01	1489.1	1.2E+02	-215.3	1.1E+02	5.7E+02	117.0	7.7E+01	2	76.1	1.6E+00	134.9	1.0E+01	153.5	1.1E+01
3	3S---------	B3run33-9	-708.3	7.2E+01	1074.5	9.2E+01	-233.1	7.1E+01	4.7E+02	76.6	8.1E+01	2	79.3	1.5E+00	113.2	9.8E+00	103.1	8.5E+00
3	3S---------	B3run33-10	-1623.6	9.6E+01	2449.2	1.7E+02	-889.5	1.0E+02	1.3E+03	140.1	1.0E+02	3	115.9	2.4E+00	116.1	1.2E+01	117.4	1.4E+01
3	3S---------	B3run34-1	-572.7	8.2E+01	978.2	1.0E+02	139.6	9.6E+01	1.5E+02	96.2	6.0E+01	1	52.1	1.3E+00	145.1	9.8E+00	137.4	1.0E+01
3	3S---------	B3run34-2	-1960.0	1.3E+02	3278.0	3.0E+02	-1031.8	1.4E+02	1.6E+03	226.1	1.2E+02	2	127.5	2.3E+00	182.2	2.1E+01	172.1	2.2E+01
3	3S---------	B3run34-3	-972.6	9.2E+01	1486.8	1.3E+02	-227.5	8.8E+01	5.7E+02	93.4	8.2E+01	2	85.8	2.0E+00	139.8	1.4E+01	150.3	1.1E+01
3	3S---------	B3run34-4	-462.4	6.4E+01	770.6	8.0E+01	141.5	8.6E+01	1.1E+02	85.8	5.6E+01	1	50.6	1.2E+00	115.1	9.2E+00	115.4	9.7E+00
3	3S---------	B3run34-5	-1130.9	1.1E+02	1771.3	1.6E+02	-241.5	1.0E+02	6.5E+02	114.8	8.4E+01	2	85.5	1.8E+00	160.3	1.3E+01	176.4	1.4E+01
3	3S---------	B3run34-6	-2464.7	1.3E+02	4641.5	3.8E+02	-1340.3	1.4E+02	2.3E+03	256.1	1.1E+02	2	133.4	2.4E+00	236.4	2.3E+01	232.7	2.4E+01
3	3S---------	B3run34-7	-1436.6	1.1E+02	2242.6	1.9E+02	-719.8	9.4E+01	1.1E+03	128.4	1.2E+02	3	125.1	2.4E+00	148.8	1.6E+01	113.1	1.2E+01
3	3S---------	B3run34-8	-1359.3	1.3E+02	2208.5	2.5E+02	-299.8	1.4E+02	8.0E+02	174.7	7.9E+01	2	81.3	1.6E+00	186.3	1.7E+01	209.5	1.7E+01
3	3S---------	B3run34-9	-934.1	1.4E+02	1660.2	2.3E+02	248.4	1.3E+02	1.2E+02	126.0	6.7E+01	2	47.7	1.3E+00	218.0	1.9E+01	172.0	1.3E+01
3	3S---------	B3run35-1	-427.1	7.9E+01	778.8	9.4E+01	227.6	8.6E+01	9.3E+01	87.5	5.5E+01	1	58.3	1.3E+00	134.1	9.4E+00	148.7	8.8E+00
3	3S---------	B3run35-2	-1119.7	1.1E+02	1782.5	1.7E+02	-494.5	1.4E+02	1.1E+03	170.3	7.9E+01	2	85.4	2.0E+00	171.8	1.5E+01	215.6	2.2E+01
3	3S---------	B3run35-3	-1239.8	9.2E+01	1937.3	1.6E+02	-255.4	1.2E+02	6.7E+02	135.2	8.0E+01	2	85.8	1.8E+00	159.9	1.6E+01	177.6	1.6E+01
3	3S---------	B3run35-4	-2718.6	2.0E+02	5156.8	1.6E+03	-2016.5	3.1E+02	3.5E+03	8123.9	1.0E+02	2	119.1	3.5E+00	190.8	2.7E+01	220.0	6.2E+01
3	3S---------	B3run35-5	-841.0	7.0E+01	1210.5	9.7E+01	-420.5	9.2E+01	6.6E+02	107.4	7.5E+01	2	72.3	1.8E+00	98.8	1.0E+01	93.9	1.1E+01
3	3S---------	B3run35-6	-1997.8	1.4E+02	3214.3	3.4E+02	-1332.8	1.3E+02	2.0E+03	211.5	9.8E+01	2	107.5	3.0E+00	132.6	1.7E+01	130.0	1.8E+01
3	3S---------	B3run35-7	-617.5	6.0E+01	967.6	7.8E+01	246.2	6.4E+01	6.8E+00	63.0	5.1E+01	1	56.3	1.1E+00	114.5	8.1E+00	117.6	8.2E+00
3	3S---------	B3run35-8	-703.6	8.4E+01	1238.7	1.1E+02	20.6	8.6E+01	3.3E+02	87.3	5.6E+01	2	49.4	1.2E+00	177.7	1.3E+01	161.4	9.9E+00
3	3S---------	B3run35-9	-1416.1	1.3E+02	2085.6	2.2E+02	-1019.8	1.1E+02	1.4E+03	161.6	1.0E+02	3	100.3	3.5E+00	108.9	1.7E+01	91.9	1.7E+01
3	3S---------	B3run36-1	-291.6	7.4E+01	604.3	8.4E+01	365.3	7.0E+01	-9.3E+01	66.0	5.4E+01	1	53.8	1.3E+00	125.1	9.2E+00	123.8	8.8E+00

Build	Exp Code	Run	Nu,C2,d,av	+/-	Nu,C3,u,av	+/-	Nu,C3,d,av	+/-	Nu,C4,u,av	+/-	Nush,C2	+/-	Nush,C3	+/-	finNu,D2,av	+/-	finNu,D3,av	+/-
3	3S---------	B3run37-1	-5314.6	2.5E+04	154778.8	1.9E+04	-3997.5	5.8E+04	-1.5E+05	142311.6	1.1E+02	365	109.4	1.1E+03	2777.2	2.3E+03	6843.4	2.2E+03
3	3S---------	B3run38-1	-138.1	7.3E+01	505.0	7.7E+01	408.0	5.2E+01	-1.2E+02	48.2	4.4E+01	1	17.3	9.9E-01	147.7	8.8E+00	132.7	6.0E+00
3	3S---------	B3run39-1	-18455.3	6.5E+04	-12412.0	7.1E+04	12523.5	6.4E+03	-7.5E+03	78773.6	1.1E+02	2	111.0	2.5E+00	-6119.2	2.0E+04	-3408.3	1.7E+04
3	3S---------	B3run40-1	244.4	4.8E+01	-48.0	4.7E+01	273.0	3.9E+01	-1.4E+02	36.7	2.9E+01	1	25.6	6.4E-01	81.5	4.8E+00	58.9	4.4E+00
3	3S---------	B3run44-1	-1066.3	4.6E+03	4337.9	2.5E+04	-1027.4	8.6E+03	9.9E+03	19490.9	1.1E+02	49	108.8	5.1E+01	1117.8	1.9E+03	2610.7	6.4E+03
3	3S---------	B3run44-2	-677.2	6.4E+03	1840.0	1.1E+04	-116.2	1.1E+04	1.7E+03	#####	1.0E+02	23	99.4	4.3E+01	444.9	2.7E+04	657.1	8.7E+02
3	3S---------	B3run44-3	-1045.9	2.1E+02	2154.5	3.6E+02	-11.8	4.1E+02	9.9E+02	492.7	9.5E+01	2	93.3	2.3E+00	358.9	3.4E+01	431.3	5.1E+01
3	3S---------	B3run45-1	91.4	1.2E+03	-54.5	1.9E+03	623.1	9.3E+02	-5.7E+02	767.0	2.8E+01	37	-1.7	4.8E+01	15.9	9.9E+01	1.4	1.0E+03

Build	Exp Code	Run	Tsh,C2,out (K)	+/-	Tsh,C3,out(K)	+/-	k_air(Tin)	+/-	V (m/s)	+/-
3	3S---------	B3run2-1	379	0.3	3.9E+02	0.30	2.7E-02	2.38E-05	32.97	3.3E-02
3	3S---------	B3run2-2	380	0.2	3.9E+02	0.19	2.8E-02	1.77E-05	32.97	2.5E-02
3	3S---------	B3run3-1	383	0.2	3.9E+02	0.19	2.8E-02	2.14E-05	32.00	2.9E-02
3	3S---------	B3run4-1	381	0.2	3.8E+02	0.25	2.7E-02	2.69E-05	11.46	1.3E-02
3	3S---------	B3run4-2	381	0.5	3.9E+02	0.55	2.7E-02	3.14E-05	11.50	1.6E-02
3	3S---------	B3run5-1	380	0.3	3.8E+02	0.26	2.7E-02	2.36E-05	20.03	2.0E-02
3	3S---------	B3run5-3	378	0.2	3.8E+02	0.21	2.7E-02	1.60E-05	19.69	1.4E-02
3	3S---------	B3run6-1	379	0.2	3.9E+02	0.21	2.7E-02	1.93E-05	19.90	1.7E-02
3	3S---------	B3run6-2	378	1.6	3.8E+02	1.60	2.7E-02	6.75E-05	19.81	5.8E-02
3	3S---------	B3run6-3	379	0.3	3.9E+02	0.24	2.7E-02	1.93E-05	19.88	1.7E-02
3	3S---------	B3run7-1	371	0.7	3.8E+02	0.66	2.6E-02	2.11E-05	9.36	8.8E-03
3	3S---------	B3run7-2	383	0.3	3.9E+02	0.30	2.8E-02	3.00E-05	9.59	1.2E-02
3	3S---------	B3run7-4	392	0.3	3.9E+02	0.35	2.8E-02	3.82E-05	9.71	1.6E-02
3	3S---------	B3run8-1	393	0.2	4.0E+02	0.21	2.7E-02	2.20E-05	9.14	8.6E-03
3	3S---------	B3run9-1	381	0.2	3.9E+02	0.24	2.7E-02	1.89E-05	26.58	2.2E-02
3	3S---------	B3run9-2	383	0.2	3.8E+02	0.16	2.7E-02	1.92E-05	9.74	8.0E-03
3	3S---------	B3run9-3	383	0.2	3.8E+02	0.16	2.7E-02	1.84E-05	9.74	7.6E-03
3	3S---------	B3run9-4	383	0.2	3.8E+02	0.16	2.8E-02	2.10E-05	20.38	1.8E-02
3	3S---------	B3run12-1	387	0.2	3.9E+02	0.16	2.8E-02	1.63E-05	14.87	1.0E-02
3	3S---------	B3run13-1	381	0.2	3.9E+02	0.18	2.8E-02	2.41E-05	41.44	4.2E-02
3	3S---------	B3run13-2	381	0.2	3.9E+02	0.16	2.8E-02	3.32E-05	41.40	5.8E-02
3	3S---------	B3run13-3	381	0.2	3.8E+02	0.17	2.7E-02	1.75E-05	14.92	1.1E-02
3	3S---------	B3run15-1	381	0.2	3.9E+02	0.16	2.7E-02	1.97E-05	15.71	1.3E-02
3	3S---------	B3run15-2	374	0.2	3.7E+02	0.16	2.7E-02	1.73E-05	7.94	6.0E-03
3	3S---------	B3run16-1	376	0.2	3.7E+02	0.16	2.7E-02	1.83E-05	15.71	1.2E-02

Build	Exp Code	Run	Tsh,C2,out (K)	+/-	Tsh,C3,out(K)	+/-	k_air(Tin)	+/-	V (m/s)	+/-
3	3S---------	B3run16-2	383	0.2	3.8E+02	0.18	2.8E-02	1.81E-05	15.57	1.2E-02
3	3S---------	B3run17-1	376	0.2	3.8E+02	0.16	2.7E-02	1.64E-05	30.56	2.2E-02
3	3S---------	B3run17-2	377	0.2	3.8E+02	0.16	2.7E-02	1.90E-05	30.40	2.5E-02
3	3S---------	B3run17-3	380	0.2	3.8E+02	0.17	2.7E-02	1.83E-05	30.69	2.4E-02
3	3S---------	B3run17-4	380	0.2	3.8E+02	0.16	2.8E-02	1.81E-05	30.62	2.4E-02
3	3S---------	B3run17-5	381	0.2	3.9E+02	0.16	2.7E-02	1.58E-05	8.53	5.8E-03
3	3S---------	B3run17-6	381	0.2	3.9E+02	0.18	2.7E-02	1.87E-05	8.35	6.7E-03
3	3S---------	B3run18-1	388	0.2	3.9E+02	0.19	2.7E-02	1.83E-05	9.61	7.6E-03
3	3S---------	B3run18-2	383	0.2	3.9E+02	0.19	2.8E-02	1.81E-05	9.60	7.3E-03
3	3S---------	B3run18-3	383	0.2	3.9E+02	0.17	2.8E-02	1.65E-05	20.52	1.4E-02
3	3S---------	B3run19-1	384	0.7	3.9E+02	0.77	2.8E-02	2.44E-05	19.30	2.0E-02
3	3S---------	B3run20-1	379	0.2	3.8E+02	0.18	2.8E-02	4.39E-05	15.60	2.9E-02
3	3S---------	B3run21-1	372	0.2	3.7E+02	0.17	2.7E-02	1.79E-05	15.57	1.2E-02
3	3S---------	B3run22-1	374	0.2	3.8E+02	0.16	2.7E-02	1.83E-05	8.02	6.4E-03
3	3S---------	B3run22-2	377	0.2	3.7E+02	0.25	2.8E-02	1.91E-05	14.92	1.2E-02
3	3S---------	B3run23-1	376	0.2	3.7E+02	0.17	2.8E-02	1.59E-05	19.12	1.3E-02
3	3S---------	B3run24-1	367	0.2	3.7E+02	0.23	2.7E-02	1.81E-05	15.15	1.2E-02
3	3S---------	B3run24-2	393	0.2	4.0E+02	0.22	2.9E-02	2.40E-05	15.90	1.5E-02
3	3S--------	B3run25-1	387	0.2	3.9E+02	0.21	2.8E-02	1.64E-05	32.25	2.2E-02
3	3S---------	B3run26-1	380	0.2	3.8E+02	0.16	2.8E-02	1.58E-05	7.70	5.0E-03
3	3S---------	B3run27-1	376	0.2	3.7E+02	0.17	2.8E-02	1.84E-05	35.27	2.7E-02
3	3S---------	B3run28-1	369	0.2	3.6E+02	0.19	2.7E-02	1.82E-05	17.88	1.4E-02
3	3S---------	B3run28-2	373	0.2	3.7E+02	0.16	2.7E-02	1.87E-05	8.96	7.2E-03
3	3S---------	B3run30-1	369	0.3	3.6E+02	0.28	2.7E-02	1.71E-05	34.37	2.5E-02
3	3S---------	B3run31-1	384	0.2	3.9E+02	0.16	2.8E-02	2.00E-05	34.98	2.9E-02
3	3S---------	B3run32-1	388	0.2	3.9E+02	0.17	2.7E-02	1.81E-05	17.38	1.4E-02
3	3S---------	B3run33-1	375	0.2	3.7E+02	0.22	2.7E-02	2.15E-05	16.01	1.5E-02

Build	Exp Code	Run	Tsh,C2,out (K)	+/-	Tsh,C3,out(K)	+/-	k_air(Tin)	+/-	V (m/s)	+/-
3	3S---------	B3run33-2	370	0.2	3.7E+02	0.17	2.7E-02	1.69E-05	16.08	1.2E-02
3	3S---------	B3run33-3	373	0.2	3.7E+02	0.16	2.7E-02	1.61E-05	7.70	5.4E-03
3	3S---------	B3run33-4	379	0.2	3.8E+02	0.16	2.7E-02	1.84E-05	33.19	2.6E-02
3	3S---------	B3run33-5	374	0.2	3.7E+02	0.17	2.8E-02	1.98E-05	24.76	2.1E-02
3	3S---------	B3run33-6	379	0.2	3.8E+02	0.18	2.7E-02	1.70E-05	5.13	3.7E-03
3	3S---------	B3run33-7	381	0.2	3.8E+02	0.16	2.7E-02	1.55E-05	16.60	1.1E-02
3	3S---------	B3run33-8	379	0.2	3.8E+02	0.16	2.8E-02	1.72E-05	32.79	2.4E-02
3	3S---------	B3run33-9	381	0.2	3.8E+02	0.16	2.8E-02	1.54E-05	9.02	5.9E-03
3	3S---------	B3run33-10	376	0.2	3.7E+02	0.19	2.8E-02	1.52E-05	11.24	7.2E-03
3	3S---------	B3run34-1	377	0.2	3.8E+02	0.16	2.7E-02	1.86E-05	20.27	1.6E-02
3	3S---------	B3run34-2	377	0.2	3.8E+02	0.17	2.7E-02	1.61E-05	17.25	1.2E-02
3	3S---------	B3run34-3	372	0.2	3.7E+02	0.16	2.7E-02	1.84E-05	10.51	8.3E-03
3	3S---------	B3run34-4	375	0.2	3.7E+02	0.16	2.7E-02	1.60E-05	10.67	7.3E-03
3	3S---------	B3run34-5	376	0.2	3.7E+02	0.17	2.8E-02	1.72E-05	19.49	1.4E-02
3	3S---------	B3run34-6	382	0.2	3.8E+02	0.16	2.8E-02	1.42E-05	30.96	1.8E-02
3	3S---------	B3run34-7	380	0.2	3.8E+02	0.16	2.8E-02	1.64E-05	9.57	6.6E-03
3	3S---------	B3run34-8	381	0.2	3.8E+02	0.16	2.8E-02	1.69E-05	34.92	2.5E-02
3	3S---------	B3run34-9	383	0.2	3.8E+02	0.17	2.8E-02	1.93E-05	34.95	2.8E-02
3	3S---------	B3run35-1	381	0.2	3.9E+02	0.17	2.8E-02	1.64E-05	16.59	1.2E-02
3	3S---------	B3run35-2	376	0.2	3.7E+02	0.16	2.8E-02	1.84E-05	30.22	2.3E-02
3	3S---------	B3run35-3	376	0.2	3.7E+02	0.16	2.8E-02	1.63E-05	14.97	1.0E-02
3	3S---------	B3run35-4	374	0.2	3.7E+02	0.17	2.8E-02	2.18E-05	25.27	2.3E-02
3	3S---------	B3run35-5	380	0.2	3.8E+02	0.16	2.8E-02	1.63E-05	7.76	5.3E-03
3	3S---------	B3run35-6	375	0.2	3.7E+02	0.16	2.8E-02	1.67E-05	12.74	8.8E-03
3	3S---------	B3run35-7	390	0.2	3.9E+02	0.16	2.8E-02	1.58E-05	10.38	6.8E-03
3	3S---------	B3run35-8	390	0.2	3.9E+02	0.16	2.8E-02	1.94E-05	38.86	3.1E-02
3	3S---------	B3run35-9	378	0.2	3.7E+02	0.19	2.8E-02	1.79E-05	6.46	4.7E-03
3	3S---------	B3run36-1	387	0.2	3.9E+02	0.17	2.8E-02	1.93E-05	21.53	1.7E-02

Build	Exp Code	Run	Tsh,C2,out (K)	+/-	Tsh,C3,out(K)	+/-	k_air(Tin)	+/-	V (m/s)	+/-
3	3S---------	B3run37-1	365	1.9	3.6E+02	1.88	2.8E-02	6.21E-05	12.09	3.2E-02
3	3S---------	B3run38-1	398	0.2	4.1E+02	0.19	2.8E-02	1.99E-05	36.10	3.0E-02
3	3S---------	B3run39-1	369	0.2	3.6E+02	0.16	2.8E-02	1.78E-05	12.13	8.9E-03
3	3S---------	B3run40-1	405	0.2	4.1E+02	0.16	2.8E-02	1.73E-05	13.31	9.6E-03
3	3S---------	B3run44-1	358	2.0	3.5E+02	1.99	2.7E-02	6.86E-05	32.31	9.7E-02
3	3S---------	B3run44-2	363	2.0	3.6E+02	1.92	2.7E-02	7.78E-05	32.40	1.1E-01
3	3S---------	B3run44-3	367	0.2	3.6E+02	0.18	2.7E-02	1.86E-05	32.70	2.6E-02
3	3S---------	B3run45-1	302	0.2	3.0E+02	0.18	2.7E-02	2.20E-05	10.39	1.0E-02

Appendix 6.4: Selected LDA test reports

LDA measurement		**LDA code:**	100	**rpm:**		**Perfd by:**	AA	Printed: 26/09/2008	Page 1/3
Build:	3	**ReΦ:**	1.00E+06	**Date:**		**LDA1:**	VΦ	**Comments:**	
LDA test # :	B3run4	**Rez:**	6.27E+04	**raw LDA file:**		**LDA2:**	Vz	**Traverse ref:**	
Heat Transfer run:	B3run4-1	**Ro:**	1.19	**LDA list file:**		**W (m/s):**	11.46		

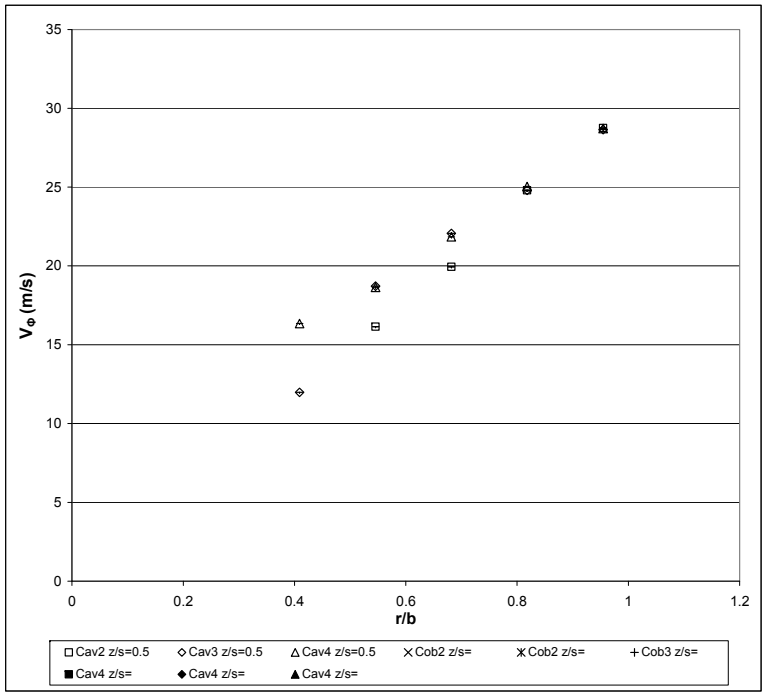

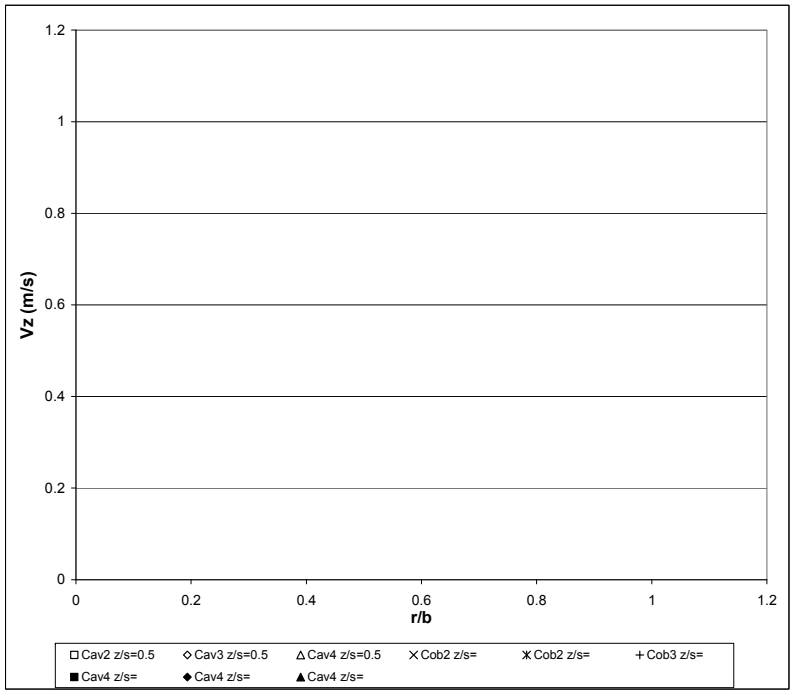

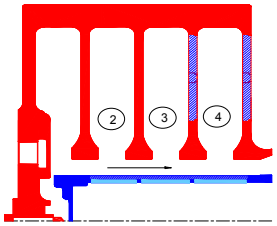

LDA measurement		**LDA code:**	101	**rpm:**	0.0	**Perfd by:**	AA	Printed: 26/09/2008	Page 2/3
Build:	3	**Re_Φ:**	1.00E+06	**Date:**	00/01/1900	**LDA1:**	VΦ	**Comments:**	0
LDA test # :	B3run4	**Re_z:**	6.27E+04	**raw LDA file:**	0	**LDA2:**	Vz	**Traverse corresp:**	0
Heat Transfer run:	B3run4-1	**Ro:**	1.19	**LDA list file:**	0	**W (m/s):**	11.46		

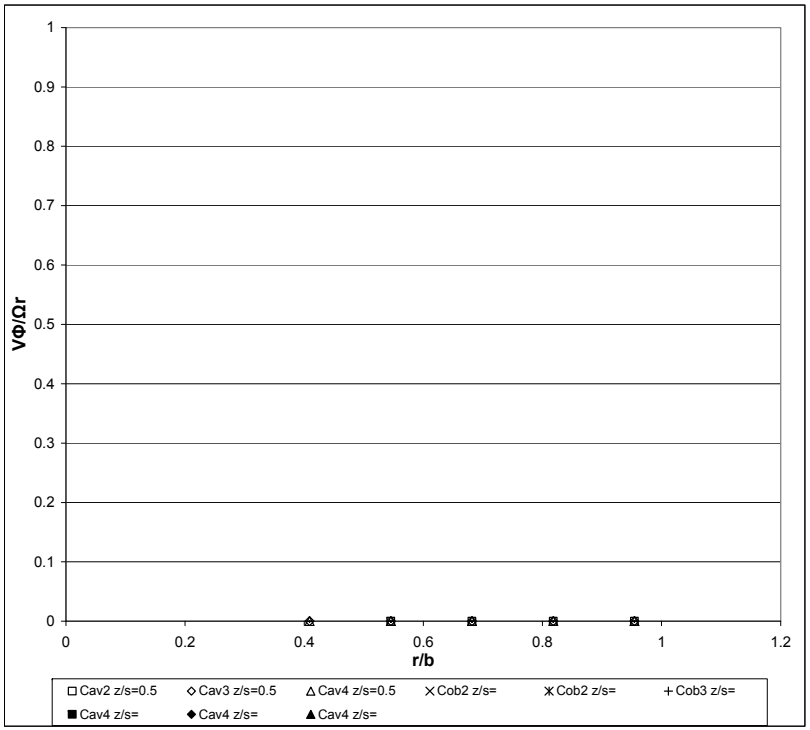

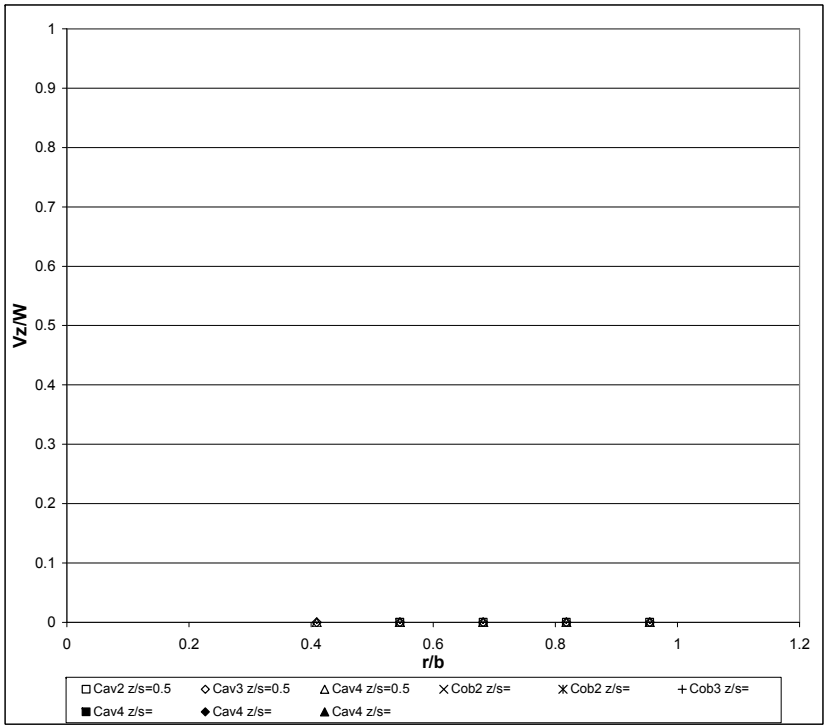

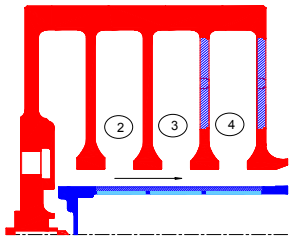

LDA measurement | **LDA code:** 100 | **rpm:** 1311.0 | **Perfd by:** AA | Printed: 26/09/2008 | Page 3/3

Build: 3 | **ReΦ:** 1.00E+06 | **Date:** 00/01/1900 | **LDA1:** VΦ | **Comments:** 0

LDA test # : B3run4 | **Rez:** 6.27E+04 | **raw LDA file:** 0 | **LDA2:** Vz | **Traverse corresp:** 0

Heat Transfer run: B3run4-1 | **Ro:** 1.19 | **LDA list file:** 0 | **W (m/s):** 11.46

X [mm]	corrected X	Y [mm]	corrected Y / Radius (mm)	Count{1}	Count{2}	Data Rate{1} [#/s]	Data Rate{2} [#/s]	Validation{1} [%]	Validation{2} [%]	LDA1 Mean [m/s]	LDA2 Mean [m/s]	LDA1 RMS [m/s]	LDA2 RMS [m/s]	LDA1 MeanConf [m/s]	LDA2 MeanConf [m/s]	LDA1 RMSConf [m/s]	LDA2 RMSConf [m/s]	Cavity	r/b	z/s	Ωr (m/s)	$V_\Phi/\Omega r$	$V_{\Phi U95\%}/\Omega r$	$V_{\Phi(RMS)}/\Omega r$	Vz/W	$Vz_{(RMS)}/W$	$Vz_{U95\%}/W$
115		140	210	100000		7211.1		70.00		28.75		0.97		0.01		0.00		2	0.955	0.500	28.83	1.00	2.09E-04	0.03	0.00	0.00	0.00E+00
115		110	180	5000		332.2		70.00		24.80		1.05		0.03		0.02		2	0.818	0.500	24.71	1.00	1.18E-03	0.04	0.00	0.00	0.00E+00
115		80	150	781		39.1		70.00		19.94		1.34		0.09		0.07		2	0.682	0.500	20.59	0.97	4.58E-03	0.07	0.00	0.00	0.00E+00
115		50	120	548		27.5		70.00		16.15		2.17		0.18		0.13		2	0.545	0.500	16.47	0.98	1.10E-02	0.13	0.00	0.00	0.00E+00
64		140	210	544		27.3		70.00		28.64		2.16		0.18		0.13		3	0.955	0.500	28.83	0.99	6.31E-03	0.07	0.00	0.00	0.00E+00
64		110	180	396		19.9		70.00		24.80		1.95		0.19		0.14		3	0.818	0.500	24.71	1.00	7.77E-03	0.08	0.00	0.00	0.00E+00
64		80	150	327		16.4				22.06		1.48		0.16		0.11		3	0.682	0.500	20.59	1.07	7.80E-03	0.07	0.00	0.00	0.00E+00
64		50	120	722		36.3				18.72		1.57		0.11		0.08		3	0.545	0.500	16.47	1.14	6.94E-03	0.10	0.00	0.00	0.00E+00
64		20	90	68		3.5				11.98		9.07		2.17		1.54		3	0.409	0.500	12.36	0.97	1.76E-01	0.73	0.00	0.00	0.00E+00
13		140	210	5000		344.2				28.72		2.23		0.06		0.04		4	0.955	0.500	28.83	1.00	2.15E-03	0.08	0.00	0.00	0.00E+00
13		110	180	5000		1990.0				25.03		2.19		0.06		0.04		4	0.818	0.500	24.71	1.01	2.46E-03	0.09	0.00	0.00	0.00E+00
13		80	150	5000		2313.3				21.85		1.49		0.04		0.03		4	0.682	0.500	20.59	1.06	2.01E-03	0.07	0.00	0.00	0.00E+00
13		50	120	5000		2781.0				18.65		1.77		0.05		0.03		4	0.545	0.500	16.47	1.13	2.99E-03	0.11	0.00	0.00	0.00E+00
13		20	90	5000		521.0				16.35		3.14		0.09		0.06		4	0.409	0.500	12.36	1.32	7.04E-03	0.25	0.00	0.00	0.00E+00

LDA measurement		**LDA code:**	100	**rpm:**	1497.8	**Perfd by:**	NM	Printed: 26/09/2008	Page 1/3
Build:	3	**ReΦ:**	1.03E+06	**Date:**	21/06/2003	**LDA1:**	VΦ	**Comments:** run OK	
LDA test # :	B3run18-3	**Rez:**	1.01E+05	**raw LDA file:**	\MCRLDA\Build3\B3run18-3.lda	**LDA2:**	Vz	**Traverse ref:**	
Heat Transfer run:	B3run18-3	**Ro:**	1.87	**LDA list file:**	\MCRLDA\Build3\B3run18-3.xls	**W (m/s):**	20.52		

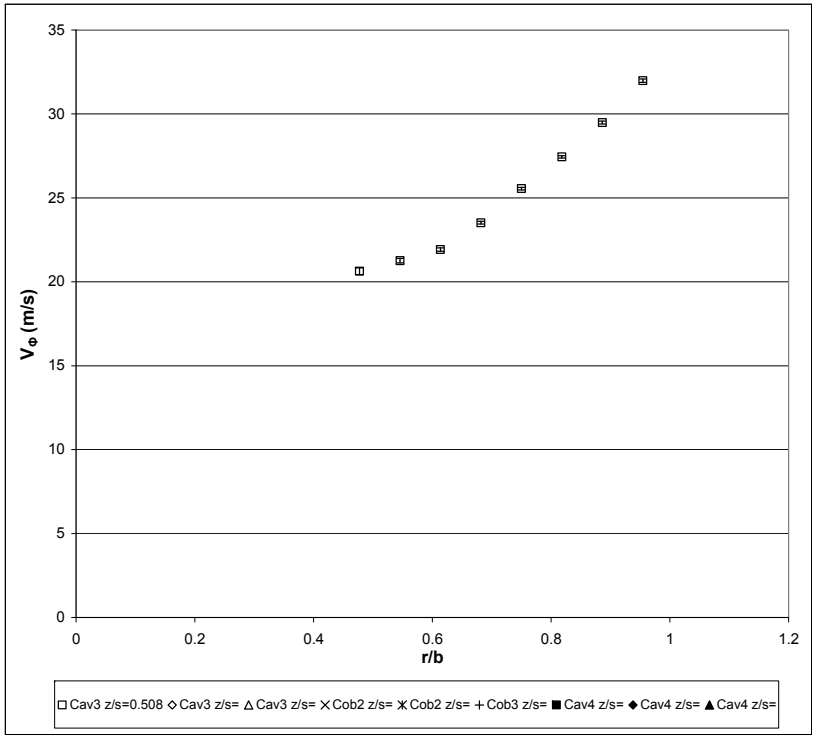

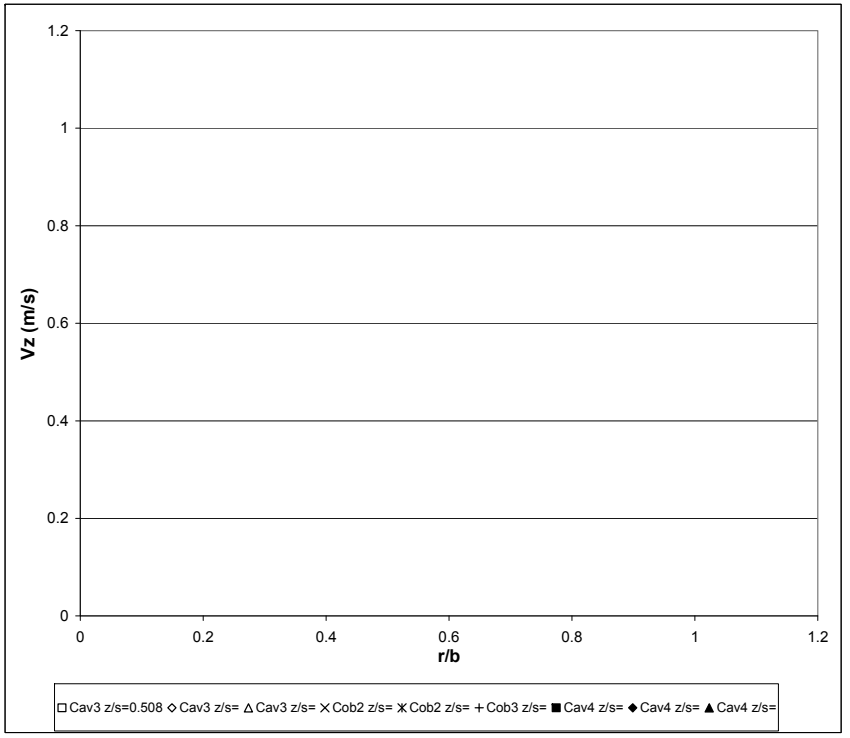

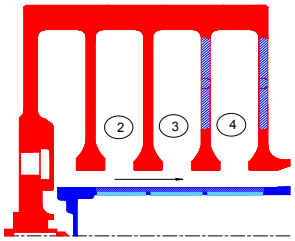

LDA measurement		**LDA code:**	101	**rpm:**	1497.8	**Perfd by:**	NM	Printed: 26/09/2008	Page 2/3
Build:	3	**Re_Φ:**	1.03E+06	**Date:**	21/06/2003	**LDA1:**	VΦ	**Comments:**	run OK
LDA test # :	B3run18-3	**Re_z:**	1.01E+05	**raw LDA file:**	\MCRLDA\Build3\B3run18-3.lda	**LDA2:**	Vz	**Traverse corresp:**	0
Heat Transfer run:	B3run18-3	**Ro:**	1.87	**LDA list file:**	\MCRLDA\Build3\B3run18-3.xls	**W (m/s):**	20.52		

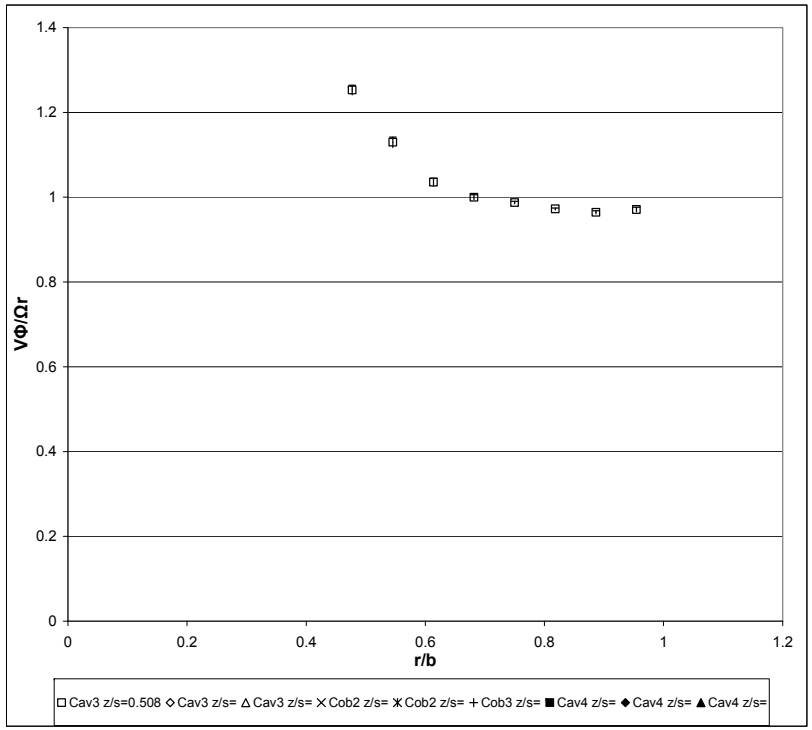

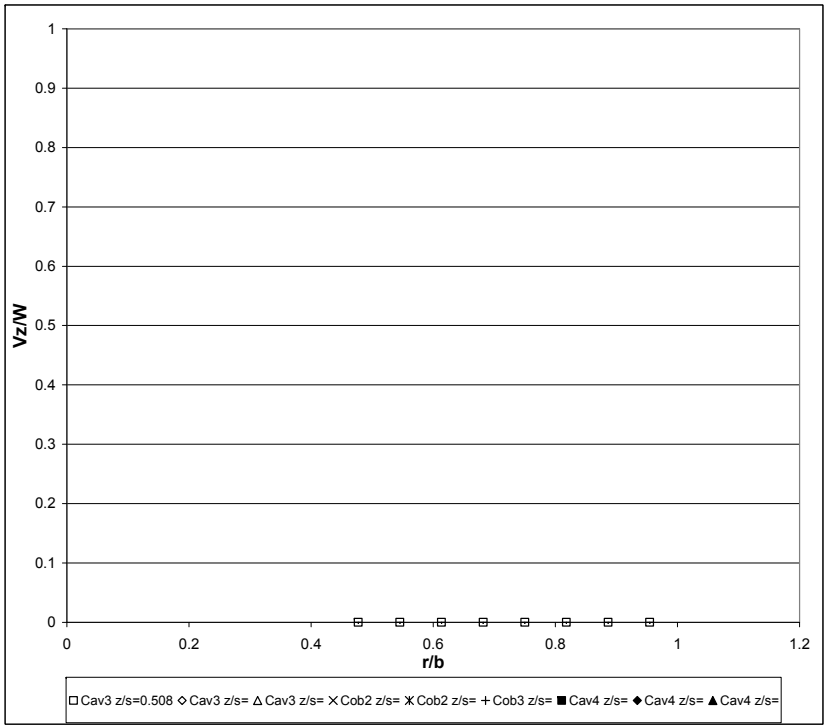

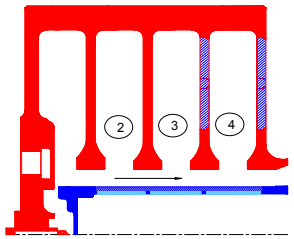

LDA measurement		**LDA code:**	100	**rpm:**	1497.8	**Perfd by:**	NM	Printed: 26/09/2008	Page 3/3
Build:	3	**ReΦ:**	1.03E+06	**Date:**	21/06/2003	**LDA1:**	VΦ	**Comments:**	run OK
LDA test # :	B3run18-3	**Rez:**	1.01E+05	**raw LDA file:**	\MCRLDA\Build3\B3run18-3.lda	**LDA2:**	Vz	**Traverse corresp:**	0
Heat Transfer run:	B3run18-3	**Ro:**	1.87	**LDA list file:**	\MCRLDA\Build3\B3run18-3.xls	**W (m/s):**	20.52		

X [mm]	corrected X	Y [mm]	corrected Y / Radius (mm)	Count{1}	Count{2}	Data Rate{1} [#/s]	Data Rate{2} [#/s]	Validation{1} [%]	Validation{2} [%]	LDA1 Mean [m/s]	LDA2 Mean [m/s]	LDA1 RMS [m/s]	LDA2 RMS [m/s]	LDA1 MeanConf [m/s]	LDA2 MeanConf [m/s]	LDA1 RMSConf [m/s]	LDA2 RMSConf [m/s]	Cavity	r/b	z/s	Ωr (m/s)	$V_\Phi/\Omega r$	$V_{\Phi U95\%}/\Omega r$	$V_{\Phi(RMS)}/\Omega r$	Vz/W	$Vz_{(RMS)}/W$	$Vz_{U95\%}/W$
64		140	210	1311		65.6				31.98		3.39		0.18		0.13		3	0.955	0.508	32.94	0.97	5.57E-03	0.10	0.00	0.00	0.00E+00
64		125	195	1998		100.2				29.49		2.52		0.11		0.08		3	0.886	0.508	30.59	0.96	3.62E-03	0.08	0.00	0.00	0.00E+00
64		110	180	4534		226.8				27.45		2.16		0.06		0.04		3	0.818	0.508	28.23	0.97	2.23E-03	0.08	0.00	0.00	0.00E+00
64		95	165	2427		121.4				25.55		1.92		0.08		0.05		3	0.750	0.508	25.88	0.99	2.95E-03	0.07	0.00	0.00	0.00E+00
64		80	150	806		40.4				23.52		1.95		0.14		0.10		3	0.682	0.508	23.53	1.00	5.74E-03	0.08	0.00	0.00	0.00E+00
64		65	135	431		21.6				21.92		2.11		0.20		0.14		3	0.614	0.508	21.18	1.04	9.40E-03	0.10	0.00	0.00	0.00E+00
64		50	120	453		22.8				21.26		2.51		0.23		0.16		3	0.545	0.508	18.82	1.13	1.23E-02	0.13	0.00	0.00	0.00E+00
64		35	105	1136		56.8				20.63		3.22		0.19		0.13		3	0.477	0.508	16.47	1.25	1.14E-02	0.20	0.00	0.00	0.00E+00

LDA measurement		**LDA code:**	101	**rpm:**	1452.2	**Perfd by:**	NM	Printed: 26/09/2008	Page 1/3
Build:	3	**ReΦ:**	1.24E+06	**Date:**	07/07/2003	**LDA1:**	VΦ	**Comments:**	run OK
LDA test # :	B3run22-1	**Rez:**	4.91E+04	**raw LDA file:**	\MCRLDA\Build3\B3run22-1.lda	**LDA2:**	Vz	**Traverse ref:**	
Heat Transfer run:	B3run22-1	**Ro:**	0.75	**LDA list file:**	\MCRLDA\Build3\B3run22-1.xls	**W (m/s):**	8.02		

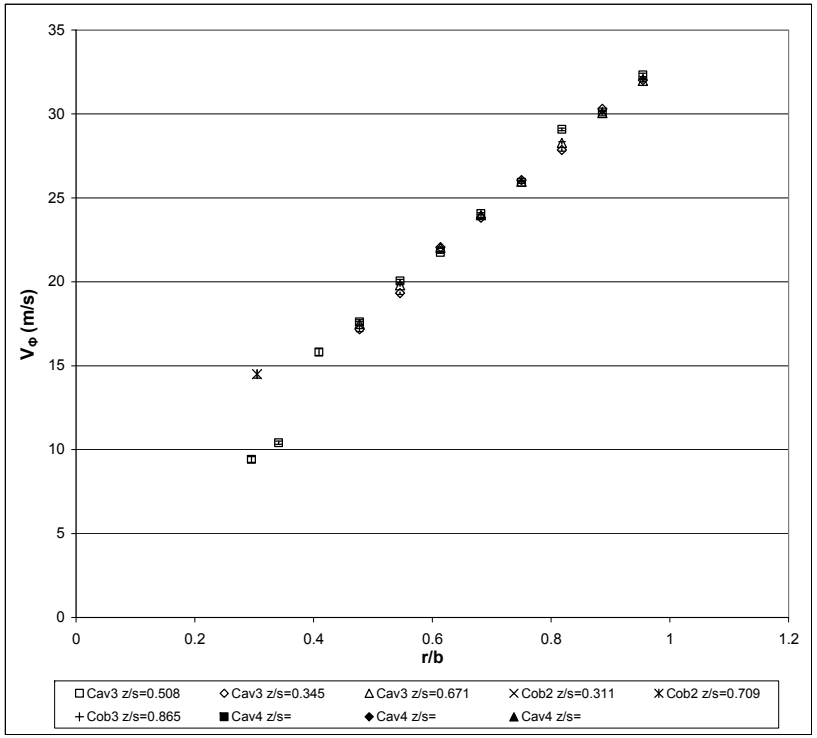

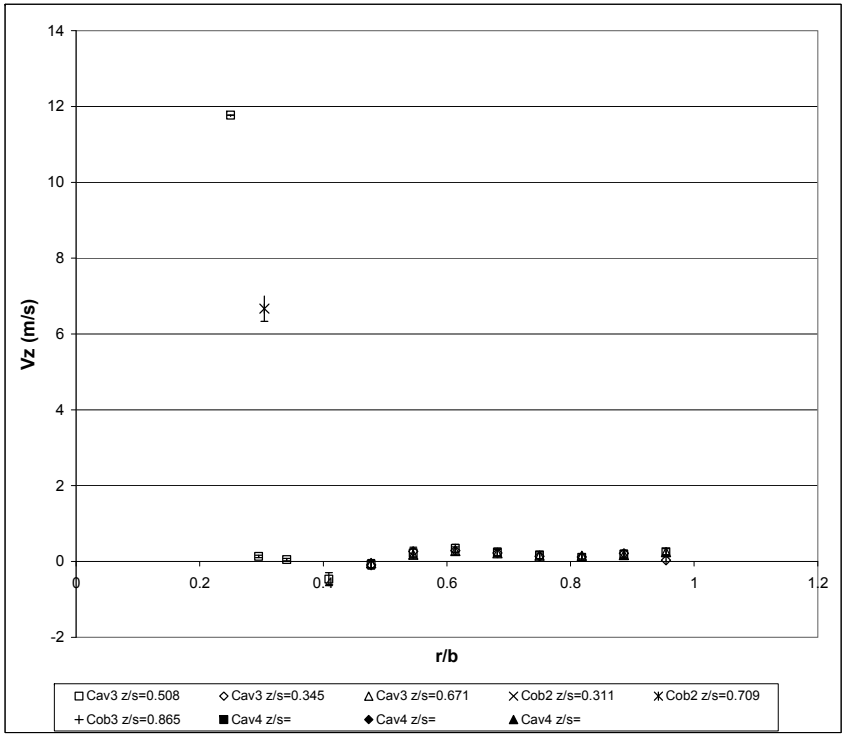

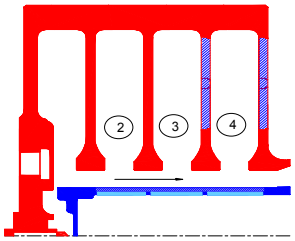

LDA measurement		**LDA code:**	101	**rpm:**	1452.2	**Perfd by:**	NM	Printed: 26/09/2008	Page 2/3
Build:	3	**Re_Φ:**	1.24E+06	**Date:**	07/07/2003	**LDA1:**	VΦ	**Comments:**	run OK
LDA test # :	B3run22-1	**Re_z:**	4.91E+04	**raw LDA file:**	\MCRLDA\Build3\B3run22-1.lda	**LDA2:**	Vz	**Traverse corresp:**	0
Heat Transfer run:	B3run22-1	**Ro:**	0.75	**LDA list file:**	\MCRLDA\Build3\B3run22-1.xls	**W (m/s):**	8.025		

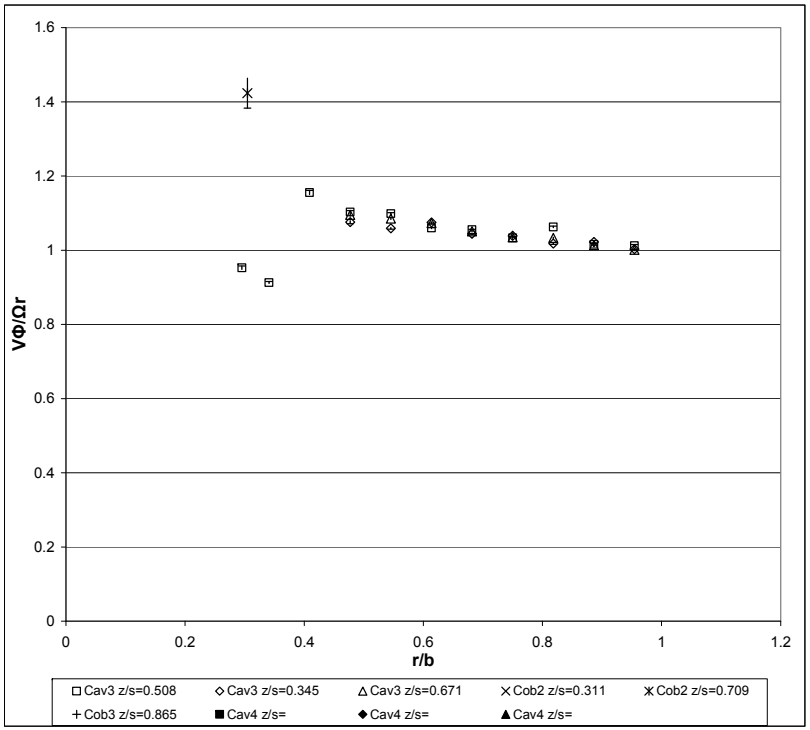

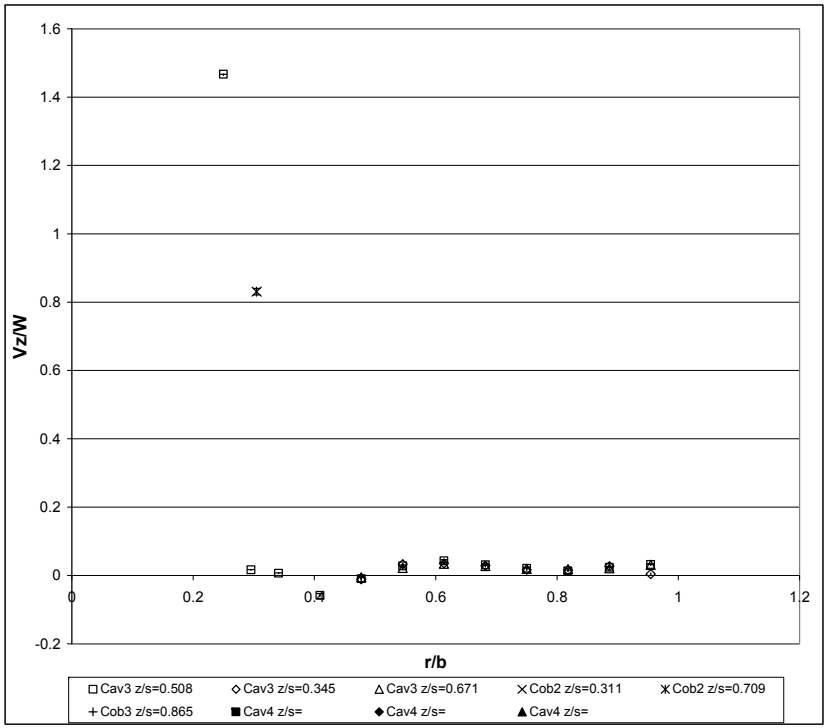

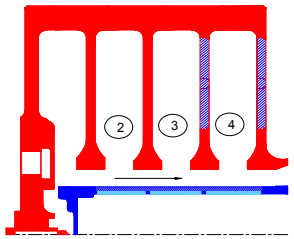

LDA measurement		**LDA code:**	101	**rpm:**	1452.2	**Perfd by:**	NM	Printed: 26/09/2008	Page 3/3
Build:	3	**ReΦ:**	1.24E+06	**Date:**	07/07/2003	**LDA1:**	VΦ	**Comments:**	run OK
LDA test # :	B3run22-1	**Rez:**	4.91E+04	**raw LDA file:**	\MCRLDA\Build3\B3run22-1.lda	**LDA2:**	Vz	**Traverse corresp:**	0
Heat Transfer run:	B3run22-1	**Ro:**	0.75	**LDA list file:**	\MCRLDA\Build3\B3run22-1.xls	**W (m/s):**	8.025		

X [mm]	corrected X	Y [mm]	corrected Y / Radius (mm)	Count{1}	Count{2}	Data Rate{1} [#/s]	Data Rate{2} [#/s]	Validation{1} [%]	Validation{2} [%]	LDA1 Mean [m/s]	LDA2 Mean [m/s]	LDA1 RMS [m/s]	LDA2 RMS [m/s]	LDA1 MeanConf [m/s]	LDA2 MeanConf [m/s]	LDA1 RMSConf [m/s]	LDA2 RMSConf [m/s]	Cavity	r/b	z/s	Ωr (m/s)	$V_\Phi/\Omega r$	$V_{\Phi U95\%}/\Omega r$	$V_{\Phi(RMS)}/\Omega r$	Vz/W	$Vz_{(RMS)}/W$	$Vz_{U95\%}/W$
64		140	210	5000	5000	23477.7	7540.6			32.33	0.26	3.25	0.67	0.09	0.02	0.06	0.01	3	0.955	0.508	31.94	1.01	2.82E-03	0.10	0.03	0.08	2.31E-03
64		125	195	5000	5000	21020.9	7589.7			30.12	0.19	2.81	0.72	0.08	0.02	0.06	0.01	3	0.886	0.508	29.65	1.02	2.63E-03	0.09	0.02	0.09	2.48E-03
64		110	180	5000	5000	23667.2	8088.8			29.08	0.11	2.12	0.76	0.06	0.02	0.04	0.01	3	0.818	0.508	27.37	1.06	2.15E-03	0.08	0.01	0.10	2.64E-03
64		95	165	5000	5000	16583.0	5873.9			25.93	0.17	1.45	0.79	0.04	0.02	0.03	0.02	3	0.750	0.508	25.09	1.03	1.60E-03	0.06	0.02	0.10	2.73E-03
64		80	150	5000	5000	2113.1	771.1			24.07	0.25	1.15	0.82	0.03	0.02	0.02	0.02	3	0.682	0.508	22.81	1.06	1.40E-03	0.05	0.03	0.10	2.83E-03
64		65	135	5000	5000	1723.7	700.0			21.75	0.35	1.10	0.85	0.03	0.02	0.02	0.02	3	0.614	0.508	20.53	1.06	1.49E-03	0.05	0.04	0.11	2.94E-03
64		50	120	5000	5000	1873.1	687.4			20.05	0.22	1.69	0.91	0.05	0.03	0.03	0.02	3	0.545	0.508	18.25	1.10	2.57E-03	0.09	0.03	0.11	3.15E-03
64		35	105	5000	5000	1800.7	745.3			17.61	-0.08	2.12	1.03	0.06	0.03	0.04	0.02	3	0.477	0.508	15.97	1.10	3.68E-03	0.13	-0.01	0.13	3.55E-03
64		20	90	5000	5000	1879.8	656.5			15.81	-0.46	2.76	1.36	0.08	0.04	0.05	0.03	3	0.409	0.508	13.69	1.16	5.59E-03	0.20	-0.06	0.17	4.68E-03
71		140	210	5000	5000	2408.5	915.8			32.02	0.03	2.87	0.77	0.08	0.02	0.06	0.02	3	0.955	0.345	31.94	1.00	2.49E-03	0.09	0.00	0.10	2.65E-03
71		125	195	5000	5000	2249.9	692.1			30.31	0.22	2.79	0.64	0.08	0.02	0.05	0.01	3	0.886	0.345	29.65	1.02	2.61E-03	0.09	0.03	0.08	2.22E-03
71		110	180	5000	5000	2396.4	670.6			27.86	0.12	2.08	0.66	0.06	0.02	0.04	0.01	3	0.818	0.345	27.37	1.02	2.11E-03	0.08	0.02	0.08	2.27E-03
71		95	165	5000	5000	2245.5	692.0			26.06	0.14	1.60	0.68	0.04	0.02	0.03	0.01	3	0.750	0.345	25.09	1.04	1.77E-03	0.06	0.02	0.08	2.36E-03
71		80	150	5000	5000	2032.7	725.3			23.82	0.23	1.03	0.75	0.03	0.02	0.02	0.01	3	0.682	0.345	22.81	1.04	1.25E-03	0.05	0.03	0.09	2.59E-03
71		65	135	5000	5000	1818.0	703.1			22.07	0.29	1.23	0.81	0.03	0.02	0.02	0.02	3	0.614	0.345	20.53	1.07	1.66E-03	0.06	0.04	0.10	2.79E-03
57		140	210	5000	5000	19186.2	569.0			31.97	0.25	3.03	0.58	0.08	0.02	0.06	0.01	3	0.955	0.671	31.94	1.00	2.63E-03	0.09	0.03	0.07	1.99E-03
57		125	195	5000	5000	15926.5	595.0			30.06	0.17	2.64	0.67	0.07	0.02	0.05	0.01	3	0.886	0.671	29.65	1.01	2.46E-03	0.09	0.02	0.08	2.31E-03
57		110	180	5000	5000	17180.4	665.9			28.27	0.15	2.05	0.69	0.06	0.02	0.04	0.01	3	0.818	0.671	27.37	1.03	2.07E-03	0.07	0.02	0.09	2.37E-03
57		95	165	5000	5000	16946.5	624.1			25.97	0.15	1.48	0.71	0.04	0.02	0.03	0.01	3	0.750	0.671	25.09	1.03	1.64E-03	0.06	0.02	0.09	2.45E-03
57		80	150	5000	5000	16872.2	667.4			23.97	0.22	1.04	0.74	0.03	0.02	0.02	0.01	3	0.682	0.671	22.81	1.05	1.27E-03	0.05	0.03	0.09	2.56E-03
57		65	135	5000	5000	15135.2	663.4			22.03	0.28	1.12	0.78	0.03	0.02	0.02	0.02	3	0.614	0.671	20.53	1.07	1.52E-03	0.05	0.03	0.10	2.70E-03
94		-3	67	#N/A	#N/A	#N/A	#N/A			#N/A	#N/A	#N/A	#N/A	#N/A	#N/A	#N/A	#N/A	cob2	0.305	0.311	10.19	#N/A	#N/A	#N/A	#N/A	#N/A	#N/A
94		-9	61	#N/A	#N/A	#N/A	#N/A			#N/A	#N/A	#N/A	#N/A	#N/A	#N/A	#N/A	#N/A	cob2	0.277	0.311	9.28	#N/A	#N/A	#N/A	#N/A	#N/A	#N/A
94		-13	57	#N/A	#N/A	#N/A	#N/A			#N/A	#N/A	#N/A	#N/A	#N/A	#N/A	#N/A	#N/A	cob2	0.259	0.311	8.67	#N/A	#N/A	#N/A	#N/A	#N/A	#N/A
84		-3	67	141	5000	7.6	429.5			14.50	6.67	2.47	2.68	0.41	0.07	0.29	0.05	cob2	0.305	0.709	10.19	1.42	4.02E-02	0.24	0.83	0.33	9.24E-03
84		-9	61	#N/A	#N/A	#N/A	#N/A			#N/A	#N/A	#N/A	#N/A	#N/A	#N/A	#N/A	#N/A	cob2	0.277	0.709	9.28	#N/A	#N/A	#N/A	#N/A	#N/A	#N/A
84		-15	55	#N/A	#N/A	#N/A	#N/A			#N/A	#N/A	#N/A	#N/A	#N/A	#N/A	#N/A	#N/A	cob2	0.250	0.709	8.36	#N/A	#N/A	#N/A	#N/A	#N/A	#N/A
131		-3	67	#N/A	#N/A	#N/A	#N/A			#N/A	#N/A	#N/A	#N/A	#N/A	#N/A	#N/A	#N/A	cob1	0.305	0.865	10.19	#N/A	#N/A	#N/A	#N/A	#N/A	#N/A
131		-9	61	#N/A	#N/A	#N/A	#N/A			#N/A	#N/A	#N/A	#N/A	#N/A	#N/A	#N/A	#N/A	cob1	0.277	0.865	9.28	#N/A	#N/A	#N/A	#N/A	#N/A	#N/A
131		-15	55	#N/A	#N/A	#N/A	#N/A			#N/A	#N/A	#N/A	#N/A	#N/A	#N/A	#N/A	#N/A	cob1	0.250	0.865	8.36	#N/A	#N/A	#N/A	#N/A	#N/A	#N/A
64		5	75	5000	5000	1429.8	226.4			10.41	0.05	1.08	0.27	0.03	0.01	0.02	0.01	3	0.341	0.508	11.41	0.91	2.63E-03	0.09	0.01	0.03	9.26E-04
64		-5	65	5000	5000	656.9	535.2			9.42	0.13	1.74	0.24	0.05	0.01	0.03	0.00	3	0.295	0.508	9.88	0.95	4.89E-03	0.18	0.02	0.03	8.43E-04
64		-15	55	0	1	#N/A	#N/A			#N/A	11.77	#N/A	0.00	#N/A	0.00	#N/A	0.00	3	0.250	0.508	8.36	#N/A	#N/A	#N/A	1.47	0.00	0.00E+00
71		50	120	5000	5000	15467.2	629.4			19.33	0.26	1.47	0.90	0.04	0.02	0.03	0.02	3	0.545	0.345	18.25	1.06	2.23E-03	0.08	0.03	0.11	3.10E-03
71		35	105	5000	5000	12501.5	584.2			17.17	-0.09	2.27	1.03	0.06	0.03	0.04	0.02	3	0.477	0.345	15.97	1.08	3.94E-03	0.14	-0.01	0.13	3.56E-03
57		50	120	5000	5000	1404.8	645.5			19.80	0.18	1.52	0.87	0.04	0.02	0.03	0.02	3	0.545	0.671	18.25	1.09	2.31E-03	0.08	0.02	0.11	2.99E-03
57		35	105	5000	5000	1616.3	619.5			17.49	-0.04	2.10	1.00	0.06	0.03	0.04	0.02	3	0.477	0.671	15.97	1.10	3.64E-03	0.13	-0.01	0.12	3.44E-03

LDA measurement		**LDA code:**	101	**rpm:**	2787.3	**Perfd by:**	NM	Printed: 26/09/2008	Page 1/3
Build:	3	**ReΦ:**	2.02E+06	**Date:**	09/07/2003	**LDA1:**	VΦ	**Comments:**	
LDA test # :	B3run23-1	**Rez:**	9.91E+04	**raw LDA file:**	\MCRLDA\Build3\B3run23-1.lda	**LDA2:**	Vz	**Traverse ref:**	
Heat Transfer run:	B3run23-1	**Ro:**	0.93	**LDA list file:**	\MCRLDA\Build3\B3run23-1.xls	**W (m/s):**	19.12		

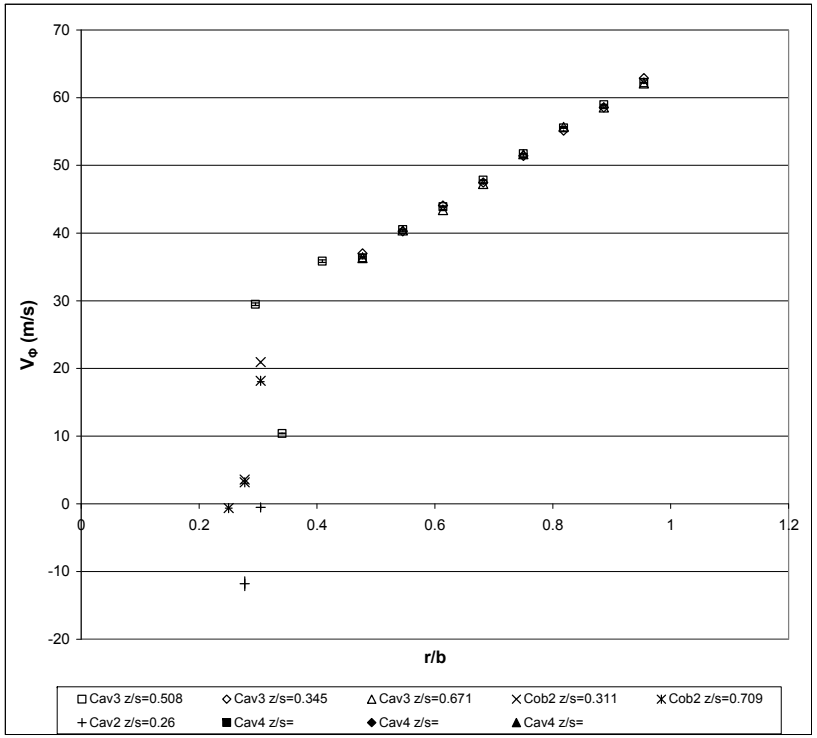

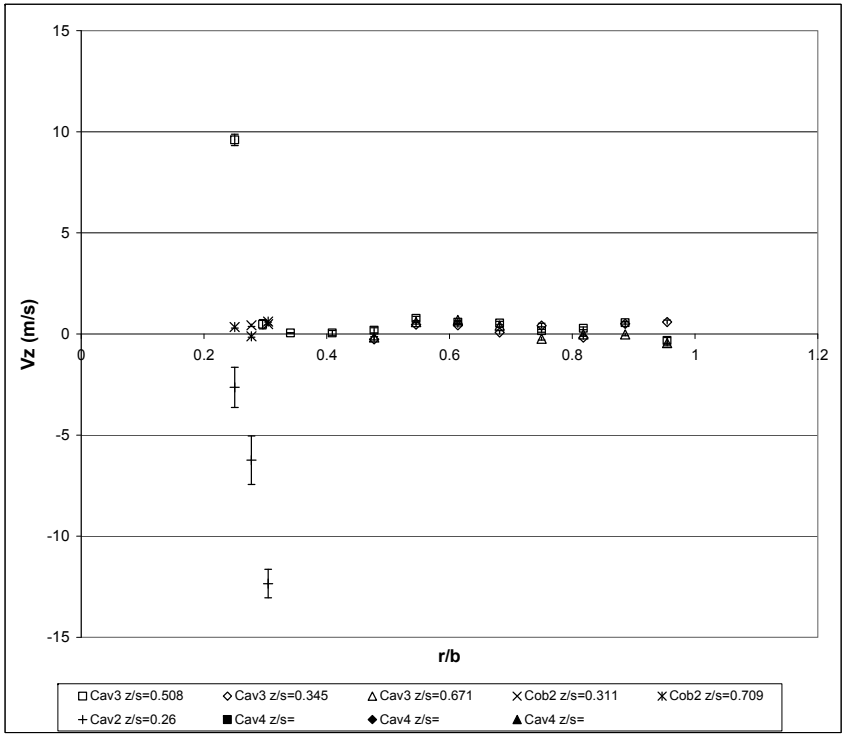

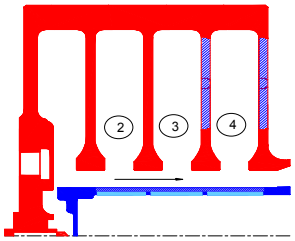

LDA measurement		**LDA code:**	101	**rpm:**	2787.3	**Perfd by:**	NM	Printed: 26/09/2008	Page 2/3
Build:	3	**Re_Φ:**	2.02E+06	**Date:**	09/07/2003	**LDA1:**	VΦ	**Comments:**	0
LDA test # :	B3run23-1	**Re_z:**	9.91E+04	**raw LDA file:**	\MCRLDA\Build3\B3run23-1.lda	**LDA2:**	Vz	**Traverse corresp:**	0
Heat Transfer run:	B3run23-1	**Ro:**	0.93	**LDA list file:**	\MCRLDA\Build3\B3run23-1.xls	**W (m/s):**	19.12		

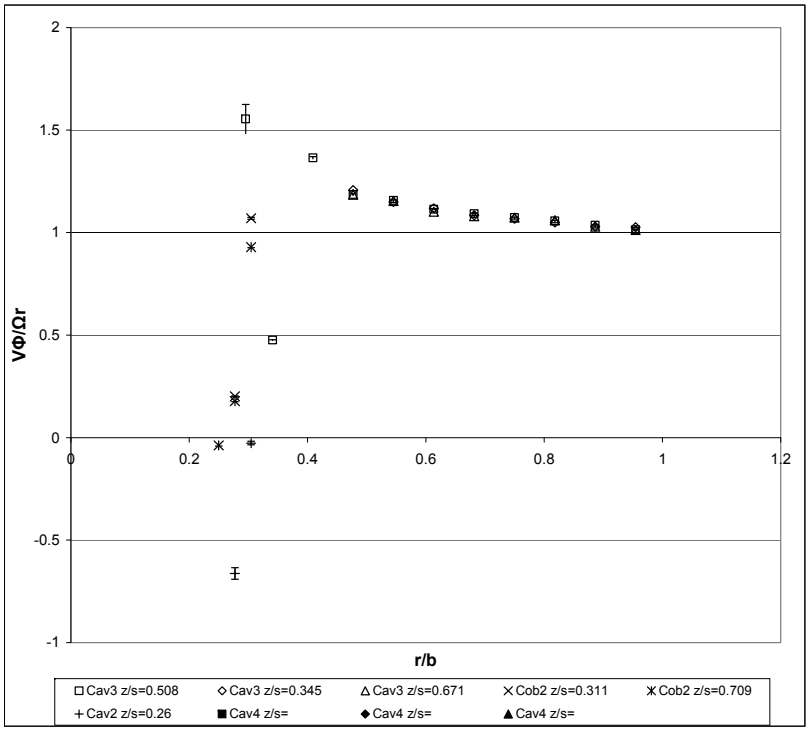

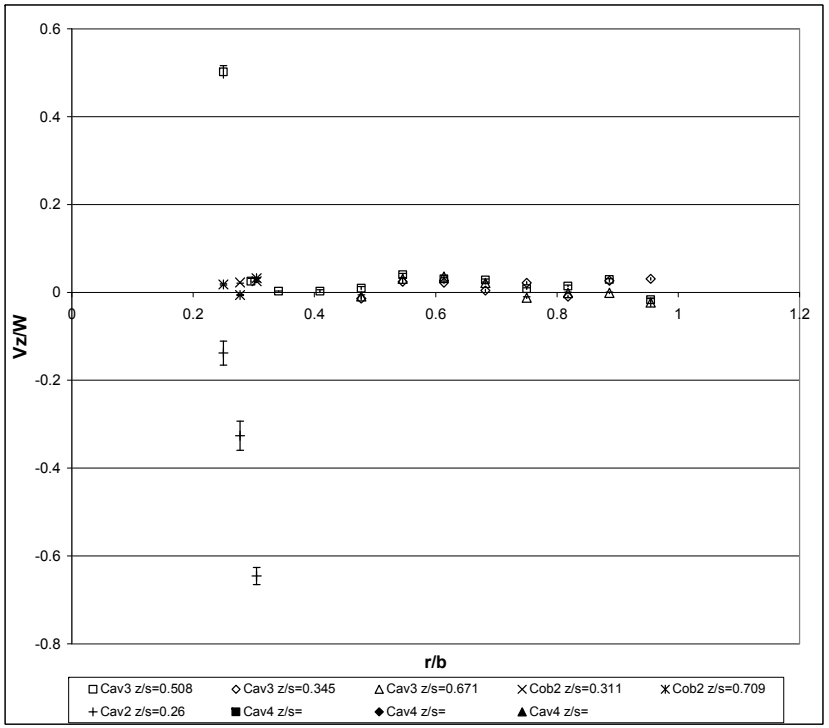

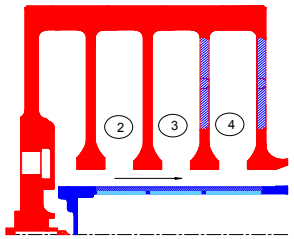

LDA measurement | **LDA code:** 101 | **rpm:** 2787.3 | **Perfd by:** NM | Printed: 26/09/2008 | Page 3/3

Build: 3 | **ReΦ:** 2.02E+06 | **Date:** 09/07/2003 | **LDA1:** VΦ | **Comments:** 0

LDA test # : B3run23-1 | **Rez:** 9.91E+04 | **raw LDA file:** \MCRLDA\Build3\B3run23-1.lda | **LDA2:** Vz | **Traverse corresp:** 0

Heat Transfer run: B3run23-1 | **Ro:** 0.93 | **LDA list file:** \MCRLDA\Build3\B3run23-1.xls | **W (m/s):** 19.12

X [mm]	corrected X	Y [mm]	corrected Y / Radius (mm)	Count{1}	Count{2}	Data Rate{1} [#/s]	Data Rate{2} [#/s]	Validation{1} [%]	Validation{2} [%]	LDA1 Mean [m/s]	LDA2 Mean [m/s]	LDA1 RMS [m/s]	LDA2 RMS [m/s]	LDA1 MeanConf [m/s]	LDA2 MeanConf [m/s]	LDA1 RMSConf [m/s]	LDA2 RMSConf [m/s]	Cavity	r/b	z/s	Ωr (m/s)	$V_\Phi/\Omega r$	$V_{\Phi U95\%}/\Omega r$	$V_{\Phi(RMS)}/\Omega r$	Vz/W	$Vz_{(RMS)}/W$	$Vz_{U95\%}/W$
64	140	210	5000	5000	2344.2	393.4			62.20	-0.32	3.97	2.71	0.11	0.07	0.08	0.05	3	0.955	0.508	61.30	1.01	1.79E-03	0.06	-0.02	0.14	3.92E-03
64	125	195	5000	5000	2645.8	284.3			58.97	0.56	4.03	1.27	0.11	0.04	0.08	0.02	3	0.886	0.508	56.92	1.04	1.96E-03	0.07	0.03	0.07	1.84E-03
64	110	180	5000	5000	2362.4	544.1			55.55	0.28	3.42	1.34	0.09	0.04	0.07	0.03	3	0.818	0.508	52.54	1.06	1.80E-03	0.07	0.01	0.07	1.94E-03
64	95	165	5000	5000	2312.0	1030.2			51.73	0.16	2.82	1.46	0.08	0.04	0.06	0.03	3	0.750	0.508	48.16	1.07	1.62E-03	0.06	0.01	0.08	2.11E-03
64	80	150	5000	5000	442.7	292.7			47.83	0.54	2.24	1.52	0.06	0.04	0.04	0.03	3	0.682	0.508	43.78	1.09	1.42E-03	0.05	0.03	0.08	2.20E-03
64	65	135	5000	5000	539.3	429.1			43.90	0.59	2.32	1.78	0.06	0.05	0.05	0.03	3	0.614	0.508	39.40	1.11	1.63E-03	0.06	0.03	0.09	2.59E-03
64	50	120	5000	5000	401.6	297.9			40.53	0.77	2.85	2.03	0.08	0.06	0.06	0.04	3	0.545	0.508	35.03	1.16	2.25E-03	0.08	0.04	0.11	2.94E-03
64	35	105	5000	5000	439.2	429.5			36.34	0.18	3.99	2.50	0.11	0.07	0.08	0.05	3	0.477	0.508	30.65	1.19	3.61E-03	0.13	0.01	0.13	3.63E-03
71	140	210	5000	5000	9160.3	1332.3			62.88	0.59	1.88	1.93	0.05	0.05	0.04	0.04	3	0.955	0.345	61.30	1.03	8.49E-04	0.03	0.03	0.10	2.80E-03
71	125	195	5000	5000	447.9	160.1			58.57	0.51	3.74	1.71	0.10	0.05	0.07	0.03	3	0.886	0.345	56.92	1.03	1.82E-03	0.07	0.03	0.09	2.48E-03
71	110	180	5000	2467	339.2	61.7			55.14	-0.18	3.41	1.39	0.09	0.05	0.07	0.04	3	0.818	0.345	52.54	1.05	1.80E-03	0.06	-0.01	0.07	2.86E-03
71	95	165	5000	5000	352.7	164.7			51.41	0.41	2.84	2.27	0.08	0.06	0.06	0.04	3	0.750	0.345	48.16	1.07	1.63E-03	0.06	0.02	0.12	3.29E-03
71	80	150	5000	5000	516.1	184.5			47.48	0.08	2.47	1.63	0.07	0.05	0.05	0.03	3	0.682	0.345	43.78	1.08	1.57E-03	0.06	0.00	0.09	2.37E-03
71	65	135	5000	5000	589.6	354.8			44.08	0.43	2.35	1.85	0.07	0.05	0.05	0.04	3	0.614	0.345	39.40	1.12	1.66E-03	0.06	0.02	0.10	2.68E-03
57	140	210	5000	876	867.9	14.6			62.11	-0.44	4.18	2.67	0.12	0.18	0.08	0.13	3	0.955	0.671	61.30	1.01	1.89E-03	0.07	-0.02	0.14	9.26E-03
57	125	195	5000	5000	1174.5	137.2			58.56	-0.02	3.97	1.20	0.11	0.03	0.08	0.02	3	0.886	0.671	56.92	1.03	1.93E-03	0.07	0.00	0.06	1.73E-03
57	110	180	5000	5000	1250.3	264.4			55.68	-0.03	3.45	1.30	0.10	0.04	0.07	0.03	3	0.818	0.671	52.54	1.06	1.82E-03	0.07	0.00	0.07	1.88E-03
57	95	165	5000	5000	1019.0	245.3			51.66	-0.23	2.91	1.46	0.08	0.04	0.06	0.03	3	0.750	0.671	48.16	1.07	1.68E-03	0.06	-0.01	0.08	2.12E-03
57	80	150	5000	5000	1061.4	115.1			47.26	0.41	2.51	1.52	0.07	0.04	0.05	0.03	3	0.682	0.671	43.78	1.08	1.59E-03	0.06	0.02	0.08	2.20E-03
57	65	135	5000	5000	929.8	356.9			43.42	0.69	2.42	1.59	0.07	0.04	0.05	0.03	3	0.614	0.671	39.40	1.10	1.70E-03	0.06	0.04	0.08	2.30E-03
94	-3	67	2930	5000	24.5	31402.5			20.92	0.49	2.63	0.66	0.10	0.02	0.07	0.01	cob2	0.305	0.311	19.56	1.07	4.87E-03	0.13	0.03	0.03	9.51E-04
94	-9	61	4834	5000	40.3	647.9			3.59	0.43	1.54	1.12	0.04	0.03	0.03	0.02	cob2	0.277	0.311	17.80	0.20	2.44E-03	0.09	0.02	0.06	1.63E-03
94	-13	57	#N/A	#N/A	#N/A	#N/A			#N/A	#N/A	#N/A	#N/A	#N/A	#N/A	#N/A	#N/A	cob2	0.259	0.311	16.64	#N/A	#N/A	#N/A	#N/A	#N/A	#N/A
84	-3	67	5000	5000	1428.1	779.7			18.17	0.62	2.31	0.65	0.06	0.02	0.05	0.01	cob2	0.305	0.709	19.56	0.93	3.28E-03	0.12	0.03	0.03	9.46E-04
84	-9	61	5000	5000	258.6	320.0			3.17	-0.12	1.87	0.74	0.05	0.02	0.04	0.01	cob2	0.277	0.709	17.80	0.18	2.91E-03	0.10	-0.01	0.04	1.07E-03
84	-15	55	133	5000	6.9	4201.4			-0.61	0.35	0.26	1.01	0.05	0.03	0.03	0.02	cob2	0.250	0.709	16.05	-0.04	2.81E-03	0.02	0.02	0.05	1.46E-03
125	-3	67	5000	5000	115.9	48.6			-0.52	-12.35	6.19	13.45	0.17	0.37	0.12	0.26	2	0.305	0.260	19.56	-0.03	8.77E-03	0.32	-0.65	0.70	1.95E-02
125	-9	61	5000	5000	65.9	1106.6			-11.80	-6.24	18.11	22.87	0.50	0.63	0.35	0.45	2	0.277	0.260	17.80	-0.66	2.82E-02	1.02	-0.33	1.20	3.32E-02
125	-15	55	0	5000	#N/A	3466.7			#N/A	-2.64	#N/A	18.92	#N/A	0.52	#N/A	0.37	2	0.250	0.260	16.05	#N/A	#N/A	#N/A	#N/A	-0.14	0.99	2.74E-02
64	20	90	5000	5000	42.1	220.3			35.85	0.05	4.82	2.24	0.13	0.06	0.09	0.04	3	0.409	0.508	26.27	1.36	5.09E-03	0.18	0.00	0.12	3.24E-03
64	5	75	5000	5000	1429.8	226.4			10.41	0.05	1.08	0.27	0.03	0.01	0.02	0.01	3	0.341	0.508	21.89	0.48	1.37E-03	0.05	0.00	0.01	3.89E-04
64	-5	65	26	5000	0.2	318.5			29.48	0.48	3.43	4.40	1.34	0.12	0.95	0.09	3	0.295	0.508	18.97	1.55	7.09E-02	0.18	0.03	0.23	6.38E-03
64	-15	55	0	1465	#N/A	12.2			#N/A	9.60	#N/A	5.30	#N/A	0.27	#N/A	0.19	3	0.250	0.508	16.05	#N/A	#N/A	#N/A	0.50	0.28	1.42E-02
71	50	120	5000	4511	189.6	75.2			40.27	0.46	2.79	2.09	0.08	0.06	0.05	0.04	3	0.545	0.345	35.03	1.15	2.21E-03	0.08	0.02	0.11	3.19E-03
71	35	105	5000	4528	138.8	75.5			36.99	-0.26	3.81	2.71	0.11	0.08	0.07	0.06	3	0.477	0.345	30.65	1.21	3.44E-03	0.12	-0.01	0.14	4.12E-03
57	50	120	5000	5000	390.5	179.8			40.42	0.59	2.99	1.91	0.08	0.05	0.06	0.04	3	0.545	0.671	35.03	1.15	2.37E-03	0.09	0.03	0.10	2.77E-03
57	35	105	5000	5000	365.5	124.4			36.32	-0.17	3.90	2.38	0.11	0.07	0.08	0.05	3	0.477	0.671	30.65	1.19	3.53E-03	0.13	-0.01	0.12	3.45E-03

LDA measurement		**LDA code:**	101	**rpm:**	1546.8	**Perfd by:**	NM	Printed: 26/09/2008	Page 1/3
Build:	3	**ReΦ:**	1.15E+06	**Date:**	27/08/2003	**LDA1:**	VΦ	**Comments:** run OK	
LDA test # :	B3run25-1	**Rez:**	1.71E+05	**raw LDA file:**	\MCRLDA\Build3\B3run25-1.lda	**LDA2:**	Vz	**Traverse ref:**	
Heat Transfer run:	B3run25-1	**Ro:**	2.84	**LDA list file:**	\MCRLDA\Build3\B3run25-1.xls	**W (m/s):**	32.25		

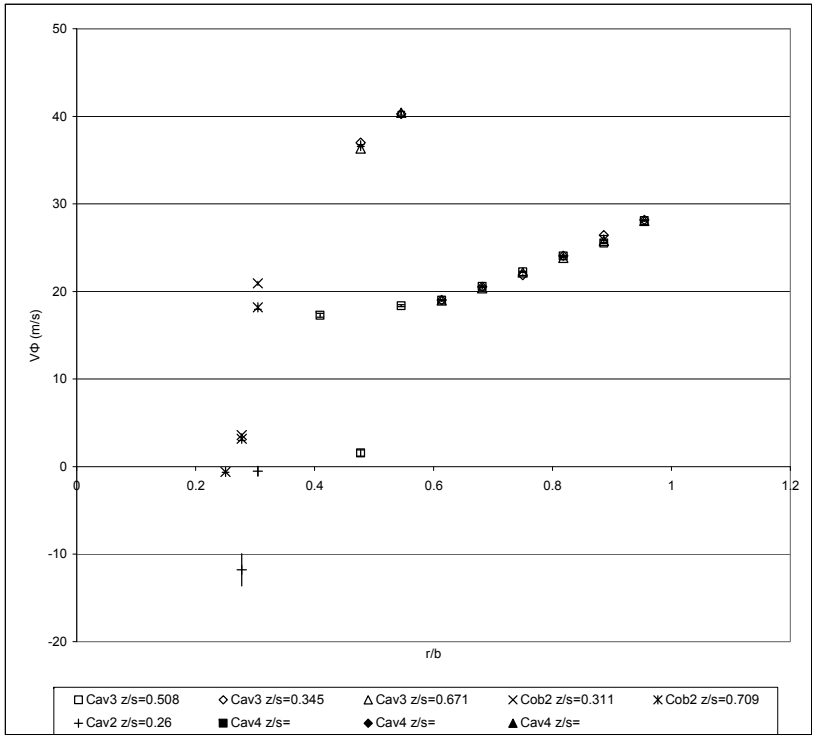

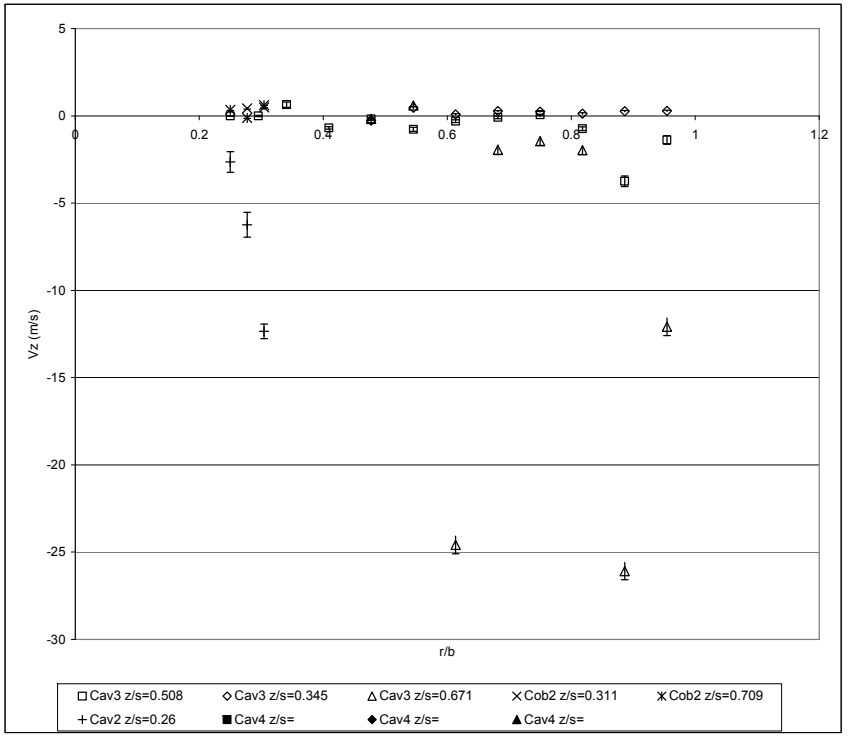

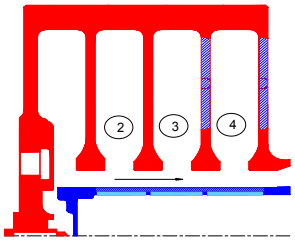

LDA measurement		**LDA code:**	101	**rpm:**	1546.8	**Perfd by:**	NM	Printed: 26/09/2008	Page 2/3
Build:	3	**Re_Φ:**	1.15E+06	**Date:**	27/08/2003	**LDA1:**	VΦ	**Comments:**	run OK
LDA test # :	B3run25-1	**Re_z:**	1.71E+05	**raw LDA file:**	\MCRLDA\Build3\B3run25-1.lda	**LDA2:**	Vz	**Traverse corresp:**	0
Heat Transfer run:	B3run25-1	**Ro:**	2.84	**LDA list file:**	\MCRLDA\Build3\B3run25-1.xls	**W (m/s):**	32.25		

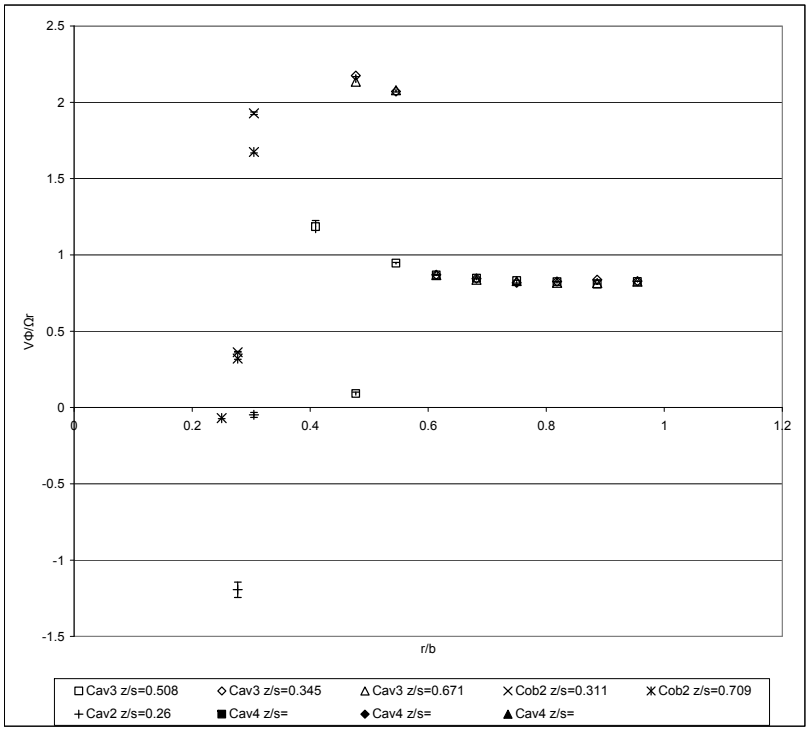

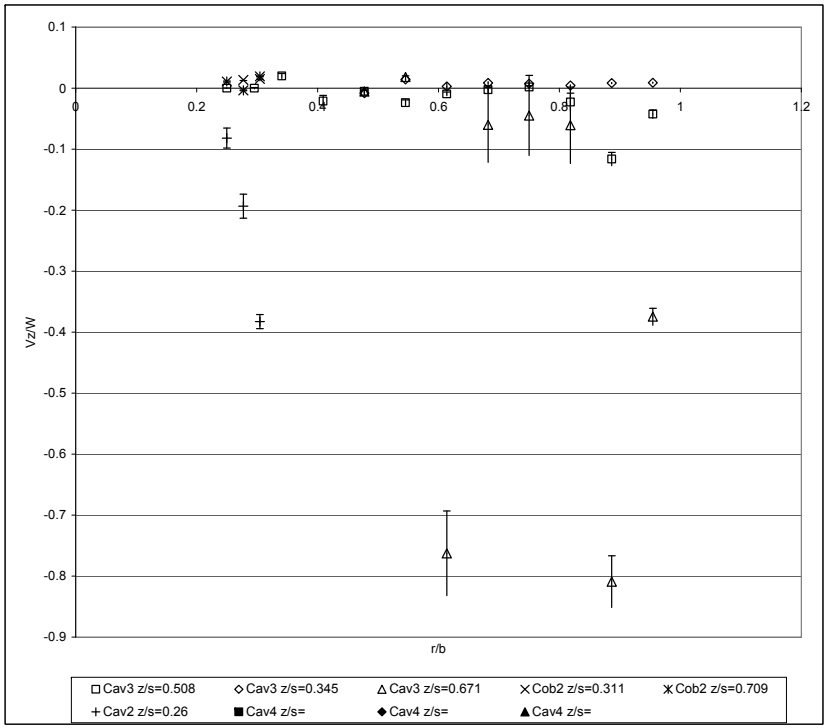

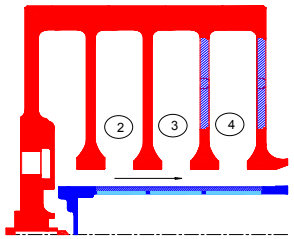

LDA measurement | LDA code: 101 | rpm: 1546.8 | Perfd by: NM | Printed: 26/09/2008 | Page 3/3

Build: 3 | ReΦ: 1.15E+06 | Date: 27/08/2003 | LDA1: VΦ | Comments: run OK

LDA test # : B3run25-1 | Rez: 1.71E+05 | raw LDA file: \MCRLDA\Build3\B3run25-1.lda | LDA2: Vz | Traverse corresp: 0

Heat Transfer run: B3run25-1 | Ro: 2.84 | LDA list file: \MCRLDA\Build3\B3run25-1.xls | W (m/s): 32.25

X [mm]	corrected X	Y [mm]	corrected Y / Radius (mm)	Count{1}	Count{2}	Data Rate{1} [#/s]	Data Rate{2} [#/s]	Validation{1} [%]	Validation{2} [%]	LDA1 Mean [m/s]	LDA2 Mean [m/s]	LDA1 RMS [m/s]	LDA2 RMS [m/s]	LDA1 MeanConf [m/s]	LDA2 MeanConf [m/s]	LDA1 RMSConf [m/s]	LDA2 RMSConf [m/s]	Cavity	r/b	z/s	Ωr (m/s)	$V_{\Phi}/\Omega r$	$V_{\Phi U95\%}/\Omega r$	$V_{\Phi(RMS)}/\Omega r$	Vz/W	$Vz_{(RMS)}/W$	$Vz_{U95\%}/W$
64		140	210	5000	5000	24481.9	1829.5			28.09	-1.38	1.93	7.99	0.05	0.22	0.04	0.16	3	0.955	0.508	34.02	0.83	1.57E-03	0.06	-0.04	0.25	6.87E-03
64		125	195	5000	2957	1577.1	49.3			25.53	-3.75	2.01	9.76	0.06	0.35	0.04	0.25	3	0.886	0.508	31.59	0.81	1.76E-03	0.06	-0.12	0.30	1.09E-02
64		110	180	5000	225	1310.1	3.8			24.05	-0.74	1.90	3.56	0.05	0.47	0.04	0.33	3	0.818	0.508	29.16	0.82	1.81E-03	0.07	-0.02	0.11	1.45E-02
64		95	165	5000	539	1159.7	9.0			22.25	0.07	1.58	0.75	0.04	0.06	0.03	0.04	3	0.750	0.508	26.73	0.83	1.64E-03	0.06	0.00	0.02	1.97E-03
64		80	150	2349	485	117.6	8.1			20.58	-0.09	1.42	2.27	0.06	0.20	0.04	0.14	3	0.682	0.508	24.30	0.85	2.36E-03	0.06	0.00	0.07	6.27E-03
64		65	135	4255	2776	212.8	46.3			19.01	-0.30	1.48	2.48	0.04	0.09	0.03	0.07	3	0.614	0.508	21.87	0.87	2.03E-03	0.07	-0.01	0.08	2.86E-03
64		50	120	1645	2412	82.3	40.3			18.38	-0.77	2.05	3.79	0.10	0.15	0.07	0.11	3	0.545	0.508	19.44	0.95	5.11E-03	0.11	-0.02	0.12	4.69E-03
64		35	105	5000	1300	5020.5	21.7			1.56	-0.17	5.99	2.22	0.17	0.12	0.12	0.09	3	0.477	0.508	17.01	0.09	9.77E-03	0.35	-0.01	0.07	3.75E-03
71		140	210	5000	5000	33613.1	19024.5			28.16	0.29	1.34	1.11	0.04	0.03	0.03	0.02	3	0.955	0.345	34.02	0.83	1.09E-03	0.04	0.01	0.03	9.52E-04
71		125	195	5000	5000	5628.0	7110.6			26.43	0.27	0.87	1.28	0.02	0.04	0.02	0.03	3	0.886	0.345	31.59	0.84	7.67E-04	0.03	0.01	0.04	1.10E-03
71		110	180	3964	5000	66.1	173.8			24.08	0.13	1.55	1.48	0.05	0.04	0.03	0.03	3	0.818	0.345	29.16	0.83	1.66E-03	0.05	0.00	0.05	1.28E-03
71		95	165	3637	179	60.7	3.0			21.86	0.24	1.50	0.73	0.05	0.11	0.03	0.08	3	0.750	0.345	26.73	0.82	1.83E-03	0.06	0.01	0.02	3.33E-03
71		80	150	3911	589	65.2	9.9			20.54	0.27	1.46	0.87	0.05	0.07	0.03	0.05	3	0.682	0.345	24.30	0.85	1.88E-03	0.06	0.01	0.03	2.17E-03
71		65	135	1548	171	25.8	2.9			19.03	0.09	1.45	1.08	0.07	0.16	0.05	0.11	3	0.614	0.345	21.87	0.87	3.31E-03	0.07	0.00	0.03	5.03E-03
57		140	210	5000	5000	2062.0	1602.4			28.06	-12.09	1.91	16.14	0.05	0.45	0.04	0.32	3	0.955	0.671	34.02	0.82	1.55E-03	0.06	-0.37	0.50	1.39E-02
57		125	195	5000	526	1124.1	8.8			25.78	-26.09	1.98	15.98	0.05	1.37	0.04	0.97	3	0.886	0.671	31.59	0.82	1.73E-03	0.06	-0.81	0.50	4.24E-02
57		110	180	5000	63	979.0	1.1			23.84	-1.96	1.75	8.10	0.05	2.02	0.03	1.43	3	0.818	0.671	29.16	0.82	1.66E-03	0.06	-0.06	0.25	6.25E-02
57		95	165	5000	52	705.8	0.9			22.17	-1.45	1.56	7.72	0.04	2.12	0.03	1.50	3	0.750	0.671	26.73	0.83	1.62E-03	0.06	-0.04	0.24	6.57E-02
57		80	150	5000	75	649.0	1.3			20.37	-1.94	1.57	8.69	0.04	1.98	0.03	1.40	3	0.682	0.671	24.30	0.84	1.79E-03	0.06	-0.06	0.27	6.14E-02
57		65	135	5000	201	166.5	3.4			18.97	-24.59	2.43	16.16	0.07	2.24	0.05	1.58	3	0.614	0.671	21.87	0.87	3.08E-03	0.11	-0.76	0.50	6.94E-02
94		-3	67	2930	5000	24.5	31402.5			20.92	0.49	2.63	0.66	0.10	0.02	0.07	0.01	cob2	0.305	0.311	10.85	1.93	8.78E-03	0.24	0.02	0.02	5.64E-04
94		-9	61	4834	5000	40.3	647.9			3.59	0.43	1.54	1.12	0.04	0.03	0.03	0.02	cob2	0.277	0.311	9.88	0.36	4.39E-03	0.16	0.01	0.03	9.65E-04
94		-13	57	#N/A	#N/A	#N/A	#N/A			#N/A	#N/A	#N/A	#N/A	#N/A	#N/A	#N/A	#N/A	cob2	0.259	0.311	9.23	#N/A	#N/A	#N/A	#N/A	#N/A	#N/A
84		-3	67	5000	5000	1428.1	779.7			18.17	0.62	2.31	0.65	0.06	0.02	0.05	0.01	cob2	0.305	0.709	10.85	1.67	5.91E-03	0.21	0.02	0.02	5.61E-04
84		-9	61	5000	5000	258.6	320.0			3.17	-0.12	1.87	0.74	0.05	0.02	0.04	0.01	cob2	0.277	0.709	9.88	0.32	5.24E-03	0.19	0.00	0.02	6.34E-04
84		-15	55	133	5000	6.9	4201.4			-0.61	0.35	0.26	1.01	0.05	0.03	0.03	0.02	cob2	0.250	0.709	8.91	-0.07	5.07E-03	0.03	0.01	0.03	8.65E-04
125		-3	67	5000	5000	115.9	48.6			-0.52	-12.35	6.19	13.45	0.17	0.37	0.12	0.26	2	0.305	0.260	10.85	-0.05	1.58E-02	0.57	-0.38	0.42	1.16E-02
125		-9	61	5000	5000	65.9	1106.6			-11.80	-6.24	18.11	22.87	0.50	0.63	0.35	0.45	2	0.277	0.260	9.88	-1.19	5.08E-02	1.83	-0.19	0.71	1.97E-02
125		-15	55	0	5000	#N/A	3466.7			#N/A	-2.64	#N/A	18.92	#N/A	0.52	#N/A	0.37	2	0.250	0.260	8.91	#N/A	#N/A	#N/A	-0.08	0.59	1.63E-02
64		20	90	113	212	1.9	3.6			17.28	-0.69	3.11	2.25	0.58	0.30	0.41	0.22	3	0.409	0.508	14.58	1.19	3.95E-02	0.21	-0.02	0.07	9.43E-03
64		5	75	0	5000	#N/A	745.7			#N/A	0.64	#N/A	4.80	#N/A	0.13	#N/A	0.09	3	0.341	0.508	12.15	#N/A	#N/A	#N/A	0.02	0.15	4.13E-03
64		-5	65	0	5000	#N/A	41222.0			#N/A	0.00	#N/A	1.22	#N/A	0.03	#N/A	0.02	3	0.295	0.508	10.53	#N/A	#N/A	#N/A	0.00	0.04	1.05E-03
64		-15	55	0	5000	#N/A	4183.2			#N/A	-0.01	#N/A	0.27	#N/A	0.01	#N/A	0.01	3	0.250	0.508	8.91	#N/A	#N/A	#N/A	0.00	0.01	2.31E-04
71		50	120	5000	4511	189.6	75.2			40.27	0.46	2.79	2.09	0.08	0.06	0.05	0.04	3	0.545	0.345	19.44	2.07	3.98E-03	0.14	0.01	0.06	1.89E-03
71		35	105	5000	4528	138.8	75.5			36.99	-0.26	3.81	2.71	0.11	0.08	0.07	0.06	3	0.477	0.345	17.01	2.17	6.20E-03	0.22	-0.01	0.08	2.44E-03
57		50	120	5000	5000	390.5	179.8			40.42	0.59	2.99	1.91	0.08	0.05	0.06	0.04	3	0.545	0.671	19.44	2.08	4.27E-03	0.15	0.02	0.06	1.64E-03
57		35	105	5000	5000	365.5	124.4			36.32	-0.17	3.90	2.38	0.11	0.07	0.08	0.05	3	0.477	0.671	17.01	2.14	6.36E-03	0.23	-0.01	0.07	2.05E-03

LDA measurement		**LDA code:**	101	**rpm:**	4552.2	**Perfd by:**	NM	Printed: 26/09/2008	Page 1/3
Build:	3	**ReΦ:**	4.12E+06	**Date:**	12/11/2003	**LDA1:**	VΦ	**Comments:** run OK	
LDA test # :	B3run28-1	**Rez:**	1.16E+05	**raw LDA file:**	\MCRLDA\Build3\B3run28-1.lda	**LDA2:**	Vz	**Traverse ref:**	
Heat Transfer run:	B3run28-1	**Ro:**	0.54	**LDA list file:**	\MCRLDA\Build3\B3run28-1.xls	**W (m/s):**	17.88		

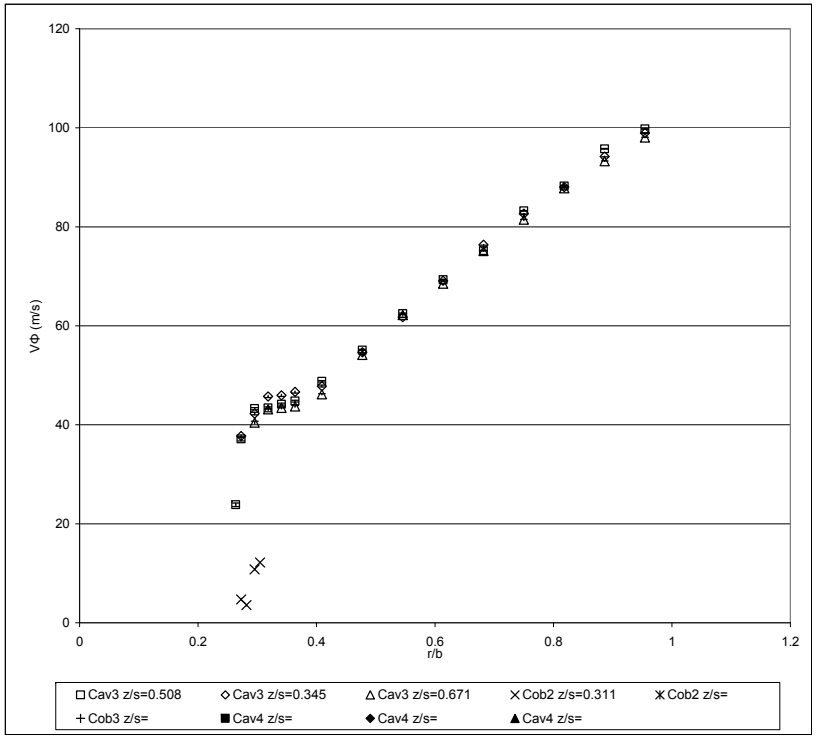

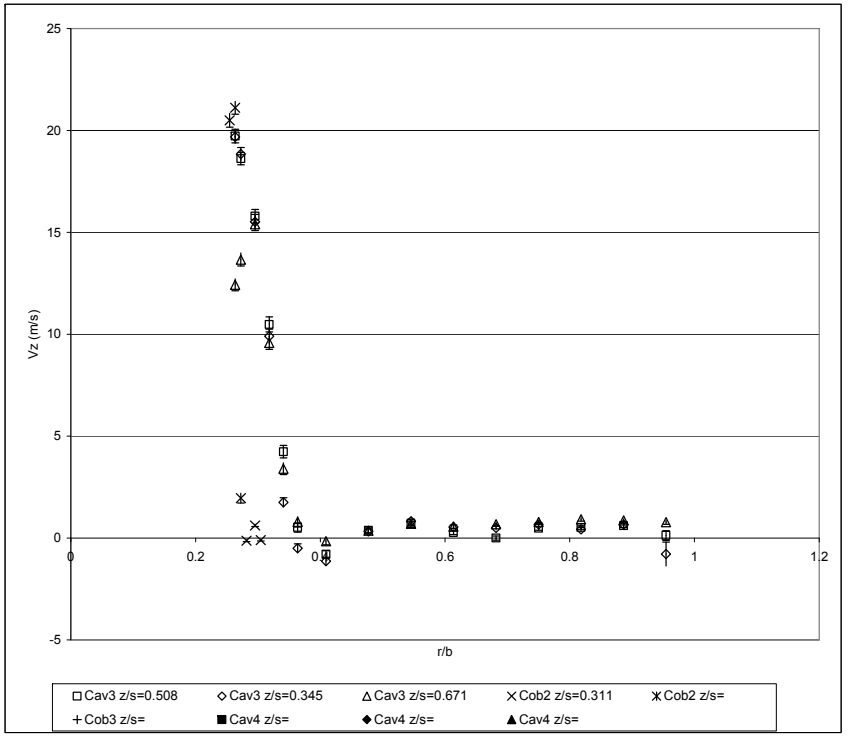

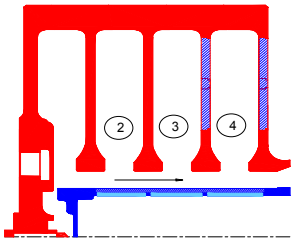

LDA measurement		**LDA code:**	101	**rpm:**	4552.2	**Perfd by:**	NM	Printed: 26/09/2008	Page 2/3
Build:	3	**Re_Φ:**	4.12E+06	**Date:**	12/11/2003	**LDA1:**	VΦ	**Comments:**	run OK
LDA test # :	B3run28-1	**Re_z:**	1.16E+05	**raw LDA file:**	\MCRLDA\Build3\B3run28-1.lda	**LDA2:**	Vz	**Traverse corresp:**	0
Heat Transfer run:	B3run28-1	**Ro:**	0.54	**LDA list file:**	\MCRLDA\Build3\B3run28-1.xls	**W (m/s):**	17.88		

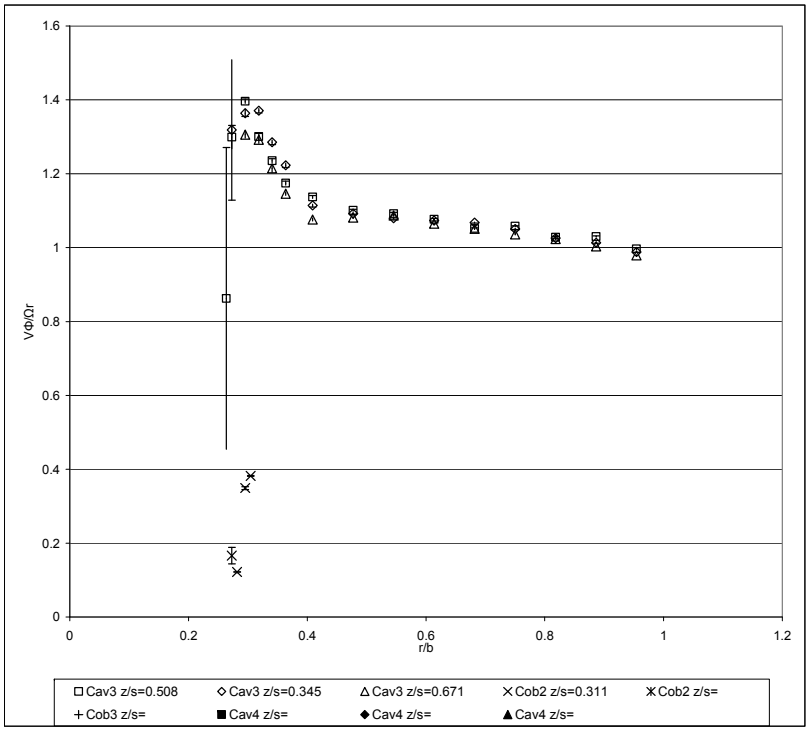

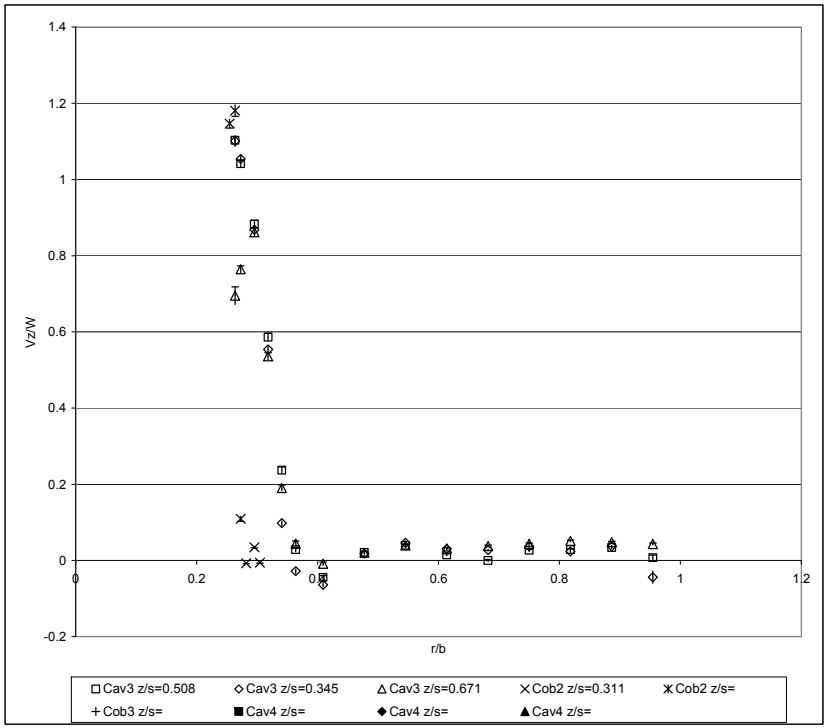

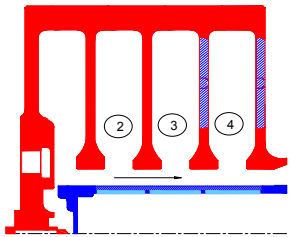

LDA measurement | LDA code: 101 | rpm: 4552.2 | Perfd by: NM | Printed: 26/09/2008 | Page 3/3

Build: 3 | **ReΦ:** 4.12E+06 | **Date:** 12/11/2003 | **LDA1:** VΦ | **Comments:** run OK

LDA test # : B3run28-1 | **Rez:** 1.16E+05 | raw LDA file: \MCRLDA\Build3\B3run28-1.lda | **LDA2:** Vz | **Traverse corresp:** 0

Heat Transfer run: B3run28-1 | **Ro:** 0.54 | LDA list file: \MCRLDA\Build3\B3run28-1.xls | **W (m/s):** 17.88

X [mm]	corrected X	Y [mm]	corrected Y / Radius (mm)	Count{1}	Count{2}	Data Rate{1} [#/s]	Data Rate{2} [#/s]	Validation{1} [%]	Validation{2} [%]	LDA1 Mean [m/s]	LDA2 Mean [m/s]	LDA1 RMS [m/s]	LDA2 RMS [m/s]	LDA1 MeanConf [m/s]	LDA2 MeanConf [m/s]	LDA1 RMSConf [m/s]	LDA2 RMSConf [m/s]	Cavity	r/b	z/s	Ωr (m/s)	$V_\Phi/\Omega r$	$V_{\Phi U95\%}/\Omega r$	$V_{\Phi(RMS)}/\Omega r$	$Vz_{(RMS)}/W$	$Vz_{U95\%}/W$
64		140	210	5000	5000	10221.0	3203.8			99.79	0.13	9.62	4.21	0.27	0.12	0.19	0.08	3	0.955	0.508	100.11	1.00	2.66E-03	0.10	0.01	0.24	6.53E-03
64		125	195	5000	5000	12325.4	4253.1			95.76	0.61	6.38	1.65	0.18	0.05	0.13	0.03	3	0.886	0.508	92.96	1.03	1.90E-03	0.07	0.03	0.09	2.57E-03
64		110	180	5000	5000	13403.7	5287.8			88.24	0.51	4.52	1.51	0.13	0.04	0.09	0.03	3	0.818	0.508	85.81	1.03	1.46E-03	0.05	0.03	0.08	2.34E-03
64		95	165	5000	5000	13316.7	5092.9			83.22	0.48	4.29	1.65	0.12	0.05	0.08	0.03	3	0.750	0.508	78.66	1.06	1.51E-03	0.05	0.03	0.09	2.56E-03
64		80	150	5000	4941	28626.4	82.4			75.20	0.00	5.08	1.78	0.14	0.05	0.10	0.04	3	0.682	0.508	71.51	1.05	1.97E-03	0.07	0.00	0.10	2.77E-03
64		65	135	5000	5000	28517.4	234.1			69.30	0.26	5.45	1.76	0.15	0.05	0.11	0.03	3	0.614	0.508	64.36	1.08	2.35E-03	0.08	0.01	0.10	2.72E-03
64		50	120	5000	5000	12005.9	596.4			62.47	0.71	6.98	2.02	0.19	0.06	0.14	0.04	3	0.545	0.508	57.20	1.09	3.38E-03	0.12	0.04	0.11	3.13E-03
64		35	105	5000	5000	396.0	1118.5			55.12	0.38	5.09	2.21	0.14	0.06	0.10	0.04	3	0.477	0.508	50.05	1.10	2.82E-03	0.10	0.02	0.12	3.43E-03
71		140	210	5000	5000	3371.3	7047.3			98.93	-0.79	5.22	10.37	0.14	0.29	0.10	0.20	3	0.955	0.345	100.11	0.99	1.44E-03	0.05	-0.04	0.58	1.61E-02
71		125	195	5000	5000	3076.8	6422.7			94.19	0.66	4.98	1.66	0.14	0.05	0.10	0.03	3	0.886	0.345	92.96	1.01	1.48E-03	0.05	0.04	0.09	2.57E-03
71		110	180	5000	5000	2985.2	5562.2			88.02	0.42	5.04	1.69	0.14	0.05	0.10	0.03	3	0.818	0.345	85.81	1.03	1.63E-03	0.06	0.02	0.09	2.62E-03
71		95	165	5000	5000	3270.3	7008.6			82.64	0.66	4.27	1.79	0.12	0.05	0.08	0.04	3	0.750	0.345	78.66	1.05	1.50E-03	0.05	0.04	0.10	2.77E-03
71		80	150	5000	5000	3670.7	8791.2			76.35	0.49	3.34	1.56	0.09	0.04	0.07	0.03	3	0.682	0.345	71.51	1.07	1.30E-03	0.05	0.03	0.09	2.42E-03
71		65	135	5000	5000	3320.9	8138.1			69.08	0.54	2.91	1.74	0.08	0.05	0.06	0.03	3	0.614	0.345	64.36	1.07	1.25E-03	0.05	0.03	0.10	2.70E-03
57		140	210	5000	5000	1064.4	1723.1			98.02	0.77	5.25	1.92	0.15	0.05	0.10	0.04	3	0.955	0.671	100.11	0.98	1.45E-03	0.05	0.04	0.11	2.97E-03
57		125	195	5000	5000	1465.3	2380.8			93.26	0.86	5.01	1.40	0.14	0.04	0.10	0.03	3	0.886	0.671	92.96	1.00	1.50E-03	0.05	0.05	0.08	2.18E-03
57		110	180	5000	5000	1861.4	2430.6			87.78	0.91	4.74	1.50	0.13	0.04	0.09	0.03	3	0.818	0.671	85.81	1.02	1.53E-03	0.06	0.05	0.08	2.33E-03
57		95	165	5000	5000	2097.1	2880.4			81.47	0.78	3.68	1.49	0.10	0.04	0.07	0.03	3	0.750	0.671	78.66	1.04	1.30E-03	0.05	0.04	0.08	2.31E-03
57		80	150	5000	5000	1958.9	3122.6			75.14	0.68	3.20	1.52	0.09	0.04	0.06	0.03	3	0.682	0.671	71.51	1.05	1.24E-03	0.04	0.04	0.08	2.36E-03
57		65	135	5000	5000	2950.1	3139.6			68.53	0.56	2.88	1.47	0.08	0.04	0.06	0.03	3	0.614	0.671	64.36	1.06	1.24E-03	0.04	0.03	0.08	2.28E-03
94		-3	67	5000	5000	54.3	1694.6			12.20	-0.10	1.46	0.80	0.04	0.02	0.03	0.02	cob2	0.305	0.311	31.94	0.38	1.27E-03	0.05	-0.01	0.04	1.24E-03
94		-5	65	5000	5000	43.8	521.3			10.81	0.62	4.42	1.00	0.12	0.03	0.09	0.02	cob2	0.295	0.311	30.99	0.35	3.95E-03	0.14	0.03	0.06	1.55E-03
94		-8	62	5000	5000	328.6	288.2			3.60	-0.13	0.48	0.79	0.01	0.02	0.01	0.02	cob2	0.282	0.311	29.56	0.12	4.50E-04	0.02	-0.01	0.04	1.22E-03
94		-10	60	352	5000	2.0	288.1			4.75	1.96	6.08	4.28	0.64	0.12	0.45	0.08	cob2	0.273	0.311	28.60	0.17	2.22E-02	0.21	0.11	0.24	6.63E-03
94		-12	58	0	1613	#N/A	13.5			#N/A	21.11	#N/A	5.57	#N/A	0.27	#N/A	0.19	cob2	0.264	0.311	27.65	#N/A	#N/A	#N/A	1.18	0.31	1.52E-02
94		-14	56	0	3321	#N/A	27.7			#N/A	20.50	#N/A	6.01	#N/A	0.20	#N/A	0.14	cob2	0.255	0.311	26.70	#N/A	#N/A	#N/A	1.15	0.34	1.14E-02
64		20	90	5000	5000	290.5	215.8			48.79	-0.80	6.10	3.02	0.17	0.08	0.12	0.06	3	0.409	0.508	42.90	1.14	3.94E-03	0.14	-0.04	0.17	4.68E-03
64		10	80	4277	5000	42.8	222.7			44.80	0.51	6.75	4.07	0.20	0.11	0.14	0.08	3	0.364	0.508	38.14	1.17	5.30E-03	0.18	0.03	0.23	6.32E-03
64		5	75	5000	5000	70.1	263.8			44.17	4.24	7.06	5.41	0.20	0.15	0.14	0.11	3	0.341	0.508	35.75	1.24	5.47E-03	0.20	0.24	0.30	8.39E-03
64		0	70	2508	5000	25.1	115.2			43.40	10.48	7.39	6.65	0.29	0.18	0.20	0.13	3	0.318	0.508	33.37	1.30	8.67E-03	0.22	0.59	0.37	1.03E-02
64		-5	65	5000	5000	62.3	104.1			43.27	15.79	6.56	6.06	0.18	0.17	0.13	0.12	3	0.295	0.508	30.99	1.40	5.87E-03	0.21	0.88	0.34	9.39E-03
64		-10	60	681	5000	4.5	187.3			37.17	18.62	11.96	5.38	0.90	0.15	0.64	0.11	3	0.273	0.508	28.60	1.30	3.14E-02	0.42	1.04	0.30	8.33E-03
64		-12	58	4	5000	0.1	142.1			23.85	19.72	9.98	5.96	11.29	0.17	7.98	0.12	3	0.264	0.508	27.65	0.86	4.08E-01	0.36	1.10	0.33	9.24E-03
71		50	120	5000	5000	1474.2	652.3			61.75	0.82	3.81	1.94	0.11	0.05	0.07	0.04	3	0.545	0.345	57.20	1.08	1.85E-03	0.07	0.05	0.11	3.01E-03
71		35	105	5000	5000	1860.7	930.4			54.67	0.32	5.05	2.30	0.14	0.06	0.10	0.05	3	0.477	0.345	50.05	1.09	2.80E-03	0.10	0.02	0.13	3.57E-03
57		50	120	5000	5000	1343.4	664.6			62.18	0.70	3.76	1.91	0.10	0.05	0.07	0.04	3	0.545	0.671	57.20	1.09	1.82E-03	0.07	0.04	0.11	2.96E-03
57		35	105	5000	5000	133.8	1185.8			54.13	0.36	5.19	2.14	0.14	0.06	0.10	0.04	3	0.477	0.671	50.05	1.08	2.88E-03	0.10	0.02	0.12	3.32E-03
71		20	90	5000	5000	86.6	102.0			47.79	-1.14	6.40	3.54	0.18	0.10	0.13	0.07	3	0.409	0.345	42.90	1.11	4.14E-03	0.15	-0.06	0.20	5.50E-03
71		10	80	4081	5000	68.0	93.3			46.64	-0.51	7.59	3.94	0.23	0.11	0.16	0.08	3	0.364	0.345	38.14	1.22	6.11E-03	0.20	-0.03	0.22	6.11E-03
71		5	75	5000	5000	88.4	119.6			45.95	1.75	8.14	4.10	0.23	0.11	0.16	0.08	3	0.341	0.345	35.75	1.29	6.31E-03	0.23	0.10	0.23	6.36E-03
71		0	70	5000	4902	106.3	81.7			45.73	9.90	6.98	6.32	0.19	0.18	0.14	0.13	3	0.318	0.345	33.37	1.37	5.80E-03	0.21	0.55	0.35	9.90E-03
71		-5	65	3050	5000	17.0	45.0			42.26	15.52	7.79	6.46	0.28	0.18	0.20	0.13	3	0.295	0.345	30.99	1.36	8.92E-03	0.25	0.87	0.36	1.00E-02
71		-10	60	7	4447	0.1	24.7			37.71	18.84	6.80	5.70	5.44	0.17	3.85	0.12	3	0.273	0.345	28.60	1.32	1.90E-01	0.24	1.05	0.32	9.38E-03
71		-12	58	0	1797	#N/A	10.0			#N/A	19.68	#N/A	5.55	#N/A	0.26	#N/A	0.18	3	0.264	0.345	27.65	#N/A	#N/A	#N/A	1.10	0.31	1.43E-02
57		20	90	5000	5000	99.3	73.2			46.17	-0.16	6.31	3.11	0.17	0.09	0.12	0.06	3	0.409	0.671	42.90	1.08	4.07E-03	0.15	-0.01	0.17	4.82E-03
57		10	80	5000	5000	115.3	80.6			43.71	0.79	6.55	4.48	0.18	0.12	0.13	0.09	3	0.364	0.671	38.14	1.15	4.76E-03	0.17	0.04	0.25	6.94E-03
57		5	75	1429	5000	7.9	71.2			43.42	3.40	7.18	5.13	0.37	0.14	0.26	0.10	3	0.341	0.671	35.75	1.21	1.04E-02	0.20	0.19	0.29	7.96E-03
57		0	70	1789	5000	10.0	66.3			43.12	9.58	7.11	5.78	0.33	0.16	0.23	0.11	3	0.318	0.671	33.37	1.29	9.87E-03	0.21	0.54	0.32	8.95E-03
57		-5	65	3017	3070	16.8	25.6			40.47	15.40	8.03	5.56	0.29	0.20	0.20	0.14	3	0.295	0.671	30.99	1.31	9.25E-03	0.26	0.86	0.31	1.10E-02
57		-10	60	0	5000	#N/A	94.3			#N/A	13.67	#N/A	5.71	#N/A	0.16	#N/A	0.11	3	0.273	0.671	28.60	#N/A	#N/A	#N/A	0.76	0.32	8.86E-03
57		-12	58	0	586	#N/A	4.9			#N/A	12.43	#N/A	5.17	#N/A	0.42	#N/A	0.30	3	0.264	0.671	27.65	#N/A	#N/A	#N/A	0.69	0.29	2.35E-02

LDA measurement		**LDA code:**	101	**rpm:**	665.6	**Perfd by:**	NM	Printed: 26/09/2008	Page 1/3
Build:	3	**ReΦ:**	4.92E+05	**Date:**	16/01/2004	**LDA1:**	VΦ	**Comments:**	run OK
LDA test # :	B3run32-1	**Rez:**	9.18E+04	**raw LDA file:**	\MCRLDA\Build3\B3run32-1.lda	**LDA2:**	Vz	**Traverse ref:**	
Heat Transfer run:	B3run32-1	**Ro:**	3.56	**LDA list file:**	\MCRLDA\Build3\B3run32-1.xls	**W (m/s):**	17.38		

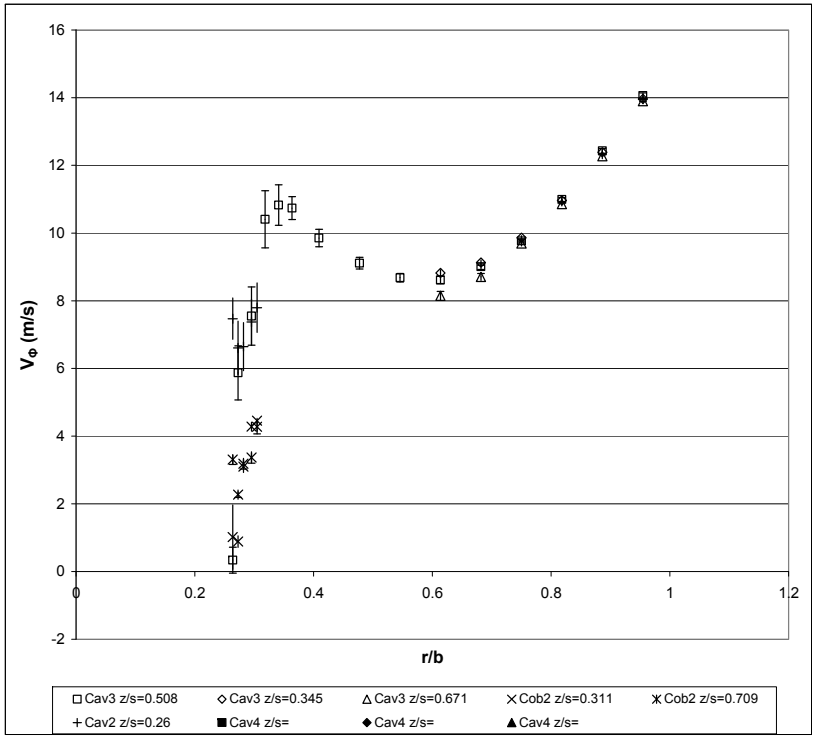

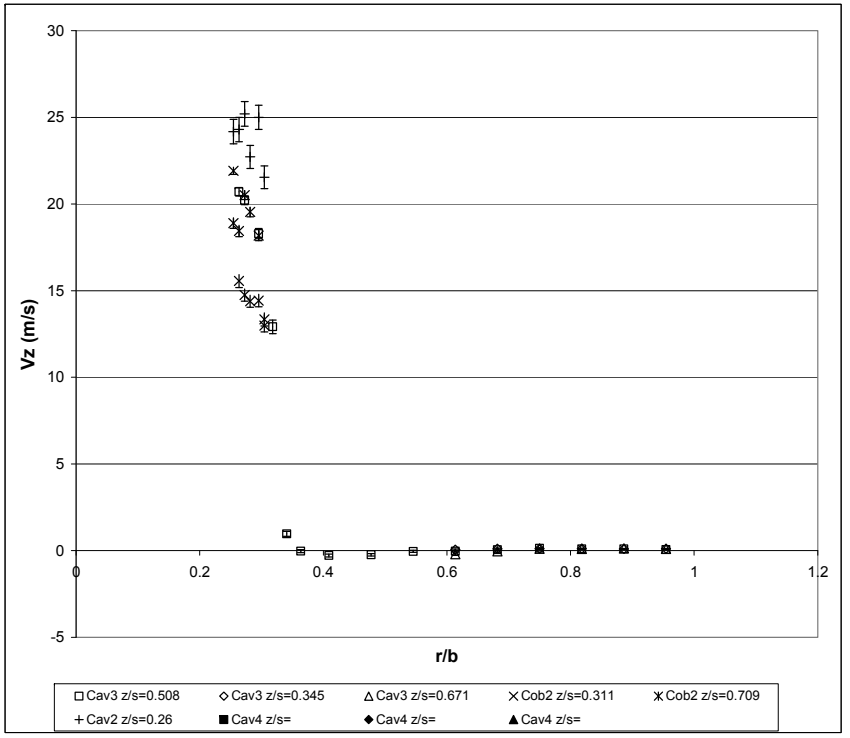

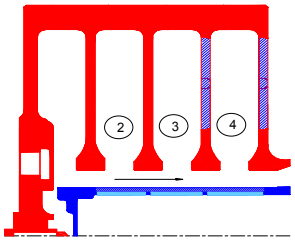

LDA measurement		**LDA code:**	101	**rpm:**	665.6	**Perfd by:**	NM	Printed: 26/09/2008	Page 2/3
Build:	3	**Re_Φ:**	4.92E+05	**Date:**	16/01/2004	**LDA1:**	VΦ	**Comments:**	run OK
LDA test # :	B3run32-1	**Re_z:**	9.18E+04	**raw LDA file:**	\MCRLDA\Build3\B3run32-1.lda	**LDA2:**	Vz	**Traverse corresp:**	0
Heat Transfer run:	B3run32-1	**Ro:**	3.56	**LDA list file:**	\MCRLDA\Build3\B3run32-1.xls	**W (m/s):**	17.38		

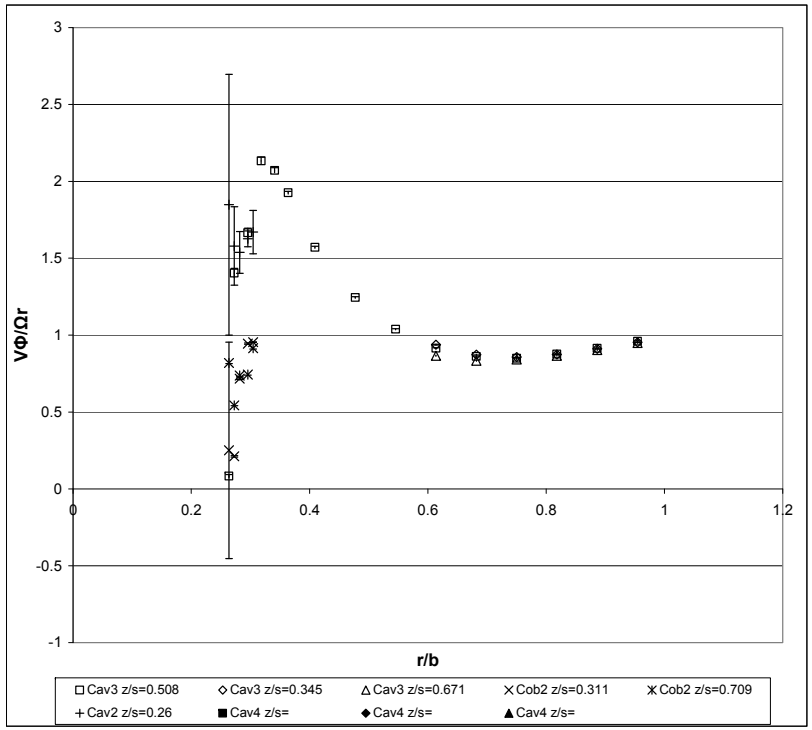

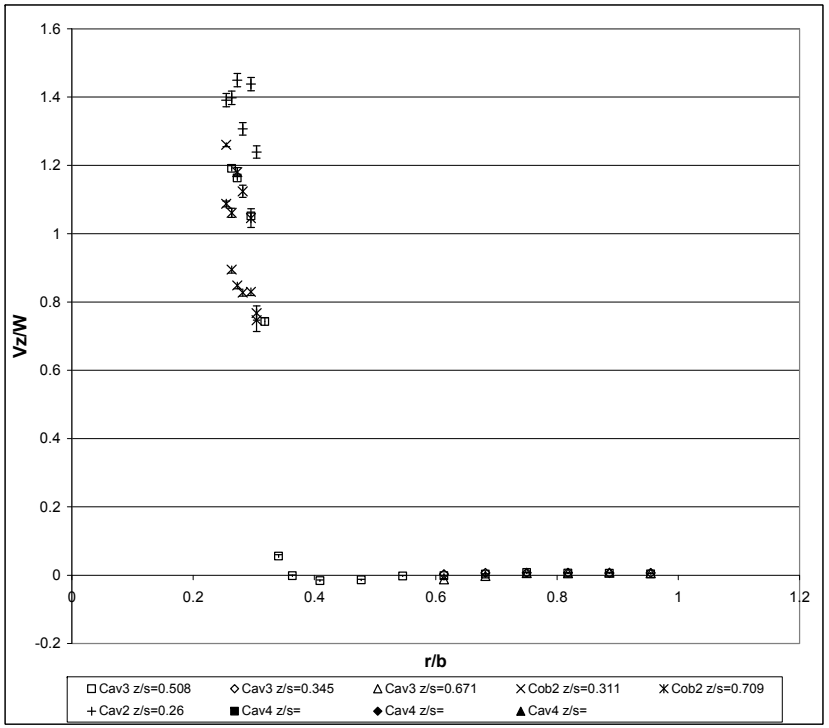

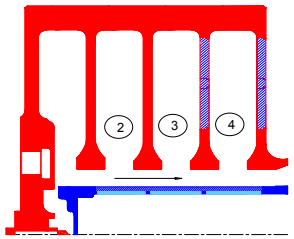

LDA measurement | LDA code: 101 | rpm: 665.6 | Perfd by: NM | Printed: 26/09/2008 | Page 3/3

Build: 3 | ReΦ: 4.92E+05 | Date: 16/01/2004 | LDA1: VΦ | Comments: run OK

LDA test # : B3run32-1 | Rez: 9.18E+04 | raw LDA file: \MCRLDA\Build3\B3run32-1.lda | LDA2: Vz | Traverse corresp: 0

Heat Transfer run: B3run32-1 | Ro: 3.56 | LDA list file: \MCRLDA\Build3\B3run32-1.xls | W (m/s): 17.38

X [mm]	corrected X	Y [mm]	corrected Y / Radius (mm)	Count{1}	Count{2}	Data Rate{1} [#/s]	Data Rate{2} [#/s]	Validation{1} [%]	Validation{2} [%]	LDA1 Mean [m/s]	LDA2 Mean [m/s]	LDA1 RMS [m/s]	LDA2 RMS [m/s]	LDA1 MeanConf [m/s]	LDA2 MeanConf [m/s]	LDA1 RMSConf [m/s]	LDA2 RMSConf [m/s]	Cavity	r/b	z/s	Ωr (m/s)	$V_\Phi/\Omega r$	$V_{\Phi U95\%}/\Omega r$	$V_{\Phi(RMS)}/\Omega r$	Vz/W	$Vz_{(RMS)}/W$	$Vz_{U95\%}/W$
64	140	210	5000	5000	87.5	83.9			14.06	0.07	1.13	0.55	0.03	0.02	0.02	0.01	3	0.955	0.508	14.64	0.96	2.13E-03	0.08	0.00	0.03	8.72E-04
64	125	195	5000	5000	131.2	116.3			12.43	0.10	0.90	0.34	0.02	0.01	0.02	0.01	3	0.886	0.508	13.59	0.91	1.83E-03	0.07	0.01	0.02	5.48E-04
64	110	180	5000	5000	860.3	621.7			10.99	0.10	0.69	0.37	0.02	0.01	0.01	0.01	3	0.818	0.508	12.55	0.88	1.53E-03	0.06	0.01	0.02	5.89E-04
64	95	165	5000	5000	82.1	75.2			9.77	0.14	0.70	0.48	0.02	0.01	0.01	0.01	3	0.750	0.508	11.50	0.85	1.68E-03	0.06	0.01	0.03	7.58E-04
64	80	150	5000	5000	274.9	325.7			9.01	0.05	0.87	0.71	0.02	0.02	0.02	0.01	3	0.682	0.508	10.46	0.86	2.31E-03	0.08	0.00	0.04	1.13E-03
64	65	135	5000	5000	105.0	120.2			8.61	-0.03	0.99	0.90	0.03	0.02	0.02	0.02	3	0.614	0.508	9.41	0.92	2.92E-03	0.11	0.00	0.05	1.44E-03
64	50	120	5000	5000	208.5	243.7			8.68	-0.04	1.05	1.04	0.03	0.03	0.02	0.02	3	0.545	0.508	8.36	1.04	3.49E-03	0.13	0.00	0.06	1.65E-03
64	35	105	5000	5000	1862.2	2793.3			9.11	-0.24	1.26	1.13	0.03	0.03	0.02	0.02	3	0.477	0.508	7.32	1.24	4.76E-03	0.17	-0.01	0.07	1.81E-03
71	140	210	5000	4909	37.8	20.8			13.96	0.11	1.12	0.30	0.03	0.01	0.02	0.01	3	0.955	0.345	14.64	0.95	2.13E-03	0.08	0.01	0.02	4.87E-04
71	125	195	5000	5000	81.1	68.0			12.39	0.10	0.94	0.33	0.03	0.01	0.02	0.01	3	0.886	0.345	13.59	0.91	1.92E-03	0.07	0.01	0.02	5.33E-04
71	110	180	5000	5000	107.7	88.8			10.97	0.12	0.75	0.36	0.02	0.01	0.01	0.01	3	0.818	0.345	12.55	0.87	1.65E-03	0.06	0.01	0.02	5.67E-04
71	95	165	5000	5000	101.0	84.5			9.86	0.12	0.70	0.42	0.02	0.01	0.01	0.01	3	0.750	0.345	11.50	0.86	1.70E-03	0.06	0.01	0.02	6.73E-04
71	80	150	5000	5000	74.2	62.0			9.13	0.11	0.81	0.58	0.02	0.02	0.02	0.01	3	0.682	0.345	10.46	0.87	2.15E-03	0.08	0.01	0.03	9.31E-04
71	65	135	5000	5000	93.5	85.4			8.82	0.05	0.88	0.77	0.02	0.02	0.02	0.02	3	0.614	0.345	9.41	0.94	2.59E-03	0.09	0.00	0.04	1.23E-03
57	140	210	5000	5000	111.3	103.4			13.90	0.10	1.18	0.32	0.03	0.01	0.02	0.01	3	0.955	0.671	14.64	0.95	2.23E-03	0.08	0.01	0.02	5.14E-04
57	125	195	5000	5000	105.7	97.5			12.27	0.13	0.96	0.33	0.03	0.01	0.02	0.01	3	0.886	0.671	13.59	0.90	1.96E-03	0.07	0.01	0.02	5.33E-04
57	110	180	5000	5000	106.8	104.7			10.86	0.10	0.72	0.40	0.02	0.01	0.01	0.01	3	0.818	0.671	12.55	0.87	1.60E-03	0.06	0.01	0.02	6.32E-04
57	95	165	5000	5000	67.7	29.1			9.69	0.11	0.82	0.53	0.02	0.01	0.02	0.01	3	0.750	0.671	11.50	0.84	1.98E-03	0.07	0.01	0.03	8.39E-04
57	80	150	5000	5000	237.8	262.3			8.71	-0.04	1.07	0.86	0.03	0.02	0.02	0.02	3	0.682	0.671	10.46	0.83	2.84E-03	0.10	0.00	0.05	1.37E-03
57	65	135	5000	5000	481.1	597.5			8.15	-0.21	1.23	1.11	0.03	0.03	0.02	0.02	3	0.614	0.671	9.41	0.87	3.62E-03	0.13	-0.01	0.06	1.77E-03
94	-3	67	5000	449	2933.8	7.5			4.46	12.98	0.32	6.24	0.01	0.58	0.01	0.41	cob2	0.305	0.311	4.67	0.95	1.93E-03	0.07	0.75	0.36	3.32E-02
94	-5	65	5000	4058	490.6	67.7			4.28	14.43	0.60	6.23	0.02	0.19	0.01	0.14	cob2	0.295	0.311	4.53	0.94	3.65E-03	0.13	0.83	0.36	1.10E-02
94	-8	62	5000	4283	300.1	71.4			3.10	14.39	0.75	6.00	0.02	0.18	0.01	0.13	cob2	0.282	0.311	4.32	0.72	4.80E-03	0.17	0.83	0.35	1.03E-02
94	-10	60	5000	5000	600.7	89.3			0.88	14.75	0.70	6.12	0.02	0.17	0.01	0.12	cob2	0.273	0.311	4.18	0.21	4.65E-03	0.17	0.85	0.35	9.76E-03
94	-12	58	5000	8	0.2	87.1			1.01	15.56	3.84	6.52	2.85	0.18	2.01	0.13	cob2	0.264	0.311	4.04	0.25	7.04E-01	0.95	0.89	0.37	1.04E-02
94	-14	56	0	5000	#N/A	838.1			#N/A	21.91	#N/A	3.62	#N/A	0.10	#N/A	0.07	cob2	0.255	0.311	3.90	#N/A	#N/A	#N/A	1.26	0.21	5.78E-03
84	-3	67	5000	1261	3333.3	21.2			4.27	13.34	0.98	6.60	0.03	0.36	0.02	0.26	cob2	0.305	0.709	4.67	0.92	5.80E-03	0.21	0.77	0.38	2.10E-02
84	-5	65	5000	452	2542.4	3.8			3.37	18.18	0.76	5.14	0.02	0.47	0.01	0.34	cob2	0.295	0.709	4.53	0.74	4.64E-03	0.17	1.05	0.30	2.73E-02
84	-8	62	5000	885	956.8	5.0			3.18	19.54	0.68	4.78	0.02	0.32	0.01	0.22	cob2	0.282	0.709	4.32	0.74	4.35E-03	0.16	1.12	0.28	1.81E-02
84	-10	60	5000	1498	8112.7	8.3			2.27	20.52	0.35	4.49	0.01	0.23	0.01	0.16	cob2	0.273	0.709	4.18	0.54	2.30E-03	0.08	1.18	0.26	1.31E-02
84	-12	58	5000	2354	2765.4	13.1			3.31	18.45	0.58	5.67	0.02	0.23	0.01	0.16	cob2	0.264	0.709	4.04	0.82	3.97E-03	0.14	1.06	0.33	1.32E-02
84	-14	56	0	5000	#N/A	31.1			#N/A	18.90	#N/A	5.32	#N/A	0.15	#N/A	0.10	cob2	0.255	0.709	3.90	#N/A	#N/A	#N/A	1.09	0.31	8.48E-03
125	-3	67	105	5000	0.6	201.1			7.80	21.54	3.42	11.33	0.66	0.31	0.46	0.22	2	0.305	0.260	4.67	1.67	1.41E-01	0.73	1.24	0.65	1.81E-02
125	-5	65	675	5000	3.8	851.0			7.37	25.00	3.09	12.13	0.23	0.34	0.16	0.24	2	0.295	0.260	4.53	1.63	5.14E-02	0.68	1.44	0.70	1.93E-02
125	-8	62	107	5000	0.6	270.1			6.64	22.72	3.07	11.61	0.58	0.32	0.41	0.23	2	0.282	0.260	4.32	1.54	1.35E-01	0.71	1.31	0.67	1.85E-02
125	-10	60	38	5000	0.2	803.3			6.61	25.20	3.31	12.29	1.07	0.34	0.75	0.24	2	0.273	0.260	4.18	1.58	2.55E-01	0.79	1.45	0.71	1.96E-02
125	-12	58	3	5000	0.0	202.2			7.47	24.30	2.47	12.25	3.43	0.34	2.42	0.24	2	0.264	0.260	4.04	1.85	8.48E-01	0.61	1.40	0.70	1.95E-02
125	-14	56	0	5000	#N/A	45.3			#N/A	24.18	#N/A	12.30	#N/A	0.34	#N/A	0.24	2	0.255	0.260	3.90	#N/A	#N/A	#N/A	1.39	0.71	1.96E-02
64	20	90	5000	5000	132.7	157.1			9.86	-0.28	1.61	1.37	0.04	0.04	0.03	0.03	3	0.409	0.508	6.27	1.57	7.10E-03	0.26	-0.02	0.08	2.19E-03
64	10	80	5000	5000	143.3	99.4			10.74	-0.03	1.88	1.51	0.05	0.04	0.04	0.03	3	0.364	0.508	5.58	1.93	9.34E-03	0.34	0.00	0.09	2.40E-03
64	5	75	5000	5000	123.1	105.0			10.83	0.97	3.12	2.43	0.09	0.07	0.06	0.05	3	0.341	0.508	5.23	2.07	1.65E-02	0.60	0.06	0.14	3.87E-03
64	0	70	5000	5000	285.2	174.0			10.41	12.92	4.13	6.88	0.11	0.19	0.08	0.13	3	0.318	0.508	4.88	2.13	2.35E-02	0.85	0.74	0.40	1.10E-02
64	-5	65	3330	5000	27.8	187.7			7.55	18.29	3.89	5.22	0.13	0.14	0.09	0.10	3	0.295	0.508	4.53	1.67	2.92E-02	0.86	1.05	0.30	8.32E-03
64	-10	60	2627	5000	21.9	299.2			5.87	20.22	3.34	4.37	0.13	0.12	0.09	0.09	3	0.273	0.508	4.18	1.40	3.06E-02	0.80	1.16	0.25	6.97E-03
64	-12	58	5000	3521	173.7	29.4			0.34	20.70	1.55	4.23	0.04	0.14	0.03	0.10	3	0.264	0.508	4.04	0.08	1.06E-02	0.38	1.19	0.24	8.04E-03
71	50	120	5000	5000	1297.9	4000.9			8.94	-0.03	0.93	0.95	0.03	0.03	0.02	0.02	cob2	0.545	0.345	8.36	1.07	3.10E-03	0.11	0.00	0.05	1.52E-03
71	35	105	5000	5000	1574.2	4345.9			9.45	-0.11	1.02	1.04	0.03	0.03	0.02	0.02	cob2	0.477	0.345	7.32	1.29	3.87E-03	0.14	-0.01	0.06	1.66E-03
57	50	120	5000	5000	1475.2	4230.0			8.05	-0.27	1.30	1.24	0.04	0.03	0.03	0.02	cob2	0.545	0.671	8.36	0.96	4.30E-03	0.16	-0.02	0.07	1.97E-03
57	35	105	5000	5000	1745.8	4581.8			8.51	-0.20	1.51	1.38	0.04	0.04	0.03	0.03	cob2	0.477	0.671	7.32	1.16	5.70E-03	0.21	-0.01	0.08	2.19E-03
71	20	90	5000	5000	3126.1	345.0			10.24	-0.32	1.24	1.04	0.03	0.03	0.02	0.02	cob2	0.409	0.345	6.27	1.63	5.46E-03	0.20	-0.02	0.06	1.65E-03
71	10	80	5000	5000	149.8	565.5			11.06	0.15	1.40	1.13	0.04	0.03	0.03	0.02	cob2	0.364	0.345	5.58	1.98	6.96E-03	0.25	0.01	0.07	1.81E-03
71	5	75	1624	5000	27.1	1058.4			11.83	-0.03	1.95	1.52	0.09	0.04	0.07	0.03	cob2	0.341	0.345	5.23	2.26	1.81E-02	0.37	0.00	0.09	2.43E-03
71	0	70	3958	5000	23.4	42.2			10.28	12.96	2.56	7.33	0.08	0.20	0.06	0.14	cob2	0.318	0.345	4.88	2.11	1.63E-02	0.52	0.75	0.42	1.17E-02
71	-5	65	2553	5000	14.2	53.5			7.44	18.70	2.96	5.17	0.11	0.14	0.08	0.10	cob2	0.295	0.345	4.53	1.64	2.54E-02	0.65	1.08	0.30	8.24E-03
71	-10	60	4	5000	0.0	46.3			5.83	19.91	0.62	4.54	0.71	0.13	0.50	0.09	cob2	0.273	0.345	4.18	1.39	1.69E-01	0.15	1.15	0.26	7.23E-03
71	-12	58	0	5000	#N/A	168.3			#N/A	19.91	#N/A	5.10	#N/A	0.14	#N/A	0.10	cob2	0.264	0.345	4.04	#N/A	#N/A	#N/A	1.15	0.29	8.14E-03
57	20	90	5000	5000	360.0	292.3			8.97	-0.15	2.09	1.27	0.06	0.04	0.04	0.02	cob2	0.409	0.671	6.27	1.43	9.22E-03	0.33	-0.01	0.07	2.02E-03
57	10	80	3445	5000	58.0	762.2			9.78	0.04	2.48	0.55	0.08	0.02	0.06	0.01	cob1	0.364	0.671	5.58	1.75	1.49E-02	0.45	0.00	0.03	8.84E-04
57	5	75	5000	5000	614.7	185.4			10.34	0.29	2.81	1.85	0.08	0.05	0.06	0.04	cob1	0.341	0.671	5.23	1.98	1.49E-02	0.54	0.02	0.11	2.95E-03
57	0	70	5000	5000	142.2	794.4			9.79	12.96	3.05	5.53	0.08	0.15	0.06	0.11	cob1	0.318	0.671	4.88	2.01	1.74E-02	0.63	0.75	0.32	8.82E-03
57	-5	65	5000	5000	162.2	310.6			8.50	16.78	2.76	5.18	0.08	0.14	0.05	0.10	cob1	0.295	0.671	4.53	1.88	1.69E-02	0.61	0.97	0.30	8.25E-03
57	-10	60	65	5000	1.1	932.9			6.71	19.42	2.60	5.05	0.64	0.14	0.45	0.10	cob1	0.273	0.671	4.18	1.60	1.52E-01	0.62	1.12	0.29	8.06E-03
57	-12	58	8	5000	0.2	311.0			4.75	18.69	1.68	6.16	1.25	0.17	0.88	0.12	cob1	0.264	0.671	4.04	1.18	3.09E-01	0.42	1.08	0.35	9.82E-03

LDA measurement		**LDA code:**	110	**rpm:**	655.0	**Perfd by:**	NM	Printed: 27/09/2008	Page 1/2
Build:	3	**ReΦ:**	3.99E+05	**Date:**	27/09/2004	**LDA1:**	Vr	**Comments:**	Probe angular error corrected -1.389deg
LDA test # :	B3run38-1	**Rez:**	1.57E+05	**raw LDA file:**	\MCRLDA\Build3\B3run38-1.lda	**LDA2:**	VΦ	**Traverse ref:**	
Heat Transfer run:	B3run38-1	**Ro:**	7.51	**LDA list file:**	\MCRLDA\Build3\B3run38-1.xls	**W (m/s):**	36.10	**CAVITY 3**	

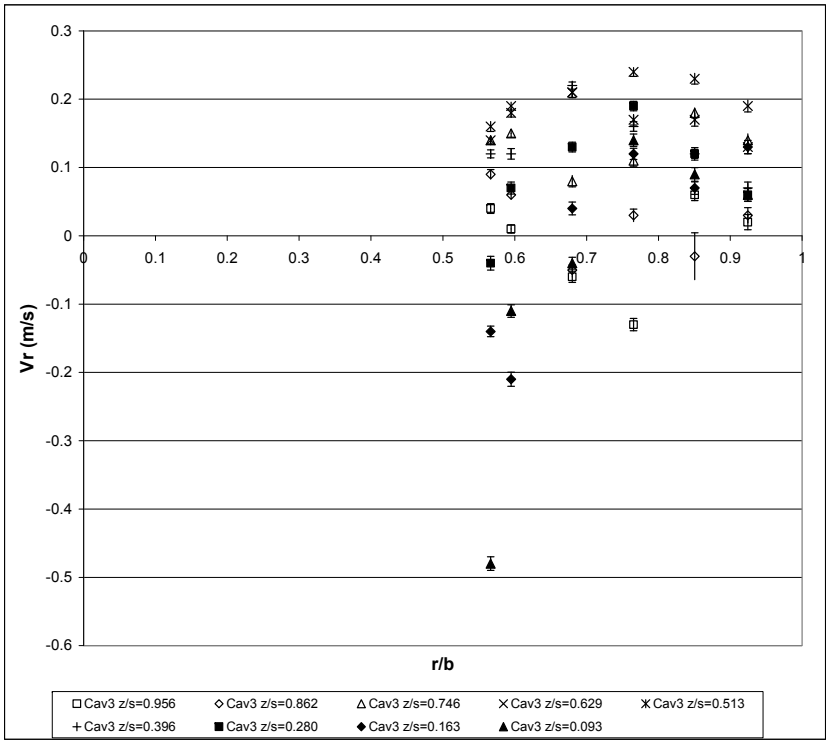

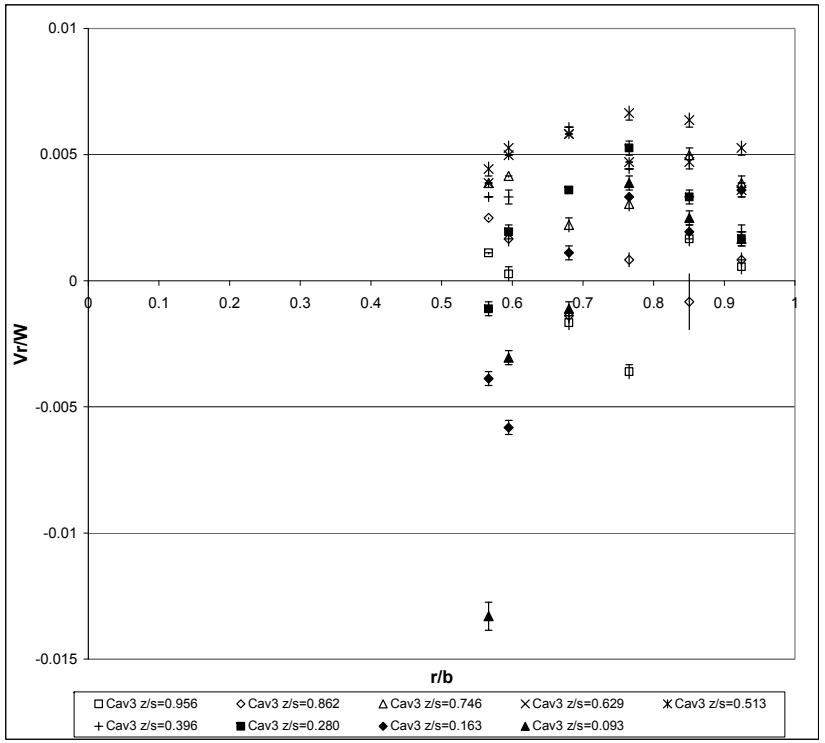

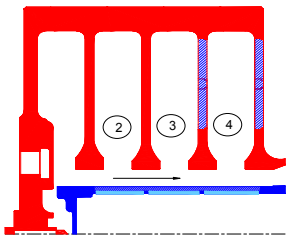

LDA measurement		**LDA code:**	110	**rpm:**	655.0	**Perfd by:**	NM	Printed: 27/09/2008	Page 1/2
Build:	3	**ReΦ:**	3.99E+05	**Date:**	27/09/2004	**LDA1:**	Vr	**Comments:**	Probe angular error corrected -1.389deg
LDA test # :	B3run38-1	**Rez:**	1.57E+05	**raw LDA file:**	\MCRLDA\Build3\B3run38-1.lda	**LDA2:**	VΦ	**Traverse ref:**	
Heat Transfer run:	B3run38-1	**Ro:**	7.51	**LDA list file:**	\MCRLDA\Build3\B3run38-1.xls	**W (m/s):**	36.10	**CAVITY 4**	

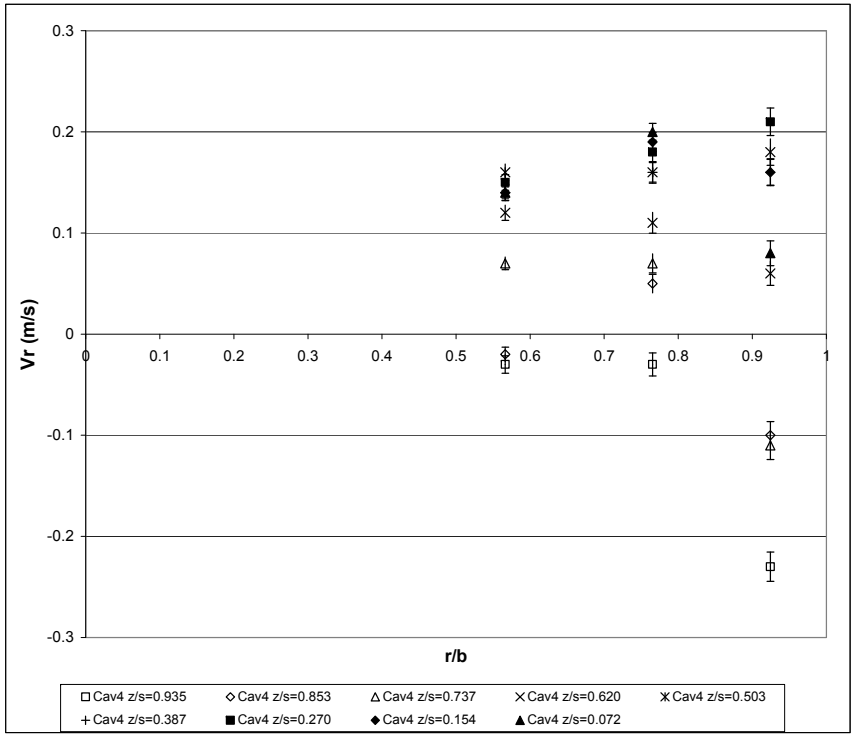

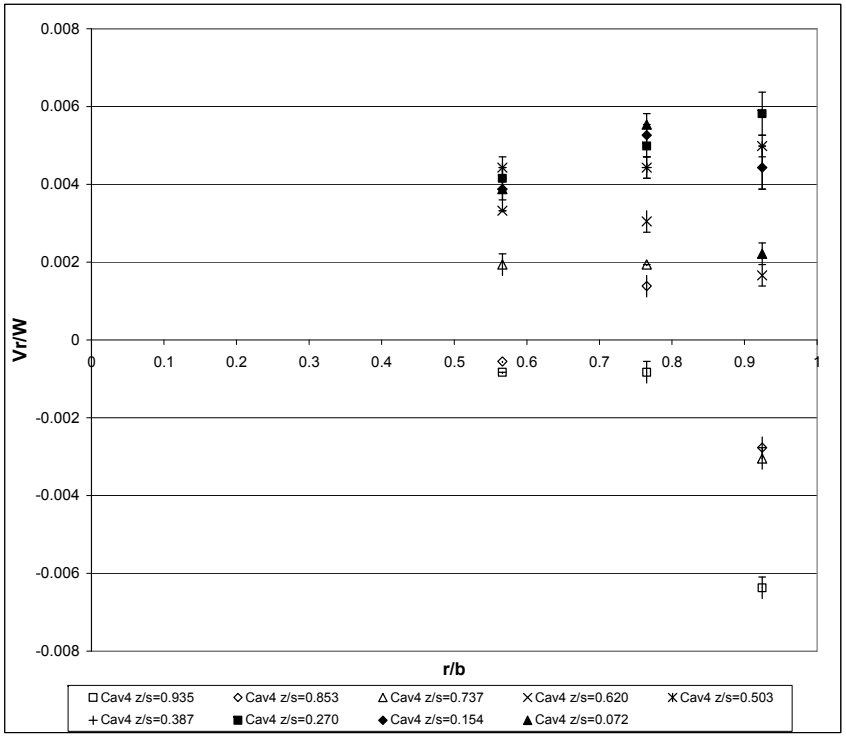

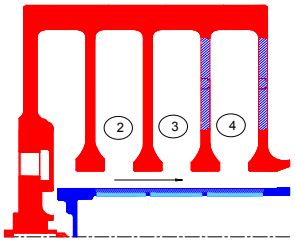

LDA measurement | **Build:** 3 | **LDA test # :** B3run38-1 | **Heat Transfer run:** B3run38-1

LDA code: 110 | **ReΦ:** 3.99E+05 | **Rez:** 1.57E+05 | **Ro:** 7.51

rpm: 655.0 | **Date:** 27/09/2004 | **raw LDA file:** \MCRLDA\Build3\B3run38-1.lda | **LDA list file:** \MCRLDA\Build3\B3run38-1.xls

Perfd by: NM | **LDA1:** Vr | **LDA2:** VΦ | **W (m/s):** 36.1

Printed: 27/09/2008 | **Comments:** Probe angular error corrected -1.389deg | **Traverse corresp:** 0

X [mm]	corrected dX	Y [mm]	corrected Y / Radius (mm)	Count{1}	Count{2}	Data Rate{1} [#/s]	Data Rate{2} [#/s]	Validation{1} [%]	Validation{2} [%]	LDA2 Mean [m/s]	LDA1 Mean [m/s]	LDA2 RMS [m/s]	LDA1 RMS [m/s]	LDA2 MeanConf [m/s]	LDA1 MeanConf [m/s]	LDA2 RMSConf [m/s]	LDA1 RMSConf [m/s]	Cavity	r/b	z/s	Ωr (m/s)	$V_\phi/\Omega r$	$V_{\phi U95\%}/\Omega r$	$V_{\phi RMS}/\Omega r$	Vz/W	Vz_{RMS}/W	$Vz_{U95\%}$/W
151	173.5	163	203.375	7142		246.6		45.61			0.02		0.40		0.01		0.01	3	0.924	0.956	13.95				0.00	0.01	2.77E-04
155	177.5	163	203.375	4472		56.1		45.49			0.03		0.41		0.01		0.01	3	0.924	0.862	13.95				0.00	0.01	2.77E-04
160	182.5	163	203.375	10054		141.3		73.83			0.14		0.33		0.01		0.00	3	0.924	0.746	13.95				0.00	0.01	2.77E-04
165	187.5	163	203.375	5266		596.7		67.60			0.19		0.31		0.01		0.01	3	0.924	0.629	13.95				0.01	0.01	2.77E-04
170	192.5	163	203.375	11583		211.6		55.95			0.13		0.35		0.01		0.00	3	0.924	0.513	13.95				0.00	0.01	2.77E-04
175	197.5	163	203.375	7101		546.6		66.17			0.07		0.32		0.01		0.01	3	0.924	0.396	13.95				0.00	0.01	2.77E-04
180	202.5	163	203.375	7190		246.8		70.09			0.06		0.33		0.01		0.01	3	0.924	0.280	13.95				0.00	0.01	2.77E-04
185	207.5	163	203.375	9604		53.4		60.77			0.13		0.35		0.01		0.00	3	0.924	0.163	13.95				0.00	0.01	2.77E-04
188	210.5	163	203.375	2801		15.6		64.77			0.06		0.35		0.01		0.01	3	0.924	0.093	13.95				0.00	0.01	2.77E-04
151	173.5	150	187.125	3550		469.3		62.28			0.06		0.31		0.01		0.01	3	0.851	0.956	12.84				0.00	0.01	2.77E-04
155	177.5	150	187.125	3205		752.4		14.72			-0.03		1.24		0.04		0.03	3	0.851	0.862	12.84				0.00	0.03	1.11E-03
160	182.5	150	187.125	7053		555.1		67.63			0.18		0.26		0.01		0.00	3	0.851	0.746	12.84				0.00	0.01	2.77E-04
165	187.5	150	187.125	10469		2020.6		60.32			0.23		0.28		0.01		0.00	3	0.851	0.629	12.84				0.01	0.01	2.77E-04
170	192.5	150	187.125	7855		1669.1		49.73			0.17		0.34		0.01		0.01	3	0.851	0.513	12.84				0.00	0.01	2.77E-04
175	197.5	150	187.125	6452		191.0		73.51			0.12		0.24		0.01		0.00	3	0.851	0.396	12.84				0.00	0.01	2.77E-04
180	202.5	150	187.125	18109		166.0		64.47			0.12		0.33		0.00		0.00	3	0.851	0.280	12.84				0.00	0.01	0.00E+00
185	207.5	150	187.125	11863		153.5		61.23			0.07		0.33		0.01		0.00	3	0.851	0.163	12.84				0.00	0.01	2.77E-04
188	210.5	150	187.125	10062		88.8		62.06			0.09		0.36		0.01		0.00	3	0.851	0.093	12.84				0.00	0.01	2.77E-04
151	173.5	135	168.375	7290		1381.9		53.29			-0.13		0.32		0.01		0.01	3	0.765	0.956	11.55				0.00	0.01	2.77E-04
155	177.5	135	168.375	3950		783.1		64.86			0.03		0.33		0.01		0.01	3	0.765	0.862	11.55				0.00	0.01	2.77E-04
160	182.5	135	168.375	3415		664.6		62.28			0.11		0.29		0.01		0.01	3	0.765	0.746	11.55				0.00	0.01	2.77E-04
165	187.5	135	168.375	4171		523.0		80.82			0.24		0.23		0.01		0.00	3	0.765	0.629	11.55				0.01	0.01	2.77E-04
170	192.5	135	168.375	13200		933.2		67.42			0.17		0.28		0.00		0.00	3	0.765	0.513	11.55				0.00	0.01	0.00E+00
175	197.5	135	168.375	14045		403.4		81.37			0.16		0.25		0.00		0.00	3	0.765	0.396	11.55				0.00	0.01	0.00E+00
180	202.5	135	168.375	4811		255.1		84.58			0.19		0.25		0.01		0.01	3	0.765	0.280	11.55				0.01	0.01	2.77E-04
185	207.5	135	168.375	13831		258.2		70.39			0.12		0.29		0.00		0.00	3	0.765	0.163	11.55				0.00	0.01	0.00E+00
188	210.5	135	168.375	13644		107.1		70.55			0.14		0.32		0.01		0.00	3	0.765	0.093	11.55				0.00	0.01	2.77E-04
151	173.5	120	149.625	3245		914.9		67.33			-0.06		0.29		0.01		0.01	3	0.680	0.956	10.26				0.00	0.01	2.77E-04
155	177.5	120	149.625	2119		478.6		72.00			-0.05		0.27		0.01		0.01	3	0.680	0.862	10.26				0.00	0.01	2.77E-04
160	182.5	120	149.625	3631		929.4		64.83			0.08		0.30		0.01		0.01	3	0.680	0.746	10.26				0.00	0.01	2.77E-04
165	187.5	120	149.625	11095		1776.0		53.80			0.21		0.26		0.00		0.00	3	0.680	0.629	10.26				0.01	0.01	0.00E+00
170	192.5	120	149.625	17084		216.7		76.35			0.21		0.28		0.00		0.00	3	0.680	0.513	10.26				0.01	0.01	0.00E+00
175	197.5	120	149.625	8683		160.1		84.94			0.22		0.19		0.00		0.00	3	0.680	0.396	10.26				0.01	0.01	0.00E+00
180	202.5	120	149.625	13733		510.1		72.37			0.13		0.26		0.00		0.00	3	0.680	0.280	10.26				0.00	0.01	0.00E+00
185	207.5	120	149.625	13002		318.8		57.09			0.04		0.34		0.01		0.00	3	0.680	0.163	10.26				0.00	0.01	2.77E-04
188	210.5	120	149.625	10449		74.0		66.23			-0.04		0.31		0.01		0.00	3	0.680	0.093	10.26				0.00	0.01	2.77E-04
151	173.5	105	130.875	2270		396.8		86.67			0.01		0.22		0.01		0.01	3	0.595	0.956	8.98				0.00	0.01	2.77E-04
155	177.5	105	130.875	6586		812.9		80.55			0.06		0.22		0.01		0.00	3	0.595	0.862	8.98				0.00	0.01	2.77E-04
160	182.5	105	130.875	11379		1650.5		79.05			0.15		0.20		0.00		0.00	3	0.595	0.746	8.98				0.00	0.01	0.00E+00
165	187.5	105	130.875	4261		543.6		82.34			0.19		0.21		0.01		0.00	3	0.595	0.629	8.98				0.01	0.01	2.77E-04
170	192.5	105	130.875	22148		599.8		80.91			0.18		0.22		0.00		0.00	3	0.595	0.513	8.98				0.00	0.01	0.00E+00
175	197.5	105	130.875	11237		1455.7		50.05			0.12		0.28		0.01		0.00	3	0.595	0.396	8.98				0.00	0.01	2.77E-04
180	202.5	105	130.875	13520		246.6		62.66			0.07		0.32		0.01		0.00	3	0.595	0.280	8.98				0.00	0.01	2.77E-04
185	207.5	105	130.875	4850		87.5		58.01			-0.21		0.37		0.01		0.01	3	0.595	0.163	8.98				-0.01	0.01	2.77E-04
188	210.5	105	130.875	8019		120.2		65.98			-0.11		0.33		0.01		0.01	3	0.595	0.093	8.98				0.00	0.01	2.77E-04
151	173.5	100	124.625	17702		538.1		62.97			0.04		0.26		0.00		0.00	3	0.566	0.956	8.55				0.00	0.01	0.00E+00
155	177.5	100	124.625	21901		493.1		67.58			0.09		0.25		0.00		0.00	3	0.566	0.862	8.55				0.00	0.01	0.00E+00
160	182.5	100	124.625	19646		767.2		67.07			0.14		0.22		0.00		0.00	3	0.566	0.746	8.55				0.00	0.01	0.00E+00
165	187.5	100	124.625	6023		344.1		41.52			0.16		0.26		0.01		0.00	3	0.566	0.629	8.55				0.00	0.01	2.77E-04
170	192.5	100	124.625	8737		917.6		80.87			0.14		0.20		0.00		0.00	3	0.566	0.513	8.55				0.00	0.01	0.00E+00
175	197.5	100	124.625	7550		999.4		73.87			0.12		0.21		0.00		0.00	3	0.566	0.396	8.55				0.00	0.01	0.00E+00
180	202.5	100	124.625	13275		441.9		57.15			-0.04		0.36		0.01		0.00	3	0.566	0.280	8.55				0.00	0.01	2.77E-04
185	207.5	100	124.625	2926		67.1		73.18			-0.14		0.28		0.01		0.01	3	0.566	0.163	8.55				0.00	0.01	2.77E-04
188	210.5	100	124.625	1860		16.1		72.22			-0.48		0.36		0.02		0.01	3	0.566	0.093	8.55				-0.01	0.01	5.54E-04
101	123.5	163	203.375	8945		1173.1		48.89			-0.23		0.52		0.01		0.01	4	0.924	0.935	13.95				-0.01	0.01	2.77E-04
104.5	127	163	203.375	6738		673.4		50.01			-0.10		0.49		0.01		0.01	4	0.924	0.853	13.95				0.00	0.01	2.77E-04
109.5	132	163	203.375	10179		623.7		51.93			-0.11		0.51		0.01		0.01	4	0.924	0.737	13.95				0.00	0.01	2.77E-04
114.5	137	163	203.375	7300		448.5		66.07			0.06		0.43		0.01		0.01	4	0.924	0.620	13.95				0.00	0.01	2.77E-04
119.5	142	163	203.375	10745		1014.0		53.59			0.18		0.47		0.01		0.01	4	0.924	0.503	13.95				0.00	0.01	2.77E-04
124.5	147	163	203.375	3193		253.7		35.82			0.16		0.46		0.02		0.01	4	0.924	0.387	13.95				0.00	0.01	5.54E-04
129.5	152	163	203.375	3533		134.8		29.00			0.21		0.49		0.02		0.01	4	0.924	0.270	13.95				0.01	0.01	5.54E-04
134.5	157	163	203.375	2281		87.2		28.25			0.16		0.48		0.02		0.01	4	0.924	0.154	13.95				0.00	0.01	5.54E-04
138	160.5	163	203.375	13663		792.4		44.06			0.08		0.44		0.01		0.01	4	0.924	0.072	13.95				0.00	0.01	2.77E-04
101	123.5	135	168.375	13764		845.83		66			-0.03		0.41		0.01		0	4	0.765	0.935	11.55				0.00	0.01	2.77E-04
104.5	127	135	168.375	15984		368.28		80.09			0.05		0.33		0.01		0	4	0.765	0.853	11.55				0.00	0.01	2.77E-04
109.5	132	135	168.375	22118		448.79		77.49			0.07		0.34		0		0	4	0.765	0.737	11.55				0.00	0.01	0.00E+00
114.5	137	135	168.375	17727		832.94		61.16			0.11		0.37		0.01		0	4	0.765	0.620	11.55				0.00	0.01	2.77E-04
119.5	142	135	168.375	4790		672.14		34.74			0.16		0.39		0.01		0.01	4	0.765	0.503	11.55				0.00	0.01	2.77E-04
124.5	147	135	168.375	9540		1169.45		43.86			0.16		0.35		0.01		0	4	0.765	0.387	11.55				0.00	0.01	2.77E-04
129.5	152	135	168.375	9749		604.87		41.29			0.18		0.34		0.01		0	4	0.765	0.270	11.55				0.00	0.01	2.77E-04
134.5	157	135	168.375	11430		789.26		42.56			0.19		0.34		0.01		0	4	0.765	0.154	11.55				0.01	0.01	2.77E-04
138	160.5	135	168.375	11370		509.38		76.65			0.2		0.3		0.01		0	4	0.765	0.072	11.55				0.01	0.01	2.77E-04
101	123.5	100	124.625	16919		2306.43		74.54			-0.03		0.31		0		0	4	0.566	0.935	8.55				0.00	0.01	0.00E+00
104.5	127	100	124.625	11850		252.06		92.11			-0.02		0.26		0		0	4	0.566	0.853	8.55				0.00	0.01	0.00E+00
109.5	132	100	124.625	5828		52.16		91.46			0.07		0.23		0.01		0	4	0.566	0.737	8.55				0.00	0.01	2.77E-04
114.5	137	100	124.625	13175		393.73		81.64			0.12		0.27		0		0	4	0.566	0.620	8.55				0.00	0.01	0.00E+00
119.5	142	100	124.625	12084		1606.01		54.81			0.16		0.3		0.01		0	4	0.566	0.503	8.55				0.00	0.01	2.77E-04
124.5	147	100	124.625	11326		515.75		61.92			0.14		0.29		0.01		0	4	0.566	0.387	8.55				0.00	0.01	2.77E-04
129.5	152	100	124.625	11784		995.39		52.48			0.15		0.28		0.01		0	4	0.566	0.270	8.55				0.00	0.01	2.77E-04
134.5	157	100	124.625	19268		1409.65		66.17			0.14		0.27		0		0	4	0.566	0.154	8.55				0.00	0.01	0.00E+00
138	160.5	100	124.625	295		2.51		95.9			0.14		0.2		0.02		0.02	4	0.566	0.072	8.55				0.00	0.01	5.54E-04

LDA measurement		**LDA code:**	110	**rpm:**	3143.4	**Perfd by:**	NM	Printed: 27/09/2008	Page 1/2
Build:	3	**ReΦ:**	1.93E+06	**Date:**	28/09/2004	**LDA1:**	Vr	**Comments:**	Probe angular error corrected -1.389deg
LDA test # :	B3run39-1	**Rez:**	5.31E+04	**raw LDA file:**	\MCRLDA\Build3\B3run39-1.lda	**LDA2:**	VΦ	**Traverse ref:**	
Heat Transfer run:	B3run39-1	**Ro:**	0.53	**LDA list file:**	\MCRLDA\Build3\B3run39-1.xls	**W (m/s):**	12.13	**CAVITY 3**	

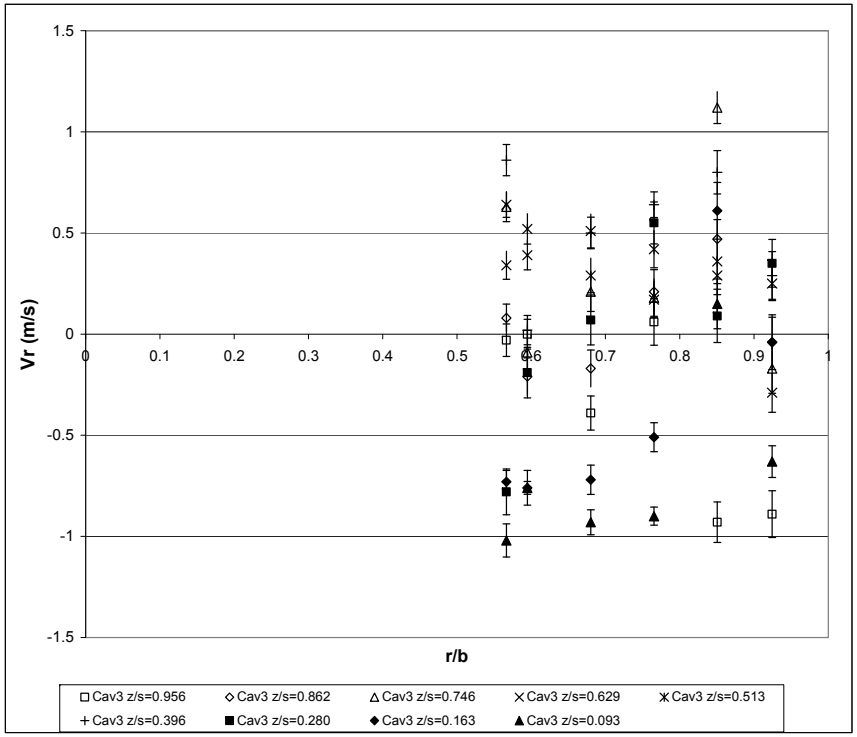

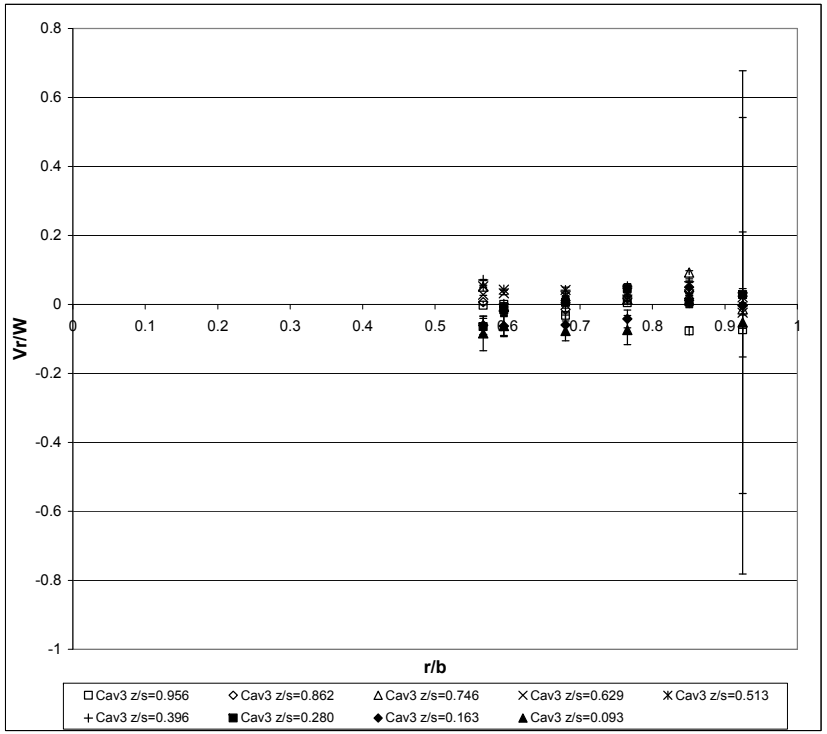

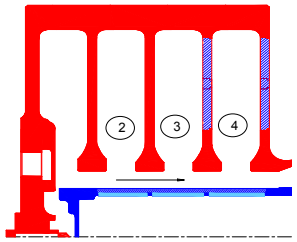

LDA measurement		LDA code:	110	rpm:	3143.4	Perfd by:	NM	Printed: 27/09/2008	Page 1/2
Build:	3	**ReΦ:**	1.93E+06	**Date:**	28/09/2004	**LDA1:**	Vr	**Comments:**	Probe angular error corrected -1.389deg
LDA test # :	B3run39-1	**Rez:**	5.31E+04	**raw LDA file:**	\MCRLDA\Build3\B3run39-1.lda	**LDA2:**	VΦ	**Traverse ref:**	
Heat Transfer run:	B3run39-1	**Ro:**	0.53	**LDA list file:**	\MCRLDA\Build3\B3run39-1.xls	**W (m/s):**	12.13	**CAVITY 4**	

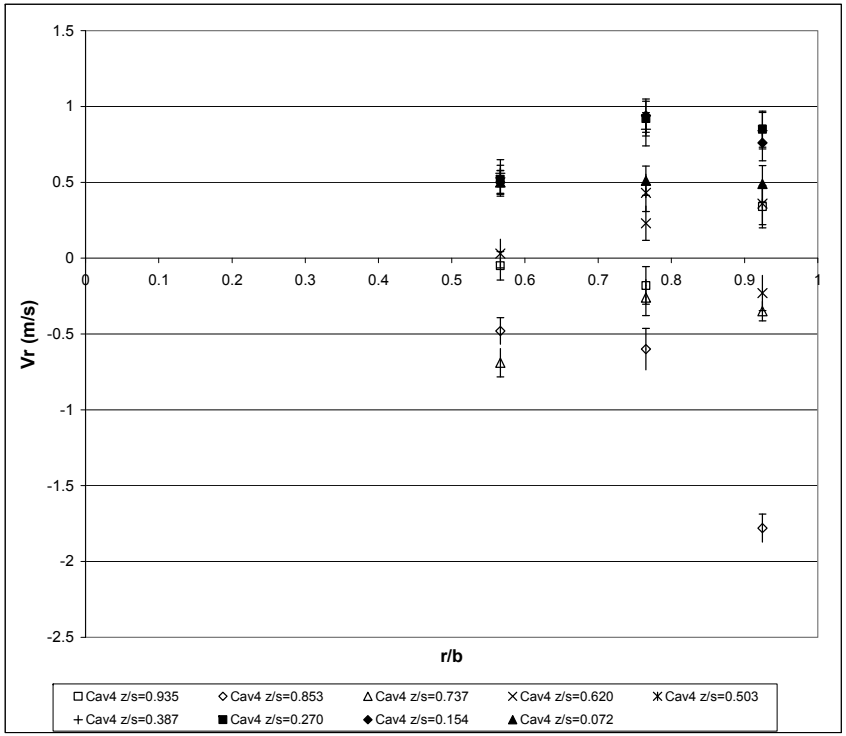

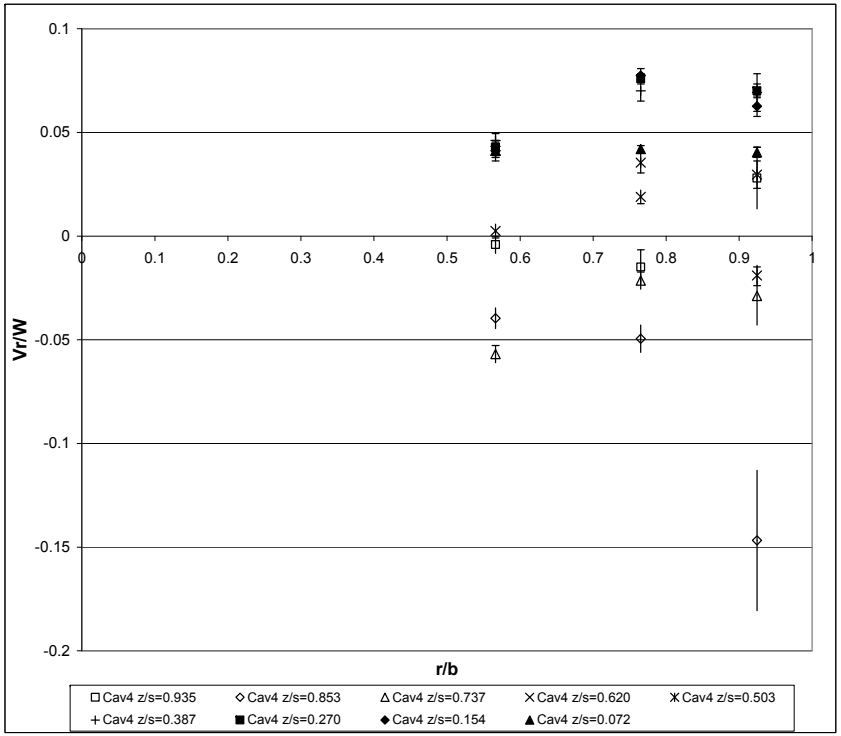

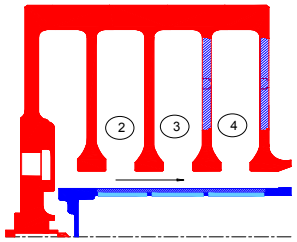

LDA measurement | LDA code: 110 | rpm: 3143.4 | Perfd by: NM | Printed: 27/09/2008 | Page 2/2

Build: 3 | **ReΦ:** 1.93E+06 | **Date:** 28/09/2004 | **LDA1:** Vr | **Comments:** Probe angular error corrected -1.389deg

LDA test # : B3run39-1 | **Rez:** 5.31E+04 | raw LDA file: \MCRLDA\Build3\B3run39-1.lda | **LDA2:** VΦ | Traverse corresp: 0

Heat Transfer run: B3run39-1 | **Ro:** 0.53 | LDA list file: \MCRLDA\Build3\B3run39-1.xls | **W (m/s):** 12.13

X [mm]	correcte d X	Y [mm]	corrected Y / Radius (mm)	Count{1}	Count{2}	Data Rate{1} [#/s]	Data Rate{2} [#/s]	Validatio n{1} [%]	Validation {2} [%]	LDA1 Mean [m/s]	LDA2 Mean [m/s]	LDA1 RMS [m/s]	LDA2 RMS [m/s]	LDA1 MeanConf [m/s]	LDA2 MeanCon f [m/s]	LDA1 RMSConf [m/s]	LDA2 RMSConf [m/s]	Cavity	r/b	z/s	Ωr (m/s)	$V_\theta/\Omega r$	$V_{\theta rRMS}/\Omega r$	$V_{\theta U95\%}/\Omega r$	$V_{zRMS}/\Omega r$	Vz/W	$Vz_{(RMS)}/W$	$Vz_{U95\%}/W$
151	173.5	163	203.375	2610		48.2		16.57		-0.89	1.40	0.05	0.04					3	0.924	0.956	66.95					-0.07	0.12	4.12E-03
155	177.5	163	203.375	3991		40.0		19.42		-0.04	1.50	0.05	0.03					3	0.924	0.862	66.95					0.00	0.12	0.00E+00
160	182.5	163	203.375	1273		55.2		19.07		-0.17	1.48	0.08	0.06					3	0.924	0.746	66.95					-0.01	0.12	0.00E+00
165	187.5	163	203.375	1466		160.7		27.42		-0.29	1.17	0.06	0.04					3	0.924	0.629	66.95					-0.02	0.10	0.00E+00
170	192.5	163	203.375	3898		50.3		36.56		0.25	1.02	0.03	0.02					3	0.924	0.513	66.95					0.02	0.08	0.00E+00
175	197.5	163	203.375	197		1.1		23.51		0.29	1.43	0.20	0.14					3	0.924	0.396	66.95					0.02	0.12	0.00E+00
180	202.5	163	203.375	101		0.6		16.61		0.35	1.43	0.28	0.20					3	0.924	0.280	66.95					0.03	0.12	0.00E+00
185	207.5	163	203.375	41		0.2		15.46		-0.04	1.64	0.51	0.36					3	0.924	0.163	66.95					0.00	0.14	0.00E+00
188	210.5	163	203.375	31		0.2		64.21		-0.63	0.95	0.34	0.24					3	0.924	0.093	66.95					-0.05	0.08	0.00E+00
151	173.5	150	187.125	1249		122.5		28.69		-0.93	1.22	0.07	0.05					3	0.851	0.956	61.60					-0.08	0.10	0.00E+00
155	177.5	150	187.125	2125		93.6		86.03		0.47	1.17	0.05	0.04					3	0.851	0.862	61.60					0.04	0.10	0.00E+00
160	182.5	150	187.125	2120		241.8		68.76		1.12	0.96	0.04	0.03					3	0.851	0.746	61.60					0.09	0.08	0.00E+00
165	187.5	150	187.125	932		397.7		77.17		0.29	1.15	0.07	0.05					3	0.851	0.629	61.60					0.02	0.09	0.00E+00
170	192.5	150	187.125	6479		190.3		79.33		0.36	1.33	0.03	0.02					3	0.851	0.513	61.60					0.03	0.11	0.00E+00
175	197.5	150	187.125	9758		195.8		46.96		0.80	1.30	0.03	0.02					3	0.851	0.396	61.60					0.07	0.11	0.00E+00
180	202.5	150	187.125	9426		156.6		51.13		0.09	1.60	0.03	0.02					3	0.851	0.280	61.60					0.01	0.13	0.00E+00
185	207.5	150	187.125	4093		294.0		78.98		0.61	1.70	0.05	0.04					3	0.851	0.163	61.60					0.05	0.14	0.00E+00
188	210.5	150	187.125	4854		75.9		53.70		0.15	1.49	0.04	0.03					3	0.851	0.093	61.60					0.01	0.12	0.00E+00
151	173.5	135	168.375	4838		1204.0		60.39		0.06	1.39	0.04	0.03					3	0.765	0.956	55.43					0.00	0.11	0.00E+00
155	177.5	135	168.375	6017		802.4		69.23		0.21	1.32	0.03	0.02					3	0.765	0.862	55.43					0.02	0.11	0.00E+00
160	182.5	135	168.375	2623		325.2		53.08		0.18	1.11	0.04	0.03					3	0.765	0.746	55.43					0.01	0.09	0.00E+00
165	187.5	135	168.375	1755		713.0		36.60		0.17	1.08	0.05	0.04					3	0.765	0.629	55.43					0.01	0.09	0.00E+00
170	192.5	135	168.375	1329		254.9		45.86		0.42	1.12	0.06	0.04					3	0.765	0.513	55.43					0.03	0.09	0.00E+00
175	197.5	135	168.375	4264		193.2		72.33		0.64	0.77	0.02	0.02					3	0.765	0.396	55.43					0.05	0.06	0.00E+00
180	202.5	135	168.375	6962		104.6		53.65		0.55	1.26	0.03	0.02					3	0.765	0.280	55.43					0.05	0.10	0.00E+00
185	207.5	135	168.375	3423		103.6		74.07		-0.51	0.87	0.03	0.02					3	0.765	0.163	55.43					-0.04	0.07	0.00E+00
188	210.5	135	168.375	1700		21.1		87.98		-0.90	0.54	0.03	0.02					3	0.765	0.093	55.43					-0.07	0.04	0.00E+00
151	173.5	120	149.625	2772		261.3		52.85		-0.39	1.02	0.04	0.03					3	0.680	0.956	49.25					-0.03	0.08	0.00E+00
155	177.5	120	149.625	7963		88.7		49.99		-0.17	1.10	0.02	0.02					3	0.680	0.862	49.25					-0.01	0.09	0.00E+00
160	182.5	120	149.625	12403		137.6		43.01		0.21	1.18	0.02	0.01					3	0.680	0.746	49.25					0.02	0.10	0.00E+00
165	187.5	120	149.625	1068		246.7		58.73		0.51	1.01	0.06	0.04					3	0.680	0.629	49.25					0.04	0.08	0.00E+00
170	192.5	120	149.625	12185		174.4		60.27		0.29	1.03	0.02	0.01					3	0.680	0.513	49.25					0.02	0.08	0.00E+00
175	197.5	120	149.625	2040		346.4		52.32		0.50	0.95	0.04	0.03					3	0.680	0.396	49.25					0.04	0.08	0.00E+00
180	202.5	120	149.625	6747		114.1		50.48		0.07	1.50	0.04	0.03					3	0.680	0.280	49.25					0.01	0.12	0.00E+00
185	207.5	120	149.625	2748		28.6		70.17		-0.72	0.88	0.03	0.02					3	0.680	0.163	49.25					-0.06	0.07	0.00E+00
188	210.5	120	149.625	1006		21.3		78.01		-0.93	0.75	0.05	0.03					3	0.680	0.093	49.25					-0.08	0.06	0.00E+00
151	173.5	105	130.875	2999		160.8		60.66		0.00	0.89	0.03	0.02					3	0.595	0.956	43.08					0.00	0.07	0.00E+00
155	177.5	105	130.875	4074		520.8		49.47		-0.21	1.13	0.03	0.02					3	0.595	0.862	43.08					-0.02	0.09	0.00E+00
160	182.5	105	130.875	3466		606.2		54.89		-0.09	1.04	0.03	0.02					3	0.595	0.746	43.08					-0.01	0.09	0.00E+00
165	187.5	105	130.875	1800		347.8		56.94		0.39	0.88	0.04	0.03					3	0.595	0.629	43.08					0.03	0.07	0.00E+00
170	192.5	105	130.875	8885		90.1		82.33		0.52	0.91	0.02	0.01					3	0.595	0.513	43.08					0.04	0.08	0.00E+00
175	197.5	105	130.875	10757		223.8		76.00		0.02	0.88	0.02	0.01					3	0.595	0.396	43.08					0.00	0.07	0.00E+00
180	202.5	105	130.875	3906		193.2		52.91		-0.19	1.52	0.05	0.03					3	0.595	0.280	43.08					-0.02	0.13	0.00E+00
185	207.5	105	130.875	3461		21.7		86.47		-0.76	1.04	0.03	0.02					3	0.595	0.163	43.08					-0.06	0.09	0.00E+00
188	210.5	105	130.875	1818		29.0		89.99		-0.76	0.38	0.02	0.01					3	0.595	0.093	43.08					-0.06	0.03	0.00E+00
151	173.5	100	124.625	9888		546.2		42.92		-0.03	0.97	0.02	0.01					3	0.566	0.956	41.02					0.00	0.08	0.00E+00
155	177.5	100	124.625	12227		349.8		54.41		0.08	0.83	0.01	0.01					3	0.566	0.862	41.02					0.01	0.07	0.00E+00
160	182.5	100	124.625	9715		1082.7		56.81		0.63	0.90	0.02	0.01					3	0.566	0.746	41.02					0.05	0.07	0.00E+00
165	187.5	100	124.625	6751		778.4		53.46		0.34	0.84	0.02	0.01					3	0.566	0.629	41.02					0.03	0.07	0.00E+00
170	192.5	100	124.625	2909		578.1		66.97		0.64	0.76	0.03	0.02					3	0.566	0.513	41.02					0.05	0.06	0.00E+00
175	197.5	100	124.625	13456		144.3		81.65		0.86	0.94	0.02	0.01					3	0.566	0.396	41.02					0.07	0.08	0.00E+00
180	202.5	100	124.625	7271		52.2		56.70		-0.78	1.37	0.03	0.02					3	0.566	0.280	41.02					-0.06	0.11	0.00E+00
185	207.5	100	124.625	1820		61.4		74.90		-0.73	0.68	0.03	0.02					3	0.566	0.163	41.02					-0.06	0.06	0.00E+00
188	210.5	100	124.625	813		6.8		80.52		-1.02	0.99	0.07	0.05					3	0.566	0.093	41.02					-0.08	0.08	0.00E+00
101	123.5	163	203.375	1915		16.0		68.31		0.34	1.69	0.08	0.05					4	0.924	0.935	66.95					0.03	0.14	0.00E+00
104.5	127	163	203.375	156		1.3		74.52		-1.78	1.12	0.18	0.12					4	0.924	0.853	66.95					-0.15	0.09	0.00E+00
109.5	132	163	203.375	142		1.2		76.83		-0.35	0.78	0.13	0.09					4	0.924	0.737	66.95					-0.03	0.06	0.00E+00
114.5	137	163	203.375	9039		75.3		75.14		-0.23	1.40	0.03	0.02					4	0.924	0.620	66.95					-0.02	0.12	0.00E+00
119.5	142	163	203.375	9253		254.9		72.93		0.36	1.69	0.03	0.02					4	0.924	0.503	66.95					0.03	0.14	0.00E+00
124.5	147	163	203.375	5781		1473.8		66.40		0.84	1.46	0.04	0.03					4	0.924	0.387	66.95					0.07	0.12	0.00E+00
129.5	152	163	203.375	7777		1481.1		58.86		0.85	1.44	0.03	0.02					4	0.924	0.270	66.95					0.07	0.12	0.00E+00
134.5	157	163	203.375	4777		968.0		71.39		0.76	1.43	0.04	0.03					4	0.924	0.154	66.95					0.06	0.12	0.00E+00
138	160.5	163	203.375	14771		237.7		67.54		0.49	1.45	0.02	0.02					4	0.924	0.072	66.95					0.04	0.12	0.00E+00
101	123.5	135	168.375	3443		1333.23		59.99		-0.18	1.5	0.05	0.04					4	0.765	0.935	55.43					-0.01	0.12	0.00E+00
104.5	127	135	168.375	5433		1007.85		62.71		-0.6	1.66	0.04	0.03					4	0.765	0.853	55.43					-0.05	0.14	0.00E+00
109.5	132	135	168.375	10055		843.62		63.95		-0.26	1.44	0.03	0.02					4	0.765	0.737	55.43					-0.02	0.12	0.00E+00
114.5	137	135	168.375	11502		1286.72		61.71		0.23	1.37	0.02	0.02					4	0.765	0.620	55.43					0.02	0.11	0.00E+00
119.5	142	135	168.375	5097		2078.68		60.21		0.43	1.49	0.04	0.03					4	0.765	0.503	55.43					0.04	0.12	0.00E+00
124.5	147	135	168.375	4299		2188.12		54.56		0.85	1.33	0.04	0.03					4	0.765	0.387	55.43					0.07	0.11	0.00E+00
129.5	152	135	168.375	6959		2220.92		52.77		0.92	1.38	0.03	0.02					4	0.765	0.270	55.43					0.08	0.11	0.00E+00
134.5	157	135	168.375	5198		1592.69		57.6		0.94	1.33	0.04	0.03					4	0.765	0.154	55.43					0.08	0.11	0.00E+00
138	160.5	135	168.375	12358		282.9		58.6		0.51	1.17	0.02	0.01					4	0.765	0.072	55.43					0.04	0.10	0.00E+00
101	123.5	100	124.625	4565		1736.72		60.83		-0.05	1.14	0.03	0.02					4	0.566	0.935	41.02					0.00	0.09	0.00E+00
104.5	127	100	124.625	3057		1605.92		63		-0.48	1.06	0.04	0.03					4	0.566	0.853	41.02					-0.04	0.09	0.00E+00
109.5	132	100	124.625	6186		1380.5		62.33		-0.69	1.13	0.03	0.02					4	0.566	0.737	41.02					-0.06	0.09	0.00E+00
114.5	137	100	124.625	11689		1554.11		59.87		0.03	1.14	0.02	0.01					4	0.566	0.620	41.02					0.00	0.09	0.00E+00
119.5	142	100	124.625	2262		1060.1		71.82		0.5	1.11	0.05	0.03					4	0.566	0.503	41.02					0.04	0.09	0.00E+00
124.5	147	100	124.625	4581		2200.99		43.41		0.56	1.09	0.03	0.02					4	0.566	0.387	41.02					0.05	0.09	0.00E+00
129.5	152	100	124.625	4767		2217.95		43.12		0.52	1.12	0.03	0.02					4	0.566	0.270	41.02					0.04	0.09	0.00E+00
134.5	157	100	124.625	3267		768.81		65.71		0.5	0.96	0.03	0.02					4	0.566	0.154	41.02					0.04	0.08	0.00E+00
138	160.5	100	124.625	6533		2111.94		52.57		0.5	0.93	0.02	0.02					4	0.566	0.072	41.02					0.04	0.08	0.00E+00

LDA measurement		**LDA code:**	110	**rpm:**	608.8	**Perfd by:**	NM	Printed: 27/09/2008	Page 1/2
Build:	3	**ReΦ:**	3.88E+05	**Date:**	05/10/2004	**LDA1:**	Vr	**Comments:**	
LDA test # :	B3run40-1	**Rez:**	6.07E+04	**raw LDA file:**	\MCRLDA\Build3\B3run40-1.lda	**LDA2:**	VΦ	**Traverse ref:**	
Heat Transfer run:	B3run40-1	**Ro:**	2.98	**LDA list file:**	\MCRLDA\Build3\B3run40-1.xls	**W (m/s):**	13.31	**CAVITY 3**	

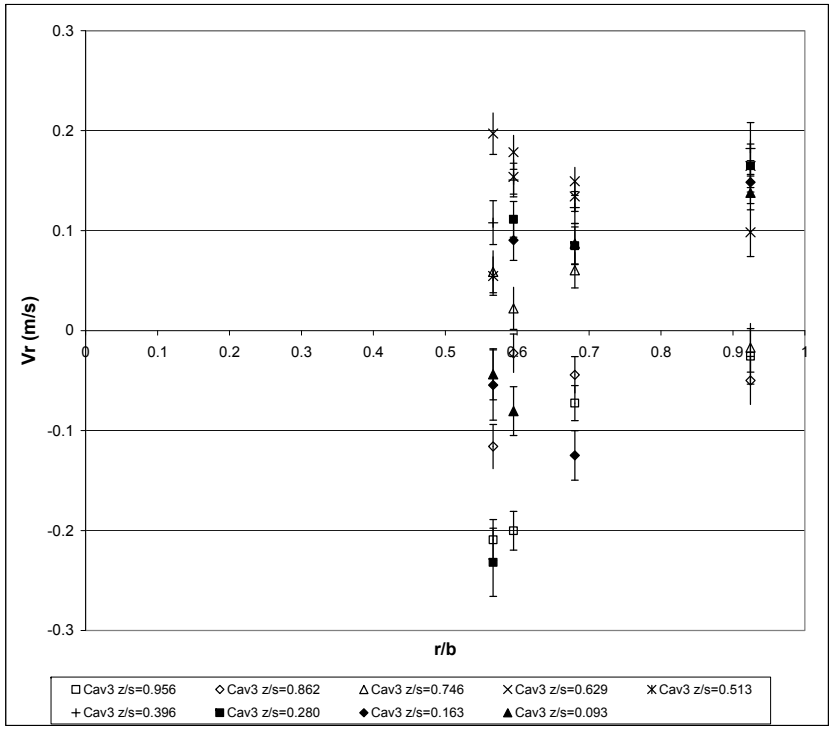

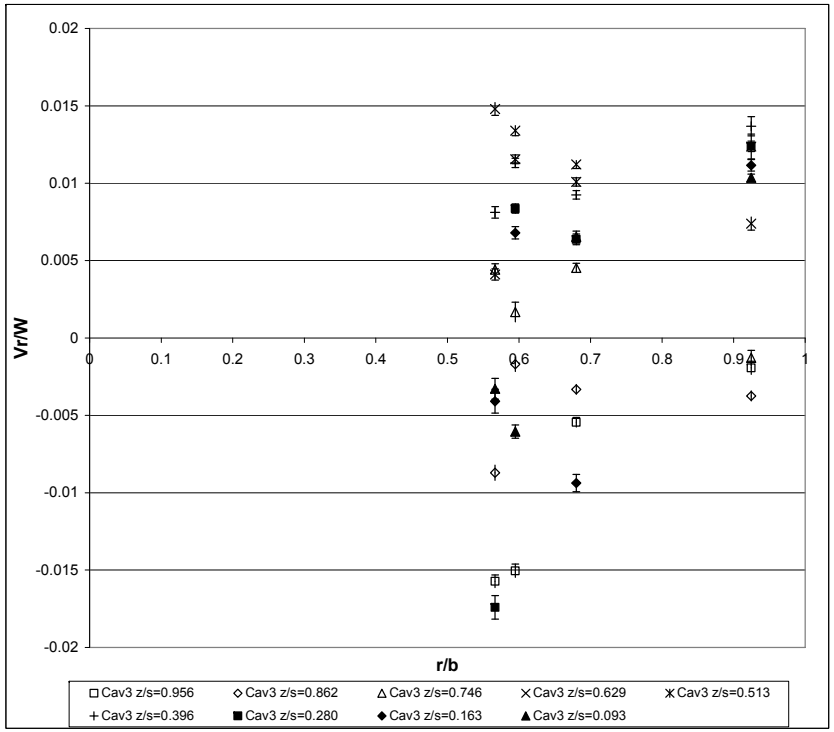

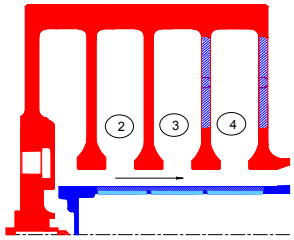

LDA measurement		LDA code:	110	rpm:	608.8	Perfd by:	NM	Printed: 27/09/2008	Page 1/2
Build:	3	**ReΦ:**	3.88E+05	**Date:**	05/10/2004	**LDA1:**	Vr	**Comments:**	
LDA test # :	B3run40-1	**Rez:**	6.07E+04	**raw LDA file:**	\MCRLDA\Build3\B3run40-1.lda	**LDA2:**	VΦ	**Traverse ref:**	
Heat Transfer run:	B3run40-1	**Ro:**	2.98	**LDA list file:**	\MCRLDA\Build3\B3run40-1.xls	**W (m/s):**	13.31	**CAVITY 4**	

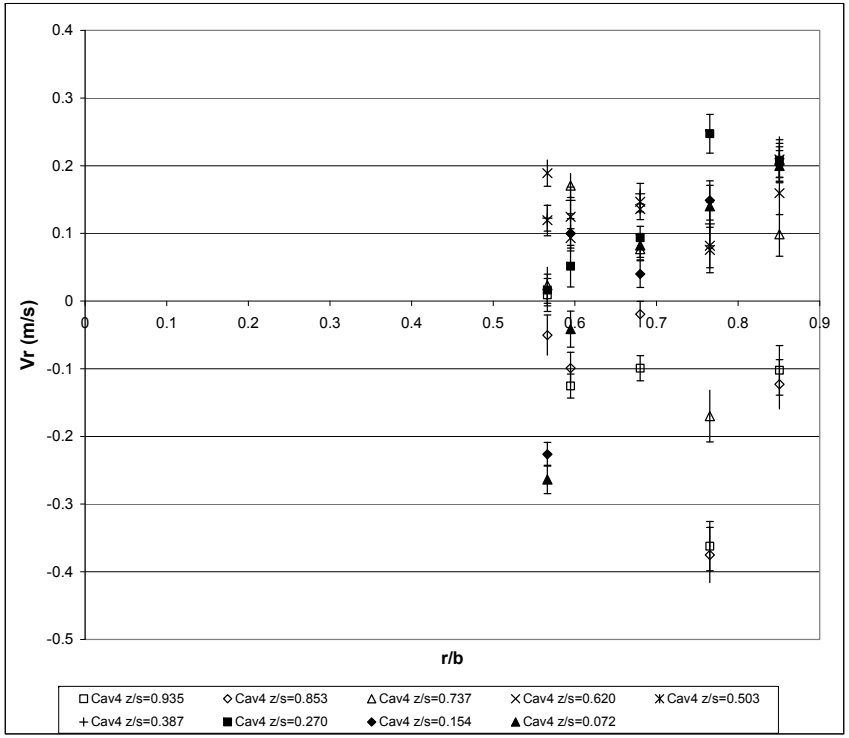

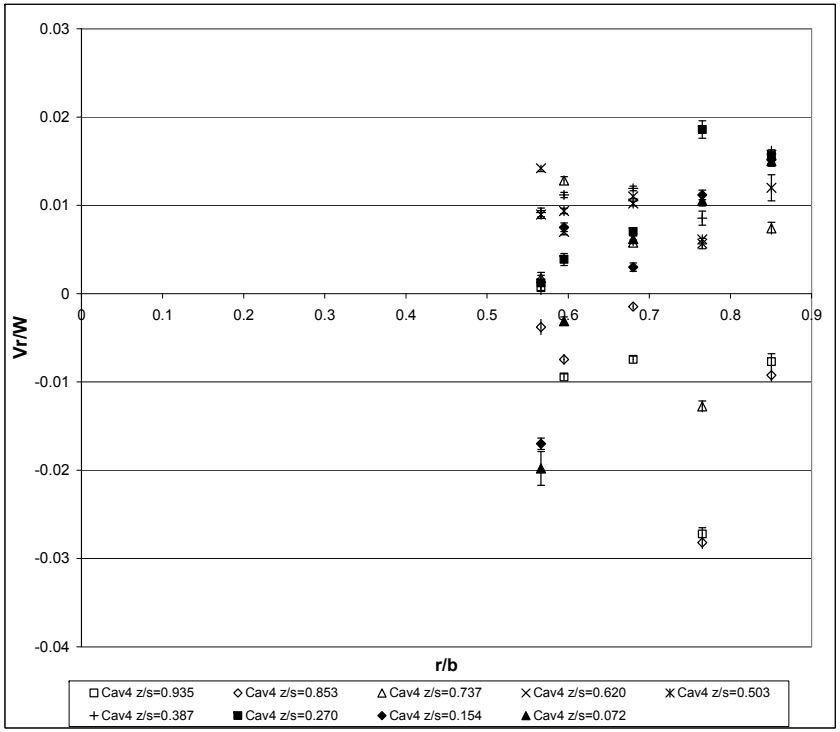

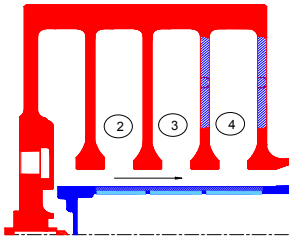

LDA measurement | LDA code: 110 | rpm: 608.8 | Perfd by: NM | Printed: 27/09/2008 | Page 2/2

Build: 3 | ReΦ: 3.88E+05 | Date: 05/10/2004 | LDA1: Vr | Comments: 0

LDA test # : B3run40-1 | Rez: 6.07E+04 | raw LDA file: \MCRLDA\Build3\B3run40-1.lda | LDA2: VΦ | Traverse corresp: 0

Heat Transfer run: B3run40-1 | Ro: 2.98 | LDA list file: \MCRLDA\Build3\B3run40-1.xls | W (m/s): 13.31

X [mm]	correcte d X	Y [mm]	corrected Y / Radius (mm)	Count{1}	Count{2}	Data Rate{1} [#/s]	Data Rate{2} [#/s]	Validatio n{1} [%]	Validation {2} [%]	LDA1 Mean [m/s]	LDA2 Mean [m/s]	LDA1 RMS [m/s]	LDA2 RMS [m/s]	LDA1 MeanConf [m/s]	LDA2 MeanCon f [m/s]	LDA1 RMSConf [m/s]	LDA2 RMSConf [m/s]	Cavity	r/b	z/s	Ωr (m/s)	$V_\Phi/\Omega r$	$V_{\Phi U95\%}/\Omega r$	$V_{\Phi RMS}/\Omega r$	Vz/W	Vz_{RMS}/W	$Vz_{U95\%}/W$
101	123.5	100	124.625	3783		15.8		41.78		0.01	0.32	0.01	0.01					4	0.566	0.935	7.95				0.00	0.02	7.74E-04
104.5	127	100	124.625	4566		19.0		43.68		-0.05	0.40	0.01	0.01					4	0.566	0.853	7.95				0.00	0.03	8.62E-04
109.5	132	100	124.625	6179		25.8		55.35		0.02	0.35	0.01	0.01					4	0.566	0.737	7.95				0.00	0.03	6.61E-04
114.5	137	100	124.625	11017		63.4		57.83		0.19	0.26	0.00	0.00					4	0.566	0.620	7.95				0.01	0.02	3.61E-04
119.5	142	100	124.625	10066		51.2		60.21		0.12	0.30	0.01	0.00					4	0.566	0.503	7.95				0.01	0.02	4.44E-04
124.5	147	100	124.625	5900		24.6		59.92		0.12	0.25	0.01	0.00					4	0.566	0.387	7.95				0.01	0.02	4.87E-04
129.5	152	100	124.625	2864		11.9		58.76		0.02	0.31	0.01	0.01					4	0.566	0.270	7.95				0.00	0.02	8.59E-04
134.5	157	100	124.625	2763		11.5		75.45		-0.23	0.23	0.01	0.01					4	0.566	0.154	7.95				-0.02	0.02	6.50E-04
138	160.5	100	124.625	459		1.9		60.53		-0.26	0.28	0.03	0.02					4	0.566	0.072	7.95				-0.02	0.02	1.91E-03
151	173.5	100	124.625	9702		40.4		59.23		-0.21	0.27	0.01	0.00					3	0.566	0.956	7.95				-0.02	0.02	4.06E-04
155	177.5	100	124.625	7645		31.9		44.79		-0.12	0.29	0.01	0.00					3	0.566	0.862	7.95				-0.01	0.02	4.96E-04
160	182.5	100	124.625	11330		77.0		56.00		0.06	0.28	0.01	0.00					3	0.566	0.746	7.95				0.00	0.02	3.86E-04
165	187.5	100	124.625	9931		96.2		64.77		0.20	0.28	0.01	0.00					3	0.566	0.629	7.95				0.01	0.02	4.09E-04
170	192.5	100	124.625	10871		87.5		65.05		0.05	0.26	0.00	0.00					3	0.566	0.513	7.95				0.00	0.02	3.62E-04
175	197.5	100	124.625	13277		82.2		57.12		0.11	0.29	0.00	0.00					3	0.566	0.396	7.95				0.01	0.02	3.73E-04
180	202.5	100	124.625	7703		46.5		36.94		-0.23	0.45	0.01	0.01					3	0.566	0.280	7.95				-0.02	0.03	7.61E-04
185	207.5	100	124.625	8009		97.8		42.99		-0.05	0.47	0.01	0.01					3	0.566	0.163	7.95				0.00	0.04	7.71E-04
188	210.5	100	124.625	5529		23.0		56.49		-0.04	0.34	0.01	0.01					3	0.566	0.093	7.95				0.00	0.03	6.74E-04
101	123.5	105	130.875	10499		53.8		64.79		-0.13	0.24	0.00	0.00					4	0.595	0.935	8.34				-0.01	0.02	3.40E-04
104.5	127	105	130.875	6710		28.0		66.00		-0.10	0.31	0.01	0.01					4	0.595	0.853	8.34				-0.01	0.02	5.58E-04
109.5	132	105	130.875	6862		28.6		73.29		0.17	0.24	0.01	0.00					4	0.595	0.737	8.34				0.01	0.02	4.20E-04
114.5	137	105	130.875	12111		95.1		60.85		0.09	0.26	0.00	0.00					4	0.595	0.620	8.34				0.01	0.02	3.44E-04
119.5	142	105	130.875	12338		85.5		64.48		0.12	0.23	0.00	0.00					4	0.595	0.503	8.34				0.01	0.02	3.10E-04
124.5	147	105	130.875	16426		110.9		75.39		0.15	0.26	0.00	0.00					4	0.595	0.387	8.34				0.01	0.02	3.03E-04
129.5	152	105	130.875	7822		43.8		44.88		0.05	0.41	0.01	0.01					4	0.595	0.270	8.34				0.00	0.03	6.81E-04
134.5	157	105	130.875	7610		33.3		51.41		0.10	0.29	0.01	0.00					4	0.595	0.154	8.34				0.01	0.02	4.89E-04
138	160.5	105	130.875	12200		113.4		40.35		-0.04	0.35	0.01	0.00					4	0.595	0.072	8.34				0.00	0.03	4.72E-04
151	173.5	105	130.875	7866		50.2		59.68		-0.20	0.26	0.01	0.00					3	0.595	0.956	8.34				-0.02	0.02	4.28E-04
155	177.5	105	130.875	6521		38.1		63.19		-0.02	0.26	0.01	0.00					3	0.595	0.862	8.34				0.00	0.02	4.67E-04
160	182.5	105	130.875	4202		17.5		70.87		0.02	0.28	0.01	0.01					3	0.595	0.746	8.34				0.00	0.02	6.37E-04
165	187.5	105	130.875	10343		146.2		62.83		0.18	0.23	0.00	0.00					3	0.595	0.629	8.34				0.01	0.02	3.26E-04
170	192.5	105	130.875	13821		146.9		66.32		0.15	0.23	0.00	0.00					3	0.595	0.513	8.34				0.01	0.02	2.87E-04
175	197.5	105	130.875	12120		80.2		70.95		0.15	0.22	0.00	0.00					3	0.595	0.396	8.34				0.01	0.02	2.99E-04
180	202.5	105	130.875	13579		68.8		62.83		0.11	0.24	0.00	0.00					3	0.595	0.280	8.34				0.01	0.02	3.02E-04
185	207.5	105	130.875	10061		72.0		59.19		0.09	0.27	0.01	0.00					3	0.595	0.163	8.34				0.01	0.02	3.95E-04
188	210.5	105	130.875	12500		208.1		36.98		-0.08	0.32	0.01	0.00					3	0.595	0.093	8.34				-0.01	0.02	4.27E-04
101	123.5	120	149.625	10257		147.0		51.08		-0.10	0.25	0.00	0.00					4	0.680	0.935	9.54				-0.01	0.02	3.60E-04
104.5	127	120	149.625	12461		173.0		54.17		-0.02	0.25	0.00	0.00					4	0.680	0.853	9.54				0.00	0.02	3.34E-04
109.5	132	120	149.625	10514		98.5		65.22		0.08	0.21	0.00	0.00					4	0.680	0.737	9.54				0.01	0.02	3.06E-04
114.5	137	120	149.625	11957		196.8		71.24		0.15	0.20	0.00	0.00					4	0.680	0.620	9.54				0.01	0.01	2.69E-04
119.5	142	120	149.625	14503		170.7		72.51		0.14	0.21	0.00	0.00					4	0.680	0.503	9.54				0.01	0.02	2.52E-04
124.5	147	120	149.625	14160		133.0		71.39		0.16	0.20	0.00	0.00					4	0.680	0.387	9.54				0.01	0.02	2.50E-04
129.5	152	120	149.625	12940		166.8		60.63		0.09	0.23	0.00	0.00					4	0.680	0.270	9.54				0.01	0.02	2.92E-04
134.5	157	120	149.625	6814		229.7		29.98		0.04	0.26	0.01	0.00					4	0.680	0.154	9.54				0.00	0.02	4.70E-04
138	160.5	120	149.625	10856		477.1		38.99		0.08	0.23	0.00	0.00					4	0.680	0.072	9.54				0.01	0.02	3.30E-04
151	173.5	120	149.625	12037		282.7		43.90		-0.07	0.23	0.00	0.00					3	0.680	0.956	9.54				-0.01	0.02	3.15E-04
155	177.5	120	149.625	12286		320.2		47.00		-0.04	0.24	0.00	0.00					3	0.680	0.862	9.54				0.00	0.02	3.23E-04
160	182.5	120	149.625	13281		181.5		56.82		0.06	0.24	0.00	0.00					3	0.680	0.746	9.54				0.00	0.02	3.00E-04
165	187.5	120	149.625	11538		140.6		74.98		0.15	0.19	0.00	0.00					3	0.680	0.629	9.54				0.01	0.01	2.55E-04
170	192.5	120	149.625	11901		110.9		74.53		0.13	0.20	0.00	0.00					3	0.680	0.513	9.54				0.01	0.02	2.70E-04
175	197.5	120	149.625	13243		148.2		72.46		0.12	0.21	0.00	0.00					3	0.680	0.396	9.54				0.01	0.02	2.73E-04
180	202.5	120	149.625	11412		262.5		48.82		0.08	0.25	0.00	0.00					3	0.680	0.280	9.54				0.01	0.02	3.47E-04
185	207.5	120	149.625	7539		159.1		28.78		-0.12	0.33	0.01	0.01					3	0.680	0.163	9.54				-0.01	0.02	5.59E-04
188	210.5	120	149.625	11782		375.7		39.21		0.09	0.27	0.00	0.00					3	0.680	0.093	9.54				0.01	0.02	3.65E-04
101	123.5	135	168.375	10208		192.1		86.82		-0.36	0.49	0.01	0.01					4	0.765	0.935	10.73				-0.03	0.04	7.07E-04
104.5	127	135	168.375	14857		708.3		68.72		-0.38	0.54	0.01	0.01					4	0.765	0.853	10.73				-0.03	0.04	6.56E-04
109.5	132	135	168.375	14995		356.7		75.39		-0.17	0.51	0.01	0.01					4	0.765	0.737	10.73				-0.01	0.04	6.13E-04
114.5	137	135	168.375	15526		489.0		81.55		0.08	0.43	0.01	0.00					4	0.765	0.620	10.73				0.01	0.03	5.13E-04
119.5	142	135	168.375	12289		706.0		74.04		0.08	0.45	0.01	0.01					4	0.765	0.503	10.73				0.01	0.03	5.96E-04
124.5	147	135	168.375	6356		139.8		64.09		0.11	0.43	0.01	0.01					4	0.765	0.387	10.73				0.01	0.03	7.97E-04
129.5	152	135	168.375	3273		272.7		53.81		0.25	0.38	0.01	0.01					4	0.765	0.270	10.73				0.02	0.03	9.83E-04
134.5	157	135	168.375	10985		678.6		75.99		0.15	0.39	0.01	0.01					4	0.765	0.154	10.73				0.01	0.03	5.41E-04
138	160.5	135	168.375	11003		640.4		68.61		0.14	0.41	0.01	0.01					4	0.765	0.072	10.73				0.01	0.03	5.70E-04
101	123.5	150	187.125	6373		816.722798		68.206		-0.10244	0.48756	0.01197	0.00847					4	0.851	0.935	11.93				-0.01	0.04	8.99E-04
104.5	127	150	187.125	11276		611.264161		68.825		-0.123	0.48373	0.00893	0.00631					4	0.851	0.853	11.93				-0.01	0.04	6.71E-04
109.5	132	150	187.125	9057		443.137818		59.42		0.09861	0.42836	0.00882	0.00624					4	0.851	0.737	11.93				0.01	0.03	6.63E-04
114.5	137	150	187.125	4677		353.401487		49.604		0.20936	0.44337	0.01271	0.00899					4	0.851	0.620	11.93				0.02	0.03	9.55E-04
119.5	142	150	187.125	1771		365.513689		42.532		0.15951	0.42294	0.0197	0.01393					4	0.851	0.503	11.93				0.01	0.03	1.48E-03
124.5	147	150	187.125	12370		1982.80094		69.092		0.21039	0.37334	0.00658	0.00465					4	0.851	0.387	11.93				0.02	0.03	4.94E-04
129.5	152	150	187.125	8167		649.763291		61.332		0.20793	0.33214	0.0072	0.00509					4	0.851	0.270	11.93				0.02	0.02	5.41E-04
134.5	157	150	187.125	5197		432.683301		53.692		0.20148	0.35307	0.0096	0.00679					4	0.851	0.154	11.93				0.02	0.03	7.21E-04
138	160.5	150	187.125	19727		1104.68374		78.665		0.19971	0.29982	0.00418	0.00296					4	0.851	0.072	11.93				0.02	0.02	3.14E-04
151	173.5	163	203.375	16538		1435.39577		77.035		-0.0257	0.36975	0.00564	0.00398					3	0.924	0.956	12.97				0.00	0.03	4.23E-04
155	177.5	163	203.375	20240		1101.46757		84.474		-0.04986	0.31952	0.0044	0.00311					3	0.924	0.862	12.97				0.00	0.02	3.31E-04
160	182.5	163	203.375	9664		659.599718		81.966		-0.01713	0.32349	0.00645	0.00456					3	0.924	0.746	12.97				0.00	0.02	4.85E-04
165	187.5	163	203.375	12731		876.514854		74.083		0.09837	0.32267	0.00561	0.00396					3	0.924	0.629	12.97				0.01	0.02	4.21E-04
170	192.5	163	203.375	4049		973.14803		53.398		0.16469	0.34671	0.01068	0.00755					3	0.924	0.513	12.97				0.01	0.03	8.02E-04
175	197.5	163	203.375	6740		375.513533		60.393		0.18218	0.34433	0.00822	0.00581					3	0.924	0.396	12.97				0.01	0.03	6.18E-04
180	202.5	163	203.375	15512		1311.59038		73.785		0.16486	0.289	0.00455	0.00322					3	0.924	0.280	12.97				0.01	0.02	3.42E-04
185	207.5	163	203.375	12659		959.855284		65.466		0.14849	0.28685	0.005	0.00353					3	0.924	0.163	12.97				0.01	0.02	3.75E-04
188	210.5	163	203.375	19211		711.376748		92.768		0.13783	0.22553	0.00319	0.00226					3	0.924	0.093	12.97				0.01	0.02	2.40E-04

LDA measurement		**LDA code:**	110	**rpm:**	2775.5	**Perfd by:**	NM	Printed: 27/09/2008	Page 1/2
Build:	3	**ReΦ:**	1.97E+06	**Date:**	20/12/2004	**LDA1:**	Vr	**Comments:** run OK	
LDA test # :	B3run44-1	**Rez:**	1.64E+05	**raw LDA file:**	\MCRLDA\Build3\B3run44-1.lda	**LDA2:**	VΦ	**Traverse ref:**	
Heat Transfer run:	B3run44-2	**Ro:**	1.59	**LDA list file:**	\MCRLDA\Build3\B3run44-1.xls	**W (m/s):**	32.31	**CAVITY 3**	

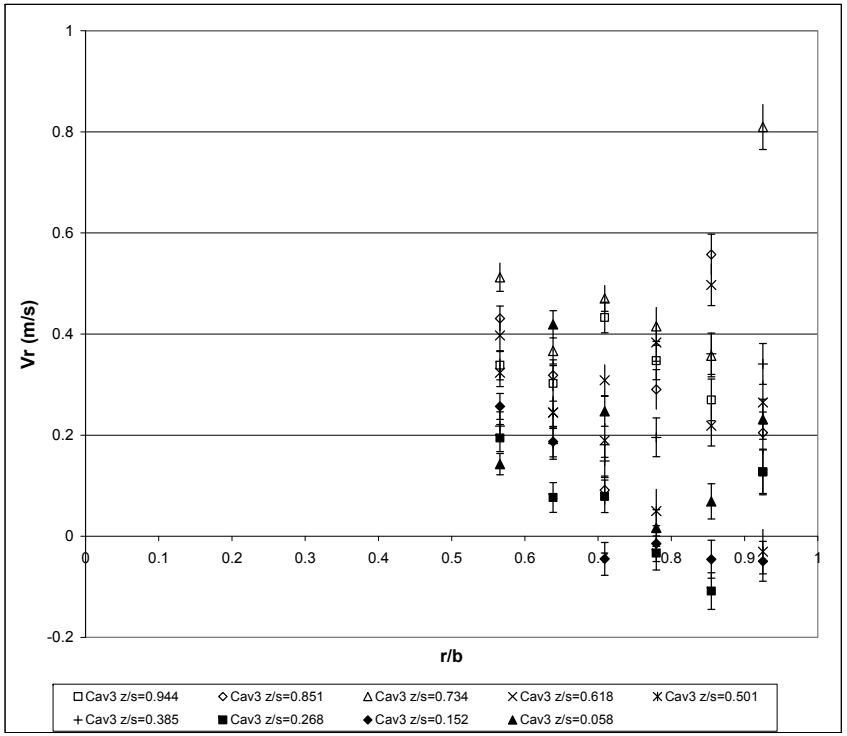

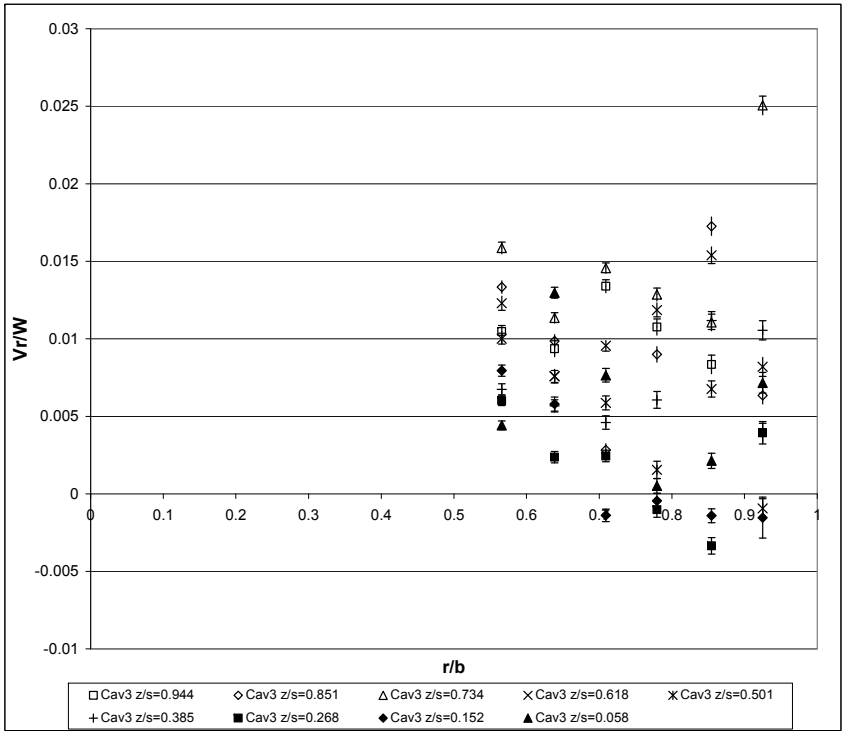

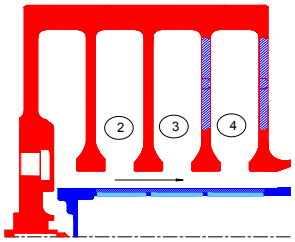

LDA measurement		**LDA code:**	110	**rpm:**	2775.5	**Perfd by:**	NM	Printed: 27/09/2008	Page 1/2
Build:	3	**ReΦ:**	1.97E+06	**Date:**	20/12/2004	**LDA1:**	Vr	**Comments:**	run OK
LDA test # :	B3run44-1	**Rez:**	1.64E+05	**raw LDA file:**	\MCRLDA\Build3\B3run44-1.lda	**LDA2:**	VΦ	**Traverse ref:**	
Heat Transfer run:	B3run44-2	**Ro:**	1.59	**LDA list file:**	\MCRLDA\Build3\B3run44-1.xls	**W (m/s):**	32.31	**CAVITY 4**	

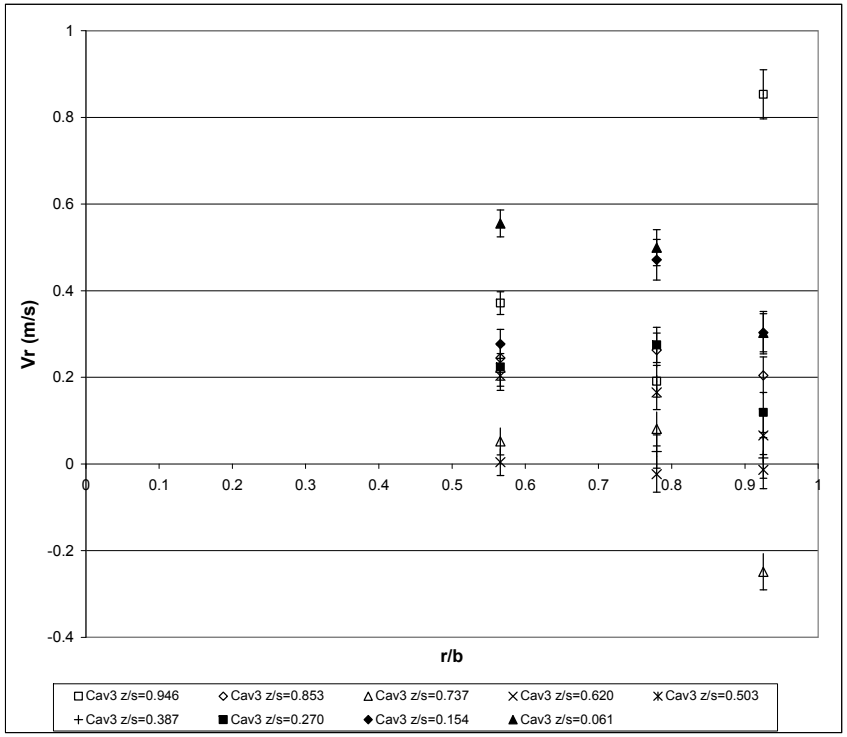

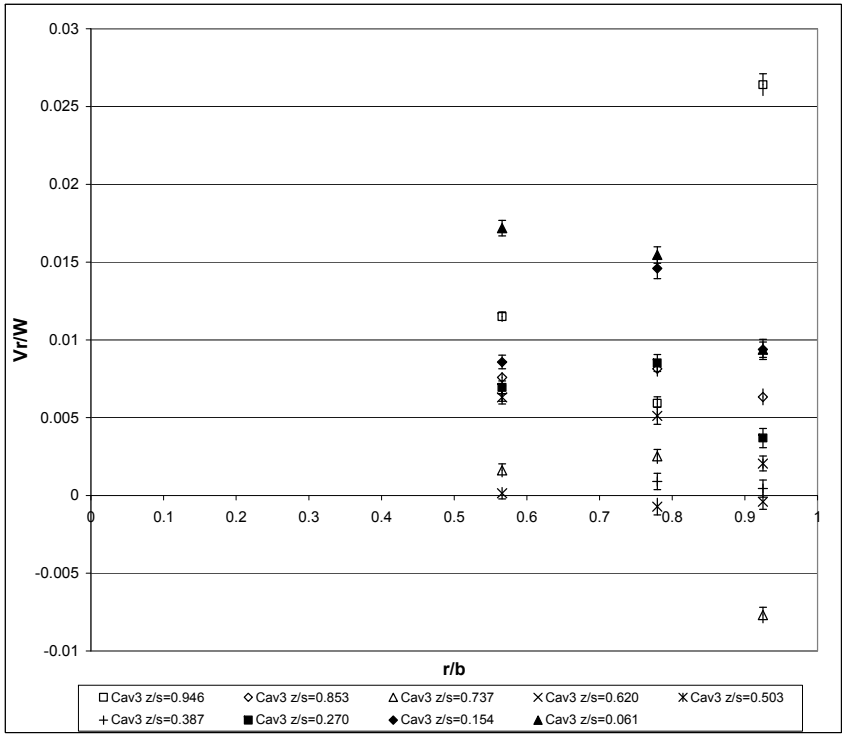

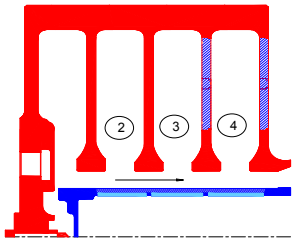

LDA measurement | LDA code: 110 | rpm: 2775.5 | Perfd by: NM | Printed: 27/09/2008 | Page 2/2

Build: 3 | ReΦ: 1.97E+06 | Date: 20/12/2004 | LDA1: Vr | Comments: run OK

LDA test # : B3run44-1 | Rez: 1.64E+05 | raw LDA file: \MCRLDA\Build3\B3run44-1.lda | LDA2: VΦ | Traverse corresp: 0

Heat Transfer run: B3run44-2 | Ro: 1.59 | LDA list file: \MCRLDA\Build3\B3run44-1.xls | W (m/s): 32.31

X [mm]	corrected X	Y [mm]	corrected Y / Radius (mm)	Count{1}	Count{2}	Data Rate{1} [#/s]	Data Rate{2} [#/s]	Validation n(1) [%]	Validation {2} [%]	LDA1 Mean [m/s]	LDA2 Mean [m/s]	LDA1 RMS [m/s]	LDA2 RMS [m/s]	LDA1 MeanConf [m/s]	LDA2 MeanConf [m/s]	LDA1 RMSConf [m/s]	LDA2 RMSConf [m/s]	Cavity	r/b	z/s	Ωr (m/s)	$V_\Phi/\Omega r$	$V_{\theta USSN}/\Omega r$	$V_{\theta RMS}/\Omega r$	Vz/W	Vz_{RMS}/W	Vz_{USSN}/W
174	203.5	20343	659.6	50.50	0.13	58.76	1.45	1.42	0.02	0.02	0.01	0.01	3	0.925	0.944	59.15	0.99	3.26E-04	0.02	0.00	0.05	6.10E-04
178	203.5	21796	661.8	52.11	0.20	58.08	1.32	1.43	0.02	0.02	0.01	0.01	3	0.925	0.851	59.15	0.98	3.22E-04	0.02	0.01	0.04	5.41E-04
183	203.5	20922	490.7	53.76	0.81	58.88	1.44	1.43	0.02	0.02	0.01	0.01	3	0.925	0.734	59.15	1.00	3.28E-04	0.02	0.03	0.04	6.02E-04
188	203.5	18447	541.6	56.56	0.26	58.51	1.37	1.46	0.02	0.02	0.01	0.01	3	0.925	0.618	59.15	0.99	3.56E-04	0.02	0.01	0.04	6.13E-04
193	203.5	18498	220.1	62.99	-0.03	58.06	1.42	1.72	0.02	0.02	0.01	0.02	3	0.925	0.501	59.15	0.98	4.20E-04	0.03	0.00	0.04	6.32E-04
198	203.5	16593	346.7	61.68	0.34	57.28	1.31	2.10	0.02	0.03	0.01	0.02	3	0.925	0.385	59.15	0.97	5.39E-04	0.04	0.01	0.04	6.15E-04
203	203.5	13717	829.5	51.17	0.13	58.04	1.39	1.63	0.02	0.03	0.02	0.02	3	0.925	0.268	59.15	0.98	4.62E-04	0.03	0.00	0.04	7.22E-04
208	203.5	3382	351.0	26.88	-0.05	59.01	1.27	1.30	0.04	0.04	0.03	0.03	3	0.925	0.152	59.15	1.00	7.39E-04	0.02	0.00	0.04	1.33E-03
212	203.5	13719	484.6	63.23	0.23	58.92	1.28	1.37	0.02	0.02	0.02	0.02	3	0.925	0.058	59.15	1.00	3.88E-04	0.02	0.01	0.04	6.64E-04
174	188	18013	900.2	55.73	0.27	54.05	1.33	1.30	0.02	0.02	0.01	0.01	3	0.855	0.944	54.64	0.99	3.48E-04	0.02	0.01	0.04	6.02E-04
178	188	17459	701.1	54.02	0.56	53.82	1.29	1.23	0.02	0.02	0.01	0.01	3	0.855	0.851	54.64	0.98	3.34E-04	0.02	0.02	0.04	5.94E-04
183	188	23184	925.3	56.26	0.36	54.10	1.35	1.43	0.02	0.02	0.01	0.01	3	0.855	0.734	54.64	0.99	3.36E-04	0.03	0.01	0.04	5.39E-04
188	188	21743	946.7	60.44	0.50	54.00	1.31	1.30	0.02	0.02	0.01	0.01	3	0.855	0.618	54.64	0.99	3.16E-04	0.02	0.02	0.04	5.41E-04
193	188	22954	744.4	62.71	0.22	53.65	1.29	1.52	0.02	0.02	0.01	0.01	3	0.855	0.501	54.64	0.98	3.60E-04	0.03	0.01	0.04	5.17E-04
198	188	19169	1576.6	63.61	0.36	52.88	1.32	2.06	0.02	0.03	0.01	0.02	3	0.855	0.385	54.64	0.97	5.33E-04	0.04	0.01	0.04	5.70E-04
203	188	17983	851.7	66.81	-0.11	54.25	1.17	1.50	0.02	0.02	0.01	0.02	3	0.855	0.268	54.64	0.99	4.02E-04	0.03	0.00	0.04	5.31E-04
208	188	26439	1297.2	74.20	-0.05	54.32	1.21	1.20	0.01	0.01	0.01	0.01	3	0.855	0.152	54.64	0.99	2.65E-04	0.02	0.00	0.04	4.51E-04
212	188	19033	670.5	75.20	0.07	54.03	1.12	1.30	0.02	0.02	0.01	0.01	3	0.855	0.058	54.64	0.99	3.38E-04	0.02	0.00	0.03	4.93E-04
174	171.5	20154	551.5	52.94	0.35	49.40	1.22	1.09	0.02	0.02	0.01	0.01	3	0.780	0.944	49.85	0.99	3.02E-04	0.02	0.01	0.04	5.21E-04
178	171.5	23055	810.5	55.52	0.29	48.96	1.26	1.26	0.02	0.02	0.01	0.01	3	0.780	0.851	49.85	0.98	3.27E-04	0.03	0.01	0.04	5.04E-04
183	171.5	29342	905.4	58.68	0.42	49.15	1.21	1.19	0.01	0.01	0.01	0.01	3	0.780	0.734	49.85	0.99	2.73E-04	0.02	0.01	0.04	4.27E-04
188	171.5	25735	616.4	58.73	0.38	49.29	1.19	1.16	0.01	0.01	0.01	0.01	3	0.780	0.618	49.85	0.99	2.85E-04	0.02	0.01	0.04	4.51E-04
193	171.5	22723	839.3	55.31	0.05	48.86	1.39	1.30	0.02	0.02	0.01	0.01	3	0.780	0.501	49.85	0.98	3.40E-04	0.03	0.00	0.04	5.57E-04
198	171.5	19260	1369.4	56.71	0.20	48.18	1.24	1.96	0.02	0.03	0.01	0.02	3	0.780	0.385	49.85	0.97	5.55E-04	0.04	0.01	0.04	5.42E-04
203	171.5	18618	1344.4	66.90	-0.03	49.36	1.09	1.34	0.02	0.02	0.01	0.01	3	0.780	0.268	49.85	0.99	3.87E-04	0.03	0.00	0.03	4.86E-04
208	171.5	21424	1631.7	66.32	-0.01	49.59	1.14	1.15	0.02	0.02	0.01	0.01	3	0.780	0.152	49.85	0.99	3.10E-04	0.02	0.00	0.04	4.74E-04
212	171.5	22492	1042.3	75.80	0.02	49.37	1.17	1.24	0.02	0.02	0.01	0.01	3	0.780	0.058	49.85	0.99	3.25E-04	0.02	0.00	0.04	4.75E-04
174	156	20233	571.4	63.75	0.43	44.96	0.98	1.03	0.01	0.01	0.01	0.01	3	0.709	0.944	45.34	0.99	3.14E-04	0.02	0.01	0.03	4.18E-04
178	156	17012	525.8	77.17	0.09	44.96	0.89	0.94	0.01	0.01	0.01	0.01	3	0.709	0.851	45.34	0.99	3.13E-04	0.02	0.00	0.03	4.15E-04
183	156	22604	345.9	85.63	0.47	44.67	0.83	0.97	0.01	0.01	0.01	0.01	3	0.709	0.734	45.34	0.99	2.78E-04	0.02	0.01	0.03	3.33E-04
188	156	31591	768.5	76.76	0.31	44.80	0.98	1.18	0.01	0.01	0.01	0.01	3	0.709	0.618	45.34	0.99	2.86E-04	0.03	0.01	0.03	3.36E-04
193	156	21173	683.1	65.77	0.19	44.58	1.09	1.50	0.01	0.02	0.01	0.01	3	0.709	0.501	45.34	0.98	4.44E-04	0.03	0.01	0.03	4.54E-04
198	156	21339	1314.7	60.61	0.15	43.67	1.05	1.73	0.01	0.02	0.01	0.02	3	0.709	0.385	45.34	0.96	5.13E-04	0.04	0.00	0.03	4.38E-04
203	156	29254	1712.5	67.71	0.08	45.05	1.04	1.22	0.01	0.01	0.01	0.01	3	0.709	0.268	45.34	0.99	3.10E-04	0.03	0.00	0.03	3.70E-04
208	156	24957	1680.6	71.28	-0.04	45.04	1.04	0.99	0.01	0.01	0.01	0.01	3	0.709	0.152	45.34	0.99	2.71E-04	0.02	0.00	0.03	4.01E-04
212	156	17096	702.9	76.31	0.25	45.00	0.95	1.07	0.01	0.02	0.01	0.01	3	0.709	0.058	45.34	0.99	3.54E-04	0.02	0.01	0.03	4.41E-04
174	140.5	17791	923.9	61.28	0.30	40.66	1.13	1.11	0.02	0.02	0.01	0.01	3	0.639	0.944	40.84	1.00	3.99E-04	0.03	0.01	0.04	5.15E-04
178	140.5	20936	932.3	69.67	0.32	40.38	0.99	0.90	0.01	0.01	0.01	0.01	3	0.639	0.851	40.84	0.99	2.99E-04	0.02	0.01	0.03	4.14E-04
183	140.5	22669	932.0	78.58	0.37	40.53	0.83	1.07	0.01	0.01	0.01	0.01	3	0.639	0.734	40.84	0.99	3.42E-04	0.03	0.01	0.03	3.34E-04
188	140.5	20323	891.3	78.93	0.25	40.44	1.03	1.16	0.01	0.02	0.01	0.01	3	0.639	0.618	40.84	0.99	3.89E-04	0.03	0.01	0.03	4.40E-04
193	140.5	19568	719.7	80.26	0.24	39.84	0.91	1.47	0.01	0.02	0.01	0.01	3	0.639	0.501	40.84	0.98	5.04E-04	0.04	0.01	0.03	3.93E-04
198	140.5	24318	2225.9	70.02	0.18	39.63	1.00	1.60	0.01	0.02	0.01	0.01	3	0.639	0.385	40.84	0.97	4.94E-04	0.04	0.01	0.03	3.86E-04
203	140.5	25227	2699.3	67.89	0.08	40.63	0.95	1.01	0.01	0.01	0.01	0.01	3	0.639	0.268	40.84	0.99	3.04E-04	0.02	0.00	0.03	3.64E-04
208	140.5	16836	872.0	82.77	0.19	40.62	0.98	0.81	0.01	0.01	0.01	0.01	3	0.639	0.152	40.84	0.99	3.01E-04	0.02	0.01	0.03	4.57E-04
212	140.5	22333	977.7	85.72	0.42	40.47	0.87	0.91	0.01	0.01	0.01	0.01	3	0.639	0.058	40.84	0.99	2.94E-04	0.02	0.01	0.03	3.54E-04
174	124.5	20986	1262.8	67.05	0.34	35.96	0.93	0.97	0.01	0.01	0.01	0.01	3	0.566	0.944	36.19	0.99	3.62E-04	0.03	0.01	0.03	3.91E-04
178	124.5	14622	640.7	76.79	0.43	35.75	0.80	0.84	0.01	0.01	0.01	0.01	3	0.566	0.851	36.19	0.99	3.75E-04	0.02	0.01	0.02	3.99E-04
183	124.5	21305	634.0	75.07	0.51	35.71	0.91	0.93	0.01	0.01	0.01	0.01	3	0.566	0.734	36.19	0.99	3.44E-04	0.03	0.02	0.03	3.76E-04
188	124.5	18972	624.8	77.62	0.40	35.60	1.03	0.80	0.01	0.01	0.01	0.01	3	0.566	0.618	36.19	0.98	3.16E-04	0.02	0.01	0.03	4.55E-04
193	124.5	22829	1190.3	79.68	0.32	35.39	0.88	1.08	0.01	0.01	0.01	0.01	3	0.566	0.501	36.19	0.98	3.88E-04	0.03	0.01	0.03	3.54E-04
198	124.5	24639	5352.6	66.62	0.22	35.19	0.91	1.19	0.01	0.01	0.01	0.01	3	0.566	0.385	36.19	0.97	4.10E-04	0.03	0.01	0.03	3.52E-04
203	124.5	27644	2475.3	77.57	0.19	35.68	0.87	0.81	0.01	0.01	0.01	0.01	3	0.566	0.268	36.19	0.99	2.64E-04	0.02	0.01	0.03	3.17E-04
208	124.5	19150	507.4	92.08	0.26	35.98	0.82	0.66	0.01	0.01	0.01	0.01	3	0.566	0.152	36.19	0.99	2.57E-04	0.02	0.01	0.03	3.61E-04
212	124.5	20961	574.9	92.52	0.14	36.01	0.68	0.74	0.01	0.01	0.01	0.01	3	0.566	0.058	36.19	1.00	2.77E-04	0.02	0.00	0.02	2.86E-04
123	203.5	24903	598.1	72.15	0.85	58.03	1.83	1.57	0.02	0.02	0.02	0.01	4	0.925	0.946	59.15	0.98	3.30E-04	0.03	0.03	0.06	7.03E-04
127	203.5	27356	563.1	72.44	0.20	58.47	1.39	1.64	0.02	0.02	0.01	0.01	4	0.925	0.853	59.15	0.99	3.29E-04	0.03	0.01	0.04	5.09E-04
132	203.5	26919	844.4	81.29	-0.25	58.27	1.35	1.56	0.02	0.02	0.01	0.01	4	0.925	0.737	59.15	0.99	3.14E-04	0.03	-0.01	0.04	5.00E-04
137	203.5	30944	1310.5	78.19	-0.01	58.46	1.41	1.48	0.02	0.02	0.01	0.01	4	0.925	0.620	59.15	0.99	2.79E-04	0.03	0.00	0.04	4.86E-04
142	203.5	32520	1979.8	70.56	0.07	58.27	1.44	1.52	0.02	0.02	0.01	0.01	4	0.925	0.503	59.15	0.99	2.80E-04	0.03	0.00	0.04	4.83E-04
147	203.5	27835	1542.8	64.24	0.01	58.26	1.52	1.51	0.02	0.02	0.01	0.01	4	0.925	0.387	59.15	0.98	3.00E-04	0.03	0.00	0.05	5.54E-04
152	203.5	21645	2219.4	60.39	0.12	58.24	1.49	1.67	0.02	0.02	0.01	0.02	4	0.925	0.270	59.15	0.98	3.77E-04	0.03	0.00	0.05	6.16E-04
157	203.5	21759	1538.6	53.14	0.30	58.67	1.58	1.47	0.02	0.02	0.01	0.01	4	0.925	0.154	59.15	0.99	3.30E-04	0.02	0.01	0.05	6.51E-04
161	203.5	30724	2603.4	66.17	0.30	58.26	1.42	1.45	0.02	0.02	0.01	0.01	4	0.925	0.061	59.15	0.98	2.74E-04	0.02	0.01	0.04	4.91E-04
123	171.5	29710	2985.89309	80.205	0.19121	48.845	1.1839	0.97475	0.01346	0.0111	0.00952	0.00784	4	0.780	0.946	49.85	0.98	2.22E-04	0.02	0.01	0.04	4.17E-04
127	171.5	27148	1924.84798	73.37	0.26297	49.1753	1.26657	1.33066	0.01507	0.0158	0.01065	0.01119	4	0.780	0.853	49.85	0.99	3.18E-04	0.03	0.01	0.04	4.66E-04
132	171.5	29093	1718.52538	79.95	0.08113	49.145	1.26997	1.34522	0.01459	0.0155	0.01032	0.01093	4	0.780	0.737	49.85	0.99	3.10E-04	0.03	0.00	0.04	4.52E-04
137	171.5	23293	1770.18556	79.75	-0.02337	49.0692	1.34671	1.39351	0.0173	0.0179	0.01223	0.01265	4	0.780	0.620	49.85	0.98	3.59E-04	0.03	0.00	0.04	5.35E-04
142	171.5	19889	2048.61781	70.515	0.16522	49.1443	1.27844	1.37447	0.01777	0.0191	0.01256	0.01351	4	0.780	0.503	49.85	0.99	3.83E-04	0.03	0.01	0.04	5.50E-04
147	171.5	20445	2295.07708	69.479	0.02893	49.2701	1.2331	1.30806	0.0169	0.0179	0.01195	0.01268	4	0.780	0.387	49.85	0.99	3.60E-04	0.03	0.00	0.04	5.23E-04
152	171.5	21321	3956.53761	63.923	0.27496	49.2681	1.31505	1.28543	0.01765	0.0173	0.01248	0.0122	4	0.780	0.270	49.85	0.99	3.46E-04	0.03	0.01	0.04	5.46E-04
157	171.5	19406	1900.62742	59.646	0.47152	49.5471	1.51374	1.23308	0.0213	0.0173	0.01506	0.01227	4	0.780	0.154	49.85	0.99	3.48E-04	0.02	0.01	0.05	6.59E-04
161	171.5	23385	4053.74975	61.363	0.49945	49.4461	1.34268	1.36104	0.01721	0.0174	0.01217	0.01234	4	0.780	0.061	49.85	0.99	3.50E-04	0.03	0.02	0.04	5.33E-04
123	124.5	28165	2637.87899	94.63	0.37144	35.6157	0.84789	0.74657	0.0099	0.0087	0.007	0.00617	4	0.566	0.946	36.19	0.98	2.41E-04	0.02	0.01	0.03	3.06E-04
127	124.5	31614	5359.00925	85.217	0.24495	35.6915	0.92865	0.98082	0.01024	0.0108	0.00724	0.00765	4	0.566	0.853	36.19	0.99	2.99E-04	0.03	0.01	0.03	3.17E-04
132	124.5	21489	4135.98865	79.814	0.05224	35.5536	1.00361	0.99008	0.01342	0.0132	0.00949	0.00936	4	0.566	0.737	36.19	0.98	3.66E-04	0.03	0.00	0.03	4.15E-04
137	124.5	27101	5268.15001	71.881	0.00436	35.6188	0.99481	0.96148	0.01184	0.0114	0.00838	0.00809	4	0.566	0.620	36.19	0.98	3.16E-04	0.03	0.00	0.03	3.67E-04
142	124.5	24148	5254.42134	63.402	0.20367	35.7509	1.08626	0.97566	0.0137	0.0123	0.00969	0.0087	4	0.566	0.503	36.19	0.99	3.40E-04	0.03	0.01	0.03	4.24E-04
147	124.5	16649	4520.8941	57.343	0.21161	35.8222	1.04325	0.96692	0.01585	0.0147	0.01121	0.01039	4	0.566	0.387	36.19	0.99	4.06E-04	0.03	0.01	0.03	4.91E-04
152	124.5	20677	4432.81944	64.82	0.22428	35.8756	0.99431	0.86527	0.01355	0.0118	0.00958	0.00834	4	0.566	0.270	36.19	0.99	3.26E-04	0.02	0.01	0.03	4.19E-04
157	124.5	22906	3580.8491	65.225	0.27711	35.9002	1.09198	0.86119	0.01414	0.0112	0.01	0.00789	4	0.566	0.154	36.19	0.99	3.08E-04	0.02	0.01	0.03	4.38E-04
161	124.5	14698	3482.85071	60.401	0.5553	35.977	1.00429	0.82987	0.01624	0.0134	0.01148	0.00949	4	0.566	0.061	36.19	0.99	3.71E-04	0.02	0.02	0.03	5.03E-04

LDA measurement		**LDA code:**	101	**rpm:**	1655.0	**Perfd by:**		Printed: 27/09/2008	Page 1/3
Build:	2	**ReΦ:**	1.09E+06	**Date:**	07/08/2001	**LDA1:**	VΦ	**Comments:**	
LDA test # :	test6	**Rez:**	1.14E+05	**raw LDA file:**	\MCRLDA\Build2&1\Projects\mcr3.lda , mcr2.lda	**LDA2:**	Vz	**Traverse ref:**	
Heat Transfer run:	B2t06	**Ro:**	3.56	**LDA list file:**	MCR\b2Data\LDA-results\MultiCavityRig\Test6-250mm-3cav\cav2_list.txt	**W (m/s):**	55.3		

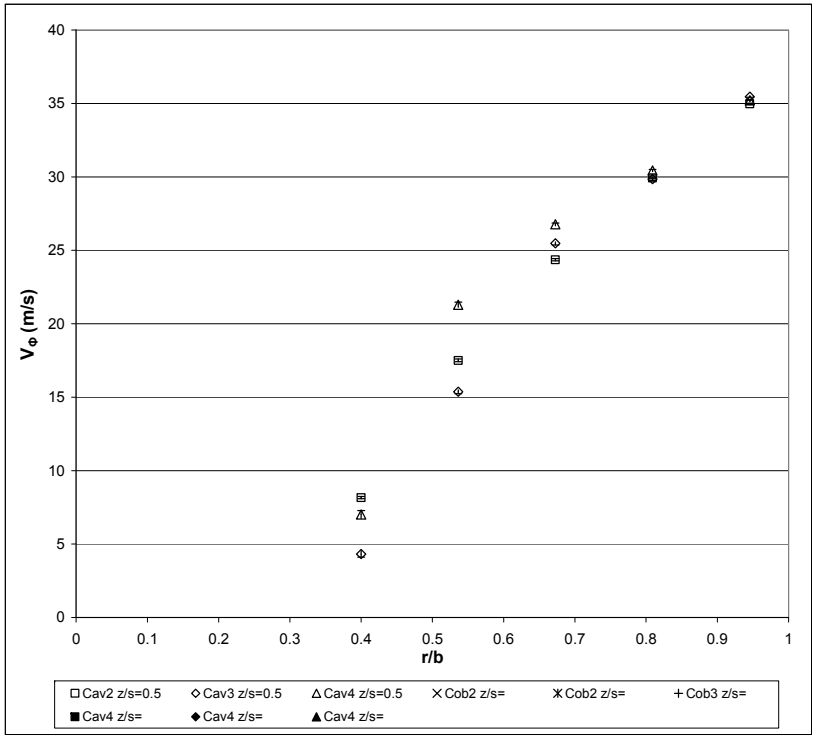

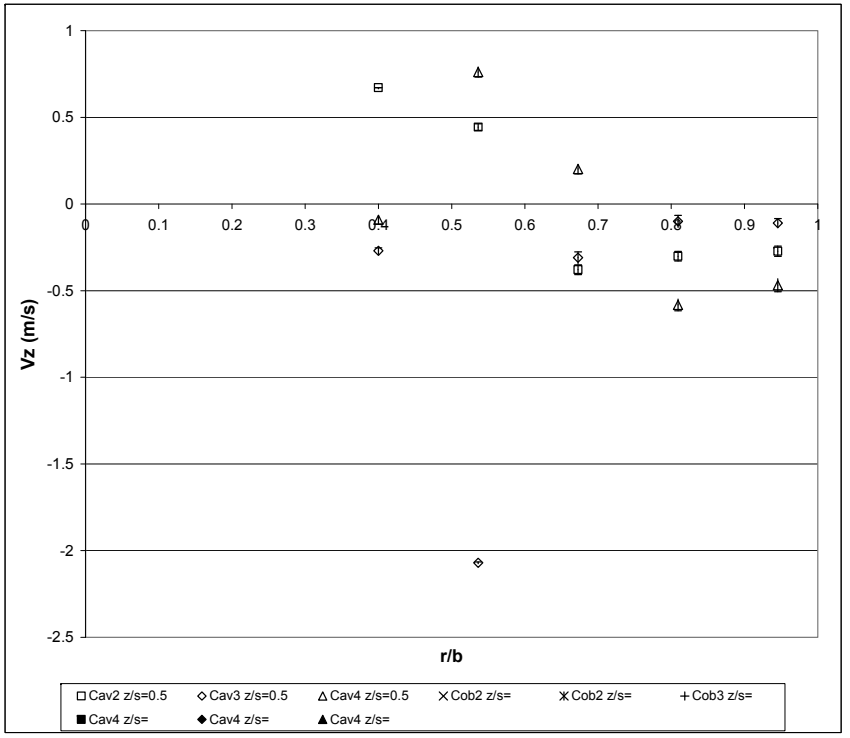

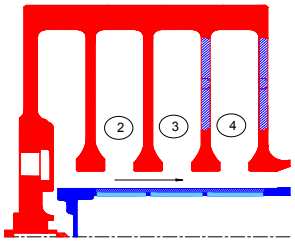

LDA measurement		**LDA code:**	101	**rpm:**	1655.0	**Perfd by:**	0	Printed: 27/09/2008	Page 2/3
Build:	2	**Re_Φ:**	1.09E+06	**Date:**	07/08/2001	**LDA1:**	VΦ	**Comments:**	0
LDA test # :	test6	**Re_z:**	1.14E+05	**raw LDA file:**	\MCRLDA\Build2&1\Projects\mcr3.lda , m	**LDA2:**	Vz	**Traverse corresp:**	0
Heat Transfer run:	B2t06	**Ro:**	3.56	**LDA list file:**	MCR\b2Data\LDA-results\MultiCavityRig\1	**W (m/s):**	55.3		

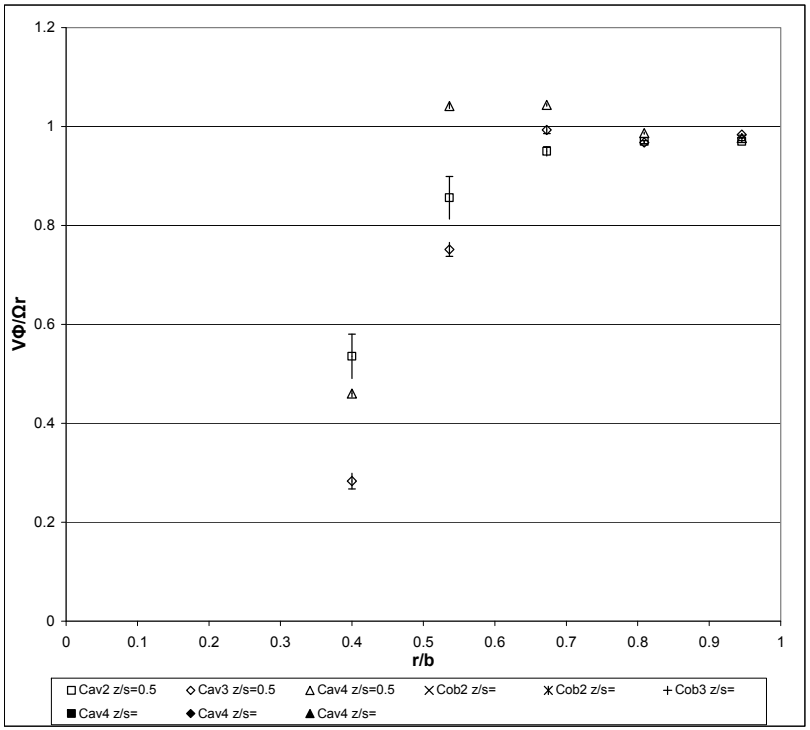

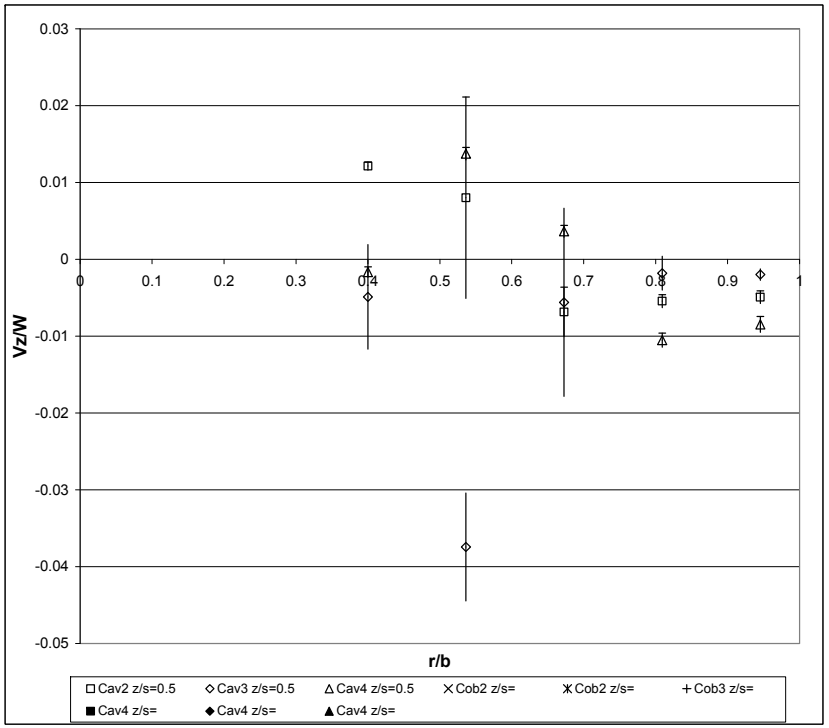

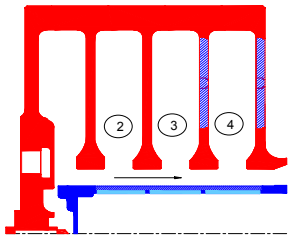

LDA measurement | LDA code: 101 | rpm: 1655.0 | Perfd by: 0 | Printed: 27/09/2008 | Page 3/3

Build: 2 | **ReΦ:** 1.09E+06 | **Date:** 07/08/2001 | **LDA1:** VΦ | **Comments:** 0

LDA test # : test6 | **Rez:** 1.14E+05 | **raw LDA file:** \MCRLDA\Build2&1\Projects\mcr3.lda , m | **LDA2:** Vz | **Traverse corresp:** 0

Heat Transfer run: B2t06 | **Ro:** 3.56 | **LDA list file:** MCR\b2Data\LDA-results\MultiCavityRig\T | **W (m/s):** 55.3

X [mm]	corrected X	Y [mm]	corrected Y / Radius (mm)	Count{1}	Count{2}	Data Rate{1} [#/s]	Data Rate{2} [#/s]	Validation{1} [%]	Validation{2} [%]	LDA1 Mean [m/s]	LDA2 Mean [m/s]	LDA1 RMS [m/s]	LDA2 RMS [m/s]	LDA1 MeanConf [m/s]	LDA2 MeanConf [m/s]	LDA1 RMSConf [m/s]	LDA2 RMSConf [m/s]	Cavity	r/b	z/s	Ωr (m/s)	$V_{\Phi}/\Omega r$	$V_{\Phi U95\%}/\Omega r$	$V_{\Phi(RMS)}/\Omega r$	$Vz_{(RMS)}/W$		$Vz_{U95\%}/W$
75		53	88	12	2	1.6	2.4			8.17	0.67	1.16	0.01	0.68	0.03	0.48	0.02	2	0.400	0.500	15.25	0.54	4.48E-02	0.08	0.01	0.00	5.26E-04
75		83	118	19	9	2.2	1.2			17.51	0.44	1.91	1.05	0.88	0.72	0.62	0.51	2	0.536	0.500	20.45	0.86	4.31E-02	0.09	0.01	0.02	1.31E-02
75		113	148	246	291	24.8	29.5			24.36	-0.38	1.92	1.55	0.24	0.18	0.17	0.13	2	0.673	0.500	25.65	0.95	9.37E-03	0.07	-0.01	0.03	3.22E-03
75		143	178	5000	4197	797.0	421.7			29.93	-0.30	1.67	1.53	0.05	0.05	0.03	0.03	2	0.809	0.500	30.85	0.97	1.50E-03	0.05	-0.01	0.03	8.35E-04
75		173	208	5000	5000	1747.6	3778.7			34.97	-0.27	1.57	1.63	0.04	0.05	0.03	0.03	2	0.945	0.500	36.05	0.97	1.21E-03	0.04	0.00	0.03	8.16E-04
130		53	88	670	23	67.4	2.6			4.32	-0.27	3.18	0.92	0.24	0.38			3	0.400	0.500	15.25	0.28	1.58E-02	0.21	0.00	0.02	6.80E-03
130		83	118	320	2	32.2	0.2			15.37	-2.07	2.60	0.28	0.28	0.39			3	0.536	0.500	20.45	0.75	1.39E-02	0.13	-0.04	0.01	7.02E-03
130		113	148	688	29	68.9	2.9			25.47	-0.31	2.52	1.86	0.19	0.68			3	0.673	0.500	25.65	0.99	7.34E-03	0.10	-0.01	0.03	1.22E-02
130		143	178	5000	945	4999.5	94.5			29.85	-0.10	2.38	1.91	0.07	0.12			3	0.809	0.500	30.85	0.97	2.14E-03	0.08	0.00	0.03	2.20E-03
130		173	208	5000	5000	24737.0	10899.2			35.46	-0.11	1.37	1.47	0.04	0.04			3	0.945	0.500	36.05	0.98	1.05E-03	0.04	0.00	0.03	7.37E-04
175		53	88	5000	5000	1074.2	853.9			7.02	-0.09	4.09	1.32	0.11	0.04	0.08	0.03	4	0.400	0.500	15.25	0.46	7.43E-03	0.27	0.00	0.02	6.63E-04
175		83	118	5000	5000	518.5	632.7			21.30	0.76	3.51	1.61	0.10	0.04	0.07	0.03	4	0.536	0.500	20.45	1.04	4.76E-03	0.17	0.01	0.03	8.06E-04
175		113	148	5000	5000	887.9	2633.0			26.77	0.20	2.33	1.52	0.06	0.04	0.05	0.03	4	0.673	0.500	25.65	1.04	2.52E-03	0.09	0.00	0.03	7.64E-04
175		143	178	5000	5000	8111.5	2777.0			30.44	-0.58	2.23	1.84	0.06	0.05	0.04	0.04	4	0.809	0.500	30.85	0.99	2.01E-03	0.07	-0.01	0.03	9.25E-04
175		173	208	5000	5000	30104.5	28704.6			35.21	-0.47	2.40	2.07	0.07	0.06	0.05	0.04	4	0.945	0.500	36.05	0.98	1.84E-03	0.07	-0.01	0.04	1.04E-03

LDA measurement		**LDA code:**	101	**rpm:**	2925.0	**Perfd by:**		Printed: 27/09/2008	Page 1/3
Build:	2	**ReΦ:**	2.02E+06	**Date:**	13/08/2001	**LDA1:**	VΦ	**Comments:**	
LDA test # :	Test7b	**Rez:**	1.23E+05	**raw LDA file:**		**LDA2:**	Vz	**Traverse ref:**	
Heat Transfer run:	B2t07-b	**Ro:**	2.07	**LDA list file:**	\MCR\b2Data\LDA-results\MultiCavityRig\Test7-250mm\test7b\avrg2.txt	**W (m/s):**	55.4		

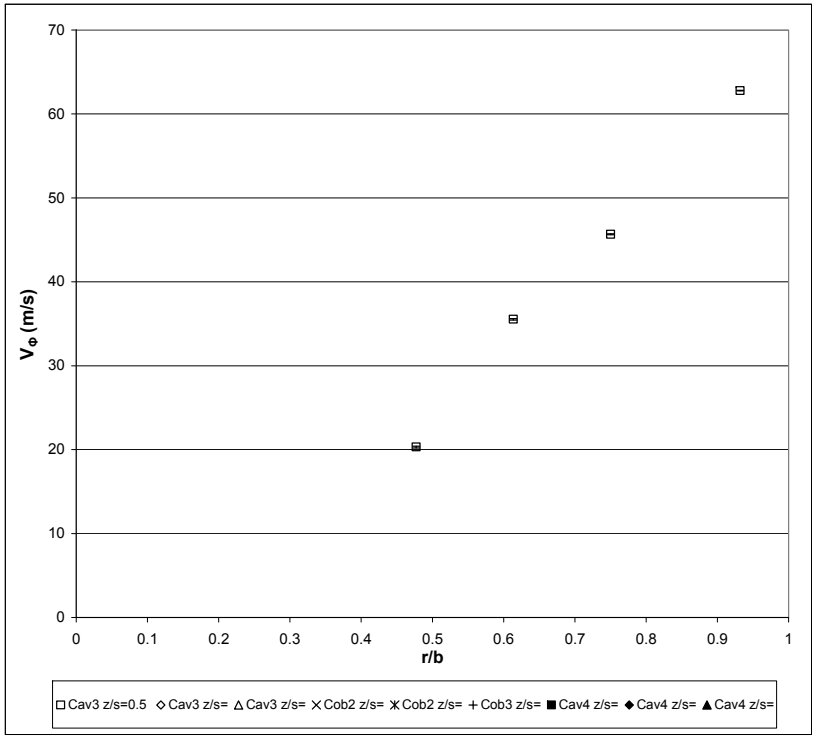

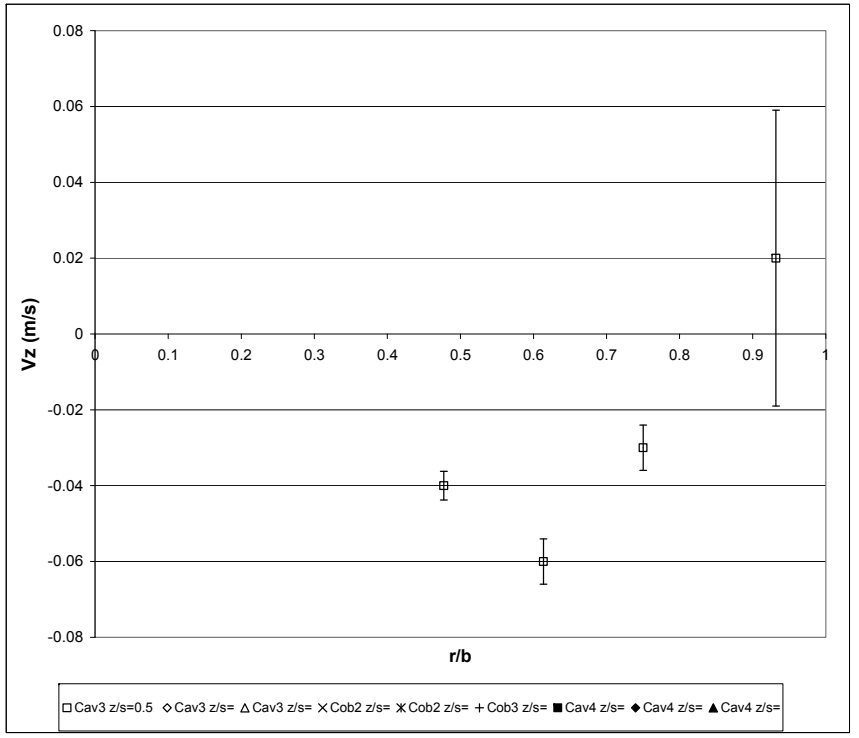

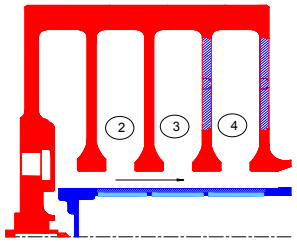

LDA measurement		**LDA code:**	101	**rpm:**	2925.0	**Perfd by:**	0	Printed: 27/09/2008	Page 2/3
Build:	2	**Re_Φ:**	2.02E+06	**Date:**	13/08/2001	**LDA1:**	VΦ	**Comments:**	0
LDA test # :	Test7b	**Re_z:**	1.23E+05	**raw LDA file:**	0	**LDA2:**	Vz	**Traverse corresp:**	0
Heat Transfer run:	B2t07-b	**Ro:**	2.07	**LDA list file:**	\MCR\b2Data\LDA-results\MultiCavityRig\	**W (m/s):**	55.4		

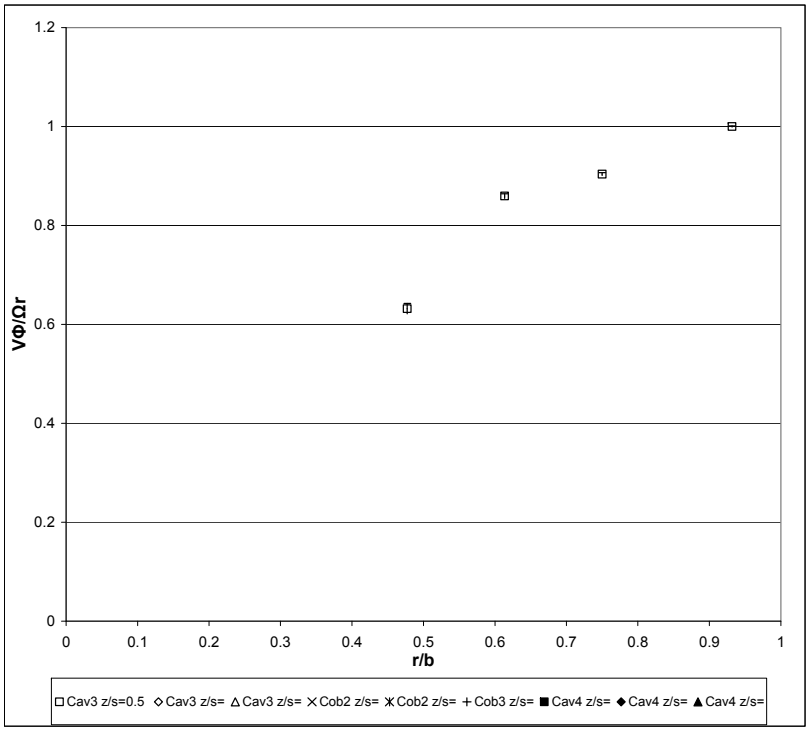

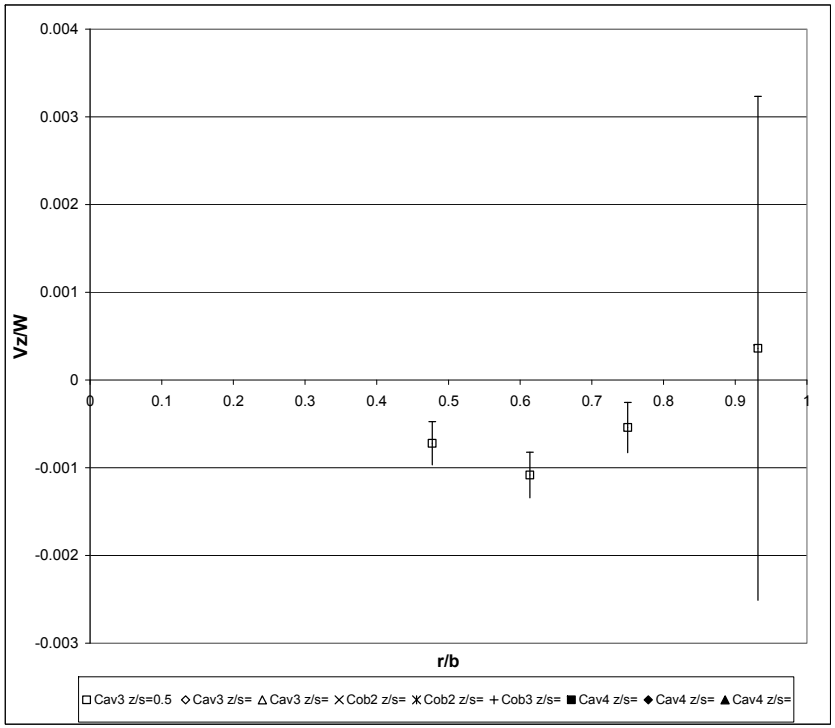

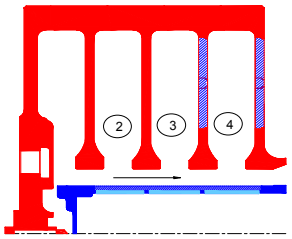

LDA measurement | LDA code: 101 | rpm: 2925.0 | Perfd by: 0 | Printed: 27/09/2008 | Page 3/3

Build: 2 | **ReΦ:** 2.02E+06 | **Date:** 13/08/2001 | **LDA1:** VΦ | **Comments:** 0

LDA test # : Test7b | **Rez:** 1.23E+05 | **raw LDA file:** 0 | **LDA2:** Vz | **Traverse corresp:** 0

Heat Transfer run: B2t07-b | **Ro:** 2.07 | **LDA list file:** \MCR\b2Data\LDA-results\MultiCavityRig\ | **W (m/s):** 55.4

X [mm]	corrected X	Y [mm]	corrected Y / Radius (mm)	Count{1}	Count{2}	Data Rate{1} [#/s]	Data Rate{2} [#/s]	Validation{1} [%]	Validation{2} [%]	LDA1 Mean [m/s]	LDA2 Mean [m/s]	LDA1 RMS [m/s]	LDA2 RMS [m/s]	LDA1 MeanConf [m/s]	LDA2 MeanConf [m/s]	LDA1 RMSConf [m/s]	LDA2 RMSConf [m/s]	Cavity	r/b	z/s	Ωr (m/s)	$V_{\Phi}/\Omega r$	$V_{\Phi U95\%}/\Omega r$	$V_{\Phi(RMS)}/\Omega r$	Vz/W	$Vz_{(RMS)}/W$	$Vz_{U95\%}/W$
125		70	105	373	911	6.4	15.3			20.32	-0.04	3.34	0.21	0.34	0.01			3	0.477	0.500	32.16	0.63	1.05E-02	0.10	0.00	0.00	2.46E-04
125		100	135	1225	2000	20.4	91.4			35.54	-0.06	3.52	0.33	0.20	0.01			3	0.614	0.500	41.35	0.86	4.77E-03	0.09	0.00	0.01	2.61E-04
125		130	165	1578	1671	26.3	27.9			45.67	-0.03	2.88	0.33	0.14	0.02			3	0.750	0.500	50.54	0.90	2.81E-03	0.06	0.00	0.01	2.86E-04
125		170	205	2000	708	52.7	11.8			62.79	0.02	1.52	2.16	0.07	0.16			3	0.932	0.500	62.79	1.00	1.06E-03	0.02	0.00	0.04	2.87E-03

LDA measurement		**LDA code:**	100	**rpm:**	1485.0	**Perfd by:**		Printed: 27/09/2008	Page 1/3
Build:	2	**ReΦ:**	1.05E+06	**Date:**	17/10/2001	**LDA1:**	VΦ	**Comments:**	
LDA test # :	Test13	**Rez:**	1.25E+05	**raw LDA file:**		**LDA2:**		**Traverse ref:**	
Heat Transfer run:	B2t13-b	**Ro:**	4.10	**LDA list file:**	MCR\b2Data\LDA-results\MultiCavityRig\Test13\avgr	**W (m/s):**	56.1		

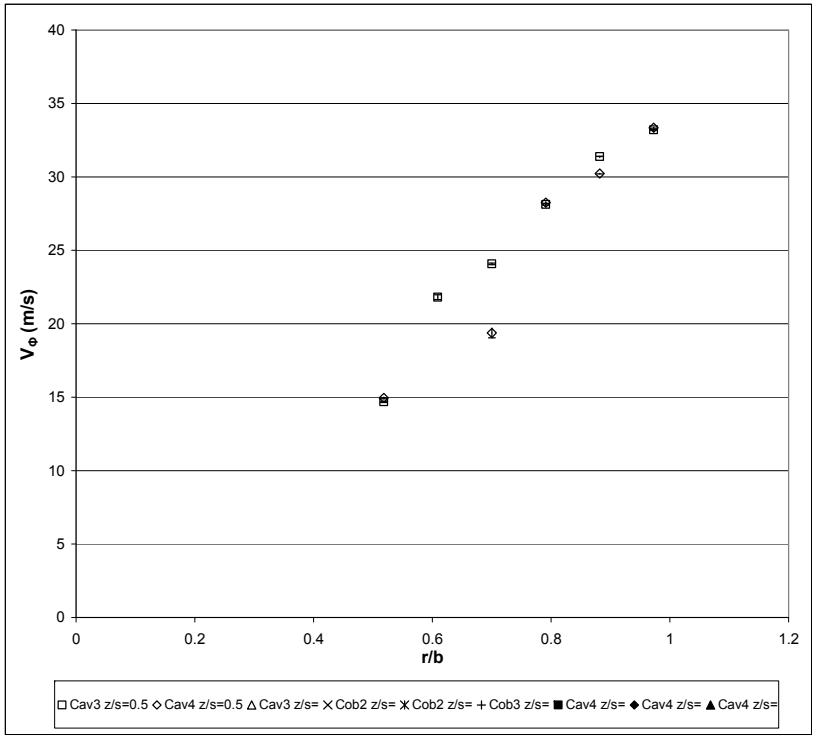

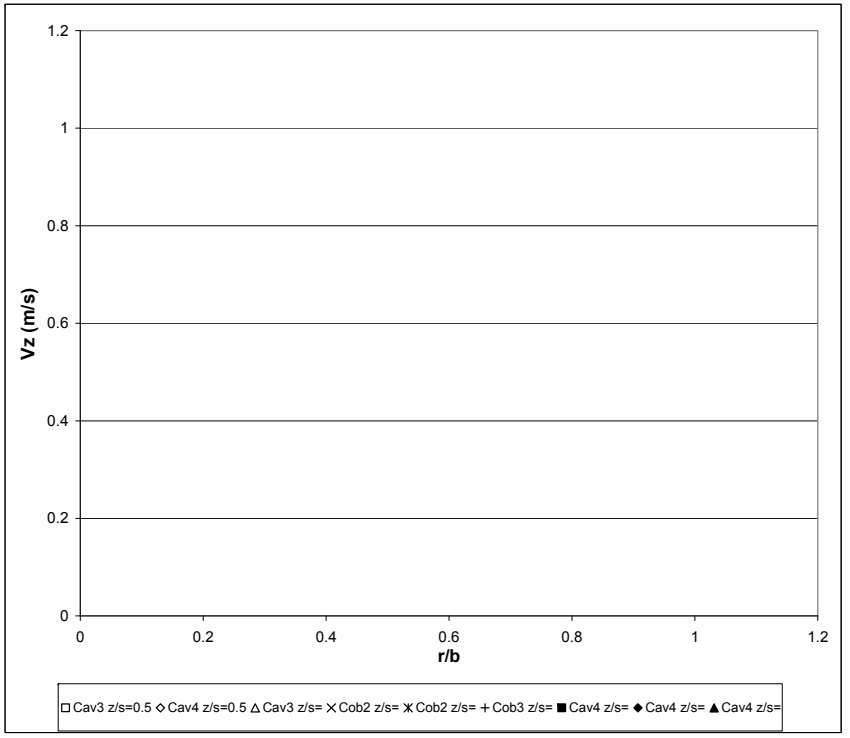

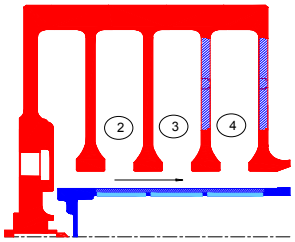

LDA measurement		**LDA code:**	101	**rpm:**	1485.0	**Perfd by:**	0	Printed: 27/09/2008	Page 2/3
Build:	2	**Re_Φ:**	1.05E+06	**Date:**	17/10/2001	**LDA1:**	VΦ	**Comments:**	0
LDA test # :	Test13	**Re_z:**	1.25E+05	**raw LDA file:**	0	**LDA2:**	0	**Traverse corresp:**	0
Heat Transfer run:	B2t13-b	**Ro:**	4.10	**LDA list file:**	MCR\b2Data\LDA-results\MultiCavityRig\1	**W (m/s):**	56.1		

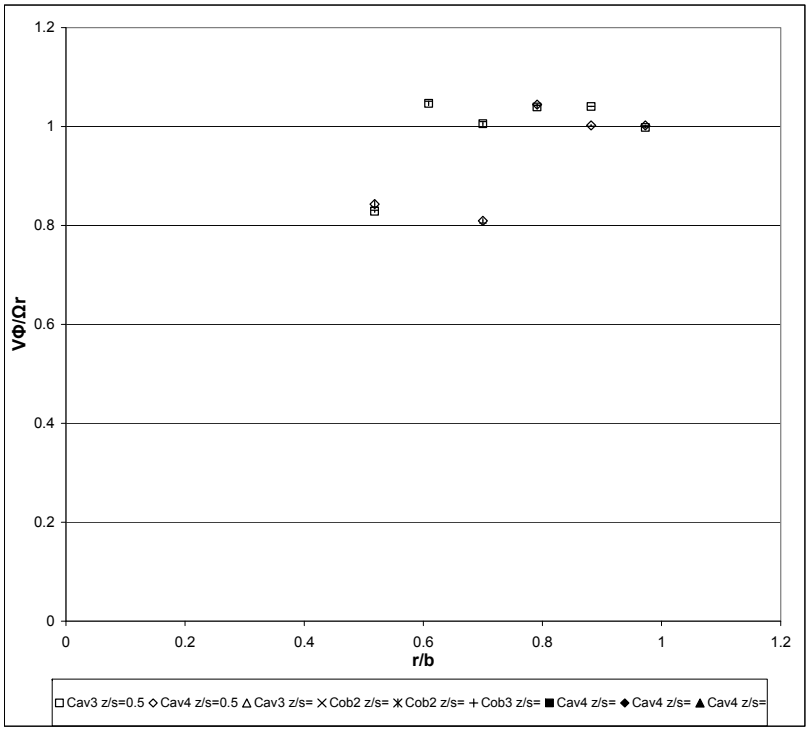

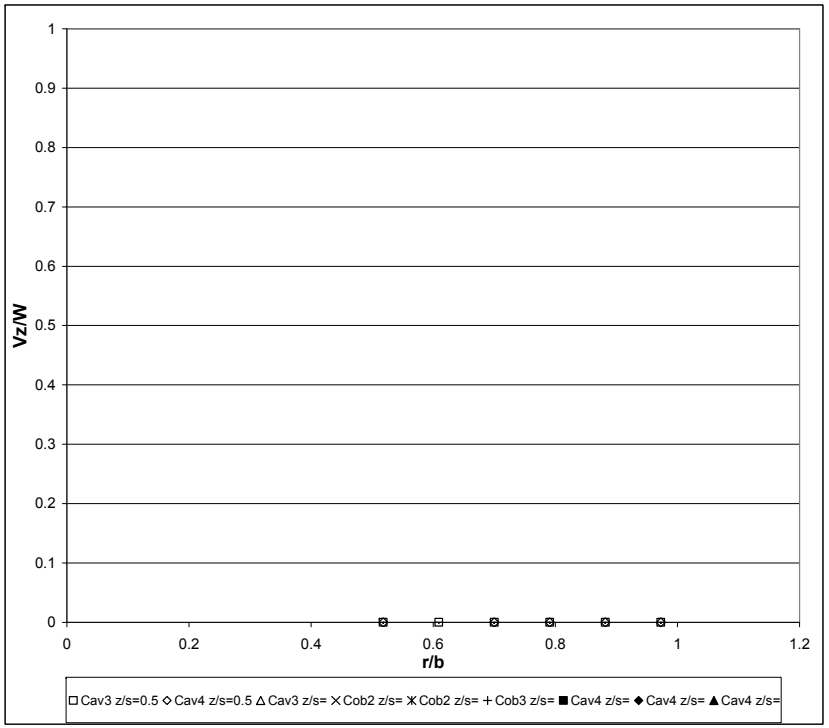

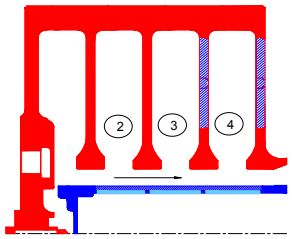

LDA measurement | **LDA code:** 100 | **rpm:** 1485.0 | **Perfd by:** 0 | Printed: 27/09/2008 | Page 3/3

Build: 2 | **ReΦ:** 1.05E+06 | **Date:** 17/10/2001 | **LDA1:** VΦ | **Comments:** 0

LDA test # : Test13 | **Rez:** 1.25E+05 | **raw LDA file:** 0 | **LDA2:** 0 | **Traverse corresp:** 0

Heat Transfer run: B2t13-b | **Ro:** 4.10 | **LDA list file:** MCR\b2Data\LDA-results\MultiCavityRig\T | **W (m/s):** 56.1

X [mm]	corrected X	Y [mm]	corrected Y / Radius (mm)	Count{1}	Count{2}	Data Rate{1} [#/s]	Data Rate{2} [#/s]	Validation{1} [%]	Validation{2} [%]	LDA1 Mean [m/s]	LDA2 Mean [m/s]	LDA1 RMS [m/s]	LDA2 RMS [m/s]	LDA1 MeanConf [m/s]	LDA2 MeanConf [m/s]	LDA1 RMSConf [m/s]	LDA2 RMSConf [m/s]	Cavity	r/b	z/s	Ωr (m/s)	$V_\Phi/\Omega r$	$V_{\Phi U95\%}/\Omega r$	$V_{\Phi(RMS)}/\Omega r$	Vz/W	$Vz_{(RMS)}/W$	$Vz_{U95\%}/W$
175		180	214	5000		7861.8				33.35		0.89		0.02				4	0.973	0.500	33.28	1.00	7.41E-04	0.03	0.00	0.00	0.00E+00
175		160	194	745		24.8				30.23		0.64		0.05				4	0.882	0.500	30.17	1.00	1.52E-03	0.02	0.00	0.00	0.00E+00
175		140	174	5000		206.1				28.25		1.43		0.04				4	0.791	0.500	27.06	1.04	1.46E-03	0.05	0.00	0.00	0.00E+00
175		120	154	20000		3204.5				19.38		7.86		0.11				4	0.700	0.500	23.95	0.81	4.55E-03	0.33	0.00	0.00	0.00E+00
175		100	134	216		7.3				21.10		3.61		0.48				4	0.609	0.520	20.84	1.01	2.31E-02	0.17	0.00	0.00	0.00E+00
175		80	114	360		12.0				14.95		0.98		0.10				4	0.518	0.500	17.73	0.84	5.71E-03	0.06	0.00	0.00	0.00E+00
125		180	214	5000		21080.9				33.21		1.08		0.03				3	0.973	0.500	33.28	1.00	9.00E-04	0.03	0.00	0.00	0.00E+00
125		160	194	863		14.4				31.39		0.15		0.01				3	0.882	0.500	30.17	1.04	3.32E-04	0.00	0.00	0.00	0.00E+00
125		140	174	824		13.8				28.13		1.37		0.09				3	0.791	0.500	27.06	1.04	3.46E-03	0.05	0.00	0.00	0.00E+00
125		120	154	567		19.0				24.08		1.32		0.11				3	0.700	0.500	23.95	1.01	4.54E-03	0.06	0.00	0.00	0.00E+00
125		100	134	5000		90.9				21.81		3.36		0.09				3	0.609	0.500	20.84	1.05	4.47E-03	0.16	0.00	0.00	0.00E+00
125		80	114	1690		28.2				14.69		0.77		0.04				3	0.518	0.500	17.73	0.83	2.07E-03	0.04	0.00	0.00	0.00E+00

Appendix 6.5: Spectral analysis plots

r/b=0.924

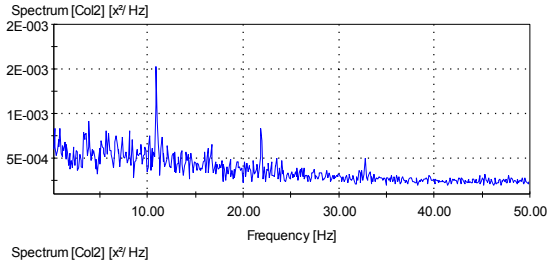

r/b=0.851

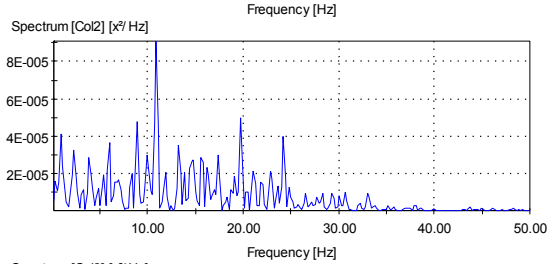

r/b=0.763

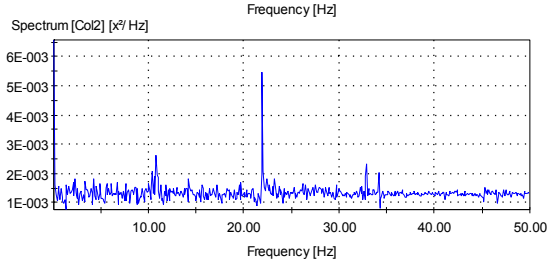

r/b=0.680

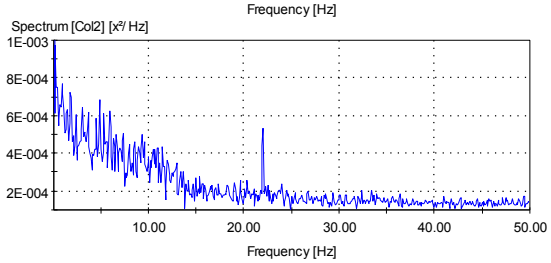

r/b=0.595

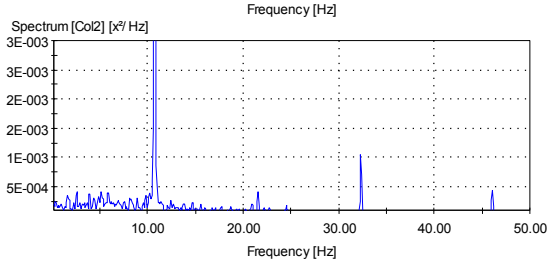

r/b=0.566

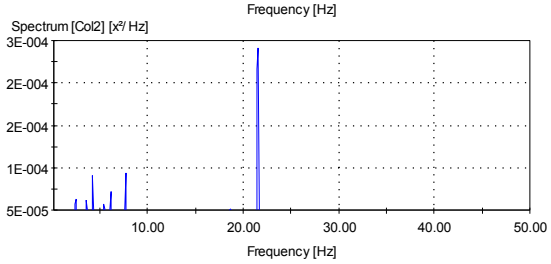

Build 3, Run 38-1, Cavity 3, r/b=0.508, $Re_{\Phi}=0.4x10^{6}$, $Re_{z}=1.57x10^{5}$, Ro=7.51

r/b=0.924

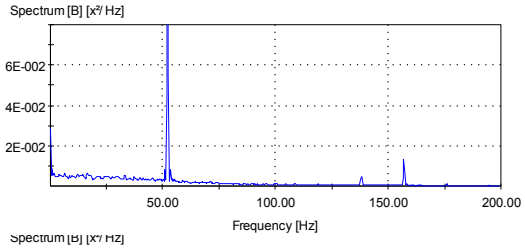

r/b=0.851

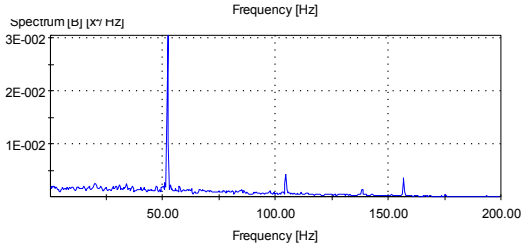

r/b=0.763

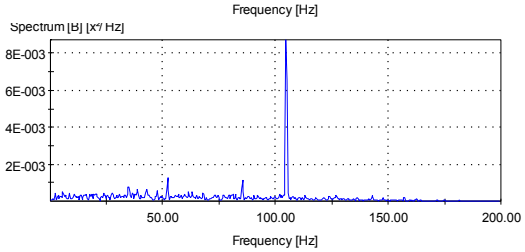

r/b=0.680

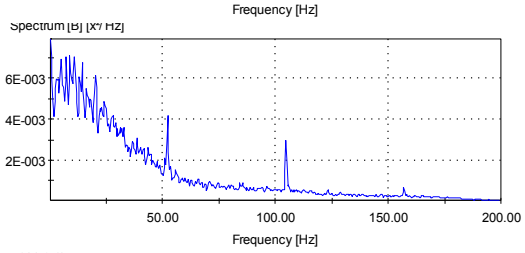

r/b=0.595

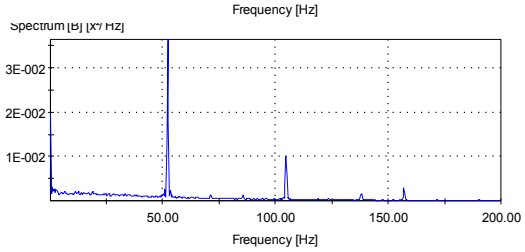

r/b=0.566

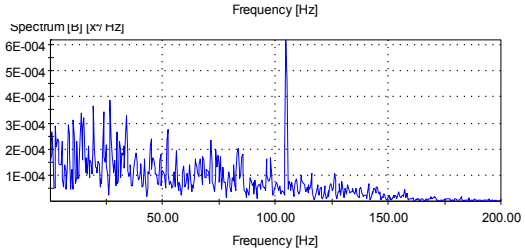

Build 3, Run 39-1, Cavity 3, r/b=0.508, $Re_{\Phi}=1.93x10^{6}$, $Re_{z}=0.53x10^{5}$, Ro=0.53

r/b=0.924

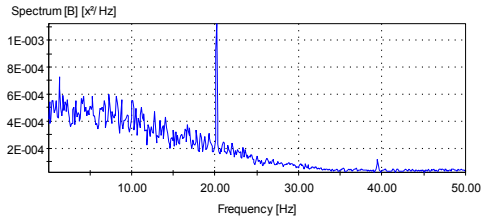

r/b=0.851

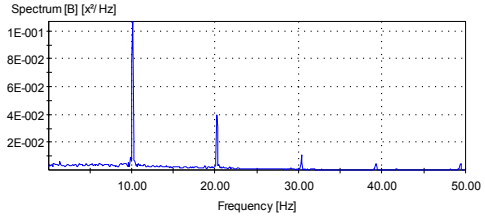

r/b=0.763

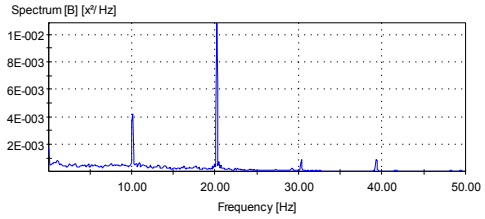

r/b=0.680

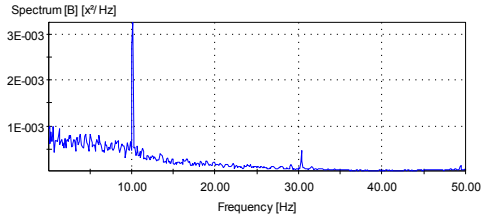

r/b=0.595

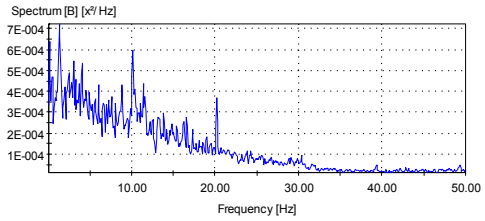

r/b=0.566

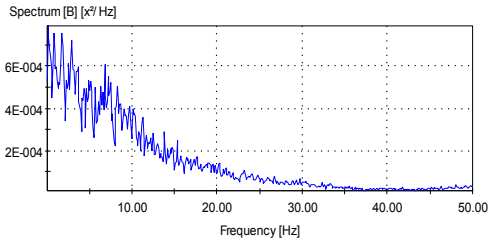

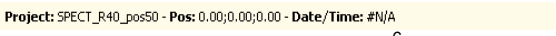

Build 3, Run 40-1, Cavity 3, r/b=0.508, $Re_{\Phi}=0.39x10^{6}$, $Re_{z}=0.61x10^{5}$, Ro=2.98

r/b=0.924

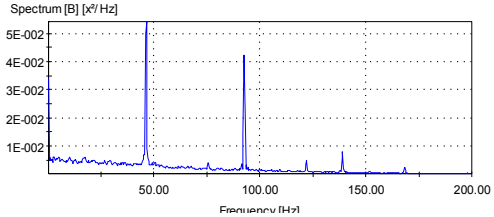

r/b=0.851

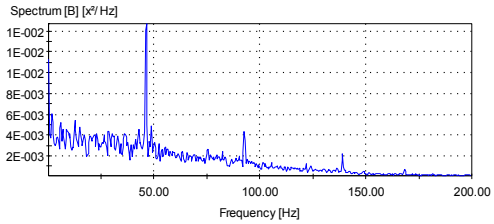

r/b=0.763

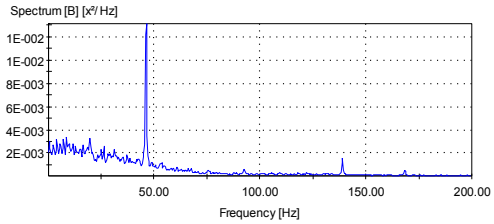

r/b=0.680

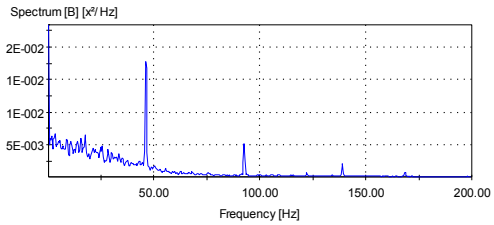

r/b=0.595

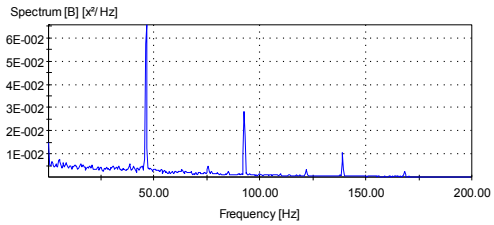

r/b=0.566

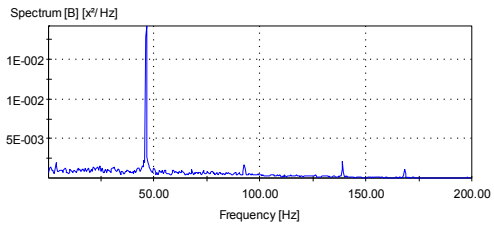

Project: SPECT_R44_pos50 - **Pos:** 0.00;0.00;0.00 - **Date/Time:** #N/A

Build 3, Run 44-1, Cavity 3, r/b=0.508, Re_{Φ}=1.99x10^{6}, Re_{z}=1.65x10^{5}, Ro=1.58

Appendix 7.1: Selected heat transfer test reports

MULTIPLE CAVITY RIG

Page 1/4

Build: 3 **ExpDate:** 11/12/2003

Printed: 27/09/2008

Exp Code: 3S--------- **Run:** B3run28-1

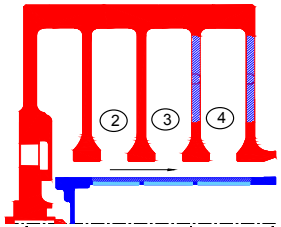

Rez:	1.16E+05	±	6.9E+01	ReΦ:	4.12E+06	±	5.7E+03
Ro:	0.54	±	4.4E-04	RotSpeed (rpm):	4552.2	±	1.0E-01
Mflow (kg/s):	0.425			Pcav (abs Pa):	3.094E+05		
Bo*:	0.308	±	4.7E-03	Pr:	0.706	±	3.9E-05
Tinlet (K):	314.83	±	2.4E-01	Texit(K):	318.29	±	2.6E-01
Tcav2 (K):	324.92	±	6.7E-01	Tcav3 (K):	319.62	±	6.7E-01
ΔTmeas (K):	3.45	±	3.3E-01	ΔTcalc (K):	3.28	±	5.5E-02
βΔTav:	0.027	±	7.7E-04	finβΔT av:	0.027	±	7.7E-04
Ø:	1.646	±	4.8E+00	finØ:	1.119	±	5.1E+00
Ts,C2, d,av(K):	325.12	±	1.4E-01	Ts,C3, u,av(K):	321.97	±	1.2E-01
Ts,C3, d,av(K):	324.19	±	1.4E-01	Ts,C4, u,av(K):	322.26	±	1.6E-01
finTs, D2,av(K):	323.54	±	8.9E-02	finTS, D3,av(K):	323.22	±	1.1E-01
Nu,C2, d,av:	-2103.6	±	1.3E+02	Nu,C3, u,av:	3453.3	±	2.8E+02
Nu,C3, d,av:	-1331.1	±	1.5E+02	Nu,C4, u,av:	2076.0	±	2.6E+02
finNu, D2,av:	152.0	±	1.9E+01	finNu, D3,av:	168.5	±	1.9E+01
Tsh,C2 (K):	354.86	±	2.4E-01	Tsh,C3 (K):	349.15	±	2.3E-01
Nush,C2:	99.7	±	2.5E+00	Nush,C3:	113.2	±	3.0E+00
Grsh,C2:	1.63E+09	±	1.9E+07	Grsh,C3:	1.37E+09	±	1.7E+07
θ2:	1.34	±	2.9E-02	θ3:	1.16	±	2.5E-02

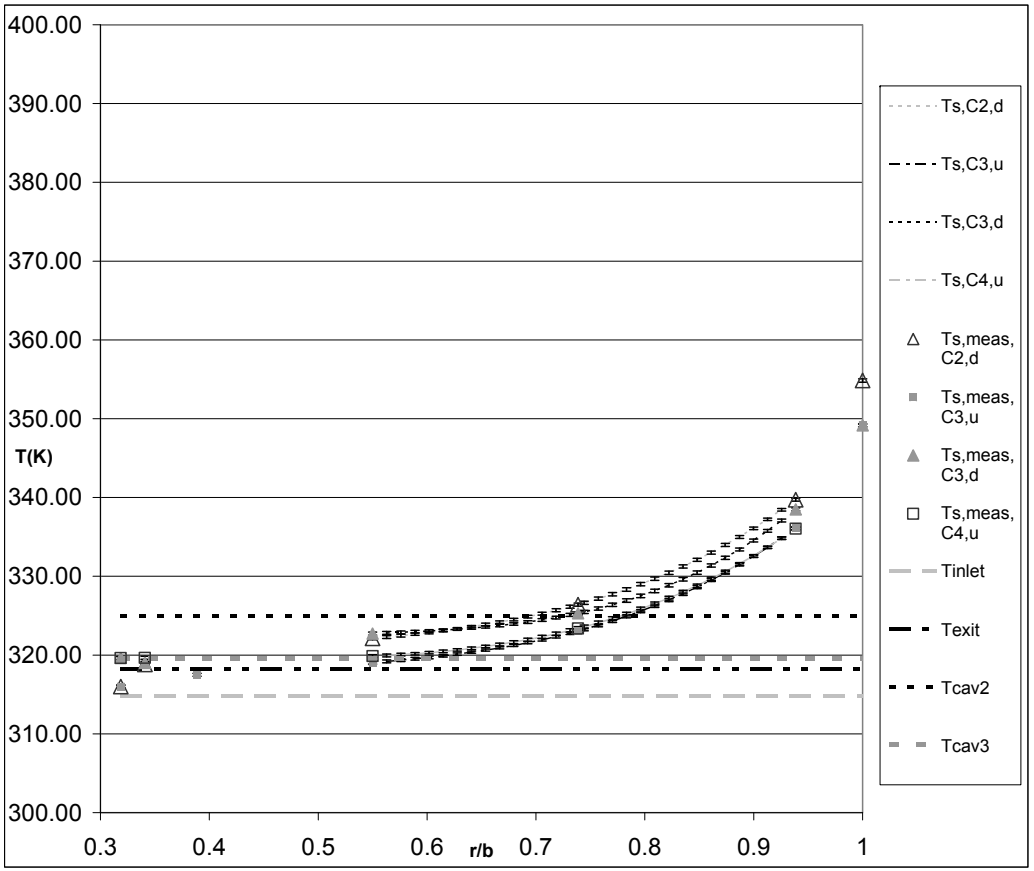

MULTIPLE CAVITY RIG

Page 2/4

Build: 3 **ExpDate:** 11/12/2003

Exp Code: 3S--------- **Run:** B3run28-1

Printed: 27/09/2008

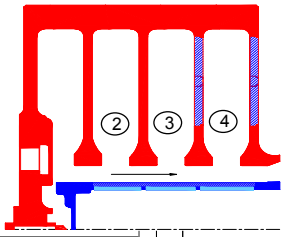

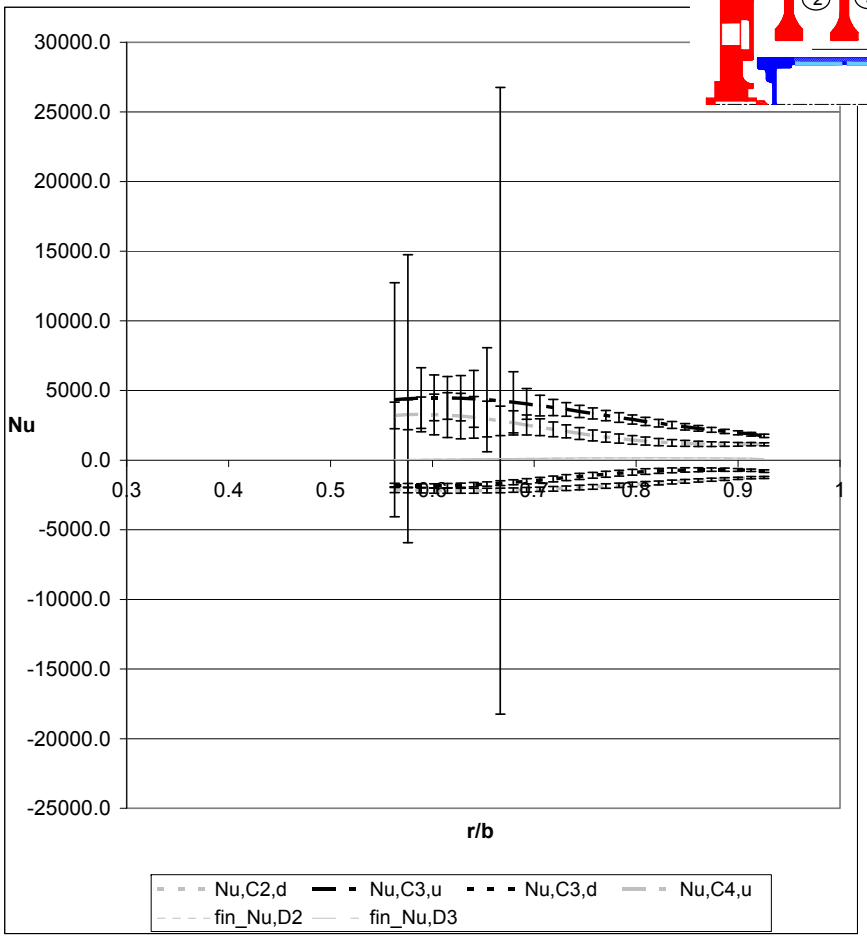

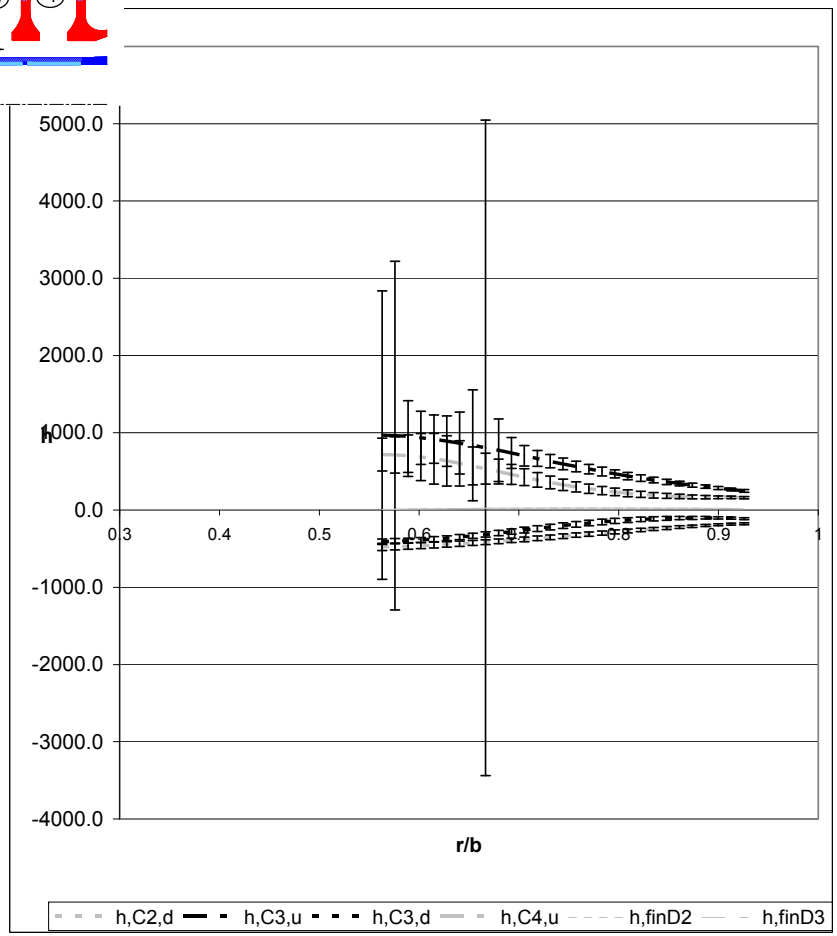

MULTIPLE CAVITY RIG

Build: 3 **ExpDate:** 11/12/2003
Exp Code: 3S--------- **Run:** B3run28-1

Radius(m)	non-dim radius	Tsh/cob D2	±	Tsh/cob D3	±	TC,C2, dn (K)	±	TC,C3, up (K)	±	TC,C3, dn (K)	±	TC,C4, up (K)	±	Ts,C2, dn (K)	±	Ts,C3, up (K)	±	Ts,C3, dn (K)	±	Ts,C4, up (K)	±	finTs, D2 (K)	±	finTs, D3 (K)	±
0.0701	0.31864	316.01	0.18	319.63	0.20																				
0.075	0.34091					318.82	0.20			319.00	0.20	319.65	0.20												
0.0855	0.38864							317.50	0.18																
0.121	0.55					322.12	0.19	319.07	0.19	322.73	0.20	319.88	0.18												
0.12385	0.56295													322.29	0.18	319.21	0.19	322.81	0.19	319.96	0.18	320.75	0.12	321.39	0.14
0.1267	0.57591													322.47	0.17	319.36	0.18	322.89	0.18	320.06	0.17	320.92	0.12	321.47	0.13
0.12955	0.58886													322.67	0.17	319.53	0.17	322.98	0.17	320.17	0.16	321.10	0.11	321.57	0.12
0.1324	0.60182													322.88	0.16	319.71	0.16	323.07	0.16	320.31	0.16	321.29	0.11	321.69	0.12
0.13525	0.61477													323.10	0.16	319.91	0.15	323.17	0.15	320.47	0.16	321.50	0.10	321.82	0.11
0.1381	0.62773													323.34	0.16	320.12	0.15	323.29	0.15	320.65	0.16	321.73	0.10	321.97	0.11
0.14095	0.64068													323.60	0.16	320.36	0.14	323.42	0.15	320.86	0.16	321.98	0.10	322.14	0.11
0.1438	0.65364													323.88	0.16	320.62	0.14	323.57	0.15	321.09	0.17	322.25	0.10	322.33	0.11
0.14665	0.66659													324.19	0.16	320.91	0.14	323.75	0.15	321.35	0.17	322.55	0.10	322.55	0.12
0.1495	0.67955													324.52	0.17	321.23	0.14	323.95	0.16	321.64	0.18	322.87	0.10	322.80	0.12
0.15235	0.6925													324.87	0.18	321.57	0.15	324.19	0.16	321.96	0.19	323.22	0.11	323.08	0.13
0.1552	0.70545													325.26	0.18	321.94	0.15	324.45	0.17	322.32	0.20	323.60	0.11	323.39	0.13
0.15805	0.71841													325.68	0.19	322.35	0.16	324.76	0.18	322.71	0.21	324.02	0.12	323.73	0.14
0.1609	0.73136													326.14	0.20	322.79	0.17	325.10	0.19	323.13	0.22	324.46	0.12	324.11	0.15
0.1625	0.73864					326.41	0.20	323.05	0.18	325.31	0.20	323.39	0.22												
0.16375	0.74432													326.63	0.20	323.27	0.18	325.48	0.20	323.59	0.23	324.95	0.13	324.54	0.16
0.1666	0.75727													327.16	0.21	323.78	0.19	325.91	0.21	324.09	0.23	325.47	0.14	325.00	0.16
0.16945	0.77023													327.72	0.21	324.34	0.20	326.39	0.21	324.63	0.24	326.03	0.14	325.51	0.17
0.1723	0.78318													328.34	0.22	324.93	0.20	326.92	0.22	325.21	0.24	326.63	0.15	326.07	0.17
0.17515	0.79614													328.99	0.22	325.58	0.21	327.51	0.22	325.84	0.24	327.28	0.15	326.67	0.17
0.178	0.80909													329.69	0.22	326.26	0.21	328.15	0.22	326.51	0.24	327.98	0.15	327.33	0.17
0.18085	0.82205													330.44	0.21	327.00	0.21	328.85	0.22	327.23	0.23	328.72	0.15	328.04	0.17
0.1837	0.835													331.24	0.21	327.79	0.20	329.62	0.22	327.99	0.23	329.52	0.15	328.81	0.16
0.18655	0.84795													332.10	0.20	328.62	0.20	330.46	0.21	328.81	0.22	330.36	0.14	329.63	0.16
0.1894	0.86091													333.01	0.19	329.52	0.19	331.37	0.20	329.67	0.20	331.26	0.14	330.52	0.15
0.19225	0.87386													333.97	0.18	330.46	0.18	332.35	0.20	330.59	0.19	332.22	0.13	331.47	0.14
0.1951	0.88682													335.00	0.17	331.47	0.17	333.41	0.19	331.57	0.17	333.23	0.12	332.49	0.13
0.19795	0.89977													336.08	0.17	332.53	0.15	334.55	0.18	332.60	0.16	334.31	0.11	333.57	0.12
0.2008	0.91273													337.23	0.16	333.66	0.15	335.77	0.18	333.68	0.15	335.44	0.11	334.73	0.11
0.20365	0.92568													338.45	0.17	334.85	0.15	337.08	0.18	334.83	0.15	336.65	0.11	335.95	0.11
0.2065	0.93864					339.73	0.18	336.10	0.17	338.48	0.19	336.03	0.17												
0.22	1	354.86	0.22	349.15	0.18																				
0.24565		369.07	0.19	362.66	0.19																				

MULTIPLE CAVITY RIG

Build: 0 **ExpDate:** 11/12/2003
Exp Code: 0 **Run:** B3run28-1

Radius(m)	non-dim radius	Nu_r, C2,d	±	Nu_r, C3,u	±	Nu_r, C3,d	±	Nu_r, C4,u	±	finNu_r, D2	±	finNu_r, D3	±	h_r, C2,d	±	h_r, C3,u	±	h_r, C3,d	±	h_r, C4,u	±	fin-h, D2	±	fin-h, D3	±
0.0701	0.31864																								
0.075	0.34091																								
0.0855	0.38864																								
0.121	0.55																								
0.12385	0.56295	-2117.9	204.5	4340.5	8400.7	-1815.1	155.2	3206.4	952.2	38.7	770.3	27.9	646.8	-477.0	46.1	969.5	1867.5	-409.3	35.1	717.6	212.5	8.7	172.6	6.3	145.3
0.1267	0.57591	-2141.0	200.9	4410.1	10335.3	-1833.4	153.7	3264.4	1074.6	55.2	192.3	42.3	163.2	-471.6	44.3	963.3	2256.9	-404.2	33.9	714.4	234.6	12.1	42.1	9.3	35.8
0.12955	0.58886	-2163.2	196.3	4452.7	2174.2	-1842.4	152.6	3285.5	1254.8	66.2	67.8	53.6	54.6	-466.2	42.4	951.6	463.5	-397.4	33.0	703.4	267.9	14.2	14.5	11.5	11.7
0.1324	0.60182	-2181.1	190.9	4472.5	1647.8	-1840.6	152.3	3274.1	1456.9	75.2	30.1	64.0	20.1	-460.2	40.3	935.7	343.7	-388.5	32.2	686.1	304.5	15.8	6.3	13.5	4.2
0.13525	0.61477	-2193.4	184.8	4470.4	1532.6	-1827.1	153.2	3232.2	1606.0	83.6	18.2	74.2	9.3	-453.3	38.2	916.1	313.0	-377.7	31.7	663.3	328.6	17.2	3.7	15.3	1.9
0.1381	0.62773	-2199.5	178.5	4446.7	1626.4	-1801.7	155.6	3162.5	1623.2	91.5	14.3	84.4	6.6	-445.5	36.2	892.9	325.4	-364.9	31.6	635.9	325.4	18.5	2.9	17.0	1.3
0.14095	0.64068	-2199.0	172.5	4401.9	2040.0	-1764.6	159.6	3067.9	1493.3	99.1	12.6	94.4	6.3	-436.7	34.3	866.6	400.1	-350.2	31.7	604.8	293.4	19.6	2.5	18.7	1.2
0.1438	0.65364	-2191.8	167.2	4337.1	3730.7	-1716.3	165.3	2952.2	1277.9	106.2	11.7	104.3	6.4	-426.9	32.6	837.5	717.5	-334.0	32.2	570.8	246.2	20.6	2.3	20.2	1.2
0.14665	0.66659	-2177.9	163.3	4253.8	22498.0	-1657.7	172.4	2819.6	1053.1	112.9	11.1	113.8	6.7	-416.3	31.3	806.1	4243.3	-316.5	33.0	534.9	199.0	21.5	2.1	21.7	1.3
0.1495	0.67955	-2157.4	161.0	4154.1	2194.6	-1590.0	180.6	2674.6	861.7	119.0	10.7	122.9	7.1	-404.9	30.3	772.8	406.4	-297.9	33.9	498.1	159.9	22.2	2.0	23.0	1.3
0.15235	0.6925	-2130.6	160.3	4040.3	1100.9	-1514.6	189.2	2521.9	714.6	124.5	10.5	131.4	7.6	-392.7	29.6	738.3	200.2	-278.7	34.9	461.3	130.2	22.9	1.9	24.1	1.4
0.1552	0.70545	-2097.8	161.1	3915.0	743.7	-1433.4	197.5	2365.8	606.7	129.4	10.3	139.1	8.0	-380.0	29.2	702.9	132.9	-259.1	35.8	425.2	108.6	23.3	1.9	25.1	1.4
0.15805	0.71841	-2059.7	162.7	3780.7	581.8	-1348.5	205.0	2210.4	528.3	133.7	10.2	146.0	8.5	-366.8	29.0	667.3	102.3	-239.5	36.5	390.5	93.0	23.7	1.8	25.9	1.5
0.1609	0.73136	-2016.7	164.5	3640.1	495.0	-1262.0	210.9	2059.3	470.5	137.3	10.2	152.1	8.9	-353.2	28.9	631.8	85.6	-220.4	36.9	357.8	81.4	23.9	1.8	26.5	1.5
0.1625	0.73864																								
0.16375	0.74432	-1969.5	166.0	3495.5	441.6	-1175.9	214.7	1915.4	426.0	140.3	10.1	157.3	9.3	-339.3	28.6	596.9	75.1	-202.0	36.9	327.4	72.6	24.1	1.7	26.9	1.6
0.1666	0.75727	-1918.8	166.4	3349.1	403.9	-1092.5	216.0	1781.0	390.0	142.6	10.1	161.5	9.6	-325.4	28.3	562.9	67.6	-184.7	36.5	299.6	65.4	24.1	1.7	27.2	1.6
0.16945	0.77023	-1865.2	165.5	3202.8	373.6	-1013.7	214.6	1658.1	359.1	144.3	10.1	164.8	9.9	-311.4	27.7	530.0	61.6	-168.7	35.7	274.6	59.3	24.0	1.7	27.4	1.6
0.1723	0.78318	-1809.4	162.9	3058.1	346.8	-941.1	210.4	1547.7	331.3	145.5	10.0	167.2	10.0	-297.6	26.8	498.5	56.3	-154.2	34.5	252.5	53.9	23.8	1.6	27.3	1.6
0.17515	0.79614	-1752.2	158.6	2916.4	321.3	-876.2	203.5	1450.8	305.3	146.1	9.9	168.8	10.1	-284.0	25.8	468.5	51.4	-141.5	32.9	233.2	48.9	23.6	1.6	27.2	1.6
0.178	0.80909	-1694.1	152.5	2778.8	296.2	-820.0	194.2	1367.5	280.3	146.3	9.8	169.6	10.1	-270.7	24.4	440.0	46.7	-130.5	30.9	216.7	44.3	23.3	1.6	26.9	1.6
0.18085	0.82205	-1635.7	144.8	2646.0	271.3	-773.2	182.8	1298.0	256.1	146.0	9.7	169.8	10.1	-257.7	22.9	413.2	42.2	-121.3	28.7	202.8	39.9	22.9	1.5	26.6	1.6
0.1837	0.835	-1577.4	135.7	2518.6	246.4	-736.2	169.7	1242.0	232.3	145.3	9.5	169.3	10.0	-245.2	21.2	388.0	37.8	-114.0	26.3	191.4	35.7	22.5	1.5	26.1	1.5
0.18655	0.84795	-1519.9	125.6	2396.9	221.7	-709.2	155.4	1199.0	209.2	144.3	9.3	168.2	9.8	-233.2	19.3	364.4	33.6	-108.3	23.8	182.4	31.7	22.0	1.4	25.6	1.5
0.1894	0.86091	-1463.5	114.7	2281.1	197.7	-692.2	140.5	1168.3	186.8	142.8	9.2	166.5	9.5	-221.7	17.4	342.4	29.5	-104.4	21.2	175.4	28.0	21.5	1.4	25.1	1.4
0.19225	0.87386	-1408.7	103.8	2171.1	174.9	-685.0	125.7	1149.1	165.6	140.9	9.3	164.1	9.4	-210.7	15.6	321.8	25.8	-102.0	18.7	170.4	24.5	21.0	1.4	24.4	1.4
0.1951	0.88682	-1356.2	93.7	2066.2	154.2	-687.7	111.9	1140.0	146.3	138.0	11.7	160.5	11.6	-200.4	13.9	302.6	22.5	-101.2	16.5	167.0	21.4	20.3	1.7	23.6	1.7
0.19795	0.89977	-1307.5	85.4	1965.0	137.3	-701.2	100.2	1138.6	130.1	132.8	23.8	154.2	24.1	-191.0	12.5	284.4	19.8	-102.0	14.6	164.8	18.8	19.3	3.5	22.4	3.5
0.2008	0.91273	-1266.0	80.4	1863.0	126.0	-729.0	92.1	1139.6	118.6	121.6	65.3	140.9	67.6	-182.8	11.7	266.6	17.9	-104.9	13.3	163.1	16.9	17.5	9.4	20.2	9.7
0.20365	0.92568	-1242.2	79.8	1747.9	122.4	-783.0	88.8	1129.3	114.0	93.4	245.9	108.0	255.9	-177.4	11.4	247.4	17.2	-111.4	12.7	159.8	16.1	13.3	35.0	15.3	36.3
0.2065	0.93864																								
0.22	1																								
0.24565																									

MULTIPLE CAVITY RIG

Build: 3 **ExpDate:** 1/16/2004

Exp Code: 3S--------- **Run:** B3run32-1

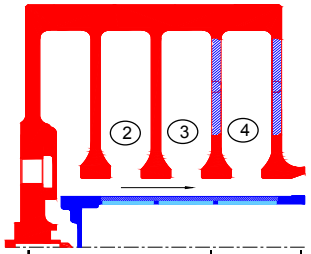

Rez:	9.18E+04	±	5.5E+01	ReΦ:	4.92E+05	±	6.9E+02
Ro:	3.56	±	2.9E-03	RotSpeed (rpm):	665.6	±	1.7E-02
Mflow (kg/s):	0.333			Pcav (abs Pa):	2.453E+05		
Bo*:	0.084	±	4.5E-04	Pr:	0.707	±	3.7E-05
Tinlet (K):	309.75	±	2.4E-01	Texit(K):	313.60	±	2.6E-01
Tcav2 (K):	317.27	±	1.3E+00	Tcav3 (K):	328.33	±	1.0E+00
ΔTmeas (K):	3.85	±	3.3E-01	ΔTcalc (K):	3.42	±	6.3E-02
βΔTav:	0.089	±	8.3E-04	finβΔT av:	0.089	±	8.3E-04
Ø:	0.404	±	5.5E-02	finØ:	0.283	±	3.3E-02
Ts,C2, d,av(K):	333.50	±	1.3E-01	Ts,C3, u,av(K):	333.65	±	1.3E-01
Ts,C3, d,av(K):	340.66	±	1.4E-01	Ts,C4, u,av(K):	341.55	±	1.2E-01
finTs, D2,av(K):	333.57	±	9.3E-02	finTS, D3,av(K):	341.11	±	9.2E-02
Nu,C2, d,av:	166.7	±	5.6E+01	Nu,C3, u,av:	108.7	±	5.5E+01
Nu,C3, d,av:	299.5	±	4.5E+01	Nu,C4, u,av:	-136.4	±	4.2E+01
finNu, D2,av:	117.8	±	7.4E+00	finNu, D3,av:	75.6	±	5.8E+00
Tsh,C2 (K):	377.70	±	2.0E-01	Tsh,C3 (K):	383.50	±	1.5E-01
Nush,C2:	39.0	±	1.1E+00	Nush,C3:	31.8	±	7.5E-01
Grsh,C2:	4.89E+07	±	3.8E+05	Grsh,C3:	5.30E+07	±	3.8E+05
θ2:	1.12	±	2.7E-02	θ3:	1.34	±	2.6E-02

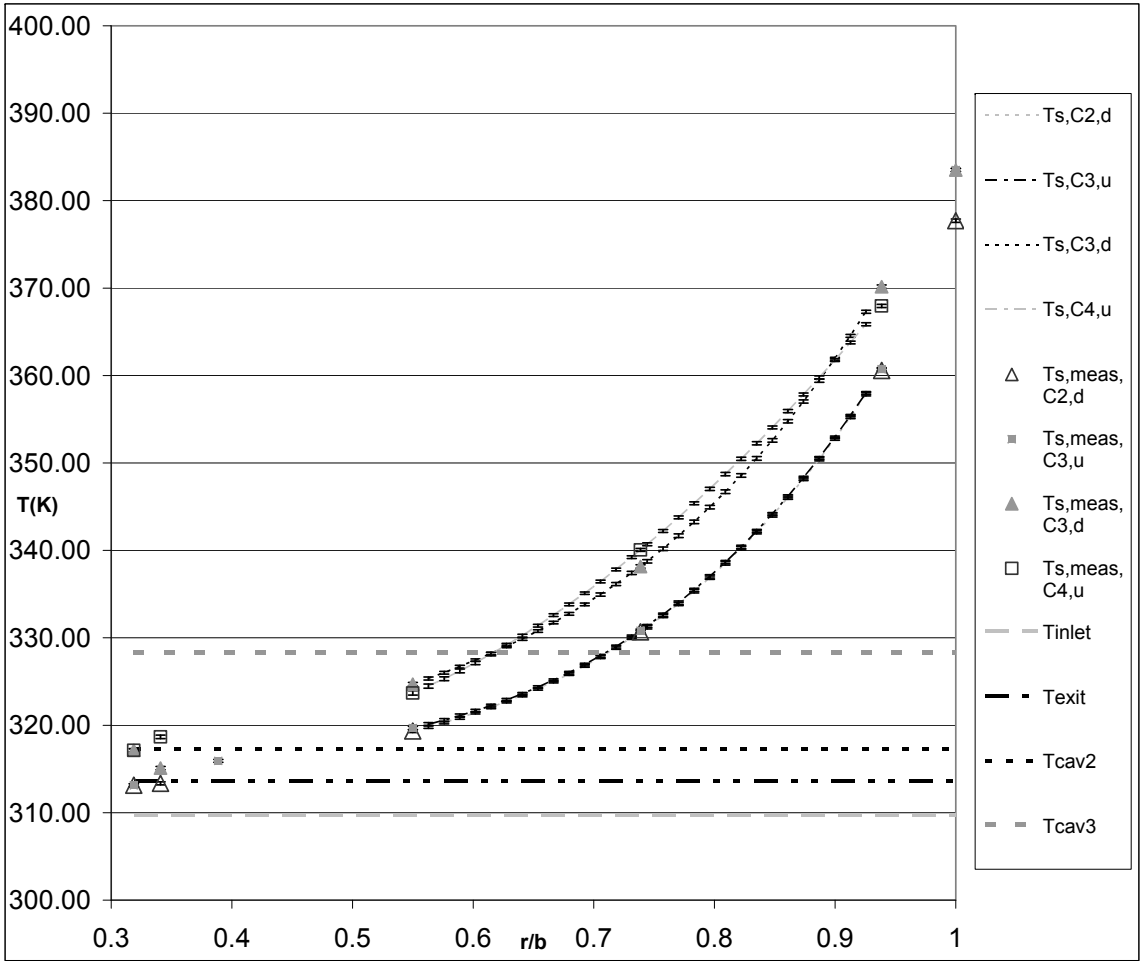

MULTIPLE CAVITY RIG

Page 2/4

Build: 3 **ExpDate:** 1/16/2004

Printed: 27/09/2008

Exp Code: 3S--------- **Run:** B3run32-1

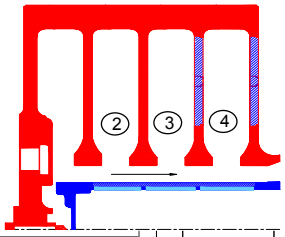

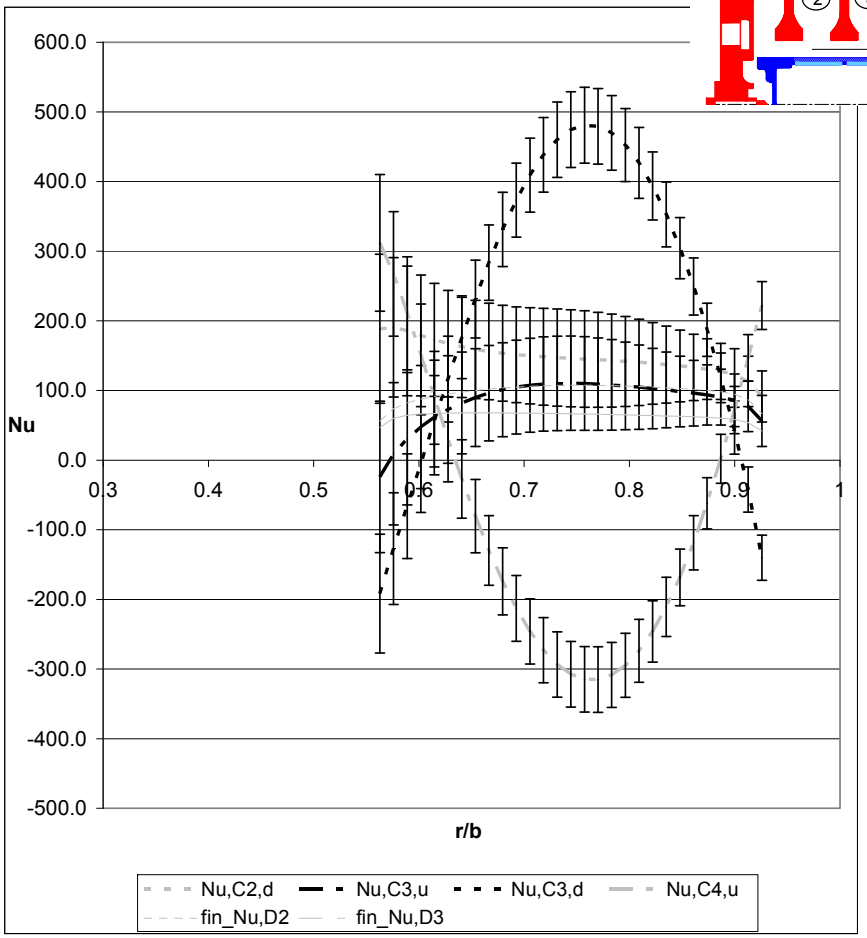

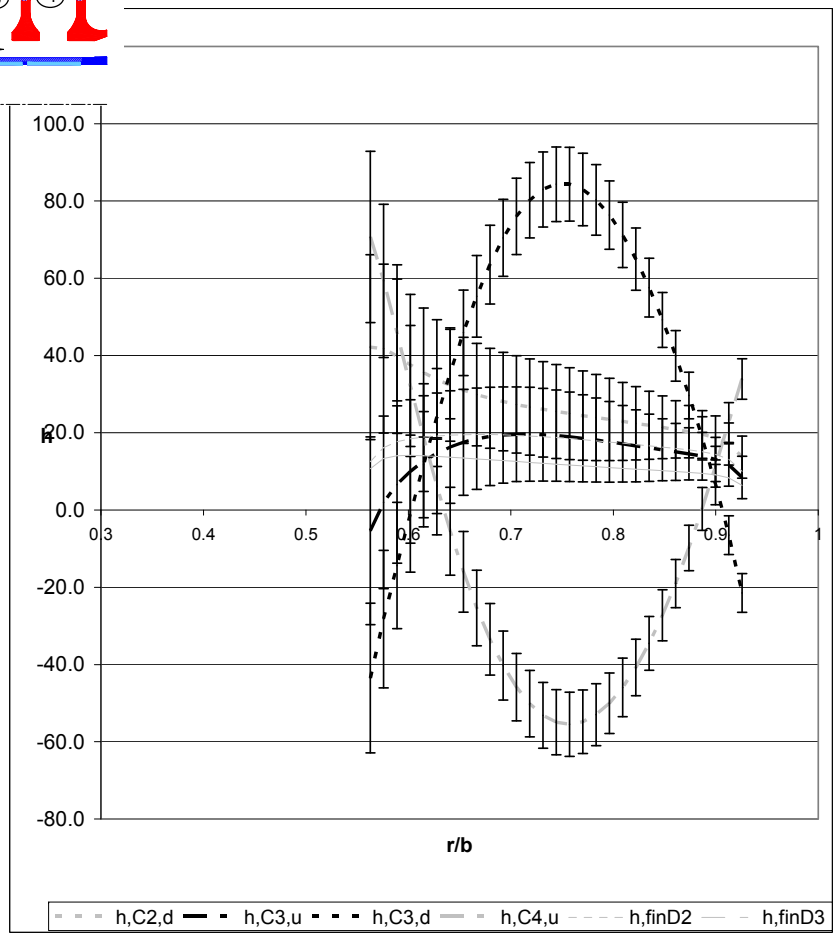

MULTIPLE CAVITY RIG

Build: 3 **ExpDate:** 1/16/2004
Exp Code: 3S--------- **Run:** B3run32-1

Radius(m)	non-dim radius	Tsh/cob D2	±	Tsh/cob D3	±	TC,C2, dn (K)	±	TC,C3, up (K)	±	TC,C3, dn (K)	±	TC,C4, up (K)	±	Ts,C2, dn (K)	±	Ts,C3, up (K)	±	Ts,C3, dn (K)	±	Ts,C4, up (K)	±	finTs, D2 (K)	±	finTs, D3 (K)	±
0.0701	0.31864	313.15	0.17	317.14	0.18																				
0.075	0.34091					313.36	0.17			315.11	0.18	318.68	0.20												
0.0855	0.38864							315.92	0.17																
0.121	0.55					319.35	0.17	319.68	0.19	324.70	0.18	323.70	0.24												
0.12385	0.56295													319.82	0.17	320.12	0.19	325.34	0.17	324.49	0.23	319.97	0.13	324.91	0.14
0.1267	0.57591													320.32	0.16	320.59	0.18	326.01	0.17	325.32	0.22	320.45	0.13	325.66	0.14
0.12955	0.58886													320.85	0.16	321.10	0.18	326.71	0.16	326.21	0.21	320.98	0.13	326.46	0.13
0.1324	0.60182													321.43	0.15	321.65	0.17	327.44	0.15	327.14	0.20	321.54	0.12	327.29	0.12
0.13525	0.61477													322.05	0.15	322.25	0.17	328.21	0.15	328.13	0.19	322.15	0.12	328.17	0.12
0.1381	0.62773													322.71	0.15	322.90	0.16	329.02	0.15	329.17	0.18	322.80	0.12	329.09	0.11
0.14095	0.64068													323.42	0.15	323.59	0.16	329.87	0.14	330.26	0.17	323.50	0.12	330.07	0.11
0.1438	0.65364													324.18	0.15	324.34	0.16	330.78	0.15	331.40	0.16	324.26	0.12	331.09	0.11
0.14665	0.66659													324.99	0.15	325.15	0.16	331.73	0.15	332.58	0.16	325.07	0.12	332.16	0.11
0.1495	0.67955													325.86	0.16	326.01	0.16	332.74	0.16	333.82	0.15	325.94	0.12	333.28	0.11
0.15235	0.6925													326.80	0.16	326.94	0.16	333.82	0.16	335.10	0.15	326.87	0.12	334.46	0.11
0.1552	0.70545													327.80	0.17	327.94	0.16	334.95	0.17	336.43	0.15	327.87	0.12	335.69	0.11
0.15805	0.71841													328.86	0.17	329.00	0.17	336.15	0.18	337.81	0.15	328.93	0.12	336.98	0.12
0.1609	0.73136													330.00	0.18	330.14	0.17	337.42	0.19	339.23	0.16	330.07	0.13	338.33	0.12
0.1625	0.73864					330.67	0.18	330.81	0.17	338.16	0.19	340.05	0.16												
0.16375	0.74432													331.21	0.18	331.35	0.18	338.76	0.19	340.70	0.16	331.28	0.13	339.73	0.13
0.1666	0.75727													332.50	0.19	332.65	0.18	340.18	0.20	342.22	0.17	332.58	0.13	341.20	0.13
0.16945	0.77023													333.88	0.19	334.02	0.18	341.68	0.20	343.78	0.17	333.95	0.13	342.73	0.13
0.1723	0.78318													335.33	0.20	335.48	0.19	343.27	0.21	345.38	0.18	335.40	0.14	344.33	0.14
0.17515	0.79614													336.87	0.20	337.02	0.19	344.94	0.21	347.03	0.18	336.95	0.14	345.99	0.14
0.178	0.80909													338.51	0.19	338.66	0.19	346.70	0.21	348.73	0.18	338.58	0.13	347.72	0.14
0.18085	0.82205													340.24	0.19	340.39	0.19	348.56	0.21	350.46	0.18	340.31	0.13	349.51	0.14
0.1837	0.835													342.06	0.19	342.22	0.18	350.52	0.20	352.24	0.18	342.14	0.13	351.38	0.14
0.18655	0.84795													343.99	0.18	344.15	0.18	352.58	0.20	354.06	0.18	344.07	0.12	353.32	0.13
0.1894	0.86091													346.02	0.18	346.18	0.17	354.75	0.19	355.93	0.17	346.10	0.12	355.34	0.13
0.19225	0.87386													348.16	0.17	348.32	0.16	357.02	0.18	357.83	0.17	348.24	0.11	357.43	0.12
0.1951	0.88682													350.41	0.16	350.57	0.15	359.41	0.18	359.78	0.16	350.49	0.11	359.59	0.12
0.19795	0.89977													352.77	0.16	352.93	0.15	361.92	0.17	361.76	0.16	352.85	0.11	361.84	0.11
0.2008	0.91273													355.25	0.17	355.41	0.15	364.54	0.17	363.79	0.16	355.33	0.11	364.16	0.11
0.20365	0.92568													357.85	0.18	358.01	0.15	367.29	0.18	365.85	0.17	357.93	0.12	366.57	0.12
0.2065	0.93864					360.57	0.21	360.73	0.17	370.17	0.20	367.95	0.18												
0.22	1	377.70	0.20	383.50	0.18																				
0.24565		388.15	0.17	392.76	0.17																				

MULTIPLE CAVITY RIG

Build: 0 **ExpDate:** 1/16/2004

Exp Code: 0 **Run:** B3run32-1

Radius(m)	non-dim radius	Nu_r, C2,d	±	Nu_r, C3,u	±	Nu_r, C3,d	±	Nu_r, C4,u	±	finNu_r, D2	±	finNu_r, D3	±	h_r, C2,d	±	h_r, C3,u	±	h_r, C3,d	±	h_r, C4,u	±	fin-h, D2	±	fin-h, D3	±
0.0701	0.31864																								
0.075	0.34091																								
0.0855	0.38864																								
0.121	0.55																								
0.12385	0.56295	188.5	107.0	-24.0	108.8	-191.6	85.3	312.0	98.1	55.9	256.8	47.1	202.4	42.2	23.9	-5.4	24.3	-43.5	19.4	70.7	22.2	12.5	57.4	10.7	45.9
0.1267	0.57591	190.9	100.0	9.1	102.1	-127.0	80.2	267.3	89.5	73.9	63.1	60.0	49.4	41.8	21.9	2.0	22.3	-28.2	17.8	59.3	19.8	16.2	13.8	13.3	11.0
0.12955	0.58886	185.6	93.1	30.8	95.1	-66.1	75.1	210.8	81.2	82.4	21.1	64.4	16.2	39.8	20.0	6.6	20.4	-14.4	16.3	45.9	17.6	17.7	4.5	14.0	3.5
0.1324	0.60182	179.0	86.8	47.5	88.4	-5.2	70.1	150.4	73.6	87.6	8.4	66.2	5.9	37.6	18.2	10.0	18.6	-1.1	15.0	32.1	15.7	18.4	1.8	14.1	1.3
0.13525	0.61477	172.7	81.2	61.1	82.3	55.9	65.6	89.5	66.8	91.6	4.5	67.0	2.6	35.6	16.7	12.6	17.0	11.7	13.7	18.7	14.0	18.9	0.9	14.0	0.6
0.1381	0.62773	167.2	76.5	72.6	77.2	116.4	61.6	29.9	61.0	94.8	3.3	67.4	1.6	33.8	15.5	14.7	15.6	23.9	12.7	6.2	12.5	19.2	0.7	13.9	0.3
0.14095	0.64068	162.7	73.0	82.1	73.2	175.3	58.3	-27.1	56.2	97.6	2.8	67.7	1.2	32.3	14.5	16.3	14.5	35.4	11.8	-5.5	11.4	19.4	0.6	13.7	0.2
0.1438	0.65364	159.0	70.6	89.9	70.3	231.4	55.8	-80.5	52.6	100.0	2.6	67.8	1.1	31.0	13.8	17.5	13.7	45.9	11.1	-16.0	10.4	19.5	0.5	13.5	0.2
0.14665	0.66659	155.9	69.3	96.2	68.5	283.7	54.2	-129.7	49.9	102.0	2.4	67.8	1.0	29.9	13.3	18.4	13.1	55.3	10.5	-25.3	9.8	19.5	0.5	13.2	0.2
0.1495	0.67955	153.5	68.7	101.2	67.5	331.3	53.3	-174.0	48.2	103.7	2.3	67.8	1.0	28.9	12.9	19.1	12.7	63.5	10.2	-33.5	9.3	19.5	0.4	13.0	0.2
0.15235	0.6925	151.5	68.8	104.9	67.2	373.4	53.0	-212.8	47.2	105.0	2.3	67.6	1.0	28.1	12.7	19.4	12.5	70.5	10.0	-40.3	8.9	19.5	0.4	12.8	0.2
0.1552	0.70545	149.9	69.1	107.5	67.4	409.3	53.2	-245.9	46.8	106.1	2.2	67.5	1.1	27.3	12.6	19.6	12.3	76.0	9.9	-45.9	8.7	19.3	0.4	12.6	0.2
0.15805	0.71841	148.5	69.5	109.2	67.6	438.4	53.6	-272.9	46.7	106.8	2.3	67.2	1.2	26.7	12.5	19.6	12.1	80.2	9.8	-50.1	8.6	19.2	0.4	12.3	0.2
0.1609	0.73136	147.3	69.8	110.2	67.8	460.2	54.1	-293.5	46.9	107.3	2.3	67.0	1.2	26.1	12.3	19.5	12.0	83.0	9.7	-53.2	8.5	19.0	0.4	12.1	0.2
0.1625	0.73864																								
0.16375	0.74432	146.2	69.7	110.4	67.7	474.5	54.4	-307.5	47.0	107.5	2.3	66.6	1.3	25.5	12.1	19.3	11.8	84.4	9.6	-54.9	8.4	18.8	0.4	11.9	0.2
0.1666	0.75727	145.2	69.2	110.1	67.3	481.0	54.5	-314.7	47.1	107.5	2.4	66.3	1.4	25.0	11.9	18.9	11.6	84.3	9.5	-55.5	8.3	18.5	0.4	11.7	0.2
0.16945	0.77023	144.1	68.2	109.3	66.4	479.4	54.3	-315.1	47.1	107.3	2.4	65.9	1.5	24.4	11.5	18.5	11.3	83.0	9.4	-54.8	8.2	18.2	0.4	11.4	0.3
0.1723	0.78318	143.0	66.6	108.1	65.0	469.9	53.6	-308.4	46.7	106.9	2.5	65.4	1.6	23.9	11.1	18.1	10.9	80.3	9.1	-53.0	8.0	17.9	0.4	11.2	0.3
0.17515	0.79614	141.7	64.5	106.6	63.0	452.3	52.5	-294.7	46.1	106.4	2.5	65.0	1.7	23.4	10.7	17.6	10.4	76.4	8.8	-50.0	7.8	17.6	0.4	11.0	0.3
0.178	0.80909	140.4	61.9	104.8	60.6	426.8	50.9	-273.9	45.2	105.7	2.5	64.5	1.7	22.9	10.1	17.1	9.9	71.2	8.5	-45.9	7.6	17.3	0.4	10.8	0.3
0.18085	0.82205	138.9	58.8	102.9	57.7	393.6	48.9	-245.9	44.0	104.9	2.5	64.0	1.8	22.4	9.5	16.6	9.3	64.9	8.0	-40.8	7.3	17.0	0.4	10.6	0.3
0.1837	0.835	137.2	55.3	100.8	54.4	352.8	46.6	-210.7	42.5	104.0	2.6	63.4	1.8	21.9	8.8	16.1	8.7	57.6	7.6	-34.5	7.0	16.6	0.4	10.4	0.3
0.18655	0.84795	135.3	51.5	98.6	50.8	304.6	43.9	-168.3	40.7	102.9	2.6	62.9	1.9	21.4	8.1	15.6	8.0	49.2	7.1	-27.3	6.6	16.3	0.4	10.2	0.3
0.1894	0.86091	133.2	47.5	96.2	47.0	249.3	41.1	-118.7	38.8	101.7	2.6	62.2	1.9	20.9	7.4	15.1	7.4	39.9	6.6	-19.0	6.2	15.9	0.4	10.0	0.3
0.19225	0.87386	130.7	43.7	93.6	43.4	187.2	38.2	-61.9	36.9	100.3	2.8	61.5	1.9	20.3	6.8	14.5	6.7	29.7	6.1	-9.8	5.9	15.6	0.4	9.8	0.3
0.1951	0.88682	127.4	40.2	90.5	40.1	118.3	35.6	1.8	35.2	98.2	3.9	60.4	2.6	19.6	6.2	13.9	6.2	18.6	5.6	0.3	5.5	15.1	0.6	9.5	0.4
0.19795	0.89977	122.5	37.6	85.9	37.6	42.3	33.6	71.9	33.9	94.7	8.8	58.4	6.6	18.7	5.7	13.1	5.7	6.6	5.2	11.2	5.3	14.4	1.3	9.1	1.0
0.2008	0.91273	113.2	36.2	77.1	36.3	-42.2	32.4	146.9	33.5	86.9	24.7	53.8	20.2	17.1	5.5	11.7	5.5	-6.5	5.0	22.6	5.2	13.1	3.7	8.3	3.1
0.20365	0.92568	91.5	36.5	56.3	36.7	-140.2	32.5	222.0	34.4	66.9	93.9	41.7	79.5	13.7	5.5	8.4	5.5	-21.5	5.0	33.9	5.2	10.0	14.1	6.4	12.2
0.2065	0.93864																								
0.22	1																								
0.24565																									